

Calculation of the Cutting Forces when Cutting Water Saturated Sand.

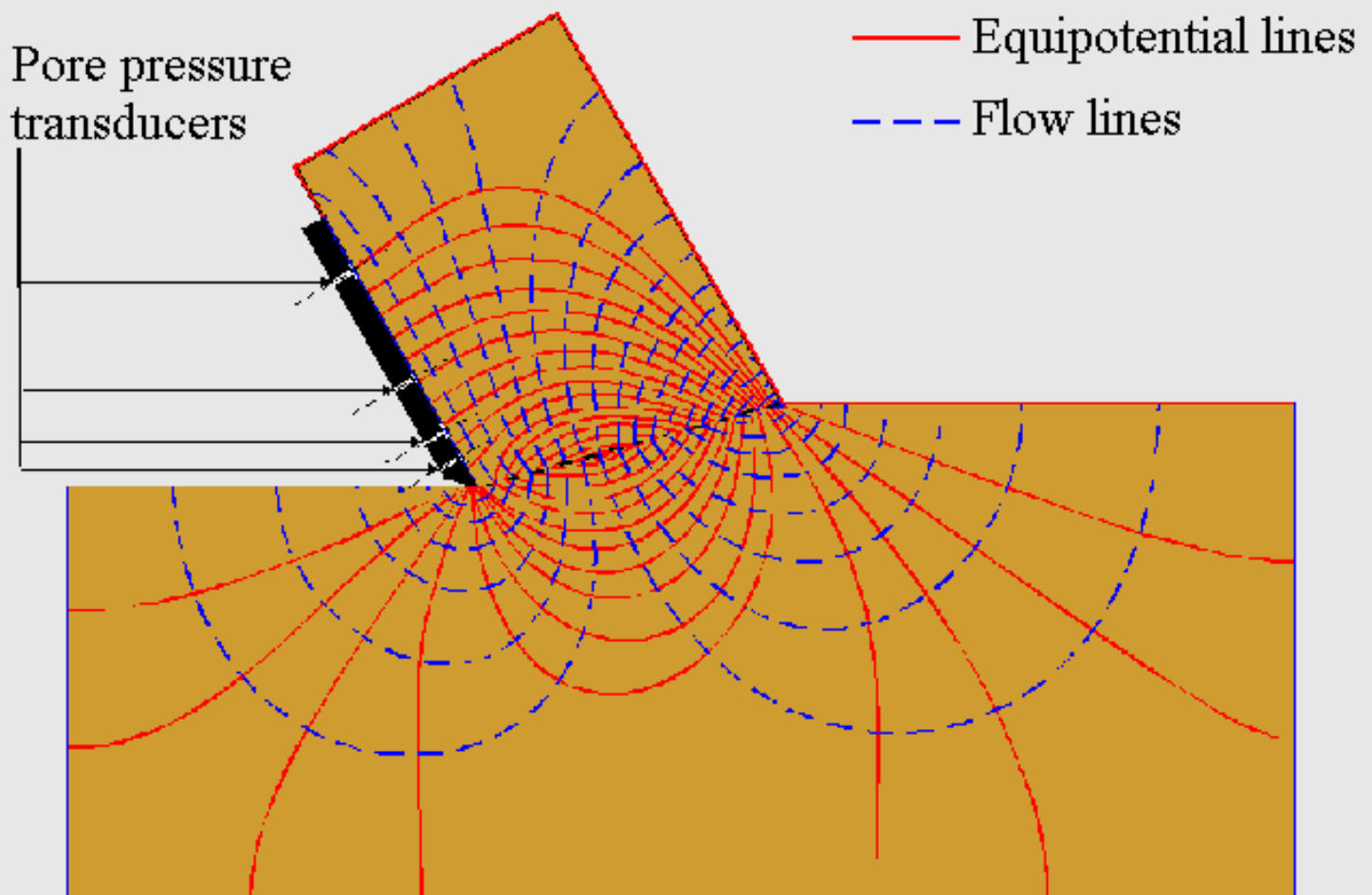
[Contents](#)

*Basic Theory and Applications for 3-D Blade Movements
and Periodically Varying Velocities for, in Dredging
Commonly used Excavating Means.*

Dr.ir. Sape Andries Miedema

Dissertation Contents

September 15th 1987



This dissertation is dedicated to:
Esther & Erik Miedema

[Back to top](#)

This is a translation of the dissertation of Dr.ir. S.A. Miedema, dated September 15th 1987 .
The dissertation was originally published in Dutch by the:
Delft University of Technology
Faculty of Mechanical Engineering and Marine Technology
Chair of Dredging Technology
Mekelweg 2
2628 CD, Delft
The Netherlands

It is advised to also read the papers following this dissertation, since the theory developed has been refined and extended.

Last modified Wednesday May 24, 2000 by: [Sape A. Miedema](#)

Translation by: [Laurens de Jonge](#)

Figures, equations and tables by: [Erik Miedema](#)

Copyright © May, 2000 Dr.ir. S.A. Miedema



[Download Adobe Acrobat Reader V4.0](#)

- [Preface](#)
 - [Summary](#)
 - [Contents](#)
 - [Introduction](#)
1. DREDMO (Dredge in Motions)
 1. [Equilibrium Equations of Motion of a Ship](#)
 2. [Solution Method of Equilibrium Equations of Motion](#)
 3. [The \$t=0\$ problem](#)
 4. [Discontinuities](#)
 2. The Two Dimensional Cutting Theory
 1. [Description of The Process](#)
 2. [Literature Survey](#)
 3. [Determination of the Underpressure around the Blade](#)
 4. [Numerical Pore Pressure Calculations](#)
 5. [The Tip of the Blade Problem](#)
 6. [The Forces on the Blade](#)
 7. [Determination of the Shear Angle \$\beta\$](#)
 8. [The Coefficients \$a_1\$ and \$a_2\$](#)
 9. [Determination of the Coefficients \$c_1\$, \$c_2\$, \$d_1\$ and \$d_2\$](#)
 10. [Determination of \$\phi\$ and \$\delta\$ from Cutting Tests](#)

11. [The Effect of a Transversal Velocity Component](#)
12. [Wear and Side Effects](#)
13. [Specific Cutting Energy](#)
14. Tables
 1. [Dimensionless Pore Pressures \(2.01\)](#)
 2. [The Non-Cavitating Cutting Process, \$\beta\$, \$d_1\$, \$d_2\$, \$a_1\$ for \$h_b/h_i=1\$ \(2.02, 2.14, 2.20 & 2.08,
without underpressure behind the blade\)](#)
 3. [The Non-Cavitating Cutting Process, \$\beta\$, \$d_1\$, \$d_2\$, \$a_1\$ for \$h_b/h_i=2\$ \(2.03, 2.15, 2.21, & 2.09,
without underpressure behind the blade\)](#)
 4. [The Non-Cavitating Cutting Process, \$\beta\$, \$d_1\$, \$d_2\$, \$a_1\$ for \$h_b/h_i=3\$ \(2.04, 2.16, 2.22, & 2.10,
without underpressure behind the blade\)](#)
 5. [The Cavitating Cutting Process, \$\beta\$, \$d_1\$, \$d_2\$ for \$h_b/h_i=1\$ \(2.05, 2.26 & 2.32,
without underpressure behind the blade\)](#)
 6. [The Cavitating Cutting Process, \$\beta\$, \$d_1\$, \$d_2\$ for \$h_b/h_i=2\$ \(2.06, 2.27 & 2.33,
without underpressure behind the blade\)](#)
 7. [The Cavitating Cutting Process, \$\beta\$, \$d_1\$, \$d_2\$ for \$h_b/h_i=3\$ \(2.07, 2.28 & 2.34,
without underpressure behind the blade\)](#)
 8. [The Non-Cavitating Cutting Process, \$\beta\$, \$d_1\$, \$d_2\$, \$a_1\$ for \$h_b/h_i=1\$ \(2.02, 2.17, 2.23 & 2.11,
with underpressure behind the blade\)](#)

9. [The Non-Cavitating Cutting Process, \$\beta\$, \$d_1\$, \$d_2\$, \$a_1\$ for \$h_b/h_i=2\$ \(2.03, 2.18, 2.24, & 2.12,](#)
with underpressure behind the blade)
10. [The Non-Cavitating Cutting Process, \$\beta\$, \$d_1\$, \$d_2\$, \$a_1\$ for \$h_b/h_i=3\$ \(2.04, 2.19, 2.25, & 2.13,](#)
with underpressure behind the blade)
11. [The Cavitating Cutting Process, \$\beta\$, \$d_1\$, \$d_2\$ for \$h_b/h_i=1\$ \(2.05, 2.29](#)
& 2.35,
with underpressure behind the blade)
12. [The Cavitating Cutting Process, \$\beta\$, \$d_1\$, \$d_2\$ for \$h_b/h_i=2\$ \(2.06, 2.30](#)
& 2.36,
with underpressure behind the blade)
13. [The Cavitating Cutting Process, \$\beta\$, \$d_1\$, \$d_2\$ for \$h_b/h_i=3\$ \(2.07, 2.31](#)
& 2.37,
with underpressure behind the blade)

3. Verification of the Cutting Theory

1. [Description of the Test Stand](#)
2. [Testing Program](#)
3. [Water Resistance](#)
4. [The Influence of the Width of the Blade](#)
5. [Side Effects](#)
6. [Scaling Effects](#)
7. [Comparison of Measurements versus Theory](#)
8. [Location of the Resulting Cutting Force](#)
9. [Verification of Forces & Pore Pressures in a 200 \$\mu\text{m}\$ Sand](#)

10. [Verification of Forces & Pore Pressures in a 105 \$\mu\text{m}\$ Sand](#)
 11. [Determination of \$\phi\$ and \$\delta\$ from Measurements](#)
 12. [General Conclusions](#)
-
4. Analytical Model of the Forces on a Cutterhead
 1. [Introduction](#)
 2. [Simplifications and Basic Equations](#)
 3. [Transformation of the Forces to the Cutterhead Related Axis System](#)
 4. [Integration of Momentary Cutting Forces and Cutting Torque](#)
 5. [The Derived Quantities](#)
 6. [Simplification of the Equations](#)
 7. [Specific Cutting Energy](#)
 8. Tables
 1. [Table 4.01: The coefficients \$f_1\$, \$f_2\$ and \$f_5\$ as a function of the angle \$\Omega_1\$.](#)
 2. [Table 4.02: The coefficients \$f_3\$, \$f_4\$ and \$f_6\$ as a function of \$\Omega_0\$ and \$\Omega_1\$.](#)
 3. [Table 4.03: The coefficients \$f_3\$, \$f_4\$ and \$f_6\$ as a function of \$\Omega_0\$ and \$\Omega_1\$.](#)
 4. [Table 4.04: The coefficients \$f_3\$, \$f_4\$ and \$f_6\$ as a function of \$\Omega_0\$ and \$\Omega_1\$.](#)
 5. [Table 4.05: The coefficients \$f_3\$, \$f_4\$ and \$f_6\$ as a function of \$\Omega_0\$ and \$\Omega_1\$.](#)

5. Analytical Model of the Forces on a Dredging Wheel

1. [Introduction](#)
2. [The Non-Cavitating Cutting Process](#)
3. [The Cavitating Cutting Process](#)
4. [Simplification of the Equations](#)
5. [Specific Cutting Energy](#)
6. [The Partly Cavitating Cutting Process](#)
7. [Correction for the Direction of the Forces](#)
8. [The Alternative Bank Cut](#)
9. Tables
 1. [Table 5.01: Coefficients \$f_{xgc}\$, \$f_{ygc}\$, \$f_{zgc}\$ and \$m_{gc}\$ at \$S=0.1 \cdot R\$, \$\Omega_2=-3^\circ\$, non-cavitating](#)
 2. [Table 5.02: Coefficients \$f_{xgc}\$, \$f_{ygc}\$, \$f_{zgc}\$ and \$m_{gc}\$ at \$S=0.2 \cdot R\$, \$\Omega_2=-6^\circ\$, non-cavitating](#)
 3. [Table 5.03: Coefficients \$f_{xgc}\$, \$f_{ygc}\$, \$f_{zgc}\$ and \$m_{gc}\$ at \$S=0.3 \cdot R\$, \$\Omega_2=-9^\circ\$, non-cavitating](#)
 4. [Table 5.04: Coefficients \$f_{xgc}\$, \$f_{ygc}\$, \$f_{zgc}\$ and \$m_{gc}\$ at \$S=0.4 \cdot R\$, \$\Omega_2=-11^\circ\$, non-cavitating](#)
 5. [Table 5.05: Coefficients \$f_{xgc}\$, \$f_{ygc}\$, \$f_{zgc}\$ and \$m_{gc}\$ at \$S=0.5 \cdot R\$, \$\Omega_2=-14^\circ\$, non-cavitating](#)
 6. [Table 5.06: Coefficients \$f_{xca}\$, \$f_{yca}\$, \$f_{zca}\$ and \$m_{ca}\$ at \$S=0.1 \cdot R\$, \$\Omega_2=-3^\circ\$, cavitating](#)
 7. [Table 5.07: Coefficients \$f_{xca}\$, \$f_{yca}\$, \$f_{zca}\$ and \$m_{ca}\$ at \$S=0.2 \cdot R\$,](#)

[8. \$\Omega_2 = -6^\circ\$, cavitating](#)

8. [Table 5.08: Coefficients \$f_{x_{ca}}\$, \$f_{y_{ca}}\$, \$f_{z_{ca}}\$ and \$m_{ca}\$ at \$S=0.3 \cdot R\$, \$\Omega_2 = -9^\circ\$, cavitating](#)

9. [Table 5.09: Coefficients \$f_{x_{ca}}\$, \$f_{y_{ca}}\$, \$f_{z_{ca}}\$ and \$m_{ca}\$ at \$S=0.4 \cdot R\$, \$\Omega_2 = -11^\circ\$, cavitating](#)

10. [Table 5.10: Coefficients \$f_{x_{ca}}\$, \$f_{y_{ca}}\$, \$f_{z_{ca}}\$ and \$m_{ca}\$ at \$S=0.5 \cdot R\$, \$\Omega_2 = -14^\circ\$, cavitating](#)

6. Scale Rules

1. [Scale Rules](#)

7. Verification of the Analytical Models for Cutterhead and Dredging Wheel

1. [Introduction](#)

2. [Test Stand Cutterhead Experiments](#)

3. [Forces and Torque on the Cutterhead](#)

4. [Test Stand Dredging Wheel Experiments](#)

5. [Mechanical and Hydraulical Losses](#)

6. [Driving Torque](#)

7. [Conclusions](#)

8. [Figures Cutterhead Tests](#)

9. [Figures Dredging Wheel Tests](#)

8. Numerical Model of the Forces on a Rotating Excavating Element (Cutterhead or Dredging Wheel)

1. [Introduction](#)

2. [Definitions](#)

3. [Transformations](#)
4. [Velocity Vectors](#)
5. [Layer Thickness, Blade Angle and Blade Height](#)
6. [Forces in Densily Packed and Water Saturated Sand](#)
7. [Transformation to the Fixed Axis System](#)
9. Comparison of the Numerical Force Model versus the Analytical Models
 1. [Introduction](#)
 2. [Numerical Calculations of the Forces on a Disc Bottom Cutterhead](#)
 3. [Conclusions](#)
 4. [Figures Disc Bottom Cutterhead Tests](#)
10. The Three Dimensional Moving Cutterhead
 1. [Introduction](#)
 2. [Determination of the Shape and the Dimensions of the Bank](#)
 3. [The Influence of Radial Velocity Variations on the Loads on the Cutterhead](#)
 4. [The Influence of Axial Velocity Variations on the Loads on the Cutterhead](#)
 5. [Specific Energy and Conclusions](#)
11. Verification of the Loads on a Three Dimensional Moving Cutterhead
 1. [Description of the Test Stand](#)
 2. [The Test Program](#)
 3. [The Signals Measured](#)

4. [Signal Processing](#)
5. [Macroscopic Cutting Behavior](#)
6. [Parameters of Influence](#)
7. [Conclusions Macroscopic Behavior](#)
8. [Verification Radial Velocity Variations](#)
9. [Verification Axial Velocity Variations](#)
10. [Conclusions](#)
12. Conclusions
 1. [Verification Two-Dimensional Cutting Theory](#)
 2. [Verification Cutterhead and Dredging Wheel](#)
 3. [Verification Three-Dimensional Moving Cutterhead](#)
 4. [Possible Further Research](#)
13. Bibliography
 1. [Bibliography](#)
14. List of Symbols Used.
 1. [General List of Symbols Used](#)
 2. [List of Symbols Used in Chapter 1](#)
 3. [List of Symbols Used in Chapter 8](#)
- Appendix B1: Definition of Axis Systems
 1. [The Fixed Axis System](#)
 2. [The Ladder Related Axis System](#)
 3. [The Cutterhead Related Axis System](#)

4. [The Dredging Wheel Related Axis System](#)
 5. [The Blade Related Axis System](#)
- Appendix B2: Derivation of the DREDMO Solution Method
 1. [The theta integration method](#)
 2. [The prediction step](#)
 3. [The correction step](#)
 4. [The convolution integral](#)
 - Appendix B3: [Soil Mechanical Properties of the 200 \$\mu\text{m}\$ Sand](#)
 - Appendix B4: [Soil Mechanical Properties of the 105 \$\mu\text{m}\$ Sand](#)
 - Appendix B5: The Measured Forces
 1. [The Measured Horizontal and Vertical Cutting Forces, Table 3.4, Chapter 3.7, Scaled to a Blade with Blade Width 200 mm and Blade Height 200 mm](#)
 2. [The Measured Horizontal and Vertical Cutting Forces, Table 3.2, Chapter 3.5, Scaled to a Blade with Blade Width 200 mm and Blade Height 200 mm](#)
 3. [The Measured Horizontal and Vertical Cutting Forces, Table 3.7-3.8, Chapter 3.9, Scaled to a Blade with Blade Width 200 mm and Blade Height 200 mm](#)
 - [Curriculum Vitae](#)
 - [Statements](#)

[Back to top](#)

**This is a translation of the dissertation of Dr.ir. S.A. Miedema, dated September 15th 1987 .
The dissertation was originally published in Dutch by the:
Delft University of Technology
Faculty of Mechanical Engineering and Marine Technology
Chair of Dredging Technology**

**Mekelweg 2
2628 CD, Delft
The Netherlands**

It is advised to also read the papers following this dissertation, since the theory developed has been refined and extended.

Last modified Thursday June 01, 2000 by: [Sape A. Miedema](#)

Translation by: [Laurens de Jonge](#)

Figures, equations and tables by: [Erik Miedema](#)

Copyright © June, 2000 Dr.ir. S.A. Miedema



[Download Adobe Acrobat Reader V4.0](#)

Preface.

From a chance concurrence of circumstances, chances are offered and possibilities are created.

Seizing the chances and using the possibilities leads to the creation of new possibilities and chances.

This dissertation is the result of the possibilities offered by the Faculty of Mechanical Engineering & Marine Technology of the Delft University of Technology and especially the chair of Dredging Technology.

I like to use this opportunity to thank everybody who contributed to the realization of this dissertation

Especially to the following people I owe my gratitude:

Prof.ir. J. de Koning for stimulating my scientific development and supplying an efficient method of approach.

Ir. L.W.F. Joanknecht for stimulating my first steps on the path of science.

Ir. S.H. Gillebaard en ing. J. van der Maas for their mental and material support.

Ing. J. Brouwer for discussions on sand cutting.

Ing. A. Zwartbol en ing. R.J. Rootzand for their assistance during the experiments.

O. Reinicke for preparing the test stand.

A. Klein for his illustrations in the dissertation.

Mevr. V. L. van Dam for translating publications.

The employees of Delft Hydraulics and the Ship Hydromechanics Laboratory for their cooperation during the development of DREDMO.

Delft Soil Mechanics for carrying out the soil mechanics research.

Zanen Verstoep n.v. for making available the dredging wheel research.

The members of the PhD committee for the time and trouble they had to go through, reading the dissertation.

The PhD committee consisted of:

Prof.ir. H. Wiggerts, Rector Magnificus T.U. Delft.

Prof.ir. J. de Koning, promotor (Mechanical Engineering).

Prof.ir. J. Gerritsma (Marine Technology).
Prof.ir. B.P.Th. Veltman (Physics).
Prof.dr.ir. A. Verruijt (Civil Engineering).
Prof.dr.ir. L. van Wijngaarden, T.U. Twente (Mechanical Engineering).
Prof.dr.ir. A.D. de Pater (Mechanical Engineering).
Ir. L.W.F. Joanknecht, guest.

Copyright (©) S.A. Miedema

Nothing from this dissertation (with exception of the summary) is allowed to be multiplied and/or published by means of print, photocopy, microfilm or any other way, without written permission of the author.

[Back to top](#)

This is a translation of the dissertation of Dr.ir. S.A. Miedema, dated September 15th 1987 .
The dissertation was originally published in Dutch by the:
Delft University of Technology
Faculty of Mechanical Engineering and Marine Technology
Chair of Dredging Technology
Mekelweg 2
2628 CD, Delft
The Netherlands

Last modified Wednesday May 24, 2000 by: [Sape A. Miedema](#)

Translation by: [Laurens de Jonge](#)

Figures, equations and tables by: [Erik Miedema](#)

Copyright © May, 2000 **Dr.ir. S.A. Miedema**



[Download Adobe Acrobat Reader V4.0](#)

Summary.

The aim of the research described in this thesis is to develop a scientifically based mathematical model with which the loads on blades moving in three dimensions and cutting sand which is saturated with water can be determined. The need to be able to provide a mathematical description of the loads occurring on the excavating element of a dredging vessel working at sea arose from the development of the simulation program DREDMO. This program was designed to predict the behaviour of specific sea-going dredgers such as cutter suction dredgers and bucket wheel dredgers in swell. The numerical methods used in the DREDMO program placed demands on the modelling of these loads. The modelling itself takes place in three phases, the model formation in each phase being verified with the aid of model tests.

In the first phase a fundamental model of cutting forces based on minimising the specific cutting energy is derived. The cutting process in sand saturated with water is dominated by the phenomena of dilatation. In consequence of the dilatation, water underpressures are generated in the sand and, with large strain rates these can reach saturated water vapour pressure, in which case cavitation occurs. Cavitating and non-cavitating cutting processes can be distinguished although an intermediate transition zone between these also occurs. The effects of inertial forces, water resistance, gravity, adhesion and cohesion are included in this two-dimensional theory.

The second phase consists of simplified analytical models to determine the loads on a cutterhead and a dredging wheel based on the theory of the first phase. Only the part of the loading caused by dilatation is included in this phase. Model rules for the execution of model tests based on the transition between cavitating and non-cavitating cutting processes are derived from the analytical models for the cutterhead and the dredging wheel. In addition to the simplified analytical models, a numerical model has been developed in which an excavating element with three-dimensional curved blades is approached through a finite number of blade elements to which the complete two-dimensional cutting theory can be applied. The modelling of the loads on a three-dimensional moving excavating element, resulting from swell is realised in the third phase, which is based on the analytical models of the second phase. The model thus developed is suitable for the calculation in the time domain and satisfies the demands of the DREDMO program. The model also permits the user to take an existing dredged breach profile as the starting condition for a

calculation with the DREDMO program.

Comparison of the models developed with the results of the model tests which have been made has, in general, led to a moderate to good correlation in which it must be realised that:

Modelling is an attempt to describe reality without having any presumption of being reality.

[Back to top](#)

This is a translation of the dissertation of Dr.ir. S.A. Miedema, dated September 15th 1987 .
The dissertation was originally published in Dutch by the:
Delft University of Technology
Faculty of Mechanical Engineering and Marine Technology
Chair of Dredging Technology
Mekelweg 2
2628 CD, Delft
The Netherlands

Last modified Wednesday May 24, 2000 by: [Sape A. Miedema](#)

Translation by: [Laurens de Jonge](#)

Figures, equations and tables by: [Erik Miedema](#)

Copyright © May, 2000 Dr.ir. S.A. Miedema



[Download Adobe Acrobat Reader V4.0](#)

Introduction.

Working under seagoing conditions with cutter suction or bucket wheel dredgers is a difficult task for dredgers, certainly when the significant wave height is over a half meter. Several directions for a solution can be indicated that prevent dredging down-time as a result of the wave conditions. The use of self-elevating platforms eliminates the influence of the waves on the dredger, but the wave influence on the ladder is still present. One could also eliminate the swell by shielding the dredger with artificial wave traps. A third possible solution is to compensate the movements of the ship in such a way that these movements not or hardly influence the excavating element, in this case the cutter or the bucket wheel.

The computer program DREDMO (Dredge in Motions) simulates the motions of the cutting suction dredger in swell. With that ability it can be an important tool for the development of swell abatement systems (for instance active controlled winches), but also for the development and design of new dredgers under sea-going conditions. An important advantage of DREDMO is the determination of the loads on subsystems or parts so that the design process can be started with better founded data. Through its modular structure it can be easily used for other purposes like anchored pontoons and semi-submersibles. The program has been developed in the workgroup Offshore Technology of the Delft University (70's & 80's). The workgroup was a cooperation of the Delft Hydraulics in Delft, that exploits the program, the section Ship Hydromechanics of Marine Technology and the section Dredging Technology within Transportation Technology of Mechanical Engineering. Financial aid for the development of DREDMO has been given by the Vereniging Aannemers Combinatie Baggerbedrijf (VACB), the T.U. Delft and Delft Hydraulics Delft.

To determine the motions of ships computer programs have been developed in the past based upon a system of coupled linear equations of motion with the solution in the frequency domain. Because a ship has six degrees of freedom (three rotations and three translations) a system of six coupled linear equations of motions has to be solved. The motions of the ship can be determined as the response on a single uniform wave. Because the superposition principle is valid within a linear system, the response on a non-uniform wave can be determined by superposition of the responses of the ship on single components of the wave. This solution method is however not suitable for a dredger because there are

several strong non-linear effects which make a solution in the frequency domain impossible.

In 1962 [13] Cummins developed equations of motion that give a solution in the time domain instead of the frequency domain. Solving equations of motion in the time domain asks for a totally different approach than solving for the frequency domain. The responses of a ship on external loads are now determined as functions of time and not as functions of the wave frequency, like in the frequency domain. This also implies that another description of the external forces has to be found. The external forces need to be a function of the displacements, velocities and accelerations of the ship and/or the time.

To determine the responses of a ship during a certain time-interval, this time-interval has to be divided into small time-steps, with if necessary a variable interval time. In every time-step the equations of motion have to be solved iterative at the cost of a lot of computing time. DREDMO uses a calculation method with a very effective prediction method to reduce the computing time and costs.

One of the most important non-linear effects on a dredger is the interaction between the excavating element and the soil. On a cutter suction or a bucket wheel dredger the excavating element is attached to the pontoon with a ladder. The ladder motions are largely determined by the reactions of the soil on the movement of the excavating element. The excavating element can move in three directions in the breach, that is:

1. In the swing direction, perpendicular to the longitudinal plane of the pontoon, as a result of the sway, roll and yaw of the pontoon.
2. Radial, in the longitudinal plane of the pontoon, as a result of the surge, pitch and heave of the pontoon and as a result of the rotation of the ladder around the ladder hinge.
3. Axial, in the longitudinal plane of the pontoon, as a result of the surge, pitch and heave of the pontoon.

These three oscillating motions have to be superposed on the regular swing motion of the excavating element. Because the forces on the excavating element exerted by the soil are a function of the three oscillating motions, the excavating element causes a coupling between the longitudinal and transverse motions of the pontoon. This coupling is not present in a free floating ship. A

closer analysis of the behavior of the soil reactions on the excavating element is therefore necessary.

In this thesis the development of a mathematical model of the interaction between the excavating element and the soil will be discussed. As a starting-point for the soil densely packed sand is chosen. With the developed force models it is possible to determine the loads on the cutter and the bucket wheel while in motion under the influence of swell.

First, however, the prediction, correction and integration method in DREDMO will be discussed. The prediction method has been developed during the research. Also discussed are the consequences of the solution method in DREDMO on the mathematical model development of the excavating element/soil interaction.

The following reports, publications and programs form the basis for this thesis:

32. Journee, J.M.J. & Miedema, S.A. & Keuning, J.A. "Dredmo, A Computer Program for the Calculation of the Behaviour of a Cutter Suction Dredger Operating in Irregular Waves". T.U. Delft & Delft Hydraulics Laboratory, Delft 1983.
36. Koning, J de & Miedema, S.A. & Zwartbol, A., "Soil/Cutterhead Interaction under Wave Conditions". Proc. WODCON X, Singapore, 1983.
44. Miedema, S.A., "De grondreactiekrachten op een kroonsnijkop die via een ladder is opgehangen in een deiningscompensator". LaO/81/97, T.H.Delft 1981.
45. Miedema, S.A., "Computerprogramma ter bepaling van de reactiekrachten op de snijkop, als gevolg van de bewegingen van de snijkop". Stagerapport Waterloopkundig Laboratorium 1981 Delft.
46. Miedema, S.A., "De modellering van de grondreacties op een snijkop en het operationeel maken van het computerprogramma DREDMO. CO/82/125, T.H.Delft 1982.
47. Miedema, S.A., "De interactie tussen snijkop en grond in zeegang". Proc. Baggerdag 19/11/1982, T.H. Delft, 1982.
48. Miedema, S.A., "Principe ontwerp van een deiningsgecompenseerde

snijkopzuiger met axiale en radiale compensatie op de snijkop".
CO/82/134, T.H.Delft 1983.

49. Miedema, S.A., "Snijkopzuiger voor het buitengaatse baggeren met een deiningsgecompenseerde ladder". IO/83/107, T.H.Delft 1983.
50. Miedema, S.A., "Computersimulatie baggerschepen". De Ingenieur, Dec. 1983. (Kivi/Misset).
51. Miedema, S.A., "Mathematische modelvorming t.a.v. een snijkopzuiger in zeegang". T.H. Delft 1984. (Kivi September 1984), The Netherlands.
52. Miedema, S.A., "The cutting of densely compacted sand under water". Terra et Aqua No. 28, October 1984 pp. 4-10.
53. Miedema, S.A., "Dwarsscheepse en langsscheepse deiningscompensatie van een snijkopzuiger". Proc. Baggerdag 9/11/1984, T.H. Delft 1984.
54. Miedema, S.A., "Mathematical Modelling of the Cutting of Densely Compacted Sand Under Water". Dredging & Port Construction, July 1985, pp. 22-26.
55. Miedema, S.A., "Derivation of the Differential Equation for Sand Pore Pressures". Dredging & Port Construction, September 1985, pp. 35.
56. Miedema, S.A., "The Application of a Cutting Theory on a Dredging Wheel". Proc. WODCON XI, Brighton 1986.
57. Miedema, S.A., "Underwater soil cutting: a study in continuity". Dredging & Port Construction, June 1986, pp. 47-53.
58. Miedema, S.A., "SAMTEXT & SAMBASE, wetenschappelijk tekstbewerkingssysteem voor Personal Computers". Delft 1986, public domain software

[Back to top](#)

This is a translation of the dissertation of Dr.ir. S.A. Miedema, dated September 15th 1987 .

The dissertation was originally published in Dutch by the:

Delft University of Technology

Faculty of Mechanical Engineering and Marine Technology

Chair of Dredging Technology

Mekelweg 2

2628 CD, Delft

The Netherlands

Last modified Wednesday May 24, 2000 by: [Sape A. Miedema](#)

Translation by: [Laurens de Jonge](#)

Figures, equations and tables by: [Erik Miedema](#)

Copyright © May, 2000 Dr.ir. S.A. Miedema



[Download Adobe Acrobat Reader V4.0](#)

1.01 Equilibrium equations of motion of a ship.

For the modeling of the interaction between the excavating element and the soil, for dredging vessels in swell, the solution method of the equilibrium equations of motion is important. The choice between frequency domain or time domain, and with the last method the choice of the prediction, correction and iteration method, determines whether or not the mathematical model needs to be non-linear and/or differentiable. The ship motions can be determined, if the system is linear, with the following equilibrium equations of motion, known from marine hydrodynamics (Gerritsma [16], see also appendix B1):

$$\sum_{j=1}^6 \left[(M_{jk} + a_{jk}(\omega)) \cdot A_j + b_{jk}(\omega) \cdot V_j + C_{jk} \cdot X_j \right] = F_k(t) \quad (1.1)$$

In which:	M	The mass matrix.
	a(w)	The frequency dependent added mass matrix.
	A	The acceleration vector.
	b(w)	The frequency dependent damping matrix.
	V	The velocity vector.
	C	The hydrostatic spring terms matrix.
	X	The displacement vector.
	F(t)	The excitation load vector.

These equations give the motions of a ship as function of the wave frequency (frequency domain). Free floating ships or ships at a constant speed can be considered as linear systems. As soon as a ship has a connection with the shore or the bottom of the sea, non-linear effects will set in. Active controlled positioning systems can also have a non-linear character. The degree of non-linearity determines whether solving the equilibrium equations of motion, if necessary by a linearisation, can take place in the frequency domain. For strong non-linear systems a method is developed by Cummins [13] in 1962 with which the equilibrium equations of motion can be solved in the time domain.

Dredging vessels under operational circumstances, especially cutter-suction dredgers and cutter-wheel dredgers, are connected with the bottom of the sea by their excavating element and eventually by their mooring. Especially the connection of the excavating element and the sea bottom introduces a strong non-linear effect in the equilibrium equations of motion. To solve the equilibrium equations of motion for dredging vessels in DREDMO is therefore chosen to use the Cummins equations, widely used in marine

hydrodynamics (Keuning & Journee [35] en Wichers [78]). This method leads to the following set of coupled non-linear integrodifferential equations of the second order:

$$\sum_{j=1}^6 \left[(M_{jk} + m_{jk}) \cdot A_j + \int_{-\infty}^t K_{jk}(t-\tau) \cdot V_j(\tau) \cdot d\tau + C_{jk} \cdot X_j \right] = F_k(A_j, V_j, X_j, t) \quad (1.2)$$

In which: K The retardation functions.
 m The frequency independent added mass matrix.

In this set of equations can be recognized:

1. The acceleration term (product of mass + added mass and acceleration).
2. The damping term as a result of the potential damping (convolution-integral of the retardation function and the velocity history).
3. The spring term (product of the hydrostatic spring term and displacement).
4. The external loads as function of the acceleration, velocity and displacement of the ship and of the time.

The terms on the right side of equation (1.2) can not be solved explicit and therefore make an implicit method necessary. With respect to the solution method used in DREDMO a second subdivision of the loads on the dredging vessel can be made.

The wave forces on the cutter-suction dredger can be assumed independent of the ship motions, when the velocities of the cutter-suction dredger are small in comparison with the orbital velocities of the water. This can also be assumed for the wind loads.

The potential damping (convolution integral) is only very slightly dependent on the momentary motions of the cutter-suction dredger. The larger part of the potential damping is determined by the velocity history of the cutter-suction dredger.

Mooring forces, soil reaction forces etc. possess a more interactive character. These loads are determined by the ship motions, while the ships motions are influenced by the forces at the same time. Therefore a numerical equilibrium has to be found iterative.

The external forces on the cutter-suction dredger can now be divided in:

I. Momentary independent loads, like:

- . Wave forces.

B. Wind forces.

II. Momentary partly independent loads, like:

- . The potential damping (convolution-integral).

III. Momentary interactive loads, like:

- . Hydrostatic spring loads

B. Viscous damping loads.

C. Mooring loads (spud or cables).

D. Loads executed by floating piping.

E. Loads executed by a positioning system.

F. The interaction between the ladder and the pontoon, determined by:

1. Cutting forces.
2. Hoist cable forces.
3. Haul cable forces.
4. Ladder bearing forces.
5. Current forces on the ladder.
6. Wave forces on the ladder.
7. De mass + added mass inertia of the ladder.
8. The submerged weight of the ladder.

9. The ladder angle.

The ladder adds a degree of freedom to the system: the rotation of the ladder around the ladder hinge. It is possible to model the cutter-suction dredger as a system with seven degrees of freedom (Wichers [78]). In DREDMO however it is chosen to consider the ladder as an external load on a pontoon with 6 degrees of freedom (Journee, Keuning & Vis [31]). This allows the ladder module to be deactivated in a simple way, making it possible to calculate other floating constructions with DREDMO, for instance pipe laying barges and crane ships.

The choice for a ladder as an external force in the equilibrium equations of motion implies however that the interaction between the ladder and the pontoon also depends on the accelerations of the pontoon. This has consequences for the method with which the equilibrium equations of motion are solved.

[Back to top](#)

This is a translation of the dissertation of Dr.ir. S.A. Miedema, dated September 15th 1987 .

The dissertation was originally published in Dutch by the:

Delft University of Technology

Faculty of Mechanical Engineering and Marine Technology

Chair of Dredging Technology

Mekelweg 2

2628 CD, Delft

The Netherlands

Last modified Wednesday May 24, 2000 by: [Sape A. Miedema](#)

Translation by: [Laurens de Jonge](#)

Figures, equations and tables by: [Erik Miedema](#)

Copyright © May, 2000 [Dr.ir. S.A. Miedema](#)



[Download Adobe Acrobat Reader V4.0](#)

1.02 Solution method of equilibrium equations of motion.

The solution of a set of non-linear equilibrium equations of motion in the time domain consists, in short, of:

Iterative solving, for each time-step, of the equilibrium equations of motion during a certain time, whether or not with a variable time-step.

This iteration process can be subdivided in the following phases:

1. For each time-step first the acceleration vector of the cutter-suction dredger is predicted, the so-called prediction step.
2. Integration of the acceleration vector gives the velocity vector and the displacement vector.
3. The loads on the cutter-suction dredger are determined with the predicted motions.
4. From these loads the calculated acceleration vector is determined, according Newton's second law.
5. This calculated acceleration vector has to be equal to the predicted acceleration vector, within a certain tolerance.
6. If the difference is not within tolerance, a new prediction of the acceleration vector of the cutter-suction dredger has to be performed and the process is repeated from step 2 (the iteration process). If the difference is within tolerance the equilibrium in the next time-step can be determined.

The iteration process is shown in figure 1.1. Considering figure 1.1 the vectors can be called: an in-going (predicted) acceleration vector and an out-going (according to Newton's second law calculated) acceleration vector.

Equation (1.2) can be modified according:

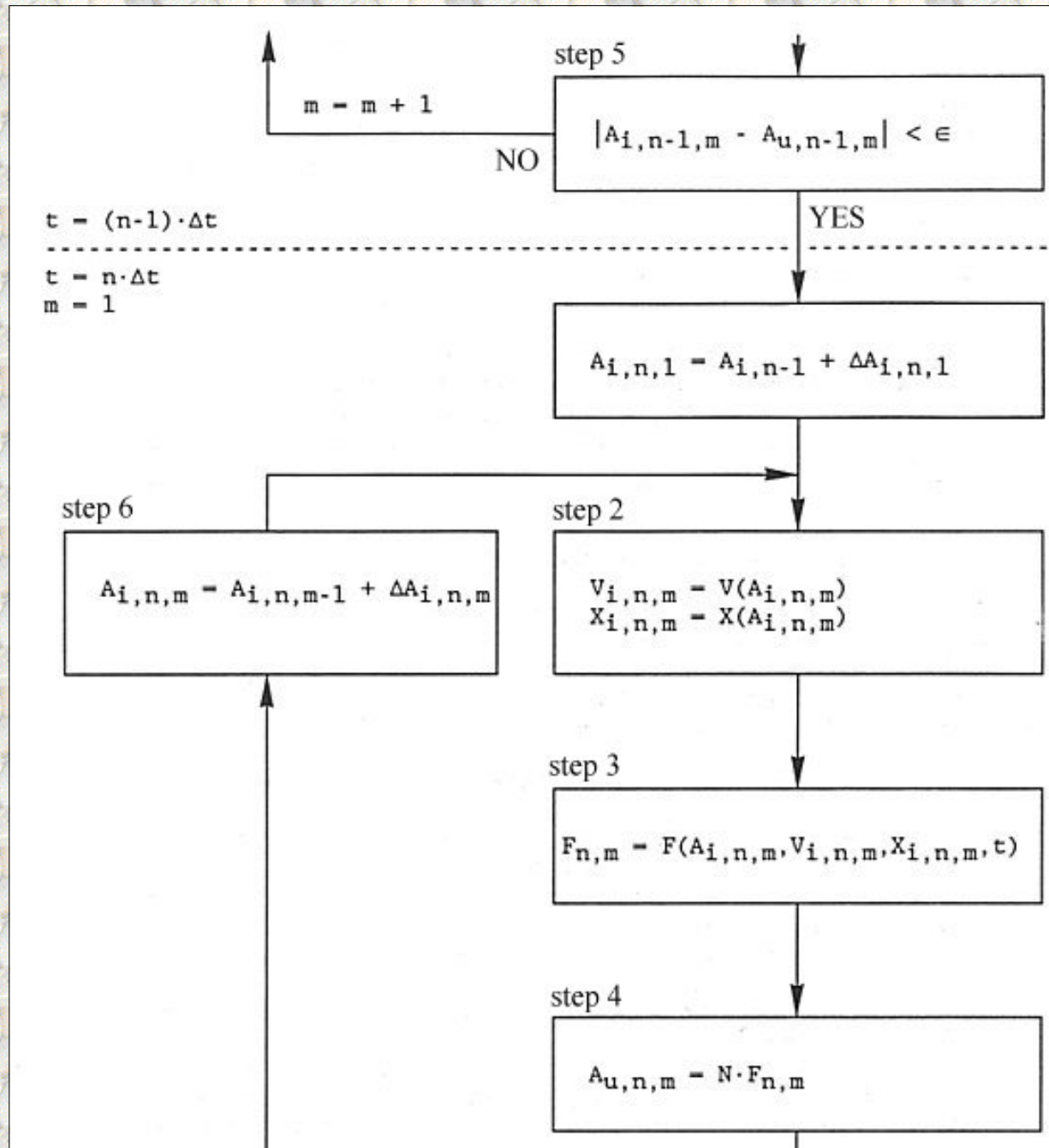
$$A_{j,u,n,1} = \sum_{k=1}^6 N_{k,j} \left(F'_k(A_{j,i,n,1}) + F''_k(t, A_{j,i,<n}, V_{j,i,<n}, X_{j,i,<n}) \right) \quad (1.3)$$

In which: $N = (M + m)^{-1}$ the inverse mass matrix.
 u index for out-going vector.
 i index for in-going vector.
 n index for the time-step.

<n

index for time-steps smaller than n.

The index 1 indicates the first iteration step or the prediction step.



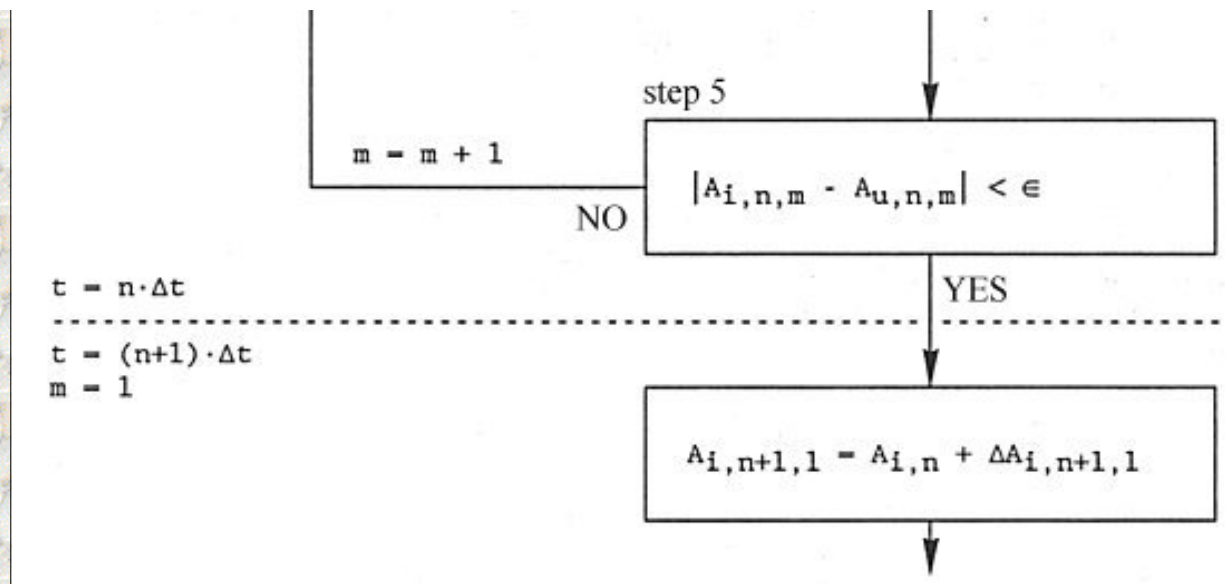


Figure 1-1: Flow diagram of the solution method of DREDMO, with the prediction step (1), the integration step (2), the determination of the loads (3), Newton's second law (4), the convergence criterion (5) and the correction step (6).

With this modification a division is made between the interactive- (first term on the right) and the independent loads (second term on the right). The in-going acceleration vector is implicitly called on the right side, while the out-going acceleration vector is called on the left side.

The iteration process is in fact a zero determination of the difference between the in-going and the out-going acceleration vectors. In DREDMO the Newton-Raphson method is used in combination with the theta-integration method (Lambert [83], see appendix B2 for further details). Because the Jacobean matrix (derivatives matrix) is not determined for every time-step or iteration, the method is also known as the so-called "modified Newton-Raphson iteration". The theta-integration method prevents numerical hunting.

The prediction step can also be seen as a zero determination. However the checked difference here is between the acceleration vector from the preceding time-step summed with the effects on the acceleration vector caused by the independent loads, and the independent part of the partly dependent loads with the out-going acceleration vector in the present time-step. In other words, the prediction step can be seen as an iteration step, provided that the time dependent influences on the zero determination are taken into account. Figure 1.2 shows this.

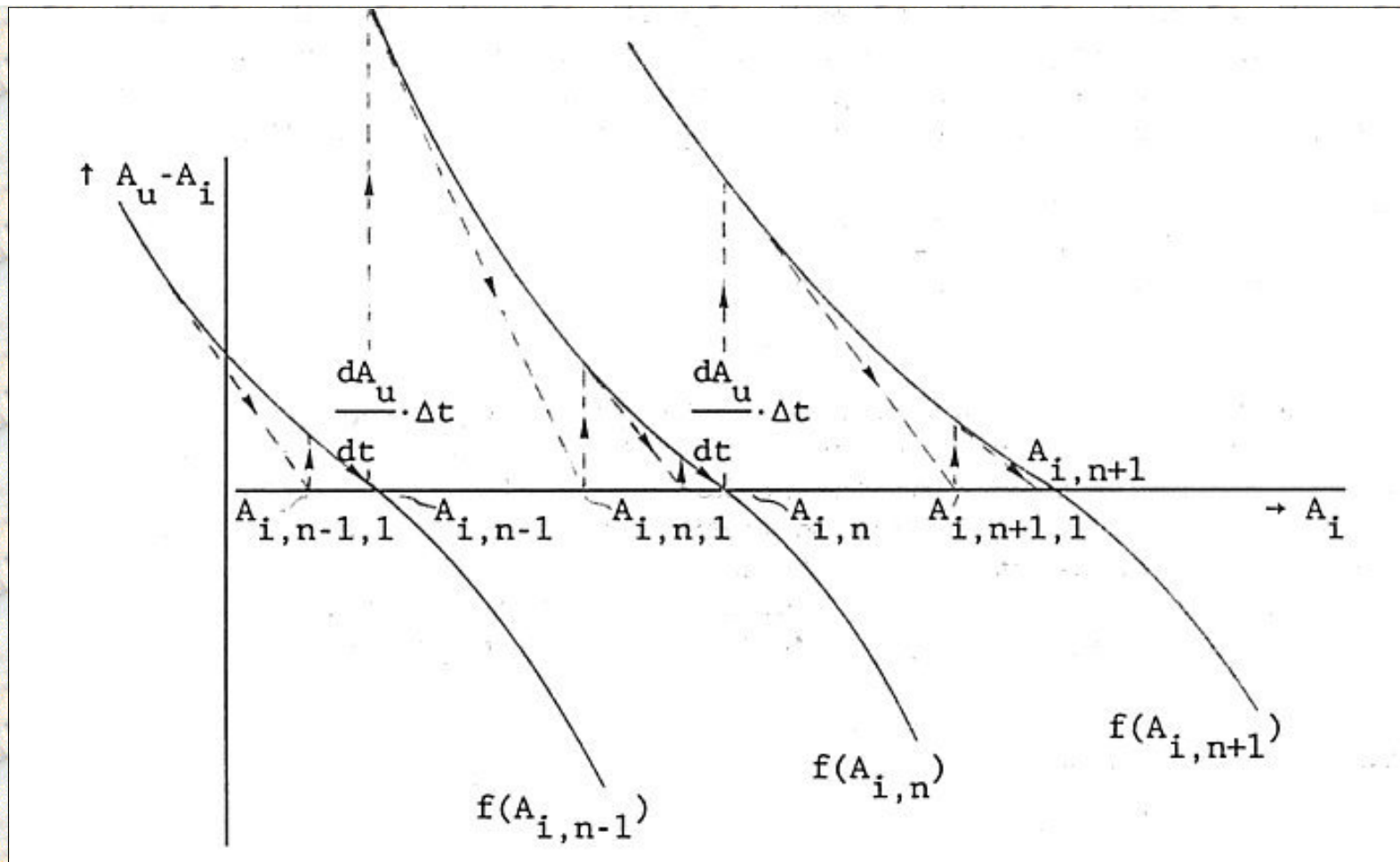


Figure 1-2: The iteration process with the prediction step as an iteration step. In this figure is indicated the difference between the out-going and the in-going acceleration $A_u - A_i$, along the vertical axis as function of the in-going acceleration vector A , along the horizontal axis, for three time steps.

The increase of the out-going acceleration vector in the prediction step (the first iteration step) is obtained by differentiating the out-going acceleration vector $A_{u,n,1}$ from equation (1.3) with respect to the time. The indices "j" and "k" are left out in the next equations, so the equations are valid for systems with one degree of freedom.

In the next equations the first index, "i" or "u", indicates the in- or out-going vector, the second index "n" indicates the time-step and the index "m" indicates the iteration step. If the third index is left out, the term does not change during the iteration process and is therefore only time dependent.

$$\frac{dA_u}{dt} \cdot \Delta t = \frac{\partial_1 A_u}{\partial_1 A_i} \cdot \frac{\partial A_i}{\partial t} \cdot \Delta t + \frac{\partial_2 A_u}{\partial_2 V_i} \cdot \frac{\partial V_i}{\partial t} \cdot \Delta t + \frac{\partial A_u}{\partial X_i} \cdot \frac{\partial X_i}{\partial t} \cdot \Delta t + \frac{\partial A_u}{\partial F_i} \cdot \frac{\partial F_i''}{\partial t} \cdot \Delta t \quad (1.4)$$

With, for a random variable α :

$$\frac{\partial \alpha}{\partial t} \cdot \Delta t = \Delta \alpha \quad (1.5)$$

This gives:

$$\Delta A_{u,n,1} = \frac{\partial_1 A_u}{\partial_1 A_i} \cdot \Delta A_{i,n,1} + \frac{\partial_2 A_u}{\partial_2 V_i} \cdot \Delta V_{i,n} + \frac{\partial A_u}{\partial X_i} \cdot \Delta X_{i,n} + \frac{\partial A_u}{\partial F_i} \cdot \Delta F_{i,n}'' \quad (1.6)$$

The first term on the right of equation (1.6) is the change of the out-going acceleration vector as a result of the change of the in-going acceleration vector. This term contains therefore also the influences of the changes in the velocity vector and the displacement vector as a result of the integration method used.

$$\frac{\partial_1 A_u}{\partial_1 A_i} = \frac{\partial A_u}{\partial A_i} + \frac{\partial A_u}{\partial V_i} \cdot \frac{\partial V_i}{\partial A_i} + \frac{\partial A_u}{\partial X_i} \cdot \frac{\partial X_i}{\partial V_i} \cdot \frac{\partial V_i}{\partial A_i} \quad (1.7)$$

The second term on the right in equation (1.6) is the change of the out-going acceleration vector as a result of the change of the acceleration independent part of the in-going velocity vector, e.g. the part of the convolution integral that can be determined from the previous time-steps. This term contains therefore also influences from the change of the displacement vector as a result of the used integration method.

$$\frac{\partial_2 A_u}{\partial_2 V_i} = \frac{\partial A_u}{\partial V_i} + \frac{\partial A_u}{\partial X_i} \cdot \frac{\partial X_i}{\partial V_i} \quad (1.8)$$

The third term on the right in equation (1.6) is the change of the out-going acceleration vector as a result of the acceleration and velocity independent part of the in-going displacement vector.

The fourth term on the right in equation (1.6) is the change of the out-going acceleration vector as a result of the change of the independent part of the load vector.

It is desired that:

$$A_{u,n,1} = A_{u,n-1} + \Delta A_{u,n,1} = A_{i,n-1} + \Delta A_{i,n,1} = A_{i,n,1} \quad (1.9)$$

Substitution of $\Delta A_{u,n,1}$ from equation (1.6) in equation (1.9), results in:

$$A_{u,n-1} + \frac{\partial_1 A_u}{\partial_1 A_i} \cdot \Delta A_{i,n,1} + \frac{\partial_2 A_u}{\partial_2 V_i} \cdot \Delta V_{i,n} + \frac{\partial A_u}{\partial X_i} \cdot \Delta X_{i,n} + \frac{\partial A_u}{\partial F_i} \cdot \Delta F_{i,n}'' = A_{i,n-1} + \Delta A_{i,n,1} \quad (1.10)$$

So:

$$\Delta A_{i,n,1} = \left(1 - \frac{\partial_1 A_u}{\partial_1 A_i} \right)^{-1} \cdot \left(A_{u,n-1} - A_{i,n-1} + \frac{\partial_2 A_u}{\partial_2 V_i} \cdot \Delta V_{i,n} + \frac{\partial A_u}{\partial X_i} \cdot \Delta X_{i,n} + \frac{\partial A_u}{\partial F_i} \cdot \Delta F_{i,n}'' \right) \quad (1.11)$$

The acceleration vector in the prediction step can now be determined with:

$$A_{i,n,1} = A_{i,n-1} + \Delta A_{i,n,1} \quad (1.12)$$

The velocity vector and the displacement vector can now be obtained by integration.

A similar deduction can be made for the iteration process. For use in the iteration process, equation (1.3) can be rewritten as:

$$A_{j,u,n,m} = \sum_{k=1}^6 N_{k,j} \cdot \left(F'_k(A_{j,i,n,m}) + F''_k \left(t, A_{j,i,n,m}, V_{j,i,n,m}, X_{j,i,n,m} \right) \right) \quad (1.13)$$

If no numerical equilibrium is reached after m-1 iteration steps, a correction on the in-going acceleration vector has to be made, such that the with this calculated out-going acceleration vector is equal to the corrected in-going acceleration vector, so:

$$A_{u,n,m} = A_{u,n,m-1} + \Delta A_{u,n,m} = A_{i,n,m-1} + \Delta A_{i,n,m} = A_{i,n,m} \quad (1.14)$$

After differentiation of $A_{u,n,m}$ from equation (1.13) to $A_{i,n,m}$, is found:

$$A_{u,n,m-1} + \frac{\partial_1 A_u}{\partial_1 A_i} \cdot \Delta A_{i,n,m} = A_{i,n,m-1} + \Delta A_{i,n,m} \quad (1.15)$$

So:

$$\Delta A_{i,n,m} = \left(1 - \frac{\partial_1 A_u}{\partial_1 A_i} \right)^{-1} \cdot (A_{u,n,m-1} - A_{i,n,m-1}) \quad (1.16)$$

The equations (1.11) and (1.16) are similar. In the second term on the left of equation (1.15) the expression according to equation

(1.7) can be substituted.

The new in-going acceleration vector can now be determined with:

$$\mathbf{A}_{i,n,m} = \mathbf{A}_{i,n,m-1} + \Delta \mathbf{A}_{i,n,m} \quad (1.17)$$

When switching to the system of coupled differential equations, the scalar 1 in equations (1.11) and (1.16) has to be substituted with the identity matrix I. Within the prediction and correction method three Jacobean matrices are used:

$$1. \quad \frac{\partial_1 A_{k,u}}{\partial_1 A_{j,i}} \quad 2. \quad \frac{\partial_2 A_{k,u}}{\partial_2 V_{j,i}} \quad 3. \quad \frac{\partial A_{k,u}}{\partial X_{j,i}}$$

The consequences of this solution method for the modeling of the cutterhead-soil interaction are:

1. The mathematical model of the soil reactions has to be formulated such that the soil reactions are a function of the acceleration vector, velocity vector and the displacement vector.
2. In the mathematical model the soil reactions have to be differentiable to the acceleration vector, velocity vector, displacement vector and the time. These derivatives have to be continuous and may therefore not contain step functions.

The soil reaction forces in DREDMO are implemented as a module within the ladder module and are considered as external loads on the ladder.

[Back to top](#)

This is a translation of the dissertation of Dr.ir. S.A. Miedema, dated September 15th 1987 .

The dissertation was originally published in Dutch by the:

Delft University of Technology

Faculty of Mechanical Engineering and Marine Technology

Chair of Dredging Technology

Mekelweg 2

2628 CD, Delft

The Netherlands

Last modified Wednesday May 24, 2000 by: [Sape A. Miedema](#)

Translation by: [Laurens de Jonge](#)

Figures, equations and tables by: [Erik Miedema](#)

Copyright © May, 2000 Dr.ir. S.A. Miedema



[Download Adobe Acrobat Reader V4.0](#)

1.03 The t=0 problem.

At time $t=0$ the motions of the dredging vessel have to be known. In DREDMO the ship is considered to be in rest at $t=0$ (the accelerations and the velocities equal zero). A first problem is the determination of the static equilibrium. Because of the complicated modeling within DREDMO it is almost impossible to determine a static equilibrium for every equation of motion. During the development of DREDMO two methods are used to determine the static equilibrium. In the first method DREDMO determines the equilibrium itself, by letting the ship search for equilibrium during a certain run-up time. This method requires however a lot of computing time, which is not preferable on personal computers. In the second method a pseudo-equilibrium situation is used, by not using the real loads in step 4 of the iteration process for the calculations, but the difference between the real loads and the loads determined at $t=0$ (except for the wave loads). This method can only be used, if and only if the pseudo-equilibrium situation is virtually similar to the static equilibrium, because of the non-linear character of the equilibrium equations of motion.

At $t=0$ equation (1.3) can be written:

$$A_{j,u,0,1} = \sum_{k=1}^6 N_{kj} \cdot [F_k''(t, X_{j,i,0,1})] = \sum_{k=1}^6 N_{kj} \cdot F_{k,0,1} \approx 0 \quad (1.18)$$

With: $F_{k,0,1}$ = the sum of the static loads in the k-direction at $t=0$, by approximation zero.

The equation to solve in the prediction step now becomes:

$$A_{j,u,n,1} = \sum_{k=1}^6 N_{kj} \cdot [F_k'(A_{j,i,n,1}) + F_{k,n,1}'' - F_{k,0,1}] \quad (1.19)$$

With:

$$F_{k,n,1}'' = F_k''(t, A_{j,i,n}, V_{j,i,n}, X_{j,i,n}) \quad (1.20)$$

Equation (1.13) can now be written:

$$A_{j,u,n,m} = \sum_{k=1}^6 N_{kj} \cdot [F'_k(A_{j,i,n,m}) + F''_{k,n,1} - F_{k,0,1}] \quad (1.21)$$

A second problem is formed by the harmonic character of the wave loads and therefore can not be included in the static equilibrium. In addition these wave loads can have a fairly random value at $t=0$, dependent on the chosen wave spectrum. As a result step loads can occur at $t=0$. To prevent this the wave loads are multiplied during a certain run-up time t_{rel} by a relaxation factor r_{t0} , for which the following formulation is used:

$$r_{t0} = \left(1 - \cosh \left(5.3 \cdot \frac{t}{t_{rel}} \right)^{-1} \right) \quad (1.22)$$

At $t=t_{rel}$ r_{t0} has a value of 0.99. A run-up time of 20 to 50 seconds "real time" is enough. If a spectral analyses of the DREDMO output is needed it should be realized that the above mentioned relaxation has an influence on the real used wave spectrum. For a spectral analysis it is advised not to consider the time from $t=0$ to $t=t_{rel}$.

[Back to top](#)

This is a translation of the dissertation of Dr.ir. S.A. Miedema, dated September 15th 1987 .

The dissertation was originally published in Dutch by the:

Delft University of Technology

Faculty of Mechanical Engineering and Marine Technology

Chair of Dredging Technology

Mekelweg 2

2628 CD, Delft

The Netherlands

Last modified Wednesday May 24, 2000 by: [Sape A. Miedema](#)

Translation by: [Laurens de Jonge](#)

Figures, equations and tables by: [Erik Miedema](#)

Copyright © May, 2000 Dr.ir. S.A. Miedema



[Download Adobe Acrobat Reader V4.0](#)



1.04 Discontinuities.

Although the in chapter 1.2 mentioned solution method of DREDMO does not allow for step functions, it is inevitable for such a simulation program, that processes are captured in the modeling in which step functions can occur. For instance the dry friction between the spud and the spud holders or the force difference over a pulley, quantified by the pulley efficiency. Such a step function is caused by the turn over of the force as a result of a rotation of the direction of velocity. With the dry friction of the spud and the spud holders this is about the rotation of the relative speed between the spud and the spud holders, while with the pulley it is about the rotation of the direction of rotation of the pulley. If necessary the step functions are approximated with the following function (in case of spud friction):

$$F_w = \left(1 - e^{\left[\frac{-C \cdot |V_r|}{H_s^2 \cdot \mu} \right]} \right) \cdot F_{w,w} = r_{sp} \cdot F_{w,w} \quad (1.23)$$

In which:	$F_{w,w}$	The real friction force.
	r_{sp}	The relaxation factor for the step functions.
	F_w	The friction force used in the equilibrium equations of motion.
	C	A constant (approximately 5 for spud friction).
	V_r	The relative speed between spud and spud holders.
	H_s	The significant wave-height.
	μ	The friction coefficient between spud and spud holders.

The arising friction force $F_{w,w}$ is directly proportional to the friction coefficient μ . It also appeared that the loads are in general proportional to the wave energy and therefore with the square of the significant wave-height H_s . The presence of the friction coefficient μ and the significant wave-height H_s in the denominator of the exponent, restricts therefore the maximum slope of the resulting function. Although the step functions is approximated with a continuous function it is still possible that the iteration

process does not lead to convergence but oscillates between two values of the acceleration vector (Ping-Pong effect). This can also happen as a result of the motion of the cutter in and out of the breach.

The introduction of the relaxation factor r_{it} with $\Delta A_i \cdot r_{it}$ in equations (1.12) en (1.17) with a value of approximately 0.5 prevents this effect. This is shown in figure 1.3:

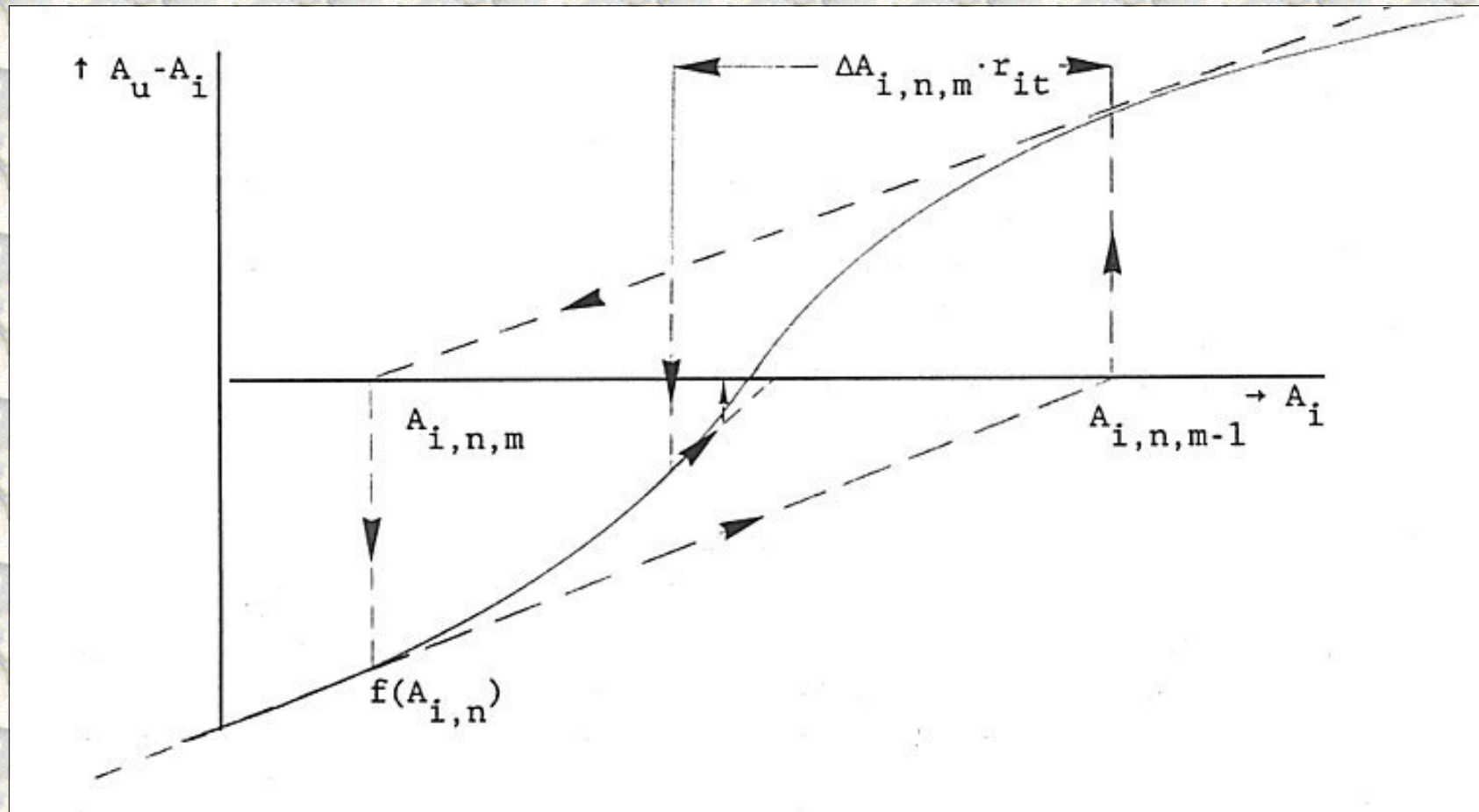


Figure 1-3: The ping-pong effect and the result of the introduction of a relaxation factor. In this figure the difference between the in-going and out-going acceleration $A_u - A_i$ is put along the vertical axis as a function of the in-going acceleration vector A_i along the horizontal axis, for the iteration process.

This is a translation of the dissertation of Dr.ir. S.A. Miedema, dated September 15th 1987 .

The dissertation was originally published in Dutch by the:

Delft University of Technology

Faculty of Mechanical Engineering and Marine Technology

Chair of Dredging Technology

Mekelweg 2

2628 CD, Delft

The Netherlands

Last modified Wednesday May 24, 2000 by: [Sape A. Miedema](#)

Translation by: [Laurens de Jonge](#)

Figures, equations and tables by: [Erik Miedema](#)

Copyright © May, 2000 Dr.ir. S.A. Miedema



[Download Adobe Acrobat Reader V4.0](#)

2.01 The two-dimensional cutting theory, process description.

[Contents](#)

One of the strong non-linear effects in the equilibrium equations of motion for the determination of the cutter-suction and dredging-wheel dredger motions, is the interaction between the excavating element and the soil. A good description of the cutting process is essential for a reliable simulation of the ship motions, in order to be able to predict the usability and the design of sea-going dredging vessels.

Although calculation models for the determination of the cutting forces for dry sand were available for a long time (Hettiaratchi & Reece [20,21,22,23,24,66], Hatamura & Chiiwa [18] etc.) it is only since the seventies and the eighties that the cutting process in saturated sand is extensively researched at the Delft Hydraulics in Delft (WL, CSB), at the Delft University of Technology and at the Mineral Technological Instituut (MTI, IHC).

First the process is described, for a good understanding of the terminology used in the literature discussion.

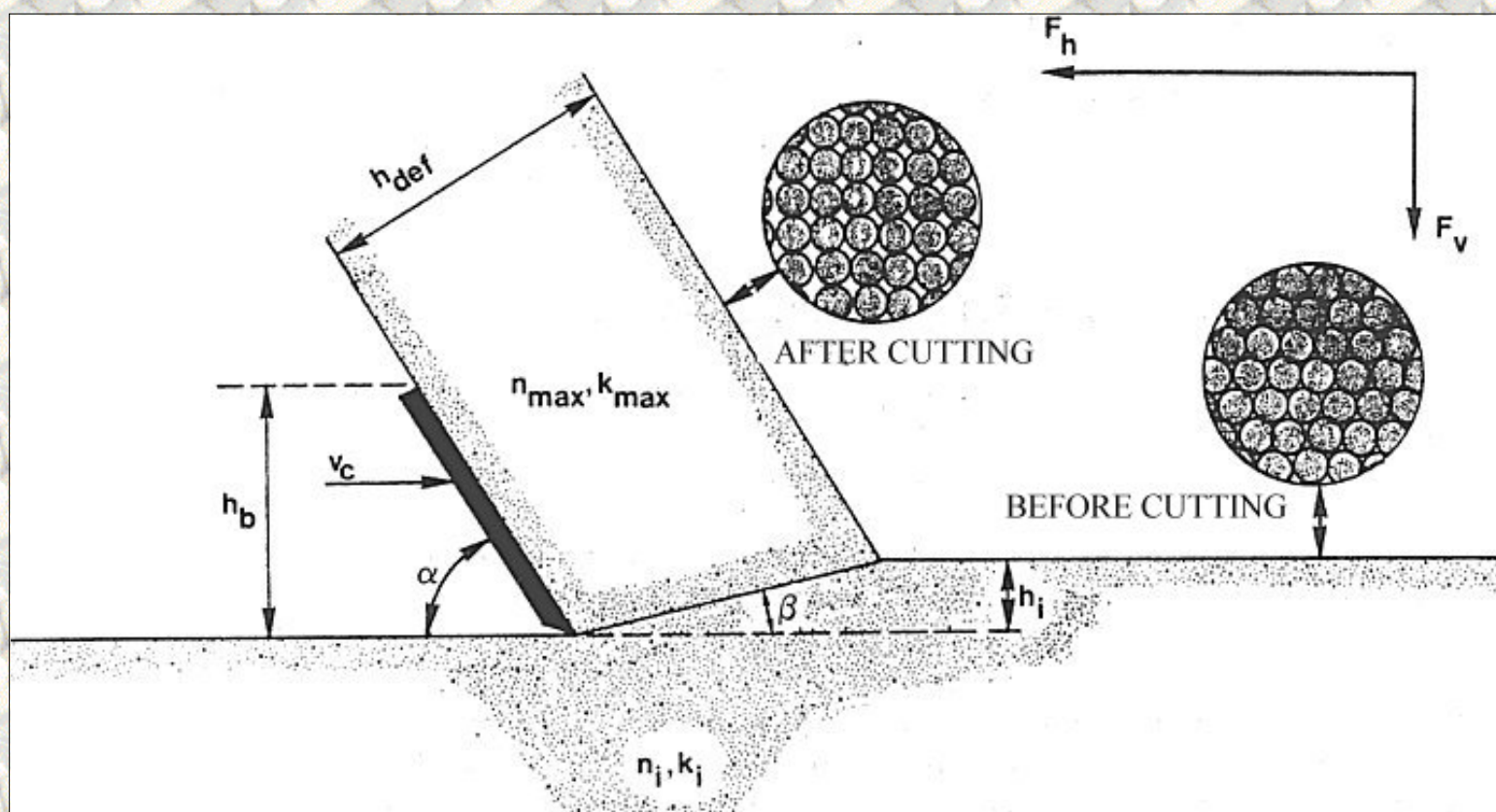


Figure 2.1: The cutting process modeled as a continuous process.

From literature it is known that, during the cutting process, the sand increases in volume (see figure 2.1). This increase in volume is accredited to dilatancy. This is the change of the pore volume as a result of shear in the sand package. This increase of the pore volume has to be filled with water. The flowing water experiences a certain resistance, which causes under-pressure in the pore water in the sand package. As a result the grain stresses increase and therefore the needed cutting forces. The speed of the increase of the pore volume in the dilatancy zone, the volume strain rate, is proportional to the cutting velocity. If the volume strain rate is high, there is a chance that the pore pressure reaches the saturated vapor pressure and cavitation occurs. A further increasing volume strain rate will not be able to cause a further decrease of the pore pressure. This also implies that, with a further increasing cutting velocity, the cutting forces cannot increase as a result of the

dilatancy properties of the sand. The cutting forces can, however, still increase with an increasing cutting velocity as a result of the inertia forces and the flow resistance.

The cutting process can be subdivided in 5 areas in relation with the cutting forces:

1. Very low cutting velocities, a quasi static cutting process. The cutting forces are determined by the gravitation, cohesion and adhesion.
2. The volume strain rate is high in relation to the permeability of the sand. The volume strain rate is however so small that inertia forces can be neglected. The cutting forces are dominated by the dilatancy properties of the sand.
3. A transition region, with local cavitation. With an increasing volume strain rate, the cavitation area will increase so that the cutting forces increase slightly as a result of dilatancy.
4. Cavitation occurs almost everywhere around and on the blade. The cutting forces do not increase anymore as a result of the dilatancy properties of the sand.
5. Very high cutting velocities. The inertia forces part in the total cutting forces can no longer be neglected but form a substantial part.

[Back to top](#)

This is a translation of the dissertation of Dr.ir. S.A. Miedema, dated September 15th 1987 .

The dissertation was originally published in Dutch by the:

Delft University of Technology

Faculty of Mechanical Engineering and Marine Technology

Chair of Dredging Technology

Mekelweg 2

2628 CD, Delft

The Netherlands

It is advised to also read the papers following this dissertation, since the theory developed has been refined and extended.

Last modified Saturday May 27, 2000 by: [Sape A. Miedema](#)

Translation by: [Laurens de Jonge](#)

Figures, equations and tables by: [Erik Miedema](#)

Copyright © May, 2000 Dr.ir. S.A. Miedema



[Download Adobe Acrobat Reader V4.0](#)

2.02 Cutting theory, literature survey.

In the seventies extensive research is carried out on the forces that occur while cutting sand under water. A conclusive cutting theory has however not been published in this period. However qualitative relations have been derived by several researchers, with which the dependability of the cutting forces with the soil properties and the blade geometry are described (Joanknecht [27], van Os [62,63]).

Afterwards it turned out that, in non-published reports for the confidential research program CSB, as indicated in the reference list of [40], Van Os had already developed the basic theory for the cutting of saturated packed sand. Ahead of the real publication [40] is provided by the Delft Hydraulics Laboratory in August 1986.

A process that has a lot of similarities with the cutting of sand as far as water pressure development is concerned, is the, with uniform velocity, forward moving breach. Meijer and van Os [41] 1976 and Meijer [42,43] 1981/1985 have transformed the storage equation for the, with the breach, forward moving coordinate system.

$$\left| \frac{\partial^2 p}{\partial x^2} \right| + \left| \frac{\partial^2 p}{\partial y^2} \right| = \frac{\rho_w \cdot g \cdot v_c}{k} \cdot \left| \frac{\partial e}{\partial x} \right| - \frac{\rho_w \cdot g}{k} \cdot \left| \frac{\partial e}{\partial t} \right| \quad (2.1)$$

In case of a stationary process, the second term on the right hand side is zero, resulting:

$$\left| \frac{\partial^2 p}{\partial x^2} \right| + \left| \frac{\partial^2 p}{\partial y^2} \right| = \frac{\rho_w \cdot g \cdot v_c}{k} \cdot \left| \frac{\partial e}{\partial x} \right| \quad (2.2)$$

Van Os [62,63] 1977 describes the basic principles of the cutting process, with special attention for the determination of the water under-pressures and the cavitation. Van Os uses the non-transformed storage equation for the

determination of the water under-pressures.

$$\left| \frac{\partial^2 p}{\partial x^2} \right| + \left| \frac{\partial^2 p}{\partial y^2} \right| = \frac{\rho_w \cdot g}{k} \cdot \left| \frac{\partial e}{\partial t} \right| \quad (2.3)$$

The average volume strain rate has to be substituted in the term $\partial e / \partial t$ on the right hand side. The average volume strain rate is the product of the average volume strain of the sand package and the cutting velocity and arises from the volume balance over the shear zone. Van Os gives a qualitative relation between the water sub-pressures and the average volume strain rate:

$$p \propto \frac{v_c \cdot h_i \cdot e}{k} \quad (2.4)$$

The problem of the solution of the storage equation for the cutting of sand under water is a mixed boundary-value problem, for which the water under-pressures along the boundaries are known (hydrostatic).

Joanknecht [26,27] 1973 assumes that the cutting forces are determined by the under-pressure in the sand package. A distinction is made between the parts of the cutting force caused by the inertia forces, the under-pressure behind the blade and the soil mechanical properties of the sand. The influence of the geometrical parameters gives the following qualitative relation:

$$F_{ci} \propto v_c \cdot h_i^2 \cdot b \quad (2.5)$$

The cutting force is proportional to the cutting velocity, the blade width and the square of the initial layer-thickness. A relation with the pore percentage and the permeability is also mentioned. A relation between the cutting force and these soil mechanical properties is however not given. It is observed that the cutting forces increase with an increasing blade angle.

In the eighties research has led to more quantitative relations. In 1984 Van

Leussen and Nieuwenhuis [39] discuss the soil mechanical aspects of the cutting process. The forces models of Miedema [54,57] and Steeghs [72,73] are published 1985/86, while the CSB (Combinatie Speurwerk Baggertechniek) model (van Leussen en van Os [40]), however developed in the early seventies at the Delft Hydraulics Laboratory (van Os [62,63]), will be published in 1987.

Brakel [5] 1982 derives a relation for the determination of the water under-pressures based upon, over each other rolling, round grains in the shear zone. The force part resulting from this is added to the model of Hettiaratchi and Reece [23].

Miedema [52] 1983 has combined the qualitative relations of Joanknecht [26,27] and Van Os [62,63] to the following relation:

$$F_{ci} :: \frac{\rho_w \cdot g \cdot v_c \cdot h_i^2 \cdot b \cdot e}{k_m} \quad (2.6)$$

With this basic equation calculation models are developed for a cutterhead and for the periodical moving cutterhead in the breach. The proportionality constants are determined empirically. The soil module of the DREDMO program is also developed from these models (Miedema [36,47]). This will be discussed in the appropriate chapters.

Van Leussen and Nieuwenhuis [39] 1984 discuss the soil mechanical aspects of the cutting process. Important in the cutting process is the way shear takes place and the shape or angle of the shear plane, respectively shear zone. In literature no unambiguous image could be found. Cutting tests along a windowpane gave an image in which the shape of the shear plane was more in accordance with the so-called "stress characteristics" than with the so-called "zero-extension lines". Therefore, for the calculation of the cutting forces, the "stress characteristics method" is used (Mohr-Coulomb failure criterion). For the calculation of the water under-pressures, however, the "zero-extension lines" are used, which are lines with a zero linear strain. A closer description has not been given for both calculations.

Although the cutting process is considered as being two-dimensional, Van Leussen and Nieuwenhuis found, that the angle of internal friction, measured at

low deformation rates in a triaxial apparatus, proved to be sufficient for dredging processes. Although the cutting process can be considered as a two-dimensional process and therefore it should be expected that the angle of internal friction has to be determined with a "plane deformation test". A sufficient explanation has not been found.

Little is known about the value of the angle of friction between sand and steel. Van Leussen and Nieuwenhuis don't give an unambiguous method to determine this soil mechanical parameter. It is, however, remarked that at low cutting velocities (0.05 mm/s), the soil/steel angle of friction can have a statistical value which is 1.5 to 2 times larger than the dynamic soil/steel angle of friction. The influence of the initial density on the resulting angle of friction is not clearly present, because loose packed sand moves over the blade. The angles of friction measured on the blades are much larger than the angles of friction measured with an adhesion cell, while also a dependency with the blade angle is observed.

With regard to the permeability of the sand, Van Leussen and Nieuwenhuis found that no large deviations of Darcy's law occur with the water flow through the pores. The found deviations are in general smaller than the accuracy with which the permeability can be determined in situ.

The size of the area where $\partial e / \partial t$ from equation (2.5) is zero can be clarified by the figures published by Van Leussen and Nieuwenhuis. The basis is formed by a cutting process where the density of the sand is increased in a shear band with a certain width. The undisturbed sand has the initial density while the sand after passage of the shear band possesses a critical density. This critical density appeared to be in good accordance with the wet critical density of the used types of sand. This implies that outside the shear band the following equation is valid:

$$\left| \frac{\partial^2 p}{\partial x^2} \right| + \left| \frac{\partial^2 p}{\partial y^2} \right| = 0 \quad (2.7)$$

Values for the various densities are given for three types of sand. Differentiation of the residual density as a function of the blade angle is not given. A verification of the water pressures calculations is given for a 60° blade

with a blade-height/layer-thickness ratio of 1.

Miedema [51,52] 1984 gives a formulation for the determination of the water under-pressures. The deformation rate is determined by taking the volume balance over the shear zone, as Van Os [62,63] did. The deformation rate is modeled as a boundary condition in the shear zone, while the shear zone is modeled as a straight line instead of a shear band as with Van Os [62,63] and Van Leussen and Nieuwenhuis [39]. The influence of the water depth on the cutting forces is clarified. Also explained are the forces on the cutterhead on the basis of equation (2.6) and a survey is given of the possibilities of DREDMO.

Steeghs [72] 1985 developed a theory for the determination of the volume strain rate, based upon a cyclic deformation of the sand in a shear band. This implies that not an average value is taken for the volume strain rate but a cyclic, with time varying, value, based upon the dilatancy angle theory.

Miedema [54,55] 1985 derives equations for the determination of the water under-pressures and the cutting forces, based upon [46,51,52]. The water under-pressures are determined with a finite element method. Explained are the influence of the permeability of the disturbed and undisturbed sand and the determination of the shear angle. The derived theory is verified with model tests. On basis of this research n_{\max} is chosen for the residual pore percentage instead of the wet critical density.

Steeghs [72,73] 1985/1986 derives equations for the determination of the water under-pressures according an analytical approximation method. With this approximation method the water under-pressures are determined with a modification of equation (2.4) derived by Van Os [62,63] and the storage equation (2.7). Explained is how cutting forces can be determined with the force equilibrium on the cut layer. Also included are the gravity force, the inertia forces and the under-pressure behind the blade. For the last influence factor no formulation is given. Discussed is the determination of the shear angle. Some examples of the cutting forces are given as a function of the cutting velocity, the water depth and the sub-pressure behind the blade. A verification of this theory is not given.

Miedema [56] 1986 develops a calculation model for the determination of the cutting forces on a dredging-wheel based upon [54,55]. This will be discussed in the appropriate section. Also nomograms are published with which the

cutting forces and the shear angle can be determined in a simple way. Explained is the determination of the weighted average permeability from the permeability of the disturbed and undisturbed sand. Based upon the calculations it is concluded that the average permeability forms a good estimation.

Miedema [57] 1986 extends the theory with adhesion, cohesion, inertia forces, gravity, and under-pressure behind the blade. The method for the calculation of the coefficients for the determination of a weighed average permeability are discussed. It is concluded that the additions to the theory lead to a better correlation with the tests results.

Van Os and Van Leussen [40] 1986 summarize the publications of Van Os [62,63] and of Van Leussen and Nieuwenhuis [39] and give a formulation of the theory developed in the early seventies at the Delft Hydraulics Laboratory. Discussed are the water pressures calculation, cavitation, the weighed average permeability, the angle of internal friction, the soil/steel angle of friction, the permeability, the volume strain and the cutting forces. Verification is given of a water pressures calculation and the cutting forces. The water under-pressures are determined with equation (2.4) derived by Van Os [62,63]. The water pore pressure calculation is performed with the finite difference method, in which the height of the shear band is equal to the mesh width of the grid. The size of this mesh width is considered to be arbitrary. From an example, however, it can be seen that the shear band has a width of 13% of the layer-thickness. Discussed is the determination of a weighed average permeability. The forces are determined with Coulomb's method.

[Back to top](#)

This is a translation of the dissertation of Dr.ir. S.A. Miedema, dated September 15th 1987 .
The dissertation was originally published in Dutch by the:
Delft University of Technology
Faculty of Mechanical Engineering and Marine Technology
Chair of Dredging Technology
Mekelweg 2
2628 CD, Delft
The Netherlands

It is advised to also read the papers following this dissertation, since the theory developed has been refined and extended.

Last modified Saturday May 27, 2000 by: [Sape A. Miedema](#)

Translation by: [Laurens de Jonge](#)

Figures, equations and tables by: [Erik Miedema](#)

Copyright © May, 2000 Dr.ir. S.A. Miedema



[Download Adobe Acrobat Reader V4.0](#)

2.03 Determination of the pore under-pressure around the blade.

[Contents](#)

The cutting process can be modeled as a two-dimensional process, in which a straight blade cuts a small layer of sand (figure 2.1). The sand is deformed in the shear zone, also called deformation zone or dilatancy zone. During this deformation the volume of the sand changes as a result of the shear stresses in the shear zone. In soil mechanics this phenomenon is called dilatancy. In densely packed sand the pore volume is increased as a result of the shear stresses in the deformation zone. This increase in the pore volume is thought to be concentrated in the deformation zone, with the deformation zone modeled as a straight line (line sink). Water has to flow to the deformation zone to fill up the increase of the pore volume in this zone. As a result of this water flow the grain stresses increase and the water pressures decrease. Therefore there are water under-pressures.

This implies that the forces necessary for cutting densely packed sand under water will be determined for an important part by the dilatancy properties of the sand. At low cutting velocities these cutting forces are also determined by the gravity, the cohesion and the adhesion for as far as these last two soil mechanical parameters are present in the sand. Is the cutting at high velocities, than the inertia forces will have an important part in the total cutting forces.

If the cutting process is assumed to be stationary, the water flow through the pores of the sand can be described in a blade motions related coordinate system. The determination of the water under-pressures in the sand around the blade is then limited to a mixed boundary conditions problem. The potential theory can be used to solve this problem. For the determination of the water under-pressures it is necessary to have a proper formulation of the boundary condition in the shear zone. Miedema [52] 1984 derived the basic equation for this boundary condition. In 1985 [54,55] and 1986 [57] a more extensive derivation is published.

If it is assumed that no deformations take place outside the deformation zone, then:

$$\left| \frac{\partial^2 p}{\partial x^2} \right| + \left| \frac{\partial^2 p}{\partial y^2} \right| = 0 \quad (2.8)$$

applies for the sand package around the blade.

The boundary condition is in fact a specific flow rate (fig. 2.2) that can be determined with the following hypothesis.

For a sand element in the deformation zone, the increase in the pore volume per unit of blade length, is:

$$\Delta V = e \cdot \Delta A = e \cdot \Delta x \cdot \Delta h_1 = e \cdot \Delta x \cdot \Delta l \cdot \sin(\beta) \quad (2.9)$$

In which:
$$e = \frac{n_{\max} - n_i}{1 - n_{\max}} \quad (2.10)$$

For the residual pore percentage is chosen for n_{\max} on the basis of the ability to explain the water under-pressures, measured in the laboratory tests. This is described in chapter 3.

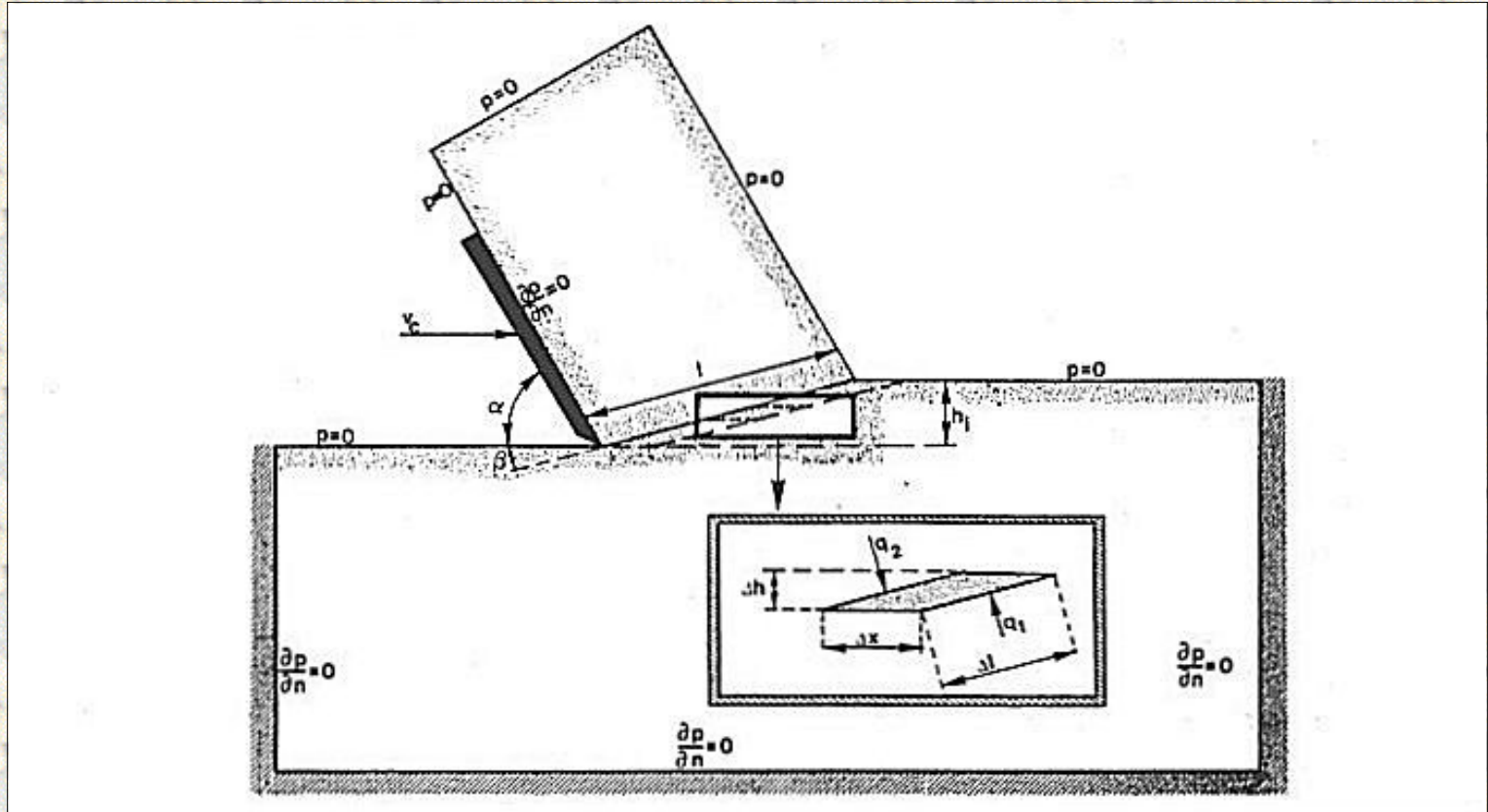


Figure 2.2: The volume balance over the shear zone.

The volume flow rate flowing to the sand element, is equal to:

$$\Delta Q = \frac{\partial V}{\partial t} = e \cdot \frac{\partial x}{\partial t} \cdot \Delta l \cdot \sin(\beta) = e \cdot v_c \cdot \Delta l \cdot \sin(\beta) \quad (2.11)$$

With the aid of Darcy's law the next differential equation can be derived for the specific flow rate, perpendicular to the deformation zone:

$$q = \frac{\partial Q}{\partial l} = q_1 + q_2 = \frac{k_i}{\rho_w \cdot g} \cdot \left| \frac{\partial p}{\partial n} \right|_1 + \frac{k_{\max}}{\rho_w \cdot g} \cdot \left| \frac{\partial p}{\partial n} \right|_2 = e \cdot v_c \cdot \sin(\beta) \quad (2.12)$$

The partial derivative $\partial p / \partial n$ is the derivative of the water under-pressures perpendicular on the boundary of the area, in which the water under-pressures are calculated (in this case the deformation zone). The boundary conditions on the other boundaries of this area are indicated in figure 2.2. A hydrostatic pressure distribution is assumed on the boundaries between sand and

water. This pressure distribution equals zero in the calculation of the water under-pressures, if the height difference over the blade is neglected. The boundaries that form the edges in the sand package are assumed to be impermeable. This will be further discussed in chapter 2.4.

Making equation (2.12) dimensionless is similar to that of the breach equation of Meijer and Van Os [41]. In the breach problem the length dimensions are normalized by dividing them by the breach height, while in the cutting of sand they are normalized by dividing them by the cut layer thickness.

Equation (2.12) in normalized format:

$$\frac{k_i}{k_{\max}} \cdot \left| \frac{\partial p}{\partial n'} \right|_1 + \left| \frac{\partial p}{\partial n'} \right|_2 = \frac{\rho_w \cdot g \cdot v_c \cdot e \cdot h_i \cdot \sin(\beta)}{k_{\max}} \quad (2.13)$$

With: $n' = n/h_i$

This equation is made dimensionless with:

$$\left| \frac{\partial p}{\partial n} \right|' = \frac{\left| \frac{\partial p}{\partial n'} \right|}{\rho_w \cdot g \cdot v_c \cdot e \cdot h_i / k_{\max}} \quad (2.14)$$

The accent indicates that a certain variable or partial derivative is dimensionless. The next dimensionless equation is now valid as a boundary condition in the deformation zone:

$$\frac{k_i}{k_{\max}} \cdot \left| \frac{\partial p}{\partial n} \right|'_1 + \left| \frac{\partial p}{\partial n} \right|'_2 = \sin(\beta) \quad (2.15)$$

The storage equation also has to be made dimensionless, which results in the next equation :

$$\left| \frac{\partial^2 p}{\partial x^2} \right|' + \left| \frac{\partial^2 p}{\partial y^2} \right|' = 0 \quad (2.16)$$

Because the right hand side of this equation equals zero, it is similar to equation (2.8)

The water under-pressures distribution in the sand package can now be determined using the storage equation and the boundary conditions. Because the calculation of the water under-pressures is dimensionless the next transformation has to be performed to determine the real

water under-pressures.

The real water under-pressures can be determined by integrating the derivative of the water under-pressures in the direction of a flow line, along a flow line, so:

$$p_{\text{calc}} = \int_s \left| \frac{\partial p}{\partial s} \right| \cdot ds' \text{ over een stroomlijn } s' \quad (2.17)$$

This is illustrated in figure 2.3.

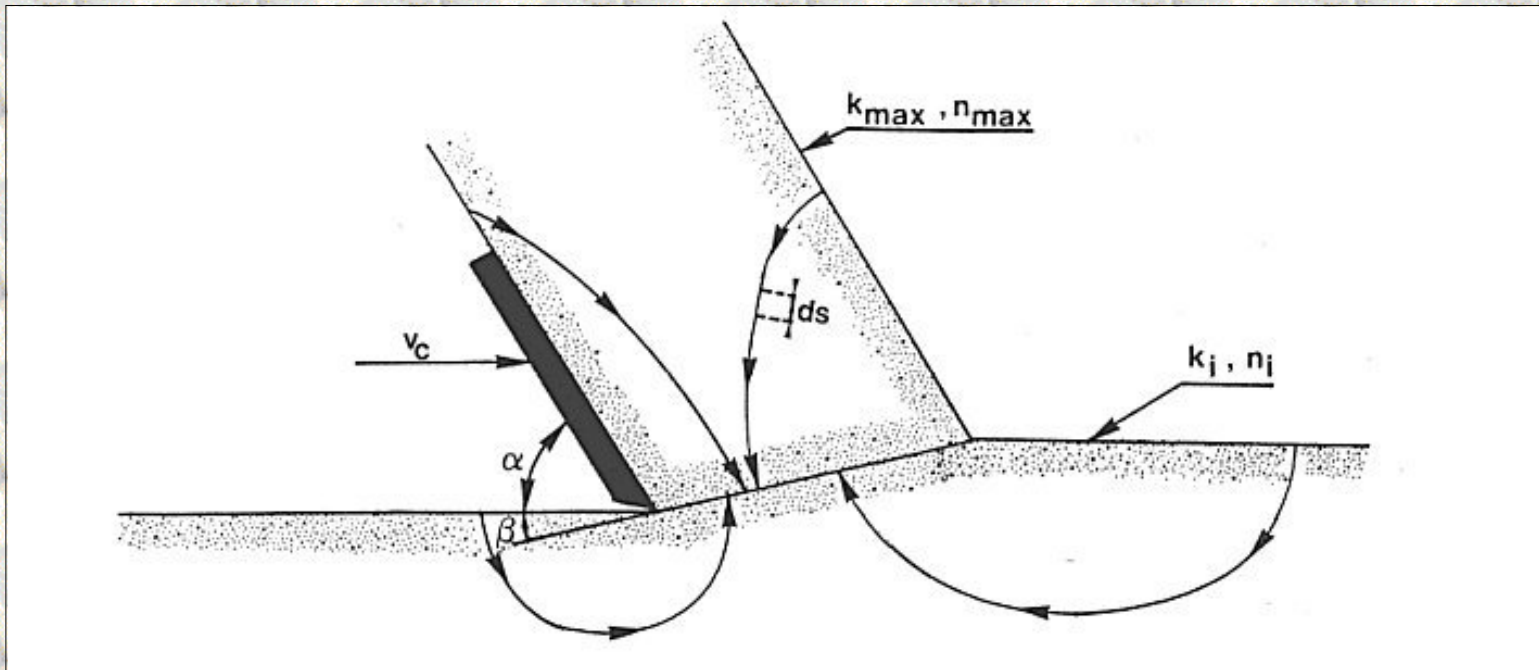


Figure 2.3: The flow of the pore water towards the shear zone.

Using equation (2.14) this can be written as:

$$p_{\text{real}} = \int_s \left| \frac{\partial p}{\partial s} \right| \cdot ds = \int_s \frac{\rho_w \cdot g \cdot v_c \cdot e \cdot h_i}{k_{\text{max}}} \cdot \left| \frac{\partial p}{\partial s} \right| \cdot ds' \quad (2.18)$$

With: $s' = s/h_i$

This gives the flowing relation between the really emerging water under-pressures and the calculated water under-pressures:

$$p_{\text{real}} = \frac{\rho_w \cdot g \cdot v_c \cdot e \cdot h_i}{k_{\text{max}}} \cdot p_{\text{calc}} \quad (2.19)$$

In table 2.1 (see appendix B5) the calculated water under-pressures are listed in relation with the blade angle, the shear angle, the blade-height/layer-thickness ratio and the ratio between the

permeability of the disturbed and undisturbed sand. Using equation (2.19) or equation (2.14) also the water under-pressures, measured in the cutting tests, can be made dimensionless. To be independent of the ratio between the initial permeability k_i and the maximum permeability k_{\max} , k_{\max} has to be replaced with the weighed average permeability k_m before making the measured water under-pressures dimensionless. This will be discussed in chapter 2.8.

[Back to top](#)

This is a translation of the dissertation of Dr.ir. S.A. Miedema, dated September 15th 1987 .
The dissertation was originally published in Dutch by the:
Delft University of Technology
Faculty of Mechanical Engineering and Marine Technology
Chair of Dredging Technology
Mekelweg 2
2628 CD, Delft
The Netherlands

It is advised to also read the papers following this dissertation, since the theory developed has been refined and extended.

Last modified Saturday May 27, 2000 by: [Sape A. Miedema](#)

Translation by: [Laurens de Jonge](#)

Figures, equations and tables by: [Erik Miedema](#)

Copyright © May, 2000 Dr.ir. S.A. Miedema



[Download Adobe Acrobat Reader V4.0](#)

2.04 Numerical water pore pressure calculations.

Contents

The water under-pressures in the sand package on and around the blade are numerically determined using the finite element method. A standard program package is used (Segal [69]). With the in this package, available "subroutines" a program is written, with which water under-pressures can be calculated and be output graphically and numerically. The solution of such a calculation is however not only dependent on the physical model of the problem, but also on the next points:

1. The size of the area in which the calculation takes place.
2. The size and distribution of the elements
3. The boundary conditions

The choices for these three points have to be evaluated with the problem that has to be solved in mind. These calculations are about the values and distribution of the water under-pressures in the shear zone and on the blade. A variation of the values for point 1 and 2 may therefore not influence this part of the solution. This is achieved by on the one hand increasing the area in which the calculations take place in steps and on the other hand by decreasing the element size until the variation in the solution was less than 1%.

The distribution of the elements is chosen such that a finer mesh is present around the blade tip, the shear zone and on the blade, also because of the blade tip problem (chapter 2.5).

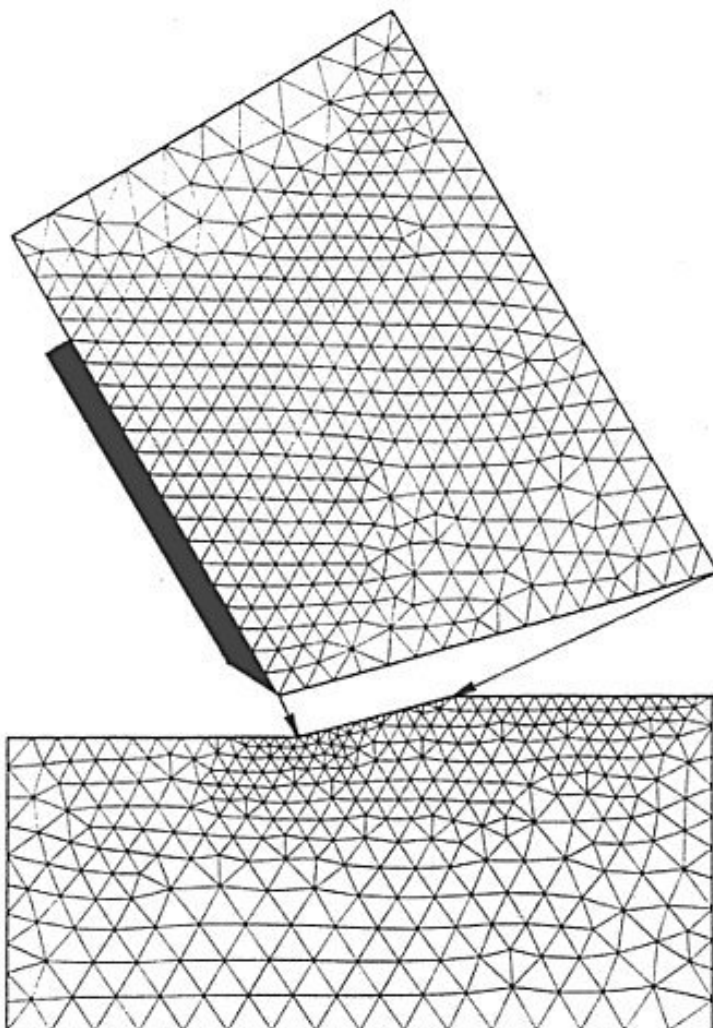


Figure 2.4: The mesh as applied in the water under-pressure calculations.

A number of boundary conditions follow from the physical model of the cutting process, these are:

1. The boundary condition in the shear zone. This is described by equation (2.15).
2. The boundary condition along the free sand surface. The hydrostatic pressure at which the process takes place, can be chosen, when neglecting the dimensions of the blade and the layer in relation to the hydrostatic pressure head. Because these calculations are meant to obtain the difference between the water under-pressures and the hydrostatic pressure it is valid to take a zero pressure as the boundary condition.

The boundary conditions along the boundaries of the area where the calculation takes place, that are located in the sand package, are not determined by the physical process. For this boundary condition there is a choice between:

1. A hydrostatic pressure along the boundary.
2. A boundary as an impermeable wall.
3. A combination of a known pressure and a known specific flow rate.

None of these choices complies with the real process. Water from outside the calculation area will flow through the boundary. This also implies, however, that the pressure along this boundary is not hydrostatic. If, however, the boundary is chosen with enough distance from the real cutting process the boundary condition may not have an influence on the solution. The impermeable wall is chosen although this choice is arbitrary. Figure 2.2 gives an impression of the size of the area and the boundary conditions, while figure 2.4 shows the element mesh. Figure 2.5 shows the two-dimensional distribution of the water under-pressures.

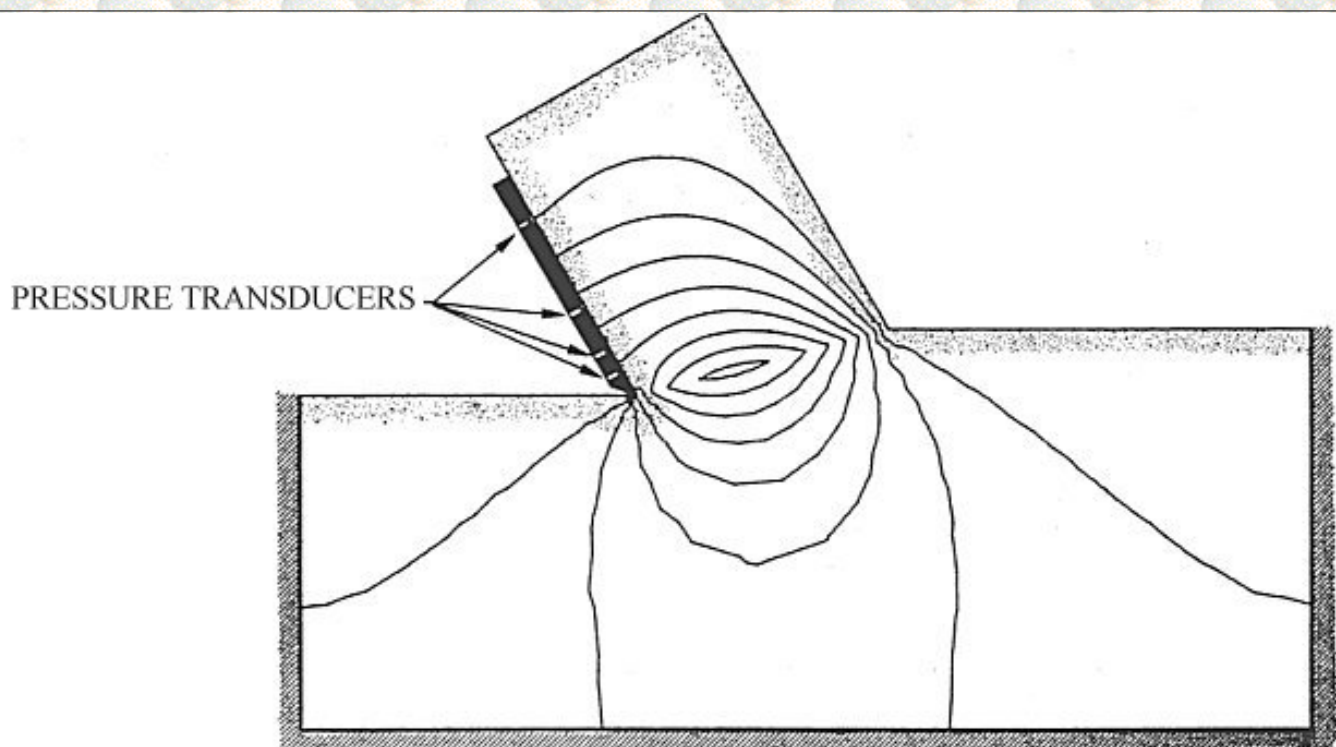


Figure 2.5: The distribution of the water under-pressures in the sand around the blade.

[Back to top](#)

This is a translation of the dissertation of Dr.ir. S.A. Miedema, dated September 15th 1987 .

The dissertation was originally published in Dutch by the:

Delft University of Technology

Faculty of Mechanical Engineering and Marine Technology

Chair of Dredging Technology

Mekelweg 2

2628 CD, Delft

The Netherlands

It is advised to also read the papers following this dissertation, since the theory developed has been refined and extended.

Last modified Saturday May 27, 2000 by: [Sape A. Miedema](#)

Translation by: [Laurens de Jonge](#)

Figures, equations and tables by: [Erik Miedema](#)

Copyright © May, 2000 Dr.ir. S.A. Miedema



[Download Adobe Acrobat Reader V4.0](#)

2.05 The blade tip problem.

During the physical modeling of the cutting process it has always been assumed that the blade tip is sharp. In other words, that in the numerical calculation, from the blade tip, a hydrostatic pressure can be introduced as the boundary condition along the free sand surface behind the blade. In practice this is never valid, because of the following reasons:

1. The blade tip always has a certain rounding, so that the blade tip can never be considered really sharp.
2. Trough wear of the blade a flat section develops behind the blade tip, which runs against the sand surface (clearance angle \leq zero)
3. If there is also dilatancy in the sand underneath the blade tip it is possible that the sand runs against the flank after the blade has passed.
4. There will be a certain sub-pressure behind the knife as a result of the blade speed and the cutting process.

A combination of these factors determines the distribution of the water under-pressures, especially around the blade tip. The first three factors can be accounted for in the numerical calculation as an extra boundary condition behind the blade tip. Along the free sand surface behind the blade tip an impenetrable line element is put in, in the calculation. The length of this line element is varied with $0.0 \cdot h_i$, $0.1 \cdot h_i$ and $0.2 \cdot h_i$. It showed from these calculations that especially the water under-pressures on the knife are strongly determined by the choice of this boundary condition as indicated in figure 2.6.

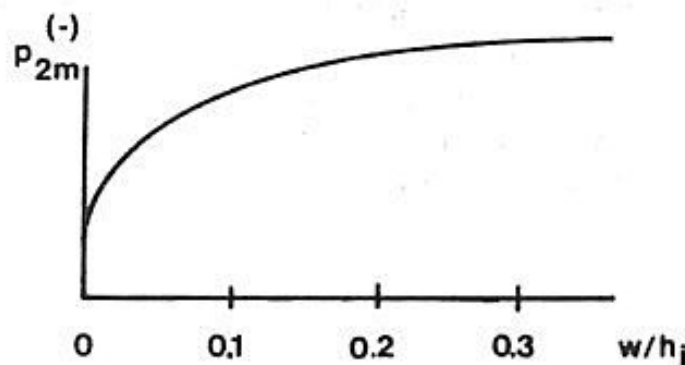


Figure 2.6a: The water sub-pressures distribution on the blade as function of the length of the flat wear section w .

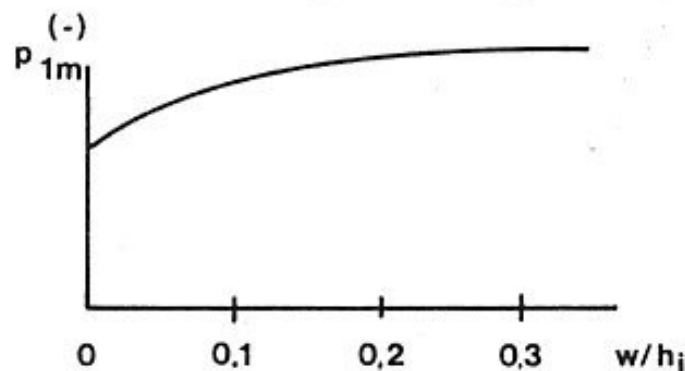


Figure 2.6b: The water sub-pressures distribution in the shear zone as function of the length of the flat wear section w .

It is hard to estimate to what degree the influence of the under-pressure behind the blade on the water under-pressures around the blade tip can be taken into account with these extra boundary condition. Since there is no clear formulation for the under-pressure behind the blade available, it will be assumed that the extra boundary condition at the blade tip describes this influence. The laboratory research will have to make this more evident.

[Back to top](#)

This is a translation of the dissertation of Dr.ir. S.A. Miedema, dated September 15th 1987 .

The dissertation was originally published in Dutch by the:
Delft University of Technology
Faculty of Mechanical Engineering and Marine Technology
Chair of Dredging Technology
Mekelweg 2
2628 CD, Delft
The Netherlands

It is advised to also read the papers following this dissertation, since the theory developed has been refined and extended.

Last modified Saturday May 27, 2000 by: [Sape A. Miedema](#)

Translation by: [Laurens de Jonge](#)

Figures, equations and tables by: [Erik Miedema](#)

Copyright © May, 2000 Dr.ir. S.A. Miedema



[Download Adobe Acrobat Reader V4.0](#)

2.06 The forces on the blade.

The forces that act on the blade during the cutting of soil, are transmitted on the blade through grain stresses and water pressures. These forces are caused by:

1. Normal stress, resulting in the force N_2 .
2. Shear stress as a result of the soil/steel friction, resulting in S_2 .
3. Shear stress as a result of the adhesion between the soil and the blade, resulting in the force A .
4. Water under-pressures on the blade p_{2m} , resulting in the force W_2 .
5. Under-pressure behind the blade p_{3m} , resulting in the force W_3 .

These forces are indicated in figure 2.7.

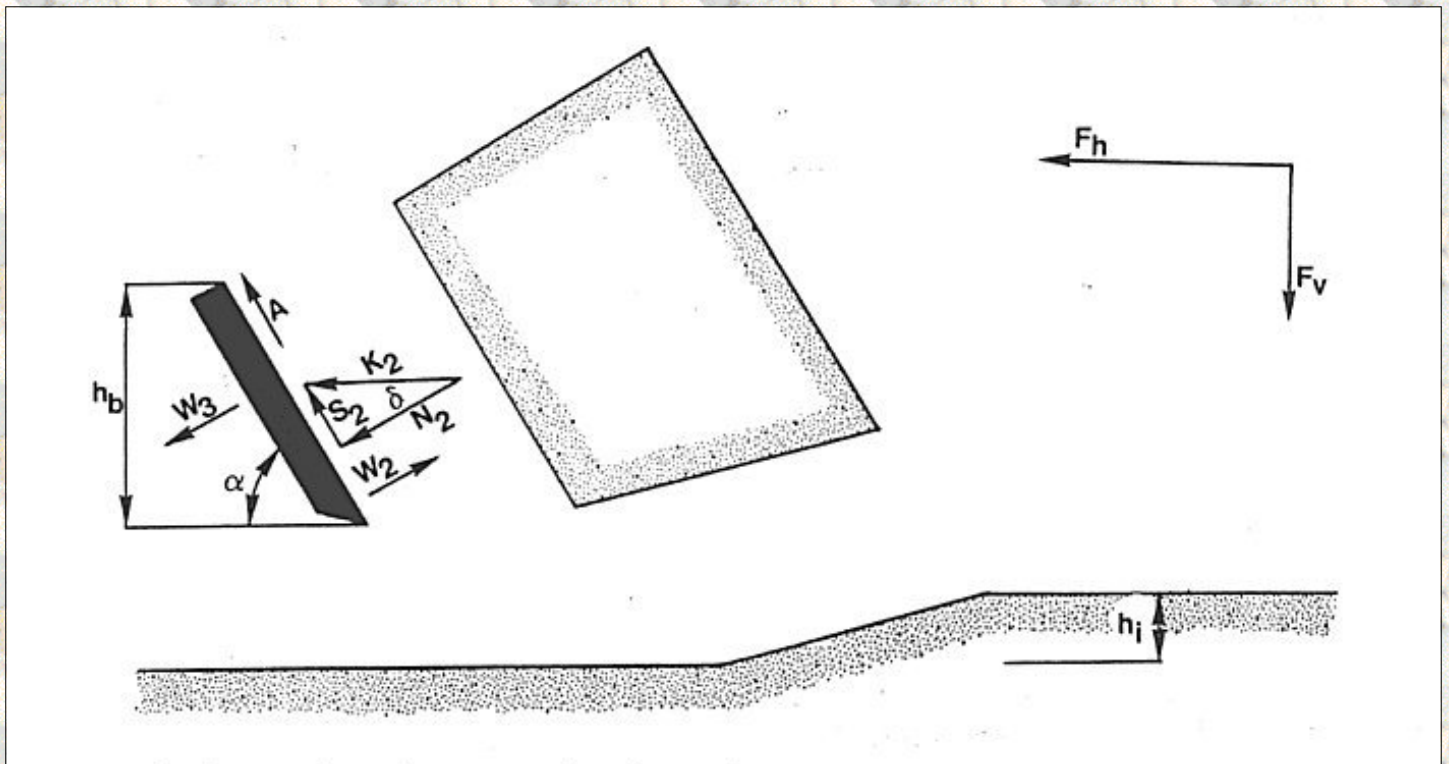


Figure 2.7: The forces acting on the blade.

The normal force N_2 and the shear force S_2 are related as follows:

$$S_2 = N_2 \cdot \tan(\delta) \quad K_2 = \sqrt{S_2^2 + N_2^2} \quad (2.20)$$

The resulting water force on the blade W_2 can be determined theoretically (see chapter 2.3). The resulting water force W_3 behind the blade results from measurements and from the determination of the angle of internal friction from measurements (see chapter 3.11). This implies that the resulting grain force K_2 is the only unknown force on the blade. This resulting force can be determined from the force equilibrium on the cut layer according the method of Coulomb [76] extended with the water pressure forces. These forces on the cut layer are shown in figure 2.8. These forces are:

1. The earlier mentioned forces W_2 , N_2 , S_2 and A .

2. The force W_1 resulting from the water pressures in the shear zone p_{1m} .
3. The force N_1 resulting from the normal stress on the shear zone.
4. The force S_1 resulting from the shear stress as a result of the internal friction of the sand.
5. The force resulting from the cohesion of the sand C .
6. The force as a result of the mass of the sand G .
7. The force as a result of the acceleration of the sand T .
8. The force W_4 as a result of the water resistance.

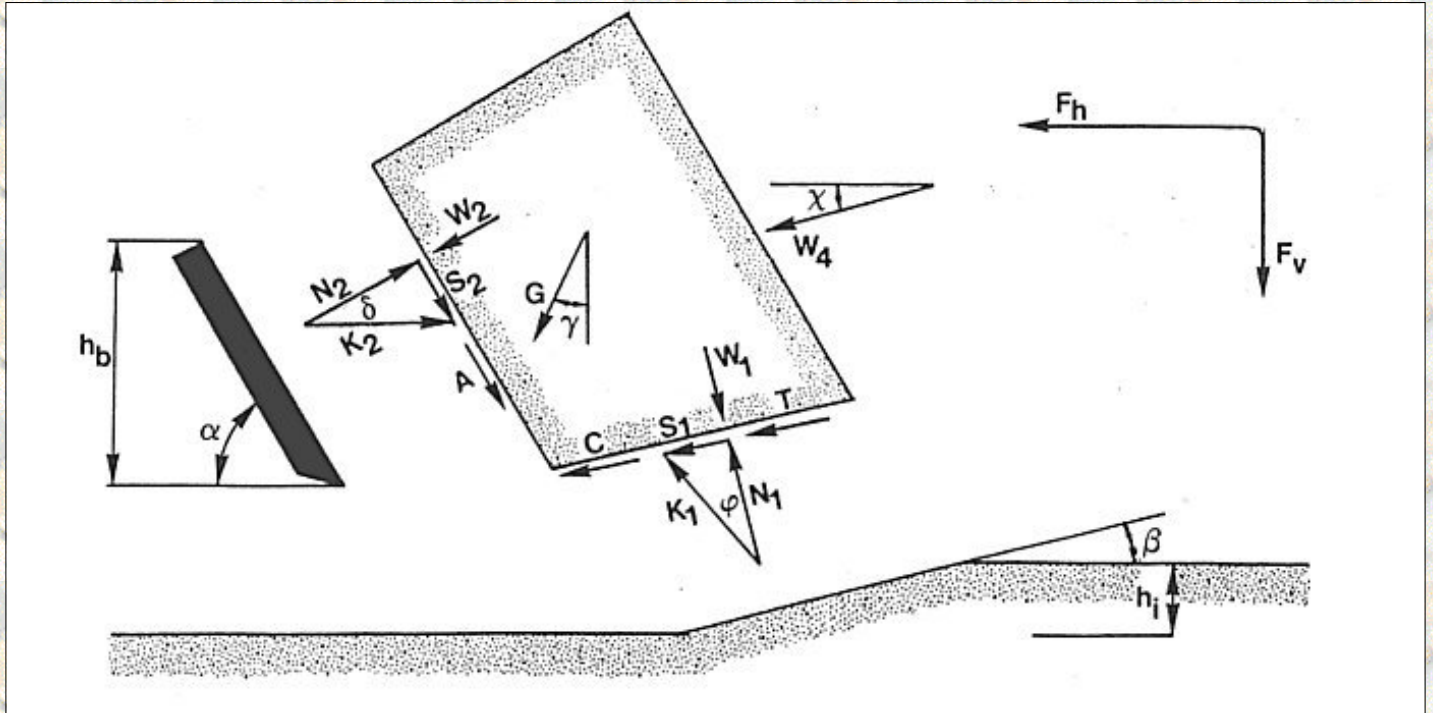


Figure 2.8: The forces acting on the layer cut.

The normal force N_1 and the shear force S_1 are related according:

$$S_1 = N_1 \cdot \tan(\varphi) \quad K_1 = \sqrt{(S_1^2 + N_1^2)} \quad (2.21)$$

From the horizontal and the vertical force equilibrium on the cut layer, the grain forces K_1 and K_2 can be determined. The horizontal and vertical expressions are related to the direction of the cutting velocity such that the horizontal axis points in the direction of the cutting velocity and the vertical axis is perpendicular to this. This means that the gravity force is not necessarily directed vertically in the figures, but can make an angle γ with the vertical. This is done to ease the determination of the vertical and horizontal equilibrium.

For the horizontal force equilibrium can now be found:

$$K_1 \cdot \sin(\beta + \varphi) - W_1 \cdot \sin(\beta) + C \cdot \cos(\beta) + T \cdot \cos(\beta) + G \cdot \sin(\gamma) + W_4 \cdot \cos(\chi) \\ - A \cdot \cos(\alpha) + W_2 \cdot \sin(\alpha) - K_2 \cdot \sin(\alpha + \delta) = 0 \quad (2.22)$$

And for the vertical force equilibrium can be found:

$$-K_1 \cdot \cos(\beta + \varphi) + W_1 \cdot \cos(\beta) + C \cdot \sin(\beta) + T \cdot \sin(\beta) + G \cdot \cos(\gamma) + W_4 \cdot \sin(\chi) \\ + A \cdot \sin(\alpha) + W_2 \cdot \cos(\alpha) - K_2 \cdot \cos(\alpha + \delta) = 0 \quad (2.23)$$

For the determination of the forces on the blade only the force K_2 is of importance. For this force can now be derived ($K_2 = K_{21} + K_{22}$):

$$K_{21} = \frac{W_2 \cdot \sin(\alpha + \beta + \varphi) + W_1 \cdot \sin(\varphi)}{\sin(\alpha + \beta + \delta + \varphi)} \quad (2.24)$$

$$K_{22} = \frac{G \cdot \sin(\beta + \varphi + \gamma) + T \cdot \cos(\varphi) + C \cdot \cos(\varphi) - A \cdot \cos(\alpha + \beta + \varphi) + W_4 \cdot \cos(\beta + \varphi - \chi)}{\sin(\alpha + \beta + \varphi + \delta)} \quad (2.25)$$

The force K_{21} is the water under-pressures part, while force K_{22} is the part of the gravity, the inertia forces, the cohesion, the adhesion and the water resistance in the force K_2 .

The following forces act on the blade:

1. The horizontal force F_h .

$$F_h = -W_2 \cdot \sin(\alpha) + K_2 \cdot \sin(\alpha + \delta) + A \cdot \cos(\alpha) + W_3 \cdot \sin(\alpha) \quad (2.26)$$

2. De vertical force F_v .

$$F_v = -W_2 \cdot \cos(\alpha) + K_2 \cdot \cos(\alpha + \delta) - A \cdot \sin(\alpha) + W_3 \cdot \cos(\alpha) \quad (2.27)$$

If there is no cavitation the water pressures forces W_1 and W_2 can be written as:

$$W_1 = \frac{p_{1m} \cdot \rho_w \cdot g \cdot v_c \cdot e \cdot h_1^2 \cdot b}{(a_1 \cdot k_i + a_2 \cdot k_{\max}) \cdot \sin(\beta)} \quad (2.28)$$

and

$$W_2 = \frac{p_{2m} \cdot \rho_w \cdot g \cdot v_c \cdot e \cdot h_1 \cdot b}{(a_1 \cdot k_i + a_2 \cdot k_{\max}) \cdot \sin(\alpha)} \quad (2.29)$$

For W_3 an empirical relation is found, namely:

$$W_3 = 0.3 \cdot \cot(\alpha) \cdot W_2 \quad (2.30)$$

With the limitation that W_3 can never be higher than W_2 . This relation suffices well for blade angles between 30° to 60° . This under-pressure behind the blade will be discussed in chapter 3.11. In case of cavitation W_1 and W_2 become:

$$W_1 = \rho_w \cdot g \cdot (z+10) \cdot h_i \cdot b / \sin(\beta) \quad (2.31)$$

and

$$W_2 = \rho_w \cdot g \cdot (z+10) \cdot h_b \cdot b / \sin(\alpha) \quad (2.32)$$

The effect of cavitation on the under-pressure behind the blade is yet unknown. For the moment the above stated equation is used.

Wismer and Luth [80] in 1972 researched the inertia forces part of the total cutting forces. The following equation is derived:

$$T = \rho_g \cdot v_c^2 \cdot \frac{\sin(\alpha)}{\sin(\alpha+\beta)} \cdot h_i \cdot b \quad (2.33)$$

The cohesion and the adhesion can be determined with soil mechanical experiments. For the cohesion and adhesion forces the following equations are valid:

$$C = c \cdot h_i \cdot b / \sin(\beta) \quad (2.34)$$

and

$$A = a \cdot h_b \cdot b / \sin(\alpha) \quad (2.35)$$

The gravitational force (weight) follows from:

$$G = (\rho_s - \rho_w) \cdot g \cdot h_i \cdot b \cdot \frac{\sin(\alpha+\beta)}{\sin(\beta)} \cdot \left\{ \frac{(h_b + h_i \cdot \sin(\alpha))}{\sin(\alpha)} + \frac{h_i \cdot \cos(\alpha+\beta)}{2 \cdot \sin(\beta)} \right\} \quad (2.36)$$

This is in accordance with the area that is used for the water pressures calculations (see figure 2.4).

The flow resistance is included explicit in equation (2.24), although this term will have to be introduced as a boundary condition in the water pressures calculations. Since the flow resistance is proportional with the square of the cutting velocity, while the volume strain rate is proportional with the cutting velocity, it is impossible to include the flow resistance in the dimensionless water pressures calculations. It is proposed to include the flow resistance as an external force in the force equilibrium, according:

$$W_4 = C_w \cdot 0.5 \cdot \rho_w \cdot v_c^2 \cdot b \cdot \left(\frac{(h_b + h_i \cdot \sin(\alpha))}{\sin(\alpha)} + \frac{h_i \cdot \cos(\alpha + \beta)}{2 \cdot \sin(\beta)} \right) \quad (2.37)$$

In which the force W_4 has an angle χ with the direction of the velocity. The values of C_w and χ will have to be determined experimentally. The term behind the blade width b is in accordance with the cut layer, as is used in the water pressures calculations.

[Back to top](#)

This is a translation of the dissertation of Dr.ir. S.A. Miedema, dated September 15th 1987 .

The dissertation was originally published in Dutch by the:

Delft University of Technology

Faculty of Mechanical Engineering and Marine Technology

Chair of Dredging Technology

Mekelweg 2

2628 CD, Delft

The Netherlands

It is advised to also read the papers following this dissertation, since the theory developed has been refined and extended.

Last modified Saturday May 27, 2000 by: [Sape A. Miedema](#)

Translation by: [Laurens de Jonge](#)

Figures, equations and tables by: [Erik Miedema](#)

Copyright © May, 2000 Dr.ir. S.A. Miedema



[Download Adobe Acrobat Reader V4.0](#)

[Contents](#) **2.07 The determination of the shear angle β .**

In chapter 2.6 the equations are derived with which the forces on a straight blade can be determined according the method of Coulomb [76]. Unknown in these equations is the shear angle β .

In literature several methods are used to determine this shear angle.

The oldest is perhaps the method of Coulomb [76]. This method is widely used in sheet pile wall calculations. Since passive earth pressure is the cause for failure here, it is necessary to find the shear angle at which the total, on the earth, exerted force by the sheet pile wall is at a minimum.

When the water pressures are not taken into account, an analytical solution for this problem can be found.

Another failure criterion is used by Hettiaratchi and Reece [23]. This principle is based upon the cutting of dry sand. The shear plane is not assumed to be straight as in the method of Coulomb, but the shear plane is composed of a logarithmic spiral from the blade tip that changes into a straight shear plane under an angle of $45^\circ - 0.5 \cdot \varphi$ with the horizontal to the sand surface. The straight part of the shear plane is part of the so-called passive Rankine zone. The origin of the logarithmic spiral is chosen such that the total force on the blade is minimal.

There are perhaps other failure criteria for sheet pile wall calculations known in literature, but these mechanisms are only suited for a one-time failure of the earth. In the cutting of soil the process of building up stresses and next the collapse of the earth, is a continuous process.

Another criterion for the collapse of earth, is the determination of those failure conditions for which the total required strain energy is minimal. Rowe [67] uses this principle for the determination of the angle under which local shear takes place. From this point of view it seems plausible to assume that those failure criteria for the cutting of sand have to be chosen, for which the cutting work is minimal. This implies that the angle of friction has to be chosen for which the cutting work and therefore the horizontal force, exercised by the knife on the soil, is minimal. Miedema [54,57] and Steeghs [72,73] have chosen this method.

Assuming that the water pressures are dominant in the cutting of packed sand, and thus neglecting adhesion, cohesion, gravity, inertia forces, flow resistance and sub-pressure behind the blade, the derivative of the force F_h (equation (2.26)) to the shear angle β becomes:

$$\begin{aligned} \frac{\partial F_h'}{\partial \beta} = & -p_{1m} \cdot h_i \cdot \frac{\sin(\varphi) \sin(\alpha + 2 \cdot \beta + \delta + \varphi)}{\sin^2(\beta) \sin(\alpha + \beta + \delta + \varphi)} + p_{2m} \cdot h_b \cdot \frac{\sin(\delta)}{\sin(\alpha) \sin(\alpha + \beta + \delta + \varphi)} \\ & + \frac{\partial p_{1m}}{\partial \beta} \cdot h_i \cdot \frac{\sin(\varphi)}{\sin(\beta)} + \frac{\partial p_{2m}}{\partial \beta} \cdot h_b \cdot \left\{ \frac{\sin(\alpha + \beta + \varphi)}{\sin(\alpha)} - \frac{\sin(\alpha + \beta + \delta + \varphi)}{\sin(\alpha + \delta)} \right\} \end{aligned} \quad (2.38)$$

With the following simplification:

$$\frac{\partial F_h'}{\partial \beta} = \frac{\partial F_h}{\partial \beta} \cdot \frac{\sin(\alpha + \beta + \delta + \varphi)}{\sin(\alpha + \delta)} \quad (2.39)$$

Since the value of the shear angle β , for which the horizontal force is minimal, has to be found, equation (2.38) is set equal to zero, so the simplification according equation (2.39) is allowed. It is clear that this problem has to be solved iterative, because an analytical solution is impossible.

The Newton-Rhapson method works very well for this problem. In tables 2.2 to 2.7 (see appendix B5) the resulting shear angles, calculated with this method, can be found for several values of δ , φ , α , several ratios of h_b/h_i and for the non-cavitating and cavitating cutting process.

Interesting are now the results if another method is used. To check this the shear angles have also been determined according Coulomb's criterion: there is failure at the shear angle for which the total force, exerted by the blade on the soil, is minimal. The maximum deviation of these shear angles with the shear angles according tables 2.2 to 2.7 (see Appendix B5) has a value of only 3° at a blade angle of 15° . The average deviation is approximately 1.5° for blade angles to 60° .

The forces have a maximum deviation of less than 1%. It can therefore be concluded that it does not matter if the total force, exercised by the soil on the blade, is minimized, or the horizontal force. Next these calculations showed that the cutting forces, as a function of the shear angle, vary only slightly with the shear angles, found using equation (2.38). This sensitivity increases with an increasing blade angle. Figure 2.9 shows this for the following conditions:

$\alpha = 15^\circ, 30^\circ, 45^\circ$ and 60° , $\delta = 24^\circ$, $\varphi = 42^\circ$, $h_b/h_i = 1$ and a non-cavitating cutting process.

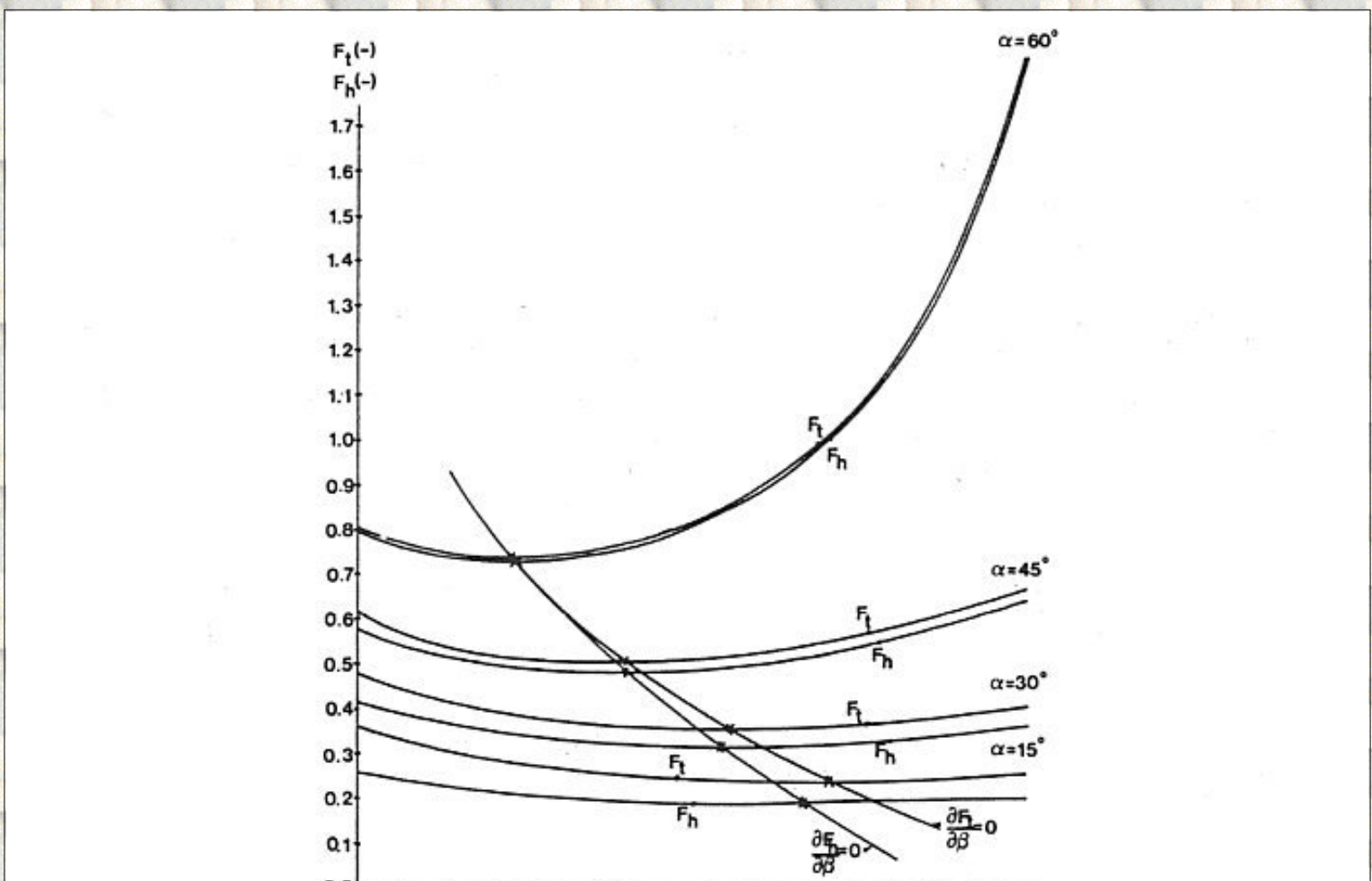




Figure 2.9: The forces F_h and F_t as a function of the shear angle β and as a function of the blade angle α , determined according to the principle of minimal specific cutting energy and according to the minimal total cutting force F_t .

[Back to top](#)

This is a translation of the dissertation of Dr.ir. S.A. Miedema, dated September 15th 1987 .
The dissertation was originally published in Dutch by the:
Delft University of Technology
Faculty of Mechanical Engineering and Marine Technology
Chair of Dredging Technology
Mekelweg 2
2628 CD, Delft
The Netherlands

It is advised to also read the papers following this dissertation, since the theory developed has been refined and extended.

Last modified Saturday May 27, 2000 by: [Sape A. Miedema](#)

Translation by: [Laurens de Jonge](#)

Figures, equations and tables by: [Erik Miedema](#)

Copyright © May, 2000 Dr.ir. S.A. Miedema



[Download Adobe Acrobat Reader V4.0](#)

2.08 The weighed average permeability.

In the derivation of the calculation of the water under-pressures around the blade, resulting in equations (2.28) and (2.29), it already showed that the water under-pressures are determined by the permeability of the undisturbed sand and the permeability of the disturbed sand. Equation (2.15) of chapter 2.3 shows this dependence. The water under-pressures are determined for several ratios of the initial permeability of the undisturbed sand to the maximum permeability of the disturbed sand:

$$k_i/k_{\max} = 1$$

$$k_i/k_{\max} = 0.5$$

$$k_i/k_{\max} = 0.25$$

The average water sub-pressures p_{1m} en p_{2m} can be put against the ratio k_i/k_{\max} , for a certain shear angle β . A hyperbolic relation emerges between the average water under-pressures and the ratio of the permeabilities. If the reciproke values of the average water under-pressures are put against the ratio of the permeabilities a linear relation emerges.

The derivatives of p_{1m} and p_{2m} to the ratio k_i/k_{\max} are, however, not equal to each other. This implies that a relation for the forces as a function of the ratio of permeabilities can not be directly derived from the found average water under-pressures.

This is in contrast with the method used by Van Leussen and Van Os [40]. In [40] it is assumed that the average pore pressure on the blade has the same dependability on the ratio of permeabilities as the average pore pressure in the shear zone. No mathematical background is given for this assumption.

For the several ratios of the permeabilities it is possible with the shear angles, determined in chapter 2.7, to determine the dimensionless forces F_h and F_v . If these dimensionless forces are put against the ratio of the permeabilities, also a hyperbolic relation is found (Miedema [57]), shown in figure 2.10.

A linear relation can therefore also be found if the reciproke values of the dimensionless forces are taken. This relation can be represented by:

$$1/F_h = a + b \cdot k_i / k_{\max} \quad (2.40)$$

With the next transformations an equation can be derived for a weighed average permeability k_m :

$$a_1 = \frac{b}{a+b} \quad a_2 = \frac{a}{a+b} \quad (2.41)$$

Thus:

$$k_m = a_1 \cdot k_i + a_2 \cdot k_{max} \quad (2.42)$$

With: $a_1 + a_2 = 1$

Since the sum of the coefficients a_1 en a_2 is equal to 1 only coefficient a_1 is given in the tables 2.8 to 2.13 (see appendix B5). It also has to be remarked that this coefficient is determined on the basis of the linear relation of F_h (dimensionless c_1), because the horizontal force gives more or less the same relation as the vertical force, but has besides a much higher value. Only for the 60° blade, where the vertical force is very small and can change direction, differences occur between the linear relations of the horizontal and the vertical force as function of the ratio of the permeabilities.

From table 2.8 to 2.13 (see Appendix B5) can be concluded, that the influence of the undisturbed soil increases when the blade-height/layer-thickness ratio increases. This can be explained by the fact that the water that flows to the shear zone over the blade has to cover a larger distance with an increasing blade height and therefore has to overcome a higher resistance. Relatively more water will have to flow through the undisturbed sand to the shear zone with an increasing blade height.

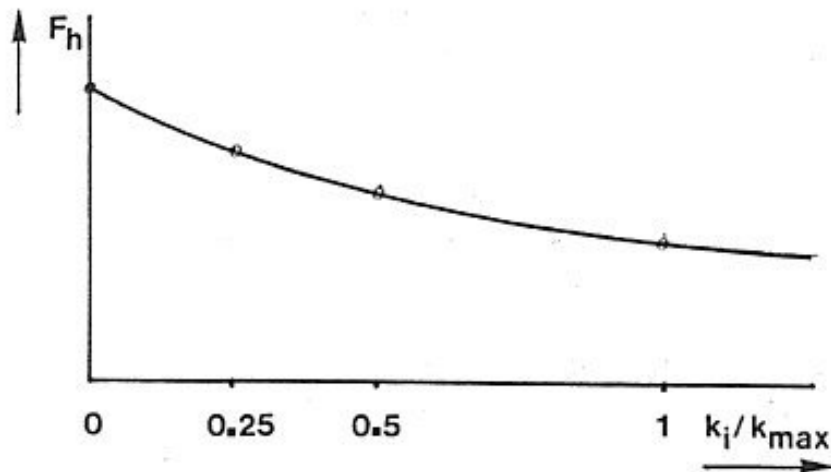


Figure 2.10a: The force F_h as a function of the ratio between the initial permeability k_i and the residual permeability k_{max} .

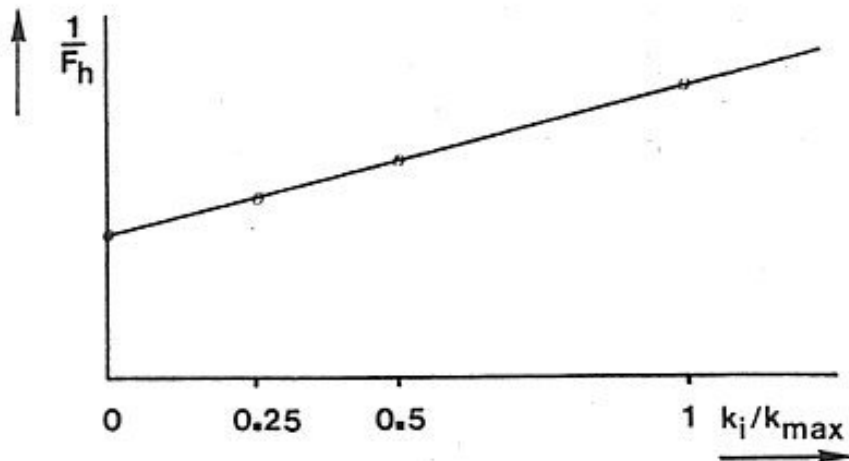


Figure 2.10b: The reciprocal of the force F_h as a function of the ratio between the initial permeability k_i and the residual permeability k_{\max} .

[Back to top](#)

This is a translation of the dissertation of Dr.ir. S.A. Miedema, dated September 15th 1987 .

The dissertation was originally published in Dutch by the:

Delft University of Technology

Faculty of Mechanical Engineering and Marine Technology

Chair of Dredging Technology

Mekelweg 2

2628 CD, Delft

The Netherlands

It is advised to also read the papers following this dissertation, since the theory developed has been refined and extended.

Last modified Saturday May 27, 2000 by: [Sape A. Miedema](#)

Translation by: [Laurens de Jonge](#)

Figures, equations and tables by: [Erik Miedema](#)

Copyright © May, 2000 Dr.ir. S.A. Miedema



[Download Adobe Acrobat Reader V4.0](#)

2.09 The dimensionless cutting force coefficients.

Contents

If only the influence of the water under-pressures on the forces that occur with the cutting of saturated packed sand under water is taken in to account, equations (2.26) and (2.27) can be simplified. It will be assumed that the non-cavitating process switches to the cavitating process for that cutting velocity v_c , for which the force in the direction of the cutting velocity F_h is equal for both processes.

In reality, however, there is a transition region between both processes, where locally cavitation starts in the shear zone. Although this transition region starts at about 65% of the cutting velocity at which, theoretically, full cavitation takes place, it shows from the results of the cutting tests that for the determination of the cutting forces the existence of a transition region can be neglected.

In the simplified equations the coefficients c_1 en d_1 represent the dimensionless horizontal force (or the force in the direction of the cutting velocity) in the non-cavitating and the cavitating cutting process. The coefficients c_2 and d_2 represent the dimensionless vertical force or the force perpendicular to the direction of the cutting velocity in the non-cavitating and the cavitating cutting process.

For the non-cavitating cutting process:

$$F_{ci} = c_i \cdot \rho_w \cdot g \cdot v_c \cdot h_i^2 \cdot b \cdot e / k_m \quad (2.43)$$

In which:

$$c_1 = \frac{\left[P_{1m} \cdot \frac{\sin(\varphi)}{\sin(\beta)} + P_{2m} \cdot \frac{h_b}{h_i} \cdot \frac{\sin(\alpha + \beta + \varphi)}{\sin(\alpha)} \right] \cdot \sin(\alpha + \delta)}{\sin(\alpha + \beta + \delta + \varphi)}$$

$$-P_{2m} \cdot \frac{h_b}{h_i} \cdot \frac{\sin(\alpha)}{\sin(\alpha)} + P_{3m} \cdot \frac{h_b}{h_i} \cdot \frac{\sin(\alpha)}{\sin(\alpha)} \quad (2.44)$$

and,

$$c_2 = \frac{\left(P_{1m} \cdot \frac{\sin(\varphi)}{\sin(\beta)} + P_{2m} \cdot \frac{h_b}{h_i} \cdot \frac{\sin(\alpha + \beta + \varphi)}{\sin(\alpha)} \right) \cdot \cos(\alpha + \delta)}{\sin(\alpha + \beta + \delta + \varphi)}$$

$$-P_{2m} \cdot \frac{h_b}{h_i} \cdot \frac{\cos(\alpha)}{\sin(\alpha)} + P_{3m} \cdot \frac{h_b}{h_i} \cdot \frac{\cos(\alpha)}{\sin(\alpha)} \quad (2.45)$$

And for the cavitating cutting process it yields:

$$F_{ci} = d_i \cdot \rho_w \cdot g \cdot (z+10) \cdot h_i \cdot b \quad (2.46)$$

In which:

$$d_1 = \frac{\left(\frac{\sin(\varphi)}{\sin(\beta)} + \frac{h_b}{h_i} \cdot \frac{\sin(\alpha + \beta + \varphi)}{\sin(\alpha)} \right) \cdot \sin(\alpha + \delta)}{\sin(\alpha + \beta + \delta + \varphi)}$$

$$- \frac{h_b}{h_i} \cdot \frac{\sin(\alpha)}{\sin(\alpha)} + P_{3m} \cdot \frac{h_b}{h_i} \cdot \frac{\sin(\alpha)}{\sin(\alpha)} \quad (2.47)$$

And:

$$d_2 = \frac{\left[\frac{\sin(\varphi)}{\sin(\beta)} + \frac{h_b}{h_i} \cdot \frac{\sin(\alpha + \beta + \varphi)}{\sin(\alpha)} \right] \cdot \cos(\alpha + \delta)}{\sin(\alpha + \beta + \delta + \varphi)} - \frac{h_b}{h_i} \cdot \frac{\cos(\alpha)}{\sin(\alpha)} + p_{3m} \cdot \frac{h_b}{h_i} \cdot \frac{\cos(\alpha)}{\sin(\alpha)} \quad (2.48)$$

The values of the 4 coefficients are determined by minimising the cutting work, or that is at that shear angle β where the derivative of the horizontal force to the shear angle is zero (see chapter 2.7).

For the non-cavitating cutting process the coefficients c_1 and c_2 are given in the tables 2.14 t/m 2.25 (see appendix B5). For the cavitating cutting process the values of d_1 and d_2 are given in the tables 2.26 t/m 2.37 (see appendix B5). The coefficients c_1 , c_2 , d_1 en d_2 are given in these tables as functions of α , δ , φ and the ratio h_b/h_i .

The tables are printed for the case without under-pressure behind the blade and for the case where the under-pressure behind the blade is calculated according equation (2.30), according next list:

Tables 2.14 t/m 2.16: c_1 without under-pressure behind the blade.

Tables 2.17 t/m 2.19: c_1 with under-pressure behind the blade.

Tables 2.20 t/m 2.22: c_2 without under-pressure behind the blade.

Tables 2.23 t/m 2.25: c_2 with under-pressure behind the blade.

Tables 2.26 t/m 2.28: d_1 without under-pressure behind the blade.

Tables 2.29 t/m 2.31: d_1 with under-pressure behind the blade.

Tables 2.32 t/m 2.34: d_2 without under-pressure behind the blade.

Tables 2.35 t/m 2.37: d_2 with under-pressure behind the blade.

Equations (2.43) en (2.46) form the basis of the simplified analytical models for the cutterhead (chapter 4) and the dredging-wheel (chapter 5).

[Back to top](#)

This is a translation of the dissertation of Dr.ir. S.A. Miedema, dated September 15th 1987 .

The dissertation was originally published in Dutch by the:

Delft University of Technology

Faculty of Mechanical Engineering and Marine Technology

Chair of Dredging Technology

Mekelweg 2

2628 CD, Delft

The Netherlands

It is advised to also read the papers following this dissertation, since the theory developed has been refined and extended.

Last modified Saturday May 27, 2000 by: [Sape A. Miedema](#)

Translation by: [Laurens de Jonge](#)

Figures, equations and tables by: [Erik Miedema](#)

Copyright © May, 2000 Dr.ir. S.A. Miedema



[Download Adobe Acrobat Reader V4.0](#)

2.10 Determination of φ and δ from cutting tests.

[Contents](#)

The soil/steel angle of friction and the angle of internal friction can be determined from cutting tests. Sand without cohesion or adhesion is assumed in the next derivations, while the mass of the cut layer has no influence on the determination of the soil/steel angle of friction. In figure 2.11 is indicated which on the blade acting forces have to be measured to determine the soil /steel angle of friction.

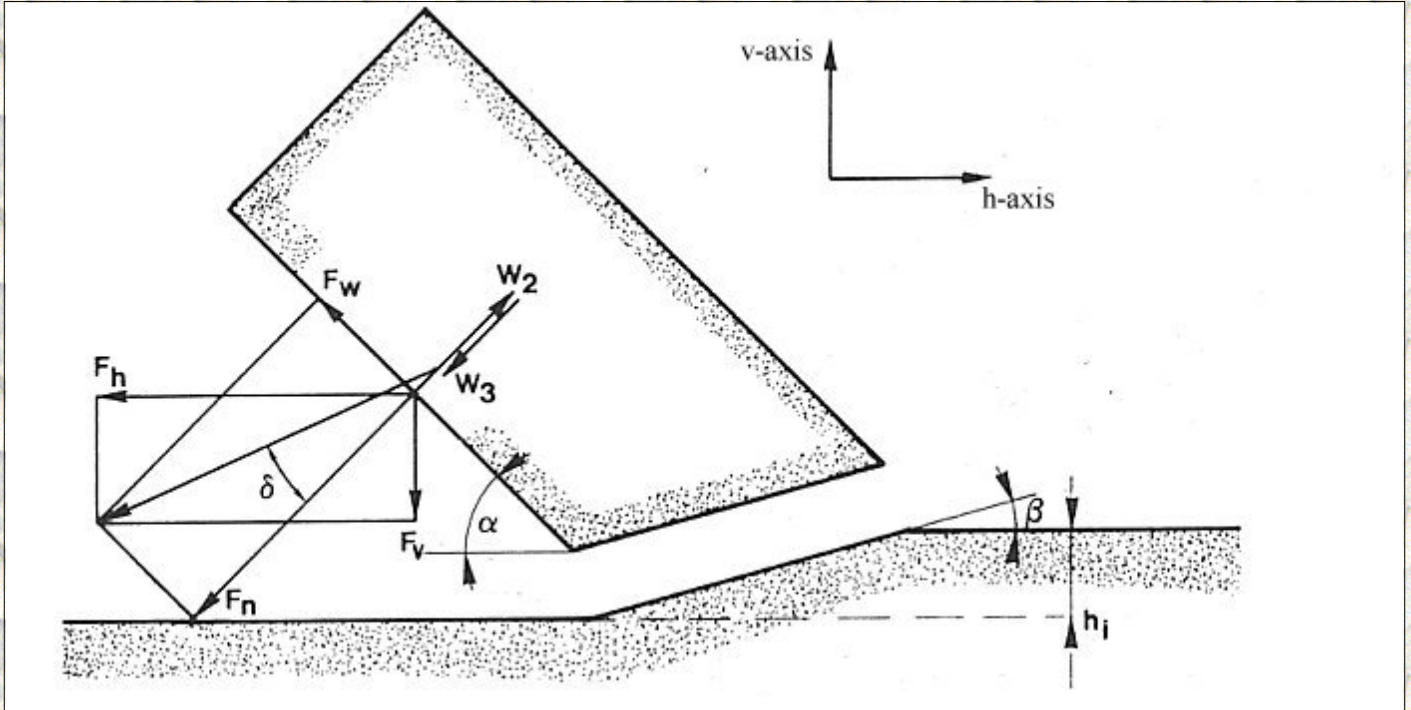


Figure 2.11: The forces from which the soil/blade friction angle can be determined.

The forces F_h and F_v can be measured directly. Force W_2 results from the integration of the measured water pressures on the blade. Force W_3 will be discussed in chapter 3.11 (see also equation (2.30)). From this figure the normal force on the blade, resulting from the grain stresses on the blade, becomes:

$$F_n = W_2 - W_3 + F_h \cdot \sin(\alpha) + F_v \cdot \cos(\alpha) \quad (2.49)$$

The friction force, resulting from the grain stresses on the blade, becomes:

$$F_w = F_h \cdot \cos(\alpha) - F_v \cdot \sin(\alpha) \quad (2.50)$$

The soil/steel angle of friction now becomes:

$$\delta = \arctan \left(\frac{F_w}{F_n} \right) \quad (2.51)$$

Determination of the angle of internal friction from the cutting tests is slightly more complicated. In figure 2.12 is indicated which forces, acting on the cut layer, have to be measured to determine this angle. Directly known are the measured forces F_h and F_v , while the inertia force T has to be determined using equation (2.33). The mass of the layer G can be determined with equation (2.36). The force W_3 results from a relation derived in chapter 3.11 (equation (2.30)). The force W_4 has to be determined

cutting tests, which will be discussed in chapter 3.11..

[Back to top](#)

This is a translation of the dissertation of Dr.ir. S.A. Miedema, dated September 15th 1987 .
The dissertation was originally published in Dutch by the:
Delft University of Technology
Faculty of Mechanical Engineering and Marine Technology
Chair of Dredging Technology
Mekelweg 2
2628 CD, Delft
The Netherlands

It is advised to also read the papers following this dissertation, since the theory developed has been refined and extended.

Last modified Saturday May 27, 2000 by: [Sape A. Miedema](#)

Translation by: [Laurens de Jonge](#)

Figures, equations and tables by: [Erik Miedema](#)

Copyright © May, 2000 Dr.ir. S.A. Miedema



[Download Adobe Acrobat Reader V4.0](#)

2.11 The effect of a velocity component parallel to the edge of the blade.

[Contents](#)

Important for the equilibrium of the cut layer is the soil/steel angle of friction, which acts in the plane perpendicular to the blade edge. It is assumed to be known that the friction force, occurring between two, in relation to each other, moving planes, acts in the direction of the velocity between the two planes. This implies that as a result of a velocity component parallel to the blade edge (sliding velocity) a friction force occurs parallel to the blade edge (sliding force) but in the opposite direction of the sliding velocity. If it is geometrically possible for the sand to move parallel to the direction of the blade edge, this can happen as a result of a velocity component parallel to the blade edge.

A known example of this phenomenon is the cutting process in a so-called "grader". In figure 2.13 the involved velocity and force components are shown.

First the involved forces have to be known, before the acting forces can be discussed.

- v_t The total velocity of the blade.
- v_c The velocity component of the blade perpendicular to the blade edge.
- v_r The relative velocity between the sand and the blade.
- v_l The velocity component of the blade parallel to the blade edge.
- f_0 The factor of v_l , with which the sand moves parallel to the blade edge.

In chapter 8 the determination of these three velocities is discussed extensively.

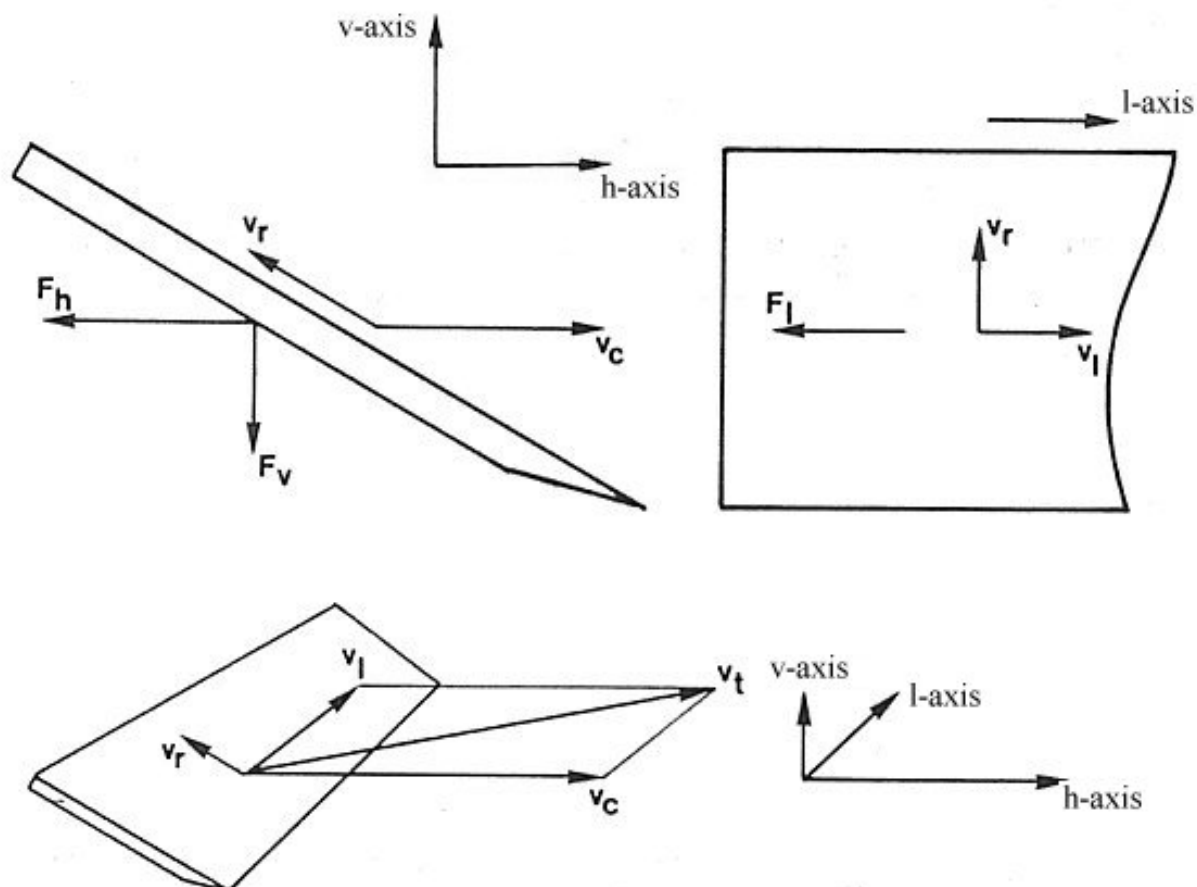


Figure 2.13: The velocity components and force components on the blade.

The velocity components perpendicular and parallel to the blade edge are assumed to be known. The relative velocity between the sand and the blade perpendicular to the blade edge can be determined according:

$$V_r = V_c \cdot \frac{\sin(\beta)}{\sin(\alpha + \beta)} \quad (2.56)$$

For the effective soil/steel angle of friction in the plane perpendicular to the blade edge can now be written:

$$\delta_e = \arctan \left(\frac{V_r}{\sqrt{(V_r^2 + V_1^2 \cdot (1 - f_0)^2)}} \cdot \tan(\delta) \right) \quad (2.57)$$

In chapter 2.7 is discussed, that the shear angle β is dependent on the soil/steel angle of friction δ , which works in the plane perpendicular to the blade edge. However when there is a velocity component parallel to the blade edge, these angles become mutual dependent (equations (2.56) and (2.57)). An iterative solution for β and δ_e has to be found. Because the shear angle β is not very sensitive to changes in the soil/steel angle of friction δ_e a simple iteration, according figure 2.14, is sufficient.

With known α , h_i , h_b , δ , and φ , the friction force between the sand and the blade in the plane perpendicular to the blade edge can be determined with:

$$F_w = F_h \cdot \cos(\alpha) - F_v \cdot \sin(\alpha) \quad (2.58)$$

The friction force parallel to the direction of the blade edge, opposite to the direction of the velocity component parallel to the blade edge, can now be determined with:

$$F_1 = F_w \cdot \frac{V_1 \cdot (1 - f_0)}{V_r} \quad (2.59)$$

In which f_0 represents the factor of the sliding speed that is forced upon the sand as a result of the sliding friction. The resistance of the sand against the acceleration in the sliding direction can be determined with:

$$F_1 = \rho_g \cdot V_c \cdot h_i \cdot b \cdot V_1 \cdot f_0 \quad (2.60)$$

Equating equations (2.59) and (2.60) gives the value for f_0 :

$$f_0 = \frac{F_w}{(F_w + \rho_g \cdot v_c \cdot h_i \cdot b \cdot v_r)} \quad (2.61)$$

Because the inertia forces can be neglected, in the cutting of saturated packed sand, in comparison with the forces as a result of the water pressures, the factor f_0 is approximately 1. This implies that the force in the sliding direction of the blade is also negligible. This force becomes only substantial at very high cutting velocities. With this the components of the cutting force in the three directions (F_h , F_v and F_l) are known.

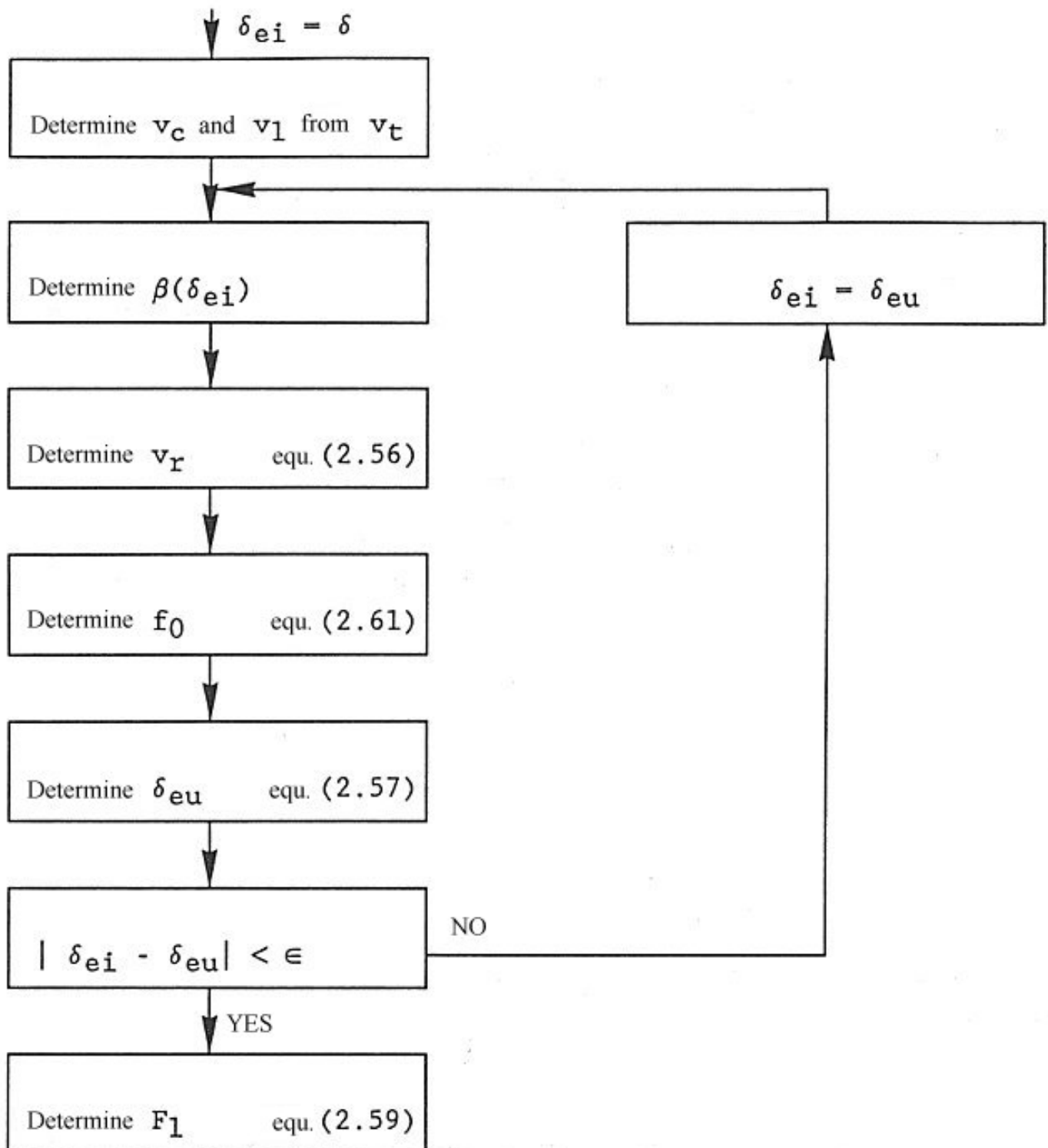


Figure 2.14: The determination of the effective soil/steel friction angle δ_e and the sliding force F_l . Within the iteration an in-going effective angle of soil/steel friction δ_{ei} and an out-going effective angle of soil/steel friction δ_{eu} are used. When these two angles are equal within a certain accuracy ϵ the effective angle of soil/steel friction is determined. With this the sliding force F_l can be determined from equation (2.59).

[Back to top](#)

This is a translation of the dissertation of Dr.ir. S.A. Miedema, dated September 15th 1987 .

The dissertation was originally published in Dutch by the:

Delft University of Technology
Faculty of Mechanical Engineering and Marine Technology
Chair of Dredging Technology
Mekelweg 2
2628 CD, Delft
The Netherlands

It is advised to also read the papers following this dissertation, since the theory developed has been refined and extended.

Last modified Saturday May 27, 2000 by: [Sape A. Miedema](#)

Translation by: [Laurens de Jonge](#)

Figures, equations and tables by: [Erik Miedema](#)

Copyright © May, 2000 Dr.ir. S.A. Miedema



[Download Adobe Acrobat Reader V4.0](#)

2.12 Wear and side effects.

In the previous chapters the blades are assumed to have a reasonable sharp blade tip and a positive clearance angle. A two dimensional cutting process has also been assumed. In dredging practice these circumstances are hardly encountered. It is however difficult to introduce a concept like wear in the theoretical model, because for every wear stage the water pressures have to be determined numerically again.

Also not clear is if the assumption that the sand shears along a straight line will also lead to a good correlation with the model tests with worn blades. Only for the case with a sharp blade and a clearance angle of -1° a model test is performed. This is discussed in chapter 3.9.

It is however possible to introduce the wear effects and the side effects simply in the theory with empirical parameters. To do this the theoretical model is slightly modified. No longer the horizontal and the vertical forces are used, but the total cutting force and its angle with the direction of the velocity component perpendicular to the blade edge. Figure 2.15 shows the dimensionless forces c_1 , c_2 , en c_t for the non-cavitating cutting process and the dimensionless forces d_1 , d_2 en d_t for the cavitating process. For the total cutting force can be written dimensionless:

non-cavitating

$$c_t = \sqrt{(c_1 \cdot c_1 + c_2 \cdot c_2)}$$

cavitating

$$d_t = \sqrt{(d_1 \cdot d_1 + d_2 \cdot d_2)} \quad (2.62)$$

For the angle the force makes with the direction of the velocity component perpendicular to the blade edge:

$$\theta_t = \text{atan} \left(\frac{c_2}{c_1} \right)$$

$$\Theta_t = \text{atan} \left(\frac{d_2}{d_1} \right) \quad (2.63)$$

It is proposed to introduce the wear and side effects according:

$$c_{ts} = c_t \cdot c_s \quad d_{ts} = d_t \cdot c_s \quad (2.64)$$

and

$$\theta_{ts} = \theta_t \cdot \theta_s \quad \Theta_{ts} = \Theta_t \cdot \Theta_s \quad (2.65)$$

For the side effects it yields:

$$c_{tr} = c_t \cdot c_r \quad d_{tr} = d_t \cdot c_r \quad (2.66)$$

and

$$\theta_{tr} = \theta_t \cdot \theta_r \quad \Theta_{tr} = \Theta_t \cdot \Theta_r \quad (2.67)$$

In chapter 4 and 5 it will appear, that in particular the angle of rotation of the total cutting force as a result of wear, has a large influence on the force needed for the haul motion of cutter-suction and cutter-wheel dredgers. Figure 2.16 gives an impression of the expected effects of the wear and the side effects.

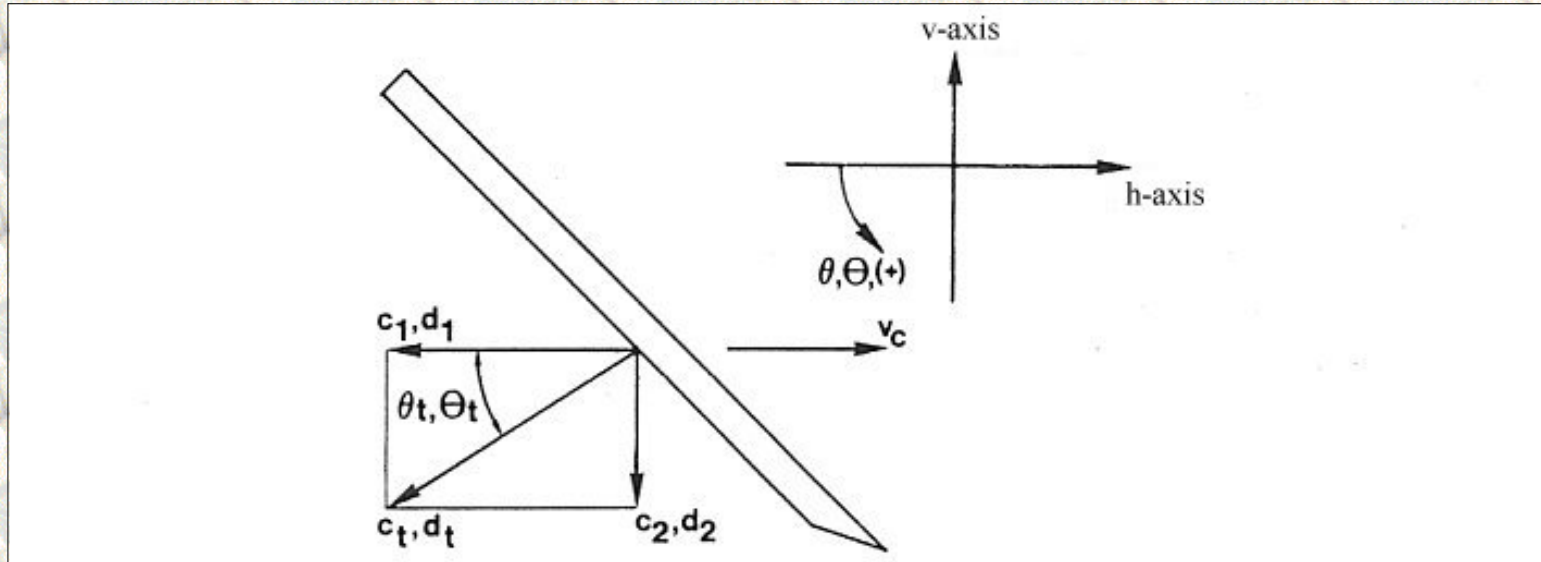


Figure 2.15: The total dimensionless cutting force c_t, d_t and the angle it makes with the velocity direction Θ_t, θ_t , where this angle is directed positive downwards.

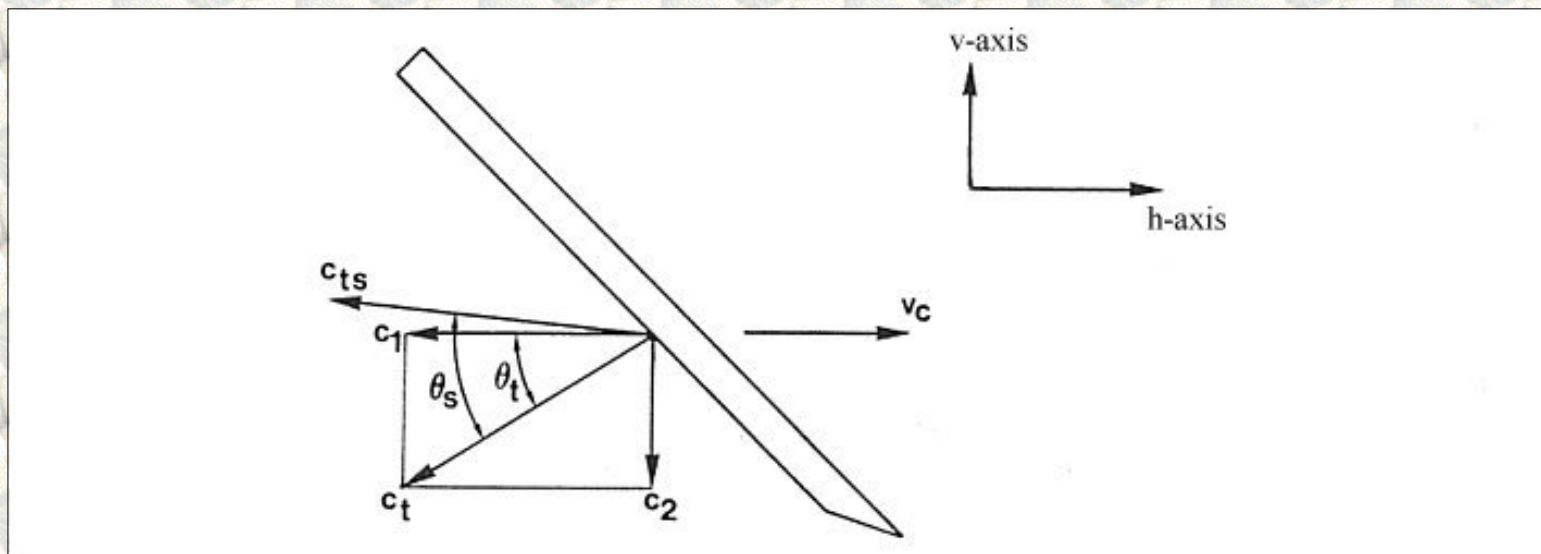


Figure 2.16a: The influence of wear on the magnitude and the direction of the dimensionless force c_t for the non-cavating cutting process.

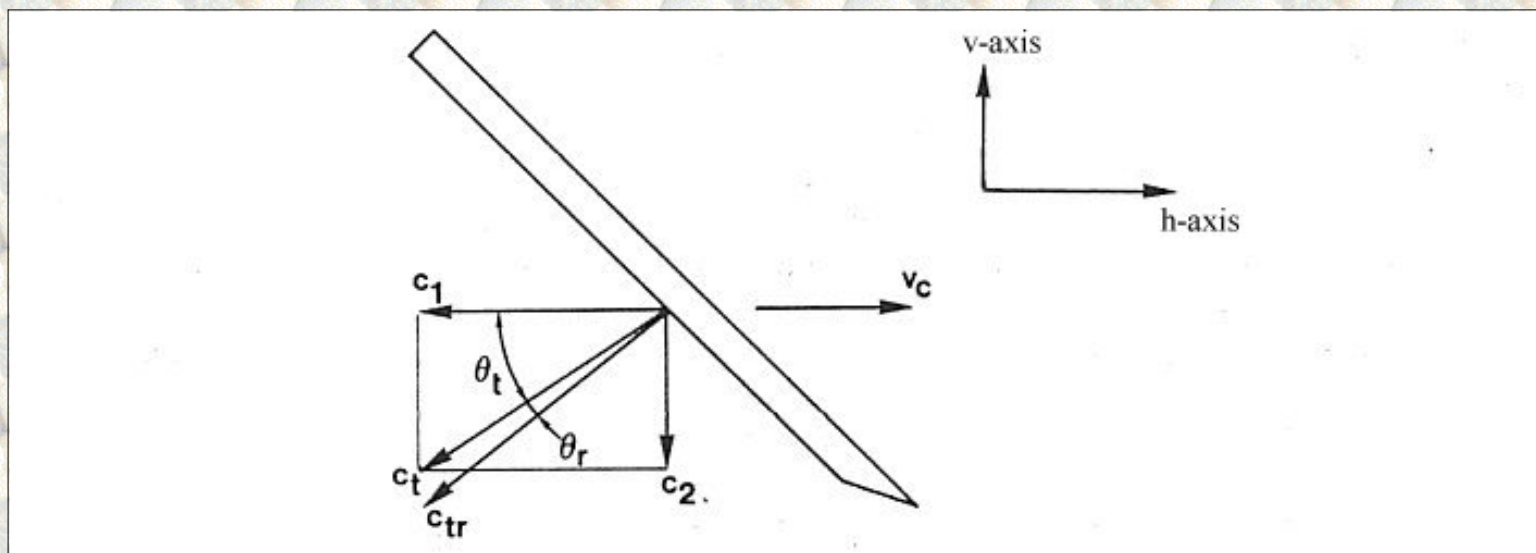


Figure 2.16b: The influence of side effects on the magnitude and the direction of the dimensionless cutting force c_t for the non-cavating cutting process.

[Back to top](#)

This is a translation of the dissertation of Dr.ir. S.A. Miedema, dated September 15th 1987 .
The dissertation was originally published in Dutch by the:
Delft University of Technology
Faculty of Mechanical Engineering and Marine Technology
Chair of Dredging Technology
Mekelweg 2
2628 CD, Delft
The Netherlands

It is advised to also read the papers following this dissertation, since the theory developed has been refined and extended.

Last modified Saturday May 27, 2000 by: [Sape A. Miedema](#)

Translation by: [Laurens de Jonge](#)

Figures, equations and tables by: [Erik Miedema](#)

Copyright © May, 2000 Dr.ir. S.A. Miedema



[Download Adobe Acrobat Reader V4.0](#)

2.13 Specific cutting energy.

In the dredging industry, the specific cutting energy is described as:

The amount of energy, that has to be added to a volume unit of soil (e.g. sand) to excavate the soil.

The dimension of the specific cutting energy is: kN/m².

Adhesion, cohesion, gravity and the inertia forces will be neglected in the determination of the specific cutting energy. For the case as described in chapter 2, cutting with a straight blade with the direction of the cutting velocity perpendicular to the blade (edge of the blade), the specific cutting energy can be written:

$$E = \frac{F_h \cdot v_c}{h_i \cdot b \cdot v_c} = \frac{F_h}{h_i \cdot b} \quad (2.68)$$

The method, with which the shear angle β is determined in chapter 2.7, is therefore equivalent with minimizing the specific cutting energy, for a certain blade geometry and certain soil mechanical parameters. For the specific energy, for the non-cavitating cutting process, can now be derived from equations (2.43) and (2.68), that:

$$E_{gc} = c_1 \cdot \rho_w \cdot g \cdot v_c \cdot h_i \cdot \frac{e}{k_m} \quad (2.69)$$

For the specific energy, for the fully cavitating cutting process, can be written from equations (2.46) and (2.68):

$$E_{ca} = d_1 \cdot \rho_w \cdot g \cdot (z+10) \quad (2.70)$$

From these equations can be derived that the specific cutting energy, for the non-cavitating cutting process is proportional to the cutting velocity, the layer-thickness, the volume strain and inversely proportional to the permeability. For the fully cavitating process the specific cutting energy is only dependent on the water depth.

Therefore it can be posed, that the specific cutting energy, for the fully cavitating cutting process is an upper limit, provided that the inertia forces, etc., can be neglected. At very high cutting velocities, however, the specific cutting energy, also for the cavitating process will increase as a result of the inertia forces and the water resistance.

A change in the specific energy occurs when the forward velocity of the blade is not perpendicular to the blade edge (chapter 2.11). Figure 2.17 shows this situation. For the non-cavitating cutting process the force F_h is not dependent on the sliding velocity, when in equation (2.43) the total velocity of the blade and the projected blade width are substituted by the cutting velocity and the blade width. The direction of this force is perpendicular to the blade edge, so that, when neglecting the sliding force F_l , for the specific cutting energy can be derived:

$$E_{gc} = \frac{F_h \cdot v_c}{h_i \cdot b \cdot v_c} = \frac{F_h \cdot \cos(\iota)}{h_i \cdot b_{pr}} = c_1 \cdot \rho_w \cdot g \cdot v_t \cdot h_i \cdot \frac{e}{k_m} \cdot \cos(\iota) \quad (2.71)$$

In this equation the total velocity of the blade v_t is included, which gives a better impression of the specific cutting energy, although $v_t \cdot \cos(\iota)$ is equal to v_c . The specific cutting energy of the cavitating cutting process does not change under influence of a sliding velocity, so equation (2.70) is still valid. However, cavitation occurs for this case at a higher total velocity, since the velocity important for the cutting process (the perpendicular velocity v_c) is smaller than the total velocity v_t .

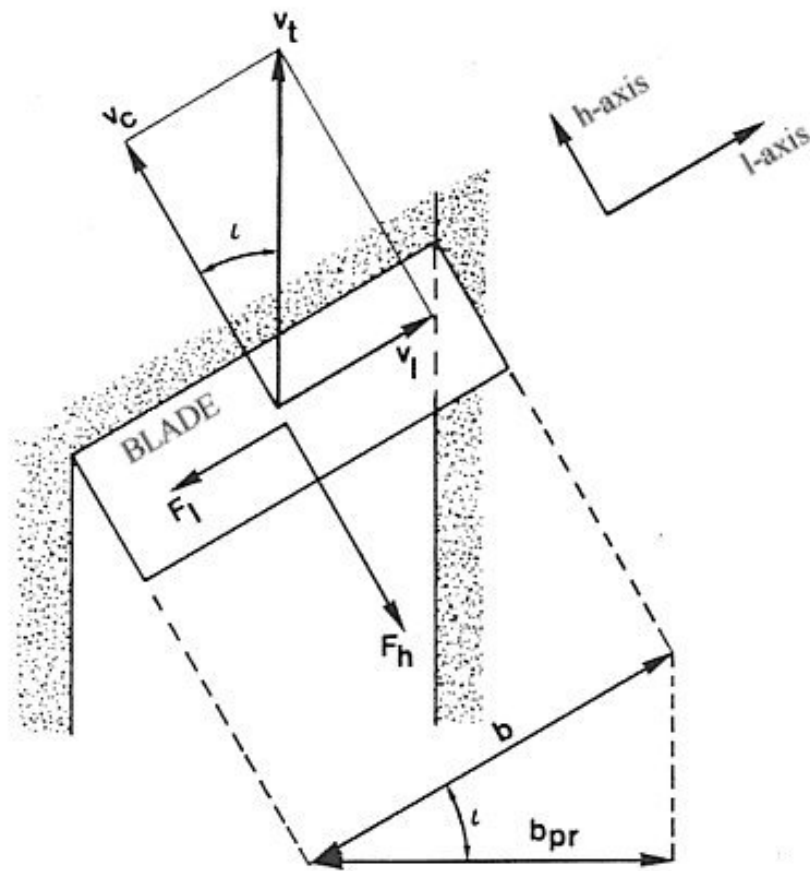


Figure 2.17: The velocity components v_t , v_c and v_l and the force F_h for a transverse component of the total blade velocity.

Also the blade width b and the projected blade width b_{pr} from above.

[Back to top](#)

This is a translation of the dissertation of Dr.ir. S.A. Miedema, dated September 15th 1987 .

The dissertation was originally published in Dutch by the:

Delft University of Technology

Faculty of Mechanical Engineering and Marine Technology

Chair of Dredging Technology

Mekelweg 2

2628 CD, Delft

The Netherlands

It is advised to also read the papers following this dissertation, since the theory developed has been refined and extended.

Last modified Saturday May 27, 2000 by: [Sape A. Miedema](#)

Translation by: [Laurens de Jonge](#)

Figures, equations and tables by: [Erik Miedema](#)

Copyright © May, 2000 Dr.ir. S.A. Miedema



[Download Adobe Acrobat Reader V4.0](#)

Table 2.01: Dimensionless Pore Pressures.Dr.ir. S.A. Miedema

	h_b/h_i	$k_i/k_{\max}=1$			$k_i/k_{\max}=0.25$		
		$\beta = 30^\circ$	37.5°	45°	30°	37.5°	45°
$\alpha = 15^\circ$	1 (s)	0.156	0.168	0.177	0.235	0.262	0.286
	2 (s)	0.157	0.168	0.177	0.236	0.262	0.286
	3 (s)	0.158	0.168	0.177	0.237	0.262	0.286
	1 (b)	0.031	0.033	0.035	0.054	0.059	0.063
	2 (b)	0.016	0.017	0.018	0.028	0.030	0.032
	3 (b)	0.011	0.011	0.012	0.019	0.020	0.021
		$\beta = 25^\circ$	30°	35°	25°	30°	35°
$\alpha = 30^\circ$	1 (s)	0.178	0.186	0.193	0.274	0.291	0.308
	2 (s)	0.179	0.187	0.193	0.276	0.294	0.310
	3 (s)	0.179	0.187	0.193	0.277	0.294	0.310
	1 (b)	0.073	0.076	0.078	0.126	0.133	0.139
	2 (b)	0.049	0.049	0.049	0.084	0.085	0.086
	3 (b)	0.034	0.034	0.033	0.059	0.059	0.059
		$\beta = 20^\circ$	25°	30°	20°	25°	30°
$\alpha = 45^\circ$	1 (s)	0.185	0.193	0.200	0.289	0.306	0.325
	2 (s)	0.190	0.198	0.204	0.304	0.322	0.339
	3 (s)	0.192	0.200	0.205	0.308	0.325	0.340
	1 (b)	0.091	0.097	0.104	0.161	0.174	0.187
	2 (b)	0.081	0.082	0.083	0.146	0.148	0.151
	3 (b)	0.067	0.065	0.063	0.120	0.116	0.114
		$\beta = 15^\circ$	20°	25°	15°	20°	25°
	1 (s)	0.182	0.192	0.200	0.278	0.303	0.324

Table 2.01

$\alpha = 60^\circ$	2 (s)	0.195	0.204	0.211	0.314	0.339	0.359
	3 (s)	0.199	0.208	0.214	0.327	0.350	0.368
	1 (b)	0.091	0.103	0.112	0.158	0.184	0.205
	2 (b)	0.100	0.106	0.109	0.182	0.196	0.204
	3 (b)	0.094	0.095	0.093	0.174	0.176	0.174

Table 2.01: The dimensionless porepressures p_{1m} in the shearzone (s) and p_{2m} on the blade surface (b) as a function of the blade angle α , de shear angle β , the ratio between the blade height h_b and the layer thickness h_i and the ratio between the permeability of the situ sand k_i and the permeability of the sand cut k_{max} , with a wear zone behind the edge of the blade of $0.2 \cdot h_i$.

[Back to top](#)

This is a translation of the dissertation of Dr.ir. S.A. Miedema, dated September 15th 1987 .

The dissertation was originally published in Dutch by the:

Delft University of Technology

Faculty of Mechanical Engineering and Marine Technology

Chair of Dredging Technology

Mekelweg 2

2628 CD, Delft

The Netherlands

It is advised to also read the papers following this dissertation, since the theory developed has been refined and extended.

Last modified Thursday November 16, 2000 by: [Sape A. Miedema](#)

Translation by: [Laurens de Jonge](#)

Figures, equations and tables by: [Erik Miedema](#)

Copyright © November, 2000 Dr.ir. S.A. Miedema



[Download Adobe Acrobat Reader V4.0](#)

Coefficients for the Non-Cavitating Cutting Process in Water Saturated Sand ($h_b/h_i=1$)

[Dr.ir. S.A. Miedema](#)

[Table 2.02: The shear angle \$\beta\$.](#)

[Table 2.14: The coefficient \$c_1\$.](#)

[Table 2.20: The coefficient \$c_2\$.](#)

[Table 2.08: The coefficient \$a_1\$.](#)

[Back to top](#)

Table 2.02: The shear angle β .

$h_b/h_i=1$	ϕ	32°	37°	42°	47°	52°
α	δ					
15°	15°	40.892	40.152	39.169	38.012	36.727
	18°	39.024	38.380	37.483	36.402	35.184
	21°	37.355	36.781	35.947	34.924	33.756
	24°	35.847	35.321	34.534	33.552	32.423
	27°	34.468	33.975	33.220	32.269	31.166
	30°	33.196	32.723	31.989	31.058	29.973
30°	15°	37.967	36.937	35.707	34.334	32.854
	18°	36.187	35.250	34.100	32.795	31.372
	21°	34.564	33.696	32.606	31.353	29.974
	24°	33.072	32.255	31.209	29.994	28.648
	27°	31.690	30.907	29.893	28.705	27.382
	30°	30.401	29.640	28.646	27.476	26.166
45°	15°	33.389	32.254	30.936	29.481	27.919
	18°	31.792	30.726	29.467	28.061	26.539
	21°	30.326	29.310	28.092	26.720	25.224
	24°	28.969	27.984	26.793	25.442	23.963
	27°	27.700	26.733	25.557	24.218	22.745

	30°	26.503	25.543	24.373	23.036	21.562
60°	15°	28.220	26.928	25.482	23.917	22.253
	18°	26.813	25.569	24.160	22.623	20.978
	21°	25.500	24.287	22.901	21.379	19.742
	24°	24.264	23.067	21.692	20.174	18.535
	27°	23.091	21.897	20.522	18.999	17.350
	30°	21.967	20.767	19.382	17.845	16.177

The shear angle β as a function of the blade angle α , the angle of internal friction ϕ , the soil/interface friction angle δ , for the non-cavitating cutting process.

[Back to top](#)

Table 2.14: The coefficient c_1 .

$h_b/h_i=1$	ϕ	32°	37°	42°	47°	52°
α	δ					
15°	15°	0.104	0.118	0.132	0.146	0.162
	18°	0.119	0.134	0.150	0.167	0.186
	21°	0.133	0.150	0.169	0.189	0.210
	24°	0.147	0.167	0.188	0.211	0.236
	27°	0.162	0.184	0.209	0.235	0.264
	30°	0.177	0.202	0.229	0.259	0.292
30°	15°	0.175	0.203	0.234	0.268	0.306
	18°	0.195	0.227	0.261	0.300	0.343
	21°	0.215	0.251	0.290	0.334	0.384
	24°	0.236	0.276	0.320	0.370	0.427
	27°	0.257	0.302	0.352	0.409	0.474
	30°	0.279	0.329	0.385	0.450	0.525
45°	15°	0.254	0.304	0.360	0.425	0.502
	18°	0.279	0.334	0.398	0.472	0.560
	21°	0.305	0.367	0.438	0.523	0.624
	24°	0.332	0.401	0.482	0.578	0.695
	27°	0.360	0.437	0.529	0.639	0.774

	30°	0.390	0.477	0.580	0.706	0.863
60°	15°	0.360	0.445	0.547	0.671	0.826
	18°	0.393	0.488	0.604	0.746	0.928
	21°	0.428	0.535	0.666	0.831	1.045
	24°	0.466	0.587	0.736	0.928	1.180
	27°	0.507	0.643	0.815	1.039	1.341
	30°	0.553	0.707	0.905	1.169	1.534

The dimensionless force c_1 , in the direction of the cutting velocity, as a function of the blade angle α , the angle of internal friction ϕ , the soil/interface friction angle δ , without under pressure behind the blade.

[Back to top](#)

Table 2.20: The coefficient c_2 .

$h_b/h_i=1$	ϕ	32°	37°	42°	47°	52°
α	δ					
15°	15°	0.113	0.137	0.161	0.187	0.215
	18°	0.110	0.134	0.159	0.186	0.215
	21°	0.106	0.130	0.156	0.184	0.214
	24°	0.101	0.126	0.152	0.181	0.213
	27°	0.096	0.121	0.148	0.178	0.211
	30°	0.090	0.116	0.143	0.174	0.208
30°	15°	0.117	0.146	0.177	0.211	0.249
	18°	0.110	0.139	0.171	0.206	0.246
	21°	0.103	0.132	0.164	0.200	0.241
	24°	0.094	0.123	0.156	0.193	0.235
	27°	0.084	0.114	0.147	0.184	0.228
	30°	0.074	0.103	0.136	0.174	0.218
45°	15°	0.101	0.130	0.164	0.202	0.247
	18°	0.090	0.119	0.152	0.191	0.237
	21°	0.078	0.106	0.139	0.178	0.224
	24°	0.064	0.092	0.124	0.162	0.208

	27°	0.049	0.075	0.106	0.143	0.188
	30°	0.032	0.056	0.085	0.120	0.164
60°	15°	0.060	0.084	0.112	0.146	0.189
	18°	0.041	0.063	0.088	0.120	0.160
	21°	0.021	0.039	0.061	0.088	0.124
	24°	-0.003	0.011	0.028	0.050	0.078
	27°	-0.030	-0.021	-0.011	0.003	0.021
	30°	-0.061	-0.059	-0.057	-0.055	-0.053

The dimensionless force c_2 , perpendicular to the cutting velocity, as a function of the blade angle α , the angle of internal friction ϕ , the soil/interface friction angle δ , without under pressure behind the blade.

[Back to top](#)

Table 2.08: The coefficient a_1 .

$h_b/h_i=1$	ϕ	32°	37°	42°	47°	52°
α	δ					
15°	15°	0.525	0.520	0.515	0.509	0.503
	18°	0.520	0.516	0.510	0.505	0.498
	21°	0.516	0.511	0.506	0.500	0.494
	24°	0.511	0.507	0.502	0.496	0.490
	27°	0.507	0.503	0.498	0.492	0.485
	30°	0.503	0.498	0.493	0.487	0.481
30°	15°	0.526	0.522	0.517	0.512	0.506
	18°	0.523	0.519	0.514	0.509	0.503
	21°	0.520	0.516	0.511	0.506	0.500
	24°	0.517	0.512	0.508	0.502	0.497
	27°	0.514	0.509	0.504	0.499	0.493
	30°	0.510	0.506	0.501	0.496	0.490
45°	15°	0.534	0.530	0.525	0.520	0.514
	18°	0.531	0.527	0.522	0.517	0.511
	21°	0.528	0.524	0.519	0.514	0.508

	24°	0.525	0.521	0.516	0.511	0.505
	27°	0.523	0.518	0.513	0.508	0.501
	30°	0.520	0.515	0.510	0.504	0.498
60°	15°	0.535	0.528	0.521	0.513	0.505
	18°	0.530	0.524	0.517	0.509	0.500
	21°	0.526	0.519	0.512	0.504	0.494
	24°	0.521	0.515	0.507	0.498	0.489
	27°	0.517	0.510	0.502	0.493	0.483
	30°	0.512	0.505	0.497	0.487	0.477

The weigh factor a_1 , for the determination of the weighed average permeability k_m , as a function of the blade angle α , the angle of internal friction ϕ , the soil/interface friction angle δ , without under pressure behind the blade.

[Back to top](#)

This is a translation of the dissertation of Dr.ir. S.A. Miedema, dated September 15th 1987 .

The dissertation was originally published in Dutch by the:

Delft University of Technology

Faculty of Mechanical Engineering and Marine Technology

Chair of Dredging Technology

Mekelweg 2

2628 CD, Delft

The Netherlands

Last modified Wednesday May 24, 2000 by: [Sape A. Miedema](#)

Translation by: [Laurens de Jonge](#)

Figures, equations and tables by: [Erik Miedema](#)

Copyright © May, 2000 Dr.ir. S.A. Miedema



[Download Adobe Acrobat Reader V4.0](#)

[Back to top](#)**Table 2.02: The shear angle β .**

$h_b/h_i=1$	ϕ	32°	37°	42°	47°	52°
α	δ					
15°	15°	40.892	40.152	39.169	38.012	36.727
	18°	39.024	38.380	37.483	36.402	35.184
	21°	37.355	36.781	35.947	34.924	33.756
	24°	35.847	35.321	34.534	33.552	32.423
	27°	34.468	33.975	33.220	32.269	31.166
	30°	33.196	32.723	31.989	31.058	29.973
30°	15°	37.967	36.937	35.707	34.334	32.854
	18°	36.187	35.250	34.100	32.795	31.372
	21°	34.564	33.696	32.606	31.353	29.974
	24°	33.072	32.255	31.209	29.994	28.648
	27°	31.690	30.907	29.893	28.705	27.382
	30°	30.401	29.640	28.646	27.476	26.166
45°	15°	33.389	32.254	30.936	29.481	27.919
	18°	31.792	30.726	29.467	28.061	26.539
	21°	30.326	29.310	28.092	26.720	25.224
	24°	28.969	27.984	26.793	25.442	23.963
	27°	27.700	26.733	25.557	24.218	22.745
	30°	26.503	25.543	24.373	23.036	21.562
60°	15°	28.220	26.928	25.482	23.917	22.253
	18°	26.813	25.569	24.160	22.623	20.978
	21°	25.500	24.287	22.901	21.379	19.742
	24°	24.264	23.067	21.692	20.174	18.535
	27°	23.091	21.897	20.522	18.999	17.350
	30°	21.967	20.767	19.382	17.845	16.177

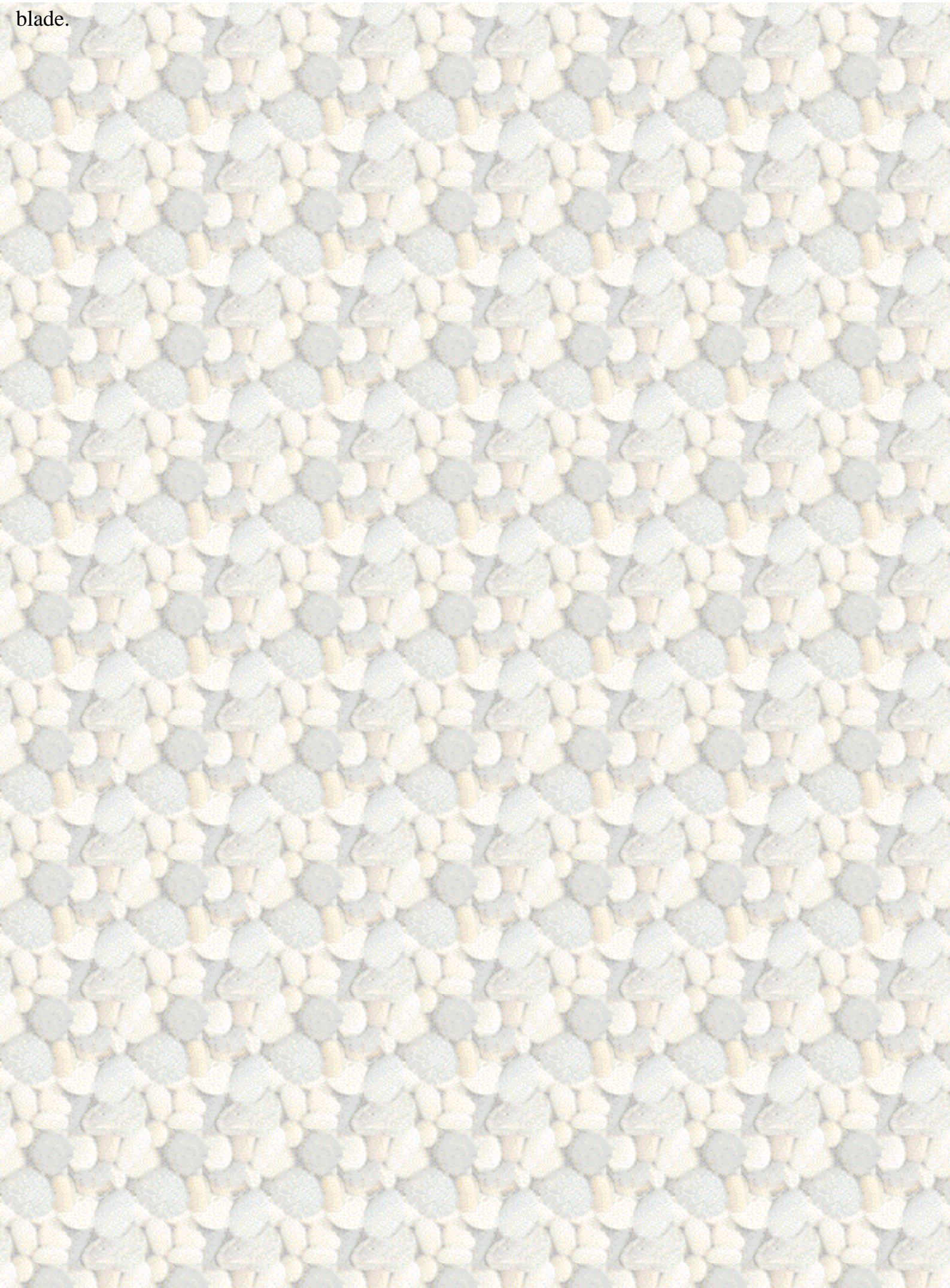
The shear angle β as a function of the blade angle α , the angle of internal friction ϕ , the soil/interface friction angle δ , for the non-cavitating cutting process.

[Back to top](#)**Table 2.14: The coefficient c_1 .**

$h_b/h_i=1$	ϕ	32°	37°	42°	47°	52°
α	δ					
15°	15°	0.104	0.118	0.132	0.146	0.162
	18°	0.119	0.134	0.150	0.167	0.186
	21°	0.133	0.150	0.169	0.189	0.210
	24°	0.147	0.167	0.188	0.211	0.236
	27°	0.162	0.184	0.209	0.235	0.264
	30°	0.177	0.202	0.229	0.259	0.292
30°	15°	0.175	0.203	0.234	0.268	0.306
	18°	0.195	0.227	0.261	0.300	0.343
	21°	0.215	0.251	0.290	0.334	0.384
	24°	0.236	0.276	0.320	0.370	0.427
	27°	0.257	0.302	0.352	0.409	0.474
	30°	0.279	0.329	0.385	0.450	0.525
45°	15°	0.254	0.304	0.360	0.425	0.502
	18°	0.279	0.334	0.398	0.472	0.560
	21°	0.305	0.367	0.438	0.523	0.624
	24°	0.332	0.401	0.482	0.578	0.695
	27°	0.360	0.437	0.529	0.639	0.774
	30°	0.390	0.477	0.580	0.706	0.863
60°	15°	0.360	0.445	0.547	0.671	0.826
	18°	0.393	0.488	0.604	0.746	0.928
	21°	0.428	0.535	0.666	0.831	1.045
	24°	0.466	0.587	0.736	0.928	1.180
	27°	0.507	0.643	0.815	1.039	1.341
	30°	0.553	0.707	0.905	1.169	1.534

The dimensionless force c_1 , in the direction of the cutting velocity, as a function of the blade angle α , the angle of internal friction ϕ , the soil/interface friction angle δ , without under pressure behind the

blade.

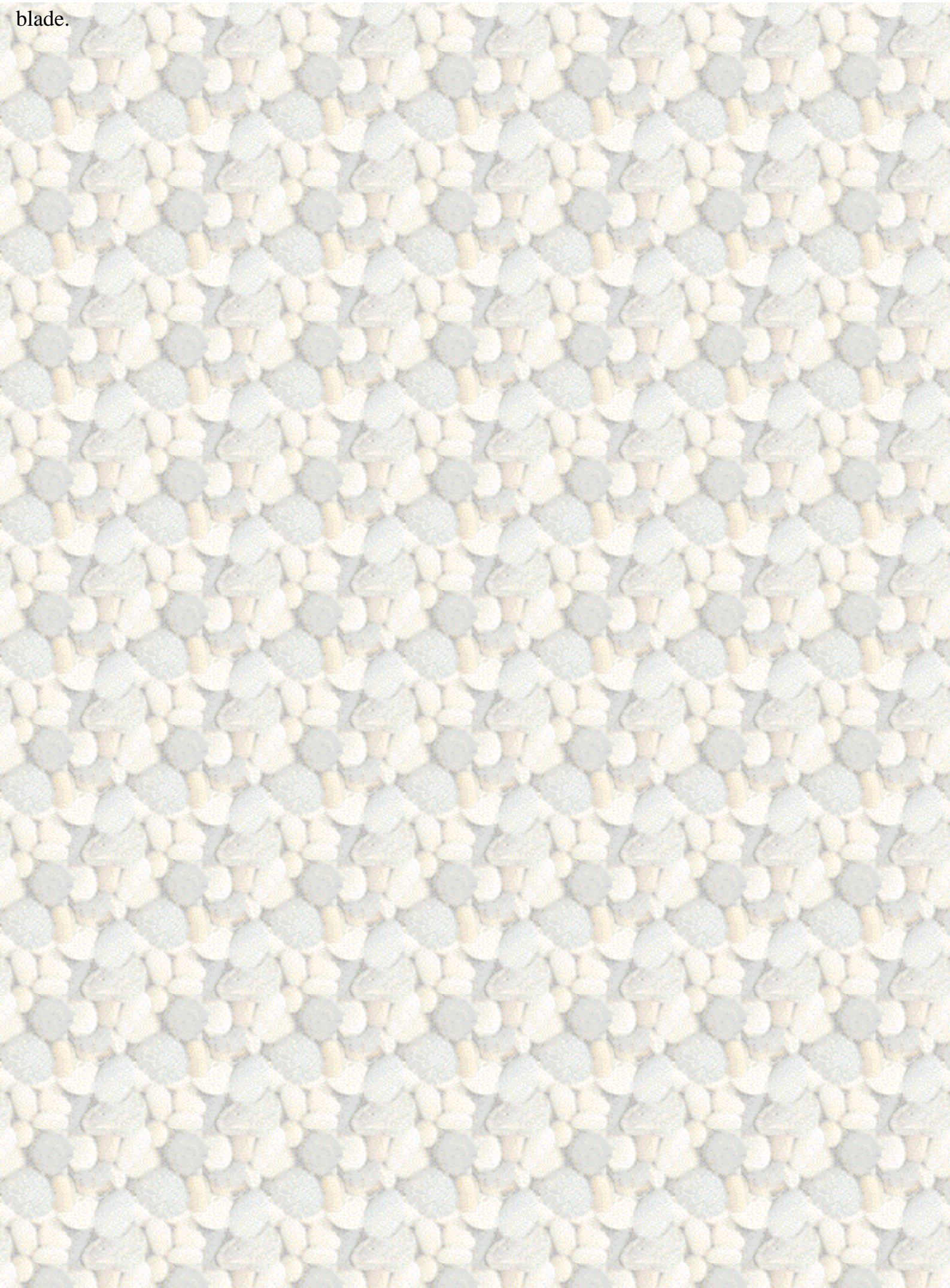


[Back to top](#)**Table 2.20: The coefficient c_2 .**

$h_b/h_i=1$	ϕ	32°	37°	42°	47°	52°
α	δ					
15°	15°	0.113	0.137	0.161	0.187	0.215
	18°	0.110	0.134	0.159	0.186	0.215
	21°	0.106	0.130	0.156	0.184	0.214
	24°	0.101	0.126	0.152	0.181	0.213
	27°	0.096	0.121	0.148	0.178	0.211
	30°	0.090	0.116	0.143	0.174	0.208
30°	15°	0.117	0.146	0.177	0.211	0.249
	18°	0.110	0.139	0.171	0.206	0.246
	21°	0.103	0.132	0.164	0.200	0.241
	24°	0.094	0.123	0.156	0.193	0.235
	27°	0.084	0.114	0.147	0.184	0.228
	30°	0.074	0.103	0.136	0.174	0.218
45°	15°	0.101	0.130	0.164	0.202	0.247
	18°	0.090	0.119	0.152	0.191	0.237
	21°	0.078	0.106	0.139	0.178	0.224
	24°	0.064	0.092	0.124	0.162	0.208
	27°	0.049	0.075	0.106	0.143	0.188
	30°	0.032	0.056	0.085	0.120	0.164
60°	15°	0.060	0.084	0.112	0.146	0.189
	18°	0.041	0.063	0.088	0.120	0.160
	21°	0.021	0.039	0.061	0.088	0.124
	24°	-0.003	0.011	0.028	0.050	0.078
	27°	-0.030	-0.021	-0.011	0.003	0.021
	30°	-0.061	-0.059	-0.057	-0.055	-0.053

The dimensionless force c_2 , perpendicular to the cutting velocity, as a function of the blade angle α , the angle of internal friction ϕ , the soil/interface friction angle δ , without under pressure behind the

blade.



[Back to top](#)**Table 2.08: The coefficient a_1 .**

$h_b/h_i=1$	ϕ	32°	37°	42°	47°	52°
α	δ					
15°	15°	0.525	0.520	0.515	0.509	0.503
	18°	0.520	0.516	0.510	0.505	0.498
	21°	0.516	0.511	0.506	0.500	0.494
	24°	0.511	0.507	0.502	0.496	0.490
	27°	0.507	0.503	0.498	0.492	0.485
	30°	0.503	0.498	0.493	0.487	0.481
30°	15°	0.526	0.522	0.517	0.512	0.506
	18°	0.523	0.519	0.514	0.509	0.503
	21°	0.520	0.516	0.511	0.506	0.500
	24°	0.517	0.512	0.508	0.502	0.497
	27°	0.514	0.509	0.504	0.499	0.493
	30°	0.510	0.506	0.501	0.496	0.490
45°	15°	0.534	0.530	0.525	0.520	0.514
	18°	0.531	0.527	0.522	0.517	0.511
	21°	0.528	0.524	0.519	0.514	0.508
	24°	0.525	0.521	0.516	0.511	0.505
	27°	0.523	0.518	0.513	0.508	0.501
	30°	0.520	0.515	0.510	0.504	0.498
60°	15°	0.535	0.528	0.521	0.513	0.505
	18°	0.530	0.524	0.517	0.509	0.500
	21°	0.526	0.519	0.512	0.504	0.494
	24°	0.521	0.515	0.507	0.498	0.489
	27°	0.517	0.510	0.502	0.493	0.483
	30°	0.512	0.505	0.497	0.487	0.477

The weigh factor a_1 , for the determination of the weighed average permeability k_m , as a function of the blade angle α , the angle of internal friction ϕ , the soil/interface friction angle δ , without under

pressure behind the blade.

Coefficients for the Non-Cavitating Cutting Process in Water Saturated Sand ($h_b/h_i=2$)

[Dr.ir. S.A. Miedema](#)

[Table 2.03: The shear angle \$\beta\$.](#)

[Table 2.15: The coefficient \$c_1\$.](#)

[Table 2.21: The coefficient \$c_2\$.](#)

[Table 2.09: The coefficient \$a_1\$.](#)

[Back to top](#)

Table 2.03: The shear angle β .

$h_b/h_i=2$	ϕ	32°	37°	42°	47°	52°
α	δ					
15°	15°	41.128	40.402	39.427	38.273	36.986
	18°	39.239	38.609	37.720	36.643	35.424
	21°	37.554	36.993	36.167	35.147	33.979
	24°	36.030	35.517	34.738	33.760	32.630
	27°	34.638	34.158	33.410	32.462	31.358
	30°	33.354	32.893	32.167	31.238	30.152
30°	15°	39.129	37.939	36.562	35.056	33.457
	18°	37.223	36.144	34.859	33.429	31.894
	21°	35.458	34.468	33.258	31.891	30.408
	24°	33.820	32.899	31.748	30.432	28.992
	27°	32.293	31.425	30.320	29.043	27.637
	30°	30.864	30.035	28.965	27.718	26.336
45°	15°	33.483	32.334	30.991	29.508	27.918
	18°	31.743	30.679	29.408	27.985	26.444
	21°	30.142	29.141	27.925	26.547	25.043
	24°	28.660	27.704	26.527	25.182	23.705
	27°	27.278	26.353	25.202	23.879	22.420

	30°	25.982	25.074	23.939	22.630	21.179
60°	15°	27.692	26.533	25.186	23.694	22.085
	18°	26.156	25.057	23.759	22.307	20.729
	21°	24.744	23.683	22.418	20.991	19.432
	24°	23.432	22.394	21.147	19.733	18.180
	27°	22.203	21.173	19.932	18.520	16.965
	30°	21.039	20.008	18.763	17.344	15.776

The shear angle β as a function of the blade angle α , the angle of internal friction ϕ , the soil/interface friction angle δ , for the non-cavitating cutting process.

[Back to top](#)

Table 2.15: The coefficient c_1 .

$h_b/h_i=2$	ϕ	32°	37°	42°	47°	52°
α	δ					
15°	15°	0.106	0.119	0.133	0.148	0.163
	18°	0.120	0.135	0.152	0.169	0.187
	21°	0.135	0.152	0.171	0.191	0.213
	24°	0.149	0.169	0.191	0.214	0.239
	27°	0.164	0.187	0.211	0.237	0.267
	30°	0.179	0.205	0.232	0.262	0.296
30°	15°	0.185	0.214	0.246	0.281	0.320
	18°	0.207	0.240	0.276	0.317	0.362
	21°	0.230	0.267	0.308	0.354	0.407
	24°	0.254	0.296	0.342	0.395	0.455
	27°	0.278	0.325	0.378	0.437	0.507
	30°	0.303	0.356	0.415	0.483	0.563
45°	15°	0.282	0.335	0.396	0.466	0.547
	18°	0.313	0.373	0.441	0.521	0.616
	21°	0.345	0.412	0.490	0.582	0.692

	24°	0.379	0.454	0.543	0.648	0.775
	27°	0.414	0.499	0.600	0.721	0.869
	30°	0.452	0.547	0.662	0.801	0.974
60°	15°	0.415	0.509	0.622	0.760	0.932
	18°	0.458	0.565	0.693	0.853	1.056
	21°	0.504	0.625	0.772	0.958	1.197
	24°	0.554	0.690	0.860	1.077	1.362
	27°	0.607	0.762	0.958	1.213	1.556
	30°	0.665	0.843	1.070	1.372	1.787

The dimensionless force c_1 , in the direction of the cutting velocity, as a function of the blade angle α , the angle of internal friction ϕ , the soil/interface friction angle δ , without under pressure behind the blade.

[Back to top](#)

Table 2.21: The coefficient c_2 .

$h_b/h_i=2$	ϕ	32°	37°	42°	47°	52°
α	δ					
15°	15°	0.113	0.136	0.161	0.187	0.215
	18°	0.109	0.133	0.159	0.186	0.216
	21°	0.105	0.130	0.156	0.184	0.215
	24°	0.101	0.126	0.153	0.182	0.214
	27°	0.095	0.121	0.148	0.178	0.212
	30°	0.089	0.115	0.143	0.174	0.209
30°	15°	0.113	0.143	0.174	0.209	0.249
	18°	0.105	0.135	0.168	0.204	0.245
	21°	0.096	0.126	0.160	0.197	0.239
	24°	0.086	0.116	0.150	0.188	0.232
	27°	0.075	0.105	0.139	0.178	0.223
	30°	0.062	0.092	0.127	0.166	0.212
	15°	0.092	0.123	0.158	0.199	0.247
	18°	0.078	0.109	0.144	0.185	0.234

45°	21°	0.062	0.092	0.127	0.168	0.217
	24°	0.044	0.073	0.107	0.148	0.197
	27°	0.023	0.051	0.084	0.124	0.173
	30°	0.001	0.027	0.058	0.096	0.143
60°	15°	0.042	0.068	0.099	0.137	0.184
	18°	0.017	0.040	0.069	0.104	0.148
	21°	-0.012	0.008	0.033	0.063	0.103
	24°	-0.044	-0.029	-0.010	0.015	0.046
	27°	-0.081	-0.071	-0.060	-0.045	-0.025
	30°	-0.123	-0.121	-0.120	-0.118	-0.116

The dimensionless force c_2 , perpendicular to the cutting velocity, as a function of the blade angle α , the angle of internal friction ϕ , the soil/interface friction angle δ , without under pressure behind the blade.

[Back to top](#)

Table 2.09: The coefficient a_1 .

$h_b/h_i=2$	ϕ	32°	37°	42°	47°	52°
α	δ					
15°	15°	0.522	0.518	0.513	0.507	0.501
	18°	0.518	0.514	0.509	0.503	0.497
	21°	0.514	0.510	0.505	0.499	0.493
	24°	0.510	0.506	0.501	0.495	0.489
	27°	0.506	0.502	0.497	0.491	0.485
	30°	0.502	0.498	0.493	0.487	0.481
30°	15°	0.531	0.526	0.521	0.516	0.511
	18°	0.527	0.523	0.518	0.513	0.508
	21°	0.524	0.520	0.515	0.510	0.505
	24°	0.521	0.517	0.512	0.507	0.501
	27°	0.518	0.514	0.509	0.504	0.498
	30°	0.514	0.510	0.506	0.500	0.495
	15°	0.554	0.550	0.546	0.541	0.536

45°	18°	0.552	0.548	0.544	0.539	0.534
	21°	0.550	0.546	0.542	0.537	0.532
	24°	0.548	0.544	0.539	0.535	0.529
	27°	0.546	0.542	0.537	0.532	0.527
	30°	0.544	0.540	0.535	0.530	0.524
60°	15°	0.575	0.569	0.563	0.556	0.549
	18°	0.571	0.566	0.559	0.552	0.545
	21°	0.568	0.562	0.556	0.549	0.541
	24°	0.565	0.559	0.552	0.545	0.536
	27°	0.561	0.555	0.548	0.541	0.532
	30°	0.558	0.552	0.544	0.536	0.527

The weigh factor a_1 , for the determination of the weighed average permeability k_m , as a function of the blade angle α , the angle of internal friction ϕ , the soil/interface friction angle δ , without under pressure behind the blade.

[Back to top](#)

This is a translation of the dissertation of Dr.ir. S.A. Miedema, dated September 15th 1987 .

The dissertation was originally published in Dutch by the:

Delft University of Technology

Faculty of Mechanical Engineering and Marine Technology

Chair of Dredging Technology

Mekelweg 2

2628 CD, Delft

The Netherlands

Last modified Wednesday May 24, 2000 by: [Sape A. Miedema](#)

Translation by: [Laurens de Jonge](#)

Figures, equations and tables by: [Erik Miedema](#)

Copyright © May, 2000 Dr.ir. S.A. Miedema



[Download Adobe Acrobat Reader V4.0](#)

[Back to top](#)**Table 2.03: The shear angle β .**

$h_b/h_i=2$	ϕ	32°	37°	42°	47°	52°
α	δ					
15°	15°	41.128	40.402	39.427	38.273	36.986
	18°	39.239	38.609	37.720	36.643	35.424
	21°	37.554	36.993	36.167	35.147	33.979
	24°	36.030	35.517	34.738	33.760	32.630
	27°	34.638	34.158	33.410	32.462	31.358
	30°	33.354	32.893	32.167	31.238	30.152
30°	15°	39.129	37.939	36.562	35.056	33.457
	18°	37.223	36.144	34.859	33.429	31.894
	21°	35.458	34.468	33.258	31.891	30.408
	24°	33.820	32.899	31.748	30.432	28.992
	27°	32.293	31.425	30.320	29.043	27.637
	30°	30.864	30.035	28.965	27.718	26.336
45°	15°	33.483	32.334	30.991	29.508	27.918
	18°	31.743	30.679	29.408	27.985	26.444
	21°	30.142	29.141	27.925	26.547	25.043
	24°	28.660	27.704	26.527	25.182	23.705
	27°	27.278	26.353	25.202	23.879	22.420
	30°	25.982	25.074	23.939	22.630	21.179
60°	15°	27.692	26.533	25.186	23.694	22.085
	18°	26.156	25.057	23.759	22.307	20.729
	21°	24.744	23.683	22.418	20.991	19.432
	24°	23.432	22.394	21.147	19.733	18.180
	27°	22.203	21.173	19.932	18.520	16.965
	30°	21.039	20.008	18.763	17.344	15.776

The shear angle β as a function of the blade angle α , the angle of internal

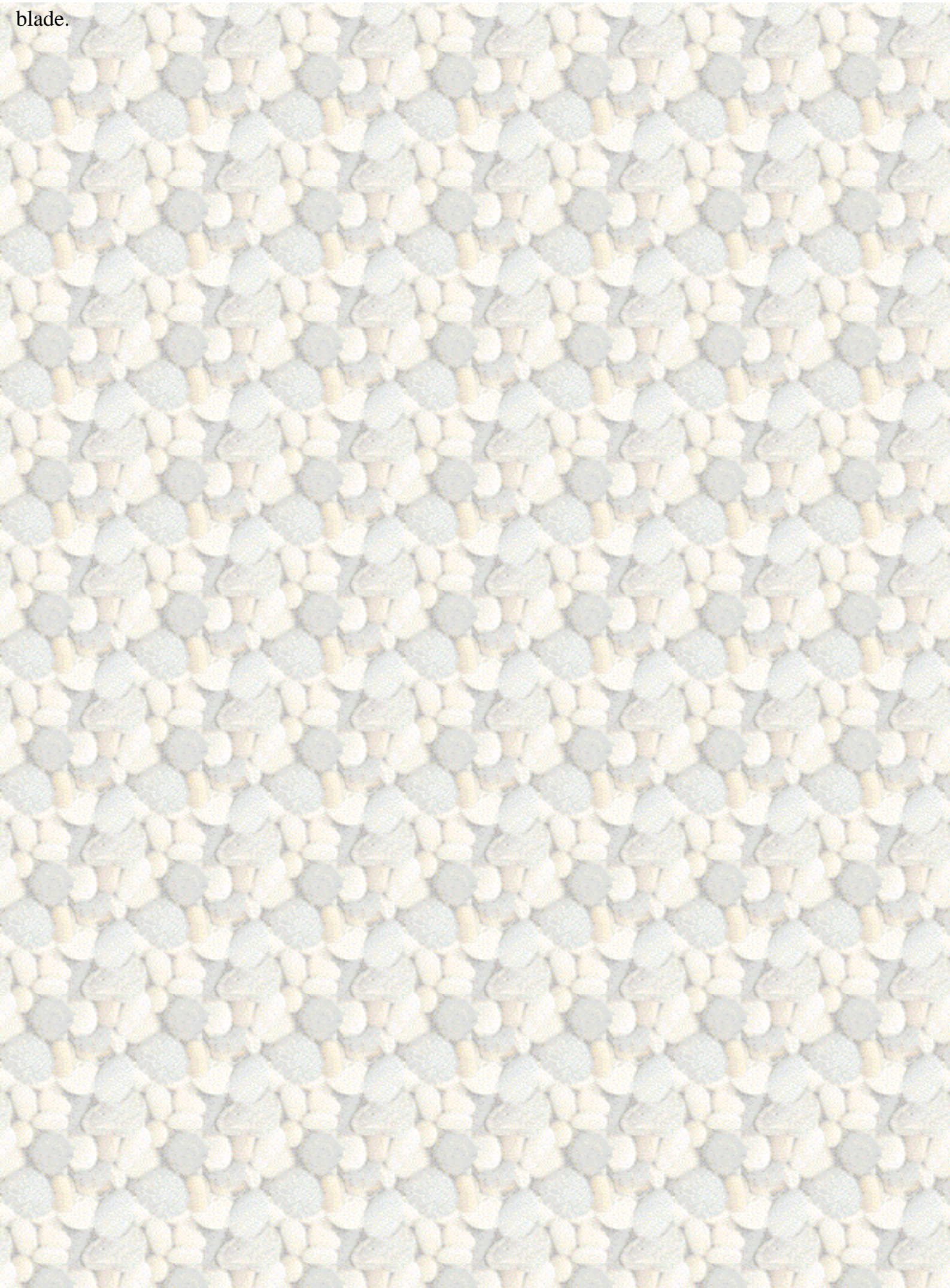
friction ϕ , the soil/interface friction angle δ , for the non-cavitating cutting process.

[Back to top](#)**Table 2.15: The coefficient c_1 .**

$h_b/h_i=2$	ϕ	32°	37°	42°	47°	52°
α	δ					
15°	15°	0.106	0.119	0.133	0.148	0.163
	18°	0.120	0.135	0.152	0.169	0.187
	21°	0.135	0.152	0.171	0.191	0.213
	24°	0.149	0.169	0.191	0.214	0.239
	27°	0.164	0.187	0.211	0.237	0.267
	30°	0.179	0.205	0.232	0.262	0.296
30°	15°	0.185	0.214	0.246	0.281	0.320
	18°	0.207	0.240	0.276	0.317	0.362
	21°	0.230	0.267	0.308	0.354	0.407
	24°	0.254	0.296	0.342	0.395	0.455
	27°	0.278	0.325	0.378	0.437	0.507
	30°	0.303	0.356	0.415	0.483	0.563
45°	15°	0.282	0.335	0.396	0.466	0.547
	18°	0.313	0.373	0.441	0.521	0.616
	21°	0.345	0.412	0.490	0.582	0.692
	24°	0.379	0.454	0.543	0.648	0.775
	27°	0.414	0.499	0.600	0.721	0.869
	30°	0.452	0.547	0.662	0.801	0.974
60°	15°	0.415	0.509	0.622	0.760	0.932
	18°	0.458	0.565	0.693	0.853	1.056
	21°	0.504	0.625	0.772	0.958	1.197
	24°	0.554	0.690	0.860	1.077	1.362
	27°	0.607	0.762	0.958	1.213	1.556
	30°	0.665	0.843	1.070	1.372	1.787

The dimensionless force c_1 , in the direction of the cutting velocity, as a function of the blade angle α , the angle of internal friction ϕ , the soil/interface friction angle δ , without under pressure behind the

blade.

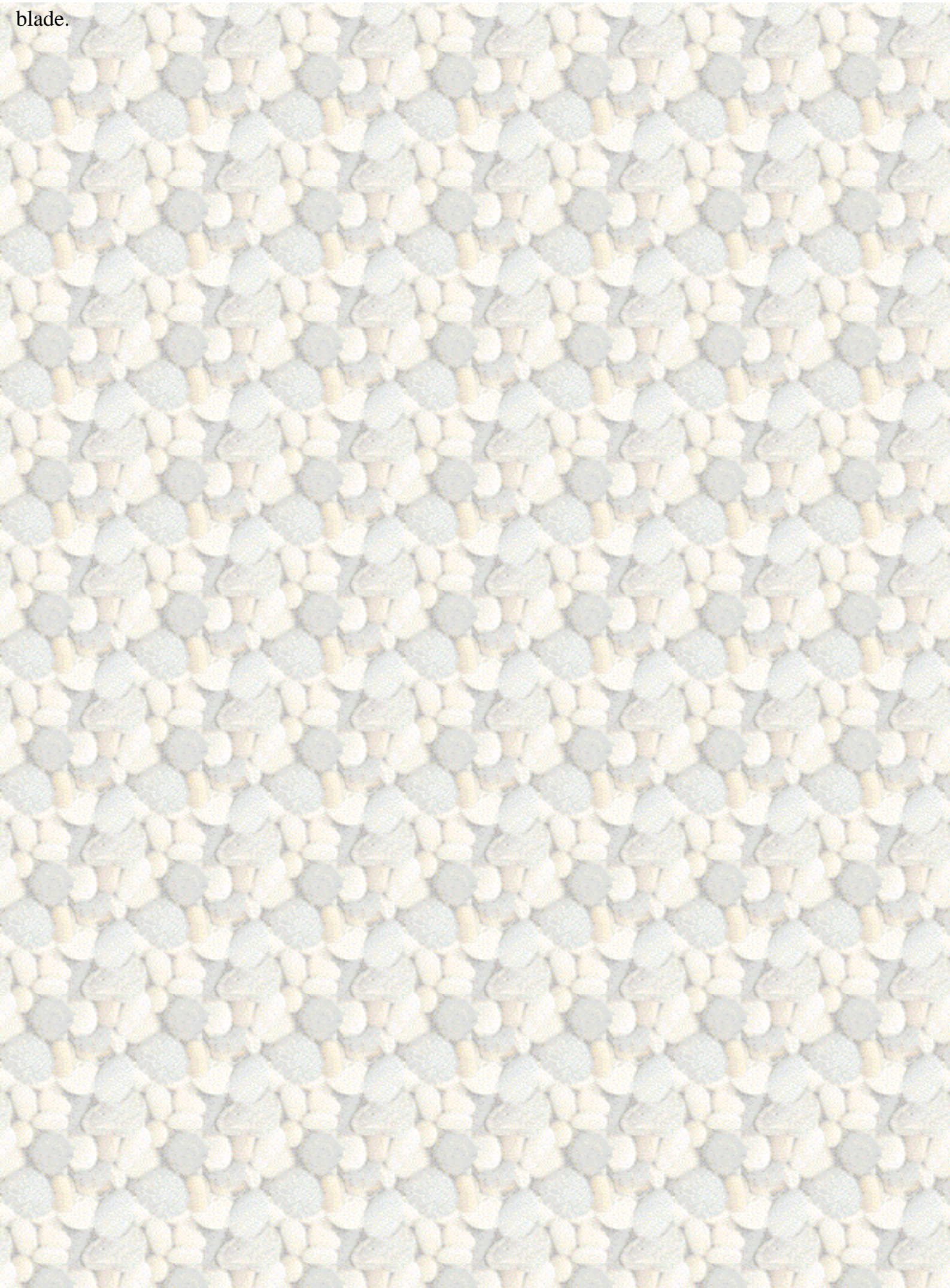


[Back to top](#)**Table 2.21: The coefficient c_2 .**

$h_b/h_i=2$	ϕ	32°	37°	42°	47°	52°
α	δ					
15°	15°	0.113	0.136	0.161	0.187	0.215
	18°	0.109	0.133	0.159	0.186	0.216
	21°	0.105	0.130	0.156	0.184	0.215
	24°	0.101	0.126	0.153	0.182	0.214
	27°	0.095	0.121	0.148	0.178	0.212
	30°	0.089	0.115	0.143	0.174	0.209
30°	15°	0.113	0.143	0.174	0.209	0.249
	18°	0.105	0.135	0.168	0.204	0.245
	21°	0.096	0.126	0.160	0.197	0.239
	24°	0.086	0.116	0.150	0.188	0.232
	27°	0.075	0.105	0.139	0.178	0.223
	30°	0.062	0.092	0.127	0.166	0.212
45°	15°	0.092	0.123	0.158	0.199	0.247
	18°	0.078	0.109	0.144	0.185	0.234
	21°	0.062	0.092	0.127	0.168	0.217
	24°	0.044	0.073	0.107	0.148	0.197
	27°	0.023	0.051	0.084	0.124	0.173
	30°	0.001	0.027	0.058	0.096	0.143
60°	15°	0.042	0.068	0.099	0.137	0.184
	18°	0.017	0.040	0.069	0.104	0.148
	21°	-0.012	0.008	0.033	0.063	0.103
	24°	-0.044	-0.029	-0.010	0.015	0.046
	27°	-0.081	-0.071	-0.060	-0.045	-0.025
	30°	-0.123	-0.121	-0.120	-0.118	-0.116

The dimensionless force c_2 , perpendicular to the cutting velocity, as a function of the blade angle α , the angle of internal friction ϕ , the soil/interface friction angle δ , without under pressure behind the

blade.



[Back to top](#)**Table 2.09: The coefficient a_1 .**

$h_b/h_i=2$	ϕ	32°	37°	42°	47°	52°
α	δ					
15°	15°	0.522	0.518	0.513	0.507	0.501
	18°	0.518	0.514	0.509	0.503	0.497
	21°	0.514	0.510	0.505	0.499	0.493
	24°	0.510	0.506	0.501	0.495	0.489
	27°	0.506	0.502	0.497	0.491	0.485
	30°	0.502	0.498	0.493	0.487	0.481
30°	15°	0.531	0.526	0.521	0.516	0.511
	18°	0.527	0.523	0.518	0.513	0.508
	21°	0.524	0.520	0.515	0.510	0.505
	24°	0.521	0.517	0.512	0.507	0.501
	27°	0.518	0.514	0.509	0.504	0.498
	30°	0.514	0.510	0.506	0.500	0.495
45°	15°	0.554	0.550	0.546	0.541	0.536
	18°	0.552	0.548	0.544	0.539	0.534
	21°	0.550	0.546	0.542	0.537	0.532
	24°	0.548	0.544	0.539	0.535	0.529
	27°	0.546	0.542	0.537	0.532	0.527
	30°	0.544	0.540	0.535	0.530	0.524
60°	15°	0.575	0.569	0.563	0.556	0.549
	18°	0.571	0.566	0.559	0.552	0.545
	21°	0.568	0.562	0.556	0.549	0.541
	24°	0.565	0.559	0.552	0.545	0.536
	27°	0.561	0.555	0.548	0.541	0.532
	30°	0.558	0.552	0.544	0.536	0.527

The weigh factor a_1 , for the determination of the weighed average permeability k_m , as a function of the blade angle α , the angle of internal friction ϕ , the soil/interface friction angle δ , without under

pressure behind the blade.

Coefficients for the Non-Cavitating Cutting Process in Water Saturated Sand ($h_b/h_i=3$)

[Dr.ir. S.A. Miedema](#)

[Table 2.04: The shear angle \$\beta\$.](#)

[Table 2.16: The coefficient \$c_1\$.](#)

[Table 2.22: The coefficient \$c_2\$.](#)

[Table 2.10: The coefficient \$a_1\$.](#)

[Back to top](#)

Table 2.04: The shear angle β .

$h_b/h_i=3$	ϕ	32°	37°	42°	47°	52°
α	δ					
15°	15°	42.346	41.502	40.418	39.164	37.786
	18°	40.414	39.674	38.681	37.507	36.198
	21°	38.673	38.010	37.086	35.973	34.718
	24°	37.087	36.481	35.609	34.542	33.328
	27°	35.631	35.064	34.230	33.197	32.013
	30°	34.283	33.742	32.934	31.926	30.763
30°	15°	40.176	38.793	37.257	35.619	33.909
	18°	38.242	36.978	35.537	33.977	32.331
	21°	36.421	35.258	33.900	32.407	30.817
	24°	34.711	33.631	32.341	30.906	29.364
	27°	33.103	32.090	30.858	29.470	27.968
	30°	31.590	30.631	29.444	28.095	26.625
45°	15°	35.406	33.895	32.248	30.509	28.703
	18°	33.548	32.142	30.578	28.907	27.156
	21°	31.788	30.472	28.981	27.368	25.665
	24°	30.126	28.885	27.455	25.891	24.230
	27°	28.557	27.376	25.996	24.474	22.845

	30°	27.075	25.941	24.600	23.111	21.509
60°	15°	28.252	26.972	25.516	23.930	22.241
	18°	26.613	25.406	24.010	22.472	20.823
	21°	25.094	23.940	22.588	21.086	19.464
	24°	23.677	22.560	21.238	19.760	18.156
	27°	22.348	21.253	19.950	18.485	16.890
	30°	21.092	20.008	18.713	17.254	15.600

The shear angle β as a function of the blade angle α , the angle of internal friction ϕ , the soil/interface friction angle δ , for the non-cavitating cutting process.

[Back to top](#)

Table 2.16: The coefficient c_1 .

$h_b/h_i=3$	ϕ	32°	37°	42°	47°	52°
α	δ					
15°	15°	0.105	0.119	0.133	0.148	0.164
	18°	0.120	0.135	0.152	0.169	0.188
	21°	0.135	0.152	0.171	0.192	0.214
	24°	0.150	0.170	0.191	0.215	0.240
	27°	0.165	0.188	0.212	0.239	0.268
	30°	0.180	0.206	0.234	0.264	0.298
30°	15°	0.185	0.215	0.247	0.282	0.322
	18°	0.208	0.241	0.278	0.318	0.364
	21°	0.232	0.269	0.310	0.357	0.410
	24°	0.256	0.298	0.345	0.398	0.459
	27°	0.280	0.328	0.381	0.441	0.511
	30°	0.306	0.359	0.419	0.488	0.569
45°	15°	0.290	0.345	0.408	0.480	0.565
	18°	0.324	0.386	0.457	0.541	0.640
	21°	0.359	0.429	0.511	0.607	0.722
	24°	0.396	0.476	0.568	0.679	0.813
	27°	0.436	0.525	0.631	0.758	0.914

	30°	0.478	0.579	0.699	0.846	1.029
60°	15°	0.439	0.538	0.657	0.802	0.983
	18°	0.489	0.601	0.737	0.906	1.120
	21°	0.542	0.670	0.826	1.024	1.278
	24°	0.599	0.744	0.926	1.157	1.461
	27°	0.660	0.827	1.037	1.310	1.676
	30°	0.728	0.918	1.163	1.487	1.933

The dimensionless force c_1 , in the direction of the cutting velocity, as a function of the blade angle α , the angle of internal friction ϕ , the soil/interface friction angle δ , without under pressure behind the blade.

[Back to top](#)

Table 2.22: The coefficient c_2 .

$h_b/h_i=3$	ϕ	32°	37°	42°	47°	52°
α	δ					
15°	15°	0.113	0.137	0.161	0.188	0.216
	18°	0.110	0.134	0.159	0.187	0.216
	21°	0.105	0.130	0.156	0.185	0.216
	24°	0.101	0.126	0.153	0.182	0.214
	27°	0.096	0.121	0.149	0.179	0.212
	30°	0.090	0.116	0.144	0.175	0.210
30°	15°	0.113	0.142	0.174	0.209	0.248
	18°	0.105	0.135	0.167	0.204	0.244
	21°	0.096	0.126	0.159	0.196	0.239
	24°	0.085	0.116	0.149	0.188	0.231
	27°	0.074	0.104	0.138	0.177	0.222
	30°	0.061	0.091	0.125	0.165	0.211
45°	15°	0.089	0.121	0.156	0.197	0.246
	18°	0.073	0.105	0.140	0.182	0.232
	21°	0.056	0.086	0.122	0.163	0.214
	24°	0.035	0.065	0.100	0.141	0.192

	27°	0.012	0.041	0.074	0.115	0.164
	30°	-0.013	0.013	0.045	0.083	0.131
60°	15°	0.032	0.058	0.090	0.129	0.177
	18°	0.002	0.026	0.055	0.091	0.136
	21°	-0.031	-0.011	0.014	0.045	0.085
	24°	-0.069	-0.054	-0.035	-0.011	0.021
	27°	-0.112	-0.104	-0.093	-0.079	-0.059
	30°	-0.162	-0.162	-0.162	-0.162	-0.162

The dimensionless force c_2 , perpendicular to the cutting velocity, as a function of the blade angle α , the angle of internal friction ϕ , the soil/interface friction angle δ , without under pressure behind the blade.

[Back to top](#)

Table 2.10: The coefficient a_1 .

$h_b/h_i=3$	ϕ	32°	37°	42°	47°	52°
α	δ					
15°	15°	0.522	0.517	0.512	0.507	0.501
	18°	0.518	0.513	0.508	0.503	0.497
	21°	0.514	0.509	0.504	0.499	0.493
	24°	0.510	0.505	0.500	0.495	0.489
	27°	0.506	0.501	0.497	0.491	0.485
	30°	0.502	0.498	0.493	0.487	0.480
30°	15°	0.534	0.529	0.524	0.519	0.514
	18°	0.531	0.526	0.521	0.516	0.511
	21°	0.528	0.523	0.519	0.513	0.508
	24°	0.525	0.520	0.516	0.511	0.505
	27°	0.522	0.517	0.513	0.508	0.502
	30°	0.519	0.514	0.510	0.504	0.499
45°	15°	0.552	0.548	0.544	0.540	0.536
	18°	0.550	0.547	0.543	0.539	0.534
	21°	0.549	0.545	0.541	0.537	0.532

	24°	0.547	0.543	0.539	0.535	0.531
	27°	0.545	0.542	0.538	0.533	0.529
	30°	0.544	0.540	0.536	0.531	0.527
60°	15°	0.580	0.575	0.570	0.565	0.559
	18°	0.578	0.573	0.568	0.563	0.557
	21°	0.576	0.571	0.566	0.560	0.554
	24°	0.573	0.569	0.564	0.558	0.551
	27°	0.571	0.566	0.561	0.555	0.548
	30°	0.569	0.564	0.558	0.552	0.545

The weigh factor a_1 , for the determination of the weighed average permeability k_m , as a function of the blade angle α , the angle of internal friction ϕ , the soil/interface friction angle δ , without under pressure behind the blade.

[Back to top](#)

This is a translation of the dissertation of Dr.ir. S.A. Miedema, dated September 15th 1987 .

The dissertation was originally published in Dutch by the:

Delft University of Technology

Faculty of Mechanical Engineering and Marine Technology

Chair of Dredging Technology

Mekelweg 2

2628 CD, Delft

The Netherlands

Last modified Wednesday May 24, 2000 by: [Sape A. Miedema](#)

Translation by: [Laurens de Jonge](#)

Figures, equations and tables by: [Erik Miedema](#)

Copyright © May, 2000 Dr.ir. S.A. Miedema



[Download Adobe Acrobat Reader V4.0](#)

[Back to top](#)**Table 2.04: The shear angle β .**

$h_b/h_i=3$	ϕ	32°	37°	42°	47°	52°
α	δ					
15°	15°	42.346	41.502	40.418	39.164	37.786
	18°	40.414	39.674	38.681	37.507	36.198
	21°	38.673	38.010	37.086	35.973	34.718
	24°	37.087	36.481	35.609	34.542	33.328
	27°	35.631	35.064	34.230	33.197	32.013
	30°	34.283	33.742	32.934	31.926	30.763
30°	15°	40.176	38.793	37.257	35.619	33.909
	18°	38.242	36.978	35.537	33.977	32.331
	21°	36.421	35.258	33.900	32.407	30.817
	24°	34.711	33.631	32.341	30.906	29.364
	27°	33.103	32.090	30.858	29.470	27.968
	30°	31.590	30.631	29.444	28.095	26.625
45°	15°	35.406	33.895	32.248	30.509	28.703
	18°	33.548	32.142	30.578	28.907	27.156
	21°	31.788	30.472	28.981	27.368	25.665
	24°	30.126	28.885	27.455	25.891	24.230
	27°	28.557	27.376	25.996	24.474	22.845
	30°	27.075	25.941	24.600	23.111	21.509
60°	15°	28.252	26.972	25.516	23.930	22.241
	18°	26.613	25.406	24.010	22.472	20.823
	21°	25.094	23.940	22.588	21.086	19.464
	24°	23.677	22.560	21.238	19.760	18.156
	27°	22.348	21.253	19.950	18.485	16.890
	30°	21.092	20.008	18.713	17.254	15.600

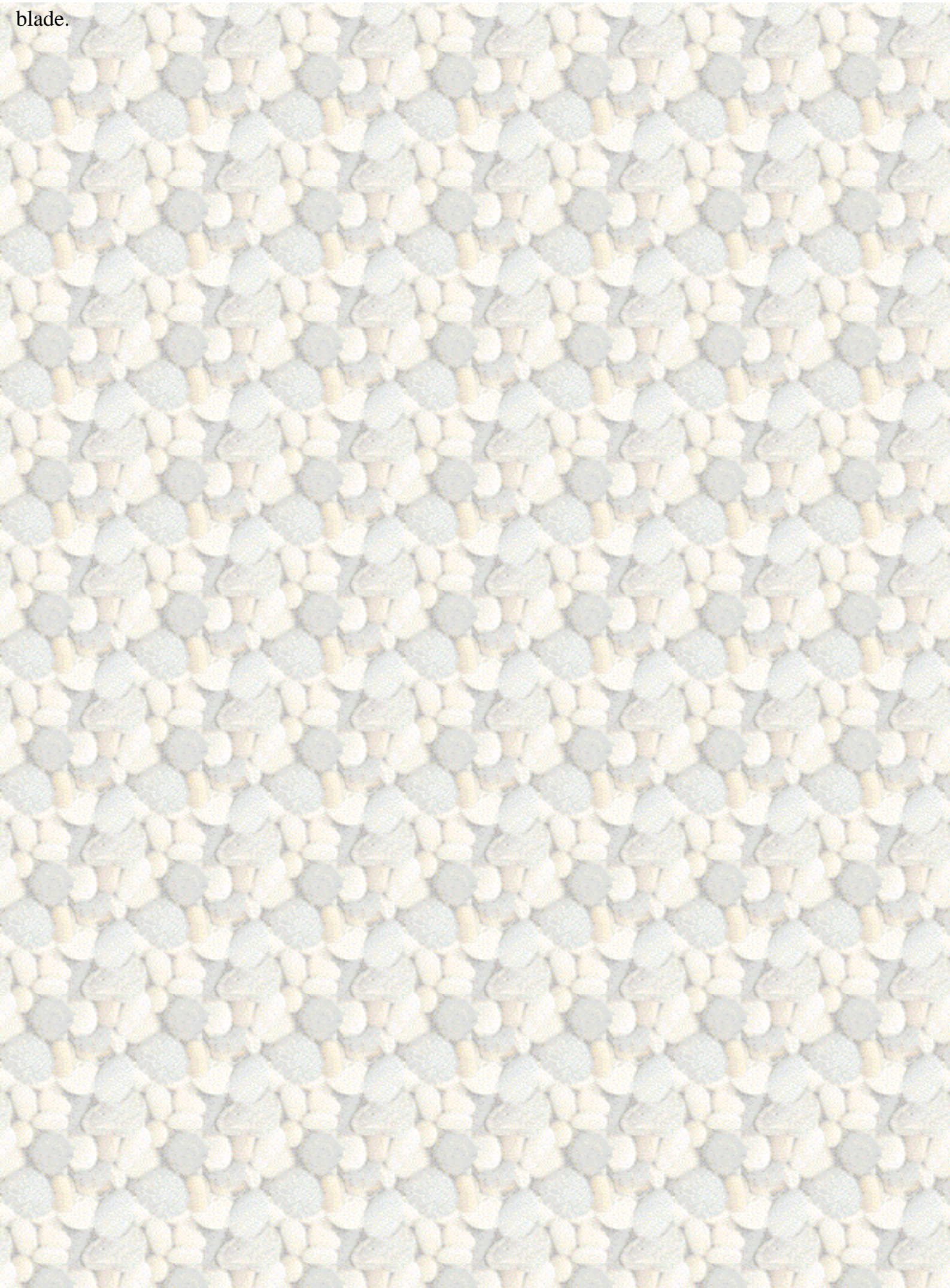
The shear angle β as a function of the blade angle α , the angle of internal friction ϕ , the soil/interface friction angle δ , for the non-cavitating cutting process.

[Back to top](#)**Table 2.16: The coefficient c_1 .**

$h_b/h_i=3$	ϕ	32°	37°	42°	47°	52°
α	δ					
15°	15°	0.105	0.119	0.133	0.148	0.164
	18°	0.120	0.135	0.152	0.169	0.188
	21°	0.135	0.152	0.171	0.192	0.214
	24°	0.150	0.170	0.191	0.215	0.240
	27°	0.165	0.188	0.212	0.239	0.268
	30°	0.180	0.206	0.234	0.264	0.298
30°	15°	0.185	0.215	0.247	0.282	0.322
	18°	0.208	0.241	0.278	0.318	0.364
	21°	0.232	0.269	0.310	0.357	0.410
	24°	0.256	0.298	0.345	0.398	0.459
	27°	0.280	0.328	0.381	0.441	0.511
	30°	0.306	0.359	0.419	0.488	0.569
45°	15°	0.290	0.345	0.408	0.480	0.565
	18°	0.324	0.386	0.457	0.541	0.640
	21°	0.359	0.429	0.511	0.607	0.722
	24°	0.396	0.476	0.568	0.679	0.813
	27°	0.436	0.525	0.631	0.758	0.914
	30°	0.478	0.579	0.699	0.846	1.029
60°	15°	0.439	0.538	0.657	0.802	0.983
	18°	0.489	0.601	0.737	0.906	1.120
	21°	0.542	0.670	0.826	1.024	1.278
	24°	0.599	0.744	0.926	1.157	1.461
	27°	0.660	0.827	1.037	1.310	1.676
	30°	0.728	0.918	1.163	1.487	1.933

The dimensionless force c_1 , in the direction of the cutting velocity, as a function of the blade angle α , the angle of internal friction ϕ , the soil/interface friction angle δ , without under pressure behind the

blade.

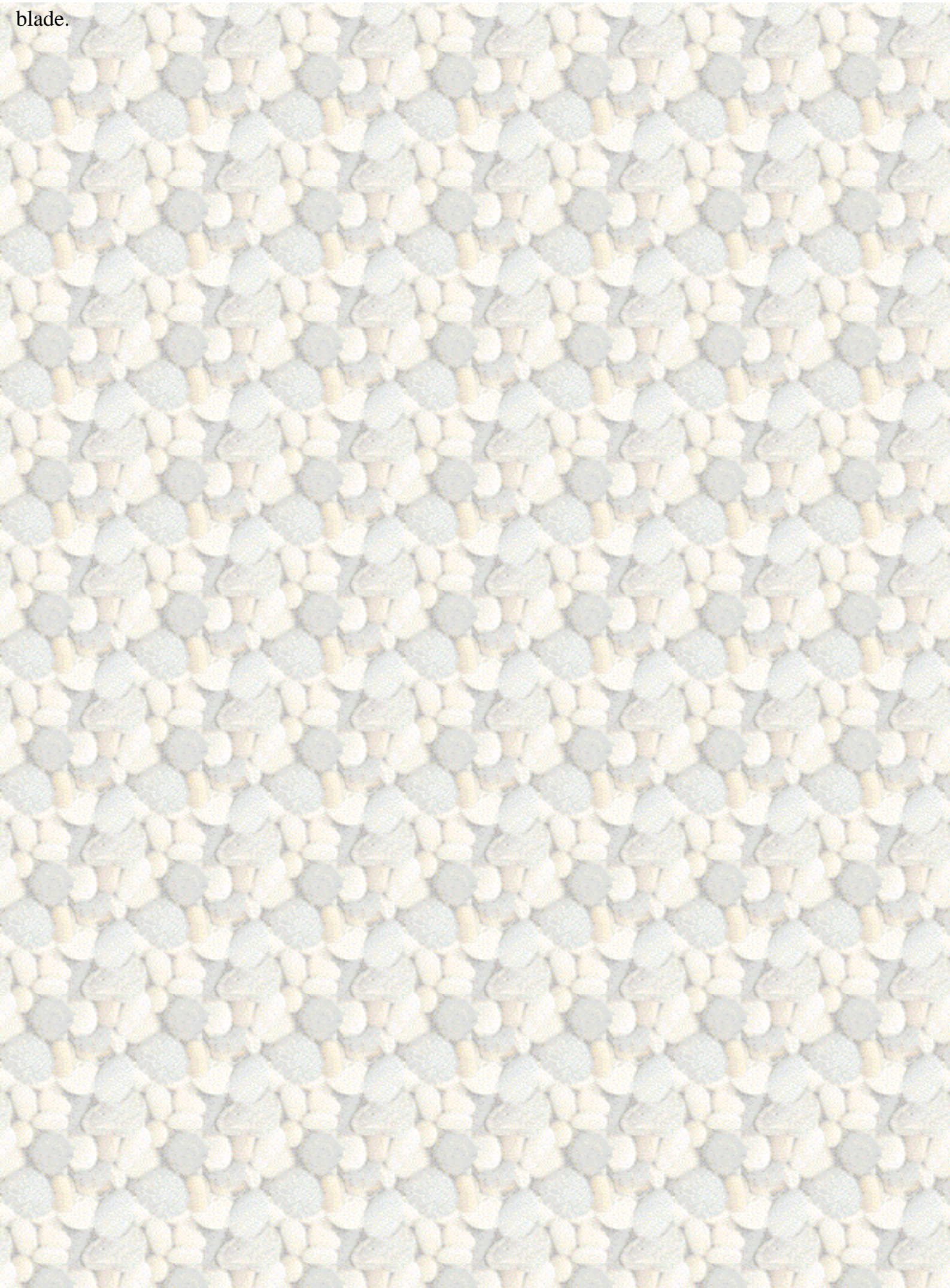


[Back to top](#)**Table 2.22: The coefficient c_2 .**

$h_b/h_i=3$	ϕ	32°	37°	42°	47°	52°
α	δ					
15°	15°	0.113	0.137	0.161	0.188	0.216
	18°	0.110	0.134	0.159	0.187	0.216
	21°	0.105	0.130	0.156	0.185	0.216
	24°	0.101	0.126	0.153	0.182	0.214
	27°	0.096	0.121	0.149	0.179	0.212
	30°	0.090	0.116	0.144	0.175	0.210
30°	15°	0.113	0.142	0.174	0.209	0.248
	18°	0.105	0.135	0.167	0.204	0.244
	21°	0.096	0.126	0.159	0.196	0.239
	24°	0.085	0.116	0.149	0.188	0.231
	27°	0.074	0.104	0.138	0.177	0.222
	30°	0.061	0.091	0.125	0.165	0.211
45°	15°	0.089	0.121	0.156	0.197	0.246
	18°	0.073	0.105	0.140	0.182	0.232
	21°	0.056	0.086	0.122	0.163	0.214
	24°	0.035	0.065	0.100	0.141	0.192
	27°	0.012	0.041	0.074	0.115	0.164
	30°	-0.013	0.013	0.045	0.083	0.131
60°	15°	0.032	0.058	0.090	0.129	0.177
	18°	0.002	0.026	0.055	0.091	0.136
	21°	-0.031	-0.011	0.014	0.045	0.085
	24°	-0.069	-0.054	-0.035	-0.011	0.021
	27°	-0.112	-0.104	-0.093	-0.079	-0.059
	30°	-0.162	-0.162	-0.162	-0.162	-0.162

The dimensionless force c_2 , perpendicular to the cutting velocity, as a function of the blade angle α , the angle of internal friction ϕ , the soil/interface friction angle δ , without under pressure behind the

blade.

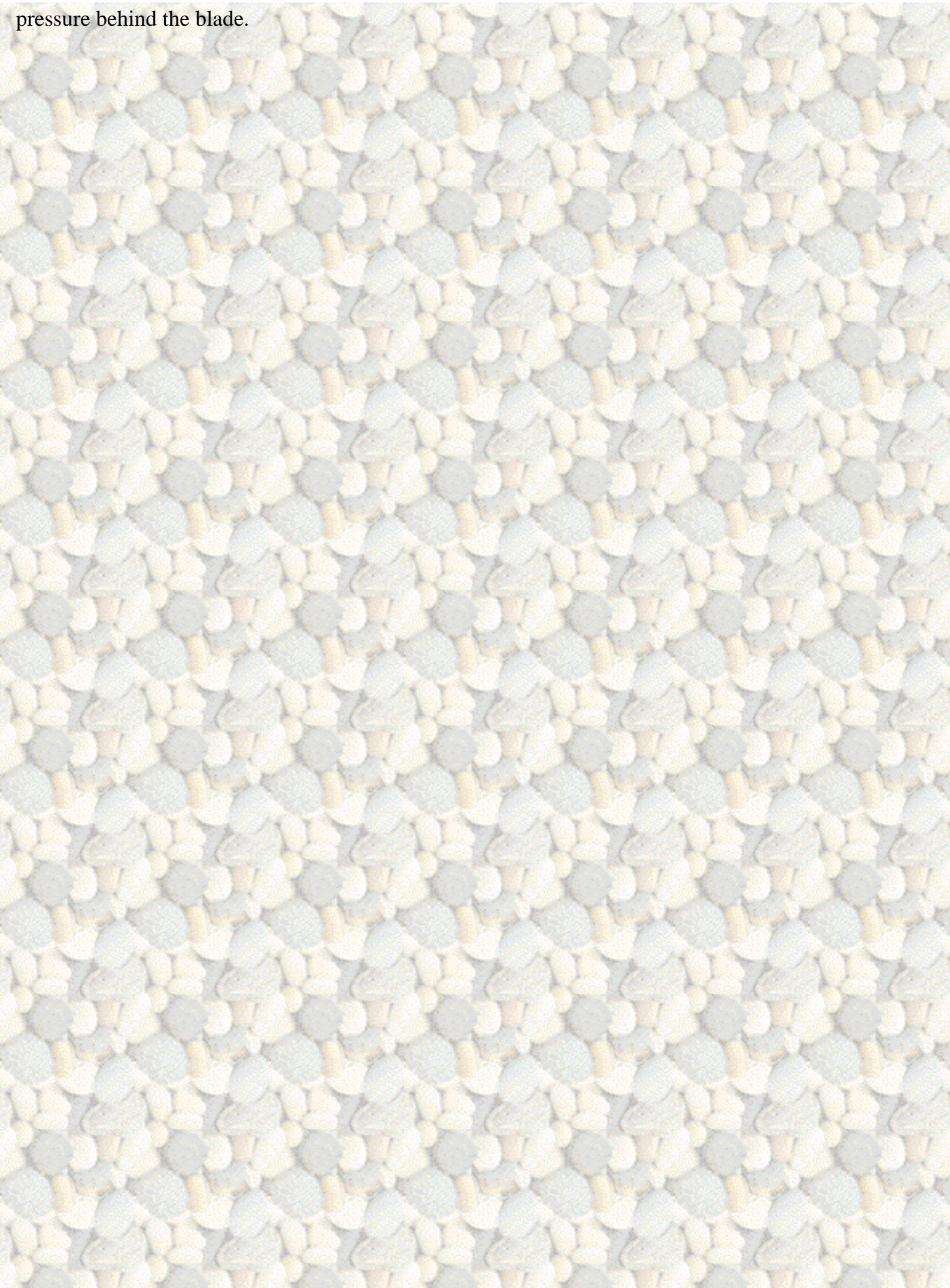


[Back to top](#)**Table 2.10: The coefficient a_1 .**

$h_b/h_i=3$	ϕ	32°	37°	42°	47°	52°
α	δ					
15°	15°	0.522	0.517	0.512	0.507	0.501
	18°	0.518	0.513	0.508	0.503	0.497
	21°	0.514	0.509	0.504	0.499	0.493
	24°	0.510	0.505	0.500	0.495	0.489
	27°	0.506	0.501	0.497	0.491	0.485
	30°	0.502	0.498	0.493	0.487	0.480
30°	15°	0.534	0.529	0.524	0.519	0.514
	18°	0.531	0.526	0.521	0.516	0.511
	21°	0.528	0.523	0.519	0.513	0.508
	24°	0.525	0.520	0.516	0.511	0.505
	27°	0.522	0.517	0.513	0.508	0.502
	30°	0.519	0.514	0.510	0.504	0.499
45°	15°	0.552	0.548	0.544	0.540	0.536
	18°	0.550	0.547	0.543	0.539	0.534
	21°	0.549	0.545	0.541	0.537	0.532
	24°	0.547	0.543	0.539	0.535	0.531
	27°	0.545	0.542	0.538	0.533	0.529
	30°	0.544	0.540	0.536	0.531	0.527
60°	15°	0.580	0.575	0.570	0.565	0.559
	18°	0.578	0.573	0.568	0.563	0.557
	21°	0.576	0.571	0.566	0.560	0.554
	24°	0.573	0.569	0.564	0.558	0.551
	27°	0.571	0.566	0.561	0.555	0.548
	30°	0.569	0.564	0.558	0.552	0.545

The weigh factor a_1 , for the determination of the weighed average permeability k_m , as a function of the blade angle α , the angle of internal friction ϕ , the soil/interface friction angle δ , without under

pressure behind the blade.



Coefficients for the Cavitating Cutting Process in Water Saturated Sand ($h_b/h_i=1$)

[Contents](#)
[Dr.ir. S.A. Miedema](#)
[Table 2.05: The shear angle \$\beta\$.](#)
[Table 2.26: The coefficient \$d_1\$.](#)
[Table 2.32: The coefficient \$d_2\$.](#)
[Back to top](#)
Table 2.05: The shear angle β .

$h_b/h_i=1$	ϕ	32°	37°	42°	47°	52°
α	δ					
15°	15°	37.217	37.520	37.355	36.831	36.026
	18°	34.461	34.854	34.790	34.370	33.669
	21°	32.163	32.598	32.594	32.243	31.613
	24°	30.212	30.661	30.689	30.379	29.796
	27°	28.530	28.973	29.012	28.726	28.173
	30°	27.060	27.483	27.520	27.243	26.707
30°	15°	39.766	39.060	38.014	36.718	35.232
	18°	37.341	36.757	35.823	34.628	33.233
	21°	35.196	34.696	33.844	32.725	31.399
	24°	33.280	32.837	32.041	30.977	29.704
	27°	31.554	31.145	30.387	29.363	28.127
	30°	29.985	29.593	28.859	27.860	26.650
45°	15°	36.853	35.599	34.097	32.412	30.591
	18°	34.768	33.616	32.202	30.594	28.839
	21°	32.866	31.789	30.441	28.892	27.188
	24°	31.119	30.094	28.794	27.288	25.623
	27°	29.502	28.512	27.246	25.770	24.132
	30°	27.996	27.026	25.781	24.325	22.705

60°	15°	31.992	30.395	28.608	26.683	24.654
	18°	30.155	28.634	26.911	25.039	23.055
	21°	28.444	26.979	25.303	23.471	21.520
	24°	26.841	25.414	23.772	21.968	20.040
	27°	25.330	23.927	22.306	20.520	18.605
	30°	23.897	22.506	20.896	19.118	17.208

The shear angle β as a function of the blade angle α , the angle of internal friction ϕ , the soil/interface friction angle δ , for the cavitating cutting process.

[Back to top](#)

Table 2.26: The coefficient d_1 .

$h_b/h_i=1$	ϕ	32°	37°	42°	47°	52°
α	δ					
15°	15°	1.390	1.505	1.625	1.753	1.890
	18°	1.626	1.766	1.913	2.069	2.238
	21°	1.860	2.028	2.205	2.393	2.597
	24°	2.092	2.291	2.501	2.726	2.970
	27°	2.324	2.557	2.803	3.068	3.358
	30°	2.556	2.826	3.112	3.423	3.764
30°	15°	1.206	1.374	1.559	1.766	2.000
	18°	1.381	1.575	1.791	2.033	2.309
	21°	1.559	1.783	2.033	2.315	2.638
	24°	1.741	1.998	2.286	2.613	2.991
	27°	1.928	2.222	2.552	2.930	3.370
	30°	2.121	2.455	2.833	3.269	3.781
45°	15°	1.419	1.688	2.000	2.365	2.800
	18°	1.598	1.905	2.262	2.685	3.192
	21°	1.784	2.133	2.543	3.032	3.625
	24°	1.980	2.376	2.846	3.411	4.105
	27°	2.186	2.636	3.174	3.829	4.642

	30°	2.404	2.916	3.533	4.292	5.249
60°	15°	1.879	2.331	2.883	3.570	4.444
	18°	2.099	2.615	3.252	4.054	5.090
	21°	2.336	2.925	3.661	4.602	5.837
	24°	2.593	3.267	4.120	5.228	6.711
	27°	2.872	3.645	4.639	5.952	7.746
	30°	3.179	4.069	5.232	6.798	8.991

The dimensionless force d_1 , in the direction of the cutting velocity, as a function of the blade angle α , the angle of internal friction ϕ , the soil/interface friction angle δ , without under pressure behind the blade.

[Back to top](#)

Table 2.32: The coefficient d_2 .

$h_b/h_i=1$	ϕ	32°	37°	42°	47°	52°
α	δ					
15°	15°	0.409	0.608	0.816	1.037	1.274
	18°	0.312	0.528	0.754	0.995	1.255
	21°	0.205	0.436	0.680	0.939	1.220
	24°	0.087	0.333	0.592	0.870	1.172
	27°	-0.040	0.219	0.493	0.788	1.110
	30°	-0.175	0.095	0.382	0.692	1.034
30°	15°	0.474	0.642	0.828	1.035	1.269
	18°	0.412	0.588	0.782	1.000	1.249
	21°	0.341	0.523	0.725	0.954	1.216
	24°	0.261	0.447	0.657	0.895	1.169
	27°	0.171	0.361	0.576	0.822	1.108
	30°	0.071	0.264	0.483	0.735	1.031
45°	15°	0.398	0.553	0.733	0.945	1.196
	18°	0.325	0.481	0.664	0.879	1.138
	21°	0.241	0.396	0.579	0.797	1.061

	24°	0.145	0.298	0.478	0.696	0.962
	27°	0.037	0.183	0.358	0.572	0.836
	30°	-0.086	0.051	0.217	0.421	0.678
60°	15°	0.195	0.317	0.465	0.650	0.885
	18°	0.083	0.193	0.329	0.500	0.721
	21°	-0.047	0.047	0.164	0.313	0.510
	24°	-0.198	-0.126	-0.036	0.081	0.238
	27°	-0.372	-0.331	-0.278	-0.208	-0.113
	30°	-0.575	-0.574	-0.573	-0.572	-0.570

The dimensionless force d_2 , perpendicular to the cutting velocity, as a function of the blade angle α , the angle of internal friction ϕ , the soil/interface friction angle δ , without under pressure behind the blade.

[Back to top](#)

This is a translation of the dissertation of Dr.ir. S.A. Miedema, dated September 15th 1987 .

The dissertation was originally published in Dutch by the:

Delft University of Technology

Faculty of Mechanical Engineering and Marine Technology

Chair of Dredging Technology

Mekelweg 2

2628 CD, Delft

The Netherlands

Last modified Wednesday May 24, 2000 by: [Sape A. Miedema](#)

Translation by: [Laurens de Jonge](#)

Figures, equations and tables by: [Erik Miedema](#)

Copyright © May, 2000 Dr.ir. S.A. Miedema



[Download Adobe Acrobat Reader V4.0](#)

[Back to top](#)**Table 2.05: The shear angle β .**

$h_b/h_i=1$	ϕ	32°	37°	42°	47°	52°
α	δ					
15°	15°	37.217	37.520	37.355	36.831	36.026
	18°	34.461	34.854	34.790	34.370	33.669
	21°	32.163	32.598	32.594	32.243	31.613
	24°	30.212	30.661	30.689	30.379	29.796
	27°	28.530	28.973	29.012	28.726	28.173
	30°	27.060	27.483	27.520	27.243	26.707
30°	15°	39.766	39.060	38.014	36.718	35.232
	18°	37.341	36.757	35.823	34.628	33.233
	21°	35.196	34.696	33.844	32.725	31.399
	24°	33.280	32.837	32.041	30.977	29.704
	27°	31.554	31.145	30.387	29.363	28.127
	30°	29.985	29.593	28.859	27.860	26.650
45°	15°	36.853	35.599	34.097	32.412	30.591
	18°	34.768	33.616	32.202	30.594	28.839
	21°	32.866	31.789	30.441	28.892	27.188
	24°	31.119	30.094	28.794	27.288	25.623
	27°	29.502	28.512	27.246	25.770	24.132
	30°	27.996	27.026	25.781	24.325	22.705
60°	15°	31.992	30.395	28.608	26.683	24.654
	18°	30.155	28.634	26.911	25.039	23.055
	21°	28.444	26.979	25.303	23.471	21.520
	24°	26.841	25.414	23.772	21.968	20.040
	27°	25.330	23.927	22.306	20.520	18.605
	30°	23.897	22.506	20.896	19.118	17.208

The shear angle β as a function of the blade angle α , the angle of internal

friction ϕ , the soil/interface friction angle δ , for the cavitating cutting process.

[Back to top](#)**Table 2.26: The coefficient d_1 .**

$h_b/h_i=1$	ϕ	32°	37°	42°	47°	52°
α	δ					
15°	15°	1.390	1.505	1.625	1.753	1.890
	18°	1.626	1.766	1.913	2.069	2.238
	21°	1.860	2.028	2.205	2.393	2.597
	24°	2.092	2.291	2.501	2.726	2.970
	27°	2.324	2.557	2.803	3.068	3.358
	30°	2.556	2.826	3.112	3.423	3.764
30°	15°	1.206	1.374	1.559	1.766	2.000
	18°	1.381	1.575	1.791	2.033	2.309
	21°	1.559	1.783	2.033	2.315	2.638
	24°	1.741	1.998	2.286	2.613	2.991
	27°	1.928	2.222	2.552	2.930	3.370
	30°	2.121	2.455	2.833	3.269	3.781
45°	15°	1.419	1.688	2.000	2.365	2.800
	18°	1.598	1.905	2.262	2.685	3.192
	21°	1.784	2.133	2.543	3.032	3.625
	24°	1.980	2.376	2.846	3.411	4.105
	27°	2.186	2.636	3.174	3.829	4.642
	30°	2.404	2.916	3.533	4.292	5.249
60°	15°	1.879	2.331	2.883	3.570	4.444
	18°	2.099	2.615	3.252	4.054	5.090
	21°	2.336	2.925	3.661	4.602	5.837
	24°	2.593	3.267	4.120	5.228	6.711
	27°	2.872	3.645	4.639	5.952	7.746
	30°	3.179	4.069	5.232	6.798	8.991

The dimensionless force d_1 , in the direction of the cutting velocity, as a

function of the blade angle α , the angle of internal friction ϕ , the soil/interface friction angle δ , without under pressure behind the blade.

[Back to top](#)**Table 2.32: The coefficient d_2 .**

$h_b/h_i=1$	ϕ	32°	37°	42°	47°	52°
α	δ					
15°	15°	0.409	0.608	0.816	1.037	1.274
	18°	0.312	0.528	0.754	0.995	1.255
	21°	0.205	0.436	0.680	0.939	1.220
	24°	0.087	0.333	0.592	0.870	1.172
	27°	-0.040	0.219	0.493	0.788	1.110
	30°	-0.175	0.095	0.382	0.692	1.034
30°	15°	0.474	0.642	0.828	1.035	1.269
	18°	0.412	0.588	0.782	1.000	1.249
	21°	0.341	0.523	0.725	0.954	1.216
	24°	0.261	0.447	0.657	0.895	1.169
	27°	0.171	0.361	0.576	0.822	1.108
	30°	0.071	0.264	0.483	0.735	1.031
45°	15°	0.398	0.553	0.733	0.945	1.196
	18°	0.325	0.481	0.664	0.879	1.138
	21°	0.241	0.396	0.579	0.797	1.061
	24°	0.145	0.298	0.478	0.696	0.962
	27°	0.037	0.183	0.358	0.572	0.836
	30°	-0.086	0.051	0.217	0.421	0.678
60°	15°	0.195	0.317	0.465	0.650	0.885
	18°	0.083	0.193	0.329	0.500	0.721
	21°	-0.047	0.047	0.164	0.313	0.510
	24°	-0.198	-0.126	-0.036	0.081	0.238
	27°	-0.372	-0.331	-0.278	-0.208	-0.113
	30°	-0.575	-0.574	-0.573	-0.572	-0.570

The dimensionless force d_2 , perpendicular to the cutting velocity, as a function

of the blade angle α , the angle of internal friction ϕ , the soil/interface friction angle δ , without under pressure behind the blade.

Coefficients for the Cavitating Cutting Process in Water Saturated Sand ($h_b/h_i=2$)

[Contents](#)
[Dr.ir. S.A. Miedema](#)
[Table 2.06: The shear angle \$\beta\$.](#)
[Table 2.27: The coefficient \$d_1\$.](#)
[Table 2.33: The coefficient \$d_2\$.](#)
[Back to top](#)
Table 2.06: The shear angle β .

$h_b/h_i=2$	ϕ	32°	37°	42°	47°	52°
α	δ					
15°	15°	28.724	29.560	29.957	29.994	29.733
	18°	26.332	27.162	27.586	27.670	27.472
	21°	24.420	25.221	25.643	25.747	25.582
	24°	22.849	23.608	24.014	24.120	23.968
	27°	21.528	22.240	22.621	22.716	22.566
	30°	20.396	21.059	21.407	21.485	21.329
30°	15°	33.398	33.367	32.937	32.198	31.215
	18°	30.972	31.019	30.677	30.027	29.134
	21°	28.922	29.011	28.721	28.131	27.299
	24°	27.161	27.265	27.004	26.451	25.659
	27°	25.622	25.725	25.476	24.944	24.177
	30°	24.259	24.349	24.101	23.576	22.823
45°	15°	32.378	31.721	30.741	29.516	28.100
	18°	30.207	29.642	28.751	27.610	26.271
	21°	28.308	27.801	26.970	25.887	24.605
	24°	26.624	26.149	25.357	24.314	23.070
	27°	25.110	24.652	23.881	22.862	21.643
	30°	23.736	23.280	22.518	21.512	20.306

60°	15°	28.906	27.806	26.445	24.886	23.174
	18°	26.993	25.974	24.686	23.194	21.540
	21°	25.276	24.309	23.072	21.626	20.014
	24°	23.716	22.781	21.576	20.159	18.574
	27°	22.283	21.364	20.176	18.776	17.204
	30°	20.955	20.038	18.855	17.461	15.892

The shear angle β as a function of the blade angle α , the angle of internal friction ϕ , the soil/interface friction angle δ , for the cavitating cutting process.

[Back to top](#)

Table 2.27: The coefficient d_1 .

$h_b/h_i=2$	ϕ	32°	37°	42°	47°	52°
α	δ					
15°	15°	2.295	2.460	2.627	2.801	2.984
	18°	2.683	2.889	3.098	3.315	3.545
	21°	3.062	3.313	3.569	3.836	4.119
	24°	3.435	3.735	4.042	4.364	4.707
	27°	3.803	4.156	4.520	4.903	5.313
	30°	4.169	4.579	5.005	5.455	5.941
30°	15°	1.729	1.934	2.156	2.401	2.674
	18°	1.997	2.239	2.503	2.794	3.122
	21°	2.267	2.550	2.860	3.205	3.593
	24°	2.539	2.868	3.230	3.634	4.093
	27°	2.815	3.195	3.614	4.085	4.625
	30°	3.097	3.532	4.015	4.563	5.195
45°	15°	1.836	2.142	2.492	2.898	3.377
	18°	2.093	2.447	2.854	3.330	3.897
	21°	2.357	2.765	3.238	3.794	4.462
	24°	2.631	3.100	3.646	4.296	5.084
	27°	2.917	3.454	4.085	4.843	5.772

	30°	3.217	3.830	4.558	5.442	6.541
60°	15°	2.269	2.764	3.364	4.104	5.038
	18°	2.567	3.139	3.837	4.710	5.827
	21°	2.883	3.543	4.357	5.388	6.728
	24°	3.221	3.982	4.933	6.154	7.771
	27°	3.586	4.464	5.578	7.031	8.995
	30°	3.982	4.998	6.306	8.047	10.453

The dimensionless force d_1 , in the direction of the cutting velocity, as a function of the blade angle α , the angle of internal friction ϕ , the soil/interface friction angle δ , without under pressure behind the blade.

[Back to top](#)

Table 2.33: The coefficient d_2 .

$h_b/h_i=2$	ϕ	32°	37°	42°	47°	52°
α	δ					
15°	15°	-0.024	0.262	0.552	0.853	1.170
	18°	-0.253	0.064	0.387	0.722	1.076
	21°	-0.496	-0.151	0.202	0.569	0.959
	24°	-0.752	-0.381	-0.001	0.396	0.820
	27°	-1.018	-0.626	-0.221	0.204	0.660
	30°	-1.294	-0.884	-0.458	-0.007	0.479
30°	15°	0.266	0.471	0.693	0.938	1.211
	18°	0.136	0.354	0.592	0.854	1.149
	21°	-0.008	0.222	0.473	0.752	1.067
	24°	-0.165	0.074	0.337	0.631	0.965
	27°	-0.336	-0.089	0.183	0.490	0.841
	30°	-0.520	-0.268	0.011	0.327	0.693
45°	15°	0.216	0.393	0.595	0.830	1.107
	18°	0.087	0.267	0.475	0.718	1.007
	21°	-0.059	0.123	0.334	0.582	0.880

	24°	-0.221	-0.040	0.170	0.420	0.723
	27°	-0.401	-0.226	-0.020	0.227	0.529
	30°	-0.600	-0.435	-0.240	-0.002	0.293
60°	15°	-0.009	0.124	0.285	0.484	0.735
	18°	-0.182	-0.060	0.089	0.275	0.513
	21°	-0.379	-0.274	-0.145	0.019	0.233
	24°	-0.603	-0.523	-0.422	-0.293	-0.122
	27°	-0.859	-0.812	-0.753	-0.676	-0.571
	30°	-1.151	-1.151	-1.150	-1.148	-1.146

The dimensionless force d_2 , perpendicular to the cutting velocity, as a function of the blade angle α , the angle of internal friction ϕ , the soil/interface friction angle δ , without under pressure behind the blade.

[Back to top](#)

This is a translation of the dissertation of Dr.ir. S.A. Miedema, dated September 15th 1987 .

The dissertation was originally published in Dutch by the:

Delft University of Technology

Faculty of Mechanical Engineering and Marine Technology

Chair of Dredging Technology

Mekelweg 2

2628 CD, Delft

The Netherlands

Last modified Wednesday May 24, 2000 by: [Sape A. Miedema](#)

Translation by: [Laurens de Jonge](#)

Figures, equations and tables by: [Erik Miedema](#)

Copyright © May, 2000 Dr.ir. S.A. Miedema



[Download Adobe Acrobat Reader V4.0](#)

[Back to top](#)**Table 2.06: The shear angle β .**

$h_b/h_i=2$	ϕ	32°	37°	42°	47°	52°
α	δ					
15°	15°	28.724	29.560	29.957	29.994	29.733
	18°	26.332	27.162	27.586	27.670	27.472
	21°	24.420	25.221	25.643	25.747	25.582
	24°	22.849	23.608	24.014	24.120	23.968
	27°	21.528	22.240	22.621	22.716	22.566
	30°	20.396	21.059	21.407	21.485	21.329
30°	15°	33.398	33.367	32.937	32.198	31.215
	18°	30.972	31.019	30.677	30.027	29.134
	21°	28.922	29.011	28.721	28.131	27.299
	24°	27.161	27.265	27.004	26.451	25.659
	27°	25.622	25.725	25.476	24.944	24.177
	30°	24.259	24.349	24.101	23.576	22.823
45°	15°	32.378	31.721	30.741	29.516	28.100
	18°	30.207	29.642	28.751	27.610	26.271
	21°	28.308	27.801	26.970	25.887	24.605
	24°	26.624	26.149	25.357	24.314	23.070
	27°	25.110	24.652	23.881	22.862	21.643
	30°	23.736	23.280	22.518	21.512	20.306
60°	15°	28.906	27.806	26.445	24.886	23.174
	18°	26.993	25.974	24.686	23.194	21.540
	21°	25.276	24.309	23.072	21.626	20.014
	24°	23.716	22.781	21.576	20.159	18.574
	27°	22.283	21.364	20.176	18.776	17.204
	30°	20.955	20.038	18.855	17.461	15.892

The shear angle β as a function of the blade angle α , the angle of internal

friction ϕ , the soil/interface friction angle δ , for the cavitating cutting process.

[Back to top](#)**Table 2.27: The coefficient d_1 .**

$h_b/h_i=2$	ϕ	32°	37°	42°	47°	52°
α	δ					
15°	15°	2.295	2.460	2.627	2.801	2.984
	18°	2.683	2.889	3.098	3.315	3.545
	21°	3.062	3.313	3.569	3.836	4.119
	24°	3.435	3.735	4.042	4.364	4.707
	27°	3.803	4.156	4.520	4.903	5.313
	30°	4.169	4.579	5.005	5.455	5.941
30°	15°	1.729	1.934	2.156	2.401	2.674
	18°	1.997	2.239	2.503	2.794	3.122
	21°	2.267	2.550	2.860	3.205	3.593
	24°	2.539	2.868	3.230	3.634	4.093
	27°	2.815	3.195	3.614	4.085	4.625
	30°	3.097	3.532	4.015	4.563	5.195
45°	15°	1.836	2.142	2.492	2.898	3.377
	18°	2.093	2.447	2.854	3.330	3.897
	21°	2.357	2.765	3.238	3.794	4.462
	24°	2.631	3.100	3.646	4.296	5.084
	27°	2.917	3.454	4.085	4.843	5.772
	30°	3.217	3.830	4.558	5.442	6.541
60°	15°	2.269	2.764	3.364	4.104	5.038
	18°	2.567	3.139	3.837	4.710	5.827
	21°	2.883	3.543	4.357	5.388	6.728
	24°	3.221	3.982	4.933	6.154	7.771
	27°	3.586	4.464	5.578	7.031	8.995
	30°	3.982	4.998	6.306	8.047	10.453

The dimensionless force d_1 , in the direction of the cutting velocity, as a

function of the blade angle α , the angle of internal friction ϕ , the soil/interface friction angle δ , without under pressure behind the blade.

[Back to top](#)**Table 2.33: The coefficient d_2 .**

$h_b/h_i=2$	ϕ	32°	37°	42°	47°	52°
α	δ					
15°	15°	-0.024	0.262	0.552	0.853	1.170
	18°	-0.253	0.064	0.387	0.722	1.076
	21°	-0.496	-0.151	0.202	0.569	0.959
	24°	-0.752	-0.381	-0.001	0.396	0.820
	27°	-1.018	-0.626	-0.221	0.204	0.660
	30°	-1.294	-0.884	-0.458	-0.007	0.479
30°	15°	0.266	0.471	0.693	0.938	1.211
	18°	0.136	0.354	0.592	0.854	1.149
	21°	-0.008	0.222	0.473	0.752	1.067
	24°	-0.165	0.074	0.337	0.631	0.965
	27°	-0.336	-0.089	0.183	0.490	0.841
	30°	-0.520	-0.268	0.011	0.327	0.693
45°	15°	0.216	0.393	0.595	0.830	1.107
	18°	0.087	0.267	0.475	0.718	1.007
	21°	-0.059	0.123	0.334	0.582	0.880
	24°	-0.221	-0.040	0.170	0.420	0.723
	27°	-0.401	-0.226	-0.020	0.227	0.529
	30°	-0.600	-0.435	-0.240	-0.002	0.293
60°	15°	-0.009	0.124	0.285	0.484	0.735
	18°	-0.182	-0.060	0.089	0.275	0.513
	21°	-0.379	-0.274	-0.145	0.019	0.233
	24°	-0.603	-0.523	-0.422	-0.293	-0.122
	27°	-0.859	-0.812	-0.753	-0.676	-0.571
	30°	-1.151	-1.151	-1.150	-1.148	-1.146

The dimensionless force d_2 , perpendicular to the cutting velocity, as a function

of the blade angle α , the angle of internal friction ϕ , the soil/interface friction angle δ , without under pressure behind the blade.

Coefficients for the Cavitating Cutting Process in Water Saturated Sand ($h_b/h_i=3$)

[Contents](#)
[Dr.ir. S.A. Miedema](#)
[Table 2.07: The shear angle \$\beta\$.](#)
[Table 2.28: The coefficient \$d_1\$.](#)
[Table 2.34: The coefficient \$d_2\$.](#)
[Back to top](#)
Table 2.07: The shear angle β .

$h_b/h_i=3$	ϕ	32°	37°	42°	47°	52°
α	δ					
15°	15°	24.046	25.019	25.609	25.872	25.856
	18°	21.976	22.900	23.476	23.751	23.765
	21°	20.350	21.217	21.763	22.030	22.053
	24°	19.031	19.838	20.348	20.596	20.615
	27°	17.932	18.680	19.150	19.374	19.381
	30°	16.996	17.687	18.117	18.313	18.303
30°	15°	29.286	29.575	29.466	29.038	28.353
	18°	26.992	27.319	27.267	26.908	26.297
	21°	25.100	25.435	25.410	25.090	24.525
	24°	23.504	23.828	23.811	23.511	22.973
	27°	22.130	22.433	22.410	22.116	21.592
	30°	20.928	21.202	21.165	20.867	20.346
45°	15°	29.236	28.919	28.257	27.325	26.179
	18°	27.101	26.853	26.266	25.411	24.339
	21°	25.277	25.065	24.524	23.719	22.699
	24°	23.690	23.493	22.977	22.203	21.215
	27°	22.288	22.091	21.584	20.825	19.857
	30°	21.031	20.823	20.315	19.561	18.600

60°	15°	26.619	25.832	24.754	23.450	21.967
	18°	24.711	23.995	22.987	21.750	20.329
	21°	23.037	22.362	21.398	20.206	18.826
	24°	21.543	20.889	19.951	18.785	17.431
	27°	20.193	19.545	18.617	17.464	16.121
	30°	18.958	18.303	17.374	16.222	14.880

The shear angle β as a function of the blade angle α , the angle of internal friction ϕ , the soil/interface friction angle δ , for the cavitating cutting process.

[Back to top](#)

Table 2.28: The coefficient d_1 .

$h_b/h_i=3$	ϕ	32°	37°	42°	47°	52°
α	δ					
15°	15°	3.145	3.362	3.578	3.799	4.028
	18°	3.672	3.945	4.218	4.497	4.789
	21°	4.185	4.519	4.855	5.200	5.562
	24°	4.687	5.087	5.492	5.910	6.351
	27°	5.180	5.652	6.132	6.631	7.159
	30°	5.667	6.216	6.778	7.366	7.993
30°	15°	2.216	2.458	2.717	3.000	3.312
	18°	2.567	2.858	3.169	3.510	3.889
	21°	2.919	3.262	3.632	4.038	4.492
	24°	3.272	3.673	4.107	4.587	5.127
	27°	3.629	4.093	4.599	5.162	5.799
	30°	3.991	4.525	5.110	5.766	6.515
45°	15°	2.222	2.566	2.954	3.402	3.925
	18°	2.549	2.951	3.408	3.938	4.562
	21°	2.883	3.350	3.885	4.509	5.252
	24°	3.228	3.768	4.391	5.123	6.004
	27°	3.585	4.207	4.929	5.788	6.831

	30°	3.958	4.671	5.508	6.513	7.750
60°	15°	2.632	3.170	3.817	4.610	5.605
	18°	2.999	3.627	4.387	5.329	6.526
	21°	3.387	4.116	5.008	6.128	7.572
	24°	3.799	4.645	5.692	7.025	8.774
	27°	4.240	5.222	6.453	8.044	10.175
	30°	4.717	5.856	7.307	9.217	11.833

The dimensionless force d_1 , in the direction of the cutting velocity, as a function of the blade angle α , the angle of internal friction ϕ , the soil/interface friction angle δ , without under pressure behind the blade.

[Back to top](#)

Table 2.34: The coefficient d_2 .

$h_b/h_i=3$	ϕ	32°	37°	42°	47°	52°
α	δ					
15°	15°	-0.552	-0.177	0.198	0.581	0.979
	18°	-0.921	-0.501	-0.080	0.350	0.800
	21°	-1.306	-0.846	-0.384	0.092	0.590
	24°	-1.703	-1.208	-0.708	-0.191	0.353
	27°	-2.111	-1.586	-1.053	-0.498	0.090
	30°	-2.528	-1.979	-1.417	-0.828	-0.201
30°	15°	0.020	0.263	0.522	0.805	1.118
	18°	-0.182	0.079	0.360	0.667	1.009
	21°	-0.402	-0.124	0.176	0.505	0.873
	24°	-0.638	-0.346	-0.030	0.319	0.711
	27°	-0.890	-0.588	-0.259	0.107	0.521
	30°	-1.158	-0.850	-0.511	-0.132	0.301
45°	15°	0.017	0.215	0.440	0.698	1.001
	18°	-0.171	0.034	0.267	0.537	0.856
	21°	-0.379	-0.171	0.068	0.346	0.677

	24°	-0.608	-0.400	-0.160	0.122	0.460
	27°	-0.858	-0.656	-0.420	-0.141	0.199
	30°	-1.133	-0.941	-0.717	-0.447	-0.114
60°	15°	-0.221	-0.076	0.097	0.310	0.578
	18°	-0.455	-0.321	-0.159	0.042	0.298
	21°	-0.718	-0.602	-0.460	-0.282	-0.052
	24°	-1.014	-0.925	-0.814	-0.673	-0.488
	27°	-1.349	-1.297	-1.231	-1.147	-1.034
	30°	-1.728	-1.727	-1.726	-1.724	-1.722

The dimensionless force d_2 , perpendicular to the cutting velocity, as a function of the blade angle α , the angle of internal friction ϕ , the soil/interface friction angle δ , without under pressure behind the blade.

[Back to top](#)

This is a translation of the dissertation of Dr.ir. S.A. Miedema, dated September 15th 1987 .

The dissertation was originally published in Dutch by the:

Delft University of Technology

Faculty of Mechanical Engineering and Marine Technology

Chair of Dredging Technology

Mekelweg 2

2628 CD, Delft

The Netherlands

Last modified Wednesday May 24, 2000 by: [Sape A. Miedema](#)

Translation by: [Laurens de Jonge](#)

Figures, equations and tables by: [Erik Miedema](#)

Copyright © May, 2000 Dr.ir. S.A. Miedema



[Download Adobe Acrobat Reader V4.0](#)

[Back to top](#)**Table 2.07: The shear angle β .**

$h_b/h_i=3$	ϕ	32°	37°	42°	47°	52°
α	δ					
15°	15°	24.046	25.019	25.609	25.872	25.856
	18°	21.976	22.900	23.476	23.751	23.765
	21°	20.350	21.217	21.763	22.030	22.053
	24°	19.031	19.838	20.348	20.596	20.615
	27°	17.932	18.680	19.150	19.374	19.381
	30°	16.996	17.687	18.117	18.313	18.303
30°	15°	29.286	29.575	29.466	29.038	28.353
	18°	26.992	27.319	27.267	26.908	26.297
	21°	25.100	25.435	25.410	25.090	24.525
	24°	23.504	23.828	23.811	23.511	22.973
	27°	22.130	22.433	22.410	22.116	21.592
	30°	20.928	21.202	21.165	20.867	20.346
45°	15°	29.236	28.919	28.257	27.325	26.179
	18°	27.101	26.853	26.266	25.411	24.339
	21°	25.277	25.065	24.524	23.719	22.699
	24°	23.690	23.493	22.977	22.203	21.215
	27°	22.288	22.091	21.584	20.825	19.857
	30°	21.031	20.823	20.315	19.561	18.600
60°	15°	26.619	25.832	24.754	23.450	21.967
	18°	24.711	23.995	22.987	21.750	20.329
	21°	23.037	22.362	21.398	20.206	18.826
	24°	21.543	20.889	19.951	18.785	17.431
	27°	20.193	19.545	18.617	17.464	16.121
	30°	18.958	18.303	17.374	16.222	14.880

The shear angle β as a function of the blade angle α , the angle of internal

friction ϕ , the soil/interface friction angle δ , for the cavitating cutting process.

[Back to top](#)**Table 2.28: The coefficient d_1 .**

$h_b/h_i=3$	ϕ	32°	37°	42°	47°	52°
α	δ					
15°	15°	3.145	3.362	3.578	3.799	4.028
	18°	3.672	3.945	4.218	4.497	4.789
	21°	4.185	4.519	4.855	5.200	5.562
	24°	4.687	5.087	5.492	5.910	6.351
	27°	5.180	5.652	6.132	6.631	7.159
	30°	5.667	6.216	6.778	7.366	7.993
30°	15°	2.216	2.458	2.717	3.000	3.312
	18°	2.567	2.858	3.169	3.510	3.889
	21°	2.919	3.262	3.632	4.038	4.492
	24°	3.272	3.673	4.107	4.587	5.127
	27°	3.629	4.093	4.599	5.162	5.799
	30°	3.991	4.525	5.110	5.766	6.515
45°	15°	2.222	2.566	2.954	3.402	3.925
	18°	2.549	2.951	3.408	3.938	4.562
	21°	2.883	3.350	3.885	4.509	5.252
	24°	3.228	3.768	4.391	5.123	6.004
	27°	3.585	4.207	4.929	5.788	6.831
	30°	3.958	4.671	5.508	6.513	7.750
60°	15°	2.632	3.170	3.817	4.610	5.605
	18°	2.999	3.627	4.387	5.329	6.526
	21°	3.387	4.116	5.008	6.128	7.572
	24°	3.799	4.645	5.692	7.025	8.774
	27°	4.240	5.222	6.453	8.044	10.175
	30°	4.717	5.856	7.307	9.217	11.833

The dimensionless force d_1 , in the direction of the cutting velocity, as a

function of the blade angle α , the angle of internal friction ϕ , the soil/interface friction angle δ , without under pressure behind the blade.

[Back to top](#)**Table 2.34: The coefficient d_2 .**

$h_b/h_i=3$	ϕ	32°	37°	42°	47°	52°
α	δ					
15°	15°	-0.552	-0.177	0.198	0.581	0.979
	18°	-0.921	-0.501	-0.080	0.350	0.800
	21°	-1.306	-0.846	-0.384	0.092	0.590
	24°	-1.703	-1.208	-0.708	-0.191	0.353
	27°	-2.111	-1.586	-1.053	-0.498	0.090
	30°	-2.528	-1.979	-1.417	-0.828	-0.201
30°	15°	0.020	0.263	0.522	0.805	1.118
	18°	-0.182	0.079	0.360	0.667	1.009
	21°	-0.402	-0.124	0.176	0.505	0.873
	24°	-0.638	-0.346	-0.030	0.319	0.711
	27°	-0.890	-0.588	-0.259	0.107	0.521
	30°	-1.158	-0.850	-0.511	-0.132	0.301
45°	15°	0.017	0.215	0.440	0.698	1.001
	18°	-0.171	0.034	0.267	0.537	0.856
	21°	-0.379	-0.171	0.068	0.346	0.677
	24°	-0.608	-0.400	-0.160	0.122	0.460
	27°	-0.858	-0.656	-0.420	-0.141	0.199
	30°	-1.133	-0.941	-0.717	-0.447	-0.114
60°	15°	-0.221	-0.076	0.097	0.310	0.578
	18°	-0.455	-0.321	-0.159	0.042	0.298
	21°	-0.718	-0.602	-0.460	-0.282	-0.052
	24°	-1.014	-0.925	-0.814	-0.673	-0.488
	27°	-1.349	-1.297	-1.231	-1.147	-1.034
	30°	-1.728	-1.727	-1.726	-1.724	-1.722

The dimensionless force d_2 , perpendicular to the cutting velocity, as a function

of the blade angle α , the angle of internal friction ϕ , the soil/interface friction angle δ , without under pressure behind the blade.

Coefficients for the Non-Cavitating Cutting Process in Water Saturated Sand ($h_b/h_i=1$), with Under Pressure behind the Blade

[Contents](#)
[Dr.ir. S.A. Miedema](#)
[Table 2.02: The shear angle \$\beta\$.](#)
[Table 2.17: The coefficient \$c_1\$.](#)
[Table 2.23: The coefficient \$c_2\$.](#)
[Table 2.11: The coefficient \$a_1\$.](#)
[Back to top](#)
Table 2.02: The shear angle β .

$h_b/h_i=1$	ϕ	32°	37°	42°	47°	52°
α	δ					
15°	15°	40.892	40.152	39.169	38.012	36.727
	18°	39.024	38.380	37.483	36.402	35.184
	21°	37.355	36.781	35.947	34.924	33.756
	24°	35.847	35.321	34.534	33.552	32.423
	27°	34.468	33.975	33.220	32.269	31.166
	30°	33.196	32.723	31.989	31.058	29.973
30°	15°	37.967	36.937	35.707	34.334	32.854
	18°	36.187	35.250	34.100	32.795	31.372
	21°	34.564	33.696	32.606	31.353	29.974
	24°	33.072	32.255	31.209	29.994	28.648
	27°	31.690	30.907	29.893	28.705	27.382
	30°	30.401	29.640	28.646	27.476	26.166
45°	15°	33.389	32.254	30.936	29.481	27.919
	18°	31.792	30.726	29.467	28.061	26.539
	21°	30.326	29.310	28.092	26.720	25.224
	24°	28.969	27.984	26.793	25.442	23.963

	27°	27.700	26.733	25.557	24.218	22.745
	30°	26.503	25.543	24.373	23.036	21.562
60°	15°	28.220	26.928	25.482	23.917	22.253
	18°	26.813	25.569	24.160	22.623	20.978
	21°	25.500	24.287	22.901	21.379	19.742
	24°	24.264	23.067	21.692	20.174	18.535
	27°	23.091	21.897	20.522	18.999	17.350
	30°	21.967	20.767	19.382	17.845	16.177

The shear angle β as a function of the blade angle α , the angle of internal friction ϕ , the soil/interface friction angle δ , for the non-cavitating cutting process.

[Back to top](#)

Table 2.17: The coefficient c_1 .

$h_b/h_i=1$	ϕ	32°	37°	42°	47°	52°
α	δ					
15°	15°	0.138	0.151	0.165	0.179	0.195
	18°	0.152	0.167	0.183	0.200	0.218
	21°	0.166	0.183	0.202	0.221	0.242
	24°	0.180	0.200	0.221	0.243	0.268
	27°	0.194	0.217	0.240	0.266	0.295
	30°	0.209	0.234	0.261	0.291	0.323
30°	15°	0.217	0.245	0.275	0.308	0.346
	18°	0.236	0.267	0.302	0.340	0.383
	21°	0.256	0.291	0.330	0.374	0.423
	24°	0.276	0.316	0.360	0.409	0.466
	27°	0.297	0.341	0.391	0.448	0.513
	30°	0.319	0.368	0.424	0.488	0.563
45°	15°	0.286	0.336	0.392	0.456	0.532
	18°	0.311	0.366	0.429	0.503	0.590
	21°	0.336	0.397	0.469	0.553	0.653
	24°	0.362	0.431	0.512	0.607	0.724

	27°	0.390	0.467	0.558	0.668	0.802
	30°	0.420	0.506	0.609	0.735	0.891
60°	15°	0.381	0.465	0.566	0.690	0.845
	18°	0.413	0.508	0.623	0.765	0.946
	21°	0.448	0.554	0.685	0.850	1.062
	24°	0.486	0.605	0.755	0.946	1.198
	27°	0.526	0.662	0.833	1.057	1.358
	30°	0.571	0.725	0.923	1.186	1.550

The dimensionless force c_1 , in the direction of the cutting velocity, as a function of the blade angle α , the angle of internal friction ϕ , the soil/interface friction angle δ , with under pressure behind the blade.

[Back to top](#)

Table 2.23: The coefficient c_2 .

$h_b/h_i=1$	ϕ	32°	37°	42°	47°	52°
α	δ					
15°	15°	0.240	0.262	0.286	0.311	0.337
	18°	0.234	0.258	0.282	0.308	0.336
	21°	0.229	0.252	0.278	0.305	0.334
	24°	0.222	0.247	0.273	0.301	0.331
	27°	0.216	0.241	0.267	0.296	0.328
	30°	0.209	0.234	0.261	0.291	0.324
30°	15°	0.189	0.217	0.248	0.281	0.319
	18°	0.181	0.210	0.241	0.276	0.315
	21°	0.173	0.202	0.233	0.269	0.310
	24°	0.164	0.193	0.225	0.261	0.303
	27°	0.153	0.182	0.215	0.252	0.295
	30°	0.142	0.171	0.204	0.241	0.285
45°	15°	0.134	0.162	0.195	0.233	0.278
	18°	0.122	0.151	0.183	0.222	0.267
	21°	0.109	0.137	0.170	0.208	0.253
	24°	0.095	0.122	0.154	0.191	0.237

	27°	0.079	0.105	0.135	0.172	0.217
	30°	0.062	0.086	0.114	0.149	0.192
60°	15°	0.072	0.095	0.123	0.157	0.200
	18°	0.053	0.074	0.099	0.131	0.170
	21°	0.032	0.050	0.072	0.099	0.134
	24°	0.008	0.022	0.039	0.060	0.088
	27°	-0.019	-0.011	0.000	0.013	0.030
	30°	-0.050	-0.049	-0.047	-0.046	-0.044

The dimensionless force c_2 , perpendicular to the cutting velocity, as a function of the blade angle α , the angle of internal friction ϕ , the soil/interface friction angle δ , with under pressure behind the blade.

[Back to top](#)

Table 2.11: The coefficient a_1 .

$h_b/h_i=1$	ϕ	32°	37°	42°	47°	52°
α	δ					
15°	15°	0.541	0.536	0.53	0.524	0.517
	18°	0.535	0.53	0.524	0.518	0.511
	21°	0.53	0.525	0.519	0.513	0.506
	24°	0.525	0.519	0.514	0.507	0.501
	27°	0.52	0.514	0.509	0.502	0.495
	30°	0.515	0.51	0.504	0.497	0.49
30°	15°	0.539	0.534	0.528	0.522	0.515
	18°	0.535	0.529	0.524	0.518	0.511
	21°	0.531	0.525	0.52	0.514	0.507
	24°	0.526	0.521	0.516	0.51	0.503
	27°	0.522	0.517	0.512	0.506	0.499
	30°	0.519	0.513	0.508	0.502	0.495
45°	15°	0.541	0.536	0.531	0.525	0.519
	18°	0.538	0.533	0.527	0.522	0.516
	21°	0.535	0.529	0.524	0.518	0.512
	24°	0.531	0.526	0.521	0.515	0.508
	27°	0.528	0.523	0.517	0.511	0.505

	30°	0.525	0.52	0.514	0.508	0.501
60°	15°	0.539	0.532	0.524	0.516	0.507
	18°	0.534	0.527	0.519	0.511	0.502
	21°	0.53	0.522	0.514	0.506	0.496
	24°	0.525	0.517	0.509	0.5	0.49
	27°	0.52	0.512	0.504	0.494	0.484
	30°	0.515	0.507	0.498	0.489	0.478

The weigh factor a_1 , for the determination of the weighed average permeability k_m , as a function of the blade angle α , the angle of internal friction ϕ , the soil/interface friction angle δ , with under pressure behind the blade.

[Back to top](#)

This is a translation of the dissertation of Dr.ir. S.A. Miedema, dated September 15th 1987 .
The dissertation was originally published in Dutch by the:
Delft University of Technology
Faculty of Mechanical Engineering and Marine Technology
Chair of Dredging Technology
Mekelweg 2
2628 CD, Delft
The Netherlands

Last modified Wednesday May 24, 2000 by: [Sape A. Miedema](#)

Translation by: [Laurens de Jonge](#)

Figures, equations and tables by: [Erik Miedema](#)

Copyright © May, 2000 Dr.ir. S.A. Miedema



[Download Adobe Acrobat Reader V4.0](#)

[Back to top](#)**Table 2.17: The coefficient c_1 .**

$h_b/h_i=1$	ϕ	32°	37°	42°	47°	52°
α	δ					
15°	15°	0.138	0.151	0.165	0.179	0.195
	18°	0.152	0.167	0.183	0.200	0.218
	21°	0.166	0.183	0.202	0.221	0.242
	24°	0.180	0.200	0.221	0.243	0.268
	27°	0.194	0.217	0.240	0.266	0.295
	30°	0.209	0.234	0.261	0.291	0.323
30°	15°	0.217	0.245	0.275	0.308	0.346
	18°	0.236	0.267	0.302	0.340	0.383
	21°	0.256	0.291	0.330	0.374	0.423
	24°	0.276	0.316	0.360	0.409	0.466
	27°	0.297	0.341	0.391	0.448	0.513
	30°	0.319	0.368	0.424	0.488	0.563
45°	15°	0.286	0.336	0.392	0.456	0.532
	18°	0.311	0.366	0.429	0.503	0.590
	21°	0.336	0.397	0.469	0.553	0.653
	24°	0.362	0.431	0.512	0.607	0.724
	27°	0.390	0.467	0.558	0.668	0.802
	30°	0.420	0.506	0.609	0.735	0.891
60°	15°	0.381	0.465	0.566	0.690	0.845
	18°	0.413	0.508	0.623	0.765	0.946
	21°	0.448	0.554	0.685	0.850	1.062
	24°	0.486	0.605	0.755	0.946	1.198
	27°	0.526	0.662	0.833	1.057	1.358
	30°	0.571	0.725	0.923	1.186	1.550

The dimensionless force c_1 , in the direction of the cutting velocity, as a

function of the blade angle α , the angle of internal friction ϕ , the soil/interface friction angle δ , with under pressure behind the blade.

[Back to top](#)**Table 2.23: The coefficient c_2 .**

$h_b/h_i=1$	ϕ	32°	37°	42°	47°	52°
α	δ					
15°	15°	0.240	0.262	0.286	0.311	0.337
	18°	0.234	0.258	0.282	0.308	0.336
	21°	0.229	0.252	0.278	0.305	0.334
	24°	0.222	0.247	0.273	0.301	0.331
	27°	0.216	0.241	0.267	0.296	0.328
	30°	0.209	0.234	0.261	0.291	0.324
30°	15°	0.189	0.217	0.248	0.281	0.319
	18°	0.181	0.210	0.241	0.276	0.315
	21°	0.173	0.202	0.233	0.269	0.310
	24°	0.164	0.193	0.225	0.261	0.303
	27°	0.153	0.182	0.215	0.252	0.295
	30°	0.142	0.171	0.204	0.241	0.285
45°	15°	0.134	0.162	0.195	0.233	0.278
	18°	0.122	0.151	0.183	0.222	0.267
	21°	0.109	0.137	0.170	0.208	0.253
	24°	0.095	0.122	0.154	0.191	0.237
	27°	0.079	0.105	0.135	0.172	0.217
	30°	0.062	0.086	0.114	0.149	0.192
60°	15°	0.072	0.095	0.123	0.157	0.200
	18°	0.053	0.074	0.099	0.131	0.170
	21°	0.032	0.050	0.072	0.099	0.134
	24°	0.008	0.022	0.039	0.060	0.088
	27°	-0.019	-0.011	0.000	0.013	0.030
	30°	-0.050	-0.049	-0.047	-0.046	-0.044

The dimensionless force c_2 , perpendicular to the cutting velocity, as a function of the blade angle α , the angle of internal friction ϕ , the soil/interface friction angle δ , with under pressure behind the blade.

[Back to top](#)**Table 2.11: The coefficient a_1 .**

$h_b/h_i=1$	ϕ	32°	37°	42°	47°	52°
α	δ					
15°	15°	0.541	0.536	0.53	0.524	0.517
	18°	0.535	0.53	0.524	0.518	0.511
	21°	0.53	0.525	0.519	0.513	0.506
	24°	0.525	0.519	0.514	0.507	0.501
	27°	0.52	0.514	0.509	0.502	0.495
	30°	0.515	0.51	0.504	0.497	0.49
30°	15°	0.539	0.534	0.528	0.522	0.515
	18°	0.535	0.529	0.524	0.518	0.511
	21°	0.531	0.525	0.52	0.514	0.507
	24°	0.526	0.521	0.516	0.51	0.503
	27°	0.522	0.517	0.512	0.506	0.499
	30°	0.519	0.513	0.508	0.502	0.495
45°	15°	0.541	0.536	0.531	0.525	0.519
	18°	0.538	0.533	0.527	0.522	0.516
	21°	0.535	0.529	0.524	0.518	0.512
	24°	0.531	0.526	0.521	0.515	0.508
	27°	0.528	0.523	0.517	0.511	0.505
	30°	0.525	0.52	0.514	0.508	0.501
60°	15°	0.539	0.532	0.524	0.516	0.507
	18°	0.534	0.527	0.519	0.511	0.502
	21°	0.53	0.522	0.514	0.506	0.496
	24°	0.525	0.517	0.509	0.5	0.49
	27°	0.52	0.512	0.504	0.494	0.484
	30°	0.515	0.507	0.498	0.489	0.478

The weigh factor a_1 , for the determination of the weighed average permeability k_m , as a function of the blade angle α , the angle of internal friction ϕ , the soil/interface friction angle δ , with under pressure behind the blade.

Coefficients for the Non-Cavitating Cutting Process in Water Saturated Sand ($h_b/h_i=2$), with Under Pressure behind the Blade

[Contents](#)
[Dr.ir. S.A. Miedema](#)
[Table 2.03: The shear angle \$\beta\$.](#)
[Table 2.18: The coefficient \$c_1\$.](#)
[Table 2.24: The coefficient \$c_2\$.](#)
[Table 2.12: The coefficient \$a_1\$.](#)
[Back to top](#)
Table 2.03: The shear angle β .

$h_b/h_i=2$	ϕ	32°	37°	42°	47°	52°
α	δ					
15°	15°	41.128	40.402	39.427	38.273	36.986
	18°	39.239	38.609	37.720	36.643	35.424
	21°	37.554	36.993	36.167	35.147	33.979
	24°	36.030	35.517	34.738	33.760	32.630
	27°	34.638	34.158	33.410	32.462	31.358
	30°	33.354	32.893	32.167	31.238	30.152
30°	15°	39.129	37.939	36.562	35.056	33.457
	18°	37.223	36.144	34.859	33.429	31.894
	21°	35.458	34.468	33.258	31.891	30.408
	24°	33.820	32.899	31.748	30.432	28.992
	27°	32.293	31.425	30.320	29.043	27.637
	30°	30.864	30.035	28.965	27.718	26.336
45°	15°	33.483	32.334	30.991	29.508	27.918
	18°	31.743	30.679	29.408	27.985	26.444
	21°	30.142	29.141	27.925	26.547	25.043
	24°	28.660	27.704	26.527	25.182	23.705

	27°	27.278	26.353	25.202	23.879	22.420
	30°	25.982	25.074	23.939	22.630	21.179
60°	15°	27.692	26.533	25.186	23.694	22.085
	18°	26.156	25.057	23.759	22.307	20.729
	21°	24.744	23.683	22.418	20.991	19.432
	24°	23.432	22.394	21.147	19.733	18.180
	27°	22.203	21.173	19.932	18.520	16.965
	30°	21.039	20.008	18.763	17.344	15.776

The shear angle β as a function of the blade angle α , the angle of internal friction ϕ , the soil/interface friction angle δ , for the non-cavitating cutting process.

[Back to top](#)

Table 2.18: The coefficient c_1 .

$h_b/h_i=2$	ϕ	32°	37°	42°	47°	52°
α	δ					
15°	15°	0.140	0.154	0.167	0.182	0.197
	18°	0.154	0.170	0.186	0.203	0.221
	21°	0.169	0.186	0.204	0.224	0.246
	24°	0.183	0.203	0.224	0.247	0.272
	27°	0.197	0.220	0.244	0.270	0.299
	30°	0.212	0.237	0.265	0.295	0.328
30°	15°	0.236	0.265	0.297	0.332	0.371
	18°	0.258	0.291	0.327	0.368	0.413
	21°	0.281	0.318	0.359	0.405	0.458
	24°	0.305	0.346	0.393	0.445	0.506
	27°	0.329	0.376	0.428	0.488	0.557
	30°	0.354	0.407	0.466	0.534	0.614
45°	15°	0.332	0.385	0.446	0.515	0.597
	18°	0.363	0.423	0.491	0.571	0.666
	21°	0.395	0.462	0.540	0.631	0.741

	24°	0.428	0.504	0.592	0.697	0.825
	27°	0.464	0.549	0.649	0.770	0.918
	30°	0.501	0.597	0.711	0.849	1.022
60°	15°	0.454	0.547	0.660	0.797	0.969
	18°	0.496	0.602	0.731	0.890	1.092
	21°	0.542	0.662	0.809	0.994	1.233
	24°	0.591	0.727	0.896	1.113	1.398
	27°	0.644	0.799	0.994	1.249	1.591
	30°	0.701	0.878	1.105	1.406	1.821

The dimensionless force c_1 , in the direction of the cutting velocity, as a function of the blade angle α , the angle of internal friction ϕ , the soil/interface friction angle δ , with under pressure behind the blade.

[Back to top](#)

Table 2.24: The coefficient c_2 .

$h_b/h_i=2$	ϕ	32°	37°	42°	47°	52°
α	δ					
15°	15°	0.243	0.266	0.290	0.315	0.342
	18°	0.238	0.261	0.286	0.312	0.340
	21°	0.232	0.256	0.282	0.309	0.338
	24°	0.226	0.250	0.277	0.305	0.336
	27°	0.219	0.244	0.271	0.300	0.332
	30°	0.212	0.238	0.265	0.295	0.328
30°	15°	0.202	0.231	0.263	0.298	0.337
	18°	0.194	0.223	0.256	0.292	0.333
	21°	0.184	0.215	0.248	0.285	0.327
	24°	0.174	0.205	0.238	0.277	0.320
	27°	0.163	0.193	0.228	0.267	0.311
	30°	0.150	0.181	0.215	0.255	0.300
45°	15°	0.142	0.173	0.208	0.249	0.296
	18°	0.128	0.159	0.194	0.235	0.283
	21°	0.112	0.142	0.177	0.218	0.267
	24°	0.093	0.123	0.157	0.197	0.247

	27°	0.073	0.101	0.134	0.173	0.222
	30°	0.050	0.076	0.107	0.145	0.191
60°	15°	0.065	0.090	0.121	0.159	0.206
	18°	0.039	0.062	0.091	0.125	0.169
	21°	0.011	0.030	0.055	0.085	0.124
	24°	-0.022	-0.007	0.012	0.036	0.067
	27°	-0.059	-0.050	-0.038	-0.024	-0.004
	30°	-0.101	-0.100	-0.098	-0.097	-0.095

The dimensionless force c_2 , perpendicular to the cutting velocity, as a function of the blade angle α , the angle of internal friction ϕ , the soil/interface friction angle δ , with under pressure behind the blade.

[Back to top](#)

Table 2.12: The coefficient a_1 .

$h_b/h_i=2$	ϕ	32°	37°	42°	47°	52°
α	δ					
15°	15°	0.538	0.533	0.528	0.522	0.516
	18°	0.533	0.528	0.523	0.517	0.511
	21°	0.528	0.523	0.518	0.512	0.506
	24°	0.523	0.519	0.513	0.507	0.501
	27°	0.519	0.514	0.509	0.503	0.496
	30°	0.514	0.51	0.504	0.498	0.491
30°	15°	0.544	0.539	0.533	0.527	0.521
	18°	0.54	0.535	0.529	0.523	0.517
	21°	0.535	0.531	0.525	0.519	0.513
	24°	0.531	0.526	0.521	0.515	0.509
	27°	0.527	0.522	0.517	0.511	0.505
	30°	0.523	0.519	0.513	0.507	0.501
45°	15°	0.562	0.557	0.552	0.547	0.542
	18°	0.559	0.554	0.549	0.544	0.539
	21°	0.556	0.551	0.547	0.541	0.536
	24°	0.553	0.549	0.544	0.538	0.533
	27°	0.55	0.546	0.541	0.536	0.53

	30°	0.548	0.543	0.538	0.533	0.526
60°	15°	0.577	0.572	0.565	0.558	0.551
	18°	0.573	0.567	0.561	0.554	0.546
	21°	0.569	0.563	0.557	0.549	0.542
	24°	0.565	0.559	0.552	0.545	0.537
	27°	0.561	0.555	0.548	0.54	0.532
	30°	0.557	0.551	0.544	0.536	0.527

The weigh factor a_1 , for the determination of the weighed average permeability k_m , as a function of the blade angle α , the angle of internal friction ϕ , the soil/interface friction angle δ , with under pressure behind the blade.

[Back to top](#)

This is a translation of the dissertation of Dr.ir. S.A. Miedema, dated September 15th 1987 .
The dissertation was originally published in Dutch by the:
Delft University of Technology
Faculty of Mechanical Engineering and Marine Technology
Chair of Dredging Technology
Mekelweg 2
2628 CD, Delft
The Netherlands

Last modified Wednesday May 24, 2000 by: [Sape A. Miedema](#)

Translation by: [Laurens de Jonge](#)

Figures, equations and tables by: [Erik Miedema](#)

Copyright © May, 2000 Dr.ir. S.A. Miedema



[Download Adobe Acrobat Reader V4.0](#)

[Back to top](#)**Table 2.18: The coefficient c_1 .**

$h_b/h_i=2$	ϕ	32°	37°	42°	47°	52°
α	δ					
15°	15°	0.140	0.154	0.167	0.182	0.197
	18°	0.154	0.170	0.186	0.203	0.221
	21°	0.169	0.186	0.204	0.224	0.246
	24°	0.183	0.203	0.224	0.247	0.272
	27°	0.197	0.220	0.244	0.270	0.299
	30°	0.212	0.237	0.265	0.295	0.328
30°	15°	0.236	0.265	0.297	0.332	0.371
	18°	0.258	0.291	0.327	0.368	0.413
	21°	0.281	0.318	0.359	0.405	0.458
	24°	0.305	0.346	0.393	0.445	0.506
	27°	0.329	0.376	0.428	0.488	0.557
	30°	0.354	0.407	0.466	0.534	0.614
45°	15°	0.332	0.385	0.446	0.515	0.597
	18°	0.363	0.423	0.491	0.571	0.666
	21°	0.395	0.462	0.540	0.631	0.741
	24°	0.428	0.504	0.592	0.697	0.825
	27°	0.464	0.549	0.649	0.770	0.918
	30°	0.501	0.597	0.711	0.849	1.022
60°	15°	0.454	0.547	0.660	0.797	0.969
	18°	0.496	0.602	0.731	0.890	1.092
	21°	0.542	0.662	0.809	0.994	1.233
	24°	0.591	0.727	0.896	1.113	1.398
	27°	0.644	0.799	0.994	1.249	1.591
	30°	0.701	0.878	1.105	1.406	1.821

The dimensionless force c_1 , in the direction of the cutting velocity, as a function of the blade angle α , the angle of internal friction ϕ , the soil/interface friction angle δ , with under pressure behind the blade.

[Back to top](#)**Table 2.24: The coefficient c_2 .**

$h_b/h_i=2$	ϕ	32°	37°	42°	47°	52°
α	δ					
15°	15°	0.243	0.266	0.290	0.315	0.342
	18°	0.238	0.261	0.286	0.312	0.340
	21°	0.232	0.256	0.282	0.309	0.338
	24°	0.226	0.250	0.277	0.305	0.336
	27°	0.219	0.244	0.271	0.300	0.332
	30°	0.212	0.238	0.265	0.295	0.328
30°	15°	0.202	0.231	0.263	0.298	0.337
	18°	0.194	0.223	0.256	0.292	0.333
	21°	0.184	0.215	0.248	0.285	0.327
	24°	0.174	0.205	0.238	0.277	0.320
	27°	0.163	0.193	0.228	0.267	0.311
	30°	0.150	0.181	0.215	0.255	0.300
45°	15°	0.142	0.173	0.208	0.249	0.296
	18°	0.128	0.159	0.194	0.235	0.283
	21°	0.112	0.142	0.177	0.218	0.267
	24°	0.093	0.123	0.157	0.197	0.247
	27°	0.073	0.101	0.134	0.173	0.222
	30°	0.050	0.076	0.107	0.145	0.191
60°	15°	0.065	0.090	0.121	0.159	0.206
	18°	0.039	0.062	0.091	0.125	0.169
	21°	0.011	0.030	0.055	0.085	0.124
	24°	-0.022	-0.007	0.012	0.036	0.067
	27°	-0.059	-0.050	-0.038	-0.024	-0.004
	30°	-0.101	-0.100	-0.098	-0.097	-0.095

The dimensionless force c_2 , perpendicular to the cutting velocity, as a function of the blade angle α , the angle of internal friction ϕ , the soil/interface friction angle δ , with under pressure behind the blade.

[Back to top](#)**Table 2.12: The coefficient a_1 .**

$h_b/h_i=2$	ϕ	32°	37°	42°	47°	52°
α	δ					
15°	15°	0.538	0.533	0.528	0.522	0.516
	18°	0.533	0.528	0.523	0.517	0.511
	21°	0.528	0.523	0.518	0.512	0.506
	24°	0.523	0.519	0.513	0.507	0.501
	27°	0.519	0.514	0.509	0.503	0.496
	30°	0.514	0.51	0.504	0.498	0.491
30°	15°	0.544	0.539	0.533	0.527	0.521
	18°	0.54	0.535	0.529	0.523	0.517
	21°	0.535	0.531	0.525	0.519	0.513
	24°	0.531	0.526	0.521	0.515	0.509
	27°	0.527	0.522	0.517	0.511	0.505
	30°	0.523	0.519	0.513	0.507	0.501
45°	15°	0.562	0.557	0.552	0.547	0.542
	18°	0.559	0.554	0.549	0.544	0.539
	21°	0.556	0.551	0.547	0.541	0.536
	24°	0.553	0.549	0.544	0.538	0.533
	27°	0.55	0.546	0.541	0.536	0.53
	30°	0.548	0.543	0.538	0.533	0.526
60°	15°	0.577	0.572	0.565	0.558	0.551
	18°	0.573	0.567	0.561	0.554	0.546
	21°	0.569	0.563	0.557	0.549	0.542
	24°	0.565	0.559	0.552	0.545	0.537
	27°	0.561	0.555	0.548	0.54	0.532
	30°	0.557	0.551	0.544	0.536	0.527

The weigh factor a_1 , for the determination of the weighed average permeability k_m , as a function of the blade angle α , the angle of internal friction ϕ , the soil/interface friction angle δ , with under pressure behind the blade.

Coefficients for the Non-Cavitating Cutting Process in Water Saturated Sand ($h_b/h_i=3$), with Under Pressure behind the Blade

[Contents](#)
[Dr.ir. S.A. Miedema](#)
[Table 2.04: The shear angle \$\beta\$.](#)
[Table 2.19: The coefficient \$c_1\$.](#)
[Table 2.25: The coefficient \$c_2\$.](#)
[Table 2.13: The coefficient \$a_1\$.](#)
[Back to top](#)
Table 2.04: The shear angle β .

$h_b/h_i=3$	ϕ	32°	37°	42°	47°	52°
α	δ					
15°	15°	42.346	41.502	40.418	39.164	37.786
	18°	40.414	39.674	38.681	37.507	36.198
	21°	38.673	38.010	37.086	35.973	34.718
	24°	37.087	36.481	35.609	34.542	33.328
	27°	35.631	35.064	34.230	33.197	32.013
	30°	34.283	33.742	32.934	31.926	30.763
30°	15°	40.176	38.793	37.257	35.619	33.909
	18°	38.242	36.978	35.537	33.977	32.331
	21°	36.421	35.258	33.900	32.407	30.817
	24°	34.711	33.631	32.341	30.906	29.364
	27°	33.103	32.090	30.858	29.470	27.968
	30°	31.590	30.631	29.444	28.095	26.625
45°	15°	35.406	33.895	32.248	30.509	28.703
	18°	33.548	32.142	30.578	28.907	27.156
	21°	31.788	30.472	28.981	27.368	25.665
	24°	30.126	28.885	27.455	25.891	24.230

	27°	28.557	27.376	25.996	24.474	22.845
	30°	27.075	25.941	24.600	23.111	21.509
60°	15°	28.252	26.972	25.516	23.930	22.241
	18°	26.613	25.406	24.010	22.472	20.823
	21°	25.094	23.940	22.588	21.086	19.464
	24°	23.677	22.560	21.238	19.760	18.156
	27°	22.348	21.253	19.950	18.485	16.890
	30°	21.092	20.008	18.713	17.254	15.600

The shear angle β as a function of the blade angle α , the angle of internal friction ϕ , the soil/interface friction angle δ , for the non-cavitating cutting process.

[Back to top](#)

Table 2.19: The coefficient c_1 .

$h_b/h_i=3$	ϕ	32°	37°	42°	47°	52°
α	δ					
15°	15°	0.140	0.153	0.167	0.182	0.198
	18°	0.154	0.170	0.186	0.203	0.222
	21°	0.169	0.186	0.205	0.225	0.247
	24°	0.183	0.203	0.225	0.248	0.273
	27°	0.198	0.221	0.245	0.272	0.301
	30°	0.213	0.239	0.267	0.297	0.331
30°	15°	0.236	0.265	0.298	0.333	0.373
	18°	0.259	0.292	0.329	0.370	0.416
	21°	0.283	0.320	0.362	0.409	0.462
	24°	0.307	0.349	0.397	0.450	0.511
	27°	0.332	0.380	0.433	0.494	0.564
	30°	0.358	0.412	0.472	0.541	0.622
45°	15°	0.344	0.400	0.463	0.536	0.622
	18°	0.379	0.441	0.513	0.598	0.697
	21°	0.415	0.485	0.567	0.664	0.780
	24°	0.453	0.532	0.626	0.737	0.872

	27°	0.493	0.583	0.689	0.817	0.974
	30°	0.535	0.637	0.758	0.905	1.089
60°	15°	0.488	0.587	0.705	0.851	1.032
	18°	0.537	0.650	0.786	0.955	1.169
	21°	0.590	0.718	0.875	1.072	1.327
	24°	0.647	0.793	0.974	1.205	1.509
	27°	0.709	0.875	1.085	1.358	1.724
	30°	0.776	0.966	1.211	1.535	1.980

The dimensionless force c_1 , in the direction of the cutting velocity, as a function of the blade angle α , the angle of internal friction ϕ , the soil/interface friction angle δ , with under pressure behind the blade.

[Back to top](#)

Table 2.25: The coefficient c_2 .

$h_b/h_i=3$	ϕ	32°	37°	42°	47°	52°
α	δ					
15°	15°	0.243	0.266	0.290	0.315	0.343
	18°	0.238	0.262	0.286	0.313	0.342
	21°	0.233	0.257	0.282	0.310	0.340
	24°	0.227	0.251	0.278	0.306	0.338
	27°	0.22	0.246	0.273	0.302	0.335
	30°	0.214	0.239	0.267	0.297	0.331
30°	15°	0.202	0.231	0.263	0.299	0.338
	18°	0.194	0.224	0.257	0.294	0.335
	21°	0.185	0.216	0.249	0.287	0.330
	24°	0.175	0.206	0.240	0.279	0.323
	27°	0.164	0.195	0.229	0.268	0.314
	30°	0.151	0.182	0.217	0.256	0.303
45°	15°	0.145	0.176	0.213	0.254	0.303
	18°	0.130	0.161	0.197	0.240	0.290
	21°	0.112	0.143	0.179	0.222	0.272
	24°	0.093	0.123	0.158	0.200	0.251

	27°	0.070	0.099	0.133	0.174	0.224
	30°	0.045	0.072	0.103	0.142	0.190
60°	15°	0.060	0.086	0.118	0.157	0.205
	18°	0.030	0.054	0.083	0.119	0.164
	21°	-0.003	0.017	0.042	0.073	0.113
	24°	-0.041	-0.026	-0.007	0.018	0.050
	27°	-0.084	-0.076	-0.065	-0.050	-0.031
	30°	-0.134	-0.134	-0.134	-0.134	-0.134

The dimensionless force c_2 , perpendicular to the cutting velocity, as a function of the blade angle α , the angle of internal friction ϕ , the soil/interface friction angle δ , with under pressure behind the blade.

[Back to top](#)

Table 2.13: The coefficient a_1 .

$h_b/h_i=3$	ϕ	32°	37°	42°	47°	52°
α	δ					
15°	15°	0.540	0.535	0.530	0.524	0.518
	18°	0.535	0.530	0.525	0.519	0.513
	21°	0.531	0.526	0.520	0.515	0.508
	24°	0.526	0.521	0.516	0.510	0.503
	27°	0.522	0.517	0.511	0.505	0.498
	30°	0.518	0.513	0.507	0.501	0.494
30°	15°	0.552	0.546	0.539	0.533	0.526
	18°	0.548	0.542	0.535	0.529	0.522
	21°	0.543	0.537	0.531	0.525	0.518
	24°	0.539	0.533	0.527	0.521	0.514
	27°	0.535	0.529	0.523	0.517	0.510
	30°	0.531	0.525	0.519	0.513	0.506
45°	15°	0.563	0.558	0.553	0.548	0.543
	18°	0.560	0.556	0.551	0.546	0.541
	21°	0.558	0.553	0.548	0.543	0.538

	24°	0.555	0.551	0.546	0.541	0.535
	27°	0.553	0.548	0.543	0.538	0.533
	30°	0.550	0.546	0.541	0.536	0.530
60°	15°	0.584	0.579	0.574	0.568	0.562
	18°	0.581	0.576	0.571	0.565	0.559
	21°	0.578	0.573	0.568	0.562	0.556
	24°	0.575	0.570	0.565	0.559	0.552
	27°	0.572	0.567	0.562	0.555	0.549
	30°	0.569	0.564	0.559	0.552	0.545

The weigh factor a_1 , for the determination of the weighed average permeability k_m , as a function of the blade angle α , the angle of internal friction ϕ , the soil/interface friction angle δ , with under pressure behind the blade.

[Back to top](#)

This is a translation of the dissertation of Dr.ir. S.A. Miedema, dated September 15th 1987 .

The dissertation was originally published in Dutch by the:

Delft University of Technology

Faculty of Mechanical Engineering and Marine Technology

Chair of Dredging Technology

Mekelweg 2

2628 CD, Delft

The Netherlands

Last modified Wednesday May 24, 2000 by: [Sape A. Miedema](#)

Translation by: [Laurens de Jonge](#)

Figures, equations and tables by: [Erik Miedema](#)

Copyright © May, 2000 Dr.ir. S.A. Miedema



[Download Adobe Acrobat Reader V4.0](#)

[Back to top](#)**Table 2.19: The coefficient c_1 .**

$h_b/h_i=3$	ϕ	32°	37°	42°	47°	52°
α	δ					
15°	15°	0.140	0.153	0.167	0.182	0.198
	18°	0.154	0.170	0.186	0.203	0.222
	21°	0.169	0.186	0.205	0.225	0.247
	24°	0.183	0.203	0.225	0.248	0.273
	27°	0.198	0.221	0.245	0.272	0.301
	30°	0.213	0.239	0.267	0.297	0.331
30°	15°	0.236	0.265	0.298	0.333	0.373
	18°	0.259	0.292	0.329	0.370	0.416
	21°	0.283	0.320	0.362	0.409	0.462
	24°	0.307	0.349	0.397	0.450	0.511
	27°	0.332	0.380	0.433	0.494	0.564
	30°	0.358	0.412	0.472	0.541	0.622
45°	15°	0.344	0.400	0.463	0.536	0.622
	18°	0.379	0.441	0.513	0.598	0.697
	21°	0.415	0.485	0.567	0.664	0.780
	24°	0.453	0.532	0.626	0.737	0.872
	27°	0.493	0.583	0.689	0.817	0.974
	30°	0.535	0.637	0.758	0.905	1.089
60°	15°	0.488	0.587	0.705	0.851	1.032
	18°	0.537	0.650	0.786	0.955	1.169
	21°	0.590	0.718	0.875	1.072	1.327
	24°	0.647	0.793	0.974	1.205	1.509
	27°	0.709	0.875	1.085	1.358	1.724
	30°	0.776	0.966	1.211	1.535	1.980

The dimensionless force c_1 , in the direction of the cutting velocity, as a function of the blade angle α , the angle of internal friction ϕ , the soil/interface friction angle δ , with under pressure behind the blade.

[Back to top](#)**Table 2.25: The coefficient c_2 .**

$h_b/h_i=3$	ϕ	32°	37°	42°	47°	52°
α	δ					
15°	15°	0.243	0.266	0.290	0.315	0.343
	18°	0.238	0.262	0.286	0.313	0.342
	21°	0.233	0.257	0.282	0.310	0.340
	24°	0.227	0.251	0.278	0.306	0.338
	27°	0.22	0.246	0.273	0.302	0.335
	30°	0.214	0.239	0.267	0.297	0.331
30°	15°	0.202	0.231	0.263	0.299	0.338
	18°	0.194	0.224	0.257	0.294	0.335
	21°	0.185	0.216	0.249	0.287	0.330
	24°	0.175	0.206	0.240	0.279	0.323
	27°	0.164	0.195	0.229	0.268	0.314
	30°	0.151	0.182	0.217	0.256	0.303
45°	15°	0.145	0.176	0.213	0.254	0.303
	18°	0.130	0.161	0.197	0.240	0.290
	21°	0.112	0.143	0.179	0.222	0.272
	24°	0.093	0.123	0.158	0.200	0.251
	27°	0.070	0.099	0.133	0.174	0.224
	30°	0.045	0.072	0.103	0.142	0.190
60°	15°	0.060	0.086	0.118	0.157	0.205
	18°	0.030	0.054	0.083	0.119	0.164
	21°	-0.003	0.017	0.042	0.073	0.113
	24°	-0.041	-0.026	-0.007	0.018	0.050
	27°	-0.084	-0.076	-0.065	-0.050	-0.031
	30°	-0.134	-0.134	-0.134	-0.134	-0.134

The dimensionless force c_2 , perpendicular to the cutting velocity, as a function of the blade angle α , the angle of internal friction ϕ , the soil/interface friction angle δ , with under pressure behind the blade.

[Back to top](#)**Table 2.13: The coefficient a_1 .**

$h_b/h_i=3$	ϕ	32°	37°	42°	47°	52°
α	δ					
15°	15°	0.540	0.535	0.530	0.524	0.518
	18°	0.535	0.530	0.525	0.519	0.513
	21°	0.531	0.526	0.520	0.515	0.508
	24°	0.526	0.521	0.516	0.510	0.503
	27°	0.522	0.517	0.511	0.505	0.498
	30°	0.518	0.513	0.507	0.501	0.494
30°	15°	0.552	0.546	0.539	0.533	0.526
	18°	0.548	0.542	0.535	0.529	0.522
	21°	0.543	0.537	0.531	0.525	0.518
	24°	0.539	0.533	0.527	0.521	0.514
	27°	0.535	0.529	0.523	0.517	0.510
	30°	0.531	0.525	0.519	0.513	0.506
45°	15°	0.563	0.558	0.553	0.548	0.543
	18°	0.560	0.556	0.551	0.546	0.541
	21°	0.558	0.553	0.548	0.543	0.538
	24°	0.555	0.551	0.546	0.541	0.535
	27°	0.553	0.548	0.543	0.538	0.533
	30°	0.550	0.546	0.541	0.536	0.530
60°	15°	0.584	0.579	0.574	0.568	0.562
	18°	0.581	0.576	0.571	0.565	0.559
	21°	0.578	0.573	0.568	0.562	0.556
	24°	0.575	0.570	0.565	0.559	0.552
	27°	0.572	0.567	0.562	0.555	0.549
	30°	0.569	0.564	0.559	0.552	0.545

The weigh factor a_1 , for the determination of the weighed average permeability k_m , as a function of the blade angle α , the angle of internal friction ϕ , the soil/interface friction angle δ , with under

pressure behind the blade.

Coefficients for the Cavitating Cutting Process in Water Saturated Sand ($h_b/h_i=1$)

[Contents](#)
[Dr.ir. S.A. Miedema](#)
[Table 2.05: The shear angle \$\beta\$.](#)
[Table 2.29: The coefficient \$d_1\$.](#)
[Table 2.35: The coefficient \$d_2\$.](#)
[Back to top](#)
Table 2.05: The shear angle β .

$h_b/h_i=1$	ϕ	32°	37°	42°	47°	52°
α	δ					
15°	15°	37.217	37.520	37.355	36.831	36.026
	18°	34.461	34.854	34.790	34.370	33.669
	21°	32.163	32.598	32.594	32.243	31.613
	24°	30.212	30.661	30.689	30.379	29.796
	27°	28.530	28.973	29.012	28.726	28.173
	30°	27.060	27.483	27.520	27.243	26.707
30°	15°	39.766	39.060	38.014	36.718	35.232
	18°	37.341	36.757	35.823	34.628	33.233
	21°	35.196	34.696	33.844	32.725	31.399
	24°	33.280	32.837	32.041	30.977	29.704
	27°	31.554	31.145	30.387	29.363	28.127
	30°	29.985	29.593	28.859	27.860	26.650
45°	15°	36.853	35.599	34.097	32.412	30.591
	18°	34.768	33.616	32.202	30.594	28.839
	21°	32.866	31.789	30.441	28.892	27.188
	24°	31.119	30.094	28.794	27.288	25.623
	27°	29.502	28.512	27.246	25.770	24.132
	30°	27.996	27.026	25.781	24.325	22.705

60°	15°	31.992	30.395	28.608	26.683	24.654
	18°	30.155	28.634	26.911	25.039	23.055
	21°	28.444	26.979	25.303	23.471	21.520
	24°	26.841	25.414	23.772	21.968	20.040
	27°	25.330	23.927	22.306	20.520	18.605
	30°	23.897	22.506	20.896	19.118	17.208

The shear angle β as a function of the blade angle α , the angle of internal friction ϕ , the soil/interface friction angle δ , for the cavitating cutting process.

[Back to top](#)

Table 2.29: The coefficient d_1 .

$h_b/h_i=1$	ϕ	32°	37°	42°	47°	52°
α	δ					
15°	15°	2.390	2.505	2.625	2.753	2.890
	18°	2.626	2.766	2.913	3.069	3.238
	21°	2.860	3.028	3.205	3.393	3.597
	24°	3.092	3.291	3.501	3.726	3.970
	27°	3.324	3.557	3.803	4.068	4.358
	30°	3.556	3.826	4.112	4.423	4.764
30°	15°	1.726	1.893	2.079	2.286	2.520
	18°	1.901	2.095	2.311	2.553	2.829
	21°	2.079	2.303	2.553	2.835	3.158
	24°	2.261	2.518	2.806	3.133	3.511
	27°	2.448	2.742	3.072	3.450	3.890
	30°	2.641	2.975	3.353	3.789	4.301
45°	15°	1.719	1.989	2.300	2.665	3.100
	18°	1.898	2.205	2.562	2.985	3.492
	21°	2.084	2.433	2.843	3.332	3.925
	24°	2.280	2.677	3.146	3.711	4.405
	27°	2.486	2.936	3.474	4.129	4.942

	30°	2.705	3.216	3.833	4.592	5.549
60°	15°	2.052	2.504	3.056	3.744	4.618
	18°	2.273	2.788	3.425	4.228	5.264
	21°	2.510	3.099	3.835	4.776	6.011
	24°	2.766	3.440	4.294	5.402	6.884
	27°	3.046	3.819	4.812	6.125	7.919
	30°	3.353	4.243	5.405	6.972	9.165

The dimensionless force d_1 , in the direction of the cutting velocity, as a function of the blade angle α , the angle of internal friction ϕ , the soil/interface friction angle δ , with under pressure behind the blade.

[Back to top](#)

Table 2.35: The coefficient d_2 .

$h_b/h_i=1$	ϕ	32°	37°	42°	47°	52°
α	δ					
15°	15°	4.143	4.342	4.550	4.771	5.008
	18°	4.046	4.262	4.488	4.729	4.989
	21°	3.939	4.170	4.414	4.673	4.954
	24°	3.821	4.067	4.326	4.604	4.906
	27°	3.694	3.953	4.227	4.522	4.844
	30°	3.559	3.829	4.116	4.426	4.768
30°	15°	1.375	1.543	1.729	1.936	2.171
	18°	1.313	1.489	1.683	1.901	2.150
	21°	1.242	1.424	1.626	1.855	2.117
	24°	1.162	1.349	1.558	1.796	2.070
	27°	1.072	1.262	1.477	1.723	2.009
	30°	0.972	1.165	1.384	1.636	1.932
45°	15°	0.698	0.854	1.034	1.245	1.496
	18°	0.625	0.782	0.964	1.180	1.439
	21°	0.541	0.697	0.880	1.098	1.362

	24°	0.446	0.598	0.779	0.996	1.263
	27°	0.337	0.484	0.659	0.872	1.137
	30°	0.214	0.352	0.517	0.721	0.978
60°	15°	0.296	0.417	0.565	0.750	0.985
	18°	0.183	0.293	0.429	0.600	0.821
	21°	0.053	0.147	0.264	0.414	0.610
	24°	-0.097	-0.026	0.064	0.181	0.338
	27°	-0.272	-0.231	-0.178	-0.108	-0.013
	30°	-0.474	-0.474	-0.473	-0.472	-0.470

The dimensionless force d_2 , perpendicular to the cutting velocity, as a function of the blade angle α , the angle of internal friction ϕ , the soil/interface friction angle δ , with under pressure behind the blade.

[Back to top](#)

This is a translation of the dissertation of Dr.ir. S.A. Miedema, dated September 15th 1987 .

The dissertation was originally published in Dutch by the:

Delft University of Technology

Faculty of Mechanical Engineering and Marine Technology

Chair of Dredging Technology

Mekelweg 2

2628 CD, Delft

The Netherlands

Last modified Wednesday May 24, 2000 by: [Sape A. Miedema](#)

Translation by: [Laurens de Jonge](#)

Figures, equations and tables by: [Erik Miedema](#)

Copyright © May, 2000 Dr.ir. S.A. Miedema



[Download Adobe Acrobat Reader V4.0](#)

[Back to top](#)**Table 2.29: The coefficient d_1 .**

$h_b/h_i=1$	ϕ	32°	37°	42°	47°	52°
α	δ					
15°	15°	2.390	2.505	2.625	2.753	2.890
	18°	2.626	2.766	2.913	3.069	3.238
	21°	2.860	3.028	3.205	3.393	3.597
	24°	3.092	3.291	3.501	3.726	3.970
	27°	3.324	3.557	3.803	4.068	4.358
	30°	3.556	3.826	4.112	4.423	4.764
30°	15°	1.726	1.893	2.079	2.286	2.520
	18°	1.901	2.095	2.311	2.553	2.829
	21°	2.079	2.303	2.553	2.835	3.158
	24°	2.261	2.518	2.806	3.133	3.511
	27°	2.448	2.742	3.072	3.450	3.890
	30°	2.641	2.975	3.353	3.789	4.301
45°	15°	1.719	1.989	2.300	2.665	3.100
	18°	1.898	2.205	2.562	2.985	3.492
	21°	2.084	2.433	2.843	3.332	3.925
	24°	2.280	2.677	3.146	3.711	4.405
	27°	2.486	2.936	3.474	4.129	4.942
	30°	2.705	3.216	3.833	4.592	5.549
60°	15°	2.052	2.504	3.056	3.744	4.618
	18°	2.273	2.788	3.425	4.228	5.264
	21°	2.510	3.099	3.835	4.776	6.011
	24°	2.766	3.440	4.294	5.402	6.884
	27°	3.046	3.819	4.812	6.125	7.919
	30°	3.353	4.243	5.405	6.972	9.165

The dimensionless force d_1 , in the direction of the cutting velocity, as a

function of the blade angle α , the angle of internal friction ϕ , the soil/interface friction angle δ , with under pressure behind the blade.

[Back to top](#)**Table 2.35: The coefficient d_2 .**

$h_b/h_i=1$	ϕ	32°	37°	42°	47°	52°
α	δ					
15°	15°	4.143	4.342	4.550	4.771	5.008
	18°	4.046	4.262	4.488	4.729	4.989
	21°	3.939	4.170	4.414	4.673	4.954
	24°	3.821	4.067	4.326	4.604	4.906
	27°	3.694	3.953	4.227	4.522	4.844
	30°	3.559	3.829	4.116	4.426	4.768
30°	15°	1.375	1.543	1.729	1.936	2.171
	18°	1.313	1.489	1.683	1.901	2.150
	21°	1.242	1.424	1.626	1.855	2.117
	24°	1.162	1.349	1.558	1.796	2.070
	27°	1.072	1.262	1.477	1.723	2.009
	30°	0.972	1.165	1.384	1.636	1.932
45°	15°	0.698	0.854	1.034	1.245	1.496
	18°	0.625	0.782	0.964	1.180	1.439
	21°	0.541	0.697	0.880	1.098	1.362
	24°	0.446	0.598	0.779	0.996	1.263
	27°	0.337	0.484	0.659	0.872	1.137
	30°	0.214	0.352	0.517	0.721	0.978
60°	15°	0.296	0.417	0.565	0.750	0.985
	18°	0.183	0.293	0.429	0.600	0.821
	21°	0.053	0.147	0.264	0.414	0.610
	24°	-0.097	-0.026	0.064	0.181	0.338
	27°	-0.272	-0.231	-0.178	-0.108	-0.013
	30°	-0.474	-0.474	-0.473	-0.472	-0.470

The dimensionless force d_2 , perpendicular to the cutting velocity, as a function

of the blade angle α , the angle of internal friction ϕ , the soil/interface friction angle δ , with under pressure behind the blade.

Coefficients for the Cavitating Cutting Process in Water Saturated Sand ($h_b/h_i=2$)

[Contents](#)
[Dr.ir. S.A. Miedema](#)
[Table 2.06: The shear angle \$\beta\$.](#)
[Table 2.30: The coefficient \$d_1\$.](#)
[Table 2.36: The coefficient \$d_2\$.](#)
[Back to top](#)
Table 2.06: The shear angle β .

$h_b/h_i=2$	ϕ	32°	37°	42°	47°	52°
α	δ					
15°	15°	28.724	29.560	29.957	29.994	29.733
	18°	26.332	27.162	27.586	27.670	27.472
	21°	24.420	25.221	25.643	25.747	25.582
	24°	22.849	23.608	24.014	24.120	23.968
	27°	21.528	22.240	22.621	22.716	22.566
	30°	20.396	21.059	21.407	21.485	21.329
30°	15°	33.398	33.367	32.937	32.198	31.215
	18°	30.972	31.019	30.677	30.027	29.134
	21°	28.922	29.011	28.721	28.131	27.299
	24°	27.161	27.265	27.004	26.451	25.659
	27°	25.622	25.725	25.476	24.944	24.177
	30°	24.259	24.349	24.101	23.576	22.823
45°	15°	32.378	31.721	30.741	29.516	28.100
	18°	30.207	29.642	28.751	27.610	26.271
	21°	28.308	27.801	26.970	25.887	24.605
	24°	26.624	26.149	25.357	24.314	23.070
	27°	25.110	24.652	23.881	22.862	21.643
	30°	23.736	23.280	22.518	21.512	20.306

60°	15°	28.906	27.806	26.445	24.886	23.174
	18°	26.993	25.974	24.686	23.194	21.540
	21°	25.276	24.309	23.072	21.626	20.014
	24°	23.716	22.781	21.576	20.159	18.574
	27°	22.283	21.364	20.176	18.776	17.204
	30°	20.955	20.038	18.855	17.461	15.892

The shear angle β as a function of the blade angle α , the angle of internal friction ϕ , the soil/interface friction angle δ , for the cavitating cutting process.

[Back to top](#)

Table 2.30: The coefficient d_1 .

$h_b/h_i=2$	ϕ	32°	37°	42°	47°	52°
α	δ					
15°	15°	4.295	4.460	4.627	4.801	4.984
	18°	4.683	4.889	5.098	5.315	5.545
	21°	5.062	5.313	5.569	5.836	6.119
	24°	5.435	5.735	6.042	6.364	6.707
	27°	5.803	6.156	6.520	6.903	7.313
	30°	6.169	6.579	7.005	7.455	7.941
30°	15°	2.769	2.974	3.196	3.440	3.714
	18°	3.037	3.279	3.543	3.834	4.162
	21°	3.307	3.590	3.900	4.244	4.633
	24°	3.579	3.908	4.270	4.674	5.133
	27°	3.855	4.235	4.654	5.125	5.665
	30°	4.137	4.572	5.055	5.603	6.235
45°	15°	2.437	2.743	3.093	3.499	3.978
	18°	2.693	3.047	3.455	3.931	4.497
	21°	2.957	3.366	3.838	4.395	5.063
	24°	3.231	3.700	4.247	4.897	5.684
	27°	3.517	4.054	4.685	5.443	6.373

	30°	3.817	4.431	5.159	6.043	7.141
60°	15°	2.616	3.111	3.711	4.451	5.385
	18°	2.914	3.485	4.184	5.056	6.173
	21°	3.230	3.889	4.704	5.734	7.075
	24°	3.568	4.329	5.280	6.501	8.118
	27°	3.933	4.811	5.924	7.378	9.342
	30°	4.329	5.345	6.653	8.394	10.800

The dimensionless force d_1 , in the direction of the cutting velocity, as a function of the blade angle α , the angle of internal friction ϕ , the soil/interface friction angle δ , with under pressure behind the blade.

[Back to top](#)

Table 2.36: The coefficient d_2 .

$h_b/h_i=2$	ϕ	32°	37°	42°	47°	52°
α	δ					
15°	15°	7.444	7.730	8.020	8.321	8.638
	18°	7.215	7.532	7.855	8.190	8.544
	21°	6.972	7.317	7.670	8.038	8.427
	24°	6.716	7.087	7.467	7.865	8.288
	27°	6.450	6.842	7.247	7.672	8.128
	30°	6.174	6.584	7.010	7.461	7.947
30°	15°	2.068	2.273	2.495	2.740	3.014
	18°	1.938	2.156	2.394	2.657	2.951
	21°	1.794	2.024	2.275	2.554	2.870
	24°	1.637	1.876	2.139	2.433	2.767
	27°	1.467	1.713	1.986	2.292	2.643
	30°	1.283	1.534	1.813	2.130	2.495
45°	15°	0.817	0.994	1.196	1.431	1.708
	18°	0.687	0.868	1.076	1.319	1.608
	21°	0.542	0.724	0.935	1.183	1.481

	24°	0.380	0.561	0.771	1.021	1.324
	27°	0.200	0.375	0.581	0.827	1.130
	30°	0.001	0.166	0.361	0.599	0.894
60°	15°	0.191	0.324	0.485	0.684	0.935
	18°	0.018	0.140	0.289	0.475	0.714
	21°	-0.179	-0.074	0.056	0.220	0.433
	24°	-0.403	-0.322	-0.222	-0.092	0.079
	27°	-0.659	-0.612	-0.553	-0.475	-0.371
	30°	-0.951	-0.950	-0.949	-0.948	-0.946

The dimensionless force d_2 , perpendicular to the cutting velocity, as a function of the blade angle α , the angle of internal friction ϕ , the soil/interface friction angle δ , with under pressure behind the blade.

[Back to top](#)

This is a translation of the dissertation of Dr.ir. S.A. Miedema, dated September 15th 1987 .

The dissertation was originally published in Dutch by the:

Delft University of Technology

Faculty of Mechanical Engineering and Marine Technology

Chair of Dredging Technology

Mekelweg 2

2628 CD, Delft

The Netherlands

Last modified Wednesday May 24, 2000 by: [Sape A. Miedema](#)

Translation by: [Laurens de Jonge](#)

Figures, equations and tables by: [Erik Miedema](#)

Copyright © May, 2000 Dr.ir. S.A. Miedema



[Download Adobe Acrobat Reader V4.0](#)

[Back to top](#)**Table 2.30: The coefficient d_1 .**

$h_b/h_i=2$	ϕ	32°	37°	42°	47°	52°
α	δ					
15°	15°	4.295	4.460	4.627	4.801	4.984
	18°	4.683	4.889	5.098	5.315	5.545
	21°	5.062	5.313	5.569	5.836	6.119
	24°	5.435	5.735	6.042	6.364	6.707
	27°	5.803	6.156	6.520	6.903	7.313
	30°	6.169	6.579	7.005	7.455	7.941
30°	15°	2.769	2.974	3.196	3.440	3.714
	18°	3.037	3.279	3.543	3.834	4.162
	21°	3.307	3.590	3.900	4.244	4.633
	24°	3.579	3.908	4.270	4.674	5.133
	27°	3.855	4.235	4.654	5.125	5.665
	30°	4.137	4.572	5.055	5.603	6.235
45°	15°	2.437	2.743	3.093	3.499	3.978
	18°	2.693	3.047	3.455	3.931	4.497
	21°	2.957	3.366	3.838	4.395	5.063
	24°	3.231	3.700	4.247	4.897	5.684
	27°	3.517	4.054	4.685	5.443	6.373
	30°	3.817	4.431	5.159	6.043	7.141
60°	15°	2.616	3.111	3.711	4.451	5.385
	18°	2.914	3.485	4.184	5.056	6.173
	21°	3.230	3.889	4.704	5.734	7.075
	24°	3.568	4.329	5.280	6.501	8.118
	27°	3.933	4.811	5.924	7.378	9.342
	30°	4.329	5.345	6.653	8.394	10.800

The dimensionless force d_1 , in the direction of the cutting velocity, as a

function of the blade angle α , the angle of internal friction ϕ , the soil/interface friction angle δ , with under pressure behind the blade.

[Back to top](#)**Table 2.36: The coefficient d_2 .**

$h_b/h_i=2$	ϕ	32°	37°	42°	47°	52°
α	δ					
15°	15°	7.444	7.730	8.020	8.321	8.638
	18°	7.215	7.532	7.855	8.190	8.544
	21°	6.972	7.317	7.670	8.038	8.427
	24°	6.716	7.087	7.467	7.865	8.288
	27°	6.450	6.842	7.247	7.672	8.128
	30°	6.174	6.584	7.010	7.461	7.947
30°	15°	2.068	2.273	2.495	2.740	3.014
	18°	1.938	2.156	2.394	2.657	2.951
	21°	1.794	2.024	2.275	2.554	2.870
	24°	1.637	1.876	2.139	2.433	2.767
	27°	1.467	1.713	1.986	2.292	2.643
	30°	1.283	1.534	1.813	2.130	2.495
45°	15°	0.817	0.994	1.196	1.431	1.708
	18°	0.687	0.868	1.076	1.319	1.608
	21°	0.542	0.724	0.935	1.183	1.481
	24°	0.380	0.561	0.771	1.021	1.324
	27°	0.200	0.375	0.581	0.827	1.130
	30°	0.001	0.166	0.361	0.599	0.894
60°	15°	0.191	0.324	0.485	0.684	0.935
	18°	0.018	0.140	0.289	0.475	0.714
	21°	-0.179	-0.074	0.056	0.220	0.433
	24°	-0.403	-0.322	-0.222	-0.092	0.079
	27°	-0.659	-0.612	-0.553	-0.475	-0.371
	30°	-0.951	-0.950	-0.949	-0.948	-0.946

The dimensionless force d_2 , perpendicular to the cutting velocity, as a function

of the blade angle α , the angle of internal friction ϕ , the soil/interface friction angle δ , with under pressure behind the blade.

Coefficients for the Cavitating Cutting Process in Water Saturated Sand ($h_b/h_i=3$)

[Contents](#)
[Dr.ir. S.A. Miedema](#)
[Table 2.07: The shear angle \$\beta\$.](#)
[Table 2.31: The coefficient \$d_1\$.](#)
[Table 2.37: The coefficient \$d_2\$.](#)
[Back to top](#)
Table 2.07: The shear angle β .

$h_b/h_i=3$	ϕ	32°	37°	42°	47°	52°
α	δ					
15°	15°	24.046	25.019	25.609	25.872	25.856
	18°	21.976	22.900	23.476	23.751	23.765
	21°	20.350	21.217	21.763	22.030	22.053
	24°	19.031	19.838	20.348	20.596	20.615
	27°	17.932	18.680	19.150	19.374	19.381
	30°	16.996	17.687	18.117	18.313	18.303
30°	15°	29.286	29.575	29.466	29.038	28.353
	18°	26.992	27.319	27.267	26.908	26.297
	21°	25.100	25.435	25.410	25.090	24.525
	24°	23.504	23.828	23.811	23.511	22.973
	27°	22.130	22.433	22.410	22.116	21.592
	30°	20.928	21.202	21.165	20.867	20.346
45°	15°	29.236	28.919	28.257	27.325	26.179
	18°	27.101	26.853	26.266	25.411	24.339
	21°	25.277	25.065	24.524	23.719	22.699
	24°	23.690	23.493	22.977	22.203	21.215
	27°	22.288	22.091	21.584	20.825	19.857
	30°	21.031	20.823	20.315	19.561	18.600

60°	15°	26.619	25.832	24.754	23.450	21.967
	18°	24.711	23.995	22.987	21.750	20.329
	21°	23.037	22.362	21.398	20.206	18.826
	24°	21.543	20.889	19.951	18.785	17.431
	27°	20.193	19.545	18.617	17.464	16.121
	30°	18.958	18.303	17.374	16.222	14.880

The shear angle β as a function of the blade angle α , the angle of internal friction ϕ , the soil/interface friction angle δ , for the cavitating cutting process.

[Back to top](#)

Table 2.31: The coefficient d_1 .

$h_b/h_i=3$	ϕ	32°	37°	42°	47°	52°
α	δ					
15°	15°	6.145	6.362	6.578	6.799	7.028
	18°	6.672	6.945	7.218	7.497	7.789
	21°	7.185	7.519	7.855	8.200	8.562
	24°	7.687	8.087	8.492	8.910	9.351
	27°	8.180	8.652	9.132	9.631	10.159
	30°	8.667	9.216	9.778	10.366	10.993
30°	15°	3.775	4.017	4.277	4.559	4.872
	18°	4.127	4.417	4.729	5.070	5.449
	21°	4.479	4.822	5.192	5.598	6.052
	24°	4.832	5.233	5.667	6.147	6.687
	27°	5.188	5.653	6.159	6.722	7.359
	30°	5.551	6.084	6.670	7.326	8.075
45°	15°	3.123	3.467	3.855	4.302	4.826
	18°	3.450	3.852	4.309	4.838	5.463
	21°	3.784	4.251	4.786	5.410	6.152
	24°	4.128	4.669	5.291	6.024	6.904
	27°	4.486	5.107	5.830	6.689	7.732

	30°	4.859	5.572	6.409	7.414	8.650
60°	15°	3.152	3.691	4.338	5.131	6.126
	18°	3.520	4.147	4.907	5.849	7.047
	21°	3.907	4.637	5.529	6.648	8.092
	24°	4.319	5.165	6.212	7.545	9.294
	27°	4.760	5.742	6.973	8.564	10.695
	30°	5.237	6.377	7.827	9.738	12.353

The dimensionless force d_1 , in the direction of the cutting velocity, as a function of the blade angle α , the angle of internal friction ϕ , the soil/interface friction angle δ , with under pressure behind the blade.

[Back to top](#)

Table 2.37: The coefficient d_2 .

$h_b/h_i=3$	ϕ	32°	37°	42°	47°	52°
α	δ					
15°	15°	10.650	11.026	11.400	11.783	12.181
	18°	10.281	10.701	11.122	11.552	12.002
	21°	9.896	10.356	10.819	11.294	11.792
	24°	9.499	9.994	10.494	11.011	11.555
	27°	9.091	9.616	10.149	10.704	11.292
	30°	8.674	9.223	9.785	10.374	11.001
30°	15°	2.724	2.966	3.226	3.508	3.821
	18°	2.521	2.783	3.064	3.371	3.712
	21°	2.301	2.579	2.879	3.209	3.576
	24°	2.065	2.357	2.673	3.022	3.414
	27°	1.813	2.115	2.444	2.81	3.225
	30°	1.545	1.854	2.192	2.571	3.004
45°	15°	0.918	1.116	1.341	1.600	1.902
	18°	0.730	0.935	1.169	1.439	1.758
	21°	0.522	0.731	0.969	1.248	1.579

	24°	0.294	0.502	0.741	1.023	1.362
	27°	0.043	0.246	0.481	0.761	1.100
	30°	-0.232	-0.040	0.185	0.455	0.787
60°	15°	0.080	0.224	0.398	0.611	0.878
	18°	-0.154	-0.020	0.142	0.343	0.598
	21°	-0.417	-0.301	-0.159	0.019	0.249
	24°	-0.714	-0.624	-0.513	-0.372	-0.187
	27°	-1.048	-0.996	-0.931	-0.846	-0.733
	30°	-1.427	-1.426	-1.425	-1.424	-1.422

The dimensionless force d_2 , perpendicular to the cutting velocity, as a function of the blade angle α , the angle of internal friction ϕ , the soil/interface friction angle δ , with under pressure behind the blade.

[Back to top](#)

This is a translation of the dissertation of Dr.ir. S.A. Miedema, dated September 15th 1987 .
The dissertation was originally published in Dutch by the:
Delft University of Technology
Faculty of Mechanical Engineering and Marine Technology
Chair of Dredging Technology
Mekelweg 2
2628 CD, Delft
The Netherlands

Last modified Wednesday May 24, 2000 by: [Sape A. Miedema](#)

Translation by: [Laurens de Jonge](#)

Figures, equations and tables by: [Erik Miedema](#)

Copyright © May, 2000 Dr.ir. S.A. Miedema



[Download Adobe Acrobat Reader V4.0](#)

[Back to top](#)**Table 2.31: The coefficient d_1 .**

$h_b/h_i=3$	ϕ	32°	37°	42°	47°	52°
α	δ					
15°	15°	6.145	6.362	6.578	6.799	7.028
	18°	6.672	6.945	7.218	7.497	7.789
	21°	7.185	7.519	7.855	8.200	8.562
	24°	7.687	8.087	8.492	8.910	9.351
	27°	8.180	8.652	9.132	9.631	10.159
	30°	8.667	9.216	9.778	10.366	10.993
30°	15°	3.775	4.017	4.277	4.559	4.872
	18°	4.127	4.417	4.729	5.070	5.449
	21°	4.479	4.822	5.192	5.598	6.052
	24°	4.832	5.233	5.667	6.147	6.687
	27°	5.188	5.653	6.159	6.722	7.359
	30°	5.551	6.084	6.670	7.326	8.075
45°	15°	3.123	3.467	3.855	4.302	4.826
	18°	3.450	3.852	4.309	4.838	5.463
	21°	3.784	4.251	4.786	5.410	6.152
	24°	4.128	4.669	5.291	6.024	6.904
	27°	4.486	5.107	5.830	6.689	7.732
	30°	4.859	5.572	6.409	7.414	8.650
60°	15°	3.152	3.691	4.338	5.131	6.126
	18°	3.520	4.147	4.907	5.849	7.047
	21°	3.907	4.637	5.529	6.648	8.092
	24°	4.319	5.165	6.212	7.545	9.294
	27°	4.760	5.742	6.973	8.564	10.695
	30°	5.237	6.377	7.827	9.738	12.353

The dimensionless force d_1 , in the direction of the cutting velocity, as a

function of the blade angle α , the angle of internal friction ϕ , the soil/interface friction angle δ , with under pressure behind the blade.

[Back to top](#)**Table 2.37: The coefficient d_2 .**

$h_b/h_i=3$	ϕ	32°	37°	42°	47°	52°
α	δ					
15°	15°	10.650	11.026	11.400	11.783	12.181
	18°	10.281	10.701	11.122	11.552	12.002
	21°	9.896	10.356	10.819	11.294	11.792
	24°	9.499	9.994	10.494	11.011	11.555
	27°	9.091	9.616	10.149	10.704	11.292
	30°	8.674	9.223	9.785	10.374	11.001
30°	15°	2.724	2.966	3.226	3.508	3.821
	18°	2.521	2.783	3.064	3.371	3.712
	21°	2.301	2.579	2.879	3.209	3.576
	24°	2.065	2.357	2.673	3.022	3.414
	27°	1.813	2.115	2.444	2.81	3.225
	30°	1.545	1.854	2.192	2.571	3.004
45°	15°	0.918	1.116	1.341	1.600	1.902
	18°	0.730	0.935	1.169	1.439	1.758
	21°	0.522	0.731	0.969	1.248	1.579
	24°	0.294	0.502	0.741	1.023	1.362
	27°	0.043	0.246	0.481	0.761	1.100
	30°	-0.232	-0.040	0.185	0.455	0.787
60°	15°	0.080	0.224	0.398	0.611	0.878
	18°	-0.154	-0.020	0.142	0.343	0.598
	21°	-0.417	-0.301	-0.159	0.019	0.249
	24°	-0.714	-0.624	-0.513	-0.372	-0.187
	27°	-1.048	-0.996	-0.931	-0.846	-0.733
	30°	-1.427	-1.426	-1.425	-1.424	-1.422

The dimensionless force d_2 , perpendicular to the cutting velocity, as a function

of the blade angle α , the angle of internal friction ϕ , the soil/interface friction angle δ , with under pressure behind the blade.

3.01 Description of the test stand.

The tests with the straight blades are performed on two locations:

1. The old laboratory of the section Grondverzet (Dredging Technology), which will be called the old laboratory GV.
2. The new laboratory of the section Grondverzet (Dredging Technology), which will be called the new laboratory GV.

The test stand in the old laboratory GV consists of a concrete tank, 30 m long, 2.5 m wide and 1.35 m high, filled with a layer of 0.5 m sand with a d_{50} of 200 μm and above the sand 0.6 m water. The properties of the sand in this tank are described in appendix B3. The test stand in the new laboratory GV consists of a concrete tank, 33m long, 3m wide and internally 1.5 m high, with a layer of 0.7 m sand with a d_{50} of 105 μm and above the sand 0.6 m water. The properties of this sand are described in appendix B4. In both laboratories a main carriage can ride over the full length of the tank, pulled by two steel cables. These steel cables are wound on the drums of a hydraulic winch, placed in the cellar and driven by a squirrel-cage motor of 35 kW in the old laboratory GV and 45 kW in the new laboratory GV.

In the old laboratory GV the velocity of the carriage could be infinitely variable controlled from 0.05 m/s to 2.50 m/s, with a pulling force of 6 kN. In the new laboratory GV the drive is equipped with a hydraulic two-way valve, which allows for the following speed ranges:

1. A range from 0.05 m/s to 1.40 m/s, with a maximum pulling force of 15 kN.
2. A range from 0.05 m/s to 2.50 m/s, with a maximum pulling force of 7.5 kN.

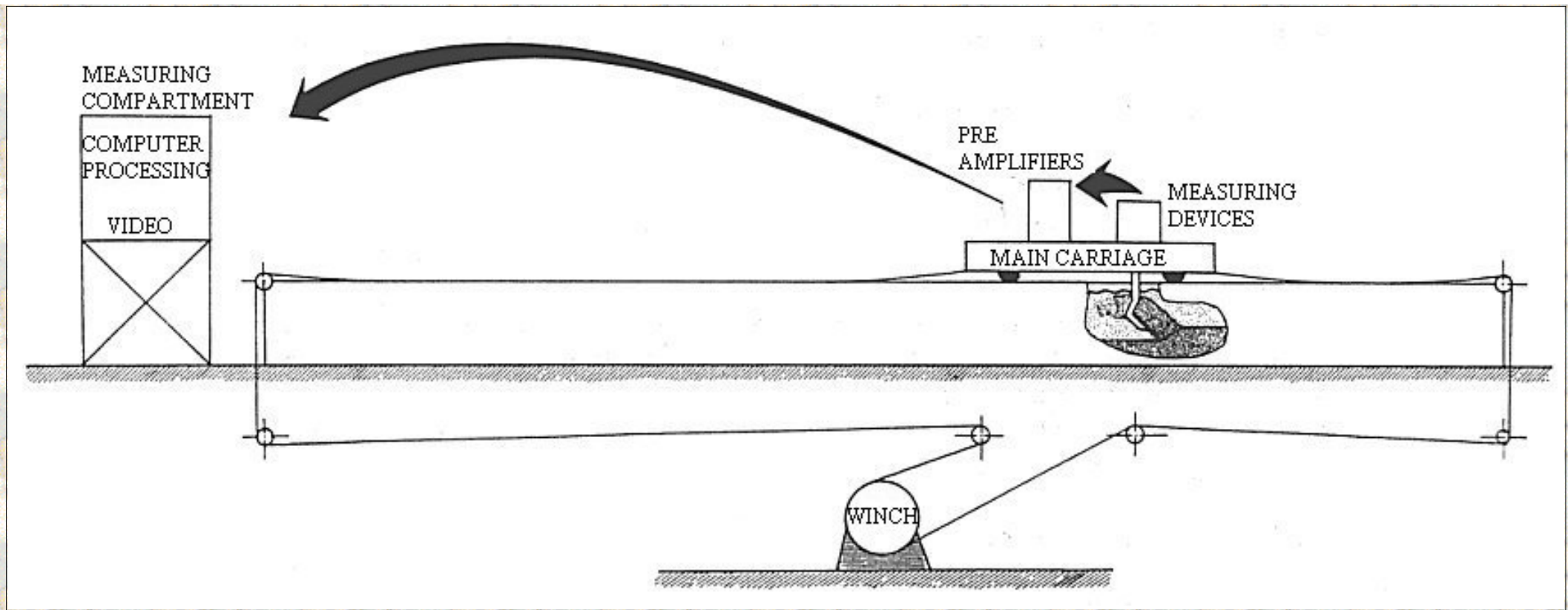


Figure 3.1: Side view of the test stand with the drive of the main carriage. The data flows are indicated with arrows with the places where data processing takes place.

An auxiliary carriage, on which the blades are mounted, can be moved transverse of the longitudinal direction on the main carriage. Hydraulic cylinders are used to adjust the cutting depth and to position the blades in the transverse direction of the tank. Figure 3.1 shows the concrete tank with the drive and figure 3.2 shows the mounting of the blades underneath the auxiliary carriage.

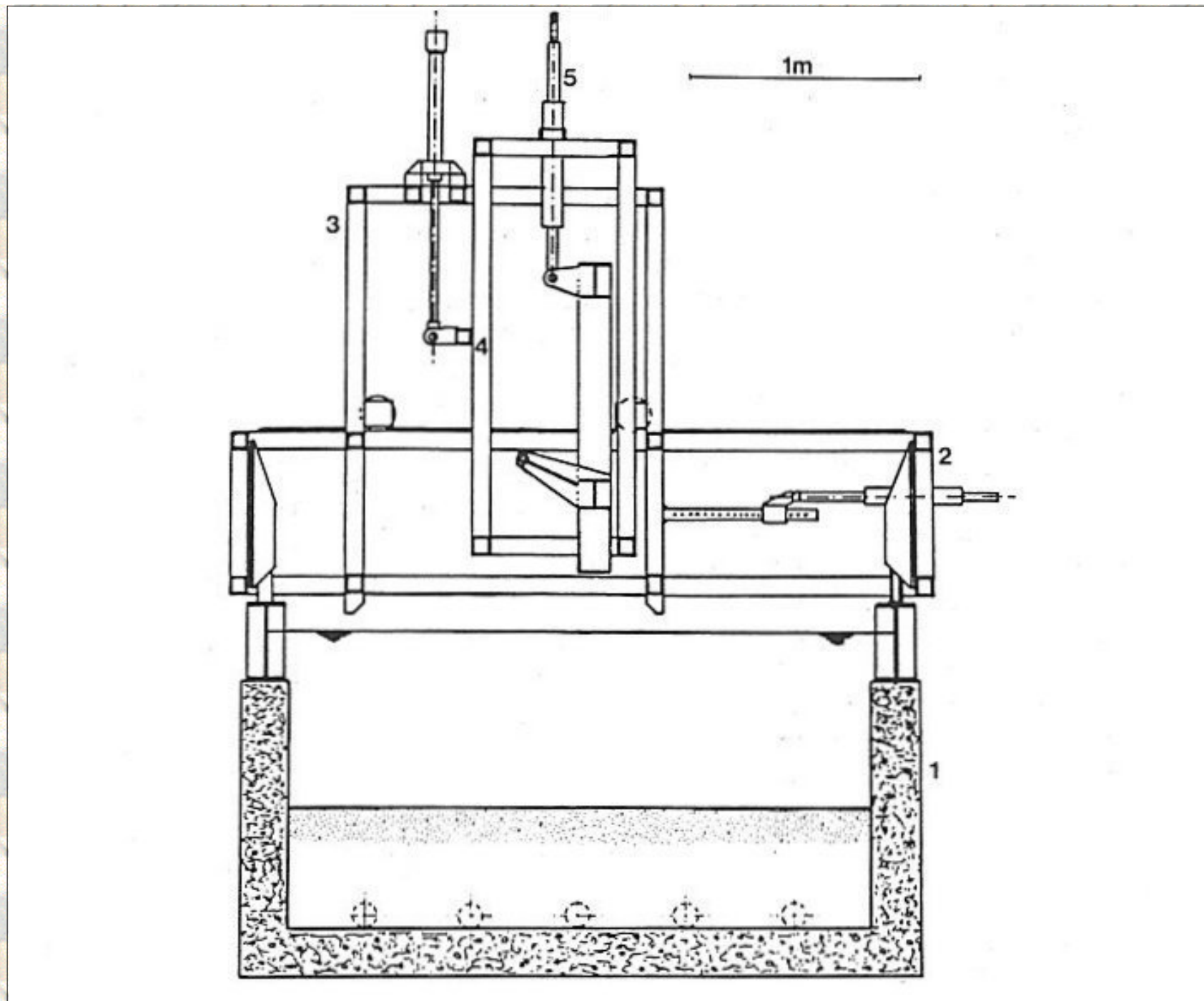


Figure 3.2: Cross section of the concrete tank and the main carriage, with:

1. The concrete tank
2. The main carriage
3. The auxiliary carriage
4. An auxiliary frame
5. Hydraulic cylinder for vertical positioning

The tests are performed using a middle blade, flanked on both sides by a side blade, in order to establish a two-dimensional cutting process on the middle blade. The middle blade is mounted in a dynamometer, with which the following loads can be measured:

1. The horizontal force
2. The vertical force
3. The transverse force
4. The bending moment

The side blades are mounted in a fork-like construction, attached to some dynamometers, with which the following loads can be measured:

1. The horizontal force
2. The vertical force

Figure 3.3 shows the mounting of the blades.

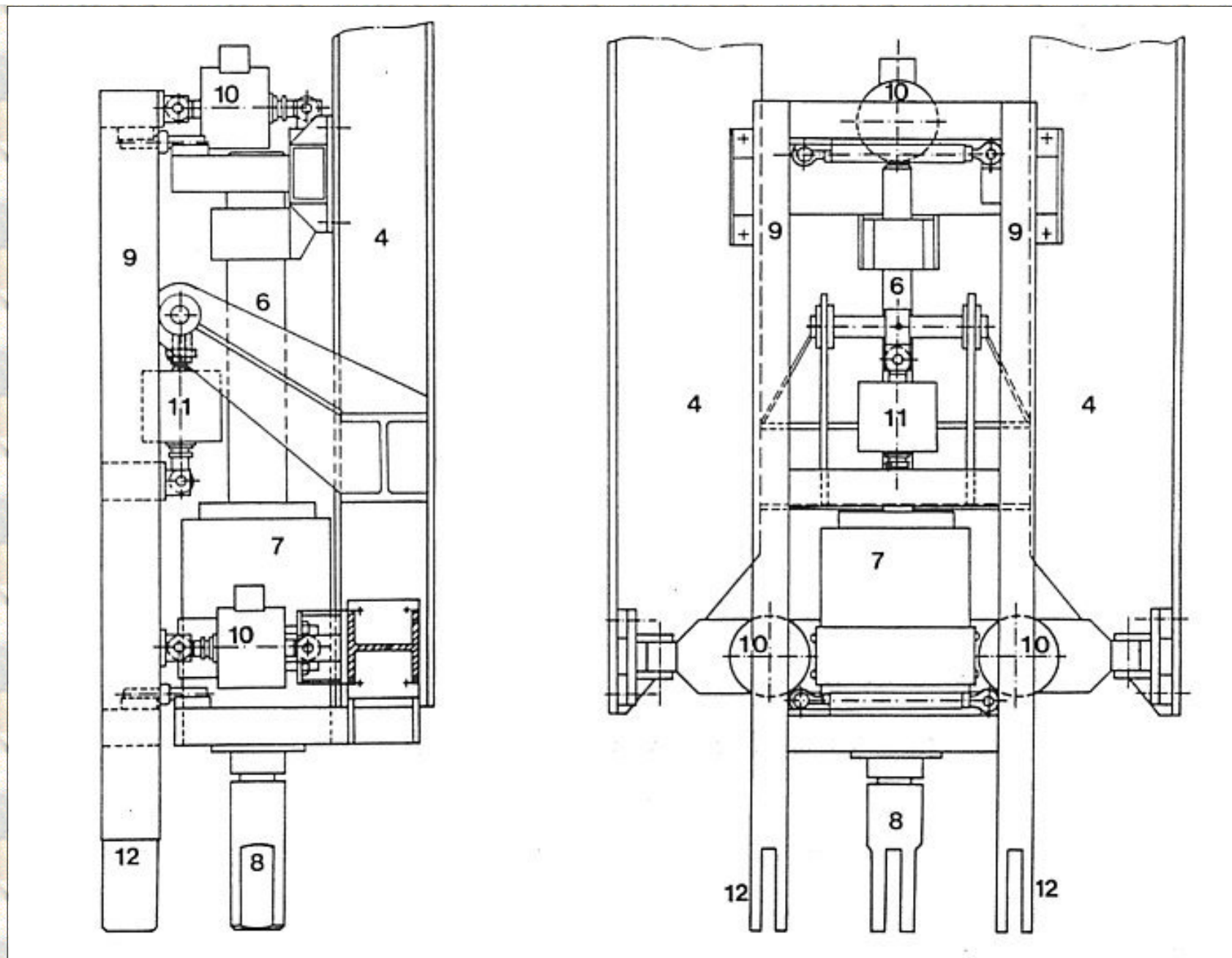


Figure 3.3: The construction of the blade mounting, with:

4. The auxiliary frame (see figure 3.2)

6. Middle blade mounting
7. Dynamometer middle blade
8. Mounting point middle blade
9. Side blade mounting
10. Dynamometers horizontal force side blades
11. Dynamometer vertical force side blades
12. Mounting point side blade

In the middle blade four pressure transducers are mounted, with which the pore pressure distribution on the blade can be measured. However no tests are performed in which the forces on the side blades and the pore pressures are measured at the same time. The measuring signals of the dynamometers and the pressure transducers are transmitted to a measurement compartment through pre amplifiers on the main carriage. In this measurement compartment the measuring signals are suited by a 12 bit, 400 Hz A/D converter for processing on a P.C. (personal computer), after which the signals are stored on a flexible disk. Figure 3.4 shows the data flow with the various intermediate processing units, where data operations are performed. Next to the blades, under water, an under water video camera is mounted to tape the cutting process. This also gave an impression of the shear angles.

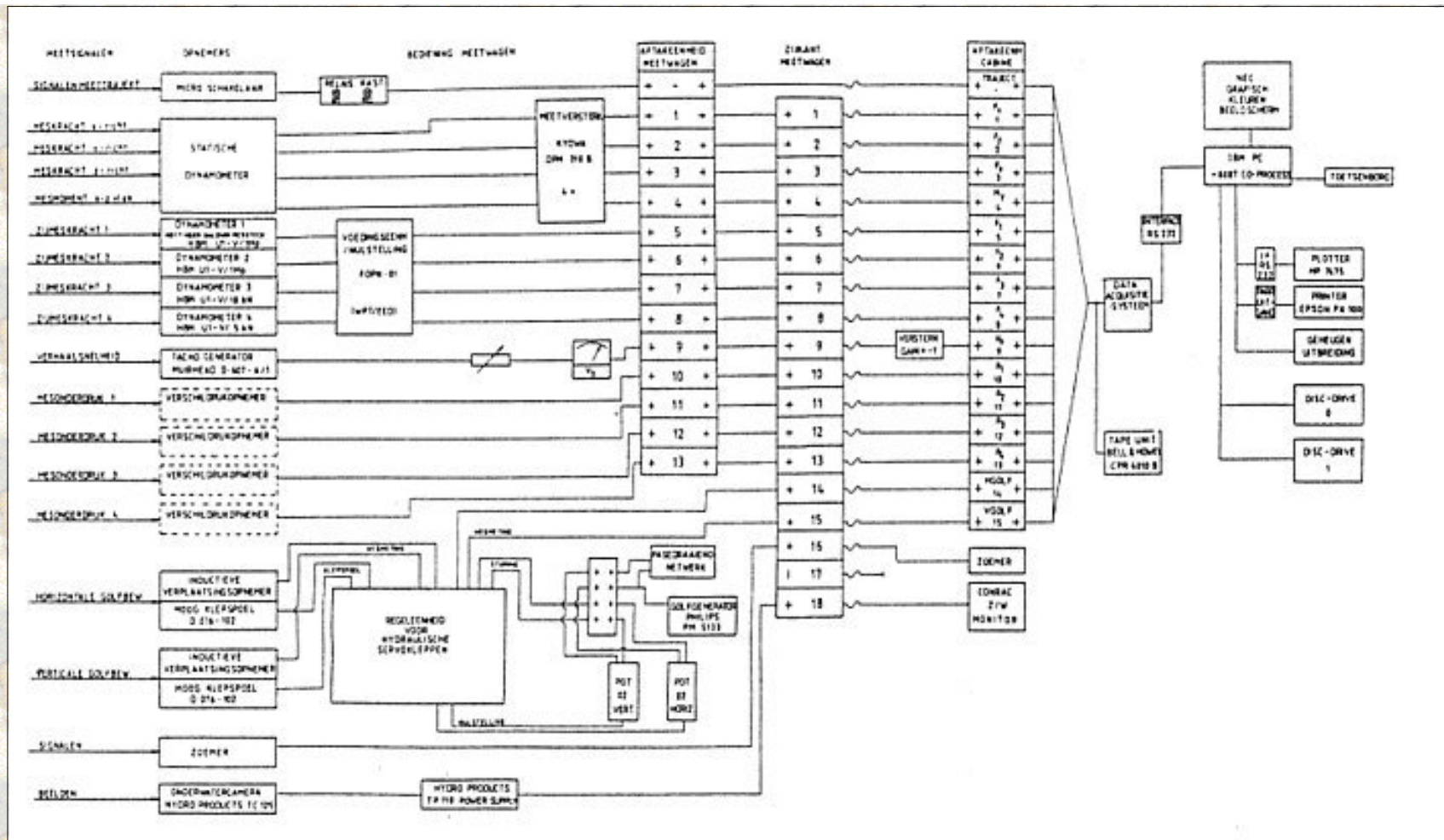


Figure 3.4: Outline of the measuring system.

With the following photo gallery an impression of the realization of this research is given.

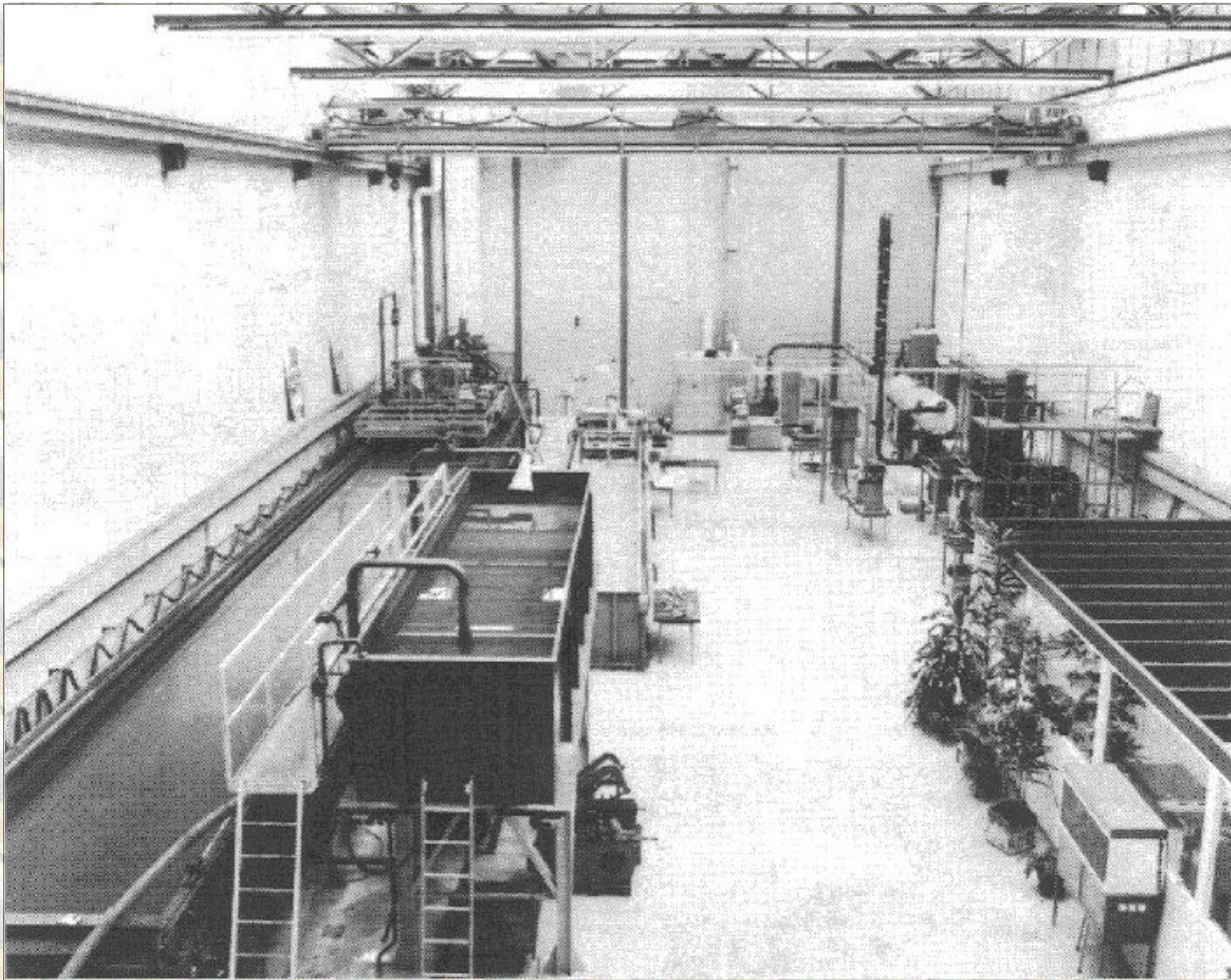


Photo 3.1: This is an overview of the test stand in which the tests are carried out.

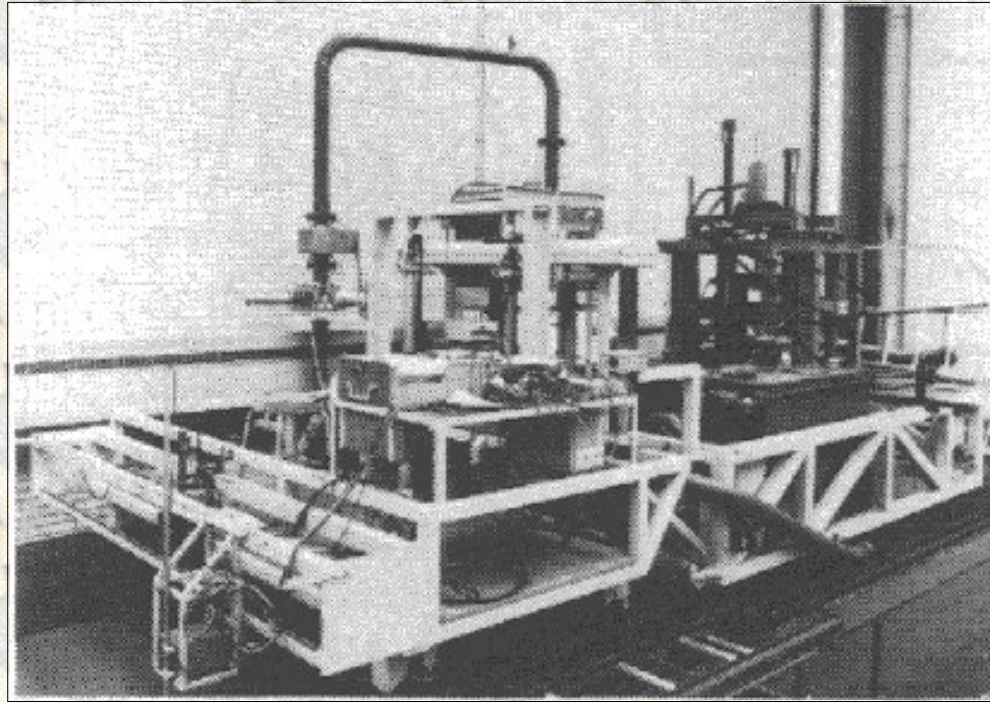


Photo 3.2: On the concrete tank, which contains the sand, a carriage can drive on which the blades are mounted.

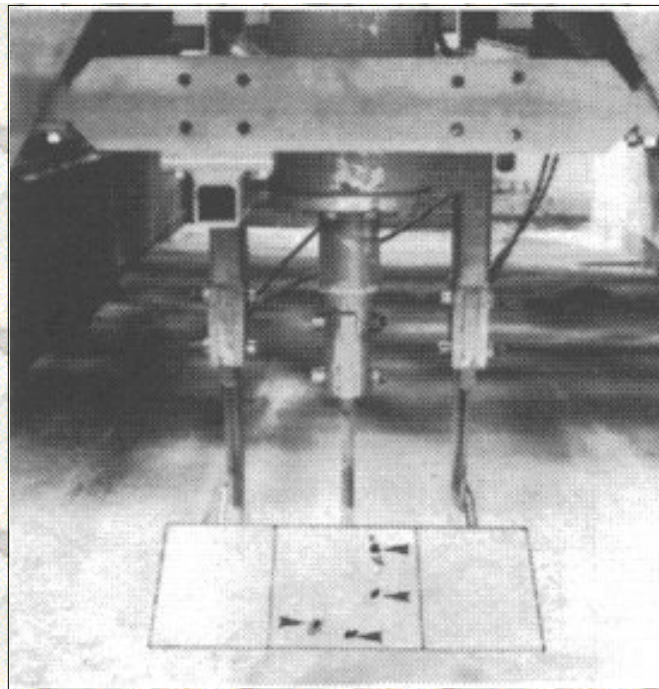


Photo 3.3: The blades used to cut the sand. The middle blade shows the pore pressure transducers.

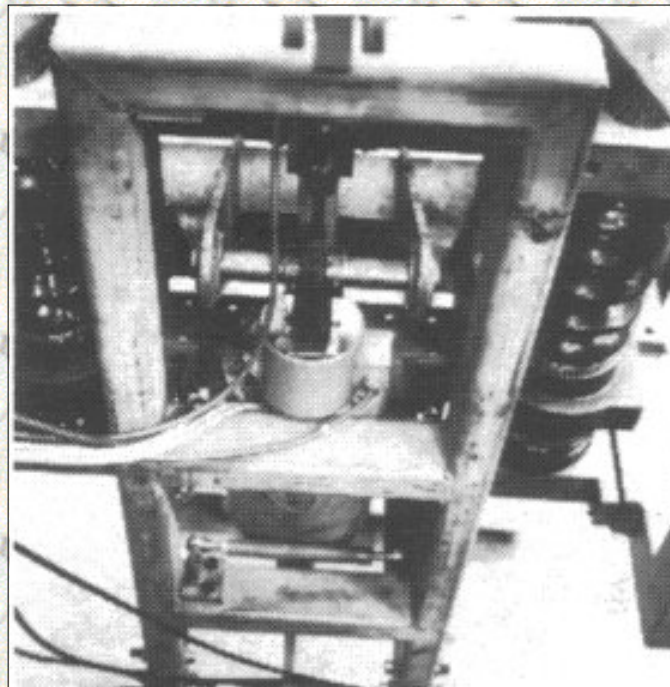


Photo 3.4: The blades are mounted in a frame with force transducers (dynamometers).

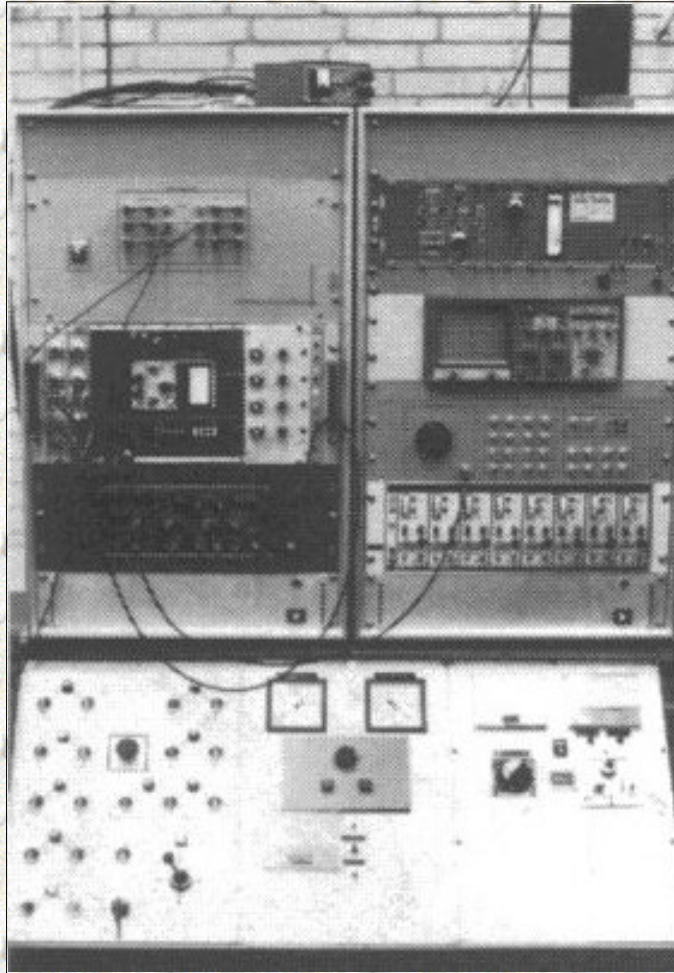


Photo 3.5: The signals from the pore pressure transducers and the force transducers are amplified with pre-amplifiers on the main carriage.

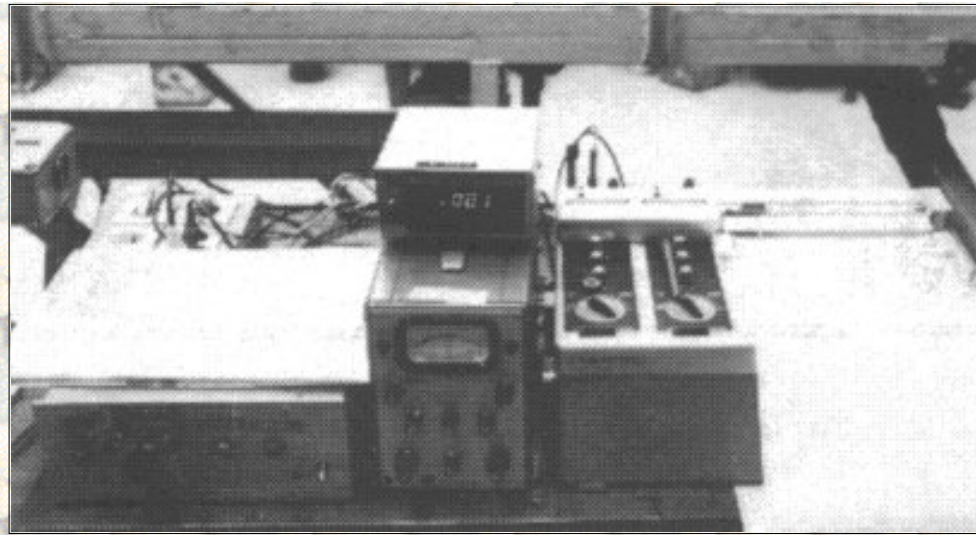


Photo 3.6: The hardness of the sand is measured before each test. This is a measure of the pore volume of the sand before it is cut during the experiment.

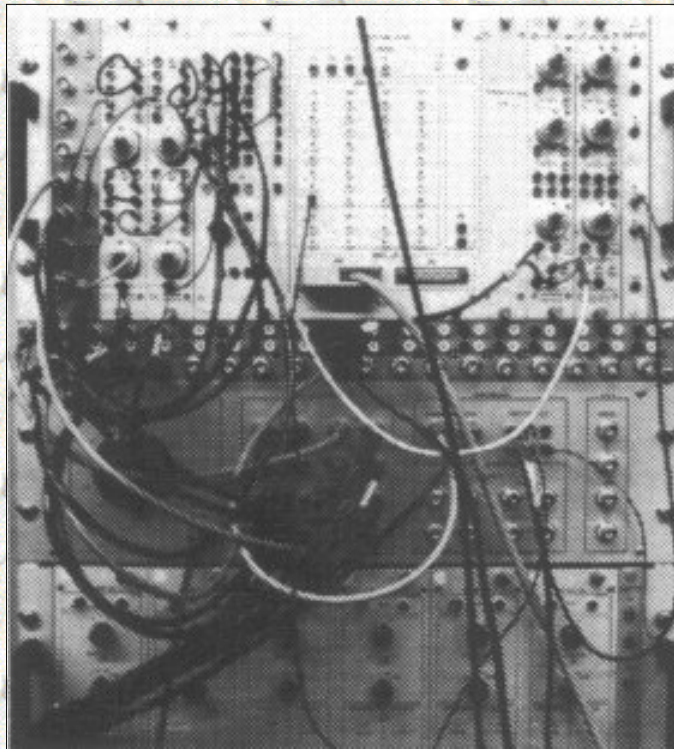


Photo 3.7: The signals are transmitted through cables to a measuring compartment, where they are pre-processed with an AD converter for further processing with a computer.

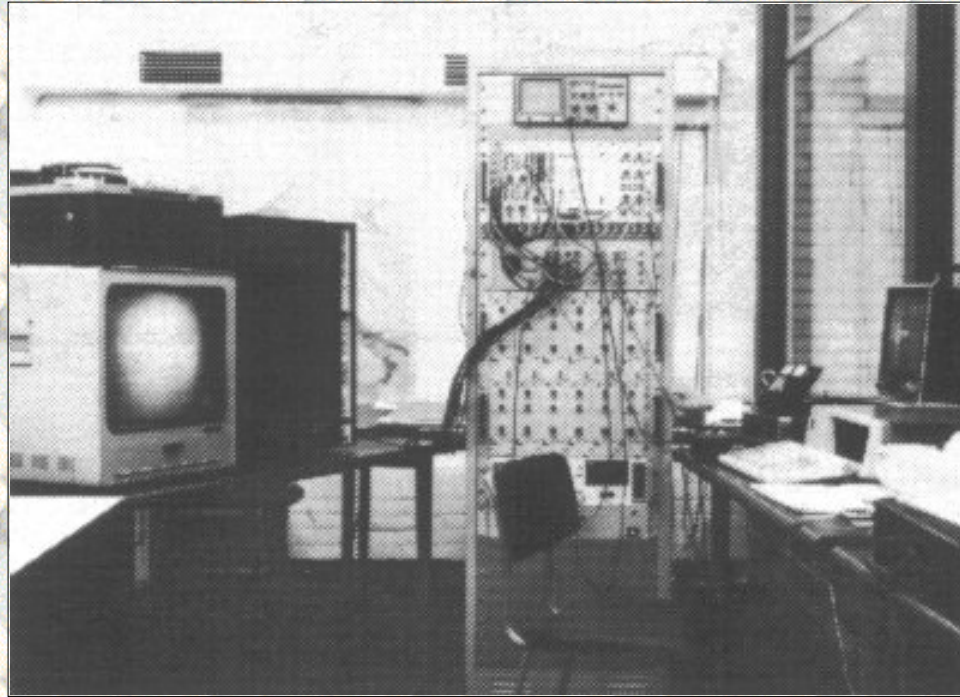


Photo 3.8: With an under water camera recordings are made of each experiment. These recordings can be viewed online by the researcher in the measuring compartment. This photo also shows the AD converter and the computer used.

[Back to top](#)

This is a translation of the dissertation of Dr.ir. S.A. Miedema, dated September 15th 1987 .
The dissertation was originally published in Dutch by the:
Delft University of Technology
Faculty of Mechanical Engineering and Marine Technology
Chair of Dredging Technology
Mekelweg 2
2628 CD, Delft
The Netherlands

It is advised to also read the papers following this dissertation, since the theory developed has been refined and extended.

Last modified Sunday May 28, 2000 by: [Sape A. Miedema](#)

Translation by: [Laurens de Jonge](#)

Figures, equations and tables by: [Erik Miedema](#)

Copyright © May, 2000 Dr.ir. S.A. Miedema



[Download Adobe Acrobat Reader V4.0](#)

3.02 Test program.

The theory for the determination of the forces that occur during the cutting of fully saturated sand with straight blades is verified in two types of sand, sand with a d_{50} of 200 μm and sand with a d_{50} of 105 μm . The soil mechanical parameters of these two types of sand can be found in appendix B3 and B4.

The research can be subdivided in a number of sub studies:

1. Research of the water resistance of the blades
2. Research of the accuracy of the assumed two-dimensional character of the cutting process on the middle blade by varying the width of the middle blade with a total width of the middle blade and the side blades of 520 mm. This research is performed in the 200 μm sand.
3. Research of the quantitative character of the side effects in relation to the size and the direction of the cutting forces. This research is performed in the 200 μm sand.
4. Research of the in the theory present scale rules. This research is performed in the 200 μm sand.
5. Research of the accuracy of the theory of the cutting forces and the water under-pressures in the non-cavitating cutting process. This research is performed in the 200 μm sand.
6. Research of the accuracy of the theory of the forces and the water under-pressures in the non-cavitating and the partly cavitating cutting process. This research is performed in the 105 μm sand.

From points 4 and 5 it has also been established that the maximum pore percentage of the sand can be chosen for the residual pore percentage. In the 200 μm the dry critical density, the wet critical density and the minimal density are determined, while in the 105 μm sand the wet critical density and the minimal density are determined. These pore values can be found in appendix B3 and B4.

For both type of sand only the minimal density (maximum pore percentage n_{max}) gave a large enough increase in volume to explain the measured water

under-pressures. This in contrast to Van Leussen and Nieuwenhuis [39] and Van Leussen and Van Os [40], where for the residual density the wet critical density is chosen.

[Back to top](#)

This is a translation of the dissertation of Dr.ir. S.A. Miedema, dated September 15th 1987 .
The dissertation was originally published in Dutch by the:
Delft University of Technology
Faculty of Mechanical Engineering and Marine Technology
Chair of Dredging Technology
Mekelweg 2
2628 CD, Delft
The Netherlands

It is advised to also read the papers following this dissertation, since the theory developed has been refined and extended.

Last modified Sunday May 28, 2000 by: [Sape A. Miedema](#)

Translation by: [Laurens de Jonge](#)

Figures, equations and tables by: [Erik Miedema](#)

Copyright © May, 2000 Dr.ir. S.A. Miedema



[Download Adobe Acrobat Reader V4.0](#)

3.03 Water resistance.

The water resistance is researched under circumstances comparable with the cutting tests as far as scale, blade width and cutting velocity are concerned. Since the water resistance during all these tests could be neglected in comparison with the cutting forces, performed under the same conditions (maximum 2%), the water resistance terms are neglected in the further verification. The water resistance could however be more significant at higher cutting velocities of probably above 2 m/s.

[Back to top](#)

This is a translation of the dissertation of Dr.ir. S.A. Miedema, dated September 15th 1987 .
The dissertation was originally published in Dutch by the:
Delft University of Technology
Faculty of Mechanical Engineering and Marine Technology
Chair of Dredging Technology
Mekelweg 2
2628 CD, Delft
The Netherlands

It is advised to also read the papers following this dissertation, since the theory developed has been refined and extended.

Last modified Sunday May 28, 2000 by: [Sape A. Miedema](#)

Translation by: [Laurens de Jonge](#)

Figures, equations and tables by: [Erik Miedema](#)

Copyright © May, 2000 **Dr.ir. S.A. Miedema**



[Download Adobe Acrobat Reader V4.0](#)

3.04 The influence of the width of the blade.

The blade on which the cutting forces are measured is embedded between two side blades. These side blades have to take care of the three-dimensional side effects, so that on the middle blade a two-dimensional cutting process takes place. The question now is how wide the side blades need to be, at a certain cutting depth, to avoid a significant presence of the side effects on the middle blade. Essential is, that at the deepest cutting depth the side effects on the middle blade are negligible.

For this research the following blade configurations are used:

1. A middle blade of 150 mm and two side blades of 185 mm each.
2. A middle blade of 200 mm and two side blades of 160 mm each.
3. A middle blade of 250 mm and two side blades of 135 mm each.

The total blade width in each configuration is therefore 520 mm. The results of this research are, scaled to a middle blade of 200 mm wide, shown in table 3.1, in which every value is the average of a number of tests. In this table the forces on the 0.20 m and the 0.25 m wide blade are listed in proportion to the 0.15 m wide blade. The change of the direction of the forces in relation to the 0.15 m wide blade are also mentioned.

		b=0.20 m (2)		b=0.25 m (3)	
α	h_b/h_i	c_{t2}/c_{t1}	$\theta_{t2}-\theta_{t1}$	c_{t3}/c_{t1}	$\theta_{t3}-\theta_{t1}$
30°	1	0.95	+1.0°	1.02	+1.0°
30°	2	1.10	+2.0°	0.93	+4.0°
30°	3	0.96	+5.0°	1.05	+7.0°
45°	1	1.08	+3.0°	1.01	+5.0°
45°	2	0.93	+3.0°	0.93	+5.0°
45°	3	0.93	-8.0°	1.07	-5.0°
60°	1	1.09	+0.0°	1.00	+1.0°
60°	2	0.90	+1.0°	0.92	+2.0°
60°	3	1.04	-5.0°	0.99	-4.0°

Table 3.1: The influence of the width ratio between the middle blade and the side blades.

The total measured cutting force c_t and the force direction θ_t , at a blade width of .20 m (c_{t2} , θ_{t2}) (2) and a blade width of .25 m (c_{t3} , θ_{t3}) (3) in proportion to the total cutting force and direction at a blade width of 0.15 m (c_{t1} , θ_{t1}) (1), according the blade configurations from chapter 3.4

From this table the following conclusions can be drawn:

1. There is no clear tendency to assume that the side effects influence the cutting forces in magnitude.
2. The widening of the middle blade, and thus narrowing the side blades, gives slightly more downward aimed forces on the middle blade at a blade angle of 30° . At a blade angle of 45° this tendency can be seen at a blade-height/layer-thickness ratio of 1 and 2, while at a blade-height/layer-thickness ratio of 3 the forces are just slightly aimed upward. The 60° blade angle gives the same image as the 45° blade angle, however with smaller differences in proportion to the 0.15 m wide blade.

[Back to top](#)

This is a translation of the dissertation of Dr.ir. S.A. Miedema, dated September 15th 1987 .

The dissertation was originally published in Dutch by the:

Delft University of Technology

Faculty of Mechanical Engineering and Marine Technology

Chair of Dredging Technology

Mekelweg 2

2628 CD, Delft

The Netherlands

It is advised to also read the papers following this dissertation, since the theory developed has been refined and extended.

Last modified Sunday May 28, 2000 by: [Sape A. Miedema](#)

Translation by: [Laurens de Jonge](#)

Figures, equations and tables by: [Erik Miedema](#)

Copyright © May, 2000 Dr.ir. S.A. Miedema



[Download Adobe Acrobat Reader V4.0](#)



3.05 Side effects.

On the outside of the side blades a three-dimensional cutting process acts, in a sense that the shear zone here is three-dimensional, but on top of that the water flows three-dimensional to the shear zone. This makes the cutting forces differ, in magnitude and direction, from the two-dimensional cutting process. Additionally it is imaginable that also forces will act on the blade in the transversal direction (internal forces in the blade). The influence of the side effects is researched by measuring the forces on both the middle blade as on the side blades. Possible present transversal forces are researched by omitting one side blade in order to be able to research the transversal forces due to the three-dimensional side effects.

For this research the following blade configurations are used:

1. A middle blade of 150 mm and two side blades of 185 mm each.
2. A middle blade of 200 mm and two side blades of 160 mm each.
3. A middle blade of 250 mm and two side blades of 135 mm each.
4. A middle blade of 200 mm and one side blade of 160 mm

The results of this research can be found in table 3.2, where every value represents the average of a number of tests. The cutting forces in this table are scaled to the 200 mm blade to simulate a middle blade without side blades.

		b=.15 m (1)		b=.20 m (2)		b=.25 m (3)		b=.20 m (4)	
α	h_b/h_i	c_r	θ_r	c_r	θ_r	c_r	θ_r	c_r	θ_r
30°	1	1.06	+26°	1.23	+14°	1.17	+11°	1.01	+13°
30°	2	0.78	+18°	0.87	+16°	0.83	+10°	1.14	+10°
30°	3	0.74	+22°	0.56	+22°	0.53	+11°	1.45	+ 6°
45°	1	1.13	+23°	1.10	+14°	1.26	+ 9°	1.04	+ 5°
45°	2	0.94	+19°	0.94	+11°	0.93	+ 7°	0.92	+ 7°
45°	3	0.79	+14°	1.10	+17°	0.98	+11°	0.85	+ 6°
60°	1	1.10	+ 8°	1.10	+ 6°	1.10	+ 5°	1.04	+ 2°

60°	2	0.94	+12°	1.10	+ 8°	1.06	+ 6°	0.91	+ 2°
60°	3	0.77	+ 8°	0.99	+15°	1.02	+11°	0.86	+ 3°

Table 3.2: The cutting force on the side blades in ratio to the cutting force on the middle blade c_r , assuming that the cutting process on the middle blade is two-dimensional. Also shown is the change of direction of the total cutting force θ_r . The cutting forces are scaled to the width of the middle blade for the blade widths .15 m (1), .20 m (2) en .25 m (3). The second column for $b=.20$ m (4) contains the results of the tests with only one side blade to measure the side effects on the middle blade. The measured cutting forces are compared to the similar tests where two side blades are used. The blade configurations are according chapter 3.5.

From this research the following conclusions can be drawn:

1. For all blade angles the cutting force on the edge is larger than follows from the two-dimensional process, for a blade-height / layer-thickness ratio of 1.
2. A blade-height / layer-thickness ratio of 2 or 3 shows a somewhat smaller cutting force with a tendency to smaller forces with a higher blade-height / layer-thickness ratio.
3. The direction of the cutting force is, for all four blade configurations, aimed more downwards on the sides than in the middle, where the differences with the middle blade decrease with a wider middle blade and therefore less wide side blades. This implies that, with the widening of the middle blade, the influence of the three-dimensional cutting process on the middle blade increases with a constant total blade width. This could be expected. It also explains that the cutting force in the middle blade is directed more downwards with an increasing middle blade width (conclusion 2 chapter 3.4).
4. Blade configuration 4 differs slightly, as far as the magnitude of the forces are concerned, from the tendency seen in the other three configurations with the 30° blade. The direction of the cutting forces match with the other configurations. It has to be remarked that in this blade configuration the side effects occur only on one side of the blade, which explains the small change of the cutting forces.

5. The measured transverse forces for blade configuration 4 are in the magnitude of 1% of the vector sum of the horizontal and the vertical cutting forces and therefore it can be concluded that the transverse forces are negligible for the used sand.

The found conclusions are on principle only valid for the used sand. The influence of the side effects on the magnitude and the direction of the expected cutting forces will depend on the ratio between the internal friction of the sand and the soil/steel friction. This is because the two-dimensional cutting process is dominated by both angles of friction, while the forces that occur on the sides of the blade, as a result of the three-dimensional shear plane, are dominated more by the internal friction of the sand.

[Back to top](#)

This is a translation of the dissertation of Dr.ir. S.A. Miedema, dated September 15th 1987 .

The dissertation was originally published in Dutch by the:

Delft University of Technology

Faculty of Mechanical Engineering and Marine Technology

Chair of Dredging Technology

Mekelweg 2

2628 CD, Delft

The Netherlands

It is advised to also read the papers following this dissertation, since the theory developed has been refined and extended.

Last modified Sunday May 28, 2000 by: [Sape A. Miedema](#)

Translation by: [Laurens de Jonge](#)

Figures, equations and tables by: [Erik Miedema](#)

Copyright © May, 2000 Dr.ir. S.A. Miedema



[Download Adobe Acrobat Reader V4.0](#)

3.06 Scale effects.

The soil mechanical research showed that the density of the sand increases slightly with the depth. Since both the permeability and the volume strain, and less significant the other soil mechanical parameters, are influenced by the density, it is important to know the size of this influence on the cutting forces (assuming that the two-dimensional cutting theory is a valid description of the process). If the two-dimensional cutting theory is a valid description of the process, the dimensionless cutting forces will have to give the same results for similar geometric ratios, independent of the dimensions and the layer-thickness, according the equations for the non-cavitating cutting process (2.43) and the cavitating cutting process (2.46).

The following blade configurations are used to research the scaling influence:

1. A blade with a width of 150 mm wide and a height of 100 mm.
2. A blade with a width of 150 mm wide and a height of 150 mm.
3. A blade with a width of 150 mm wide and a height of 200 mm.
4. A blade with a width of 150 mm wide and a height of 300 mm.

The results of this research can be found in table 3.3, where every value represents the average value of a number of tests.

Configuration		1	2	3	4
α	h_b/h_i	$h = 0.10$	0.15	0.20	0.30
30°	1	0.93	1.00	0.94	1.18
30°	2	1.23	1.00	1.06	1.13
30°	3	----	1.00	0.89	0.90
45°	1	0.95	1.00	1.13	----
45°	2	0.89	1.00	1.05	1.30
45°	3	----	1.00	1.02	1.13
60°	1	0.91	1.00	----	----
60°	2	0.90	1.00	1.19	1.04

60°	3	1.02	1.00	1.13	1.21
-----	---	------	------	------	------

Table 3.3: Influence of the scale factor. The total cutting force c_t with blade heights of .10 m (1), .15 m (2), .20 m (3) and .30 m (4) in proportion to the cutting force at a blade height .15 m (2). The blade configurations are according chapter 3.6.

Because the influences of the gravity and inertia forces can disturb the character of the dimensionless forces compared to the tables 2.14 to 2.25, the measured forces are first corrected for these influences. The forces in the table are in proportion to the forces that occurred with blade configuration 2.

The following conclusions can be drawn from the table:

1. There is a slight tendency to larger dimensionless forces with increasing dimensions of the blades and the layer-thickness, which could be expected with the slightly increasing density.
2. For a blade angle of 30° and a blade-height / layer-thickness ratio of 2, large dimensionless forces are measured for blade configuration 1. These are the tests with the thinnest layer-thickness of 25 mm. A probable cause can be that the rounding of the blade tip in proportion with the layer-thickness is relatively large, leading to a relatively large influence of this rounding on the cutting forces. This also explains the development of the dimensionless forces at a blade angle of 30° and a blade-height / layer-thickness ratio of 3.

[Back to top](#)

This is a translation of the dissertation of Dr.ir. S.A. Miedema, dated September 15th 1987 .

The dissertation was originally published in Dutch by the:

Delft University of Technology

Faculty of Mechanical Engineering and Marine Technology

Chair of Dredging Technology

Mekelweg 2

2628 CD, Delft

The Netherlands

It is advised to also read the papers following this dissertation, since the theory developed has been refined and extended.

Last modified Sunday May 28, 2000 by: [Sape A. Miedema](#)

Translation by: [Laurens de Jonge](#)

Figures, equations and tables by: [Erik Miedema](#)

Copyright © May, 2000 Dr.ir. S.A. Miedema



[Download Adobe Acrobat Reader V4.0](#)

3.07 Comparison of measurements versus theory.

Contents

The results of the preceding three researches are collected in table 3.4, compared with the theory. Every value is the average of a number of tests. In the table can be found:

1. The dimensionless forces, the average from the several scales and blade widths.
2. As 1, but corrected for the gravity and inertia forces.
3. The theoretical dimensionless forces according tables 2.14 to 2.25.

		measured				calculated	
		uncorrected		corrected		theoretical	
α	h_b/h_i	c_t	θ_t	c_t	θ_t	c_t	θ_t
30°	1	0.52	+13.3°	0.48	+17.1°	0.39	+28.3°
30°	2	0.56	+17.0°	0.53	+20.1°	0.43	+27.4°
30°	3	0.56	+24.8°	0.53	+28.2°	0.43	+27.3°
45°	1	0.71	+ 4.9°	0.63	+ 7.5°	0.49	+12.9°
45°	2	0.75	+ 6.0°	0.66	+ 8.0°	0.57	+10.7°
45°	3	0.76	+ 5.1°	0.70	+ 6.9°	0.61	+ 9.9°
60°	1	1.06	+1.2°	0.88	+ 1.9°	0.69	- 0.7°
60°	2	1.00	- 2.4°	0.84	- 3.4°	0.83	- 3.2°
60°	3	0.99	- 3.4°	0.85	- 4.2°	0.91	- 4.6°

Table 3.4: The measured total cutting force (not-corrected and corrected for the gravity and inertia forces) and the theoretical total cutting forces (all dimensionless, chapter 3.7). The theoretical values for c_t and θ_t are based on a angle of internal friction of 38° , a soil/steel angle of friction of 30° and a weighed average permeability of approximately .000242 m/s dependent on the weigh factor a_1 . The total cutting force c_t and the force direction θ_t are determined according chapter 2.12.

The following conclusions can be drawn from this table:

1. The measured and corrected cutting forces are larger than the, according to the theory, calculated cutting forces, at blade angles of 30° and 45° . The differences become smaller with an increase in the blade angle and when the blade-height / layer-thickness ratio increases.
2. For a blade angle of 60° the corrected measure forces agree well with the calculated forces.
3. The tendency towards larger forces with a larger blade-height / layer-thickness ratio (theory) is clearly present with blade angles 30° and 45° .
4. At a blade angle of 60° the forces seem to be less dependent of the blade-height / layer-thickness ratio.
5. The direction of the measured cutting forces agrees well with the theoretical determined direction. Only at the blade angle of 30° the forces are slightly aimed more upward for the blade-height / layer-thickness ratios 1 and 2.
6. Neglecting the inertia forces, gravity, etc. introduces an error of at least 15% within the used velocity range. This error occurs with the 60° blade, where the cutting velocity is the lowest of all cutting tests and is mainly due to the gravity.

Considering that the sand, in the course of the execution of the tests, as a result of segregation, has obtained a slightly coarser grain distribution and that the tests are performed with an increasing blade angle, can be concluded that the test results show a good correlation with the theory. It has to be remarked, however, that the scale and side effects can slightly disturb the good correlation between the theory and the measurements.

[Back to top](#)

**This is a translation of the dissertation of Dr.ir. S.A. Miedema, dated September 15th 1987 .
The dissertation was originally published in Dutch by the:
Delft University of Technology
Faculty of Mechanical Engineering and Marine Technology
Chair of Dredging Technology
Mekelweg 2**

2628 CD, Delft
The Netherlands

It is advised to also read the papers following this dissertation, since the theory developed has been refined and extended.

Last modified Sunday May 28, 2000 by: [Sape A. Miedema](#)

Translation by: [Laurens de Jonge](#)

Figures, equations and tables by: [Erik Miedema](#)

Copyright © May, 2000 Dr.ir. S.A. Miedema



[Download Adobe Acrobat Reader V4.0](#)

3.08 The location of the cutting force.

A quantity that is measured but has not been integrated in the theory, is the location of the resulting cutting force. This quantity can be of importance for the determination of the equilibrium of a drag head. The locations, of the in this chapter performed tests, are listed in table 3.5. Table 3.6 lists the dimensionless locations of the resulting cutting force, in relation with the layer-thickness.

Configuration		1	2	3	4
α	h_b/h_i	$h = 0.10$	0.15	0.20	0.30
30°	1	51.25	63.1	96.7	157.2
30°	2	76.00	55.7	61.3	84.8
30°	3	----	50.5	54.3	71.5
45°	1	66.38	87.5	128.0	----
45°	2	55.13	56.9	73.4	128.6
45°	3	----	62.0	56.0	82.1
60°	1	69.88	99.5	----	----
60°	2	50.00	68.4	86.1	123.9
60°	3	46.25	55.0	66.3	95.1

Table 3.5: The location of the resulting cutting force (chapter 3.8) in mm from the blade tip, for the blade configurations of chapter 3.6.

From these tables the following conclusions can be drawn:

1. The location of the resulting cutting force is closer to the blade tip (table 3.6) with larger blade dimensions.
2. The location of the resulting cutting force is closer to the blade tip (table 3.6) with a smaller blade-height / layer-thickness ratio.

The first conclusion can be based upon the fact that a possible present adhesion, on a larger scale (and therefore layer-thickness) causes, in proportion, a smaller part of the cutting force. For the second conclusion this can also be a cause, although the blade-height / layer-thickness ratio must be

seen as the main cause.

Configuration		1	2	3	4
α	h_b/h_i	$h = 0.10$	0.15	0.20	0.30
30°	1	0.51	0.42	0.48	0.59
30°	2	1.52	0.75	0.61	0.56
30°	3	----	1.01	0.82	0.71
45°	1	0.67	0.58	0.64	----
45°	2	1.11	0.76	0.63	0.73
45°	3	----	1.25	0.84	0.83
60°	1	0.70	0.66	----	----
60°	2	1.01	0.91	0.86	0.83
60°	3	1.38	1.11	0.99	0.95

Table 3.6: The location of the resulting cutting force (chapter 3.8) from the blade tip, along the blade, made dimensionless by dividing with the layer-thickness, for the blade configurations of chapter 3.6

[Back to top](#)

This is a translation of the dissertation of Dr.ir. S.A. Miedema, dated September 15th 1987 .

The dissertation was originally published in Dutch by the:

Delft University of Technology

Faculty of Mechanical Engineering and Marine Technology

Chair of Dredging Technology

Mekelweg 2

2628 CD, Delft

The Netherlands

It is advised to also read the papers following this dissertation, since the theory developed has been refined and extended.

Last modified Sunday May 28, 2000 by: [Sape A. Miedema](#)

Translation by: [Laurens de Jonge](#)

Figures, equations and tables by: [Erik Miedema](#)

Copyright © May, 2000 [Dr.ir. S.A. Miedema](#)



[Download Adobe Acrobat Reader V4.0](#)



3.09 Verification forces and water pore pressures in 200 μm sand.

[Contents](#)

The linear cutting theory is researched on three points:

1. The distribution of the water pore-pressures on the blade for a blade with a radius of rounding of 1 mm.
2. The distribution of the water pore-pressures on the blade for a blade with a flat wear face of approximately 10 mm and a clearance angle of 1° .
3. The correlation between the measured cutting forces and the theoretical cutting forces.

The dimensions of the blades and the wear faces can be found in figure 3.5. In table 3.9 the ratios of the wear face length and the layer-thickness are listed. In the preceding paragraph already a few conclusions are drawn upon the correlation between the measured and the calculated cutting forces. In this research both the forces and the water pressures are measured to increase the knowledge of the accuracy of the theory. Also it has to be mentioned that the soil mechanical parameters are determined during this research.

In figure 3.6 the results of a test are shown. The results of the whole research of the forces are listed in table 3.7 for the blade with the radius of rounding of 1 mm and in table 3.8 for the blade with the wear face. The dimensionless measured water pore-pressures are shown in figures 3.7 to 3.16, in which the theoretical distribution is represented by the solid line. The water sub-pressures are made dimensionless analogously to equation (2.14), although the weighed average permeability k_m is used instead of the permeability k_{\max} used in the equation.

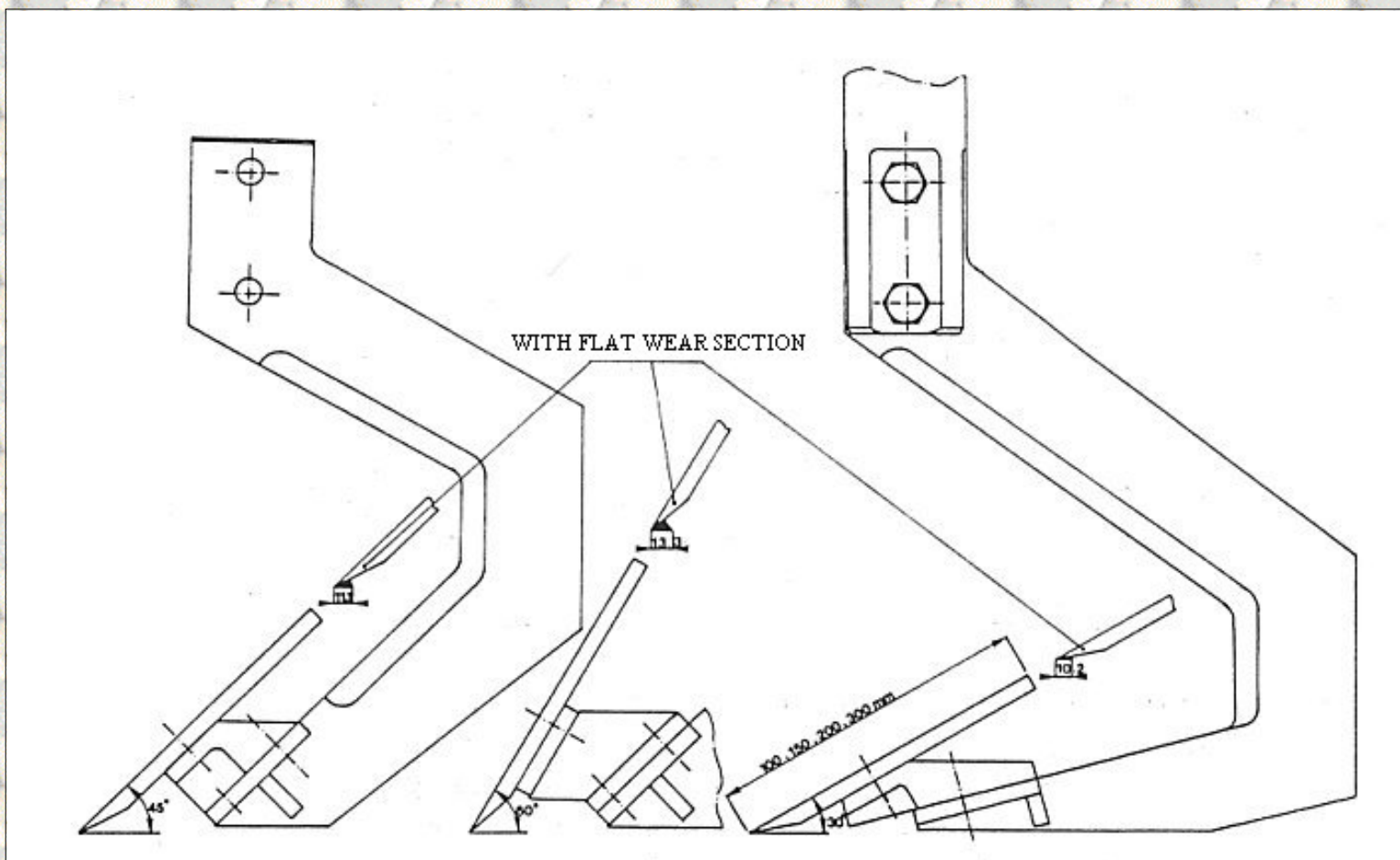


Figure 3.5: The middle blade with the blade mounting.

From this research the following conclusions can be drawn:

1. The measured forces and water pore-pressures show, in general, a good correlation with the theory.
2. The tendency towards increasing and more upward aimed forces with increasing blade angles can be observed clearly in the tables 3.7 and 3.8.
3. The ratio between the measured and calculated forces becomes smaller when the blade angle and the blade-height / layer-thickness ratio increase.
4. The cutting forces on the blade with the wear face are almost equal to the cutting forces on the blade with the radius of rounding, but are slightly aimed more upward.
5. The ratio between the measured and calculated water pore-pressures is, in general, smaller than the ratio between the measured and calculated cutting forces.
6. The measured water pore-pressures on the blade with the wear face and the blade with the radius of rounding differ slightly (table 3.9) from the water pore-pressures on the blade with the radius of rounding. On the 30° and the 45° blade, the water pore-pressures tend to smaller values for the blade with the wear face, although the differences are very small. On the 60° blade these water under-pressures are slightly higher. Therefore it can be concluded that, for water pressures calculations, the wear-section-length / layer-thickness ratio w/h_i has to be chosen dependent of the blade angle. Which was already clear during the tests because the clearance angle increased with a larger blade angle. For the determination of table 2.14 to 2.25, however, the ratio used was w/h_i , which is a good average value.

		measured				calculated	
		uncorrected		corrected		theoretical	
α	h_b/h_i	c_t	θ_t	c_t	θ_t	c_t	θ_t
30°	1	0.54	+29.3°	0.49	+29.0°	0.39	+28.3°
30°	2	0.48	+27.5°	0.46	+27.2°	0.43	+27.4°
30°	3	0.49	+27.6°	0.46	+27.3°	0.43	+27.3°
45°	1	0.78	+15.1°	0.58	+13.9°	0.49	+12.9°
45°	2	0.64	+12.3°	0.59	+11.6°	0.57	+10.7°
45°	3	0.60	+11.0°	0.55	+10.5°	0.61	+ 9.9°
60°	1	1.16	+ 0.7°	0.77	- 0.6°	0.69	+ 0.7°
60°	2	0.95	- 1.4°	0.79	- 2.2°	0.83	- 3.2°
60°	3	0.93	- 3.4°	0.82	- 4.0°	0.91	- 4.6°
60°	6	0.70	- 4.8°	0.64	- 5.7°	1.14	- 7.4°

Table 3.7: Measured dimensionless forces, not-corrected and corrected for gravity and inertia

forces and theoretical values according table 2.14 to 2.25 for the blade with the radius of rounding and the sub-pressure behind the blade (chapter 3.9). The theoretical values for c_t en θ_t are determined according chapter 2.12. They are based on values for the angle of internal friction of 38° , a soil/steel angle of friction of 30° and a weighed average permeability of 0.000242 m/s, dependent on the weigh factor a_1 .

		measured				calculated	
		uncorrected		corrected		theoretical	
α	h_b/h_i	c_t	θ_t	c_t	θ_t	c_t	θ_t
30°	1	0.53	$+26.2^\circ$	0.48	$+25.9^\circ$	0.39	$+28.3^\circ$
30°	2	0.48	$+24.0^\circ$	0.46	$+23.7^\circ$	0.43	$+27.4^\circ$
30°	3	0.49	$+24.7^\circ$	0.46	$+24.3^\circ$	0.43	$+27.3^\circ$
45°	1	0.72	$+11.9^\circ$	0.57	$+11.0^\circ$	0.49	$+12.9^\circ$
45°	2	0.66	$+ 8.8^\circ$	0.60	$+ 8.3^\circ$	0.57	$+10.7^\circ$
45°	3	0.63	$+ 7.8^\circ$	0.60	$+ 7.3^\circ$	0.61	$+ 9.9^\circ$
60°	1	-----	-----	-----	-----	-----	-----
60°	2	0.90	$- 5.6^\circ$	0.80	$- 6.2^\circ$	0.83	$- 3.2^\circ$
60°	3	0.95	$- 7.3^\circ$	0.87	$- 8.0^\circ$	0.91	$- 4.6^\circ$
60°	6	0.70	$- 9.2^\circ$	0.64	-10.1°	1.14	$- 7.4^\circ$

Table 3.8: Measured dimensionless forces, not-corrected and corrected for gravity and inertia forces and theoretical values according table 2.14 to 2.25 for the blade with the flat wear face and the sub-pressure behind the blade (chapter 3.9). The theoretical values for c_t en θ_t are determined according chapter 2.12. They are based on values for the angle of internal friction of 38° , a soil/steel angle of friction of 30° and a weighed average permeability of 0.000242 m/s, dependent on the weigh factor a_1 .

TESTNUMBER	: SC45A70	CUTTING VELOCITY (m/s)	: 0.681
TESTDATE	: 12/03/1985	INITIAL POROSITY (%)	: 38.11
TESTTIME	: 06: 48: 47		

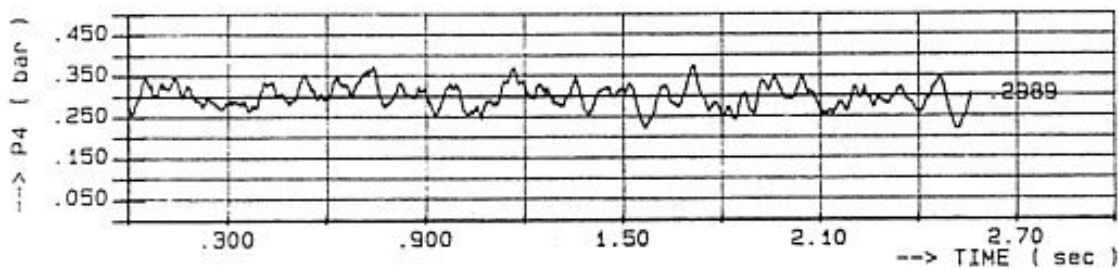
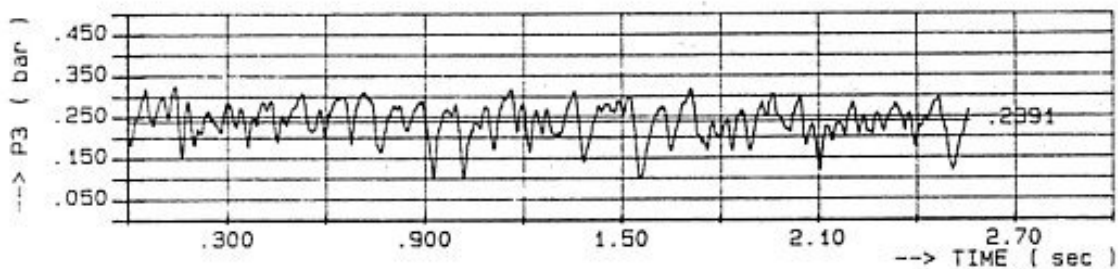
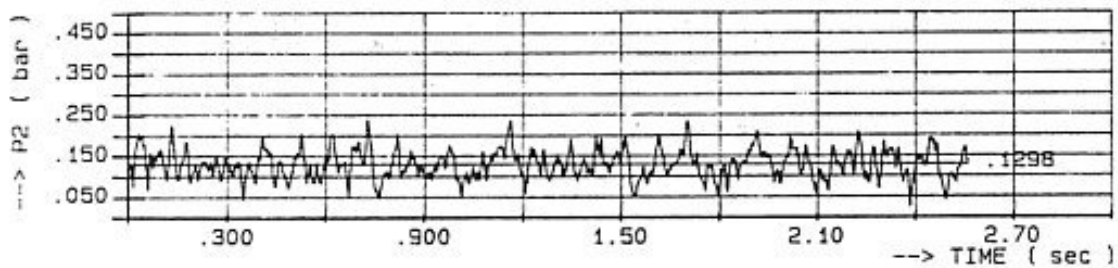
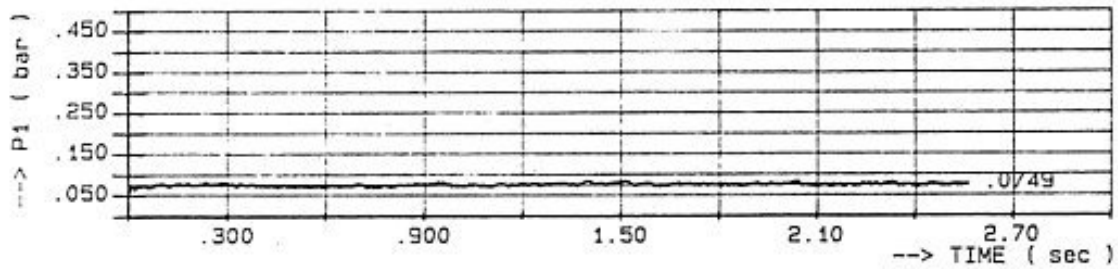
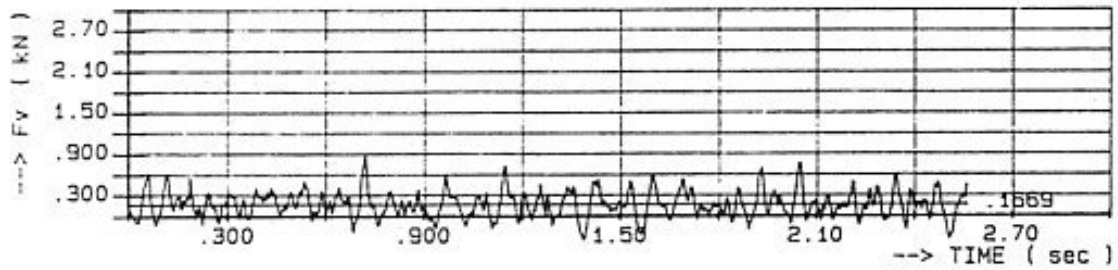
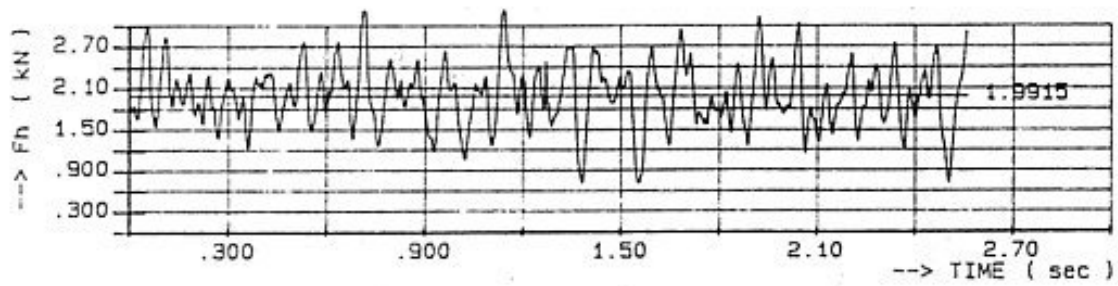


Figure 3.6: The result of a cutting test graphically. In this figure the horizontal force F_h , the vertical force F_v and the water sub-pressures on the blade P1, P2, P3 and P4 are shown (see also figure 3.8). The test is performed with a blade angle α of 45° , a layer thickness h_i of 70 mm and a cutting velocity v_c of 0.68 m/s in the 200 μ m sand.

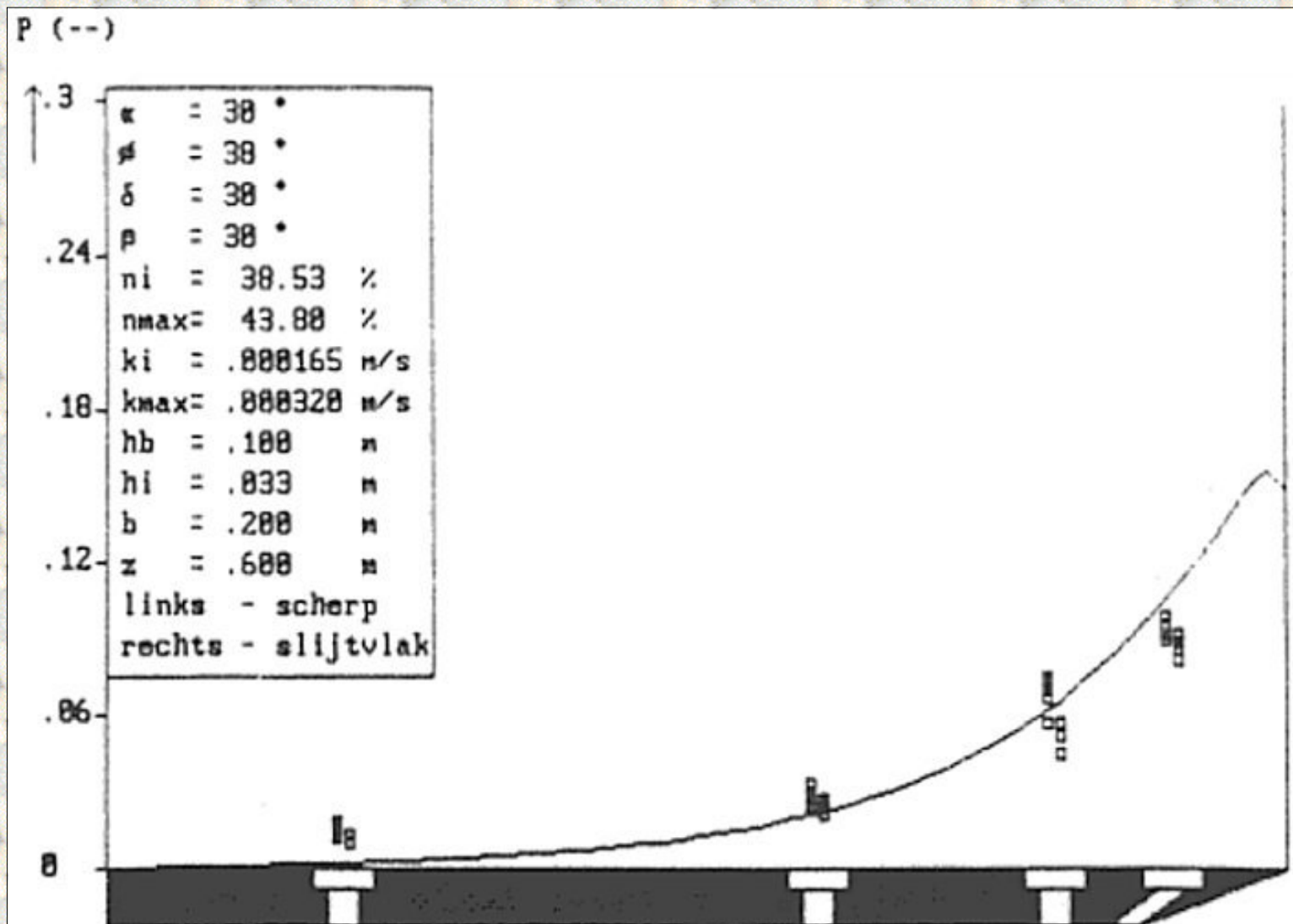


Figure 3.7 : The dimensionless water pore pressures on the blade. Experiments in 200 μ m sand with a 30° blade, layer thickness h_i of 33 mm, blade height h_b of 100 mm and a non-cavitating cutting process.

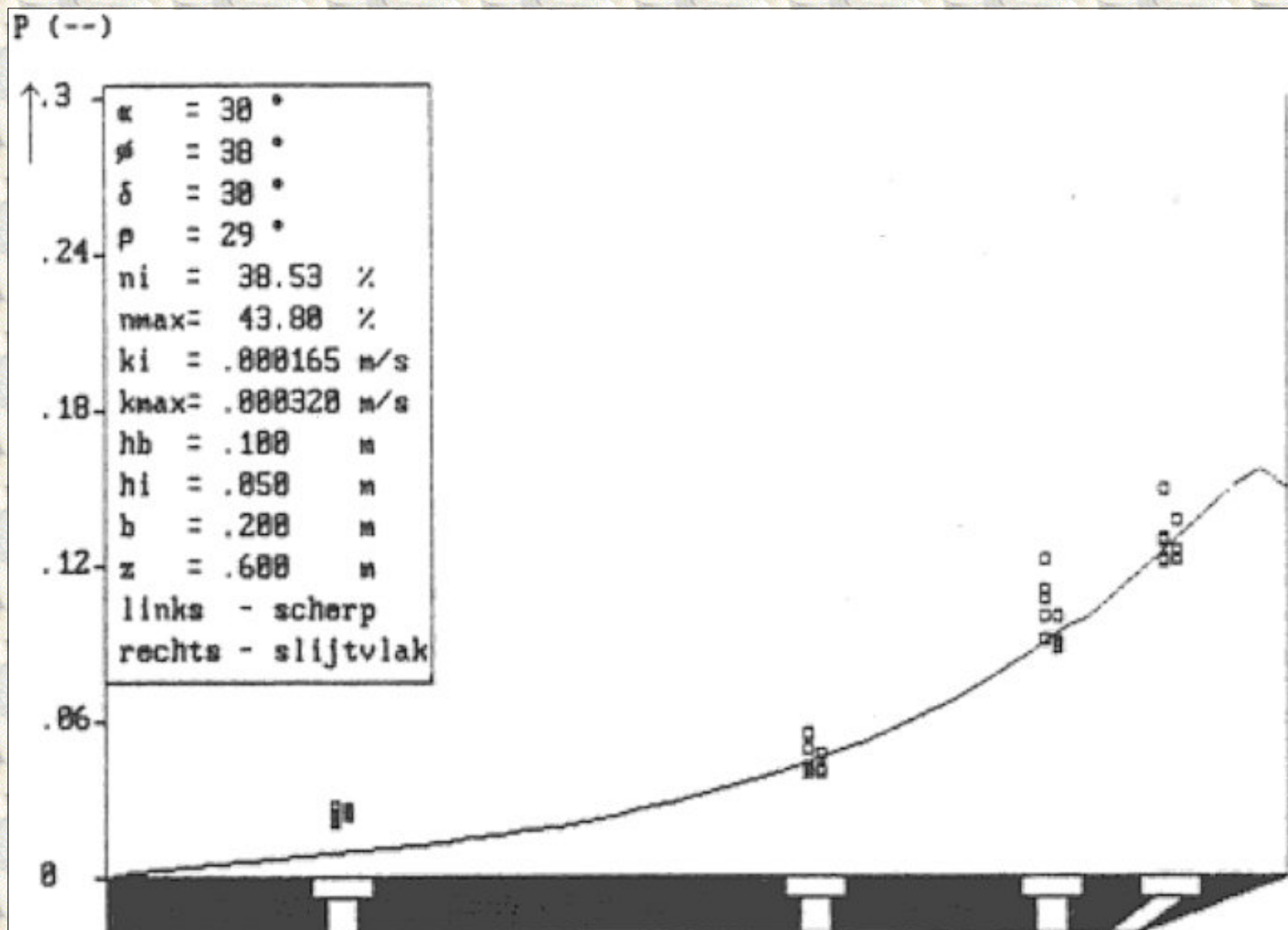


Figure 3.8 : The dimensionless water pore pressures on the blade. Experiments in 200 μ m sand with a 30° blade, layer thickness h_i of 50 mm, blade height h_b of 100 mm and a non-cavitating cutting process.

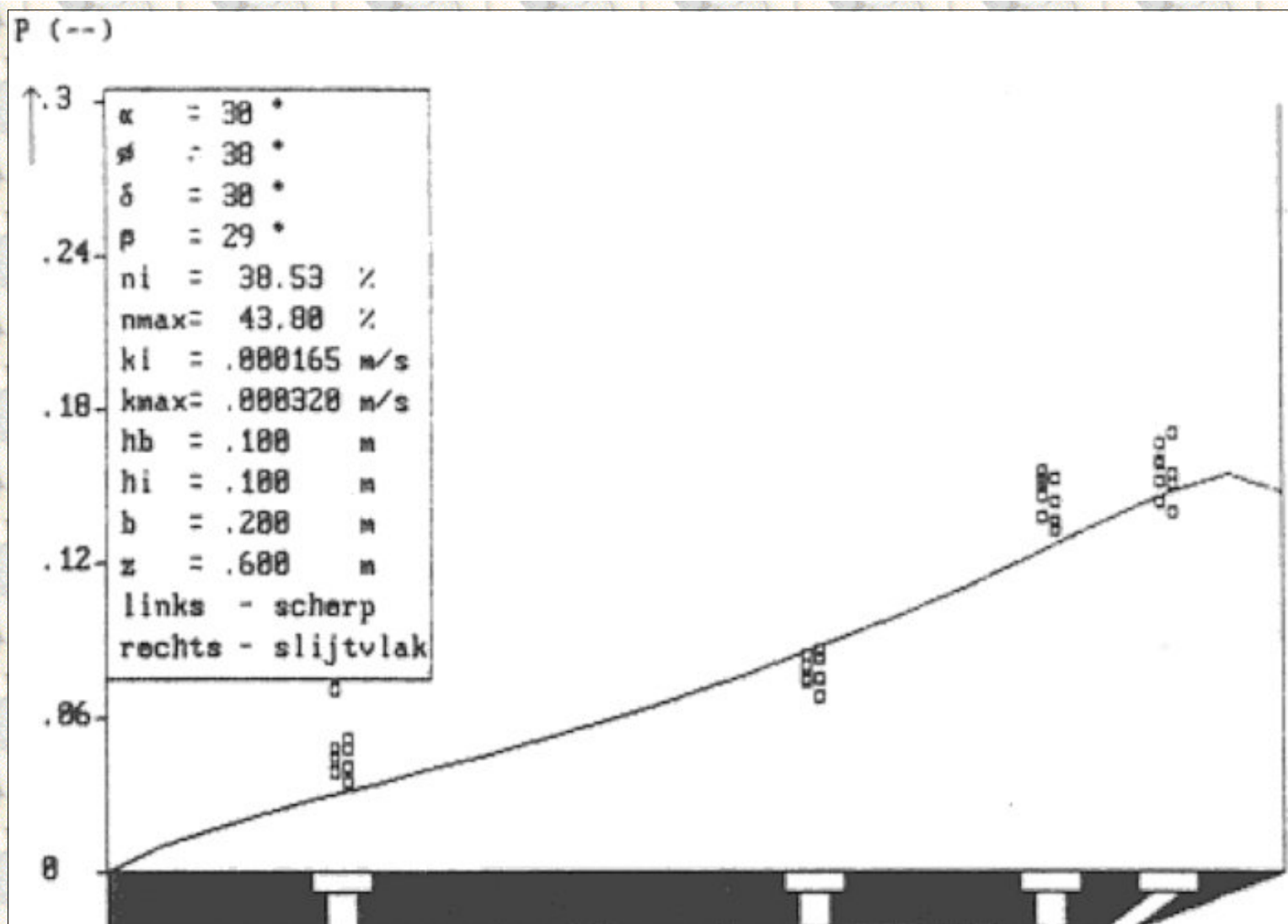


Figure 3.9 : The dimensionless water pore pressures on the blade. Experiments in 200 μm sand with a 30° blade, layer thickness h_i of 100 mm, blade height h_b of 100 mm and a non-cavitating cutting process.

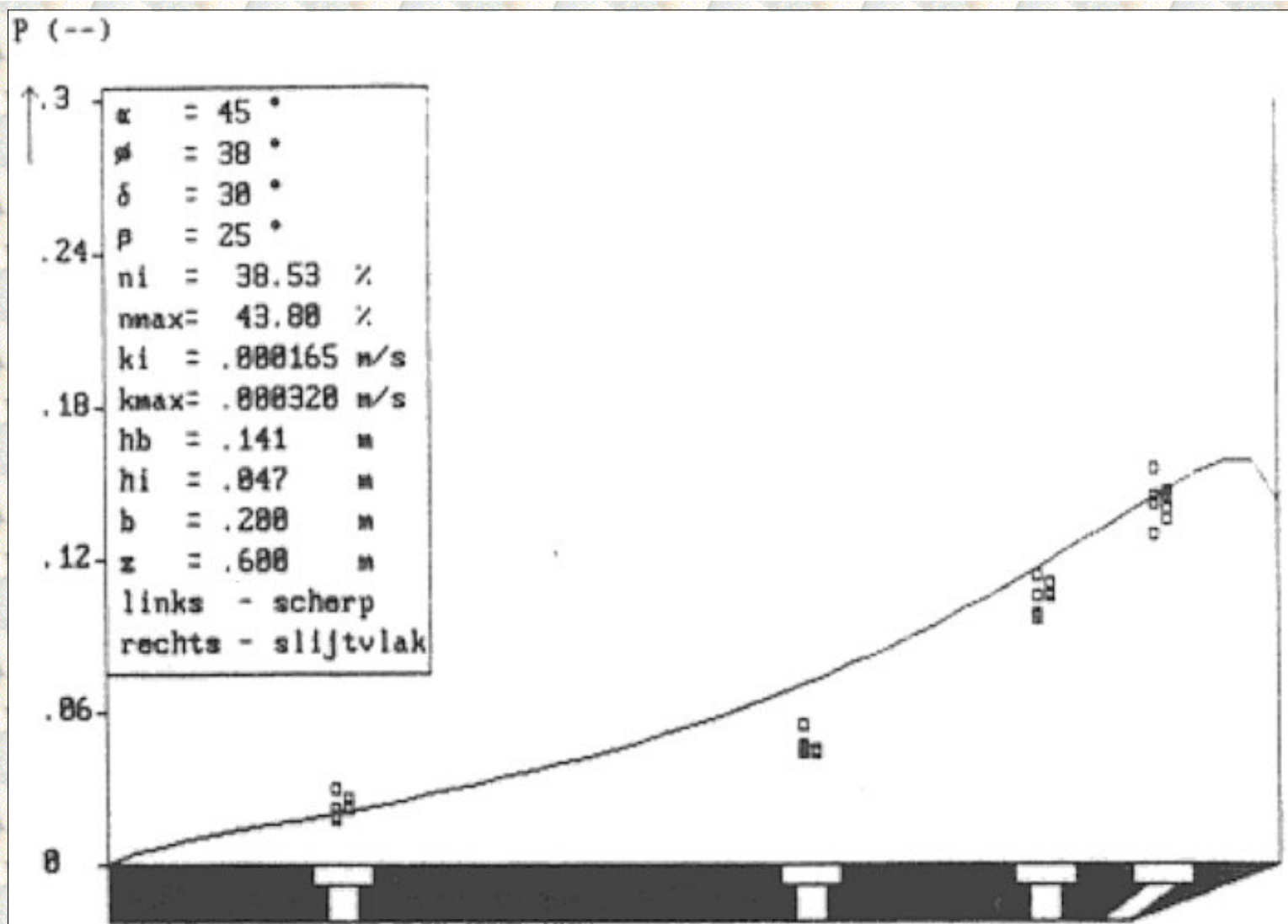


Figure 3.10 : The dimensionless water pore pressures on the blade. Experiments in 200 μm sand with a 45° blade, layer thickness h_i of 47 mm, blade height h_b of 141 mm and a non-cavitating cutting process.

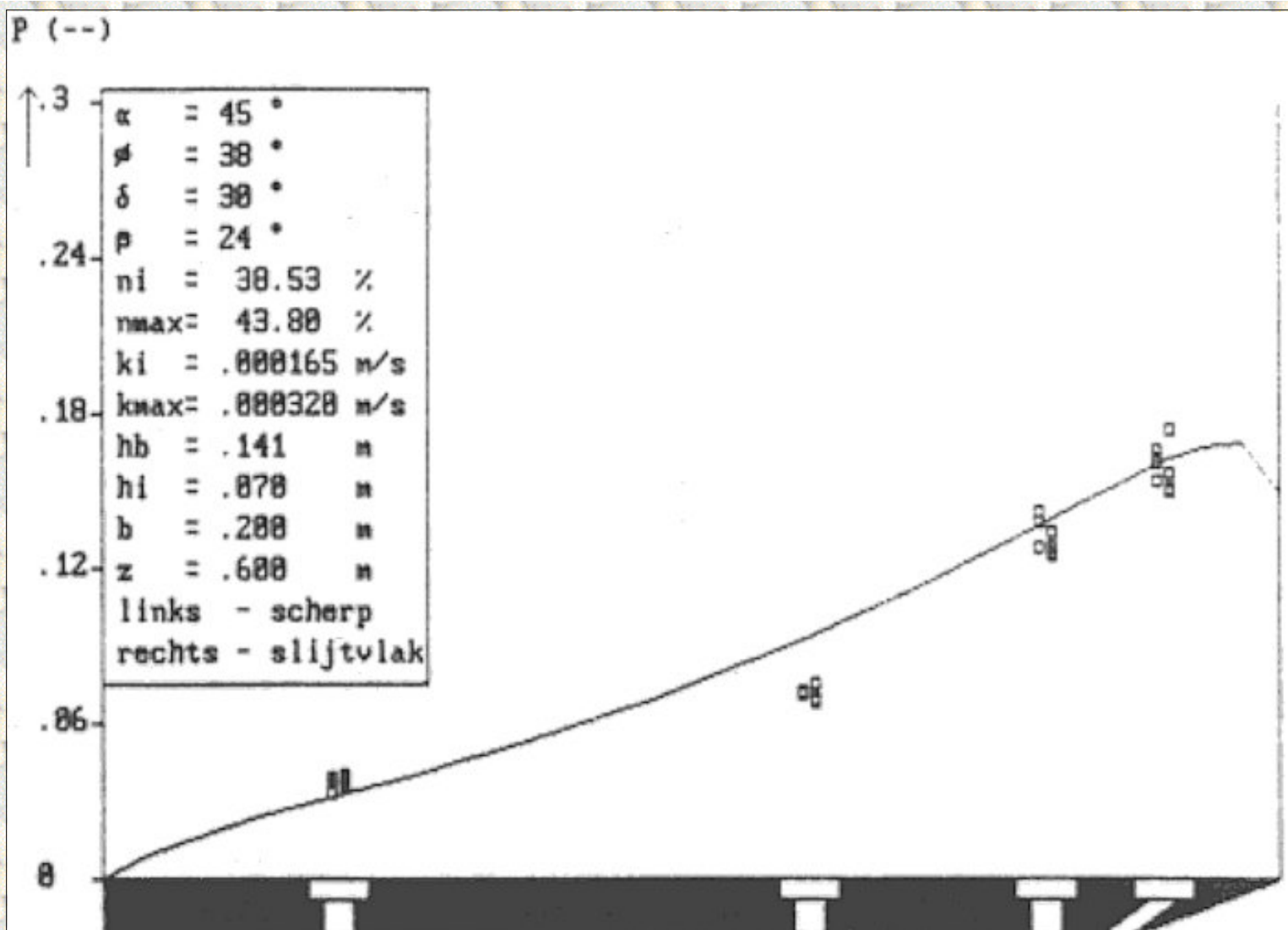


Figure 3.11 : The dimensionless water pore pressures on the blade. Experiments in 200 μ m sand with a 45° blade, layer thickness h_i of 70 mm, blade height h_b of 141 mm and a non-cavitating cutting process.

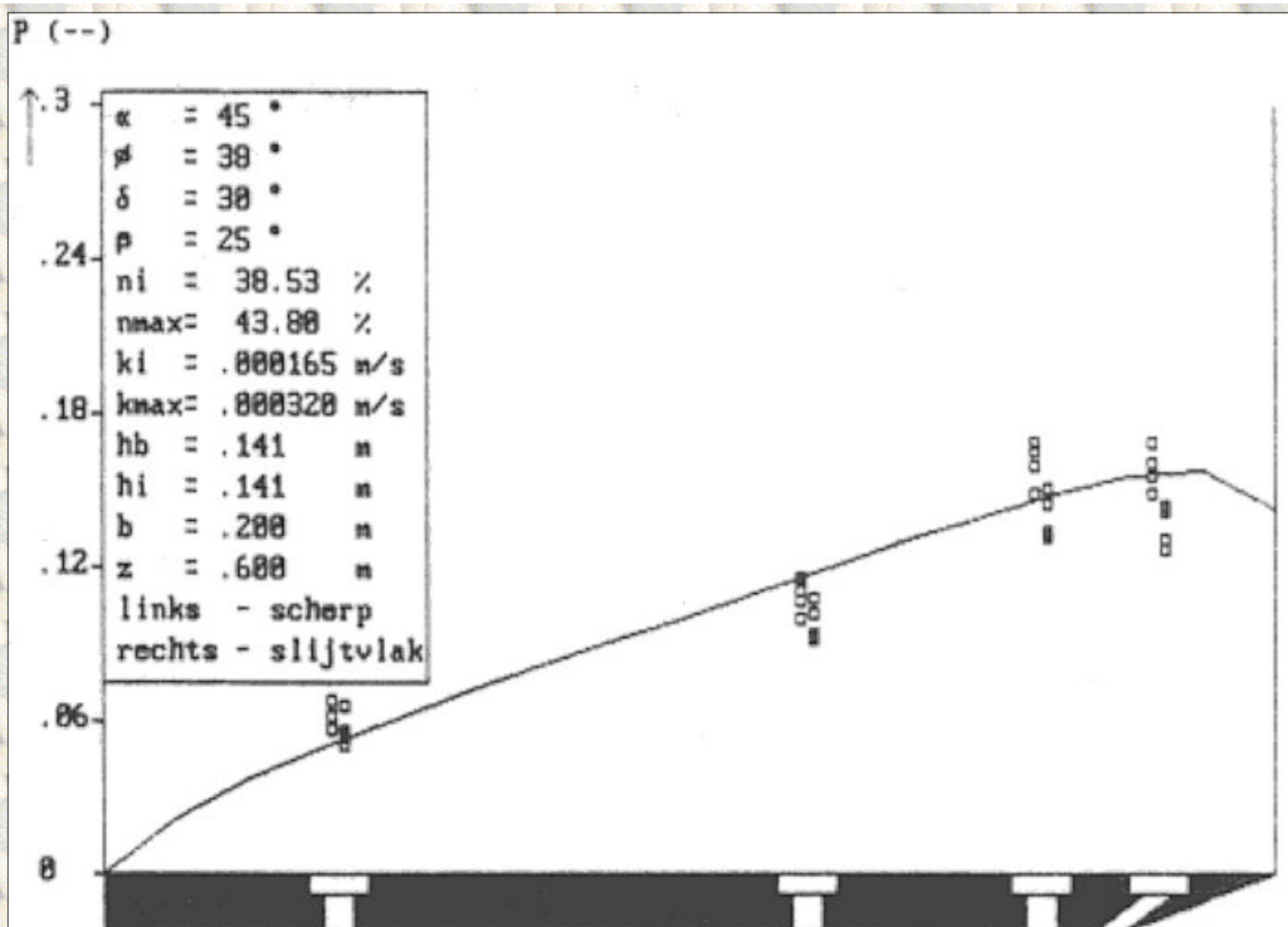


Figure 3.12 : The dimensionless water pore pressures on the blade. Experiments in $200 \mu\text{m}$ sand with a 45° blade, layer thickness h_i of 141 mm, blade height h_b of 141 mm and a non-cavitating cutting process.

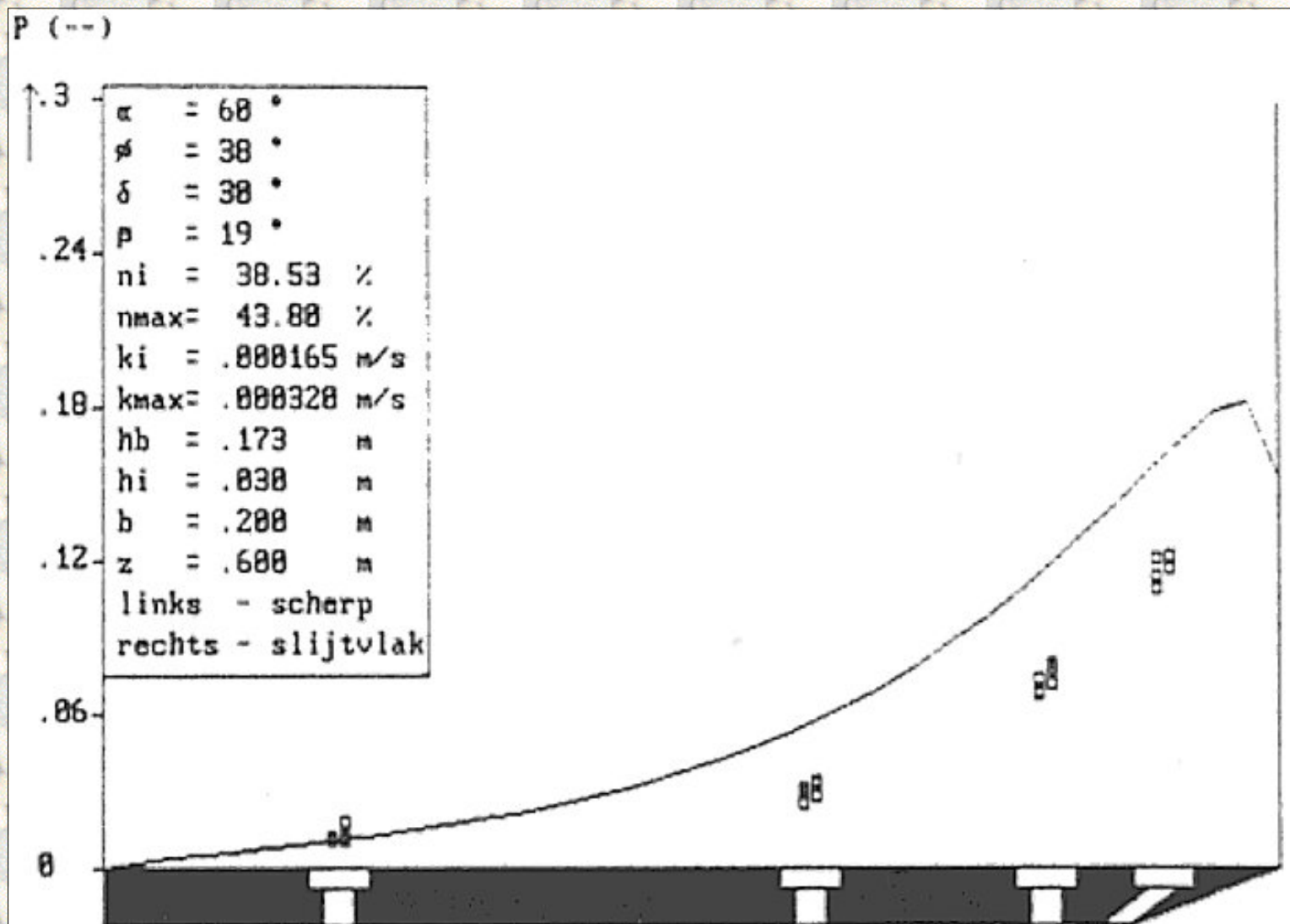


Figure 3.13 : The dimensionless water pore pressures on the blade. Experiments in 200 μm sand with a 60° blade, layer thickness h_i of 30 mm, blade height h_b of 173 mm and a non-cavitating cutting process.

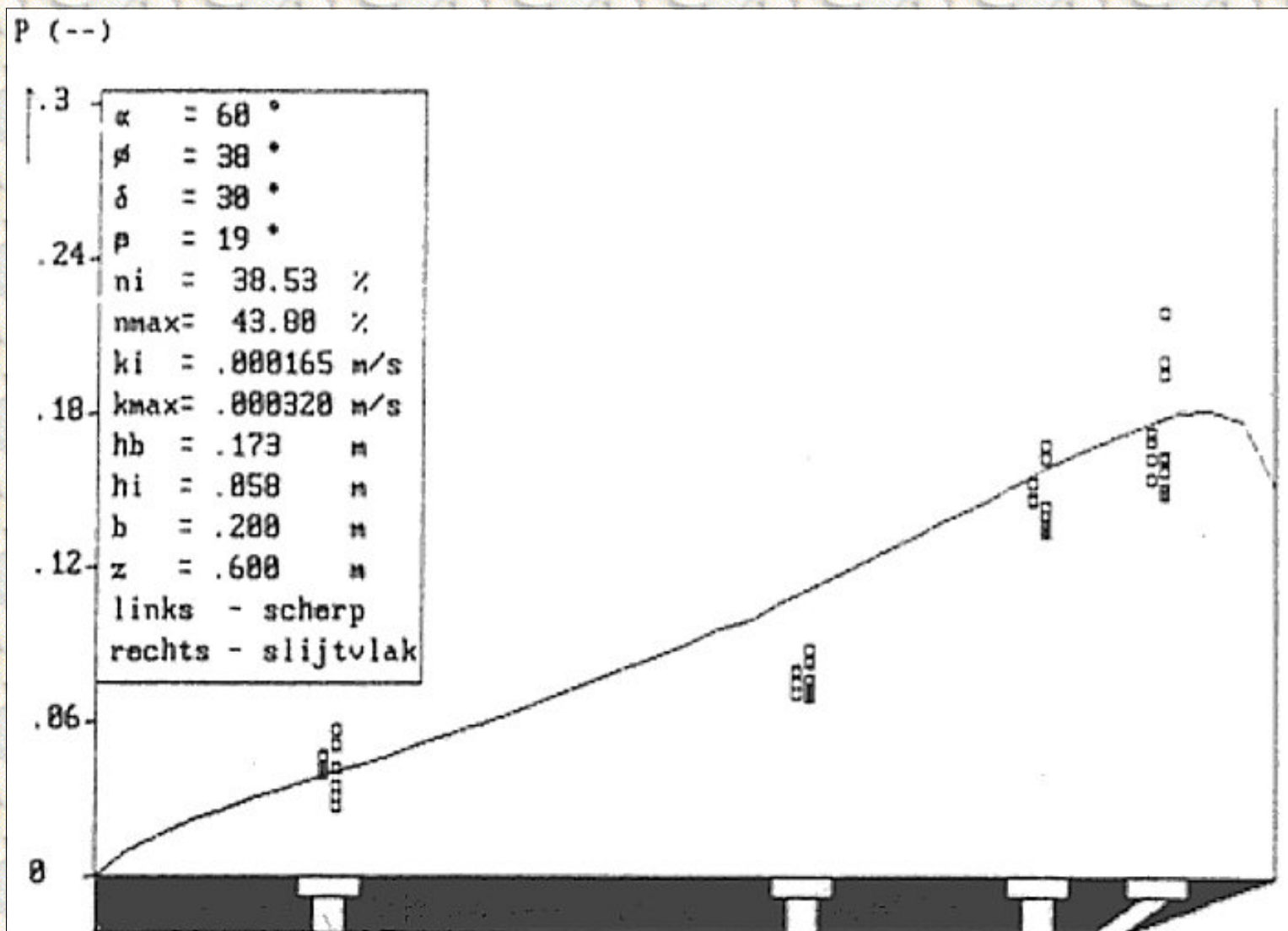


Figure 3.14 : The dimensionless water pore pressures on the blade. Experiments in 200 μ m sand with a 60° blade, layer thickness h_i of 58 mm, blade height h_b of 173 mm and a non-cavitating cutting process.

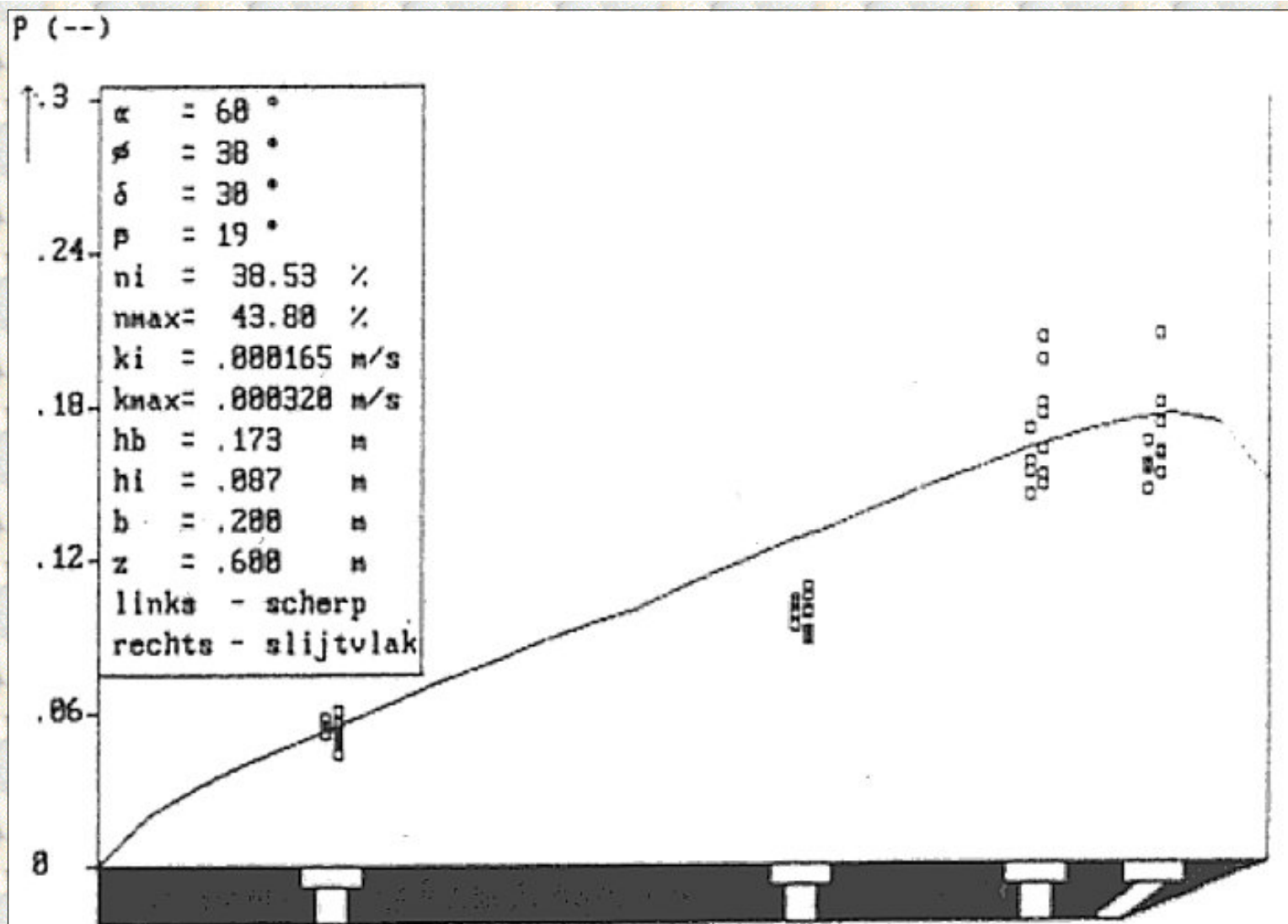


Figure 3.15 : The dimensionless water pore pressures on the blade. Experiments in 200 μm sand with a 60° blade, layer thickness h_i of 87 mm, blade height h_b of 173 mm and a non-cavitating cutting process.

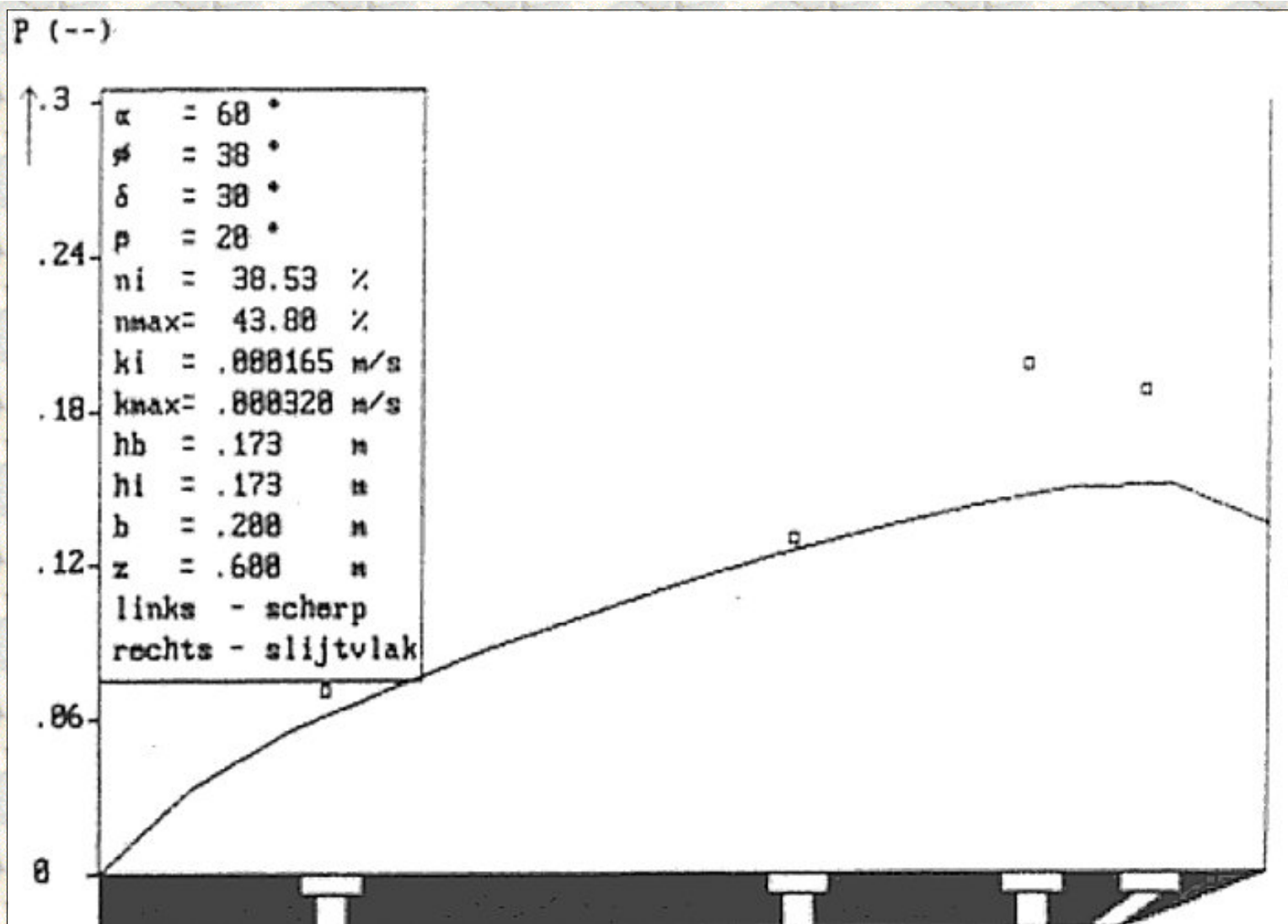


Figure 3.16 : The dimensionless water pore pressures on the blade. Experiments in 200 μm sand with a 60° blade, layer thickness h_i of 173 mm, blade height h_b of 173 mm and a non-cavitating cutting process.

α	h_b/h_i	w	h_i	w/h_i	p_{2ma}	p_{2ms}	p_{2m}	p_{2ms}/p_{2ma}
30°	1	10.2	100	0.102	0.076	0.073	0.076	0.96
30°	2	10.2	50	0.204	0.051	0.050	0.049	0.98
30°	3	10.2	33	0.308	0.034	0.030	0.034	0.88
45°	1	11.1	141	0.079	0.090	0.080	0.097	0.89
45°	2	11.1	70	0.159	0.069	0.068	0.082	0.99
45°	3	11.1	47	0.236	0.052	0.051	0.065	0.98
60°	1	13.3	173	0.077	0.107	-----	0.091	----
60°	2	13.3	87	0.153	0.083	0.090	0.100	1.08
60°	3	13.3	58	0.229	0.075	0.081	0.094	1.08
60°	6	13.3	30	0.443	0.035	0.038	0.061	1.09

Table 3.9: The average dimensionless pore pressures on the blade, on the blade with the radius of

rounding p_{2ma} and the blade with the wear face p_{2ms} , the theoretical values p_{2m} and the ratio between the sub-pressures p_{2ms} en p_{2ma} , as a function of the length of the wear face w (mm), the layer-thickness h_i (mm) and the wear-section-length / layer-thickness ratio (chapter 3.9).

[Back to top](#)

This is a translation of the dissertation of Dr.ir. S.A. Miedema, dated September 15th 1987 .
The dissertation was originally published in Dutch by the:
Delft University of Technology
Faculty of Mechanical Engineering and Marine Technology
Chair of Dredging Technology
Mekelweg 2
2628 CD, Delft
The Netherlands

It is advised to also read the papers following this dissertation, since the theory developed has been refined and extended.

Last modified Sunday May 28, 2000 by: [Sape A. Miedema](#)

Translation by: [Laurens de Jonge](#)

Figures, equations and tables by: [Erik Miedema](#)

Copyright © May, 2000 Dr.ir. S.A. Miedema



[Download Adobe Acrobat Reader V4.0](#)

3.10 Verification forces and water pore pressures in 105 μm sand.

[Contents](#)

The linear cutting theory for the 105 μm is researched on three points:

1. The distribution of the water pore-pressures on the blade in a non-cavitating cutting process.
2. The distribution of the water pore-pressures on the blade in the transition region between the non-cavitating and the cavitating cutting process.
3. The correlation between the measured cutting forces and the theoretical calculated cutting forces.

The dimensions of the blades can be found in figure 3.5. In this research only a 30° blade with a layer-thickness of 100 mm, a 45° blade with a layer-thickness of 70 mm and a 60° with a layer-thickness of 58 mm, are used, at a blade height h of 200 mm. The soil mechanical parameters of the used sand are listed in appendix B4. The results of the research regarding the cutting forces can be found in table 3.10.

		measured				calculated	
α	h_b/h_i	c_t	θ_t	c_t	θ_t	c_t	θ_t
no cavitation		uncorrected		corrected		theoretical	
30°	1	.45	$+16.5^\circ$.45	$+25.6^\circ$.41	$+25.1^\circ$
45°	2	.50	$- 3.5^\circ$.47	$+ 7.2^\circ$.62	$+ 7.6^\circ$
60°	3	.60	$- 8.8^\circ$.58	$- 6.3^\circ$	1.02	$- 7.5^\circ$
cavitation		uncorrected		corrected		theoretical	
30°	1	3.4	$+13.1^\circ$	3.4	$+24.2^\circ$	3.3	$+21.6^\circ$
45°	2	4.7	-10.3°	4.2	$+ 5.7^\circ$	4.6	$+ 2.6^\circ$
60°	3	4.9	$- 9.0^\circ$	4.8	$- 7.8^\circ$	6.8	-12.1°

Table 3.10: Measured dimensionless forces, not-corrected and corrected for gravity and inertia forces and the theoretical values according tables 2.14 to 2.25 for the non-cavitating cutting process and according tables 2.26 to 2.37 for the cavitating cutting process, calculated with a under-pressure behind the blade. The values of c_t and θ_t are calculated according chapter 2.12. They are based on values for the angle of internal friction of 38° , a soil/steel angle of friction of 30° and a weighed average permeability between 0.00011 m/s and 0.00012 m/s (chapter 3.10), dependent on the weigh factor a_1 and the initial pore percentage of the sandbed.

The dimensionless measured water pore-pressures of the non-cavitating cutting process are presented in figures 3.17 to 3.19, in which the solid line represents the theoretical distribution. The dimensionless measured water pore-pressures in the transition region are presented in figures 3.20 to 3.22. Figures 3.23 to 3.25 show the measured horizontal forces F_h , in which the solid line represents the theoretical distribution. Figure 3.26 to 3.28 show the measured vertical forces F_v , in which the solid line represents the theoretical distribution. Also shown in figures 3.23 to 3.28 is the distribution of the forces, for several water depths, during a fully cavitating cutting process (the

almost horizontal lines).

From this research the following conclusions can be drawn:

1. The tests with the 30° blade give a good correlation with the theory, both for the forces as for the water pore-pressures. For the 45° blade both the forces and the water pore-pressures are lower than the theoretical calculated values with even larger deviations for the 60° blade. For the 60° blade the forces and the water pore-pressures values are approximately 60% of the calculated values.
2. The direction of the cutting forces agrees reasonably well with the theory for all blade angles, after correction for the gravity and the inertia forces.
3. Figures 3.20 to 3.22 show that the profile of the water pore-pressures on the blade, clearly changes shape when the peak stress close to the blade tip (under-pressure) has a value of approximately 65% of the absolute pressure. An increase of the cutting velocity results in a more flattening profile, with a translation of the peak to the middle of the blade. No cavitation is observed but rather an asymptotic approach of the cavitation pressure with an increasing cutting velocity. For the 60° blade the flattening only appears near the blade tip. This can be explained with the large blade-height / layer-thickness ratio. This also explains the low cutting forces in the range where cavitation is expected. There is some cavitation but only locally in the shear zone, the process is not yet fully cavitated.
4. Since, according to the theory from chapter 2, the highest under-pressures will appear in the shear zone, cavitation will appear there first. The theoretical ratio between the highest under-pressure in the shear zone and the highest under-pressure on the blade is approximately 1.6, which is in accordance with conclusion 3. Obviously there is cavitation in the shear zone in these tests, during which the cavitation spot expands to above the blade and higher above the blade with higher cutting velocities.

In figure 3.7 this relation between the cavitation spot and the water pressures profile on the blade are shown. The water under-pressures will become smaller where the cavitation spot ends. This also implies that the measurements give an impression of the size of the cavitation spot.

As soon as cavitation occurs locally in the sand package, it becomes difficult to determine the dimensionless coefficients c_1 and c_2 or d_1 and d_2 . This is difficult because the cutting process in the transition region varies between a cavitating and a non-cavitating cutting process. The ratio between the average water pressure in the shear zone and the average water pressure on the blade surface change continuously with an increasing cutting velocity.

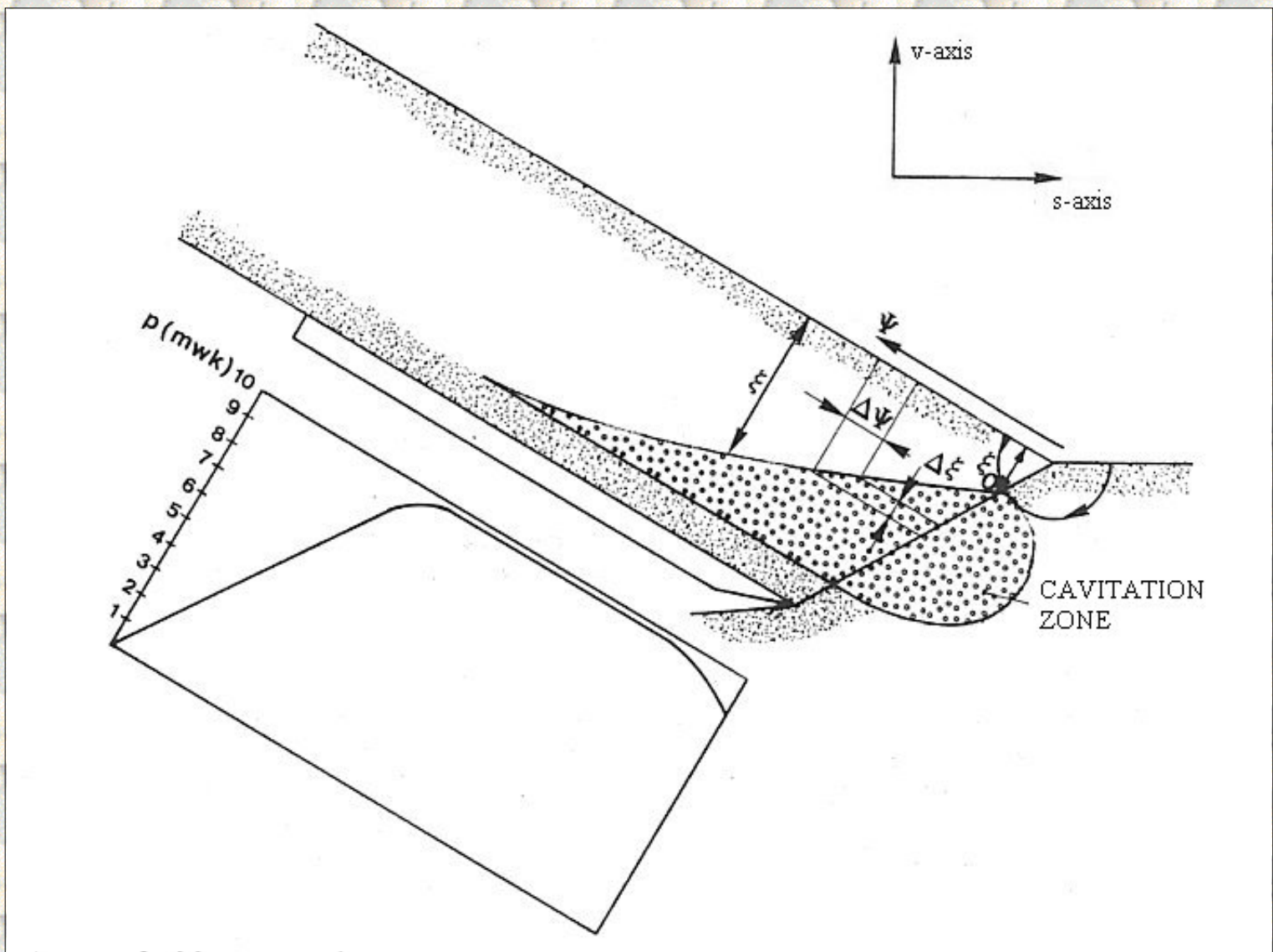


Figure 3.29: The relation between the dimensions of the cavitation spot and the water pressure profile on the blade.

On top of that the shape and the size of the area where cavitation occurs are unknown. However, to get an impression of the cutting process in the transition region, a number of simplifications regarding the water flow through the pores are carried out.

1. The flow from the free sand surface to the shear zone takes place along circular flow lines, both through the packed sand as through the cut sand. With this assumption the distance from the free sand surface to the cavitation area can be determined, according to:

$$\xi_0 = \frac{(z+10)}{v_c \cdot e \cdot \sin(\beta)} \cdot \left[\frac{k_{\max}}{\alpha + \beta} + \frac{k_i}{\pi - \beta} \right] \cdot \sin(\alpha + \beta) \quad (3.1)$$

2. The flow in the cut sand is perpendicular to the free sand surface, from the breakpoint where the shear plane reaches the free sand surface. This flow fills the water vapor bubbles with water. The distance from the free sand surface to the cavitating area can now be determined, under the assumption that the volume flow rate of the vapor bubbles equals the volume flow rate of the dilatancy, according to:

$$\frac{k_{max} \cdot (z+10)}{\xi} \cdot d\psi = v_c \cdot e \cdot \frac{\sin(\beta)}{\sin(\alpha+\beta)} \cdot d\xi \quad (3.2)$$

In which the right term represents the volume flow rate of the vapor bubbles from the dilatancy zone, while the left term represents the supply of water from the free sand surface. This is shown in figure 3.7. With the initial value from equation (3.1) the following solution can be found:

$$\xi = \sqrt{\xi_0^2 + 2 \cdot \frac{k_{max} \cdot (z+10)}{v_c \cdot \frac{\sin(\beta)}{\sin(\alpha+\beta)} \cdot e} \cdot \psi} \quad (3.3)$$

3. The distance from the blade to the cavitation spot is considered to be constant over the blade. The magnitude of this distance is however unknown.

The progressive character of the cavitation spot development results from equation (3.3). If, at a certain cutting velocity, cavitation occurs locally in the cavitation zone, then the resulting cavitation spot will always expand immediately over a certain distance above the blade as a result of the fact that a certain time is needed to fill the volume flow rate of the vapor bubbles.

The development of the water pore-pressures will, in general, be influenced by the ever in the pore water present dissolved air. As soon as water pore-pressures are developing as a result of the increase in volume in the shear zone, part of the dissolved air will form air bubbles. Since these air bubbles are compressible, a large part of the volume strain will be taken in by the expansion of the air bubbles, which results in a less fast increase of the water pore-pressures with an increasing cutting velocity. The maxima of the water pore-pressures will also be influenced by the present air bubbles. This can be illustrated with the following example:

Assume the sand contains 3 volume percent air, which takes up the full volume strain in the dilatancy zone. With a volume strain of 16%, this implies that after expansion, the volume percentage air is 19%. Since it is a quick process, it may be assumed that the expansion is adiabatic, which amounts to maximum water sub-pressures of 0.925 times the present hydrostatic pressure. In an isothermal process the maximum water under-pressures are 0.842 times the present hydrostatic pressure.

From this simple example can be concluded that the in the pore water present, either dissolved or not, air has to be taken into account. In the verification of the water pore-pressures, measured during the cutting tests in the 105 μm sand, the possibility of a presence of dissolved air is recognized but it appeared to be impossible to quantify this influence. It is however possible that the maximum reached water under-pressures (figures 3.20 to 3.22) are limited by the in the pore water present dissolved air.

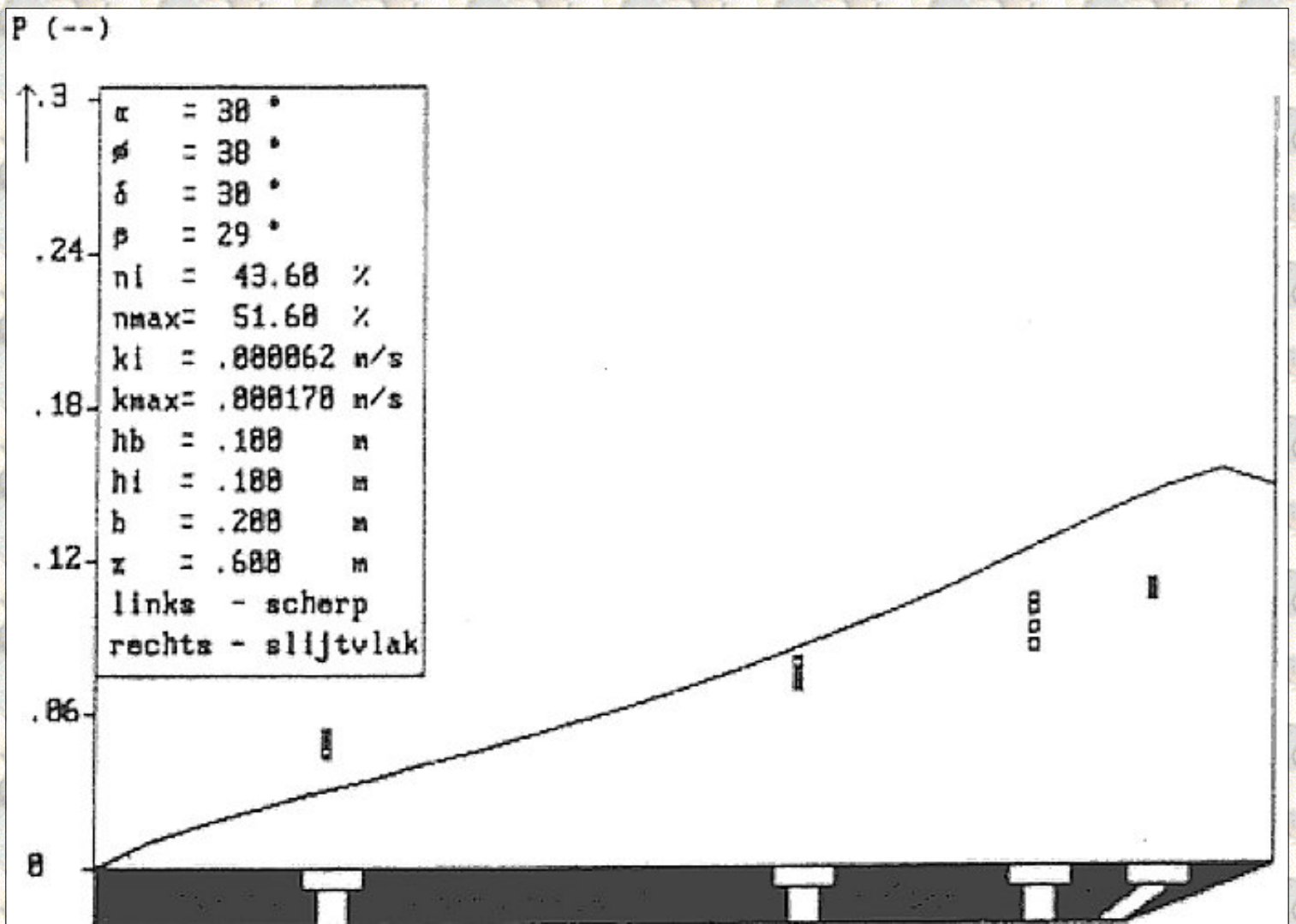


Figure 3.17: The dimensionless water pore pressures on the blade. Experiments in 105 μm sand with a 30° blade, layer thickness h_l of 100 mm, blade height h_b of 100 mm and a non-cavitating cutting process.

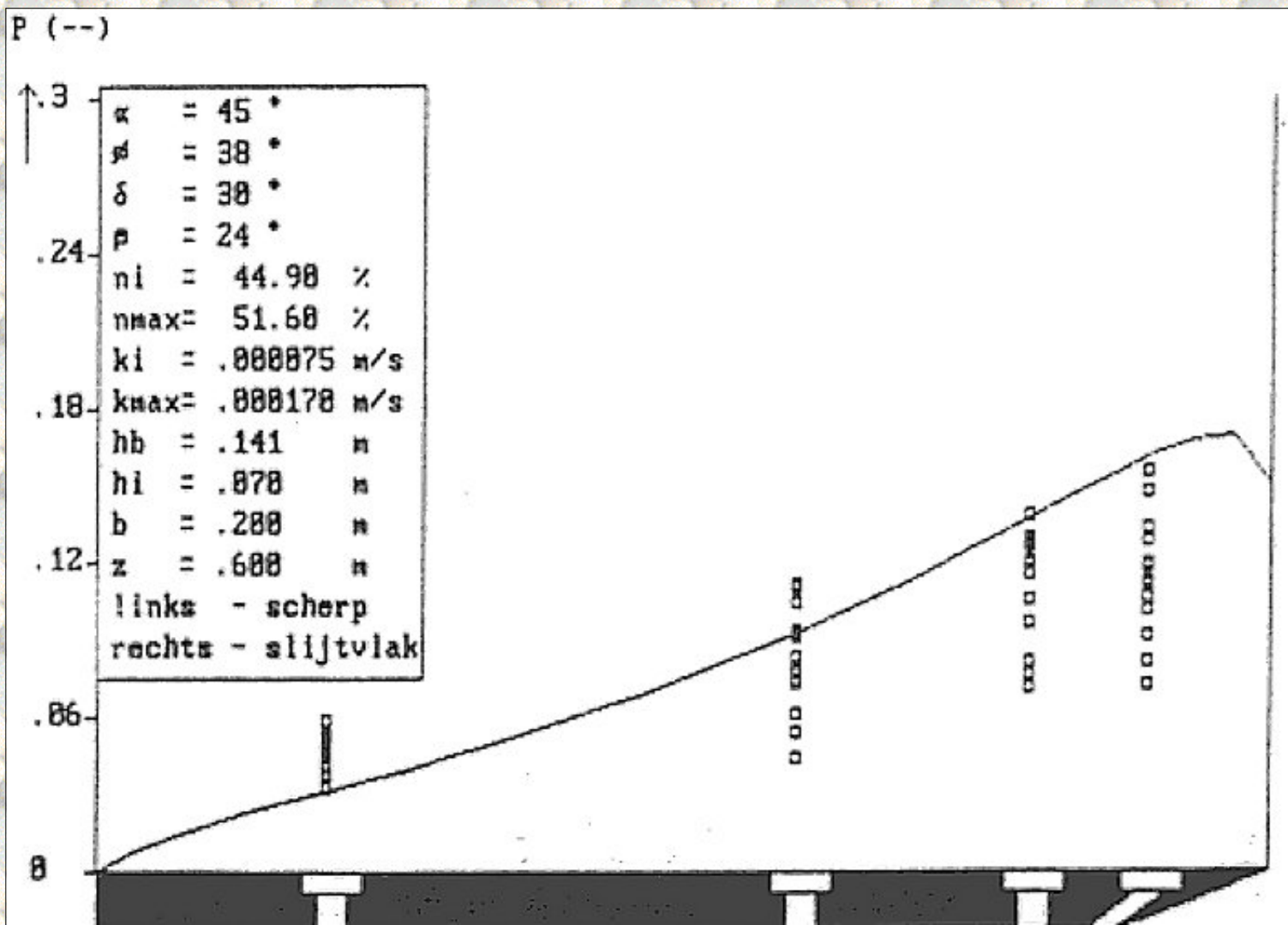


Figure 3.18: The dimensionless water pore pressures on the blade. Experiments in 105 μm sand with a 45° blade, layer thickness h_l of 70 mm, blade height h_b of 141 mm and a non-cavitating cutting process.

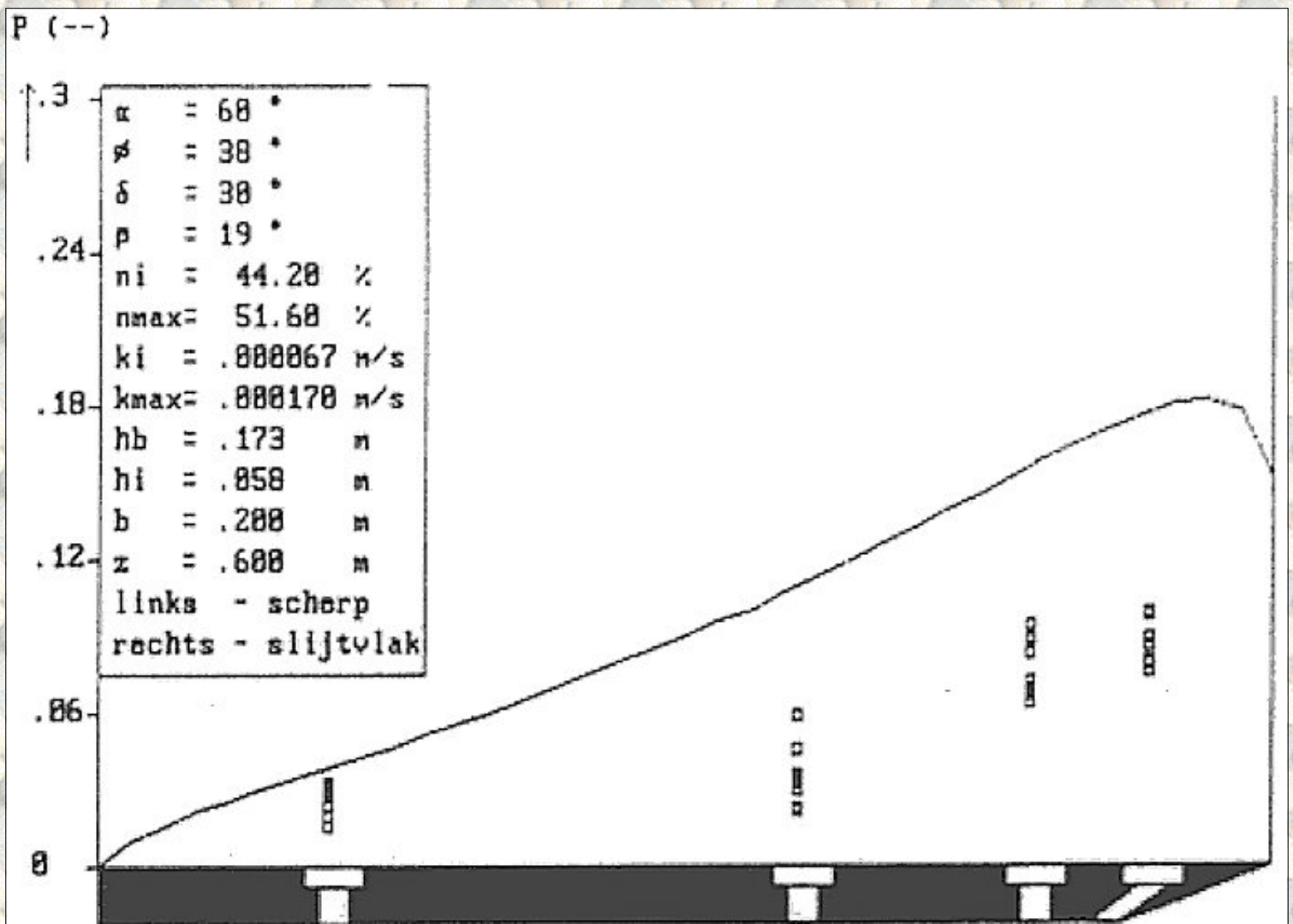


Figure 3.19: The dimensionless water pore pressures on the blade. Experiments in 105 μm sand with a 60° blade, layer thickness h_i of 58 mm, blade height h_b of 173 mm and a non-cavitating cutting process.

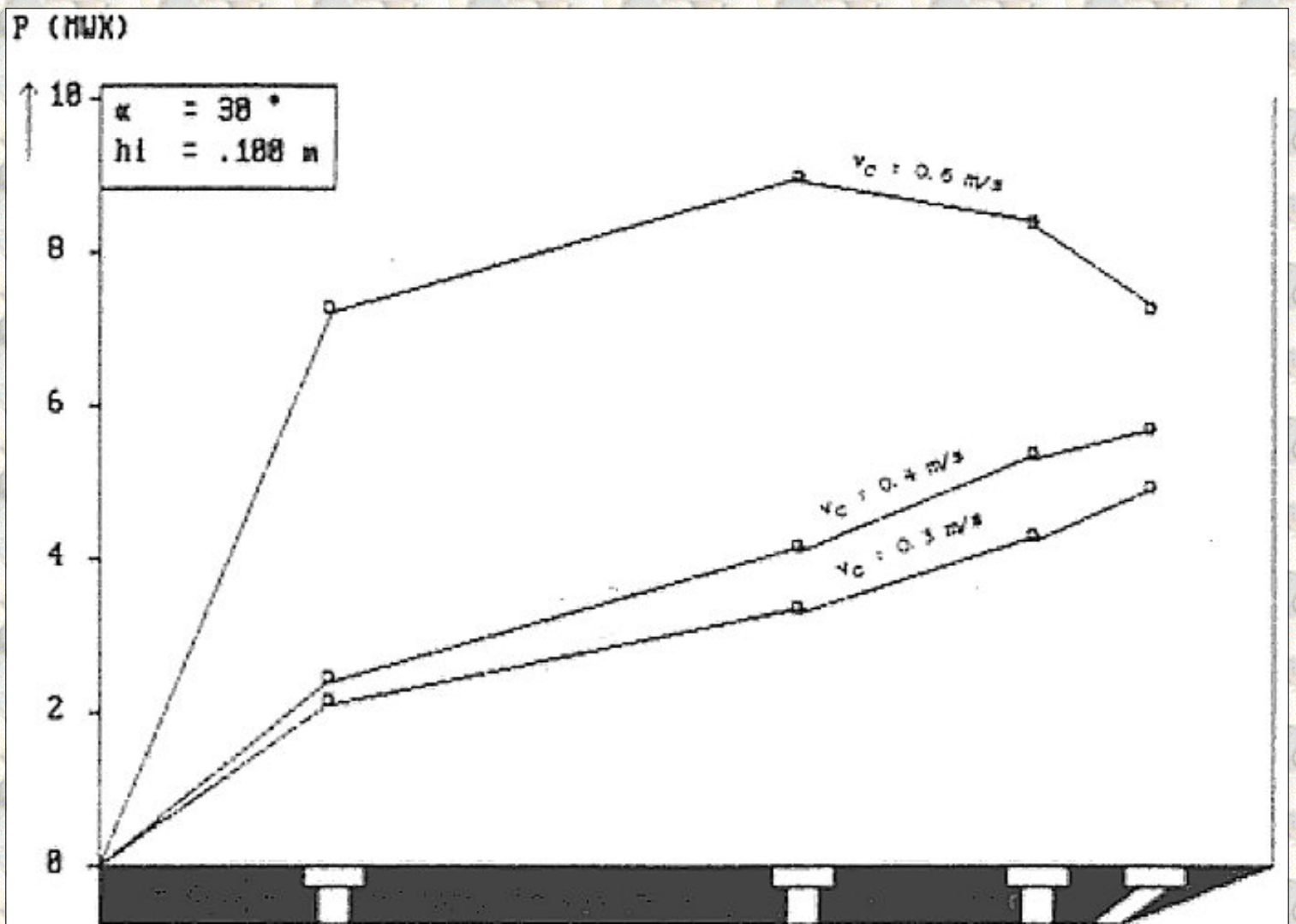


Figure 3.20: The water pore pressures on the blade. Experiments in $105 \mu\text{m}$ sand with a 30° blade, layer thickness h_l of 100 mm, blade height h_b of 100 mm, as a function of the cutting velocity v_c .

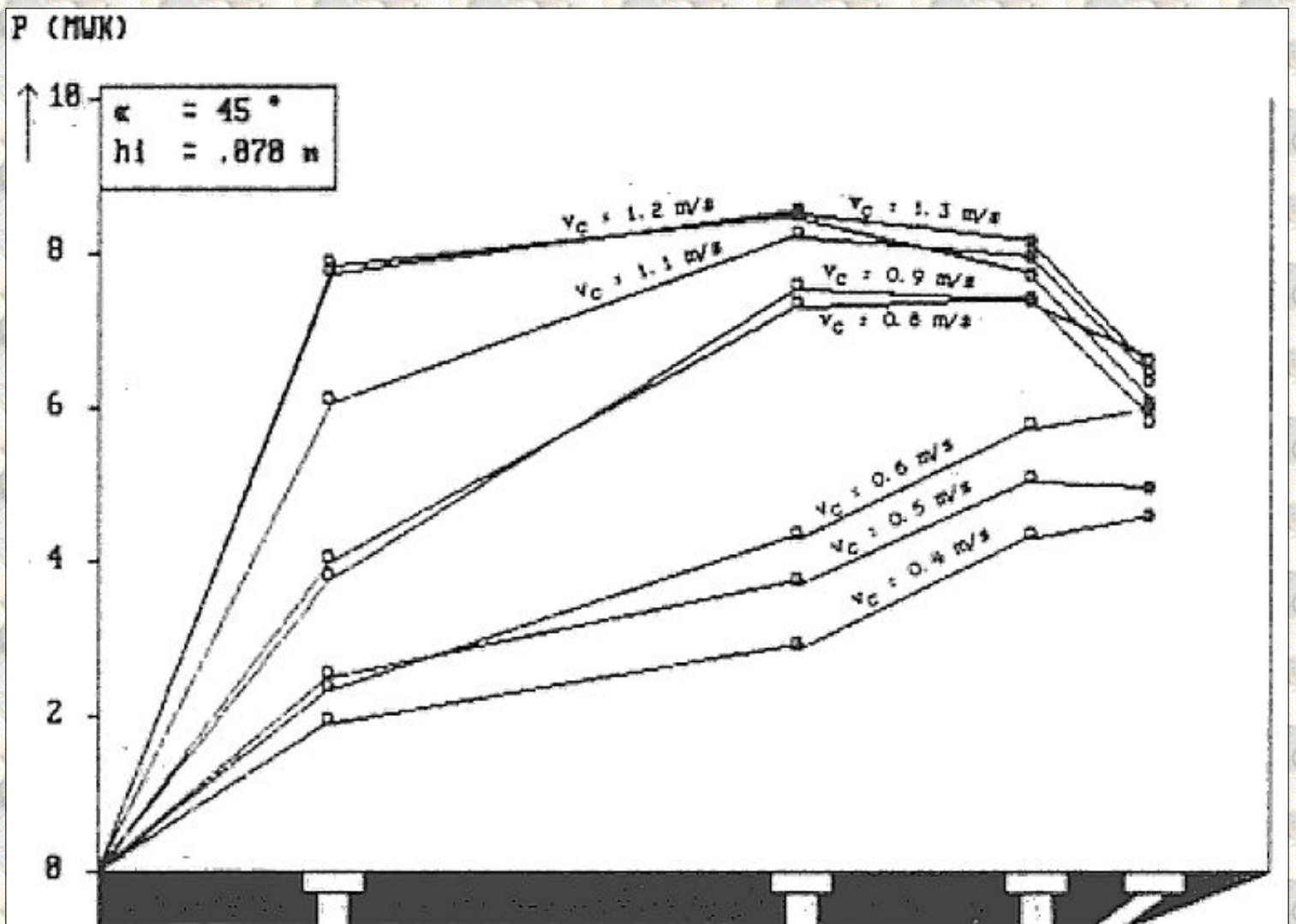


Figure 3.21: The water pore pressures on the blade. Experiments in 105 μ m sand with a 45° blade, layer thickness h_l of 70 mm, blade height h_b of 141 mm, as a function of the cutting velocity v_c .

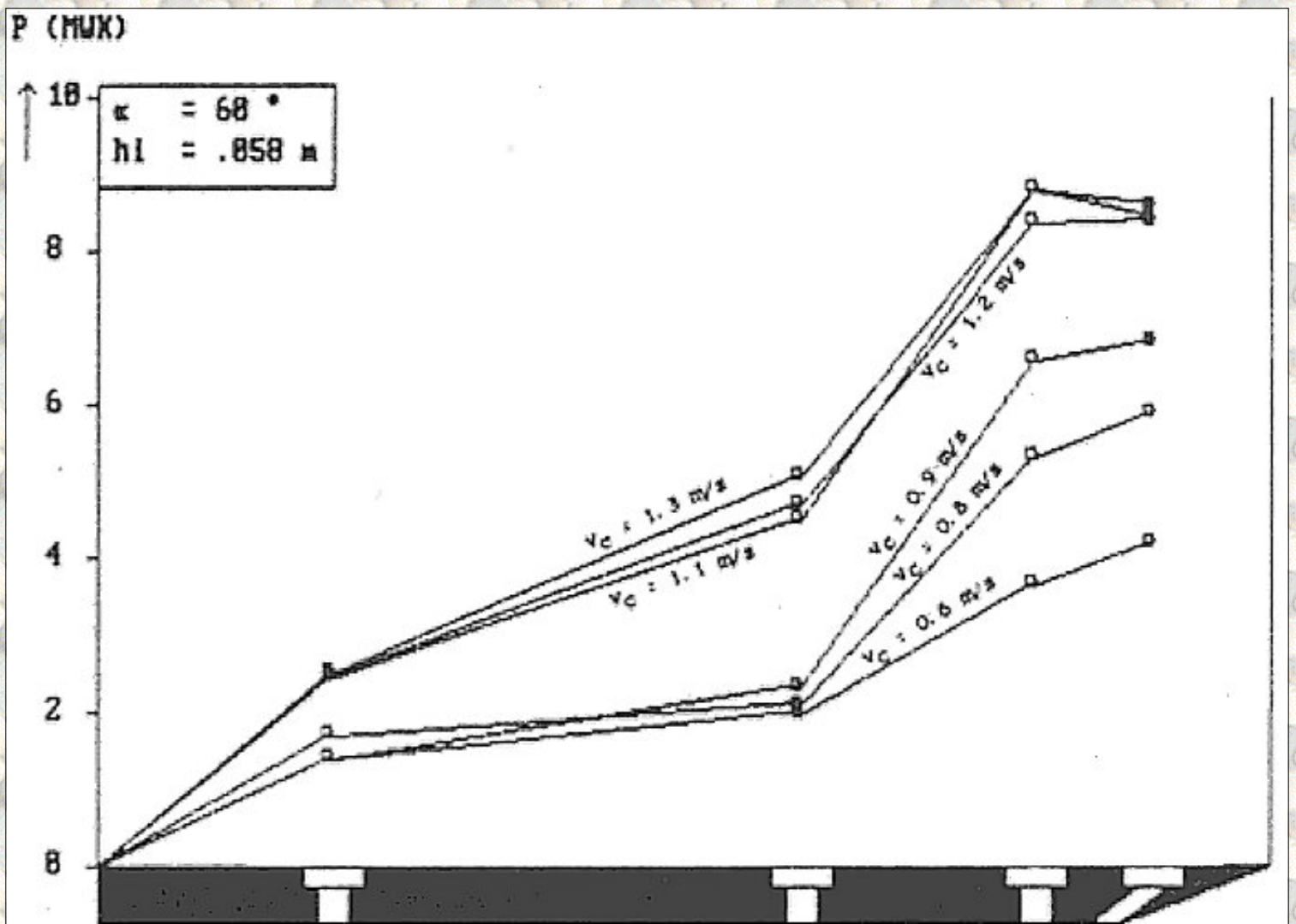


Figure 3.22: The water pore pressures on the blade. Experiments in 105 μ m sand with a 60° blade, layer thickness h_l of 58 mm, blade height h_b of 173 mm, as a function of the cutting velocity v_c .

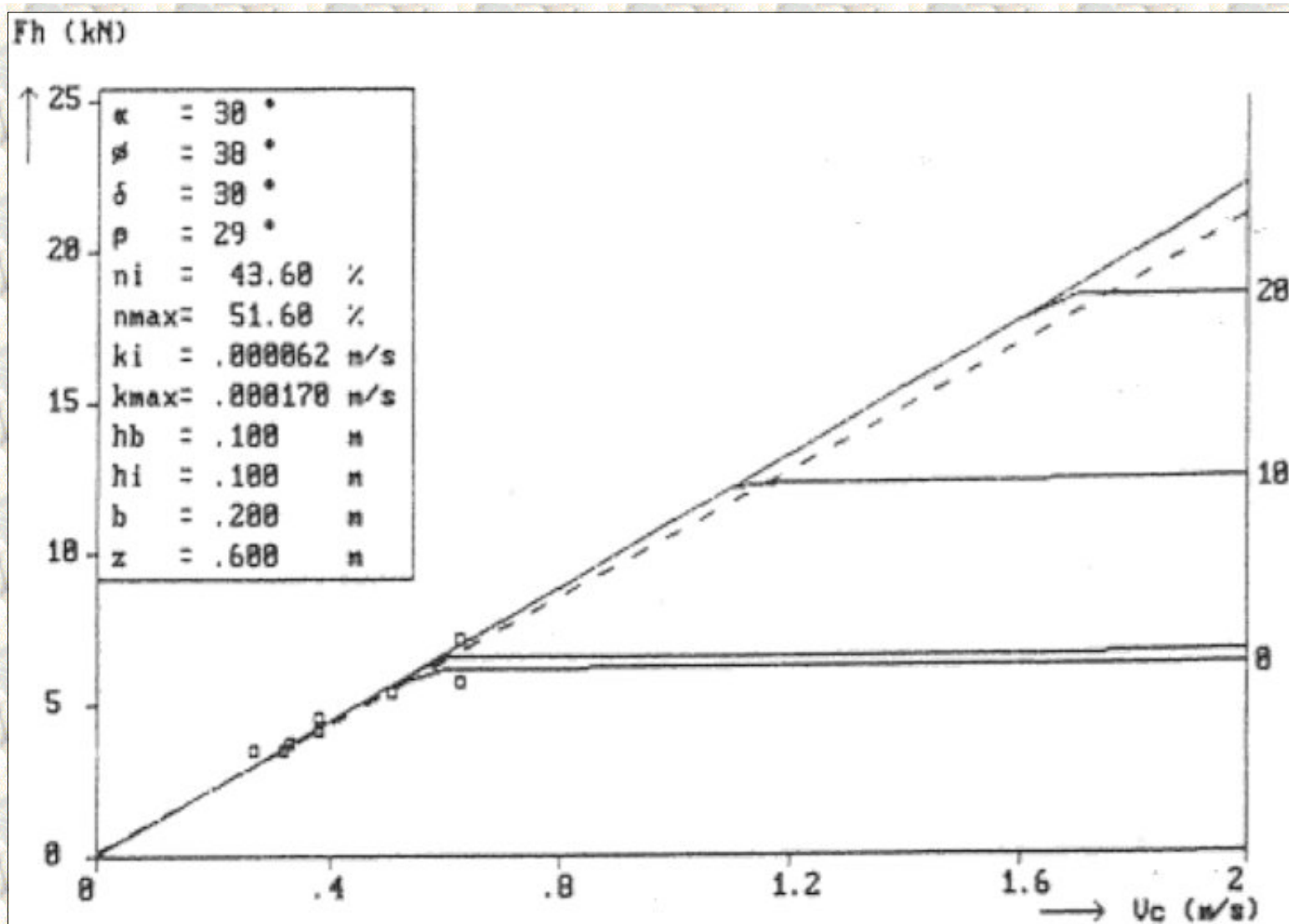


Figure 3.23: The horizontal force F_h as a function of the cutting velocity v_c , at a blade angle of 30° for the non-cavating and the partly cavating cutting process, in the $105 \mu\text{m}$ sand.

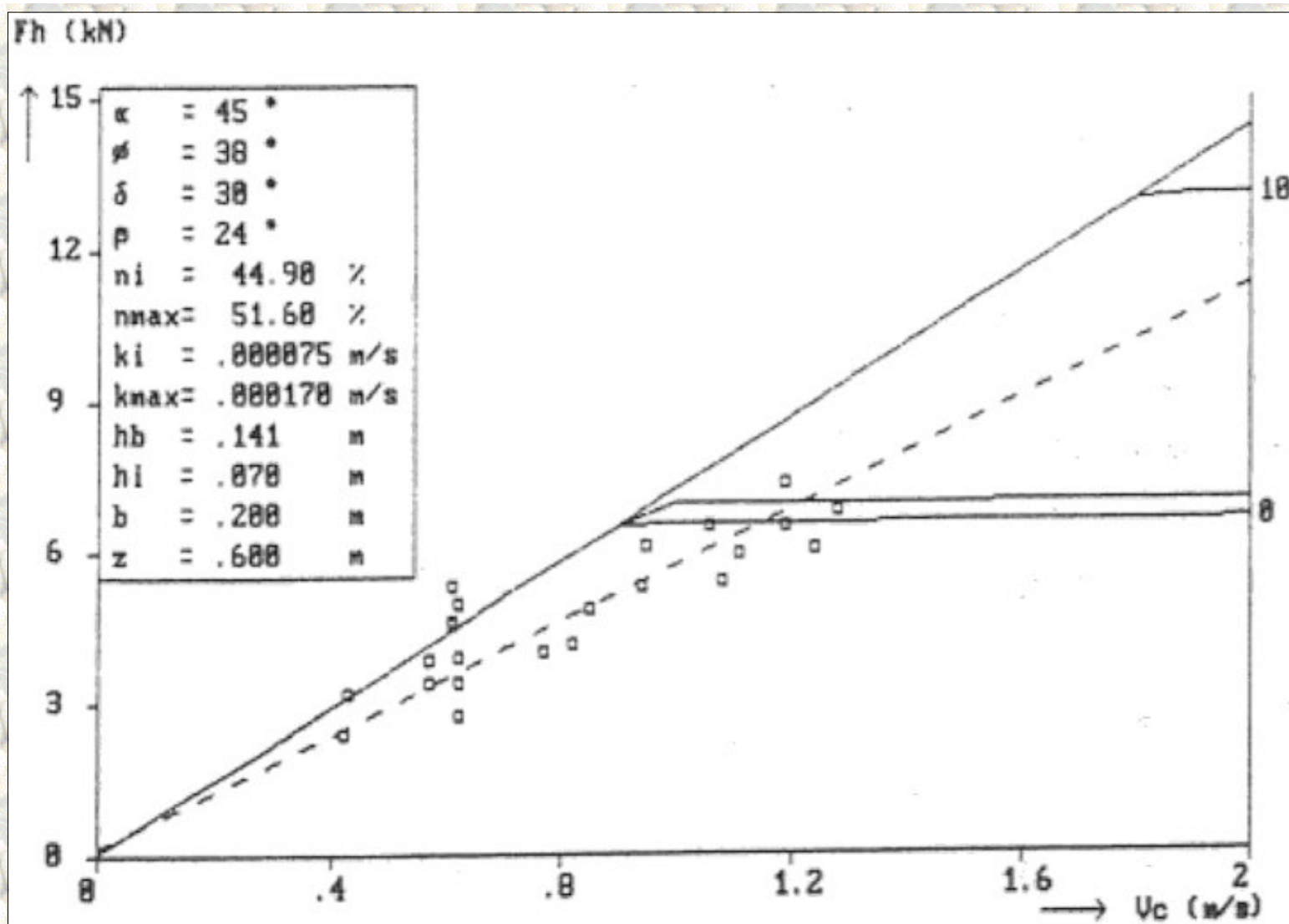


Figure 3.24: The horizontal force F_h as a function of the cutting velocity v_c , at a blade angle of 45° for the non-cavitating and the partly cavitating cutting process, in the $105 \mu\text{m}$ sand.

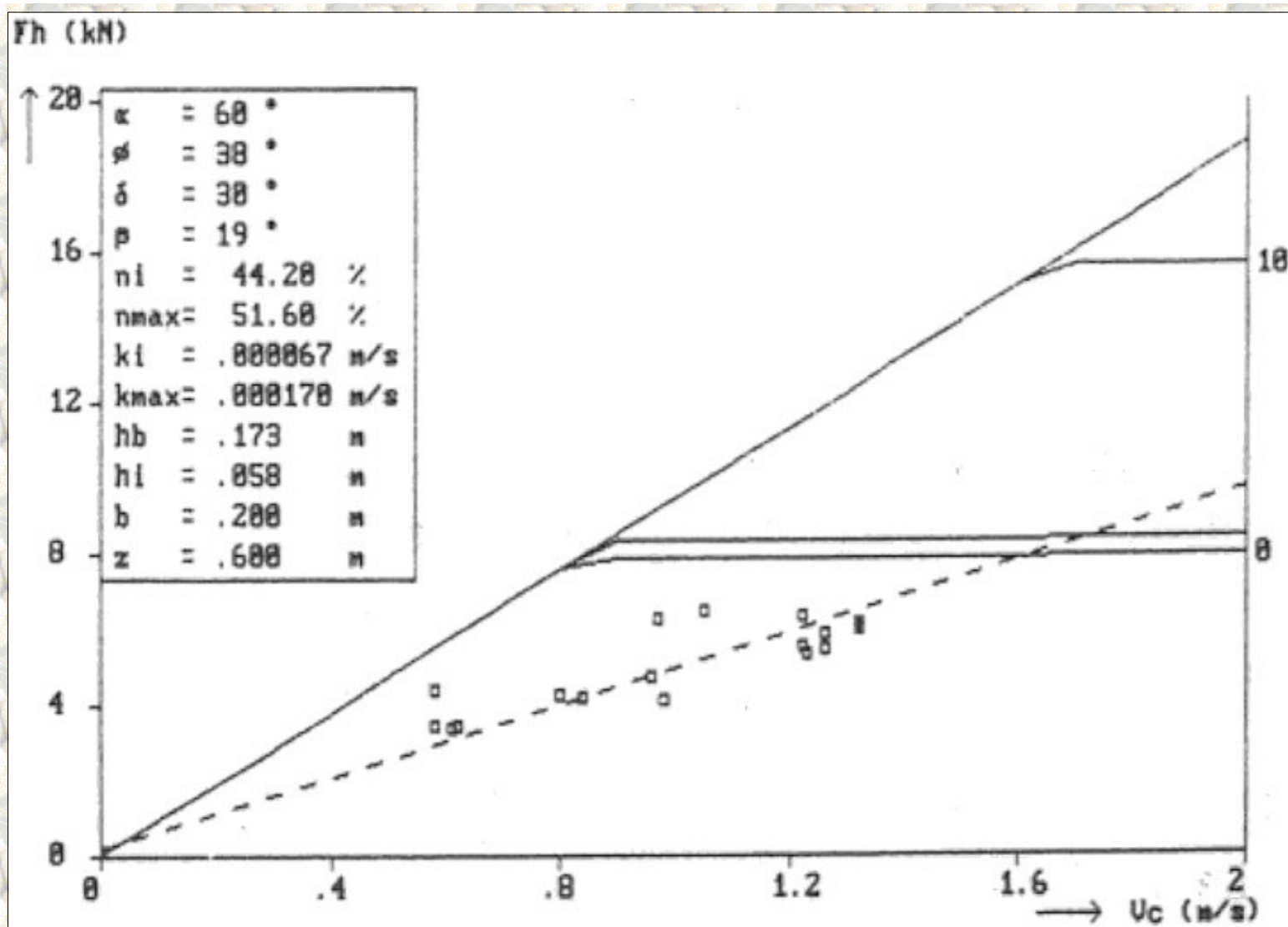


Figure 3.25: The horizontal force F_h as a function of the cutting velocity v_c , at a blade angle of 60° for the non-cavating and the partly cavating cutting process, in the $105 \mu\text{m}$ sand.

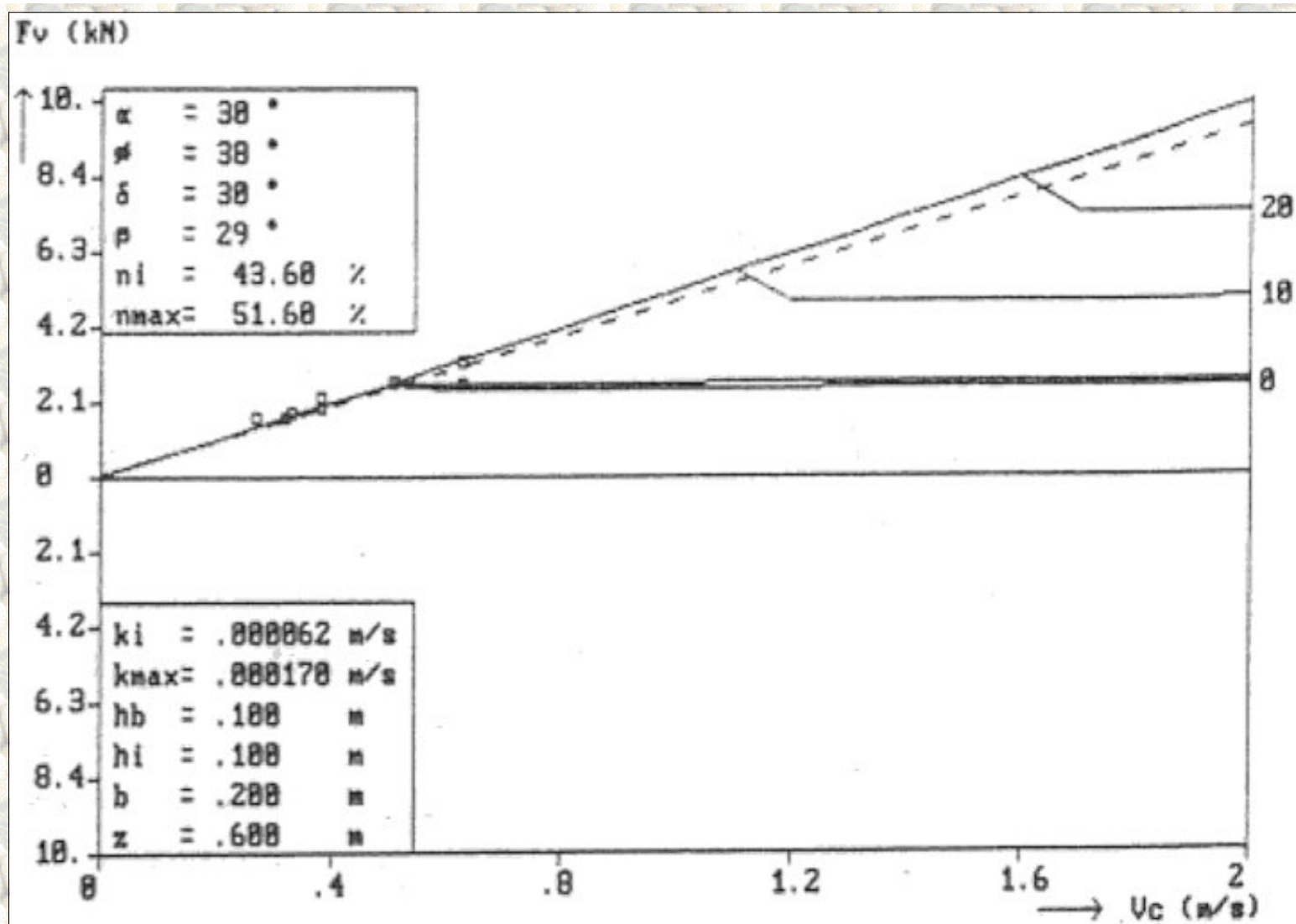


Figure 3.26: The vertical force F_v as a function of the cutting velocity v_c , at a blade angle of 30° for the non-cavitating and the partly cavitating cutting process, in the $105 \mu\text{m}$ sand.

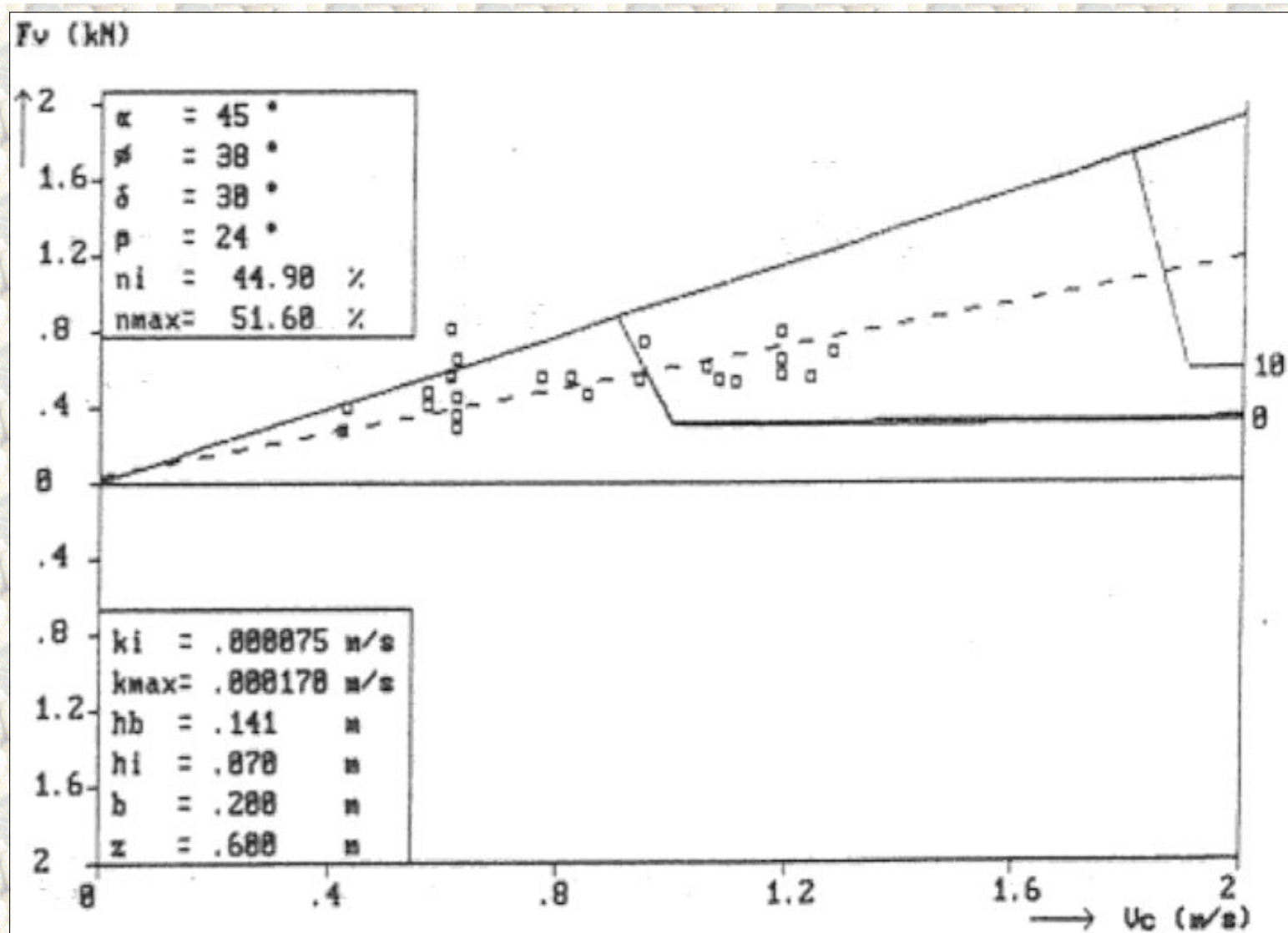


Figure 3.27: The vertical force F_v as a function of the cutting velocity v_c , at a blade angle of 45° for the non-cavating and the partly cavating cutting process, in the $105 \mu\text{m}$ sand.

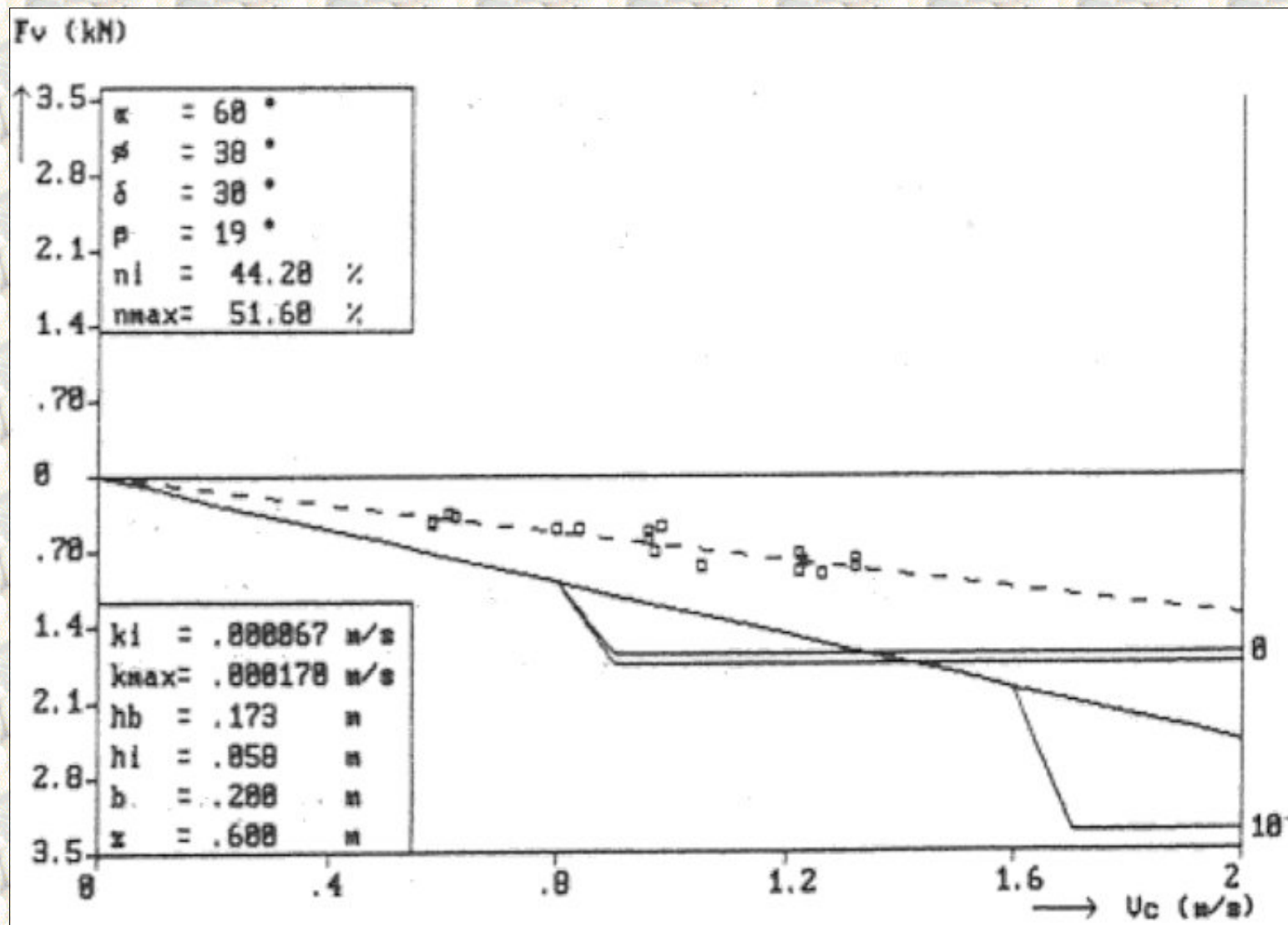


Figure 3.28: The vertical force F_v as a function of the cutting velocity v_c , at a blade angle of 60° for the non-cavitating and the partly cavitating cutting process, in the 105 μ m sand.

[Back to top](#)

This is a translation of the dissertation of Dr.ir. S.A. Miedema, dated September 15th 1987 .

The dissertation was originally published in Dutch by the:

Delft University of Technology

Faculty of Mechanical Engineering and Marine Technology

Chair of Dredging Technology

Mekelweg 2

2628 CD, Delft

The Netherlands

It is advised to also read the papers following this dissertation, since the theory developed has been refined and extended.

Last modified Sunday May 28, 2000 by: [Sape A. Miedema](#)

Translation by: [Laurens de Jonge](#)

Figures, equations and tables by: [Erik Miedema](#)

Copyright © May, 2000 Dr.ir. S.A. Miedema



[Download Adobe Acrobat Reader V4.0](#)

3.11 Determination of φ and δ from measurements.

In chapter 2.10 is indicated how φ en δ can be determined from the cutting tests. The soil/steel angle of friction can quite easily be determined using equation (2.51), with the remark that the side and wear effects can influence the results from this equation slightly. The soil/steel angle of friction, determined by this method, is therefore a gross value. This value, however, is of great practical importance, because the side and wear effects that occur in practice are included in this value.

The soil/steel angle of friction, determined by this method, varied between 24° and 35° , with an average of approximately 30° . For both types of sand almost the same results were found for the soil/steel angle of friction. A clear tendency towards stress or blade angle dependency of the soil/steel angle of friction is not observed. This in contrast to Van Leussen and Nieuwenhuis [39], who found a blade angle dependency according Hettiaratchi and Reece [24].

Harder to determine is the angle of internal friction (equation (2.55)). This is caused by the unknown under-pressure behind the blade that is present in this equation. Assuming a hydrostatic pressure behind the blade, the following average values for the angle of internal friction are found, for the $200\text{ }\mu\text{m}$ sand:

- $\alpha = 30^\circ \gg \varphi = 46.7^\circ$
- $\alpha = 45^\circ \gg \varphi = 45.9^\circ$
- $\alpha = 60^\circ \gg \varphi = 41.0^\circ$

These values are high above the angle of internal friction that is determined with soil mechanical research according appendix B3, for a pore percentage of 38.5%. From equation (2.55) can be derived that the presence of under-pressure behind the blade make the results of this equation smaller and also that this reduction is larger when the blade angle is smaller.

Within the test program space is created to perform experiments where the under-pressure is measured both on and behind the blade (figure 3.8). Pressure transducer P1 is removed from the blade and mounted behind the blade tip.

Although the number of measurements was too limited to base an theoretical or empirical model on, these measurements have slightly increased the understanding of the under-pressure behind the blade. Behind the blade tip under-pressures are measured, with a value of 30% to 60% of the peak pressure on the blade. The highest under-pressure behind the blade was measured with the 30° blade. This can be explained by the wedge shaped space behind the blade.

Equation (2.30) is derived from these measurements, with the remark that this equation is based on a very limited number of tests and that further research will have to lead to a better understanding of the under-pressure behind the blade.

The use of equation (2.30) for the determination of the angle of internal friction led to the following values:

- $\alpha = 30^\circ \gg \varphi = 36.6^\circ$

- $\alpha = 45^\circ \gg \varphi = 39.7^\circ$

- $\alpha = 60^\circ \gg \varphi = 36.8^\circ$

For the verification of the cutting tests an average value of 38° for the internal angle of friction is assumed. These values are also more in accordance with the values of internal friction mentioned in appendix B3, where a value of approximate 35° can be found with a pore percentage of 38.5%.

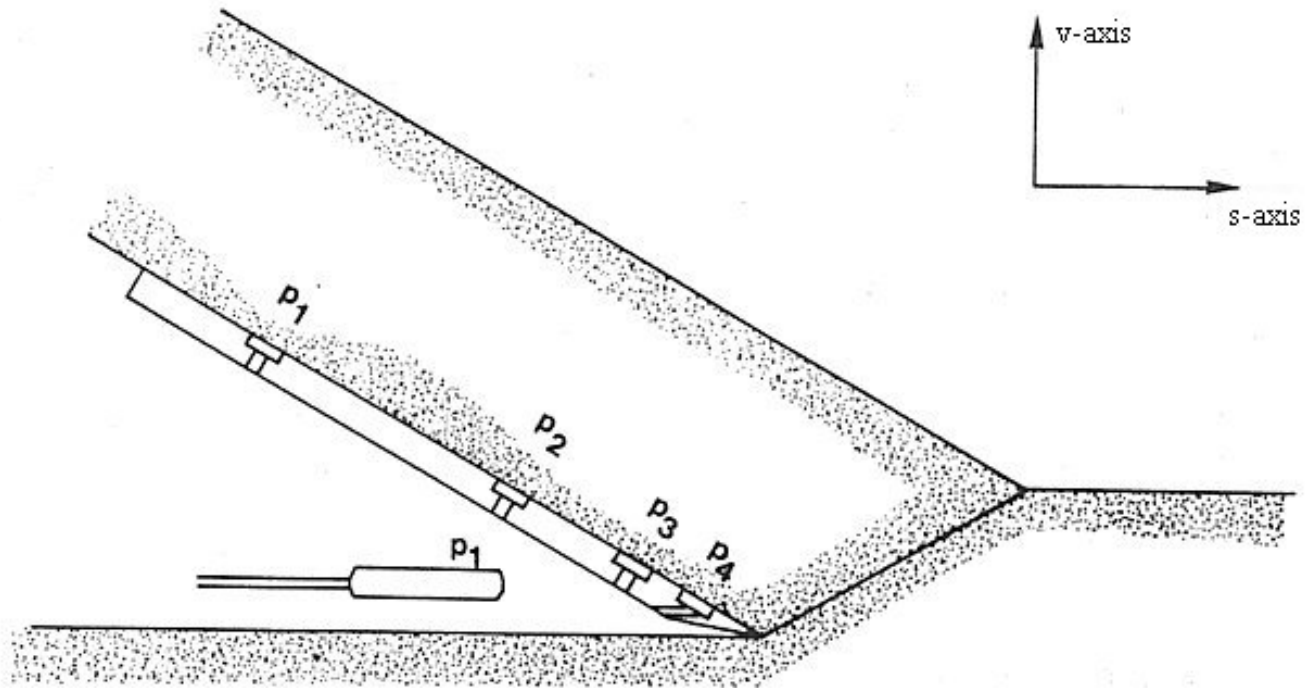


Figure 3.30: Location of the pressure transducer P1 behind the edge of the blade.

The same phenomena are observed in the determination of the angle of internal friction of the $105 \mu\text{m}$ sand. The assumption of a hydrostatic pressure behind the blade resulted also in too large values for the angle of internal friction, analogously to the calculations of the $200 \mu\text{m}$ sand. Here the following values are determined:

- $\alpha = 30^\circ \gg \varphi = 46.2^\circ$

- $\alpha = 45^\circ \gg \varphi = 38.7^\circ$

- $\alpha = 60^\circ \gg \varphi = 40.3^\circ$

Using equation (2.30) results in:

- $\alpha = 30^\circ \gg \varphi = 38.7^\circ$

- $\alpha = 45^\circ \gg \varphi = 34.0^\circ$

- $\alpha = 60^\circ \gg \varphi = 38.4^\circ$

The low value of the angle of internal friction for the 45° blade can be explained by the fact that these tests are performed for the first time in the new laboratory GV in a situation where the sand was not homogenous from top to bottom.

For the verification of the cutting forces and the water pressures is, for both sand types, chosen for a soil/steel angle of friction of 30° and an angle of internal friction of 38° , as an average value.

[Back to top](#)

This is a translation of the dissertation of Dr.ir. S.A. Miedema, dated September 15th 1987 .

The dissertation was originally published in Dutch by the:

Delft University of Technology

Faculty of Mechanical Engineering and Marine Technology

Chair of Dredging Technology

Mekelweg 2

2628 CD, Delft

The Netherlands

It is advised to also read the papers following this dissertation, since the theory developed has been refined and extended.

Last modified Sunday May 28, 2000 by: [Sape A. Miedema](#)

Translation by: [Laurens de Jonge](#)

Figures, equations and tables by: [Erik Miedema](#)

Copyright © May, 2000 Dr.ir. S.A. Miedema



[Download Adobe Acrobat Reader V4.0](#)

3.12 General conclusions.

From the performed research the following general conclusions can be drawn:

1. Both the measured cutting forces as the measured water pore-pressures agree reasonably with the theory from chapter 2.
2. For both sand types is observed that the cutting forces and the water pore-pressures become smaller in comparison with the theory, when the blade angle becomes larger. For the 30° blade the cutting forces and the water pore-pressures are larger or equal to theoretical derived values, while for the 60° blade the theory can overestimate the measurements with a factor 1.6. This can be explained by assuming that with an increasing blade angle the cutting process becomes more discontinuous and therefore decreases the average volume strain rate. Slices of sand shear off with dilatancy around the shear planes, while the dilatancy is less in the sand between the shear planes. The theory can still be pretty useful since in dredging practice the used blade angles are between 30° and 45° .
3. Side effects can considerably influence the direction of the cutting forces, although the magnitude of the cutting forces is less disturbed. As a result of the side effects the cutting forces are aimed more downward.
4. Wear effects can also influence the direction of the cutting forces considerably, while also the magnitude of the cutting forces is less disturbed. As a result of the wear the cutting forces are, however, aimed more upwards.
5. Research will have to be done on the sub-pressure behind the blade to obtain a better considered formulation.

[Back to top](#)

This is a translation of the dissertation of Dr.ir. S.A. Miedema, dated September 15th 1987 .
 The dissertation was originally published in Dutch by the:
Delft University of Technology
Faculty of Mechanical Engineering and Marine Technology
Chair of Dredging Technology
Mekelweg 2
2628 CD, Delft
The Netherlands

It is advised to also read the papers following this dissertation, since the theory developed has been refined and extended.

Last modified Sunday May 28, 2000 by: [Sape A. Miedema](#)

Translation by: [Laurens de Jonge](#)

Figures, equations and tables by: [Erik Miedema](#)

Copyright © May, 2000 [Dr.ir. S.A. Miedema](#)



[Download Adobe Acrobat Reader V4.0](#)

4.01 Introduction.

With a few simplifications it is possible to formulate an analytical model for the determination of the forces, the torque, the power and the specific cutting energy on a cutterhead. This model is developed initially for a disc bottom cutterhead but can, in its present shape, also be used for a helix cutterhead.

These simplifications are:

1. It is assumed that the coefficients c_1 , c_2 , d_1 and d_2 are constant over the run-through angle Ω_0 (figure 4.1). This implies that an average value for the layer-thickness must be chosen for the determination of the coefficients c_1 , c_2 , d_1 and d_2 .
2. The blades have to be straight and must have an angle τ with the axis of the cutterhead, the pitch angle. Also included in the model is a constant curvature angle ξ of the blades. This implies that a helix cutterhead is considered, where the model is valid for a strip according figure 4.2, with a projected width b_{pr} and a radius R . This curvature angle is included to get an impression of the influence of this angle on the loads on the cutterhead. For the determination of the loads on the cutterhead with a variable curvature angle the numerical model from chapter 8 is preferred.
3. The effects of the sliding velocity on the blades can only be taken into account, if the shear angle belonging to δ is considered and not to δ_e (the effective soil/steel angle of friction, see equation (2.57)). The error made, however, is not large.
4. Only the effects of the water pore-pressures on the cutting forces are considered.
5. Inertia effects, gravity, cohesion and adhesion are neglected.
6. Simplified expressions are used for the layer-thickness and the cutting velocity.

In figure 4.2 is indicated which forces act on the blade momentarily. These are F_h , F_v and F_l in the blade related coordinate system, F_t , F_r and F_a in the cylindrical coordinate system and F_v , F_s and F_a in the cutterhead related coordinate system. The coordinate system definitions can be found in appendix B1. The forces F_h , F_v en F_l are extensively discussed in chapter 2.

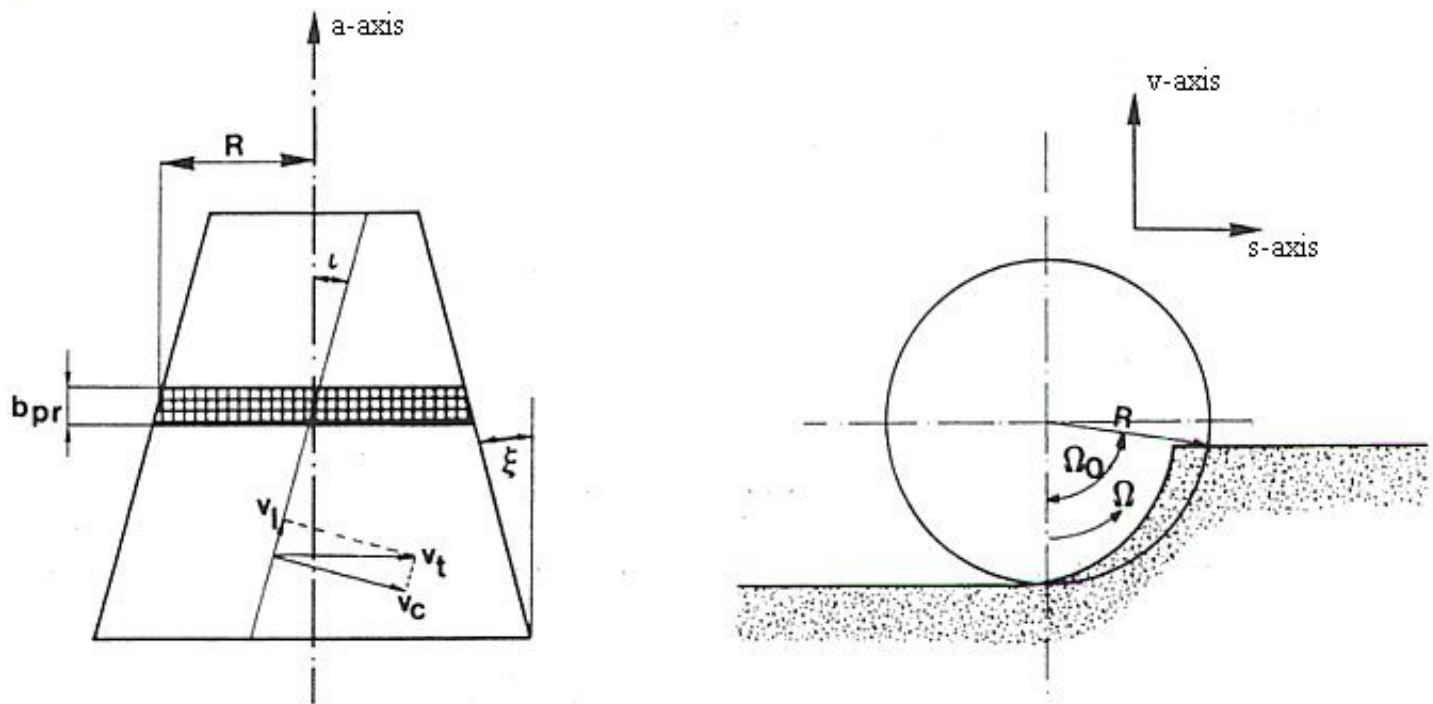


Figure 4.1: Helix cutterhead. Indicated are the curvature angle ξ , the helix angle l , the velocity components on the blade and the run-through angle Ω_0 . Also a strip is indicated for which the model is valid with a radius R and a projected blade width b_{pr} .

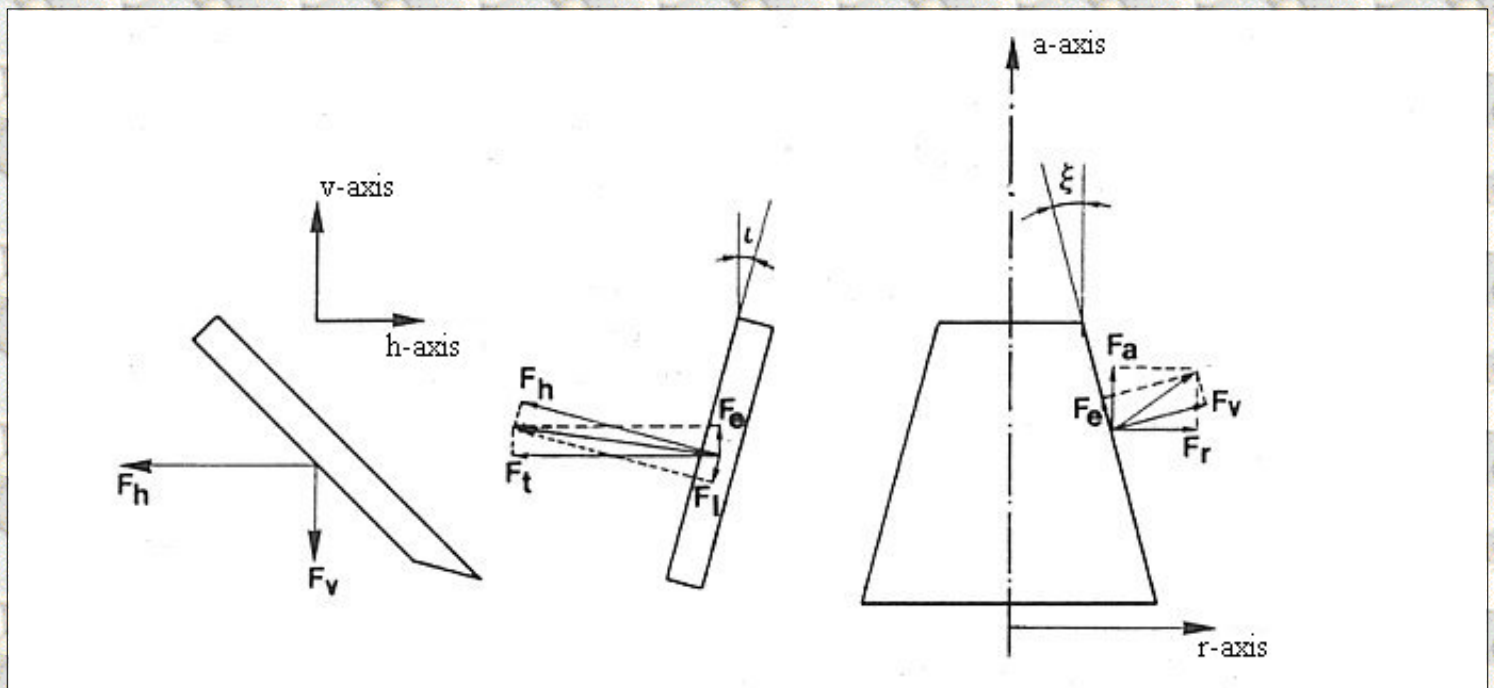


Figure 4.2: The momentary forces on the blade. Indicated are F_h , F_v and F_l in the blade related coordinate system and the forces F_t , F_r en F_a in the cylindric coordinate system.

[Back to top](#)

This is a translation of the dissertation of Dr.ir. S.A. Miedema, dated September 15th 1987 .
 The dissertation was originally published in Dutch by the:
 Delft University of Technology
 Faculty of Mechanical Engineering and Marine Technology
 Chair of Dredging Technology
 Mekelweg 2
 2628 CD, Delft

The Netherlands

It is advised to also read the papers following this dissertation, since the theory developed has been refined and extended.

Last modified Sunday May 28, 2000 by: [Sape A. Miedema](#)

Translation by: [Laurens de Jonge](#)

Figures, equations and tables by: [Erik Miedema](#)

Copyright © May, 2000 Dr.ir. S.A. Miedema



[Download Adobe Acrobat Reader V4.0](#)

4.02 Simplifications and basic equations.

The shape of the layer is dependent on the ratio between the peripheral velocity of the cutterhead and the haul velocity. Figure 4.3 shows two layer shapes at a ratio of 2.5 and a ratio of 10, for both the under cutting and over cutting dredging process. In practical cases this ratio is high (e.g. 10), so that a simplified expression can be used for the layer-thickness.

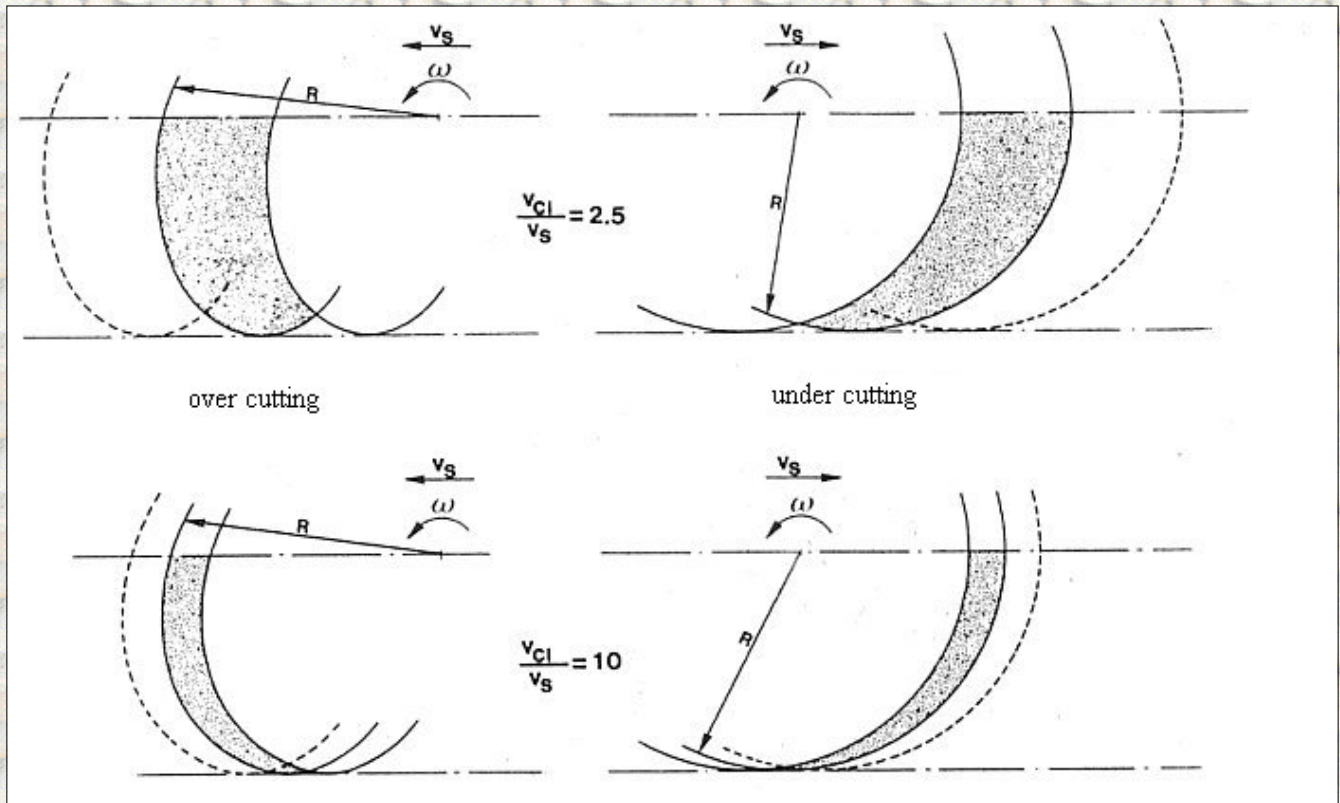


Figure 4.3: The shape of the cut layer as function of the ratio between the peripheral velocity v_{ci} and the haul velocity v_s .

For the layer-thickness now the following simplified expression can be derived (figure 4.4):

$$h_i = \frac{v_s \cdot 60}{n_o \cdot p} \cdot \sin(\Omega) \cdot \cos(\xi) \quad (4.1)$$

In which: v_s the haul velocity
 n_o the number of revolutions of the cutterhead
 p the number of blades
 Ω the run-through angle

This expression is a simplification of the equations (8.26) and (8.27) from chapter 8, where it is assumed that the haul velocity \ll peripheral velocity of the cutterhead.

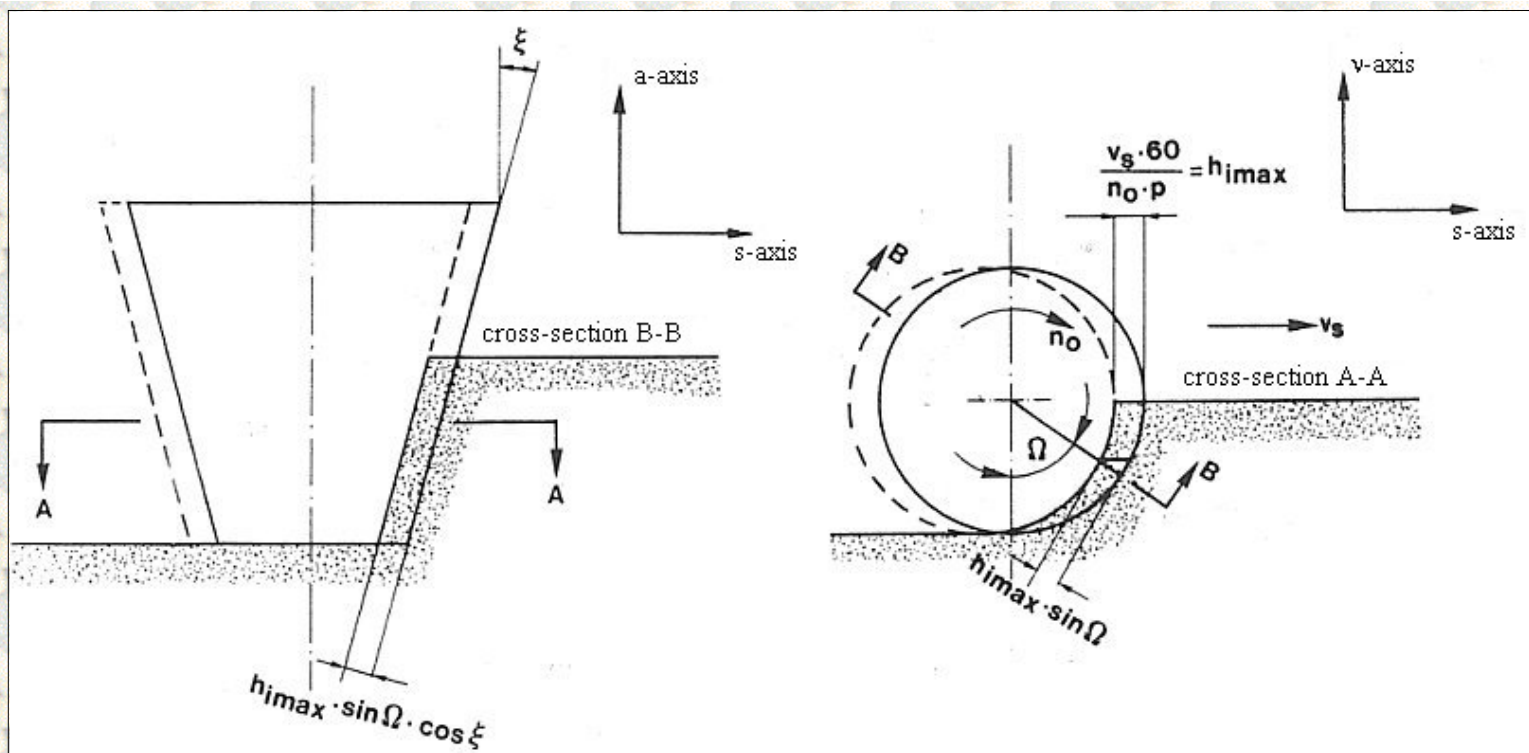


Figure 4.4: The layer thickness as function of the run-through angle Ω and the curvature angle ξ .

The width of a blade part can be expressed in the, on the axis of the cutterhead, projected width (figure 4.5), according:

$$b = \frac{b_{pr}}{\cos(\vartheta) \cdot \cos(\xi)} \quad (4.2)$$

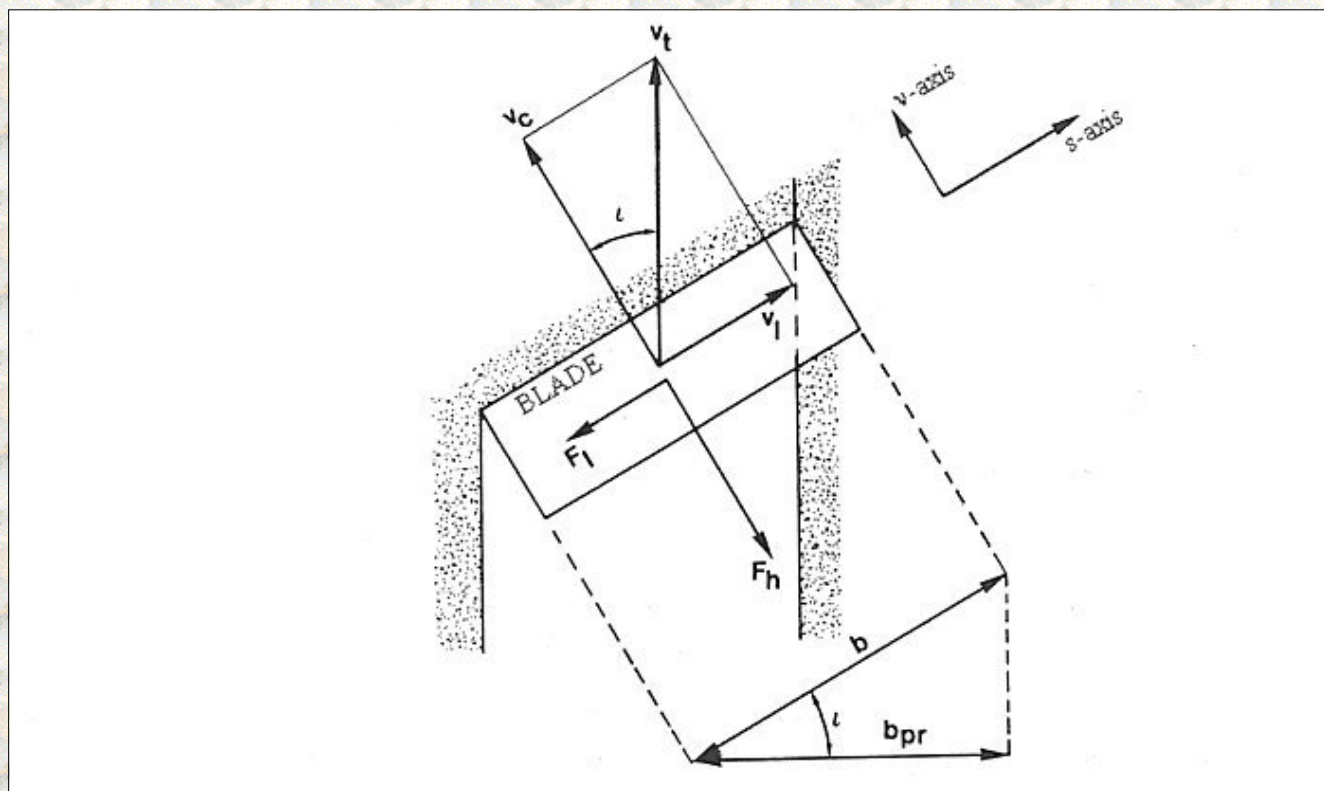


Figure 4.5: The blade width b and the projected blade width b_{pr} .

The total blade velocity v_t can be approached by the peripheral velocity v_{ci} , for high ratios between the peripheral velocity v_{ci} and the haul velocity v_s . The cutting velocity perpendicular to the blade edge can now be

approximated by the peripheral velocity of the cutterhead (figure 4.6), corrected for the pitch angle ι :

$$v_c = v_t \cdot \cos(\iota) \approx \frac{2 \cdot \pi \cdot R \cdot n_o}{60} \cdot \cos(\iota) \quad (4.3)$$

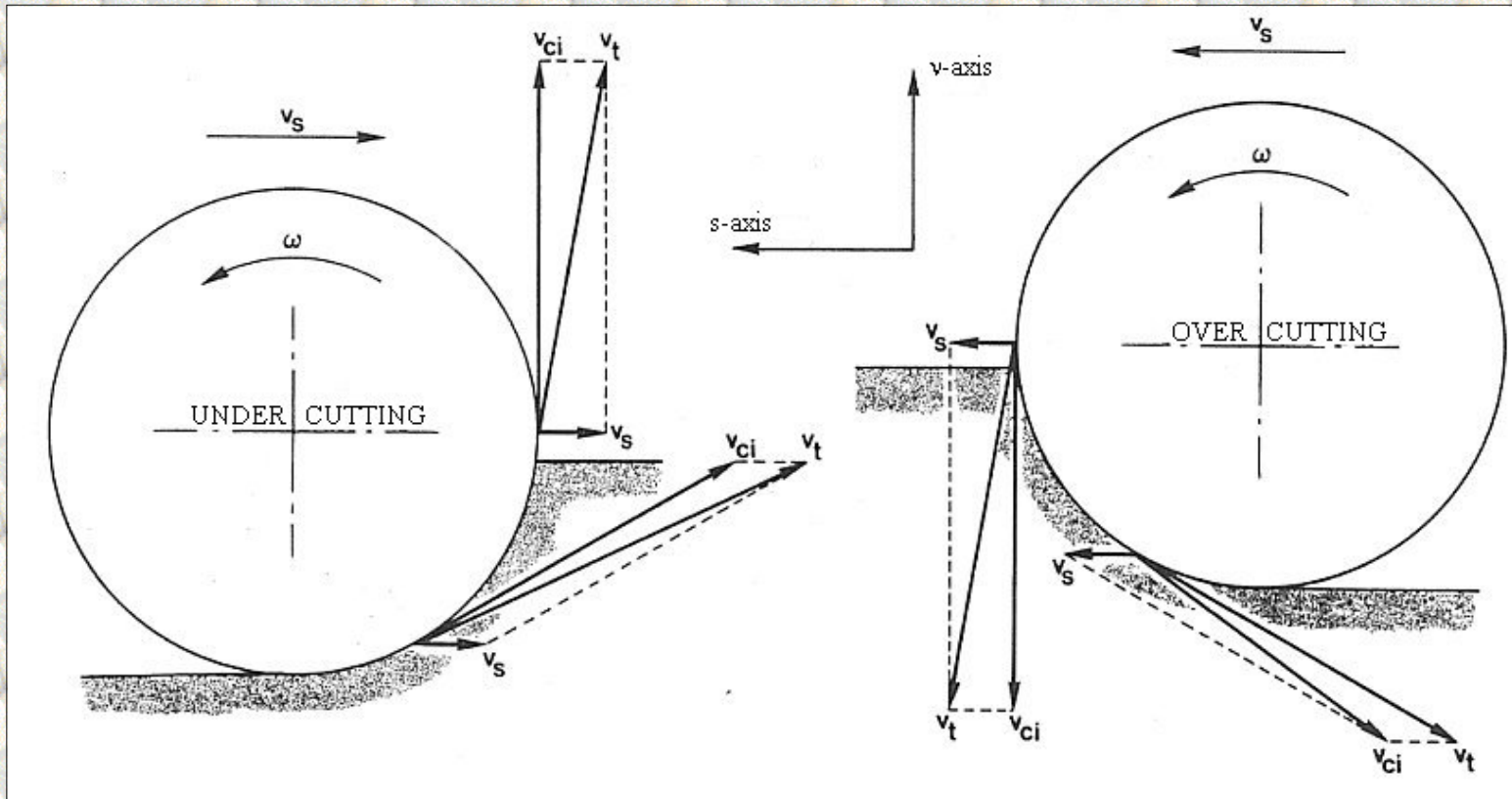


Figure 4.6: The peripheral velocity v_{ci} , the haul velocity v_s and the resulting blade velocity v_t .

The sliding velocity is approximately:

$$v_l = v_t \cdot \sin(\iota) \approx \frac{2 \cdot \pi \cdot R \cdot n_o}{60} \cdot \sin(\iota) \quad (4.4)$$

For the relative velocity between the sand and the blade can be derived (see equation (2.56)):

$$v_r = \frac{2 \cdot \pi \cdot R \cdot n_o}{60} \cdot \cos(\iota) \cdot \frac{\sin(\beta)}{\sin(\alpha + \beta)} \quad (4.5)$$

Substituting these equations in the basic equation (2.43) for the momentary cutting forces of the non-cavitating cutting process,

$$F_{ci} = c_i \cdot \rho_w \cdot g \cdot v_c \cdot h_i^2 \cdot b \cdot \frac{e}{k_m} \quad (4.6)$$

obtains with the equations (4.1), (4.2) and (4.3):

$$F_{ci} = c_i \cdot \rho_w \cdot g \cdot \left(\frac{2 \cdot \pi \cdot R \cdot n_o}{60} \cdot \cos(\vartheta) \right) \cdot \left(\frac{v_s \cdot 60}{n_o \cdot p} \cdot \sin(\Omega) \cdot \cos(\xi) \right)^2 \cdot \frac{b_{pr}}{\cos(\vartheta) \cdot \cos(\xi)} \cdot \frac{e}{k_m} \quad (4.7)$$

For the cavitating cutting process equation (2.46) is found:

$$F_{ci} = d_i \cdot \rho_w \cdot g \cdot h_i \cdot b \cdot (z+10) \quad (4.8)$$

This gives with equations (4.1), (4.2) and (4.3):

$$F_{ci} = d_i \cdot \rho_w \cdot g \cdot \frac{b_{pr}}{\cos(\vartheta) \cdot \cos(\xi)} \cdot (z+10) \cdot \frac{v_s \cdot 60}{n_o \cdot p} \cdot \sin(\Omega) \cdot \cos(\xi) \quad (4.9)$$

The force F_1 can be determined with the theory of chapter 2.11. In this analytical model it is however assumed that this force can be neglected, so:

$$F_1 = 0 \quad (4.10)$$

[Back to top](#)

This is a translation of the dissertation of Dr.ir. S.A. Miedema, dated September 15th 1987 .

The dissertation was originally published in Dutch by the:

Delft University of Technology
Faculty of Mechanical Engineering and Marine Technology
Chair of Dredging Technology
Mekelweg 2
2628 CD, Delft
The Netherlands

It is advised to also read the papers following this dissertation, since the theory developed has been refined and extended.

Last modified Sunday May 28, 2000 by: [Sape A. Miedema](#)

Translation by: [Laurens de Jonge](#)

Figures, equations and tables by: [Erik Miedema](#)

Copyright © May, 2000 Dr.ir. S.A. Miedema



[Download Adobe Acrobat Reader V4.0](#)

4.03 Transformation of the forces to the cutterhead related axis system.

[Contents](#)

The forces F_t , F_r and F_a can be derived from F_h , F_v and F_l with the following transformations (see figure 4.2).

For the tangential force can be written:

$$F_t = F_h \cdot \cos(\vartheta) + F_l \cdot \sin(\vartheta) \approx F_h \cdot \cos(\vartheta) \quad (4.11)$$

For the radial force the following equation can be derived:

$$F_r = -F_h \cdot \sin(\vartheta) \cdot \sin(\xi) + F_l \cdot \cos(\vartheta) \cdot \sin(\xi) + F_v \cdot \cos(\xi) \quad (4.12)$$

$$\approx -F_h \cdot \sin(\vartheta) \cdot \sin(\xi) + F_v \cdot \cos(\xi) \quad (4.13)$$

For the axial force the following equation can be derived:

$$F_a = F_h \cdot \sin(\vartheta) \cdot \cos(\xi) - F_l \cdot \cos(\vartheta) \cdot \cos(\xi) + F_v \cdot \sin(\xi) \quad (4.14)$$

$$\approx F_h \cdot \sin(\vartheta) \cdot \cos(\xi) + F_v \cdot \sin(\xi) \quad (4.15)$$

In this intermediate step the forces from the blade related coordinate system are transformed to a tangential, a radial and an axial force in the cylindrical coordinate system (see also appendix B1.3, the cutterhead related coordinate system).

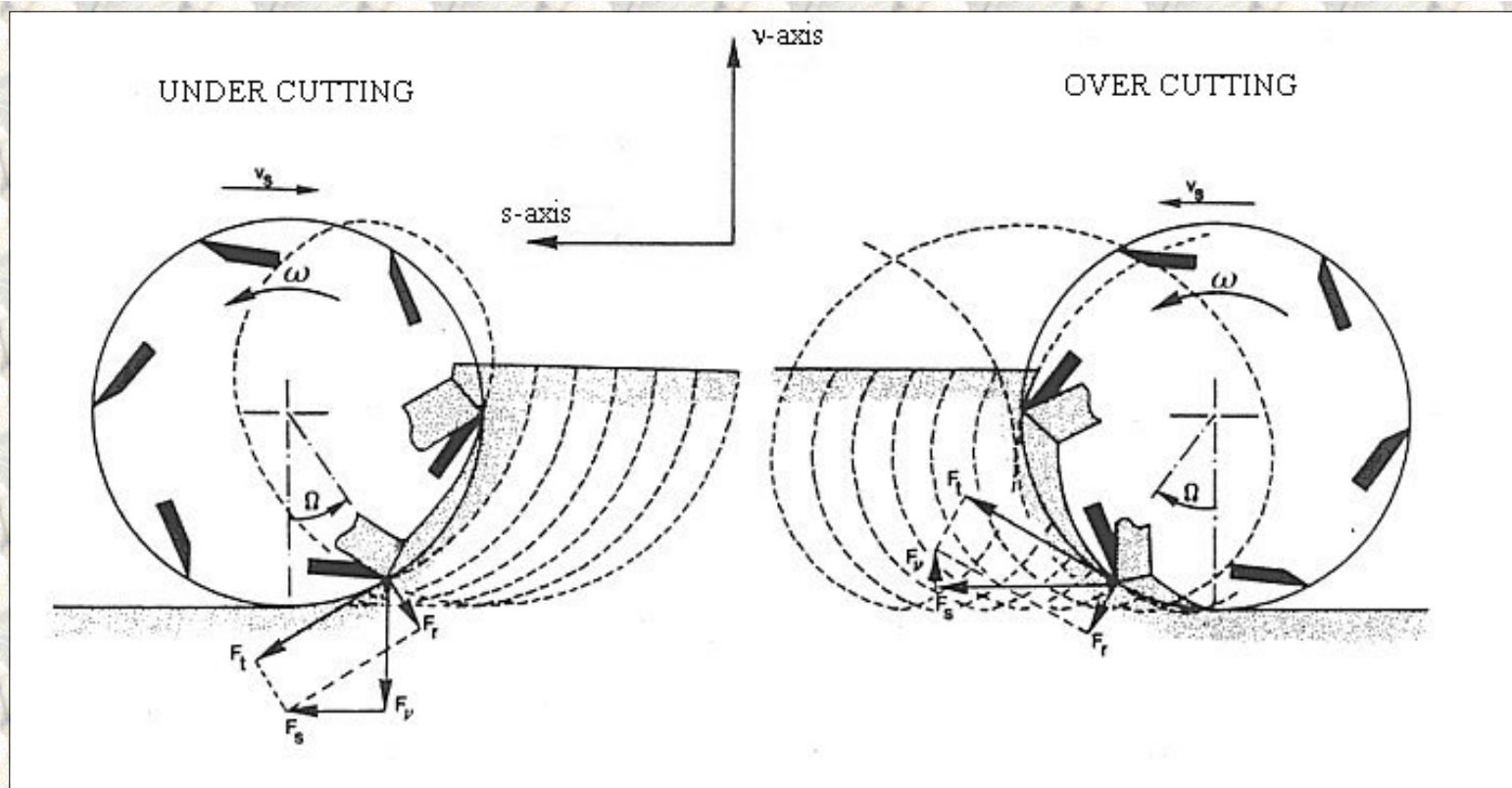


Figure 4.7: Transformation of the momentane forces on the blade to the ladder related coordinate system.

The tangential force F_t , the axial force F_a , and the radial force F_r are now known. These forces can be transformed to the ladder related coordinate system according figure 4.7 (see also appendix B1.2, the ladder related coordinate system), which results in:

$$F_s = F_t \cdot \cos(\Omega) \pm F_r \cdot \sin(\Omega) \quad (4.16)$$

and

$$F_v = F_t \cdot \sin(\Omega) \pm F_r \cdot \cos(\Omega) \quad (4.17)$$

The axial force F_a can be determined according equation (4.14). In these and a number of following equations the notation \pm is found. The upper sign indicates the over cutting process and the lower sign indicates the under cutting process. Substitution of (4.11), (4.13) and (4.14) in (4.16) and (4.17) gives:

$$F_s = F_h \cdot \cos(\varphi) \cdot \cos(\Omega) \pm \left[-F_h \cdot \sin(\varphi) \cdot \sin(\xi) + F_v \cdot \cos(\xi) \right] \cdot \sin(\Omega) \quad (4.18)$$

and

$$F_v = \int_{-}^{+} F_h \cdot \cos(\iota) \sin(\Omega) \left[-F_h \cdot \sin(\iota) \sin(\xi) + F_v \cdot \cos(\xi) \right] \cdot \cos(\Omega) \quad (4.19)$$

For the drive torque the following equation can be derived:

$$M = F_t \cdot R = F_h \cdot \cos(\iota) \cdot R \quad (4.20)$$

[Back to top](#)

This is a translation of the dissertation of Dr.ir. S.A. Miedema, dated September 15th 1987 .
The dissertation was originally published in Dutch by the:
Delft University of Technology
Faculty of Mechanical Engineering and Marine Technology
Chair of Dredging Technology
Mekelweg 2
2628 CD, Delft
The Netherlands

It is advised to also read the papers following this dissertation, since the theory developed has been refined and extended.

Last modified Sunday May 28, 2000 by: [Sape A. Miedema](#)

Translation by: [Laurens de Jonge](#)

Figures, equations and tables by: [Erik Miedema](#)

Copyright © May, 2000 Dr.ir. S.A. Miedema



[Download Adobe Acrobat Reader V4.0](#)

4.04 Integration of the momentary cutting forces and the momentary drive torque.

The total average forces in the ladder related coordinate system can be determined by integrating the momentary forces. For the determination of the average cutting forces on the total cutterhead can be derived:

$$F_{ct} = \frac{p}{2\pi} \cdot \int_0^{\Omega_0} F_c \cdot d\Omega \quad (4.21)$$

In which:	F_c	Momentary force on the cutterhead.
	F_{ct}	Total force on the cutterhead.
	Ω_0	The total run-through angle.
	Ω_1	The run-through angle where the non-cavating cutting process changes to the cavating cutting process (figure 4.8).

The determination of the coefficients c_{gc} , c_{ca} , g_1 to g_6 and the angle Ω_1 will be discussed in chapter 4.5. The forces F_{vt} , F_{st} and F_{at} and the torque M_t can now be determined with the following equations:

$$F_{st} = c_{gc} \cdot \left[g_1 \cdot \int_0^{\Omega_1} \sin^2(\Omega) \cdot \cos(\Omega) \cdot d\Omega + g_2 \cdot \int_0^{\Omega_1} \sin^3(\Omega) \cdot d\Omega \right] + c_{ca} \cdot \left[g_3 \cdot \int_1^{\Omega_0} \sin(\Omega) \cdot \cos(\Omega) \cdot d\Omega + g_4 \cdot \int_1^{\Omega_0} \sin^2(\Omega) \cdot d\Omega \right] \quad (4.22)$$

and:

$$F_{vt} = c_{gc} \cdot \left[+ g_1 \cdot \int_0^{\Omega_1} \sin^3(\Omega) \cdot d\Omega - g_2 \cdot \int_0^{\Omega_1} \sin^2(\Omega) \cdot \cos(\Omega) \cdot d\Omega \right] + c_{ca} \cdot \left[+ g_3 \cdot \int_1^{\Omega_0} \sin^2(\Omega) \cdot d\Omega - g_4 \cdot \int_1^{\Omega_0} \sin(\Omega) \cdot \cos(\Omega) \cdot d\Omega \right] \quad (4.23)$$

For the axial force the following equation can be derived:

$$F_{at} = c_{gc} \cdot g_5 \cdot \int_0^{\Omega_1} \sin^2(\Omega) \cdot d\Omega + c_{ca} \cdot g_6 \cdot \int_1^{\Omega_0} \sin(\Omega) \cdot d\Omega \quad (4.24)$$

and for the drive torque it yields:

$$M_t = c_{gc} \cdot g_1 \cdot R \cdot \int_0^{\Omega_1} \sin^2(\Omega) \cdot d\Omega + c_{ca} \cdot g_3 \cdot R \cdot \int_1^{\Omega_0} \sin(\Omega) \cdot d\Omega \quad (4.25)$$

Integration of these equations results, for the force in the haul direction, in:

$$F_{st} = c_{gc} \cdot \left[g_1 \cdot \frac{\sin^3(\Omega_1)}{3} - g_2 \cdot \left(\frac{\cos^3(\Omega_1)}{3} - \cos(\Omega_1) + \frac{2}{3} \right) \right] \\ + c_{ca} \cdot \left[g_3 \cdot \left(\frac{\sin(\Omega_0^2) - \sin(\Omega_1^2)}{2} \right) - g_4 \cdot \left(\frac{\Omega_0 - \Omega_1}{2} \cdot \frac{\sin(2 \cdot \Omega_0) - \sin(2 \cdot \Omega_1)}{4} \right) \right] \quad (4.26)$$

And for the radial force perpendicular to the haul direction:

$$F_{vt} = c_{gc} \cdot \left[+ g_1 \cdot \left(\frac{\cos(\Omega_1^3)}{3} - \cos(\Omega_1) + \frac{2}{3} \right) - g_2 \cdot \frac{\sin(\Omega_1^3)}{3} \right]$$

$$+c_{ca} \cdot \begin{bmatrix} +g_3 \cdot \left(\frac{\Omega_0 - \Omega_1}{2} \frac{\sin(2\Omega_0) - \sin(2\Omega_1)}{4} \right) - g_4 \cdot \left(\frac{\sin^2(2\Omega_0) - \sin^2(2\Omega_1)}{2} \right) \\ - \end{bmatrix} \quad (4.27)$$

For the axial force it follows that:

$$F_{at} = c_{gc} \cdot g_5 \cdot \left[\frac{\Omega_1}{2} - \frac{\sin(2\Omega_1)}{4} \right] + c_{ca} \cdot g_6 \cdot [\cos(\Omega_1) - \cos(\Omega_0)] \quad (4.28)$$

and for the drive torque it yields:

$$M_t = c_{gc} \cdot g_1 \cdot R \cdot \left[\frac{\Omega_1}{2} - \frac{\sin(2\Omega_1)}{4} \right] + c_{ca} \cdot g_3 \cdot R \cdot [\cos(\Omega_1) - \cos(\Omega_0)] \quad (4.29)$$

The drive power can be derived from the drive torque according to:

$$P_t = M_t \cdot \frac{2 \cdot \pi \cdot n_o}{60} \quad (4.30)$$

[Back to top](#)

This is a translation of the dissertation of Dr.ir. S.A. Miedema, dated September 15th 1987 .
 The dissertation was originally published in Dutch by the:
 Delft University of Technology
 Faculty of Mechanical Engineering and Marine Technology
 Chair of Dredging Technology
 Mekelweg 2
 2628 CD, Delft
 The Netherlands

It is advised to also read the papers following this dissertation, since the theory developed has been refined and extended.

Last modified Sunday May 28, 2000 by: [Sape A. Miedema](#)

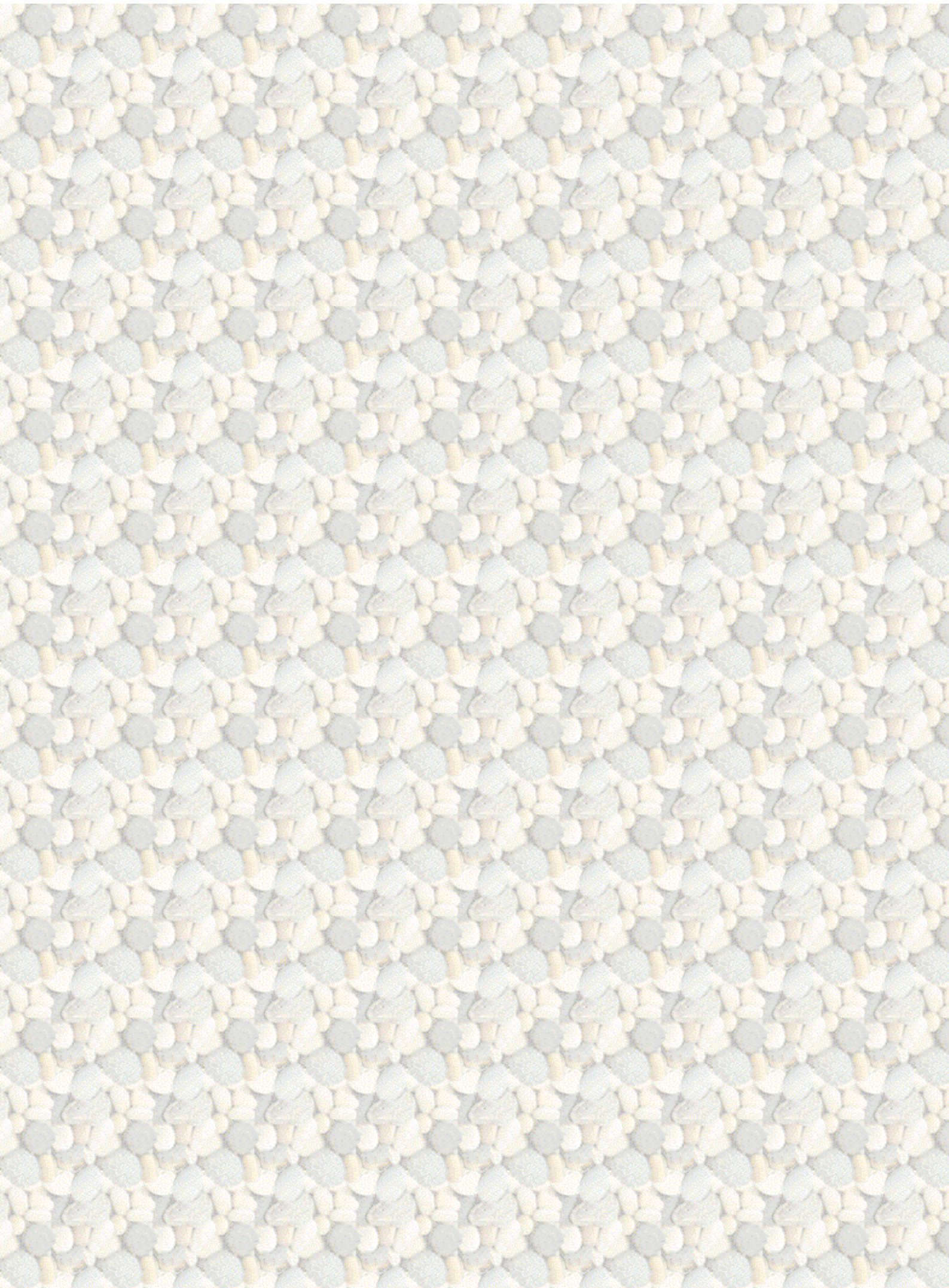
Translation by: [Laurens de Jonge](#)

Figures, equations and tables by: [Erik Miedema](#)

Copyright © May, 2000 Dr.ir. S.A. Miedema



[Download Adobe Acrobat Reader V4.0](#)



4.05 The derived quantities.

The coefficients c_{gc} and c_{ca} contain the quantities like the haul velocity, the number of revolutions and the radius of the cutterhead. These coefficients can be determined with the following equations:

$$c_{gc} = \rho_w \cdot g \cdot b_{pr} \cdot \frac{e}{k_m} \cdot R \cdot \frac{60 \cdot v_s^2}{n_o \cdot p} \quad (4.31)$$

For the part of the layer without cavitation:

$$c_{ca} = \rho_w \cdot g \cdot b_{pr} \cdot (z+10) \cdot \frac{60 \cdot v_s}{2 \cdot \pi \cdot n_o} \quad (4.32)$$

For the part of the layer with cavitation:

The angle Ω_1 where cavitation in the layer starts can be determined using the following equation:

$$\Omega_1 = \arcsin \left[\frac{d_1 \cdot (z+10) \cdot k_m \cdot p}{c_1 \cdot 2 \cdot \pi \cdot R \cdot v_s \cdot e \cdot \cos(\iota) \cdot \cos(\xi)} \right] \quad (4.33)$$

This equation is derived from equating the force F_h for the cavitating and the non-cavitating cutting process.

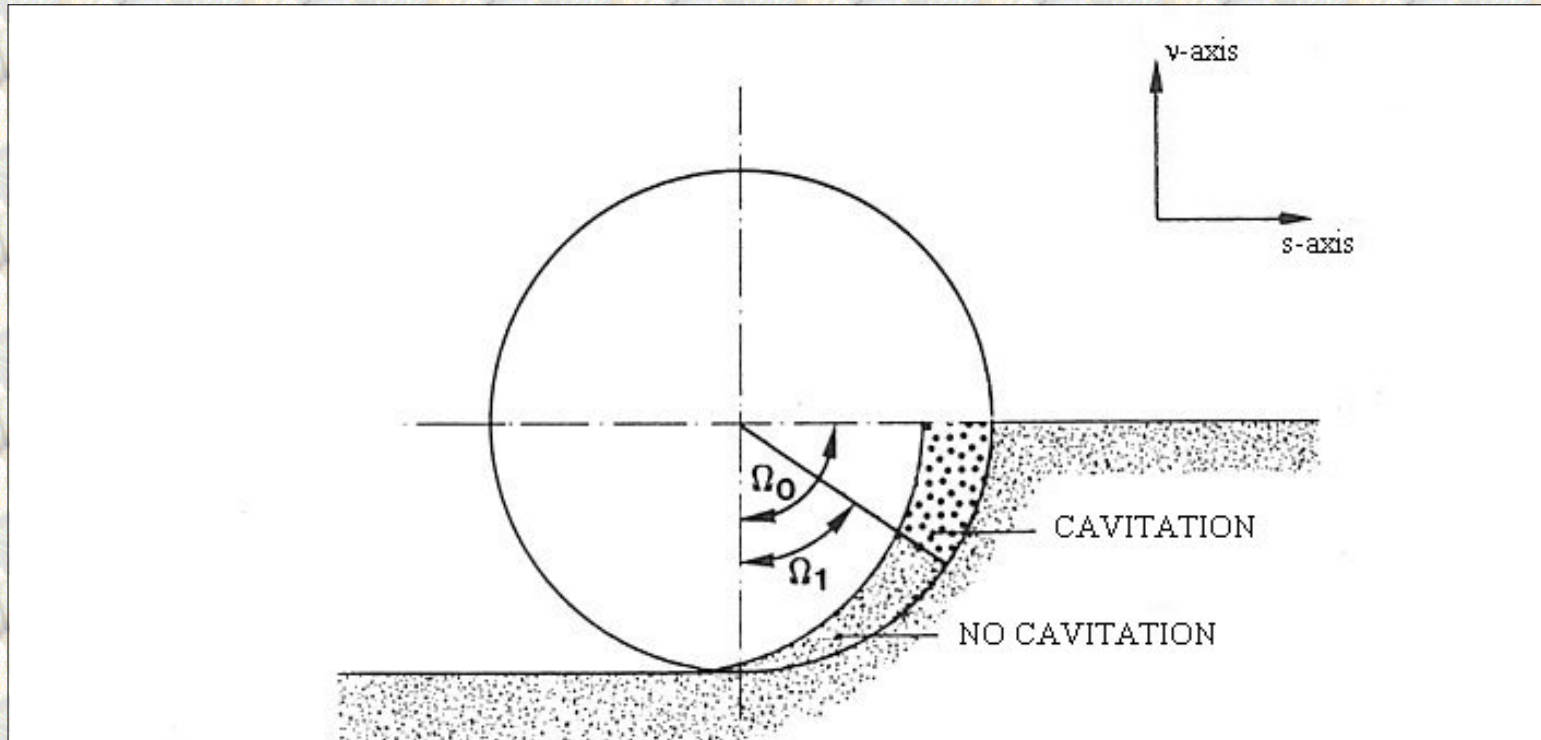


Figure 4.8: The part of the layer without cavitation and the part with cavitation.

The coefficients g_1 to g_6 give an impression of the influence of the shape of the blades, these

coefficients are:

$$g_1 = c_1 \cdot \cos(\vartheta) \cdot \cos(\xi) \quad (4.34)$$

$$g_2 = -c_1 \cdot \sin(\vartheta) \cdot \sin(\xi) \cdot \cos(\xi) + c_2 \cdot \cos^2(\xi) \quad (4.35)$$

$$g_3 = d_1 \quad (4.36)$$

$$g_4 = -d_1 \cdot \tan(\vartheta) \cdot \sin(\xi) + d_2 \cdot \frac{\cos(\xi)}{\cos(\vartheta)} \quad (4.37)$$

$$g_5 = c_1 \cdot \sin(\vartheta) \cdot \cos^2(\xi) + c_2 \cdot \sin(\xi) \cdot \cos(\xi) \quad (4.38)$$

$$g_6 = d_1 \cdot \tan(\vartheta) \cdot \cos(\xi) + d_2 \cdot \frac{\sin(\xi)}{\cos(\vartheta)} \quad (4.39)$$

[Back to top](#)

This is a translation of the dissertation of Dr.ir. S.A. Miedema, dated September 15th 1987 .

The dissertation was originally published in Dutch by the:

Delft University of Technology

Faculty of Mechanical Engineering and Marine Technology

Chair of Dredging Technology

Mekelweg 2

2628 CD, Delft

The Netherlands

It is advised to also read the papers following this dissertation, since the theory developed has been refined and extended.

Last modified Sunday May 28, 2000 by: [Sape A. Miedema](#)

Translation by: [Laurens de Jonge](#)

Figures, equations and tables by: [Erik Miedema](#)

Copyright © May, 2000 Dr.ir. S.A. Miedema



[Download Adobe Acrobat Reader V4.0](#)

4.06 Simplification of the equations.

The equations (4.26) to (4.29) can be simplified. In the notation \pm the upper sign indicates an over cutting process and the lower sign indicates an under cutting process:

$$F_{st} = c_{gc} \cdot \begin{bmatrix} f_1 \cdot g_1^+ \\ f_2 \cdot g_2^- \end{bmatrix} + c_{ca} \cdot \begin{bmatrix} f_3 \cdot g_3^+ \\ f_4 \cdot g_4^- \end{bmatrix} \quad (4.40)$$

and

$$F_{vt} = c_{gc} \cdot \begin{bmatrix} f_2 \cdot g_1^+ - f_1 \cdot g_2^- \\ - \end{bmatrix} + c_{ca} \cdot \begin{bmatrix} f_4 \cdot g_3^+ - f_3 \cdot g_4^- \\ - \end{bmatrix} \quad (4.41)$$

and

$$F_{at} = c_{gc} \cdot f_5 \cdot g_5 + c_{ca} \cdot f_6 \cdot g_6 \quad (4.42)$$

and

$$M_t = c_{gc} \cdot f_5 \cdot g_1 \cdot R + c_{ca} \cdot f_6 \cdot g_3 \cdot R \quad (4.43)$$

These equations are in principle equal to Miedema [52] equation (17).

The coefficients f_1 to f_6 follow from integration and can be found in equations (4.26) to (4.29).

$$f_1 = \frac{\sin^3(\Omega_1)}{3} \quad (4.44)$$

and

$$f_2 = \frac{\cos^3(\Omega_1)}{3} - \cos(\Omega_1) + \frac{2}{3} \quad (4.45)$$

and

$$f_3 = \frac{\sin^2(\Omega_0) - \sin^2(\Omega_1)}{2} \quad (4.46)$$

and

$$f_4 = \frac{\Omega_0 - \Omega_1}{2} - \frac{\sin(2 - \Omega_0) - \sin(2 - \Omega_1)}{4} \quad (4.47)$$

and

$$f_5 = \frac{\Omega_1}{2} - \frac{\sin(2 - \Omega_1)}{4} \quad (4.48)$$

and

$$f_6 = \cos(\Omega_1) - \cos(\Omega_0) \quad (4.49)$$

Values for the coefficients f_1 to f_6 can be found in the tables 4.1 to 4.5.

**This is a translation of the dissertation of Dr.ir. S.A. Miedema, dated September 15th 1987 .
The dissertation was originally published in Dutch by the:
Delft University of Technology
Faculty of Mechanical Engineering and Marine Technology
Chair of Dredging Technology
Mekelweg 2
2628 CD, Delft
The Netherlands**

It is advised to also read the papers following this dissertation, since the theory developed has been refined and extended.

Last modified Sunday May 28, 2000 by: [Sape A. Miedema](#)

Translation by: [Laurens de Jonge](#)

Figures, equations and tables by: [Erik Miedema](#)

Copyright © May, 2000 Dr.ir. S.A. Miedema



[Download Adobe Acrobat Reader V4.0](#)

4.07 Specific cutting energy.

The specific cutting energy can be approached from two points of view:

1. Based on the average drive torque, the average haul force and the average cut sand flow rate.
2. Based on the momentary cutting forces and the momentary cut sand flow rate, from which an average value can be obtained by integration.

The specific cutting energy, based upon the first method, can be determined with the following equation:

$$E = \frac{M_t \cdot \omega + F_{st} \cdot v_s}{v_s \cdot A} \approx \frac{M_t \cdot \omega}{v_s \cdot b_{pr} \cdot R \cdot (1 - \cos(\Omega_0))} \quad (4.50)$$

In which ω The angular velocity of the cutterhead ($2 \cdot \pi \cdot n / 60$)
 A The cut away breach surface ($R \cdot (1 - \cos(\Omega_0)) \cdot b$)

Substitution of the equations (4.29), (4.31) and (4.32) in (4.50) gives:

$$E = \rho_w \cdot g \cdot \left[\frac{f_5 \cdot c_1 \cdot \frac{e}{k_m} \cdot \left(\frac{2 \cdot \pi \cdot R \cdot n_o}{60} \cdot \cos(l) \right) \cdot \left(\frac{60 \cdot v_s}{n_o \cdot p} \cdot \cos(\xi) \right) + f_6 \cdot d_1 \cdot (z+10)}{(1 - \cos(\Omega_0))} \right] \quad (4.51)$$

The second method uses the formulation for the specific cutting energy, which is derived in chapter for the cutting with straight blades (equation (2.68)).

$$E \approx \frac{1}{\Omega_0} \cdot \int_0^{\Omega_0} \frac{M(\Omega) \cdot \omega}{v_c \cdot h_i(\Omega) \cdot b} \cdot d\Omega = \frac{1}{\Omega_0} \cdot \int_0^{\Omega_0} \frac{F_t(\Omega) \cdot v_{ci}}{v_c \cdot h_i(\Omega) \cdot b} \cdot d\Omega \quad (4.52)$$

Substitution of the equations (4.1) to (4.3), (4.31) and (4.32) gives:

$$E = \frac{1}{\Omega_0} \cdot \rho_w \cdot g \cdot \left[c_1 \cdot \frac{e}{k_m} \cdot \left(\frac{2 \cdot \pi \cdot R \cdot n_o}{60} \cdot \cos(l) \right) \cdot \left(\frac{60 \cdot v_s}{n_o \cdot p} \cdot \cos(\xi) \right) \cdot \int_0^{\Omega_0} \sin(\Omega) \cdot d\Omega \right]$$

$$\left. + d_1 \cdot (z+10) \cdot \int_{\Omega_1}^{\Omega_0} d\Omega \right] \quad (4.53)$$

This integration gives:

$$E = \frac{1}{\Omega_0} \cdot \rho_w \cdot g \cdot \left[c_1 \cdot \frac{e}{k_m} \cdot \left(\frac{2 \cdot \pi \cdot R \cdot n_o}{60} \cdot \cos(\iota) \right) \cdot \left(\frac{60 \cdot v_s}{n_o \cdot p} \cdot \cos(\xi) \right) \cdot (1 - \cos(\Omega_1)) \right. \\ \left. + d_1 \cdot (z+10) \cdot (\Omega_0 - \Omega_1) \right] \quad (4.54)$$

The first method can be used for the verification of model study, since there only the total loads on the cutterhead are known and not the momentary loads on a blade of the cutterhead.

The second method gives a better formulation of the specific cutting energy. Additionally formulations for the layer-thickness can be derived from the second method, which are needed for the determination of the coefficients c_1 , c_2 , d_1 en d_2 .

If it is assumed that the specific cutting energy in the rotating cutting process is equal to the specific cutting energy in the linear cutting process, than the following can be derived for the characteristic layer-thickness:

The average specific cutting energy in the part of the layer where no cavitation takes place, is:

$$E = \frac{1}{\Omega_0} \cdot \rho_w \cdot g \cdot c_1 \cdot \frac{e}{k_m} \cdot \left(\frac{2 \cdot \pi \cdot R \cdot n_o}{60} \cdot \cos(\iota) \right) \cdot \left(\frac{60 \cdot v_s}{n_o \cdot p} \cdot \cos(\xi) \right) \cdot (1 - \cos(\Omega_1)) \quad (4.55)$$

This is equal to the specific cutting energy in a linear cutting process, where the same path is followed, with a layer-thickness:

$$h_{igc} = \frac{60 \cdot v_s}{n_o \cdot p} \cdot \cos(\xi) \cdot \frac{1 - \cos(\Omega_1)}{\Omega_1} \quad (4.56)$$

This is the average layer-thickness in the non-cavitating area. The specific cutting energy in the cavitating part of the layer is equal to that in the linear cutting process, where it has to be remarked that the coefficient d_1 has to be chosen such that it belongs to the amount of cut sand.

The average value of the layer-thickness in this area can serve as a characteristic value for the determination of d_1 . This results in:

$$h_{ica} = \frac{60 \cdot v_s}{n_o \cdot p} \cdot \cos(\xi) \cdot \frac{\cos(\Omega_1) - \cos(\Omega_0)}{\Omega_0 - \Omega_1} \quad (4.57)$$

With this the characteristic values for the layer-thickness are found for the determination of c_1 and c_2 from tables 2.14 to 2.25 and for the determination of d_1 and d_2 from the tables 2.26 to 2.37.

[Back to top](#)

This is a translation of the dissertation of Dr.ir. S.A. Miedema, dated September 15th 1987 .
 The dissertation was originally published in Dutch by the:
 Delft University of Technology
 Faculty of Mechanical Engineering and Marine Technology
 Chair of Dredging Technology
 Mekelweg 2
 2628 CD, Delft
 The Netherlands

It is advised to also read the papers following this dissertation, since the theory developed has been refined and extended.

Last modified Sunday May 28, 2000 by: [Sape A. Miedema](#)

Translation by: [Laurens de Jonge](#)

Figures, equations and tables by: [Erik Miedema](#)

Copyright © May, 2000 Dr.ir. S.A. Miedema



[Download Adobe Acrobat Reader V4.0](#)

Table 4.01: The coefficients f_1 , f_2 and f_3 as a function of the angle Ω_1 .

[Contents](#)

Ω_1	f_1	f_2	f_3
10 °	0.002	0.000	0.002
20 °	0.013	0.004	0.014
30 °	0.042	0.017	0.045
40 °	0.089	0.050	0.103
50 °	0.150	0.112	0.190
60 °	0.217	0.208	0.307
70 °	0.277	0.338	0.450
80 °	0.318	0.495	0.613
90 °	0.333	0.667	0.785
100 °	0.318	0.839	0.958
110 °	0.277	0.995	1.121
120 °	0.217	1.125	1.264
130 °	0.150	1.221	1.381
140 °	0.089	1.283	1.468
150 °	0.042	1.316	1.526
160 °	0.013	1.330	1.557
170 °	0.002	1.333	1.569
180 °	0.000	1.333	1.571

[Back to top](#)

This is a translation of the dissertation of Dr.ir. S.A. Miedema, dated September 15th 1987 .
 The dissertation was originally published in Dutch by the:
Delft University of Technology
Faculty of Mechanical Engineering and Marine Technology
Chair of Dredging Technology

**Mekelweg 2
2628 CD, Delft
The Netherlands**

It is advised to also read the papers following this dissertation, since the theory developed has been refined and extended.

Last modified Sunday May 28, 2000 by: [Sape A. Miedema](#)

Translation by: [Laurens de Jonge](#)

Figures, equations and tables by: [Erik Miedema](#)

Copyright © May, 2000 Dr.ir. S.A. Miedema



[Download Adobe Acrobat Reader V4.0](#)

Table 4.02: The coefficients f_3 , f_4 and f_6 as a function of Ω_0 and Ω_1 .

[Contents](#)

Ω_0	Ω_1	f_3	f_4	f_6
10°	0°	0.015	0.002	0.015
20°	0°	0.058	0.014	0.060
20°	10°	0.043	0.012	0.045
30°	0°	0.125	0.045	0.134
30°	10°	0.110	0.044	0.119
30°	20°	0.067	0.031	0.074
40°	0°	0.207	0.103	0.234
40°	10°	0.192	0.101	0.219
40°	20°	0.148	0.089	0.174
40°	30°	0.082	0.058	0.100
50°	0°	0.293	0.190	0.357
50°	10°	0.278	0.188	0.342
50°	20°	0.235	0.176	0.297

50 °	30 °	0.168	0.145	0.223
50 °	40 °	0.087	0.087	0.123
60 °	0 °	0.375	0.307	0.500
60 °	10 °	0.360	0.305	0.485
60 °	20 °	0.317	0.293	0.440
60 °	30 °	0.250	0.262	0.366
60 °	40 °	0.168	0.204	0.266
60 °	50 °	0.082	0.117	0.143
70 °	0 °	0.441	0.450	0.658
70 °	10 °	0.426	0.448	0.643
70 °	20 °	0.383	0.436	0.598
70 °	30 °	0.317	0.405	0.524
70 °	40 °	0.235	0.347	0.424
70 °	50 °	0.148	0.260	0.301
70 °	60 °	0.067	0.143	0.158
80 °	0 °	0.485	0.613	0.826

80 °	10 °	0.470	0.611	0.811
80 °	20 °	0.426	0.599	0.766
80 °	30 °	0.360	0.567	0.692
80 °	40 °	0.278	0.510	0.592
80 °	50 °	0.192	0.422	0.469
80 °	60 °	0.110	0.306	0.326
80 °	70 °	0.043	0.162	0.168

[Back to top](#)

**This is a translation of the dissertation of Dr.ir. S.A. Miedema, dated September 15th 1987 .
 The dissertation was originally published in Dutch by the:
 Delft University of Technology
 Faculty of Mechanical Engineering and Marine Technology
 Chair of Dredging Technology
 Mekelweg 2
 2628 CD, Delft
 The Netherlands**

It is advised to also read the papers following this dissertation, since the theory developed has been refined and extended.

Last modified Sunday May 28, 2000 by: [Sape A. Miedema](#)

Translation by: [Laurens de Jonge](#)

Figures, equations and tables by: [Erik Miedema](#)

Copyright © May, 2000 Dr.ir. S.A. Miedema



[Download Adobe Acrobat Reader V4.0](#)

Table 4.03: The coefficients f_3 , f_4 and f_6 as a function of Ω_0 and Ω_1 .

[Contents](#)

Ω_0	Ω_1	f_3	f_4	f_6
90°	0°	0.500	0.785	1.000
90°	10°	0.485	0.784	0.985
90°	20°	0.442	0.772	0.940
90°	30°	0.375	0.740	0.866
90°	40°	0.293	0.682	0.766
90°	50°	0.207	0.595	0.643
90°	60°	0.125	0.478	0.500
90°	70°	0.059	0.335	0.342
90°	80°	0.015	0.173	0.174
100°	0°	0.485	0.958	1.174
100°	10°	0.470	0.956	1.158
100°	20°	0.426	0.944	1.113
100°	30°	0.360	0.913	1.040

100 °	40 °	0.278	0.855	0.940
100 °	50 °	0.192	0.768	0.816
100 °	60 °	0.110	0.651	0.674
100 °	70 °	0.043	0.508	0.516
100 °	80 °	0.000	0.346	0.347
100 °	90 °	-0.015	0.173	0.174
110 °	0 °	0.442	1.121	1.342
110 °	10 °	0.426	1.119	1.327
110 °	20 °	0.383	1.107	1.282
110 °	30 °	0.317	1.075	1.208
110 °	40 °	0.235	1.018	1.108
110 °	50 °	0.148	0.930	0.985
110 °	60 °	0.067	0.814	0.842
110 °	70 °	0.000	0.670	0.684
110 °	80 °	-0.043	0.508	0.516
110 °	90 °	-0.058	0.335	0.342

110 °	100 °	-0.043	0.162	0.168
120 °	0 °	0.375	1.264	1.500
120 °	10 °	0.360	1.262	1.485
120 °	20 °	0.317	1.250	1.440
120 °	30 °	0.250	1.218	1.366
120 °	40 °	0.168	1.161	1.266
120 °	50 °	0.082	1.074	1.143
120 °	60 °	0.000	0.957	1.000
120 °	70 °	-0.066	0.814	0.842
120 °	80 °	-0.110	0.651	0.674
120 °	90 °	-0.125	0.478	0.500
120 °	100 °	-0.110	0.306	0.326
120 °	110 °	-0.067	0.143	0.158

[Back to top](#)

**This is a translation of the dissertation of Dr.ir. S.A. Miedema, dated September 15th 1987 .
The dissertation was originally published in Dutch by the:
Delft University of Technology
Faculty of Mechanical Engineering and Marine Technology
Chair of Dredging Technology
Mekelweg 2**

**2628 CD, Delft
The Netherlands**

It is advised to also read the papers following this dissertation, since the theory developed has been refined and extended.

Last modified Sunday May 28, 2000 by: [Sape A. Miedema](#)

Translation by: [Laurens de Jonge](#)

Figures, equations and tables by: [Erik Miedema](#)

Copyright © May, 2000 Dr.ir. S.A. Miedema



[Download Adobe Acrobat Reader V4.0](#)

Table 4.04: The coefficients f_3 , f_4 and f_6 as a function of Ω_0 and Ω_1 .

[Contents](#)

Ω_0	Ω_1	f_3	f_4	f_6
130 °	0 °	0.293	1.381	1.643
130 °	10 °	0.278	1.379	1.628
130 °	20 °	0.235	1.367	1.582
130 °	30 °	0.168	1.335	1.509
130 °	40 °	0.087	1.278	1.409
130 °	50 °	0.000	1.191	1.286
130 °	60 °	-0.082	1.074	1.143
130 °	70 °	-0.148	0.930	0.985
130 °	80 °	-0.191	0.768	0.816
130 °	90 °	-0.207	0.595	0.643
130 °	100 °	-0.191	0.423	0.469
130 °	110 °	-0.148	0.260	0.301
130 °	120 °	-0.082	0.117	0.143
140 °	0 °	0.207	1.468	1.766
140 °	10 °	0.192	1.466	1.751
140 °	20 °	0.148	1.454	1.706
140 °	30 °	0.082	1.423	1.632
140 °	40 °	0.000	1.365	1.532
140 °	50 °	-0.087	1.278	1.409
140 °	60 °	-0.168	1.161	1.266
140 °	70 °	-0.235	1.018	1.108
140 °	80 °	-0.278	0.855	0.940

140 °	90 °	-0.293	0.683	0.766
140 °	100 °	-0.278	0.510	0.592
140 °	110 °	-0.235	0.347	0.424
140 °	120 °	-0.168	0.204	0.266
140 °	130 °	-0.087	0.087	0.123
150 °	0 °	0.125	1.525	1.866
150 °	10 °	0.110	1.524	1.851
150 °	20 °	0.067	1.512	1.806
150 °	30 °	0.000	1.480	1.732
150 °	40 °	-0.082	1.423	1.632
150 °	50 °	-0.168	1.335	1.509
150 °	60 °	-0.250	1.218	1.366
150 °	70 °	-0.316	1.075	1.208
150 °	80 °	-0.360	0.913	1.040
150 °	90 °	-0.375	0.740	0.866
150 °	100 °	-0.360	0.567	0.692
150 °	110 °	-0.316	0.405	0.524
150 °	120 °	-0.250	0.262	0.366
150 °	130 °	-0.168	0.145	0.223
150 °	140 °	-0.082	0.058	0.100

[Back to top](#)

This is a translation of the dissertation of Dr.ir. S.A. Miedema, dated September 15th 1987 .

The dissertation was originally published in Dutch by the:

Delft University of Technology

Faculty of Mechanical Engineering and Marine Technology

Chair of Dredging Technology

Mekelweg 2

2628 CD, Delft

The Netherlands

It is advised to also read the papers following this dissertation, since the theory developed has been refined and

extended.

Last modified Sunday May 28, 2000 by: [Sape A. Miedema](#)

Translation by: [Laurens de Jonge](#)

Figures, equations and tables by: [Erik Miedema](#)

Copyright © May, 2000 Dr.ir. S.A. Miedema



[Download Adobe Acrobat Reader V4.0](#)

Table 4.05: The coefficients f_3 , f_4 and f_6 as a function of Ω_0 and Ω_1 .

[Contents](#)

Ω_0	Ω_1	f_3	f_4	f_6
160°	0°	0.059	1.557	1.940
160°	10°	0.043	1.555	1.924
160°	20°	0.000	1.543	1.879
160°	30°	-0.066	1.512	1.806
160°	40°	-0.148	1.454	1.706
160°	50°	-0.235	1.367	1.582
160°	60°	-0.316	1.250	1.440
160°	70°	-0.383	1.107	1.282
160°	80°	-0.426	0.944	1.113
160°	90°	-0.441	0.772	0.940
160°	100°	-0.426	0.599	0.766
160°	110°	-0.383	0.436	0.598
160°	120°	-0.317	0.293	0.440

160 °	130 °	-0.235	0.176	0.297
160 °	140 °	-0.148	0.089	0.174
160 °	150 °	-0.067	0.031	0.074
170 °	0 °	0.015	1.569	1.985
170 °	10 °	0.000	1.567	1.970
170 °	20 °	-0.043	1.555	1.924
170 °	30 °	-0.110	1.524	1.851
170 °	40 °	-0.191	1.466	1.751
170 °	50 °	-0.278	1.379	1.628
170 °	60 °	-0.360	1.262	1.485
170 °	70 °	-0.426	1.119	1.327
170 °	80 °	-0.470	0.956	1.158
170 °	90 °	-0.485	0.784	0.985
170 °	100 °	-0.470	0.611	0.811
170 °	110 °	-0.426	0.448	0.643
170 °	120 °	-0.360	0.305	0.485

170 °	130 °	-0.278	0.188	0.342
170 °	140 °	-0.192	0.101	0.219
170 °	150 °	-0.110	0.044	0.119
170 °	160 °	-0.043	0.012	0.045
180 °	0 °	0.000	1.571	2.000
180 °	10 °	-0.015	1.569	1.985
180 °	20 °	-0.058	1.557	1.940
180 °	30 °	-0.125	1.526	1.866
180 °	40 °	-0.207	1.468	1.766
180 °	50 °	-0.293	1.381	1.643
180 °	60 °	-0.375	1.264	1.500
180 °	70 °	-0.441	1.121	1.342
180 °	80 °	-0.485	0.958	1.174
180 °	90 °	-0.500	0.785	1.000
180 °	100 °	-0.485	0.613	0.826
180 °	110 °	-0.442	0.450	0.658

180 °	120 °	-0.375	0.307	0.500
180 °	130 °	-0.293	0.190	0.357
180 °	140 °	-0.207	0.103	0.234
180 °	150 °	-0.125	0.045	0.134
180 °	160 °	-0.059	0.014	0.060
180 °	170 °	-0.015	0.002	0.015

[Back to top](#)

This is a translation of the dissertation of Dr.ir. S.A. Miedema, dated September 15th 1987 .

The dissertation was originally published in Dutch by the:

Delft University of Technology

Faculty of Mechanical Engineering and Marine Technology

Chair of Dredging Technology

Mekelweg 2

2628 CD, Delft

The Netherlands

It is advised to also read the papers following this dissertation, since the theory developed has been refined and extended.

Last modified Sunday May 28, 2000 by: [Sape A. Miedema](#)

Translation by: [Laurens de Jonge](#)

Figures, equations and tables by: [Erik Miedema](#)

Copyright © May, 2000 Dr.ir. S.A. Miedema



[Download Adobe Acrobat Reader V4.0](#)

5.01 Introduction.

For a successful application of the cutting theory, derived in chapter 2, on a dredging wheel dredger it is necessary to analyze the geometry of the cutting process first. Figure 5.1 and 5.2 show the cutting process in the axial plane and the plane perpendicular to the axis of the dredging wheel.

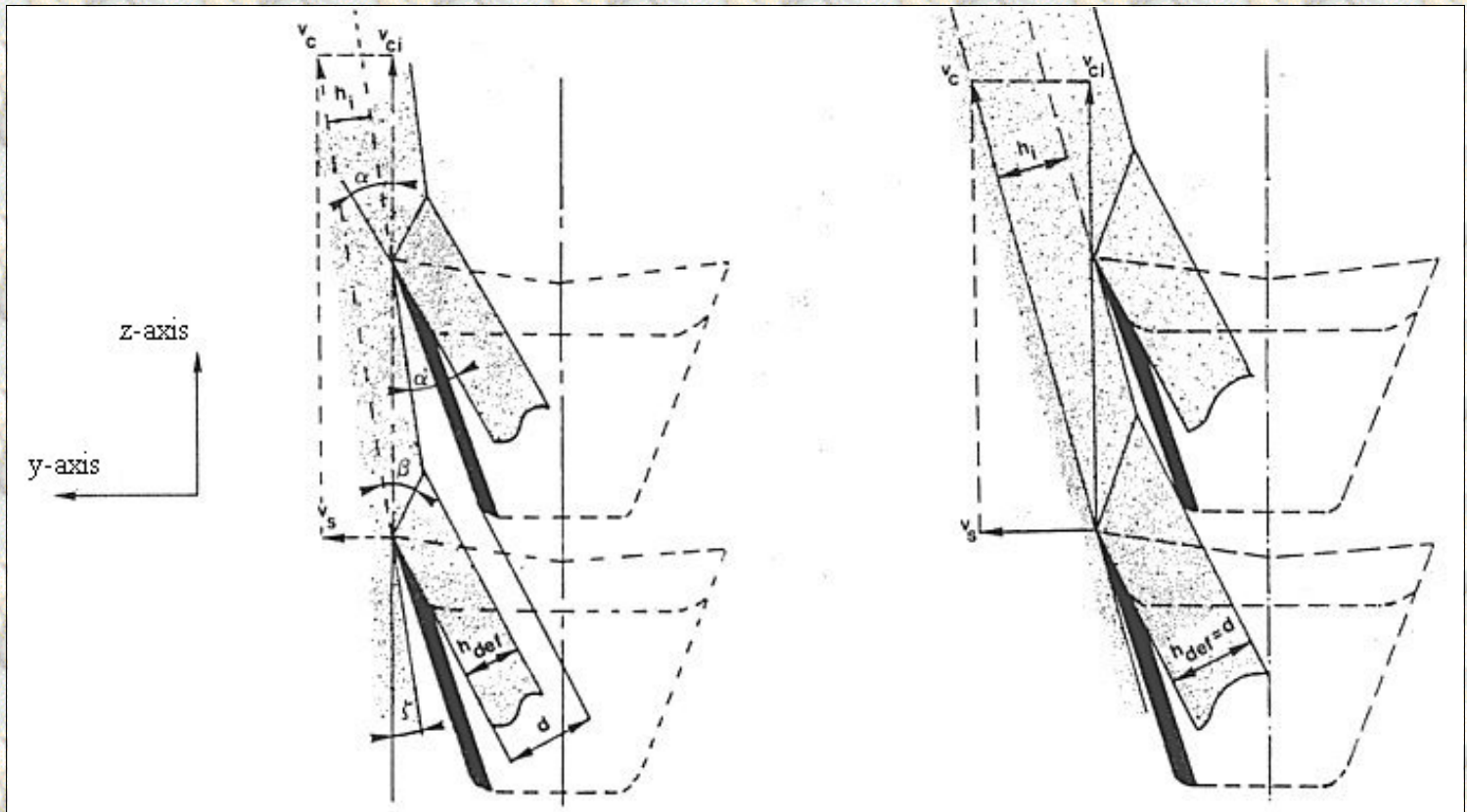


Figure 5.1: The cutting process of a dredging wheel in the axial plane, with on the right the "bulldozer" effect.

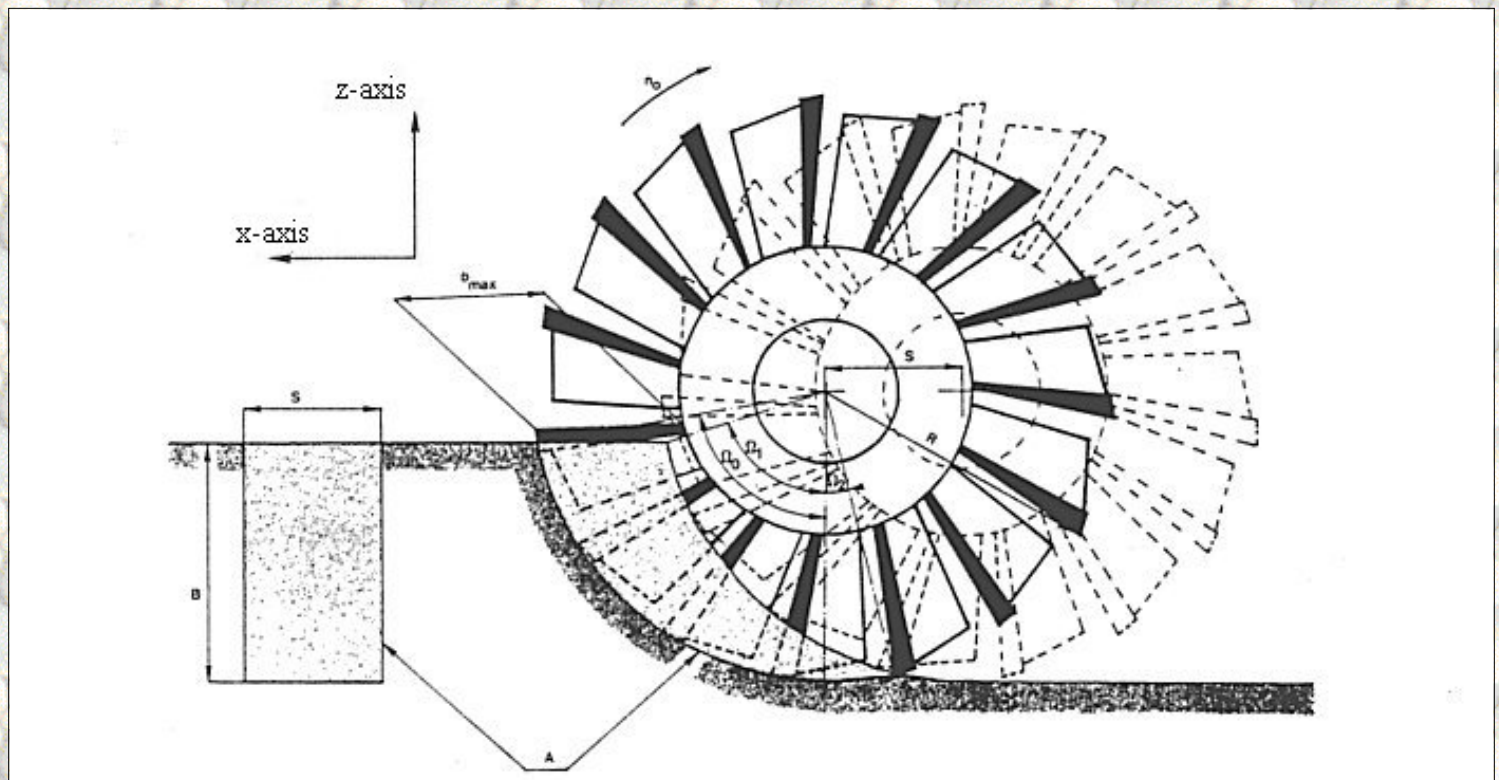


Figure 5.2: The cutting process of a dredging wheel in the radial plane.

The cutting velocity, layer-thickness and the blade width are a function of the haul velocity, the number of revolutions, the step size, the dimensions of the dredging wheel and the breach height. The blade width also varies strong with the run-through angle of the cutting edge of the bucket. The layer-thickness and the dynamic blade angle are, different from the cutterhead, not a function of the run-through angle though they are dependent on the position on the cutting edge (figure 5.3).

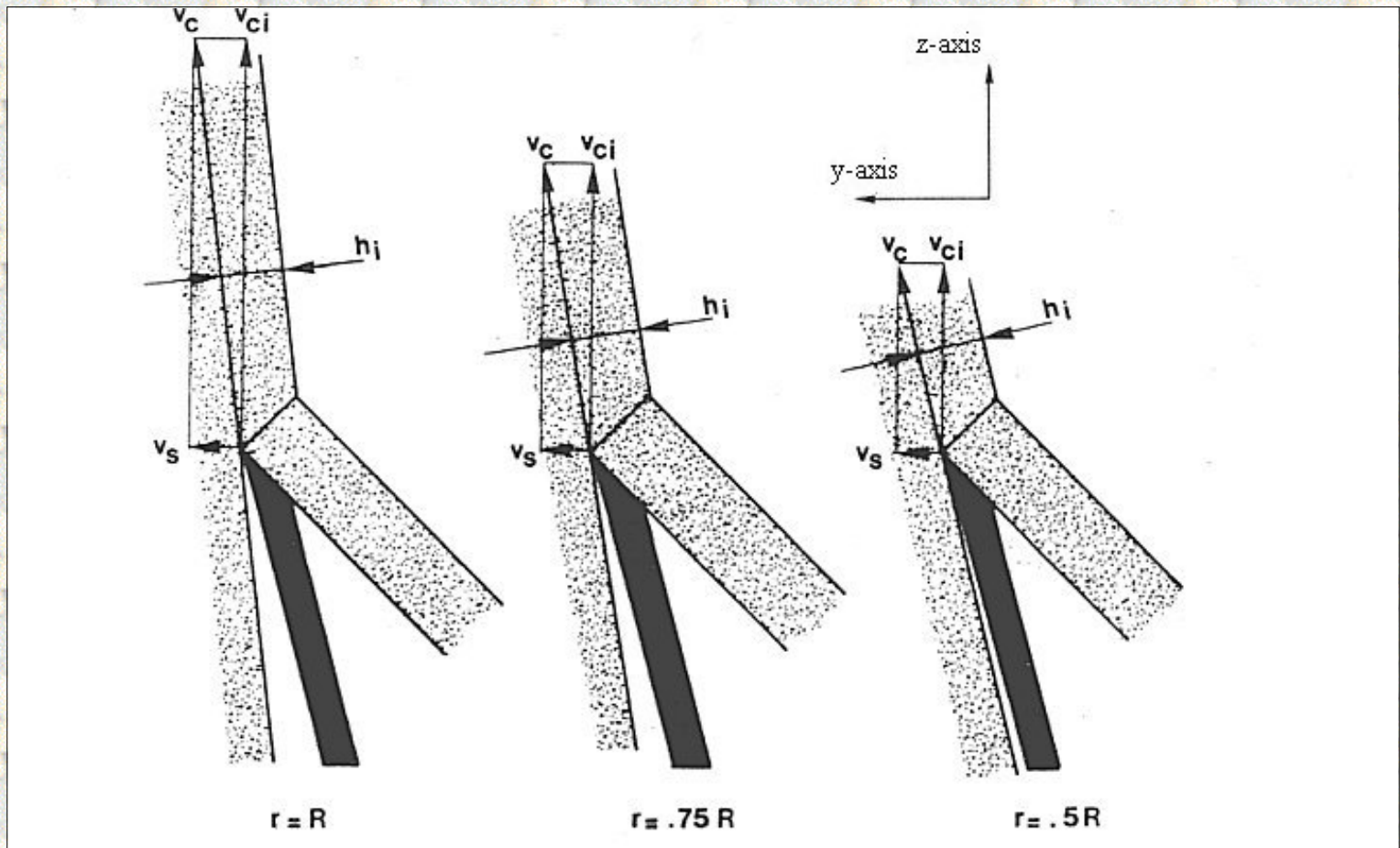


Figure 5.3: The cutting process at different radii.

The next equation can be derived for the layer-thickness as a function of the distance r to the axis of the dredging wheel:

$$h_i = \frac{v_s \cdot 60}{n_o \cdot p} \cdot \frac{v_{ci}}{\sqrt{(v_{ci}^2 + v_s^2)}} \quad (5.1)$$

In which:

$$v_{ci} = \frac{2 \cdot \pi \cdot n_o}{60} \cdot r \quad (5.2)$$

With:

v_{ci}	Peripheral velocity as a function of the radius.
v_s	Haul velocity.
n_o	Number of revolutions.
p	Number of blades.

r

Local radius.

If the haul velocity is much smaller than the peripheral velocity than the layer-thickness can be expressed by:

$$h_i = \frac{v_s \cdot 60}{n_o \cdot p} \quad (5.3)$$

The layer-thickness has become independent of the position on the cutting edge.

In figure 5.1 a "standing" cut is assumed, in which can be spoken of a horizontal "step" S and a breach height B. It is however also possible that, with a high embankment, a layer of the embankment is dredged which gives a so-called "bank" cut. This is shown in figure 5.4. For the derivation of the equations to calculate the forces, torque and power on the dredging wheel will first be assumed that the cut is a "standing" cut.

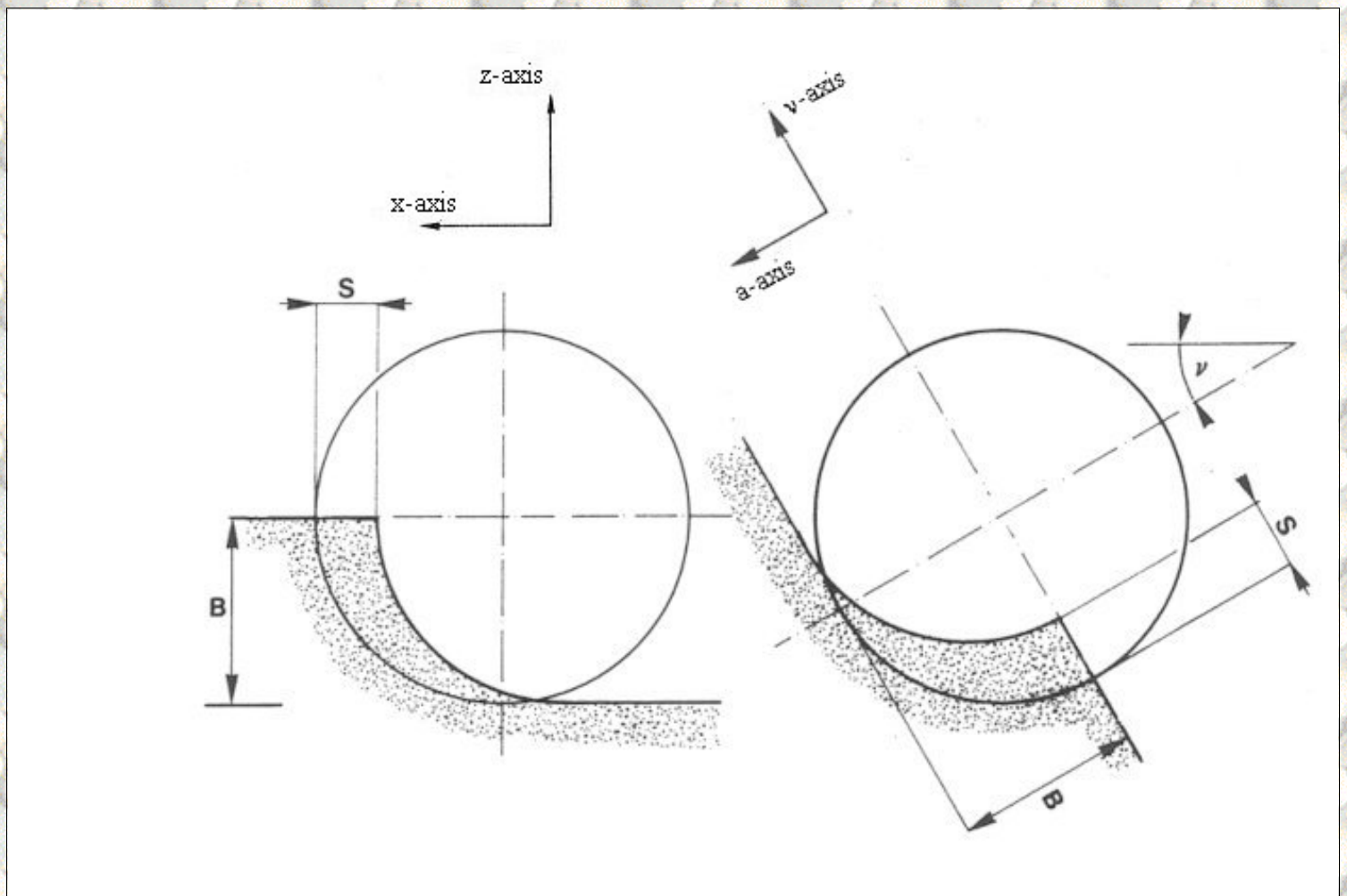


Figure 5.4: The standing cut and the bank cut.

It appears, from figure 5.1 that the part of a blade edge that participates in the cutting process is dependent on the angle that the blade edge has run-through since entering the breach. In this model it is assumed that the blade enters the breach under an angle $\Omega_2 = -S/2R$. For the width of the blade edge that participates in the cutting process can be derived:

$$b(\Omega) = S \cdot \sin(\Omega) + R \cdot \left[1 - \sqrt{1 - \cos^2(\Omega) \cdot \frac{S^2}{R^2}} \right] \quad (5.4)$$

In which:	R	Outer radius of the dredging wheel.
	Ω	Run-through angle.
	S	Step.
	$b(\Omega)$	Blade width as a function of the run-through angle.

The second term, on the right, can not be neglected. This in contrast to the similar term in equation (8.26) for the layer-thickness in the numerical model (chapter 8) for the determination of the forces on the cutterhead, where this term is neglected for use in the analytical model (chapter 4). This is because the step S is of the same order of magnitude as the radius of the dredging wheel. For the determination of the forces and the torque on the dredging wheel, the product of equation (5.4) with another function of Ω has to be integrated. Because this term is hard to integrate, a good approximation has to be found using a Taylor series development. The found approximation has only an error of 0.5% maximum for relevant values of S.

$$b(\Omega) = S \cdot \sin(\Omega) + C \cdot \cos^2(\Omega) \quad (5.5)$$

$$\Omega_2 < \Omega < \Omega_1$$

With:

$$C = \left[1 - \sqrt{1 - \frac{S^2}{R^2}} \right] \quad (5.6)$$

Equation (5.5) is valid until angle Ω_1 , as shown in figure 5.5. When Ω is between Ω_1 and Ω_0 the next equations are valid for the blade width as a function of Ω .

$$b(\Omega) = R - R \cdot \frac{\cos(\Omega_0)}{\cos(\Omega)} \quad (5.7)$$

$$\Omega_1 < \Omega < \Omega_0$$

For the angles Ω_2 , Ω_1 en Ω_0 the following can be derived:

$$\Omega_2 = -\arcsin\left(\frac{S}{2 \cdot R}\right) \quad (5.8)$$

$$\Omega_1 = \arctan\left(\frac{R \cdot \sin(\Omega_0) - S}{R \cdot \cos(\Omega_0)}\right) \quad (5.9)$$

$$\Omega_0 = \arccos\left(\frac{R - B}{R}\right) \quad (5.10)$$

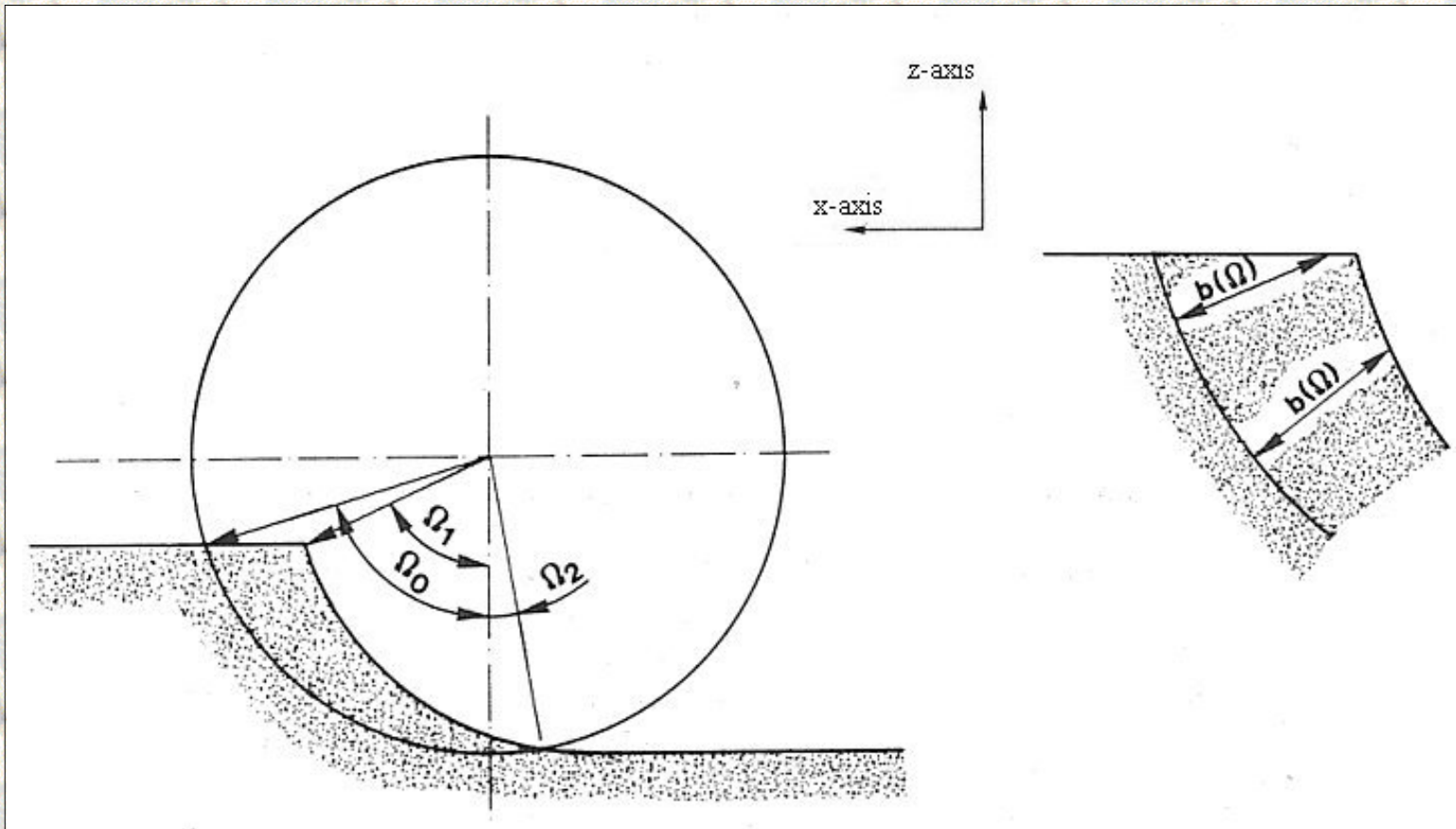


Figure 5.5: The blade width in contact with the bank as a function of the run through angle.

The radius $r(\Omega)$, the distance of the point of the blade most aimed to the axis that is in contact with the breach can be described by:

$$r(\Omega) = R - b(\Omega) \quad (5.11)$$

For the determination of the forces and the torque the non-cavitating and the cavitating process can be distinguished, though both phases of the cutting process can occur at the same time. This is because the cutting velocity increases with an increasing distance of a point on the blade edge to the

axis, while the layer-thickness is more or less constant over the blade edge.

[Back to top](#)

This is a translation of the dissertation of Dr.ir. S.A. Miedema, dated September 15th 1987 .

The dissertation was originally published in Dutch by the:

Delft University of Technology

Faculty of Mechanical Engineering and Marine Technology

Chair of Dredging Technology

Mekelweg 2

2628 CD, Delft

The Netherlands

It is advised to also read the papers following this dissertation, since the theory developed has been refined and extended.

Last modified Sunday May 28, 2000 by: [Sape A. Miedema](#)

Translation by: [Laurens de Jonge](#)

Figures, equations and tables by: [Erik Miedema](#)

Copyright © May, 2000 Dr.ir. S.A. Miedema



[Download Adobe Acrobat Reader V4.0](#)

5.02 The non-cavitating cutting process.

For the non-cavitating cutting process the forces and the torque can be determined by integrating the momentary forces and torque over the run-through angle Ω_0 . This results in the following integrals:

$$F_x = -b_{gc} \cdot c_1 \cdot \int_{\Omega_2}^{\Omega_0} \int_{r(\Omega)}^R r \cdot \cos(\Omega) \cdot dr \cdot d\Omega \quad (5.12)$$

$$F_y = b_{gc} \cdot c_2 \cdot \int_{\Omega_2}^{\Omega_0} \int_{r(\Omega)}^R r \cdot dr \cdot d\Omega = b_{gc} \cdot c_2 \cdot A \quad (5.13)$$

In which: A = The surface of the bank cross section.

$$F_z = -b_{gc} \cdot c_1 \cdot \int_{\Omega_2}^{\Omega_0} \int_{r(\Omega)}^R r \cdot \sin(\Omega) \cdot dr \cdot d\Omega \quad (5.14)$$

$$M = b_{gc} \cdot c_1 \cdot \int_{\Omega_2}^{\Omega_0} \int_{r(\Omega)}^R r^2 \cdot dr \cdot d\Omega \quad (5.15)$$

In which:

$$b_{gc} = \rho_w \cdot g \cdot \frac{v_s^2 \cdot 60 \cdot e}{n_o \cdot p \cdot k_m} \quad (5.16)$$

And c_1 and c_2 according the tables 2.14 to 2.25 from chapter 2 (see Appendix B5).

The accents in the following equations indicate that the coefficients b_{gc} , c_1 and c_2 are neglected here. The solution of the equations (5.12) to (5.15) now becomes, with the aid of equations (5.5), (5.7) and (5.11):

$$\begin{aligned} F'_x = & S \cdot R \left(\frac{\sin^2(\Omega_1) - \sin^2(\Omega_2)}{2} \right) + C \cdot R^2 \cdot \left(\sin(\Omega_1) - \sin(\Omega_2) - \frac{\sin^3(\Omega_1) - \sin^3(\Omega_2)}{3} \right) \\ & - S^2 \cdot \left(\frac{\sin^3(\Omega_1) - \sin^3(\Omega_2)}{6} \right) + C \cdot S \cdot R \cdot \left(\frac{\cos^4(\Omega_1) - \cos^4(\Omega_2)}{4} \right) \\ & - C^2 \cdot R^2 \cdot \left(\frac{\sin(\Omega_1) - \sin(\Omega_2)}{2} - \frac{\sin^3(\Omega_1) - \sin^3(\Omega_2)}{3} + \frac{\sin^5(\Omega_1) - \sin^5(\Omega_2)}{10} \right) \\ & + R^2 \cdot \left(\frac{\sin(\Omega_0) - \sin(\Omega_1)}{2} + \frac{\cos^2(\Omega_0)}{2} \cdot \ln \left(\frac{\sec(\Omega_1) + \tan(\Omega_1)}{\sec(\Omega_0) + \tan(\Omega_0)} \right) \right) \end{aligned} \quad (5.17)$$

and

$$\begin{aligned}
 F'_y = A = & R \cdot S \cdot (\cos(\Omega_2) - \cos(\Omega_1)) + C \cdot R^2 \cdot \left(\frac{\Omega_1 - \Omega_2}{2} + \frac{\sin(2 \cdot \Omega_1) - \sin(2 \cdot \Omega_2)}{4} \right) \\
 & - S^2 \cdot \left(\frac{\Omega_1 - \Omega_2}{4} - \frac{\sin(2 \cdot \Omega_1) - \sin(2 \cdot \Omega_2)}{8} \right) + C \cdot S \cdot R \cdot \left(\frac{\cos^3(\Omega_1) - \cos^3(\Omega_2)}{3} \right) \\
 & - C^2 \cdot R^2 \cdot \left(3 \cdot \frac{\Omega_1 - \Omega_2}{16} + 3 \cdot \frac{\sin(2 \cdot \Omega_1) - \sin(2 \cdot \Omega_2)}{32} + \frac{\sin(\Omega_1) \cos^3(\Omega_1) - \sin(\Omega_2) \cos^3(\Omega_2)}{8} + \right) \\
 & + R^2 \cdot \left(\frac{\Omega_0 - \Omega_1}{2} - \frac{\cos^2(\Omega_0)}{2} \cdot (\tan(\Omega_0) - \tan(\Omega_1)) \right)
 \end{aligned} \tag{5.18}$$

and

$$F'_z = S \cdot R \cdot \left(\frac{\Omega_1 - \Omega_2}{2} - \frac{\sin(2 \cdot \Omega_1) - \sin(2 \cdot \Omega_2)}{4} \right) - C \cdot R^2 \cdot \left(\frac{\cos^3(\Omega_1) - \cos^3(\Omega_2)}{3} \right)$$

$$\begin{aligned}
& -S^2 \cdot \left(\frac{\cos(\Omega_1) - \cos(\Omega_2)}{2} + \frac{\cos^3(\Omega_1) - \cos^3(\Omega_2)}{6} \right) \\
& -C \cdot S \cdot R \cdot \left(\frac{\Omega_1 - \Omega_2}{8} - \frac{\sin(4 \cdot \Omega_1) - \sin(4 \cdot \Omega_2)}{32} \right) + C^2 \cdot R^2 \cdot \left(\frac{\cos^5(\Omega_1) - \cos^5(\Omega_2)}{10} \right) \\
& + R^2 \cdot \left(\frac{\cos(\Omega_1) - \cos(\Omega_0)}{2} + \frac{\cos^2(\Omega_0)}{2} \cdot (\sec(\Omega_1) - \sec(\Omega_0)) \right) \quad (5.19)
\end{aligned}$$

and

$$\begin{aligned}
M' = & S \cdot R^2 \cdot (\cos(\Omega_2) - \cos(\Omega_1)) + C \cdot R^3 \cdot \left(\frac{\Omega_1 - \Omega_2}{2} + \frac{\sin(2 \cdot \Omega_1) - \sin(2 \cdot \Omega_2)}{4} \right) \\
& - S^2 \cdot R \cdot \left(\frac{\Omega_1 - \Omega_2}{2} - \frac{\sin(2 \cdot \Omega_1) - \sin(2 \cdot \Omega_2)}{4} \right) + C \cdot S \cdot R^2 \cdot \left(2 \cdot \frac{\cos^3(\Omega_1) - \cos^3(\Omega_2)}{3} \right)
\end{aligned}$$

$$\begin{aligned}
& -C^2 \cdot R^3 \cdot \left(3 \cdot \frac{\Omega_1 - \Omega_2}{8} + 3 \cdot \frac{\sin(2 \cdot \Omega_1) - \sin(2 \cdot \Omega_2)}{16} + \frac{\sin(\Omega_1) \cos^3(\Omega_1) - \sin(\Omega_2) \cos^3(\Omega_2)}{4} + \right) \\
& -S^3 \cdot \left(-\frac{\cos(\Omega_1) - \cos(\Omega_2)}{3} + \frac{\cos^3(\Omega_1) - \cos^3(\Omega_2)}{9} \right) \\
& + C \cdot S^2 \cdot R \cdot \left(\frac{\Omega_1 - \Omega_2}{8} - \frac{\sin(4 \cdot \Omega_1) - \sin(4 \cdot \Omega_2)}{32} \right) - C^2 \cdot S \cdot R^2 \cdot \left(\frac{\cos^5(\Omega_1) - \cos^5(\Omega_2)}{5} \right) \\
& + C^3 \cdot R^3 \cdot \left(5 \cdot \frac{\Omega_1 - \Omega_2}{48} + 5 \cdot \frac{\sin(\Omega_1) \cdot \cos(\Omega_1) - \sin(\Omega_2) \cdot \cos(\Omega_2)}{48} \right. \\
& + 5 \cdot \frac{\sin(\Omega_1) \cos^3(\Omega_1) - \sin(\Omega_2) \cos^3(\Omega_2)}{72} \\
& \left. + \frac{\sin(\Omega_1) \cos^5(\Omega_1) - \sin(\Omega_2) \cos^5(\Omega_2)}{18} \right)
\end{aligned}$$

$$+ R^3 \cdot \left(\frac{\Omega_0 - \Omega_1}{3} + \frac{\cos^3(\Omega_0)}{6} \cdot \left(\frac{\sin(\Omega_0)}{\cos^2(\Omega_0)} + \frac{\sin(\Omega_1)}{\cos^2(\Omega_1)} + \ln \left(\frac{\sec(\Omega_1) + \tan(\Omega_1)}{\sec(\Omega_0) + \tan(\Omega_0)} \right) \right) \right) \quad (5.20)$$

[Back to top](#)

This is a translation of the dissertation of Dr.ir. S.A. Miedema, dated September 15th 1987 .

The dissertation was originally published in Dutch by the:

Delft University of Technology

Faculty of Mechanical Engineering and Marine Technology

Chair of Dredging Technology

Mekelweg 2

2628 CD, Delft

The Netherlands

It is advised to also read the papers following this dissertation, since the theory developed has been refined and extended.

Last modified Sunday May 28, 2000 by: [Sape A. Miedema](#)

Translation by: [Laurens de Jonge](#)

Figures, equations and tables by: [Erik Miedema](#)

Copyright © May, 2000 Dr.ir. S.A. Miedema



[Download Adobe Acrobat Reader V4.0](#)

5.03 The cavitating cutting process.

To determine the forces and the torque on the dredging wheel from the momentary forces, for the fully cavitating cutting process, the following integrals have to be solved:

$$F_x = -b_{ca} \cdot d_1 \cdot \int_{\Omega_2}^{\Omega_0} \int_{r(\Omega)}^R \cos(\Omega) \cdot dr \cdot d\Omega \quad (5.21)$$

$$F_y = b_{ca} \cdot d_2 \cdot \int_{\Omega_2}^{\Omega_0} \int_{r(\Omega)}^R dr \cdot d\Omega \quad (5.22)$$

$$F_z = -b_{ca} \cdot d_1 \cdot \int_{\Omega_2}^{\Omega_0} \int_{r(\Omega)}^R \sin(\Omega) \cdot dr \cdot d\Omega \quad (5.23)$$

$$M = b_{ca} \cdot d_1 \cdot \int_{\Omega_2}^{\Omega_0} \int_{r(\Omega)}^R r \cdot dr \cdot d\Omega \quad (5.24)$$

In which:

$$b_{ca} = \rho_w \cdot g \cdot (z+10) \cdot \frac{v_s \cdot 60}{2 \cdot \pi \cdot n_o} \quad (5.25)$$

and d_1 and d_2 according tables 2.26 to 2.37 from chapter 2 (see Appendix B5).

The accents in the following equations indicate that the coefficients b_{ca} , d_1 and d_2 are neglected here. The solution of equations (5.21) to (5.24) now becomes:

$$\begin{aligned} F'_x = & S \cdot \left(\frac{\sin^2(\Omega_1) - \sin^2(\Omega_2)}{2} \right) + C \cdot R \cdot \left(\sin(\Omega_1) - \sin(\Omega_2) - \frac{\sin^3(\Omega_1) - \sin^3(\Omega_2)}{3} \right) \\ & + R \cdot \left(\sin(\Omega_0) - \sin(\Omega_1) - \cos(\Omega_0) \cdot (\Omega_0 - \Omega_1) \right) \end{aligned} \quad (5.26)$$

and

$$F'_y = S \cdot \left(\cos(\Omega_2) - \cos(\Omega_1) \right) + C \cdot R \cdot \left(\frac{\Omega_1 - \Omega_2}{2} + \frac{\sin(2 \cdot \Omega_1) - \sin(2 \cdot \Omega_2)}{4} \right)$$

$$+ R \cdot \left(\Omega_0 - \Omega_1 + \cos(\Omega_0) \cdot \ln \left(\frac{\sec(\Omega_1) + \tan(\Omega_1)}{\sec(\Omega_0) + \tan(\Omega_0)} \right) \right) \quad (5.27)$$

and

$$F'_z = S \cdot \left(\frac{\Omega_1 - \Omega_2}{2} \frac{\sin(2 \cdot \Omega_1) - \sin(2 \cdot \Omega_2)}{4} \right) + C \cdot R \cdot \left(\frac{\cos^3(\Omega_2) - \cos^3(\Omega_1)}{3} \right) \\ R \cdot \left(\cos(\Omega_1) - \cos(\Omega_0) + \cos(\Omega_0) \cdot \ln \left(\frac{\cos(\Omega_0)}{\cos(\Omega_1)} \right) \right) \quad (5.28)$$

While for the torque the same is found as for the force F'_y in the non-cavitating cutting process. Compare equations (5.13) and (5.24).

$$M' = F'_y \quad (5.29)$$

[Back to top](#)

This is a translation of the dissertation of Dr.ir. S.A. Miedema, dated September 15th 1987 .
 The dissertation was originally published in Dutch by the:
 Delft University of Technology
 Faculty of Mechanical Engineering and Marine Technology
 Chair of Dredging Technology
 Mekelweg 2
 2628 CD, Delft
 The Netherlands

It is advised to also read the papers following this dissertation, since the theory developed has been refined and extended.

Last modified Sunday May 28, 2000 by: [Sape A. Miedema](#)

Translation by: [Laurens de Jonge](#)

Figures, equations and tables by: [Erik Miedema](#)

Copyright © May, 2000 Dr.ir. S.A. Miedema



[Download Adobe Acrobat Reader V4.0](#)

5.04 Simplification of the equations.

The above shown analytical model is not very clear, while the purpose of an analytical model is to improve the understanding of the dredging process. This model also makes it difficult to find a simple expression for the "specific energy" for the sand.

Equations (5.17) to (5.20), for the non-cavitating cutting process can however be simplified to:

$$F_x = -b_{gc} \cdot c_1 \cdot f_{xgc} \cdot A \quad (5.30)$$

and

$$F_y = -b_{gc} \cdot c_2 \cdot f_{ygc} \cdot A \quad (5.31)$$

and

$$F_z = -b_{gc} \cdot c_1 \cdot f_{zgc} \cdot A \quad (5.32)$$

and

$$M = b_{gc} \cdot c_1 \cdot m_{gc} \cdot R \cdot A \quad (5.33)$$

Where the coefficients f_{xgc} , f_{ygc} , f_{zgc} and m_{gc} can be found in tables 5.1 to 5.5 for a number of S/R and B/R ratios.

For the fully cavitating cutting process the following simplifications can be carried out (equations (5.26) to (5.29)):

$$F_x = -b_{ca} \cdot d_1 \cdot f_{xca} \cdot A/R \quad (5.34)$$

and

$$F_y = b_{ca} \cdot d_2 \cdot f_{yca} \cdot A/R \quad (5.35)$$

and

$$F_z = -b_{ca} \cdot d_1 \cdot f_{zca} \cdot A/R \quad (5.36)$$

and

$$M = b_{ca} \cdot d_1 \cdot m_{ca} \cdot A \quad (5.37)$$

Where the coefficients f_{xca} , f_{yca} , f_{zca} and m_{ca} can be found in tables 5.6 to 5.10.

[Back to top](#)

This is a translation of the dissertation of Dr.ir. S.A. Miedema, dated September 15th 1987 .
The dissertation was originally published in Dutch by the:
Delft University of Technology
Faculty of Mechanical Engineering and Marine Technology
Chair of Dredging Technology
Mekelweg 2
2628 CD, Delft
The Netherlands

It is advised to also read the papers following this dissertation, since the theory developed has been refined and extended.

Last modified Sunday May 28, 2000 by: [Sape A. Miedema](#)

Translation by: [Laurens de Jonge](#)

Figures, equations and tables by: [Erik Miedema](#)

Copyright © May, 2000 Dr.ir. S.A. Miedema



[Download Adobe Acrobat Reader V4.0](#)

5.05 Specific cutting energy.

For the "specific cutting energy" can now be derived, with $\omega = 2 \cdot \pi \cdot n_o / 60$:

$$E_{gc} = \frac{M \cdot \omega + F_y \cdot v_s}{v_s \cdot A} = b_{gc} \cdot \frac{c_1 \cdot m_{gc} \cdot R \cdot \omega + c_2 \cdot f_{ygc} \cdot v_s}{v_s} \quad (5.38)$$

For the non-cavitating cutting process, and:

$$E_{ca} = b_{ca} \cdot \frac{d_1 \cdot \omega + d_2 \cdot f_{yca} \cdot v_s / R}{v_s} \quad (5.39)$$

For the fully cavitating cutting process.

The contribution of the haul power in the "specific energy" ($F_y \cdot v_s$) is minor and can be neglected if necessary. The next simple expressions are then found for the "specific energy":

$$E_{gc} = 2\pi \cdot \rho_w \cdot g \cdot c_1 \cdot m_{gc} \cdot R \cdot \frac{v_s \cdot e}{p \cdot k_m} \quad (5.40)$$

and

$$E_{ca} = \rho_w \cdot g \cdot (z + 10) \cdot d_1 \quad (5.41)$$

It is notable, that these equations are similar to the equations for the "specific energy" which are found in the straight cutting process, if for the determination of the cutting velocity in the non-cavitating cutting process the term $m_{gc} \cdot R$ from equation (5.40) is taken as the radius for the determination of the cutting velocity.

The dissertation was originally published in Dutch by the:
Delft University of Technology
Faculty of Mechanical Engineering and Marine Technology
Chair of Dredging Technology
Mekelweg 2
2628 CD, Delft
The Netherlands

It is advised to also read the papers following this dissertation, since the theory developed has been refined and extended.

Last modified Sunday May 28, 2000 by: [Sape A. Miedema](#)

Translation by: [Laurens de Jonge](#)

Figures, equations and tables by: [Erik Miedema](#)

Copyright © May, 2000 Dr.ir. S.A. Miedema



[Download Adobe Acrobat Reader V4.0](#)

5.06 Partial cavitation.

Since the cutting velocity on a point of the blade edge is proportional to the distance of that point to the axis of the dredging wheel, it is possible that cavitation occurs on the circumference of the dredging wheel, while there is no cavitation more towards the middle. This is shown in figure 5.6.

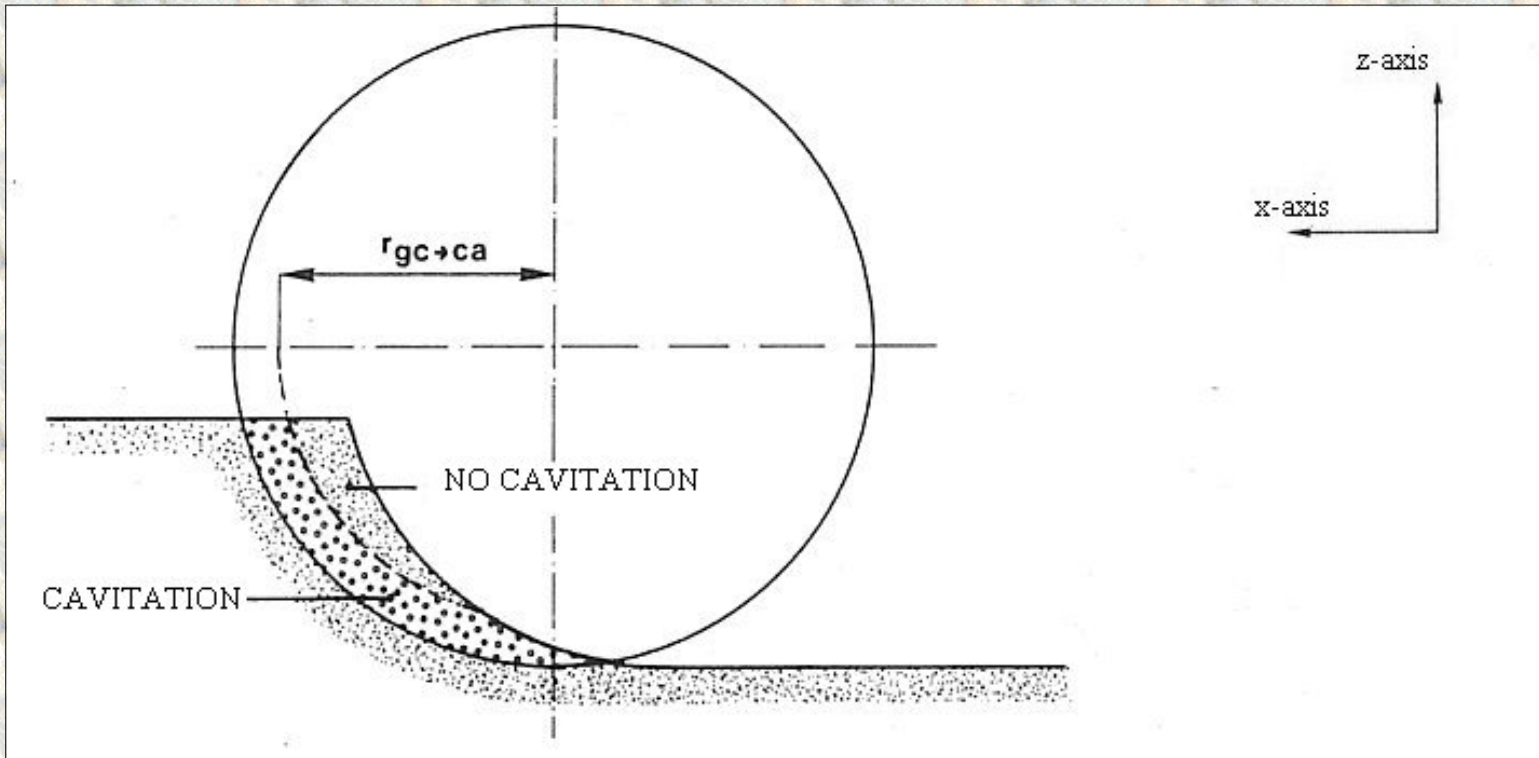


Figure 5.6: The transition between the non-cavitating and the cavitating cutting process.

If again it is assumed that the transition between a non-cavitating and a cavitating cutting process is abrupt then the radius where this transition takes place can be calculated with:

$$r_{gc \rightarrow ca} = \frac{d_1 \cdot (z+10) \cdot p \cdot k_m}{c_1 \cdot 2 \cdot \pi \cdot v_s \cdot e} \quad (5.42)$$

By integrating the forces over the non-cavitating and the cavitating area the resulting forces and the resulting torque can be determined. It is however of more use to apply the numerical model of chapter 8 for these calculations.

[Back to top](#)

This is a translation of the dissertation of Dr.ir. S.A. Miedema, dated September 15th 1987 .
The dissertation was originally published in Dutch by the:
Delft University of Technology
Faculty of Mechanical Engineering and Marine Technology
Chair of Dredging Technology
Mekelweg 2
2628 CD, Delft
The Netherlands

It is advised to also read the papers following this dissertation, since the theory developed has been refined and extended.

Last modified Sunday May 28, 2000 by: [Sape A. Miedema](#)

Translation by: [Laurens de Jonge](#)

Figures, equations and tables by: [Erik Miedema](#)

Copyright © May, 2000 Dr.ir. S.A. Miedema



[Download Adobe Acrobat Reader V4.0](#)

5.07 Correction of the direction of the forces.

[Contents](#)

Figure 5.7 shows that the direction of the forces on the blade edge are not parallel to the plane perpendicular to the axis of the dredging wheel and to the axis of the dredging wheel (the y-axis, see also figure 5.3)

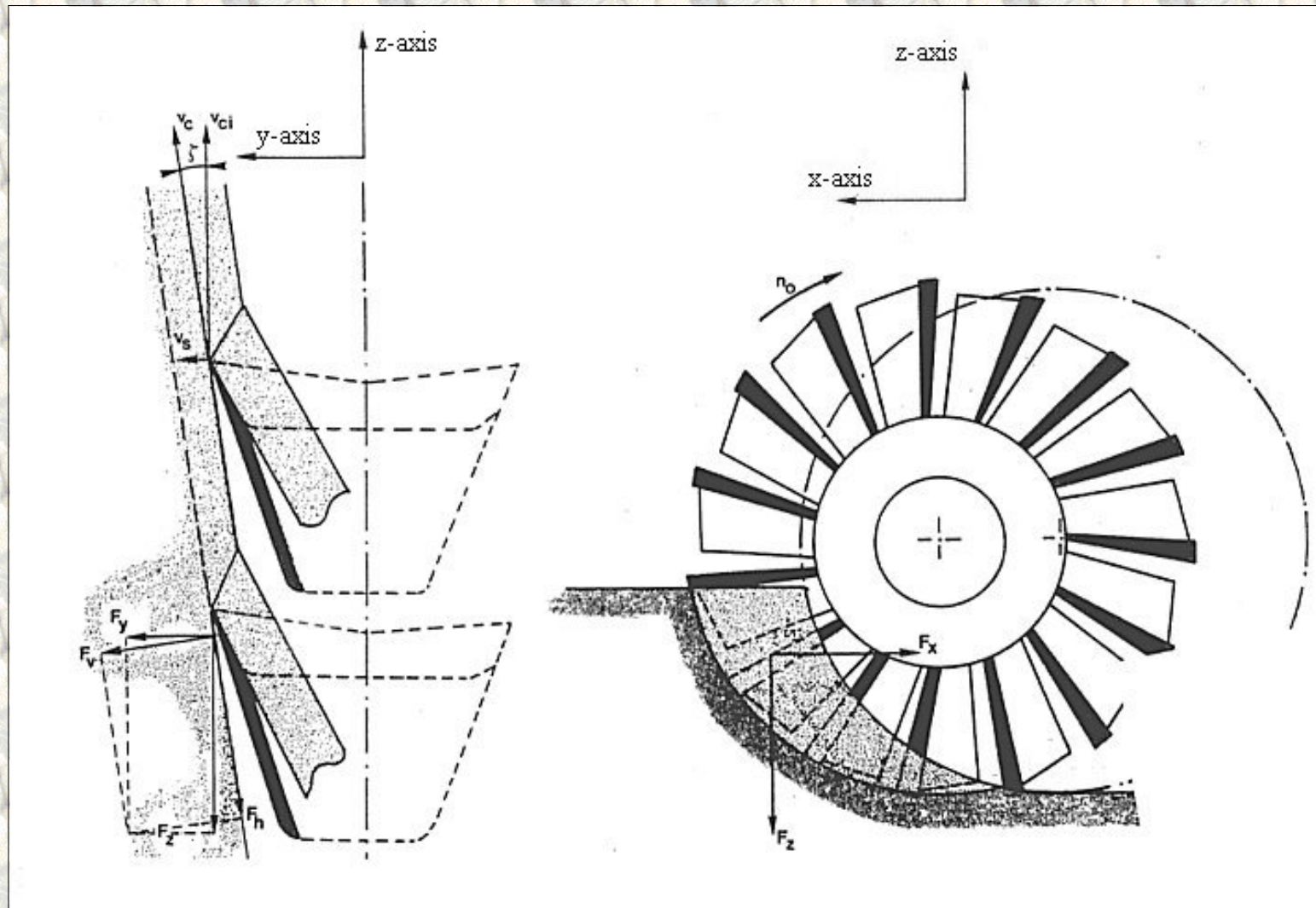


Figure 5.7: The direction of the forces F_h and F_v .

The angle between the velocity direction and the plane perpendicular to the axis of the dredging wheel is:

$$\xi = \frac{v_{ci}}{\sqrt{(v_{ci}^2 + v_s^2)}} \quad (5.43)$$

The difference between the static blade angle and the dynamic blade angle is also equal to ξ . If the peripheral velocity is much larger than the haul velocity than this angle is negligible. A complication arises however, because the force component perpendicular to the velocity direction (F_v) is also smaller than the force component in the haul direction (F_h). Figure 5.7 shows that F_v wants to drive the dredging wheel in the haul direction while F_h wants to slow it down. Dependent

on the ratio between F_v and F_h and of the angle ζ , the resulting forces can be either driving or slowing down in the haul direction. It will also be obvious that the wear of the blade edge will be very decisive for the direction of the force in the haul direction. The angle ζ can therefore not be neglected in the determination of the force in the haul direction. The angle ζ is not dependent on the run-through angle Ω , but it is on the radius of a point on the cutting edge. Including the angle ζ in the equations (5.12) to (5.15) and (5.21) to (5.24) makes the solution of the integrals so complicated, that it is better to use the numerical model. It is however possible to find a normative radius with which the angle ζ can be accounted for.

For the non-cavitating cutting process this is:

$$r_{\text{cor}} = \frac{m_{gc}}{f_{yca}} \cdot R \quad (5.44)$$

For the cavitating cutting process this is:

$$r_{\text{cor}} = \frac{m_{ca}}{f_{yca}} \cdot R \quad (5.45)$$

The correction for the angle ζ can now take place with the corrected values for c_1 and d_1 respectively c_2 and d_2 , according:

$$c_1' = c_2 \cdot \frac{V_s}{\sqrt{(V_{ci}^2 + V_s^2)}} + c_1 \cdot \frac{V_{ci}}{\sqrt{(V_{ci}^2 + V_s^2)}} \quad (5.46)$$

and

$$c_2' = c_2 \cdot \frac{V_s}{\sqrt{(V_{ci}^2 + V_s^2)}} - c_1 \cdot \frac{V_{ci}}{\sqrt{(V_{ci}^2 + V_s^2)}} \quad (5.47)$$

For the non-cavitating cutting process.

Substitution of d_1 for c_1 and d_2 for c_2 gives similar equations for the cavitating cutting process. The peripheral velocity in these equations has to be determined with a radius according equation (5.44) for the non-cavitating cutting process and equation (5.45) for the cavitating cutting process.

[Back to top](#)

Chair of Dredging Technology
Mekelweg 2
2628 CD, Delft
The Netherlands

It is advised to also read the papers following this dissertation, since the theory developed has been refined and extended.

Last modified Sunday May 28, 2000 by: [Sape A. Miedema](#)

Translation by: [Laurens de Jonge](#)

Figures, equations and tables by: [Erik Miedema](#)

Copyright © May, 2000 Dr.ir. S.A. Miedema



[Download Adobe Acrobat Reader V4.0](#)

5.08 The alternative bank cut.

The determination of the resulting cutting forces, the driving torque and the specific energy, for a bank cut, can be done using the same equations derived for the standing cut, if the breach width and the step size comply with their definitions according figure 5.8. For the forces in the x- and z-direction the following conversions have to be done:

$$F_x = -F'_x \cdot \sin(\nu) - F'_z \cdot \cos(\nu) \quad (5.48)$$

and

$$F_z = -F'_x \cdot \cos(\nu) + F'_z \cdot \sin(\nu) \quad (5.49)$$

The accents indicate the forces in the ladder-related coordinate system. These are here the forces determined with equations (5.30) to (5.33) for the non-cavitating cutting process or the equations (5.34) to (5.37) for the cavitating cutting process. The force in the y-direction, the driving torque and the specific energy are in principle equal to the concerning values for the standing cut, with a similar cutting process.

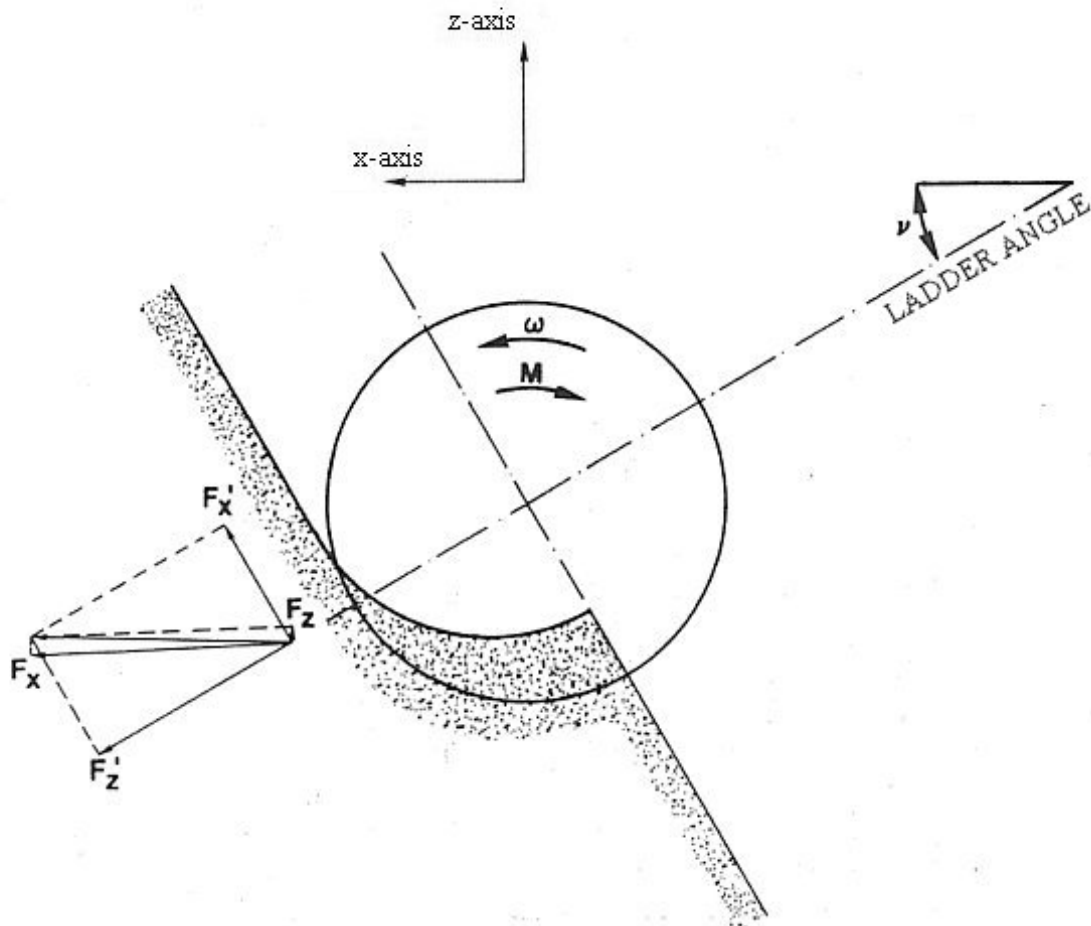


Figure 5.8: The forces occurring at the alternative bank cut.

[Back to top](#)

Mekelweg 2
2628 CD, Delft
The Netherlands

It is advised to also read the papers following this dissertation, since the theory developed has been refined and extended.

Last modified Sunday May 28, 2000 by: [Sape A. Miedema](#)

Translation by: [Laurens de Jonge](#)

Figures, equations and tables by: [Erik Miedema](#)

Copyright © May, 2000 Dr.ir. S.A. Miedema



[Download Adobe Acrobat Reader V4.0](#)

Table 5.01: Coefficients f_{xgc} , f_{ygc} , f_{zgc} and m_{gc} at $S=0.1 \cdot R$, $\Omega_2=-3^\circ$, non-cavitating.

[Contents](#)

B/R	Ω_0	Ω_1	f_{xgc}	f_{ygc}	f_{zgc}	m_{gc}
0.1	26°	20°	0.962	1.000	0.248	0.987
0.2	37°	32°	0.917	1.000	0.367	0.981
0.3	46°	41°	0.870	1.000	0.455	0.977
0.4	53°	49°	0.821	1.000	0.525	0.973
0.5	60°	57°	0.772	1.000	0.584	0.970
0.6	66°	64°	0.721	1.000	0.634	0.968
0.7	73°	71°	0.671	1.000	0.676	0.966
0.8	78°	77°	0.620	1.000	0.712	0.964
0.9	84°	84°	0.568	1.000	0.742	0.963
1.0	90°	90°	0.517	1.000	0.768	0.961
1.1	96°	96°	0.465	1.000	0.789	0.960
1.2	102°	103°	0.413	1.000	0.805	0.959
1.3	107°	109°	0.361	1.000	0.818	0.959

1.4	114 °	116 °	0.309	1.000	0.826	0.958
1.5	120 °	123 °	0.257	1.000	0.829	0.958
1.6	127 °	131 °	0.205	1.000	0.829	0.958
1.7	134 °	139 °	0.153	1.000	0.823	0.959
1.8	143 °	148 °	0.102	1.000	0.812	0.959
1.9	154 °	160 °	0.050	1.000	0.795	0.960
2.0	180 °	186 °	0.000	1.000	0.768	0.961

[Back to top](#)

This is a translation of the dissertation of Dr.ir. S.A. Miedema, dated September 15th 1987 .

The dissertation was originally published in Dutch by the:

Delft University of Technology

Faculty of Mechanical Engineering and Marine Technology

Chair of Dredging Technology

Mekelweg 2

2628 CD, Delft

The Netherlands

It is advised to also read the papers following this dissertation, since the theory developed has been refined and extended.

Last modified Sunday May 28, 2000 by: [Sape A. Miedema](#)

Translation by: [Laurens de Jonge](#)

Figures, equations and tables by: [Erik Miedema](#)

Copyright © May, 2000 Dr.ir. S.A. Miedema



[Download Adobe Acrobat Reader V4.0](#)

Table 5.02: Coefficients f_{xgc} , f_{ygc} , f_{zgc} and m_{gc} at $S=0.2 \cdot R$, $\Omega_2=-6^\circ$, non-cavitating.

[Contents](#)

B/R	Ω_0	Ω_1	f_{xgc}	f_{ygc}	f_{zgc}	m_{gc}
0.1	26°	15°	0.972	1.000	0.204	0.976
0.2	37°	27°	0.932	1.000	0.325	0.965
0.3	46°	36°	0.888	1.000	0.416	0.956
0.4	53°	45°	0.841	1.000	0.489	0.949
0.5	60°	53°	0.793	1.000	0.551	0.943
0.6	66°	61°	0.743	1.000	0.604	0.938
0.7	73°	68°	0.692	1.000	0.650	0.933
0.8	78°	76°	0.640	1.000	0.688	0.930
0.9	84°	83°	0.588	1.000	0.722	0.926
1.0	90°	90°	0.534	1.000	0.749	0.924
1.1	96°	97°	0.481	1.000	0.772	0.922
1.2	102°	104°	0.427	1.000	0.790	0.920
1.3	107°	112°	0.372	1.000	0.803	0.919

1.4	114 °	119 °	0.318	1.000	0.811	0.918
1.5	120 °	127 °	0.264	1.000	0.815	0.917
1.6	127 °	135 °	0.210	1.000	0.814	0.918
1.7	134 °	144 °	0.156	1.000	0.808	0.918
1.8	143 °	153 °	0.103	1.000	0.796	0.919
1.9	154 °	165 °	0.050	1.000	0.777	0.921
2.0	180 °	191 °	-0.001	1.000	0.748	0.924

[Back to top](#)

This is a translation of the dissertation of Dr.ir. S.A. Miedema, dated September 15th 1987 .

The dissertation was originally published in Dutch by the:

Delft University of Technology

Faculty of Mechanical Engineering and Marine Technology

Chair of Dredging Technology

Mekelweg 2

2628 CD, Delft

The Netherlands

It is advised to also read the papers following this dissertation, since the theory developed has been refined and extended.

Last modified Sunday May 28, 2000 by: [Sape A. Miedema](#)

Translation by: [Laurens de Jonge](#)

Figures, equations and tables by: [Erik Miedema](#)

Copyright © May, 2000 Dr.ir. S.A. Miedema



[Download Adobe Acrobat Reader V4.0](#)

Table 5.03: Coefficients f_{xgc} , f_{ygc} , f_{zgc} and m_{gc} at $S=0.3 \cdot R$, $\Omega_2=-9^\circ$, non-cavitating.

[Contents](#)

B/R	Ω_0	Ω_1	f_{xgc}	f_{ygc}	f_{zgc}	m_{gc}
0.1	26°	9°	0.979	1.000	0.160	0.969
0.2	37°	21°	0.945	1.000	0.281	0.951
0.3	46°	31°	0.904	1.000	0.374	0.937
0.4	53°	40°	0.860	1.000	0.451	0.926
0.5	60°	49°	0.814	1.000	0.516	0.917
0.6	66°	57°	0.765	1.000	0.572	0.909
0.7	73°	65°	0.714	1.000	0.621	0.902
0.8	78°	74°	0.661	1.000	0.663	0.897
0.9	84°	82°	0.607	1.000	0.699	0.892
1.0	90°	90°	0.552	1.000	0.729	0.887
1.1	96°	98°	0.496	1.000	0.753	0.884
1.2	102°	106°	0.440	1.000	0.772	0.881
1.3	107°	115°	0.383	1.000	0.786	0.879

1.4	114 °	123 °	0.327	1.000	0.795	0.878
1.5	120 °	131 °	0.270	1.000	0.799	0.878
1.6	127 °	140 °	0.214	1.000	0.797	0.878
1.7	134 °	149 °	0.158	1.000	0.790	0.879
1.8	143 °	159 °	0.103	1.000	0.777	0.880
1.9	154 °	171 °	0.050	1.000	0.757	0.883
2.0	180 °	197 °	-0.002	1.000	0.727	0.888

[Back to top](#)

This is a translation of the dissertation of Dr.ir. S.A. Miedema, dated September 15th 1987 .

The dissertation was originally published in Dutch by the:

Delft University of Technology

Faculty of Mechanical Engineering and Marine Technology

Chair of Dredging Technology

Mekelweg 2

2628 CD, Delft

The Netherlands

It is advised to also read the papers following this dissertation, since the theory developed has been refined and extended.

Last modified Sunday May 28, 2000 by: [Sape A. Miedema](#)

Translation by: [Laurens de Jonge](#)

Figures, equations and tables by: [Erik Miedema](#)

Copyright © May, 2000 Dr.ir. S.A. Miedema



[Download Adobe Acrobat Reader V4.0](#)

Table 5.04: Coefficients f_{xgc} , f_{ygc} , f_{zgc} and m_{gc} at $S=0.4 \cdot R$, $\Omega_2=-11^\circ$, non-cavitating.

[Contents](#)

B/R	Ω_0	Ω_1	f_{xgc}	f_{ygc}	f_{zgc}	m_{gc}
0.1	26°	9°	0.979	1.000	0.160	0.969
0.2	37°	21°	0.945	1.000	0.281	0.951
0.3	46°	31°	0.904	1.000	0.374	0.937
0.4	53°	40°	0.860	1.000	0.451	0.926
0.5	60°	49°	0.814	1.000	0.516	0.917
0.6	66°	57°	0.765	1.000	0.572	0.909
0.7	73°	65°	0.714	1.000	0.621	0.902
0.8	78°	74°	0.661	1.000	0.663	0.897
0.9	84°	82°	0.607	1.000	0.699	0.892
1.0	90°	90°	0.552	1.000	0.729	0.887
1.1	96°	98°	0.496	1.000	0.753	0.884
1.2	102°	106°	0.440	1.000	0.772	0.881
1.3	107°	115°	0.383	1.000	0.786	0.879

1.4	114 °	123 °	0.327	1.000	0.795	0.878
1.5	120 °	131 °	0.270	1.000	0.799	0.878
1.6	127 °	140 °	0.214	1.000	0.797	0.878
1.7	134 °	149 °	0.158	1.000	0.790	0.879
1.8	143 °	159 °	0.103	1.000	0.777	0.880
1.9	154 °	171 °	0.050	1.000	0.757	0.883
2.0	180 °	197 °	-0.002	1.000	0.727	0.888

[Back to top](#)

This is a translation of the dissertation of Dr.ir. S.A. Miedema, dated September 15th 1987 .

The dissertation was originally published in Dutch by the:

Delft University of Technology

Faculty of Mechanical Engineering and Marine Technology

Chair of Dredging Technology

Mekelweg 2

2628 CD, Delft

The Netherlands

It is advised to also read the papers following this dissertation, since the theory developed has been refined and extended.

Last modified Sunday May 28, 2000 by: [Sape A. Miedema](#)

Translation by: [Laurens de Jonge](#)

Figures, equations and tables by: [Erik Miedema](#)

Copyright © May, 2000 Dr.ir. S.A. Miedema



[Download Adobe Acrobat Reader V4.0](#)

Table 5.05: Coefficients f_{xgc} , f_{ygc} , f_{zgc} and m_{gc} at $S=0.5 \cdot R$, $\Omega_2=-14^\circ$, non-cavitating.

[Contents](#)

B/R	Ω_0	Ω_1	f_{xgc}	f_{ygc}	f_{zgc}	m_{gc}
0.1	26°	9°	0.979	1.000	0.160	0.969
0.2	37°	21°	0.945	1.000	0.281	0.951
0.3	46°	31°	0.904	1.000	0.374	0.937
0.4	53°	40°	0.860	1.000	0.451	0.926
0.5	60°	49°	0.814	1.000	0.516	0.917
0.6	66°	57°	0.765	1.000	0.572	0.909
0.7	73°	65°	0.714	1.000	0.621	0.902
0.8	78°	74°	0.661	1.000	0.663	0.897
0.9	84°	82°	0.607	1.000	0.699	0.892
1.0	90°	90°	0.552	1.000	0.729	0.887
1.1	96°	98°	0.496	1.000	0.753	0.884
1.2	102°	106°	0.440	1.000	0.772	0.881
1.3	107°	115°	0.383	1.000	0.786	0.879

1.4	114 °	123 °	0.327	1.000	0.795	0.878
1.5	120 °	131 °	0.270	1.000	0.799	0.878
1.6	127 °	140 °	0.214	1.000	0.797	0.878
1.7	134 °	149 °	0.158	1.000	0.790	0.879
1.8	143 °	159 °	0.103	1.000	0.777	0.880
1.9	154 °	171 °	0.050	1.000	0.757	0.883
2.0	180 °	197 °	-0.002	1.000	0.727	0.888

[Back to top](#)

This is a translation of the dissertation of Dr.ir. S.A. Miedema, dated September 15th 1987 .

The dissertation was originally published in Dutch by the:

Delft University of Technology

Faculty of Mechanical Engineering and Marine Technology

Chair of Dredging Technology

Mekelweg 2

2628 CD, Delft

The Netherlands

It is advised to also read the papers following this dissertation, since the theory developed has been refined and extended.

Last modified Sunday May 28, 2000 by: [Sape A. Miedema](#)

Translation by: [Laurens de Jonge](#)

Figures, equations and tables by: [Erik Miedema](#)

Copyright © May, 2000 Dr.ir. S.A. Miedema



[Download Adobe Acrobat Reader V4.0](#)

Table 5.06: Coefficients f_{xca} , f_{yca} , f_{zca} and m_{ca} at $S=0.1 \cdot R$, $\Omega_2=-3^\circ$, cavitating.

[Contents](#)

B/R	Ω_0	Ω_1	f_{xca}	f_{yca}	f_{zca}	m_{ca}
0.1	26°	20°	0.975	1.013	0.252	1.000
0.2	37°	32°	0.935	1.020	0.375	1.000
0.3	46°	41°	0.890	1.024	0.467	1.000
0.4	53°	49°	0.843	1.028	0.542	1.000
0.5	60°	57°	0.794	1.031	0.604	1.000
0.6	66°	64°	0.744	1.034	0.657	1.000
0.7	73°	71°	0.693	1.036	0.703	1.000
0.8	78°	77°	0.641	1.038	0.742	1.000
0.9	84°	84°	0.588	1.040	0.775	1.000
1.0	90°	90°	0.535	1.041	0.802	1.000
1.1	96°	96°	0.481	1.042	0.825	1.000
1.2	102°	103°	0.427	1.043	0.843	1.000
1.3	107°	109°	0.373	1.044	0.856	1.000

1.4	114 °	116 °	0.319	1.044	0.865	1.000
1.5	120 °	123 °	0.265	1.044	0.868	1.000
1.6	127 °	131 °	0.211	1.044	0.868	1.000
1.7	134 °	139 °	0.157	1.043	0.861	1.000
1.8	143 °	148 °	0.104	1.044	0.850	1.000
1.9	154 °	160 °	0.051	1.042	0.831	1.000
2.0	180 °	186 °	-0.000	1.041	0.802	1.000

[Back to top](#)

This is a translation of the dissertation of Dr.ir. S.A. Miedema, dated September 15th 1987 .

The dissertation was originally published in Dutch by the:

Delft University of Technology

Faculty of Mechanical Engineering and Marine Technology

Chair of Dredging Technology

Mekelweg 2

2628 CD, Delft

The Netherlands

It is advised to also read the papers following this dissertation, since the theory developed has been refined and extended.

Last modified Sunday May 28, 2000 by: [Sape A. Miedema](#)

Translation by: [Laurens de Jonge](#)

Figures, equations and tables by: [Erik Miedema](#)

Copyright © May, 2000 Dr.ir. S.A. Miedema



[Download Adobe Acrobat Reader V4.0](#)

Table 5.07: Coefficients f_{xca} , f_{yca} , f_{zca} and m_{ca} at $S=0.2 \cdot R$, $\Omega_2=-6^\circ$, cavitating.

[Contents](#)

B/R	Ω_0	Ω_1	f_{xca}	f_{yca}	f_{zca}	m_{ca}
0.1	26°	15°	0.996	1.024	0.209	1.000
0.2	37°	27°	0.967	1.037	0.338	1.000
0.3	46°	36°	0.929	1.048	0.437	1.000
0.4	53°	45°	0.887	1.056	0.520	1.000
0.5	60°	53°	0.841	1.063	0.590	1.000
0.6	66°	61°	0.791	1.069	0.651	1.000
0.7	73°	68°	0.739	1.074	0.703	1.000
0.8	78°	76°	0.686	1.079	0.749	1.000
0.9	84°	83°	0.630	1.083	0.788	1.000
1.0	90°	90°	0.573	1.086	0.820	1.000
1.1	96°	97°	0.515	1.089	0.847	1.000
1.2	102°	104°	0.457	1.091	0.868	1.000
1.3	107°	112°	0.398	1.092	0.883	1.000

1.4	114 °	119 °	0.339	1.093	0.893	1.000
1.5	120 °	127 °	0.280	1.094	0.897	1.000
1.6	127 °	135 °	0.221	1.094	0.895	1.000
1.7	134 °	144 °	0.163	1.093	0.887	1.000
1.8	143 °	153 °	0.107	1.091	0.873	1.000
1.9	154 °	165 °	0.052	1.089	0.852	1.000
2.0	180 °	191 °	-0.001	1.086	0.819	1.000

[Back to top](#)

This is a translation of the dissertation of Dr.ir. S.A. Miedema, dated September 15th 1987 .

The dissertation was originally published in Dutch by the:

Delft University of Technology

Faculty of Mechanical Engineering and Marine Technology

Chair of Dredging Technology

Mekelweg 2

2628 CD, Delft

The Netherlands

It is advised to also read the papers following this dissertation, since the theory developed has been refined and extended.

Last modified Sunday May 28, 2000 by: [Sape A. Miedema](#)

Translation by: [Laurens de Jonge](#)

Figures, equations and tables by: [Erik Miedema](#)

Copyright © May, 2000 Dr.ir. S.A. Miedema



[Download Adobe Acrobat Reader V4.0](#)

Table 5.08: Coefficients f_{xca} , f_{yca} , f_{zca} and m_{ca} at $S=0.3 \cdot R$, $\Omega_2=-9^\circ$, cavitating.

[Contents](#)

B/R	Ω_0	Ω_1	f_{xca}	f_{yca}	f_{zca}	m_{ca}
0.1	26°	9°	1.011	1.033	0.166	1.000
0.2	37°	21°	0.995	1.053	0.298	1.000
0.3	46°	31°	0.967	1.069	0.403	1.000
0.4	53°	40°	0.931	1.083	0.493	1.000
0.5	60°	49°	0.889	1.095	0.571	1.000
0.6	66°	57°	0.841	1.106	0.640	1.000
0.7	73°	65°	0.790	1.115	0.701	1.000
0.8	78°	74°	0.735	1.123	0.754	1.000
0.9	84°	82°	0.677	1.130	0.800	1.000
1.0	90°	90°	0.616	1.136	0.839	1.000
1.1	96°	98°	0.553	1.141	0.870	1.000
1.2	102°	106°	0.489	1.144	0.895	1.000
1.3	107°	115°	0.424	1.147	0.913	1.000

1.4	114 °	123 °	0.359	1.149	0.923	1.000
1.5	120 °	131 °	0.295	1.149	0.927	1.000
1.6	127 °	140 °	0.231	1.149	0.925	1.000
1.7	134 °	149 °	0.169	1.147	0.915	1.000
1.8	143 °	159 °	0.109	1.145	0.898	1.000
1.9	154 °	171 °	0.051	1.141	0.873	1.000
2.0	180 °	197 °	-0.002	1.136	0.837	1.000

[Back to top](#)

This is a translation of the dissertation of Dr.ir. S.A. Miedema, dated September 15th 1987 .

The dissertation was originally published in Dutch by the:

Delft University of Technology

Faculty of Mechanical Engineering and Marine Technology

Chair of Dredging Technology

Mekelweg 2

2628 CD, Delft

The Netherlands

It is advised to also read the papers following this dissertation, since the theory developed has been refined and extended.

Last modified Sunday May 28, 2000 by: [Sape A. Miedema](#)

Translation by: [Laurens de Jonge](#)

Figures, equations and tables by: [Erik Miedema](#)

Copyright © May, 2000 Dr.ir. S.A. Miedema



[Download Adobe Acrobat Reader V4.0](#)

Table 5.09: Coefficients f_{xca} , f_{yca} , f_{zca} and m_{ca} at $S=0.4 \cdot R$, $\Omega_2=-11^\circ$, cavitating.

[Contents](#)

B/R	Ω_0	Ω_1	f_{xca}	f_{yca}	f_{zca}	m_{ca}
0.1	26°	2°	0.021	1.039	0.123	1.000
0.2	37°	14°	0.018	1.066	0.254	1.000
0.3	46°	24°	1.001	1.089	0.363	1.000
0.4	53°	34°	0.973	1.109	0.460	1.000
0.5	60°	43°	0.938	1.127	0.546	1.000
0.6	66°	52°	0.895	1.144	0.624	1.000
0.7	73°	62°	0.845	1.158	0.695	1.000
0.8	78°	71°	0.790	1.171	0.757	1.000
0.9	84°	80°	0.729	1.182	0.812	1.000
1.0	90°	90°	0.664	1.192	0.858	1.000
1.1	96°	100°	0.596	1.199	0.896	1.000
1.2	102°	109°	0.525	1.205	0.925	1.000
1.3	107°	118°	0.453	1.210	0.946	1.000

1.4	114 °	128 °	0.381	1.212	0.958	1.000
1.5	120 °	137 °	0.310	1.213	0.961	1.000
1.6	127 °	146 °	0.240	1.212	0.957	1.000
1.7	134 °	156 °	0.173	1.209	0.944	1.000
1.8	143 °	166 °	0.110	1.205	0.923	1.000
1.9	154 °	178 °	0.050	1.199	0.894	1.000
2.0	180 °	202 °	-0.003	1.191	0.855	1.000

[Back to top](#)

This is a translation of the dissertation of Dr.ir. S.A. Miedema, dated September 15th 1987 .

The dissertation was originally published in Dutch by the:

Delft University of Technology

Faculty of Mechanical Engineering and Marine Technology

Chair of Dredging Technology

Mekelweg 2

2628 CD, Delft

The Netherlands

It is advised to also read the papers following this dissertation, since the theory developed has been refined and extended.

Last modified Sunday May 28, 2000 by: [Sape A. Miedema](#)

Translation by: [Laurens de Jonge](#)

Figures, equations and tables by: [Erik Miedema](#)

Copyright © May, 2000 Dr.ir. S.A. Miedema



[Download Adobe Acrobat Reader V4.0](#)

Table 5.10: Coefficients f_{xca} , f_{yca} , f_{zca} and m_{ca} at $S=0.5 \cdot R$, $\Omega_2=-14^\circ$, cavitating.

[Contents](#)

B/R	Ω_0	Ω_1	f_{xca}	f_{yca}	f_{zca}	m_{ca}
0.1	26°	-4°	1.026	1.042	0.083	1.000
0.2	37°	7°	1.036	1.077	0.209	1.000
0.3	46°	17°	1.031	1.107	0.320	1.000
0.4	53°	27°	1.014	1.134	0.421	1.000
0.5	60°	36°	0.987	1.159	0.514	1.000
0.6	66°	46°	0.951	1.183	0.602	1.000
0.7	73°	57°	0.905	1.204	0.683	1.000
0.8	78°	67°	0.851	1.224	0.757	1.000
0.9	84°	79°	0.788	1.241	0.823	1.000
1.0	90°	90°	0.719	1.255	0.879	1.000
1.1	96°	101°	0.644	1.267	0.925	1.000
1.2	102°	113°	0.565	1.276	0.960	1.000
1.3	107°	123°	0.484	1.283	0.984	1.000

1.4	$\frac{114}{\circ}$	$\frac{134}{\circ}$	0.403	1.286	0.996	1.000
1.5	$\frac{120}{\circ}$	$\frac{144}{\circ}$	0.324	1.287	0.999	1.000
1.6	$\frac{127}{\circ}$	$\frac{153}{\circ}$	0.248	1.285	0.991	1.000
1.7	$\frac{134}{\circ}$	$\frac{163}{\circ}$	0.176	1.281	0.975	1.000
1.8	$\frac{143}{\circ}$	$\frac{173}{\circ}$	0.109	1.274	0.950	1.000
1.9	$\frac{154}{\circ}$	$\frac{184}{\circ}$	0.049	1.265	0.917	1.000
2.0	$\frac{180}{\circ}$	$\frac{207}{\circ}$	-0.005	1.254	0.873	1.000

[Back to top](#)

This is a translation of the dissertation of Dr.ir. S.A. Miedema, dated September 15th 1987 .

The dissertation was originally published in Dutch by the:

Delft University of Technology

Faculty of Mechanical Engineering and Marine Technology

Chair of Dredging Technology

Mekelweg 2

2628 CD, Delft

The Netherlands

It is advised to also read the papers following this dissertation, since the theory developed has been refined and extended.

Last modified Sunday May 28, 2000 by: [Sape A. Miedema](#)

Translation by: [Laurens de Jonge](#)

Figures, equations and tables by: [Erik Miedema](#)

Copyright © May, 2000 Dr.ir. S.A. Miedema



[Download Adobe Acrobat Reader V4.0](#)

6.01 Scale rules.

If one wishes to perform cutting tests on scale models in order to obtain a good impression of the size and the direction of the, on the prototype, acting cutting forces, than it is desirable that the cutting process on the scale model develops similar to that on the prototype scale. Therefore it is also important that the prototype and the scale model have similar shapes and that the same sand type is used in the model tests as would be dredged in practice. This last condition is due to unpredictable effects that can arise when using different types of sand. The cutting process is determined by two quantities: the shape of the cut layer and the possible occurrence of cavitation. Effects of inertia, gravity, cohesion and adhesion are left out of consideration here.

The shape of the layer is determined by step size, breach height and the ratio between the number of revolutions of the cutterhead or cutter-wheel to the haul velocity. This ratio also determines the effective clearance angle (in relation to the changing clearance angle as function of the ratio between the peripheral velocity v_{ci} and the haul velocity v_s). It will be clear that the effective clearance angle for a cutterhead varies in time with the run-through angle Ω of the involved blade, since the peripheral velocity direction varies while the direction of the haul velocity is constant (figure 4.6). For a cutter-wheel the effective clearance angle and the layer-thickness vary with the distance of a blade element to the axis (figures 5.2 and 5.3).

A same ratio between the peripheral velocity and the haul velocity in prototype and model lead to a same shape of the layer and a same development of the effective clearance angle (the last also being important in relation with the wear). With this the following scale rule can be derived:

$$\frac{v_{ci}}{v_s} \therefore \frac{r}{h_i} = \text{constant} \quad (6.1)$$

This gives:

$$\frac{r_p}{r_m} = \frac{h_{ip}}{h_{im}} = \lambda_1 \quad (6.2)$$

Equation (6.1) follows from the equations (4.1), (4.3), (5.1) and (5.2). With this the length scale is set.

The breach height B and the step size S also have to be scaled with λ_1 to obtain a similar layer.

The second condition for a similar cutting process is that if the sub-pressure in the prototype becomes so low that cavitation occurs, it also has to occur when scaled back to the model. Cavitation occurs when:

$$\Delta p > (\rho_w \cdot g \cdot z + p_{\text{atm}} - p_{\text{damp}}) \quad (6.3)$$

Where Δp = sub-pressure in the sand packet.

Since the saturated vapor pressure is negligible in comparison with the atmospheric pressure, it will no longer be mentioned in the next equations. If, however, there is air present, dissolved or not in the pore water then this will have to be accounted for. For that case the term $p_{\text{atm}} - p_{\text{damp}}$ can no longer be equalized to p_{atm} but will become for instance $0.9 \cdot p_{\text{atm}}$. Cavitation starts when in equation (6.3) the "larger than" sign is replaced by the "equal sign". This means for the model and the prototype, when equalizing the atmospheric pressure to 10-meter water column:

$$\Delta p_p = (\rho_w \cdot g \cdot z_p + \rho_w \cdot g \cdot 10) \quad (6.4)$$

and

$$\Delta p_m = (\rho_w \cdot g \cdot z_m + \rho_w \cdot g \cdot 10) \quad (6.5)$$

Thus:

$$\frac{\Delta p_p}{\Delta p_m} = \frac{(z_p + 10)}{(z_m + 10)} = \lambda_c \quad (6.6)$$

This is the cavitation scale factor or the hydrostatic pressure factor. The cavitation scale factor is not equalized to the length scale factor for principle reasons, because there is a pressure ratio involved. That the pressure ratio is also dependent on the water depth ratio is of secondary interest. A large length scale factor will additionally lead to negative waterdepths in the model, so that an sub-pressure tank is needed. Knowing that the water sub-pressures in the non-cavitating area are proportional to the product of the cutting velocity and the layer-thickness and if it is assumed that the pore pressure ratio is equal to the cavitation scale factor than equation (6.6) leads to:

$$\frac{V_{cp} \cdot h_{ip}}{V_{cm} \cdot h_{im}} = \lambda_c \quad (6.7)$$

This gives:

$$\frac{V_{cp}}{V_{cm}} = \frac{\lambda_c}{\lambda_l} \quad (6.8)$$

The cutting velocity is approximately equal to the peripheral velocity, so:

$$V_c \approx V_{ci} \approx n_o \cdot r \quad (6.9)$$

The scale rule for the number of revolutions now becomes:

$$\frac{n_{op} \cdot r_p}{n_{om} \cdot r_m} = \frac{V_{cp}}{V_{cm}} = \frac{\lambda_c}{\lambda_l} \quad (6.10)$$

thus:

$$\frac{n_{op}}{n_{om}} = \frac{\lambda_c}{\lambda_l^2} \quad (6.11)$$

Of a similar process can be spoken for the cutterhead, if the run-through angle Ω_1 , where the cutting process changes from the non-cavitating to the cavitating process, is equal in model and prototype. This implies that equation (4.33) has to give similar answers for prototype and model:

$$\frac{\Omega_{1p}}{\Omega_{1m}} = \frac{(z_p + 10)}{(z_m + 10)} \cdot \frac{v_{sm}}{v_{sp}} \cdot \frac{r_m}{r_p} = 1 \quad (6.12)$$

thus:

$$\frac{v_{sp}}{v_{sm}} = \frac{\lambda_c}{\lambda_1} \quad (\text{cutterhead}) \quad (6.13)$$

The cutting process for the dredging-wheel is similar, if the radius $r_{gc} \gg ca$, where the cutting process changes from the non-cavitating to the cavitating cutting process, is proportional to the length scale factor for the prototype and model. Equation (5.42) then gives:

$$\frac{r_{gc \rightarrow cap}}{r_{gc \rightarrow cam}} = \frac{(z_p + 10)}{(z_m + 10)} \cdot \frac{v_{sm}}{v_{sp}} = \lambda_1 \quad (6.14)$$

Thus:

$$\frac{v_{sp}}{v_{sm}} = \frac{\lambda_c}{\lambda_1} \quad (\text{dredging wheel}) \quad (6.15)$$

So the scale rules for the number of revolutions and the haul velocity are identical for the cutterhead and the dredging-wheel. From the condition of equal layer follows the scale rule for the haul velocity:

$$\frac{v_{sp}}{v_{sm}} = \frac{h_{ip} \cdot n_{op}}{h_{im} \cdot n_{om}} = \frac{\lambda_c}{\lambda_1} \quad (6.16)$$

Now the scale rules for the cutting forces and the drive torque can be derived with the aid of the found scale rules for layer-thickness, haul velocity and number of revolutions.

For the cutting forces counts:

$$\frac{F_p}{F_m} = \frac{v_{cp} \cdot h_{ip}^2 \cdot b_p}{v_{cm} \cdot h_{im}^2 \cdot b_m} = \lambda_c \cdot \lambda_1^2 \quad (6.17)$$

In the non-cavitating case, and:

$$\frac{F_p}{F_m} = \frac{h_{ip} \cdot b_p \cdot (z_p + 10)}{h_{im} \cdot b_m \cdot (z_m + 10)} = \lambda_c \cdot \lambda_1^2 \quad (6.18)$$

In the cavitating case.

It makes therefore no difference if the cutting is cavitating or non-cavitating. This is an advantage as there is often just partial cavitation in the layer. Two different scale rules would lead to complications when the cutting forces are scaled back to the prototype. As the torque is proportional to the product of the force and the radius of the excavation element, the following scale rule applies for the torque:

$$\frac{M_p}{M_m} = \frac{F_p \cdot r_p}{F_m \cdot r_m} = \lambda_c \cdot \lambda_1^3 \quad (6.19)$$

For the drive power applies:

$$\frac{P_p}{P_m} = \frac{M_p \cdot n_{op}}{M_m \cdot n_{om}} = \lambda_c^2 \cdot \lambda_1 \quad (6.20)$$

Summarized the following scale rules are found:

$$n_{om} = \frac{\lambda_1^2}{\lambda_c} \cdot n_{op} \quad (6.21)$$

$$V_{sm} = \frac{\lambda_1}{\lambda_c} \cdot V_{sp} \quad (6.22)$$

$$F_p = \lambda_c \cdot \lambda_1^2 \cdot F_m \quad (6.23)$$

$$M_p = \lambda_c \cdot \lambda_1^3 \cdot M_m \quad (6.24)$$

$$P_p = \lambda_c^2 \cdot \lambda_1 \cdot P_m \quad (6.25)$$

Of course the scale rules are only valid when they are used correctly. A wrong choice for the haul velocity or the number of revolutions in the scale model lead to a comparison of a non-cavitating cutting process in the model with a partly cavitating cutting process in the prototype. In those cases scaling-up of the forces, the torque or the power may give much too high values.

The fact that the scale rules are independent of the type of excavating element (cutterhead or cutter-wheel) and of the type of cutting process (non-cavitating or cavitating) makes it possible to apply a combination of the analytical models for the cutterhead and the cutter-wheel in chapter 10 for the model shaping of

the three-dimensional moving cutterhead.

[Back to top](#)

This is a translation of the dissertation of Dr.ir. S.A. Miedema, dated September 15th 1987 .

The dissertation was originally published in Dutch by the:

Delft University of Technology

Faculty of Mechanical Engineering and Marine Technology

Chair of Dredging Technology

Mekelweg 2

2628 CD, Delft

The Netherlands

It is advised to also read the papers following this dissertation, since the theory developed has been refined and extended.

Last modified Sunday May 28, 2000 by: [Sape A. Miedema](#)

Translation by: [Laurens de Jonge](#)

Figures, equations and tables by: [Erik Miedema](#)

Copyright © May, 2000 Dr.ir. S.A. Miedema



[Download Adobe Acrobat Reader V4.0](#)

7.01 Introduction.

In the basic cutting theory there are a number of force components from which the cutting forces are composed. In the verification of this theory from chapter 2 a force component caused by the dilatancy is assumed. The force components caused by the water resistance, inertia forces etc. appeared to be negligible for the straight blades within the used velocity range. Dependent on the magnitude of the cutting velocities, which occur in a cutterhead or a dredging wheel, these forces can not be neglected. The model tests on the cutterhead are performed at low numbers of revolution and thus at low cutting velocities so that these forces can be neglected here. The data regarding the model tests on the cutterhead are derived from Miedema [46].

In the model tests with the dredging wheel there was also, besides the energy for the cutting, a non-negligible amount of energy needed to overcome the mechanical and hydraulical resistance, because in these tests higher numbers of revolution and thus cutting velocities are used. For a verification of the drive torque these mechanical and hydraulical losses have to be known.

In 1982 research is done on the efficiency of a dredging wheel by "MOD DREDGING", a cooperation between Philipp Holzman, Zanen Verstoep and Polensky & Zollner. This research is performed in the laboratory "De Techniek van het Grondverzet". The aim of this research was to improve the efficiency of the dredging wheel. Besides that the driving torque of the dredging wheel is measured during every measurement. The mechanical and hydraulical losses part of the total driving torque was also studied for several breach shapes. The results of this research are provided by "MOD DREDGING" for verification of the in chapter 5 developed theory. The data used in this chapter is derived from Derks [81].

Both the tests with the cutterhead as the tests with the dredging wheel are performed for the development of the scale rules in chapter 6. The measured and calculated loads can therefore not be scaled back to the prototype dimensions without difficulty. These tests are however suitable for a verification of the developed calculation models, as if the theory is valid, this has to lead to predictable loads for every combination of number of revolutions and haul velocities

**This is a translation of the dissertation of Dr.ir. S.A. Miedema, dated September 15th 1987 .
The dissertation was originally published in Dutch by the:
Delft University of Technology
Faculty of Mechanical Engineering and Marine Technology
Chair of Dredging Technology
Mekelweg 2
2628 CD, Delft
The Netherlands**

It is advised to also read the papers following this dissertation, since the theory developed has been refined and extended.

Last modified Monday May 29, 2000 by: [Sape A. Miedema](#)

Translation by: [Laurens de Jonge](#)

Figures, equations and tables by: [Erik Miedema](#)

Copyright © May, 2000 Dr.ir. S.A. Miedema



[Download Adobe Acrobat Reader V4.0](#)

7.02 Test stand cutterhead experiments.

The research is performed in the old laboratory GV in 1982, with a disc bottom cutterhead (figure 7.1).

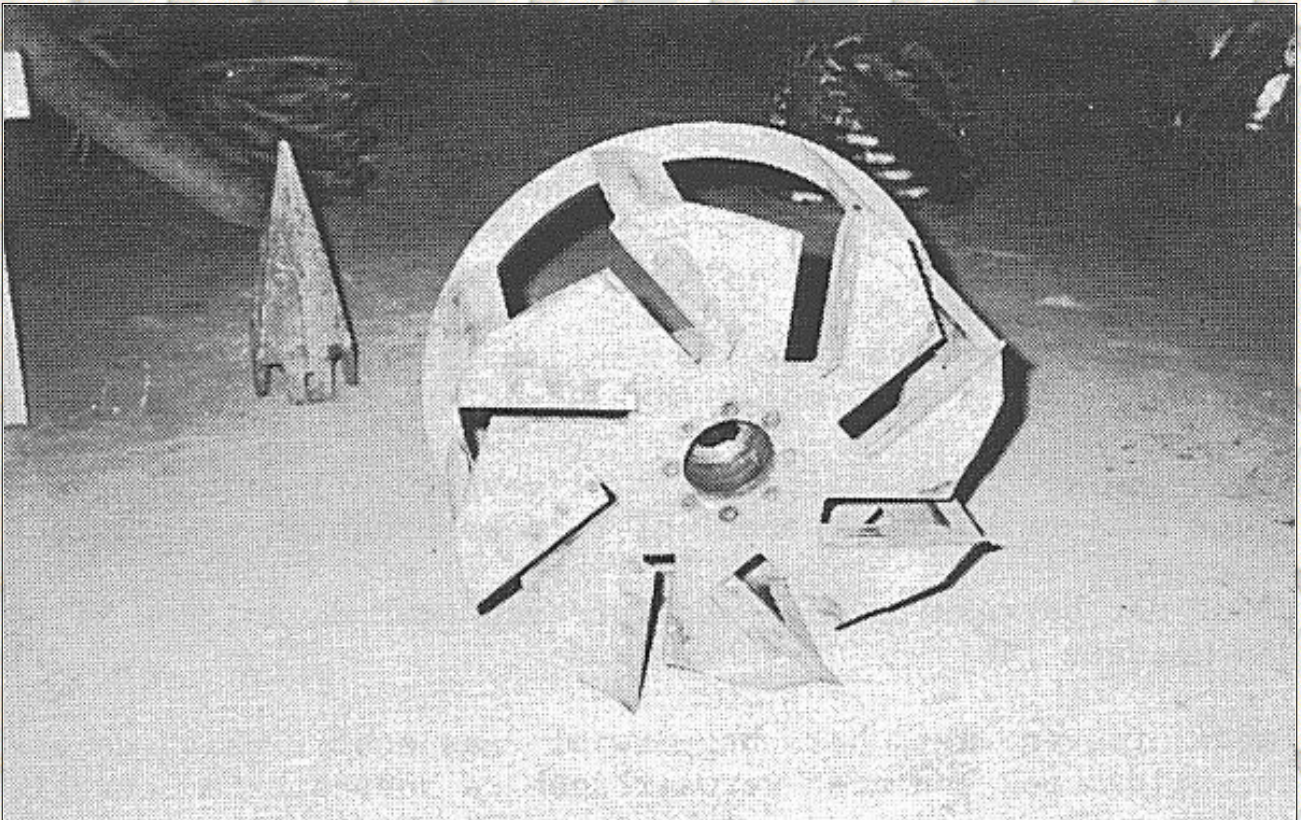
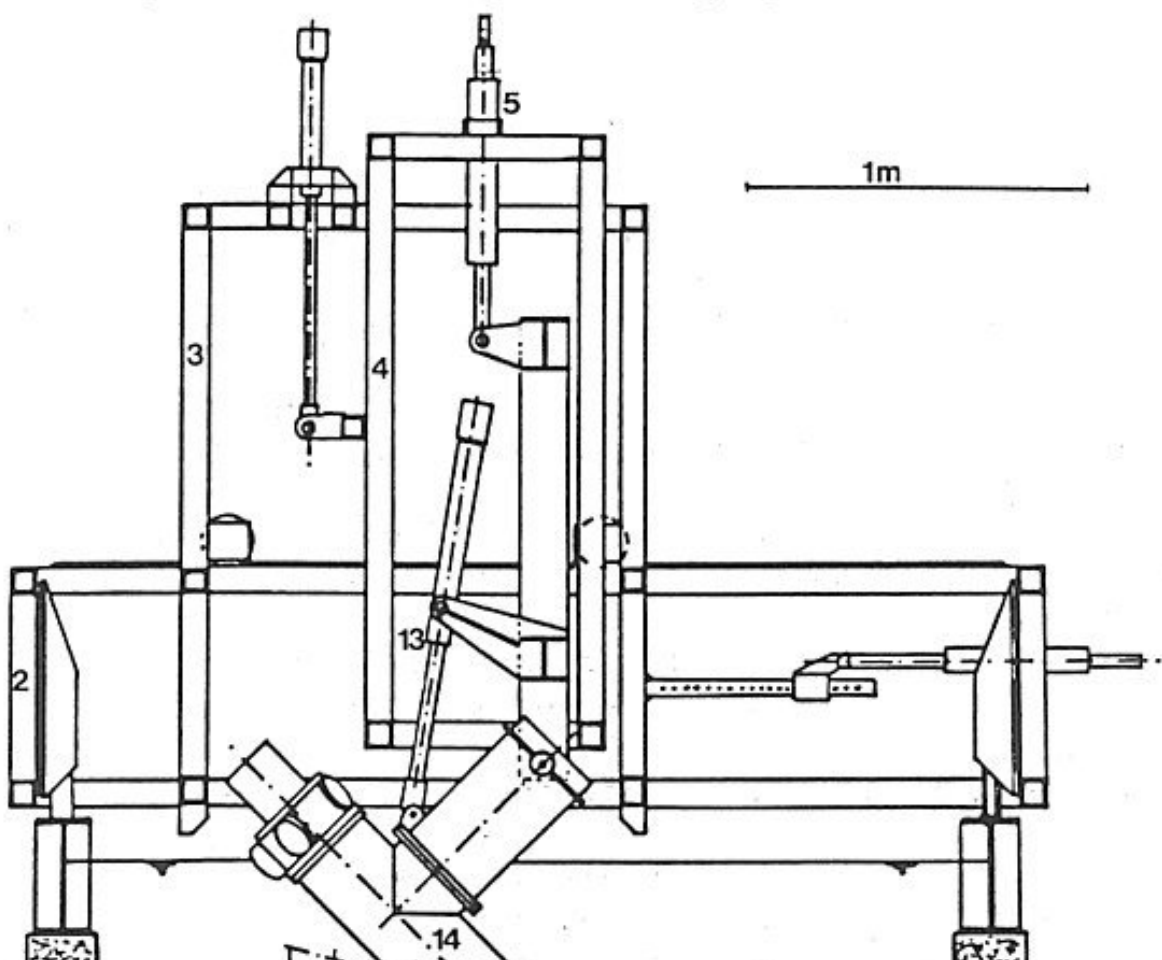


Figure 7.1: The experimental disc bottom cutterhead.



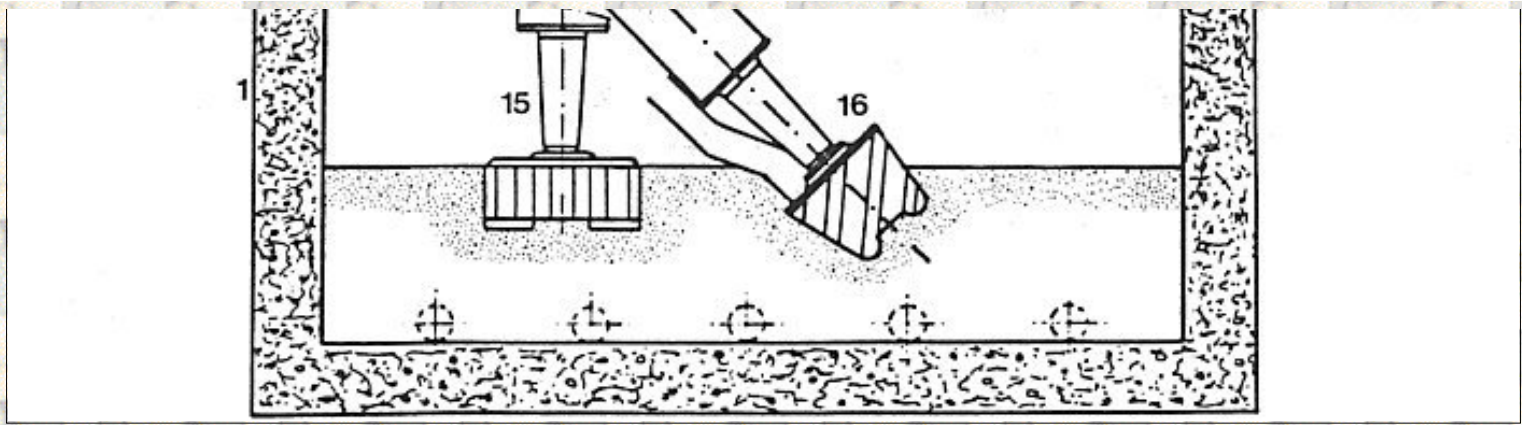


Figure 7.2: The test stand with:

1. The concrete tank.
2. The main carriage.
3. The auxiliary carriage.
4. The auxiliary frame.
5. Hydraulic cilinder for vertival positioning.
13. Hydraulic cilinder for positioning of the ladder angle.
14. Ladder.
15. Disc bottom cutterhead.
16. Helix cutterhead.

The soil mechanical parameters of the used sand can be found in appendix B3. The used disc bottom cutterhead has a rectangular cross-section with a diameter of 475 mm and a blade width of 165 mm. Eight blades are mounted in the cutterhead along the circumference. The position and the dimensions can be found in figure 7.3.

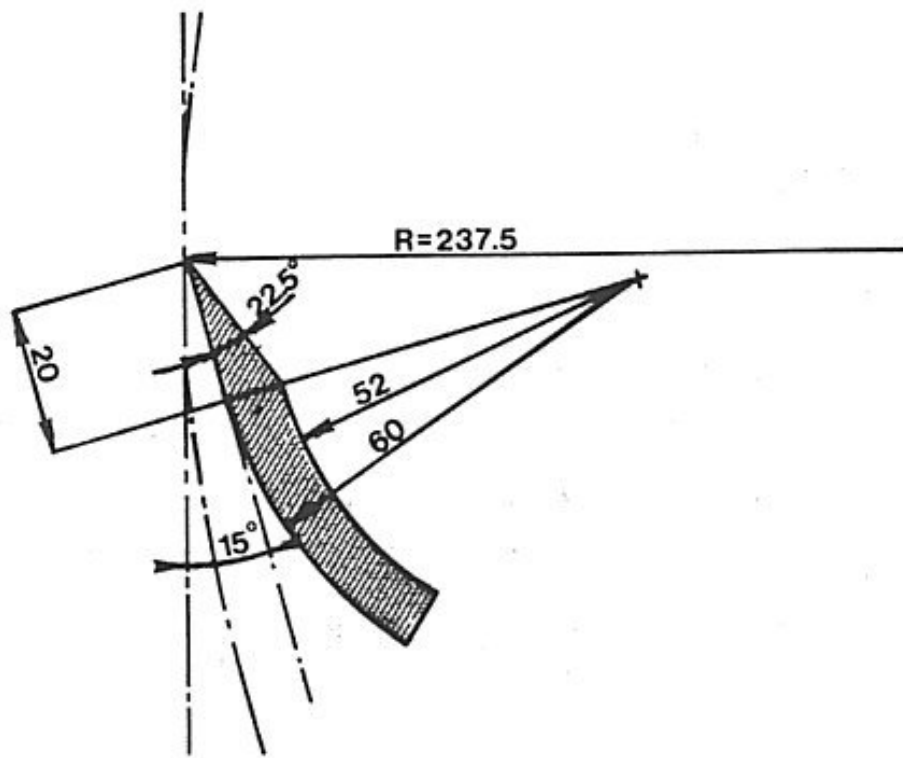


Figure 7.3: The circumferential blades.

In the bottom of the cutterhead are another 8 blades for which the data can be found in figure 7.4. These bottom blades cut the sand over a height of 19 mm so the total cutting height becomes 184 mm.

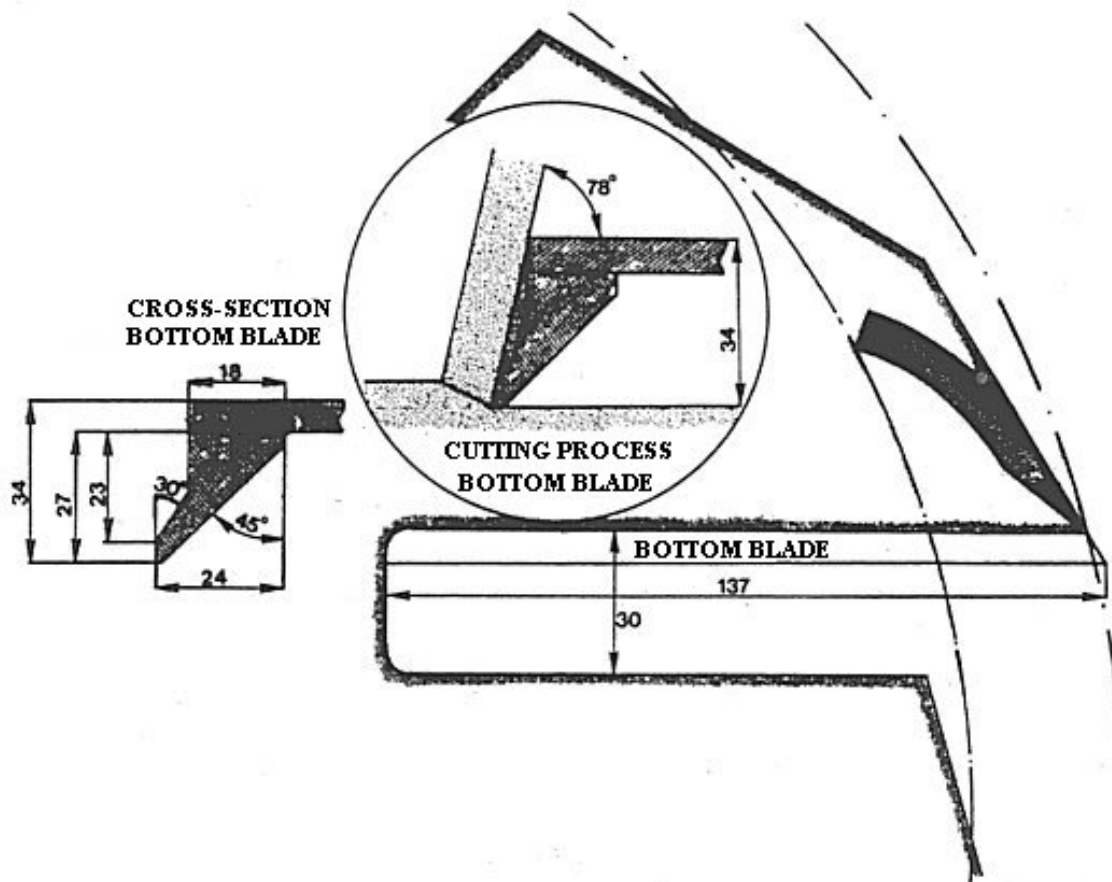


Figure 7.4: The bottom blades.

Figure 7.5 shows the cutting pattern. The middle cut is used as a penetration cut, to create a breach.

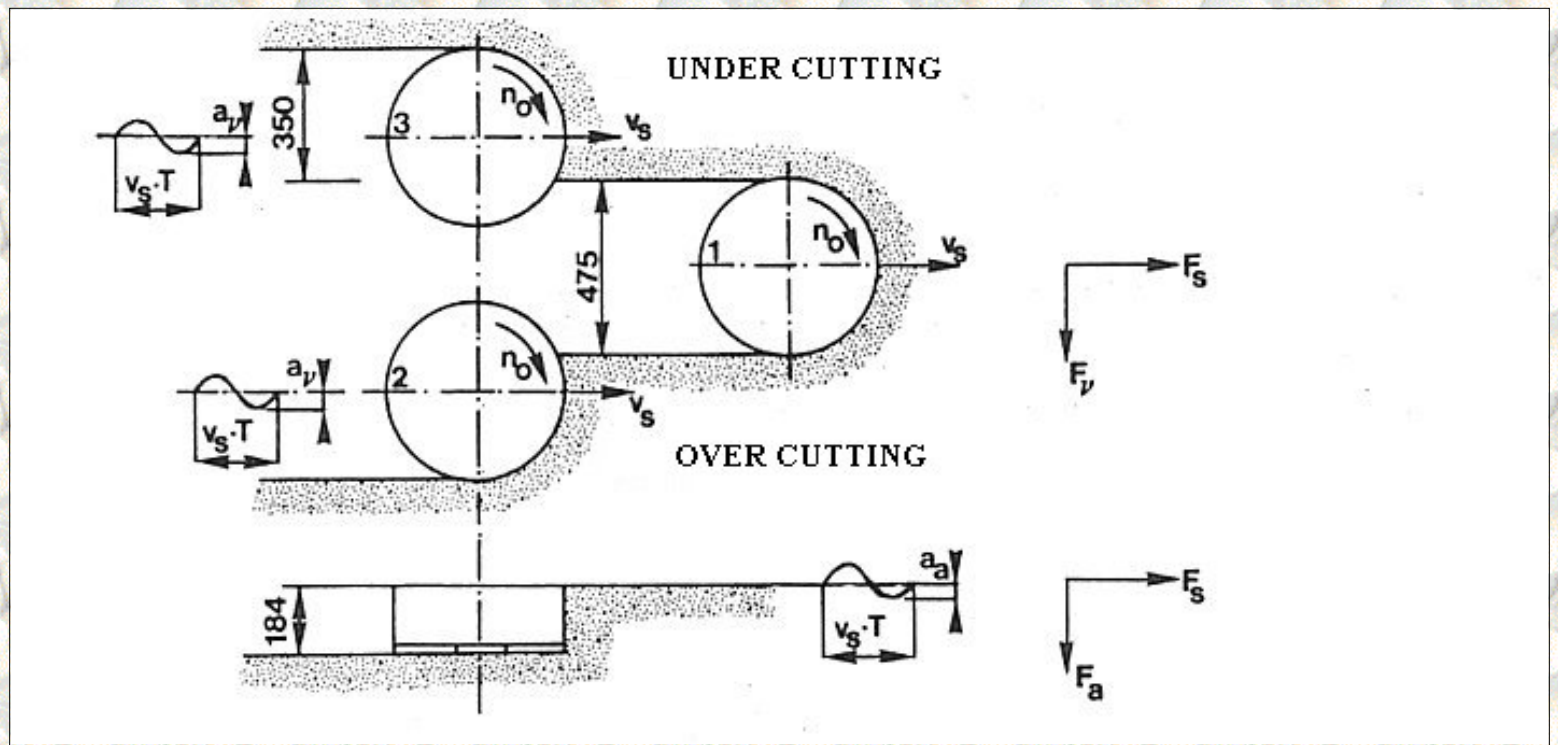


Figure 7.5: The cutting pattern.

The two side cuts are used for tests for the verification of the theory from chapter 4 and for a three-dimensional moving cutterhead. This will be discussed in chapter 11. Figure 7.5 shows that a run-through angle of 118° is used for the side cuts. This implies that only small differences can be observed between the over cutting and the under cutting tests.

During the tests are measured:

- I. The driving torque M_t .
- II. The force in the haul direction F_{st} .
- III. The horizontal force, perpendicular to the haul direction F_{vt} .
- IV. The axial force F_a .

[Back to top](#)

This is a translation of the dissertation of Dr.ir. S.A. Miedema, dated September 15th 1987 .
The dissertation was originally published in Dutch by the:
Delft University of Technology
Faculty of Mechanical Engineering and Marine Technology
Chair of Dredging Technology
Mekelweg 2
2628 CD, Delft
The Netherlands

It is advised to also read the papers following this dissertation, since the theory developed has been refined and extended.

Last modified Monday May 29, 2000 by: [Sape A. Miedema](#)

Translation by: [Laurens de Jonge](#)

Figures, equations and tables by: [Erik Miedema](#)

Copyright © May, 2000 Dr.ir. S.A. Miedema



[Download Adobe Acrobat Reader V4.0](#)

7.03 Forces and torque on the cutterhead.

The verification of the tests with the disc bottom cutterhead give the opportunity to illustrate the use of the developed theories and in particular the needed tables.

On the basis of the soil mechanical parameters of the sand, the used numbers of revolution, the used haul velocities and the blade geometry of the blades along the circumference of the cutterhead, an upper and lower limit for the coefficients c_1 en c_2 can be determined.

The number of revolutions is varied between 25 and 45 revolutions per minute, while the haul velocity is varied between 6.4 and 13.6 cm/sec.

Figure 7.3 shows that the static blade angle is 37.5° , while the blade height h_b can be estimated to be 13 mm.

The lower limit is now set by the lowest number of revolutions in combination with the highest haul velocity, which results in the lowest dynamic blade angle. A number of revolutions of 25 rpm and a haul velocity of 13.6 cm/s results in a dynamic blade angle that varies between 25° to 37.5° . The average layer-thickness can now be determined with equation (4.56). This is approximately 26 mm for the above-mentioned number of revolutions and the above mentioned haul velocity.

The upper limit is set by the highest number of revolutions in combination with the lowest haul velocity, which results in the highest dynamic blade angle. A number of revolutions of 45 rpm and a haul velocity of 6.4 cm/s results in a variation of the dynamic blade angle of 34° to 37.5° . The resulting layer-thickness is approximately 7 mm. The average dynamic blade angle at a given number of revolutions and haul velocity can be determined at that run-through angle where equation (4.56) is valid.

Although this choice is arbitrary, it will find the dynamic blade angle that connects with the determination of the specific cutting energy:

$$\Omega = \arcsin\left(\frac{1 - \cos(\Omega_1)}{\Omega_1}\right) \quad (7.1)$$

For the under and over-cutting process this results in an angle of 45.5° where the average layer-thickness occurs (figure 7.6).

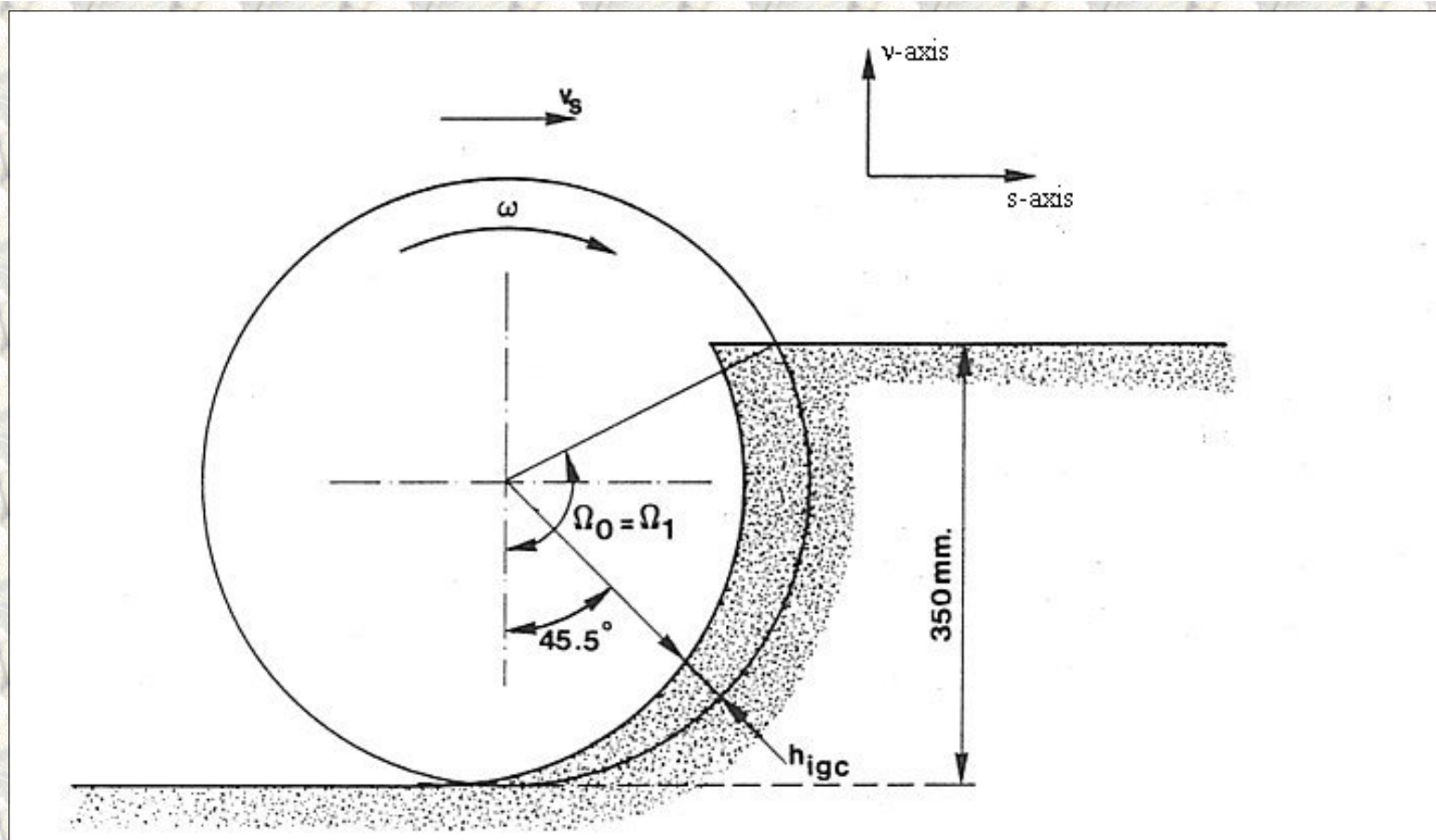


Figure 7.6: The average layer thickness according to equation (7.1).

For the lower limit an average dynamic blade angle of 29.3° is found, while for the upper limit 35.4° is found. The ratio h_b/h_i varies roughly between 0.5 and 2. With this data, an angle of internal friction of 38° and a soil/steel angle of friction of 30° the coefficients c_1 and c_2 can be looked up in the tables 2.14 to 2.25 (see Appendix B5). It will be assumed that a sub-pressure is present behind the blade and that there is no cavitation, which can be proven. The blades have a pitch angle $\iota=0$ and a curvature angle $\xi=0$. The following coefficients can now be determined, with a total run-through angle Ω_0 of 118° :

From chapter 4: general

$$\begin{array}{ll} f_1 = 0.22 & g_1 = c_1 \\ f_2 = 1.13 & g_2 = c_2 \\ f_5 = 1.26 & g_5 = 0 \end{array}$$

For the coefficient c_{gc} , equation (4.31), is found:

$$c_{gc} = 1.025 \cdot 9.81 \cdot 0.165 \cdot \frac{0.103}{0.00022} \cdot 0.2375 \cdot \frac{60}{8} \cdot \frac{v_s^2}{n_o} = 1384 \cdot \frac{v_s^2}{n_o} \quad (7.2)$$

From chapter 2:

$$\begin{array}{ll} \text{Lower limit} & \text{Upper limit} \\ c_1 = 0.35 & c_1 = 0.48 \end{array}$$

$$c_2 = 0.17$$

$$c_2 = 0.15$$

For the determination of these coefficients a cutting process on a sharp straight blade is assumed. Figure 7.3 shows however that the blades in the cutterhead have a slightly deviated shape, while additionally it is not known to what extent wear has had an influence on the model tests. During the processing of the measured data it appeared that the measured loads are best predicted with the following coefficients:

$$c_1 = 0.50$$

$$c_2 = -0.04$$

These coefficients agree with the earlier mentioned upper limit, where an angle of rotation θ_{ts} of 22° is introduced as a result of the wear, etc. To what extent this angle of rotation is caused by wear or by a deviated shape of the blades is not known. For the verification of the loads on the straight-forward moving cutterhead and the three-dimensional moving cutterhead the last mentioned coefficients c_1 and c_2 will be used. In the verification this has only influence on the force in the haul direction F_{st} . For the torque and the force perpendicular on the haul direction F_{vt} almost the same values are found as when using c_1 and c_2 according the upper limit. This shows that the ability to predict the force in the haul direction F_{st} is dependent on the insight in the effects of wear.

The bottom blades cut, as is remarked already, a layer of 19 mm, with a similar cutting process to that of the dredging wheel from chapter 5. The layer-thickness is then constant and the step S can be determined according:

$$S = \frac{v_s \cdot 60}{n_o \cdot p} \quad (7.3)$$

For the bank height B the following can be derived:

$$B = R \cdot (1 - \cos(\Omega_0)) \quad (7.4)$$

The geometry of the bottom blades (figure 7.4) is however not similar to the straight blades from chapter 2. It is proposed to approximate the bottom blade with a blade with a blade angle α of 78° and a blade height h_b of 34 mm. This implies however that it is no longer a matter of contact between the cut sand and the blade surface, but of a matter of friction between two sand surfaces, moving along each other. The accompanying angle of internal friction will have a value between the angle of internal friction belonging to the initial packing and an angle of internal friction that belongs to the loosest packing. In this verification an angle of friction of 38° is assumed, although this choice is arbitrary, as well as the chosen failure mechanism.

The various coefficients have constant values, since both the layer-thickness as the dynamic blade angle are constants. For the bottom blades can be derived, by extrapolation, from the tables 2.14 t/m 2.25, for $\delta=38^\circ$ en $\phi=38^\circ$:

$$c_1 = 1.57$$

$$c_2 = -0.52$$

From table 5.1 can be derived, assuming that $S/R \approx .1$ and $B/R \approx 1.5$, that:

$$f_{xgc} = 0.257 \text{ (} F_x \text{ from chapter 5 corresponds with } F_s \text{ chapter 4)}$$

$$f_{ygc} = 1.000 \text{ (} F_y \text{ from chapter 5 corresponds with } F_a \text{ chapter 4)}$$

$$f_{zgc} = 0.829 \text{ (} F_z \text{ from chapter 5 corresponds with } F_v \text{ chapter 4)}$$

$$m_{gc} = 0.958$$

The coefficient b_{gc} , equation (5.16), can not be used without consequences, because in this case the layer-thickness is constant. This coefficient can be written:

$$b_{gc} = \rho_w \cdot g \cdot 0.19^2 \cdot \frac{n_o \cdot p \cdot e}{60 \cdot k_m} \quad (7.5)$$

With the found coefficients and the equations (4.40) to (4.43) and (7.1) for the circumference blades and (5.30) to (5.33) and (7.2) to (7.5) for the bottom blades, the following equations can be derived for the cutting forces and the driving torque. The first term gives the contribution of the circumference blades and the second term gives the contribution of the bottom blades:

overcutting

undercutting

$$M_t = 207 \cdot \frac{v_s^2}{n_o} + 0.206 \cdot v_s \quad 207 \cdot \frac{v_s^2}{n_o} + 0.206 \cdot v_s \quad (7.6)$$

$$F_{st} = 90 \cdot \frac{v_s^2}{n_o} + 0.233 \cdot v_s \quad 215 \cdot \frac{v_s^2}{n_o} + 0.233 \cdot v_s \quad (7.7)$$

$$F_{vt} = 794 \cdot \frac{v_s^2}{n_o} + 0.752 \cdot v_s \quad 770 \cdot \frac{v_s^2}{n_o} + 0.752 \cdot v_s \quad (7.8)$$

$$F_{at} = 0 \cdot \frac{v_s^2}{n_o} + 0.300 \cdot v_s \quad 0 \cdot \frac{v_s^2}{n_o} + 0.300 \cdot v_s \quad (7.9)$$

The axial force on the blades along the circumference of the cutterhead is theoretically equal to 0, while the bottom blades cause a small upward-aimed force. Small axial forces are also measured during the measurements, but the spreading, caused by the momentary loads on the blades, as a function of time was larger than the average loads.

In figures 7.7 to 7.18 the measured values are put against the, with equations (7.6), (7.7) and (7.8), calculated, values, for the over cutting and the under cutting dredging process. The drawn lines indicate, for each figure, the contribution of the blades along the circumference of the cutterhead, while the striped lines indicate the total loads according the above mentioned equations.

From these figures can be concluded:

1. In general there is a good correlation between the measured and the calculated loads.
2. The theoretical ratios between F_{st} , F_{vt} and M_t reasonably agree with the measured values, although the measured values of F_{vt} in this ratio are slightly larger.

The cutterhead tests are performed in 1982. The sand in this period had a d_{50} of 180 μm . The tests with the straight blades (chapter 3) are performed in 1985. It has to be mentioned that the soil mechanical parameters are determined during this research (d_{50} : 200 μm). During the years a certain segregation of the sand package took place, through which the smaller particles of the sand are disposed or carried away from the measuring area. During the last measurements with the straight blades, the d_{50} was increased to 210 μm . For this reason, for the verification of the cutterhead, the soil mechanical parameters as they were known at the beginning of the straight blade research are used ($n_i = 38\%$, $k_i = 0.00012 \text{ m/s}$).

It is however not improbable that, during the cutterhead research, the soil mechanical parameters of the cutterhead research have slightly differed from the parameters used for this verification.

There are a few possibilities explanations of the second conclusion:

1. It appears from the equations (4.40) to (4.43) that M_t and F_{vt} are mainly determined by c_1 , while F_{st} is determined by c_1 and c_2 (because $g_1 = c_1$ and $g_2 = c_2$). The earlier mentioned drift of d_{50} in time could have caused a small change in the angle of internal friction and the soil/steel angle of friction. This also changes the ratio between c_1 and c_2 according tables 2.14 to 2.25.
2. Considering the construction of the blades on the cutterhead the distribution of the sub-pressure in front of and behind the blade can differ from the straight blades. This also influences the ratio between c_1 and c_2 .
3. The cut layers are very thin when compared to the possible bluntness and wear of the blades. The influence of the bluntness and wear is characterized by on the one hand a small increase of the total force on the blade and on the other hand a change in direction of the total force, which influences the ratio between c_1 and c_2 .
4. The values of c_1 and c_2 are not constant but vary with the run-through angle. The ratio between c_1 and c_2 is also not constant with the run-through angle, although this is assumed in the analytical model. This will be further discussed in chapter 9.

A quantitative estimation of these factors is hard to give, but the found small deviations of the theory are of importance for the verification of the three-dimensional moving cutterhead.

If in the tests with the used disc bottom cutterhead a run-through angle of 180° is used, a division

can be made between loads dependent on the coefficient c_1 and loads dependent on the coefficient c_2 . These tests are then also useful to determine these coefficients in combination with the permeability k_m and the dilatancy e . This results in the following coefficients, for the non-cavitating, cutting process where only the blades along the circumference of the cutterhead are involved.

$$\Pi_1 = c_1 \cdot \frac{e}{k_m} \quad (7.10)$$

and

$$\Pi_2 = c_2 \cdot \frac{e}{k_m} \quad (7.11)$$

In an almost fully cavitating cutting process, the coefficients d_1 and d_2 can be derived directly from the ratio between and the magnitude of the forces F_{vt} and F_{st} . The advantage of these coefficients is that not all soil mechanical parameters have to be determined. A condition however is that in a, for this purpose developed, disc bottom cutterhead, the possible present bottom blades don't cause hinder, like there was in the performed tests.

[Back to top](#)

This is a translation of the dissertation of Dr.ir. S.A. Miedema, dated September 15th 1987 .
 The dissertation was originally published in Dutch by the:
 Delft University of Technology
 Faculty of Mechanical Engineering and Marine Technology
 Chair of Dredging Technology
 Mekelweg 2
 2628 CD, Delft
 The Netherlands

It is advised to also read the papers following this dissertation, since the theory developed has been refined and extended.

Last modified Monday May 29, 2000 by: [Sape A. Miedema](#)

Translation by: [Laurens de Jonge](#)

Figures, equations and tables by: [Erik Miedema](#)

Copyright © May, 2000 Dr.ir. S.A. Miedema



[Download Adobe Acrobat Reader V4.0](#)

7.04 Test stand dredging wheel experiments.

[Contents](#)

The research is performed in the old laboratory GV in 1982. A model dredging wheel was mounted underneath the auxiliary carriage. In figure 7.19 this test equipment is shown:

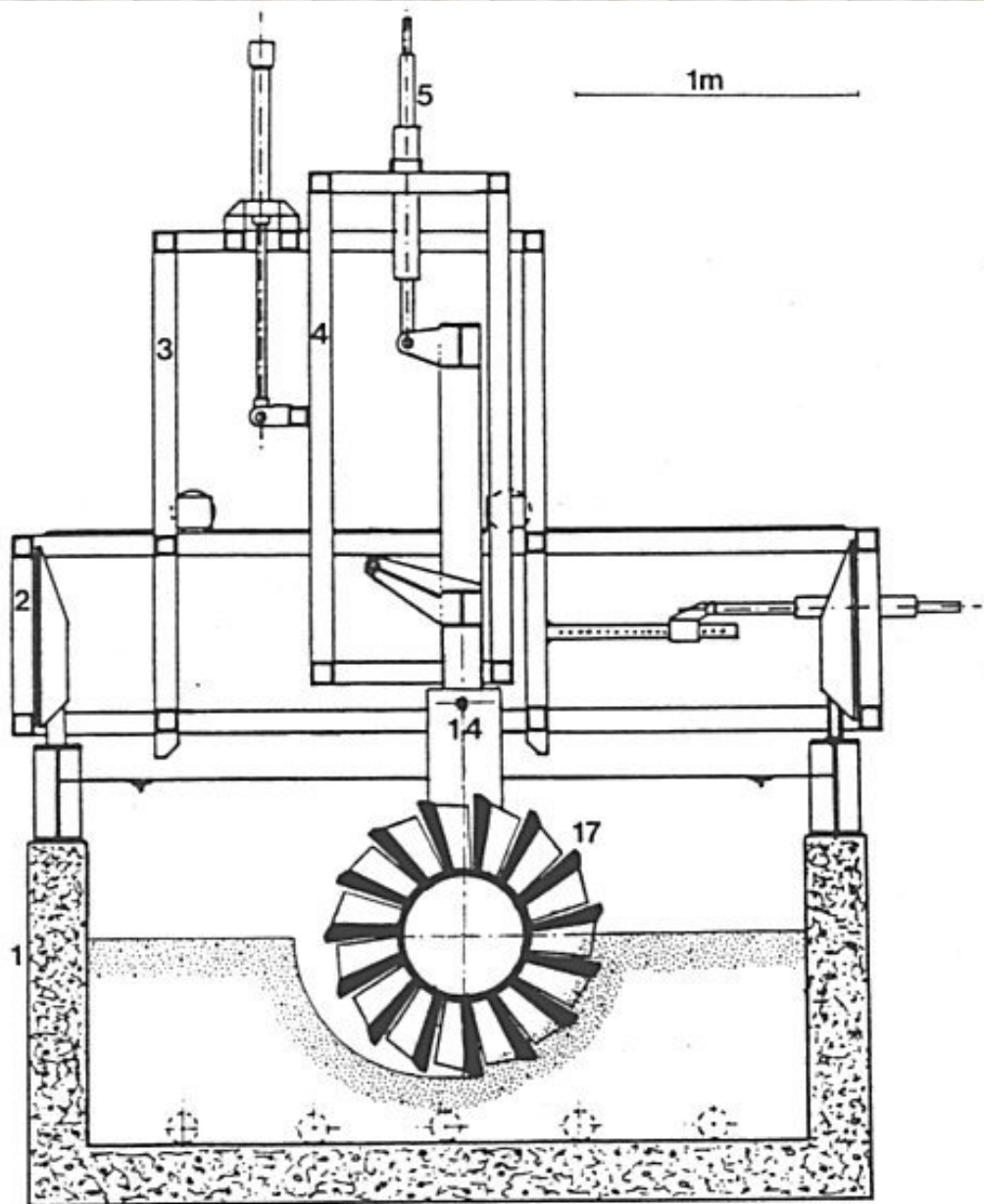


Figure 7.19: The test stand with:

1. The concrete tank.
2. The main carriage.
3. The auxiliary carriage.
4. The auxiliary frame.
5. Hydraulic cilinder for vertical positioning.
14. Ladder.

15. Dredging wheel.

The dredging wheel has a radius of 318 mm and is equipped with 15 cutting blades with a blade angle between 30° and 42° . The soil mechanical parameters of the used sand can be found in appendix B3.

Of the performed sub studies, the following sub studies are of importance for the verification:

1. Study of the mechanical and hydraulic losses in open water and with various breach shapes.
2. Study of the acting driving torques for various numbers of revolution, haul velocities and breach shapes.

The dimensions of the used model dredging wheel are indicated in figure 7.20.

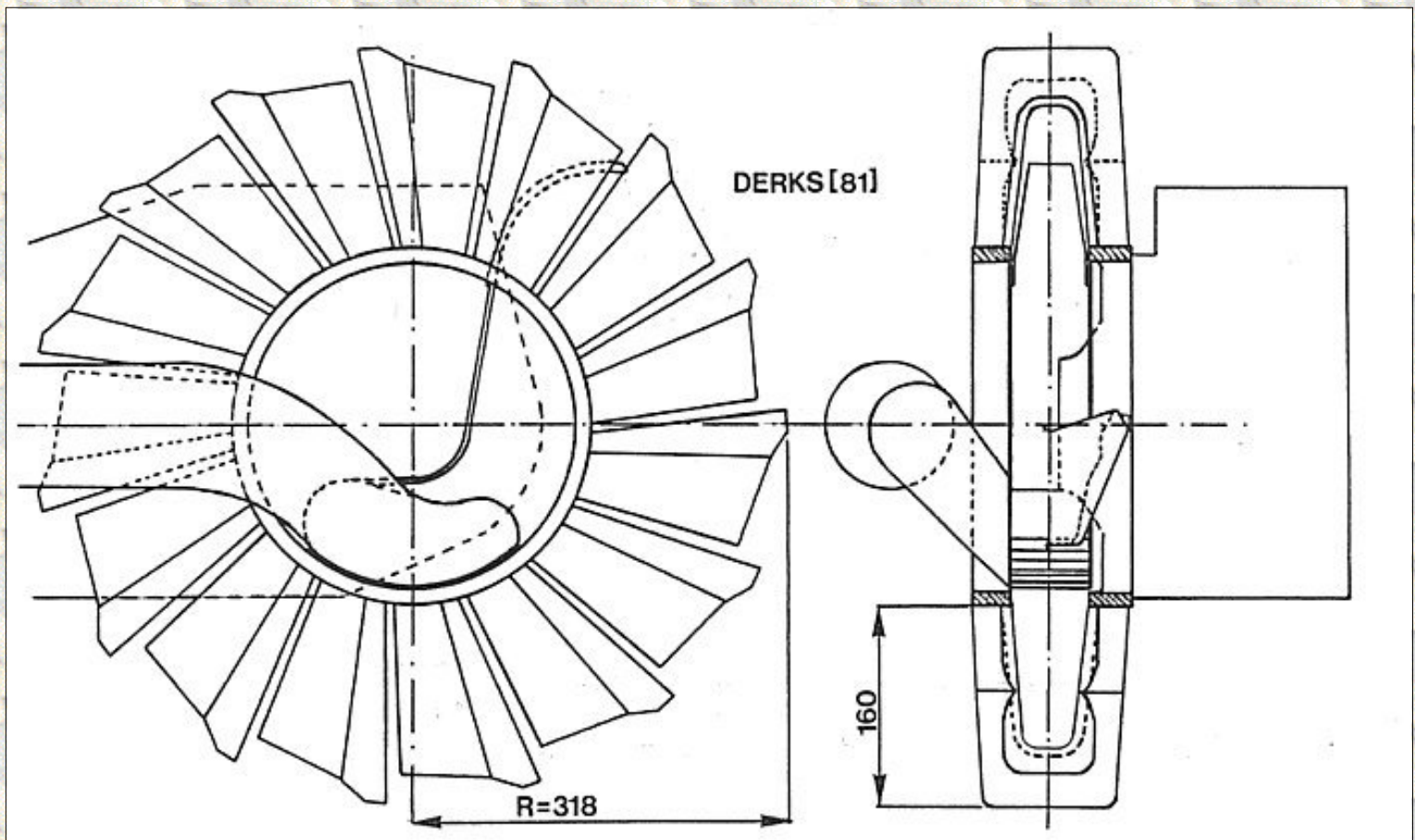


Figure 7.20: The model dredging wheel.

[Back to top](#)

This is a translation of the dissertation of Dr.ir. S.A. Miedema, dated September 15th 1987 .
The dissertation was originally published in Dutch by the:
Delft University of Technology
Faculty of Mechanical Engineering and Marine Technology
Chair of Dredging Technology
Mekelweg 2
2628 CD, Delft
The Netherlands

It is advised to also read the papers following this dissertation, since the theory developed has been refined and extended.

Last modified Monday May 29, 2000 by: [Sape A. Miedema](#)

Translation by: [Laurens de Jonge](#)

Figures, equations and tables by: [Erik Miedema](#)

Copyright © May, 2000 Dr.ir. S.A. Miedema



[Download Adobe Acrobat Reader V4.0](#)

7.05 Mechanical and hydraulical losses.

First the mechanical and the hydraulical losses have to be known, before the measured driving torques can be discussed. From Derks [81] is known that the mechanical and the hydraulical losses are proportional to the number of revolutions of the dredging wheel to the second power. The hydraulic losses are also influenced by the breach shape. To get an impression of these losses measurements are performed on two fixed concrete breach models with the dredging wheel rotating in the water. Figure 7.21 gives an impression of these breach models and the mechanical and hydraulical losses as a function of the square of the number of revolutions of the dredging wheel. From figure 7.21 can be concluded that a larger run-through breach angle decreases the hydraulic losses. For the verification of the driving torque a linear interpolation is performed between the measured mechanical and hydraulical losses for the vertical and horizontal breach. The losses are considered here as a fact, so that only the cutting torques are verified.

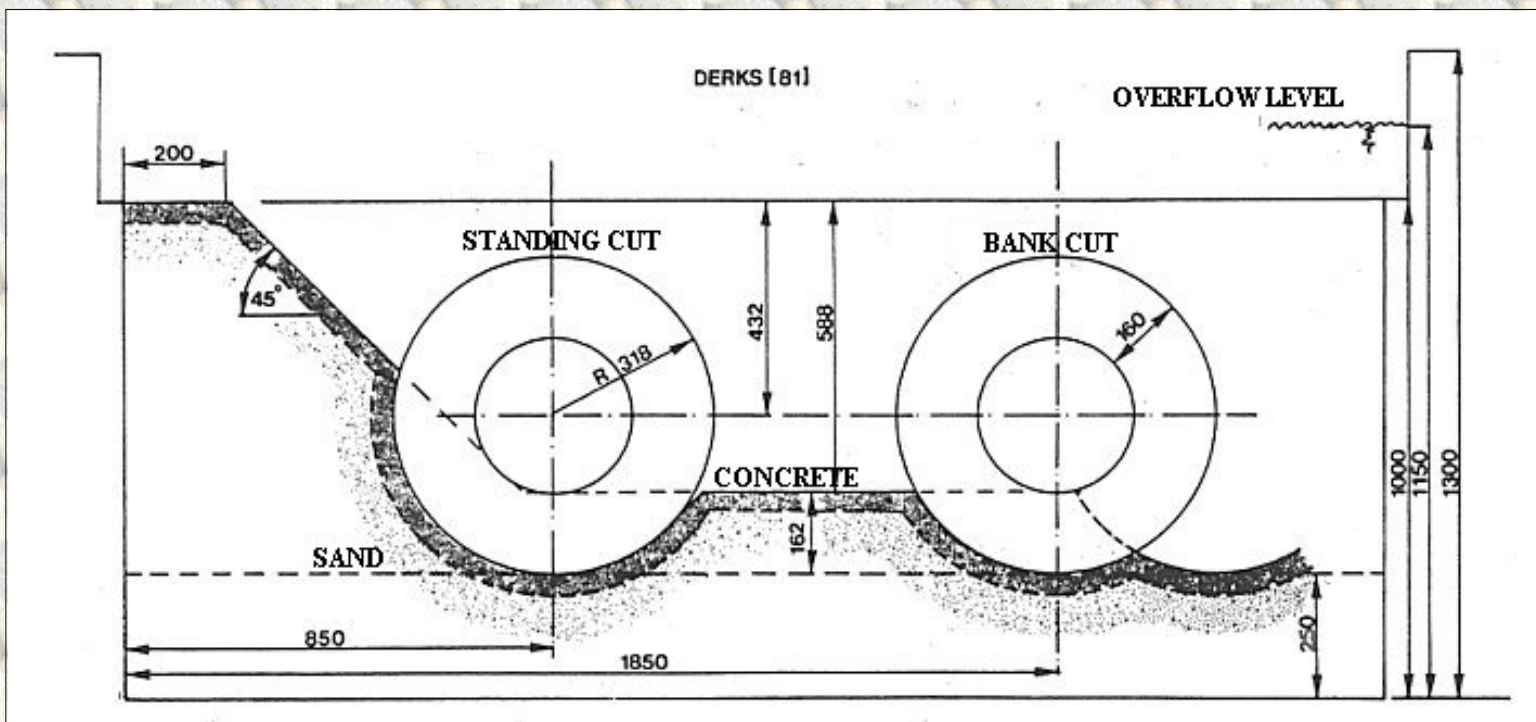


Figure 7.21a: The two fixed concrete bank shapes.

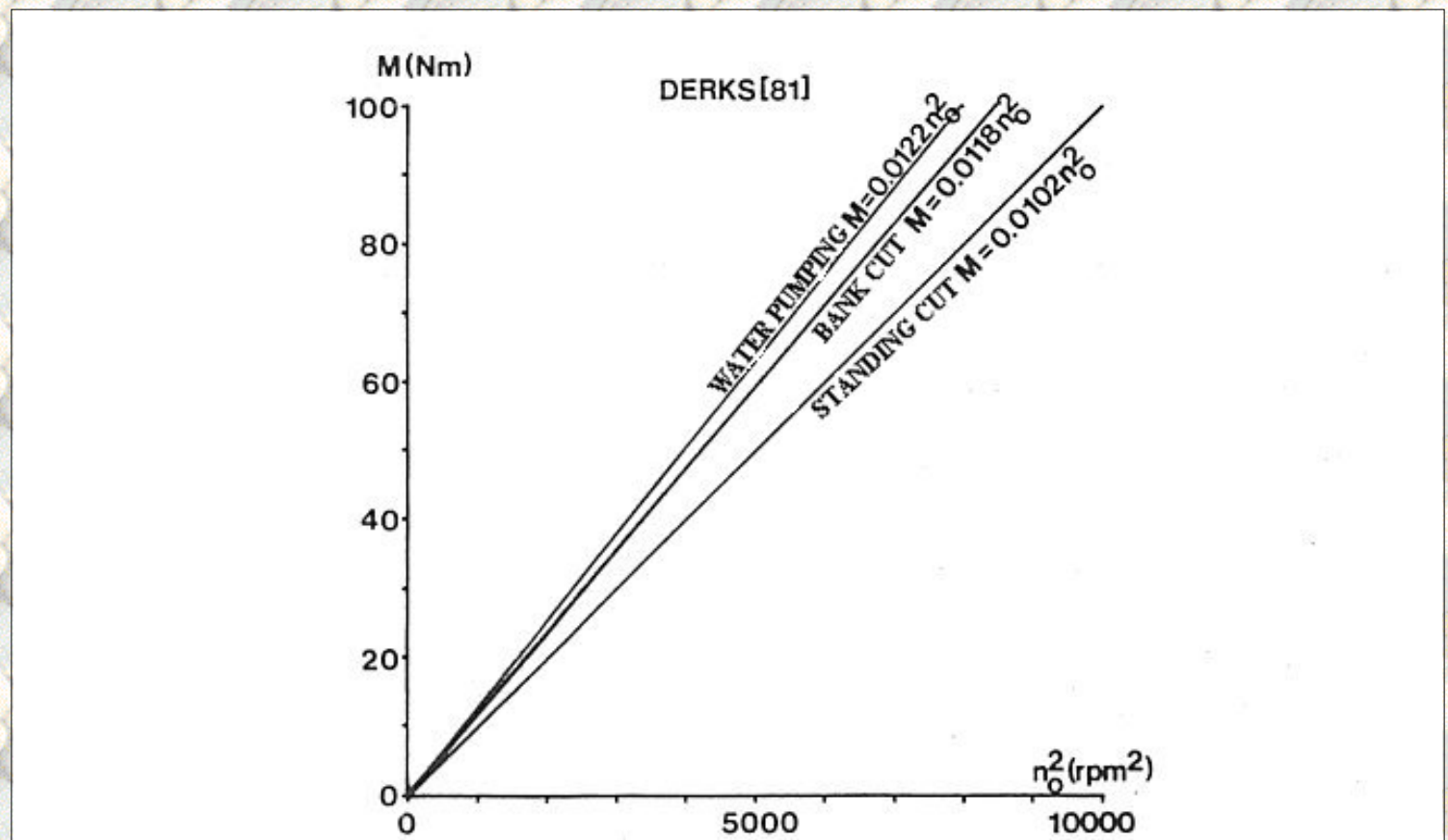


Figure 7.21b: The water pumping drive torque.

[Back to top](#)

This is a translation of the dissertation of Dr.ir. S.A. Miedema, dated September 15th 1987 .

The dissertation was originally published in Dutch by the:
Delft University of Technology
Faculty of Mechanical Engineering and Marine Technology
Chair of Dredging Technology
Mekelweg 2
2628 CD, Delft
The Netherlands

It is advised to also read the papers following this dissertation, since the theory developed has been refined and extended.

Last modified Monday May 29, 2000 by: [Sape A. Miedema](#)

Translation by: [Laurens de Jonge](#)

Figures, equations and tables by: [Erik Miedema](#)

Copyright © May, 2000 Dr.ir. S.A. Miedema



[Download Adobe Acrobat Reader V4.0](#)

7.06 Driving torques.

The following parameters are verified in the determination of the driving torques:

1. The breach shape. The various breach shapes are shown in figure 7.10. The run-through breach angles and the accompanying hydraulic and mechanical losses are listed in table 7.1.
2. The number of revolutions of the dredging wheel. The number of revolutions is varied between 25 rpm to 100 rpm with steps of 25 rpm
3. The haul velocity. The haul velocity is varied between 0.10 m/s to 0.37 m/s

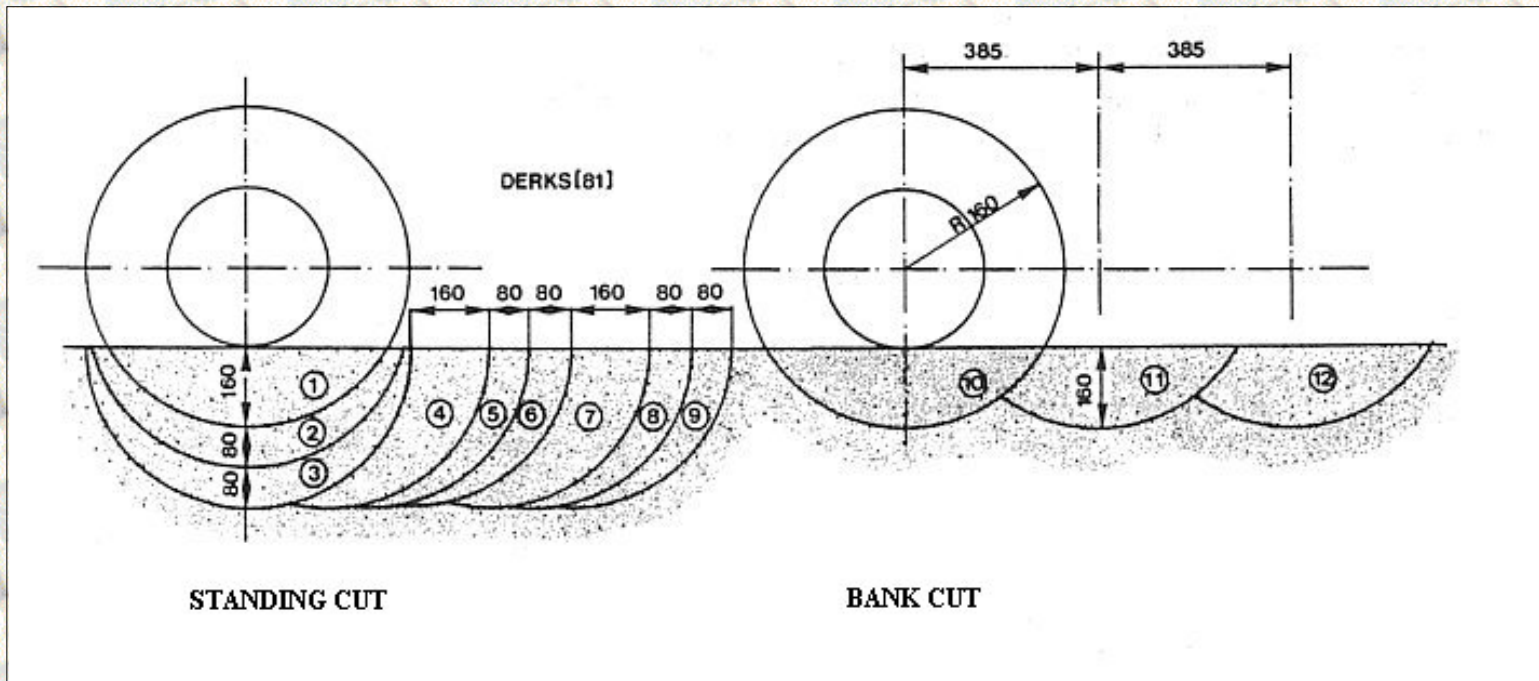


Figure 7.22: The different bank shapes with the cross sections cut.

$A_1 = 6.27 \text{ dm}^2$ $A_4 = 5.01 \text{ dm}^2$ $A_7 = 5.01 \text{ dm}^2$ $A_{10} = 6.27 \text{ dm}^2$
 $A_2 = 4.70 \text{ dm}^2$ $A_5 = 2.46 \text{ dm}^2$ $A_8 = 2.46 \text{ dm}^2$ $A_{11} = 5.41 \text{ dm}^2$
 $A_3 = 5.04 \text{ dm}^2$ $A_6 = 2.46 \text{ dm}^2$ $A_9 = 2.46 \text{ dm}^2$ $A_{12} = 5.41 \text{ dm}^2$

A (dm ²)	Ω_0	$M \cdot 0.001 \cdot n_o^2$
6.72	120°	11.2
5.41	92°	11.8
4.70	150°	10.6
5.04	180°	9.9
5.01	104°	11.5
2.46	97°	11.7

Table 7.1: The hydraulic and mechanical losses (M in Nm).

For the determination of the theoretical driving torque the next equation is derived in chapter 5, for a non-cavitating cutting process

$$M = b_{gc} \cdot c_1 \cdot m_{gc} \cdot R \cdot A \quad (7.12)$$

The coefficient b_{gc} can be determined with equation (5.16). For the determination of k_m initially the average of k_{max} en k_i (Miedema [57]) can be used.

The geometry of the dredging wheel must be known for the determination of the coefficient c_1 from the tables 2.14 to 2.25 from chapter 2 (see Appendix B5). From figure 7.11 can be seen that the blade angle varies between 30° and 42° while the blade height h varies between 37 mm and 25 mm, which corresponds to a h_b of approximately 18.5 mm to 16.7 mm. The first mentioned values are valid on the circumference of the dredging wheel, while the last mentioned values are valid for the point on the cutting edge with a radius of 158 mm. It also has to be remarked that these values are valid for the static case, that is a stationary dredging wheel.

Dynamically both the blade angle and the blade height h_b are smaller. In the performed tests the dynamic blade angle was maximum 6° smaller than the static blade angle on the circumference of the dredging wheel. A radius of 158 mm showed a maximum decrease of the blade angle of 12° . On the part of the cutting edge that was mostly in contact with the breach during the tests, an average blade angle of approximately 30° and a blade height h_b of 16 mm can be assumed. The layer-thickness varied between 4 mm and 16 mm, which is similar to the blade-height / layer-thickness ratio that varies between 4 and 1.

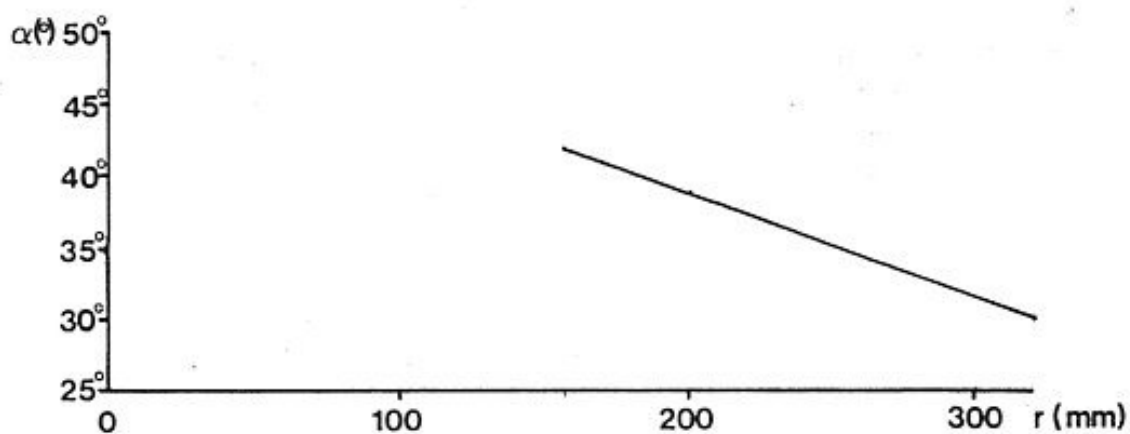


Figure 7.23: The static blade angle as a function of the radius.

With this data and the soil mechanical parameters from appendix B3 a value for c_1 is found that varies between 0.37 and 0.42. From the tables 2.2 to 2.5 from chapter 2 the shear angle β can also be determined, it can be fixed on approximately 30° .

The coefficient m_{gc} is harder to estimate, as the breach shapes, shown in figure 7.10, are not all

similar to the breach shapes from chapter 5. From the tables 5.1 to 5.5 it appears however that the coefficient m_{gc} does not vary much with a slightly varying breach shape. A value for m_{gc} between 0.82 and 0.92 is chosen, with the remark that m_{gc} decreases with an increasing breach surface.

Since only the driving torques are measured, it is impossible to make comments, on the basis of these tests, on the ratio between c_1 en c_2 , like with the cutting edges. The theoretically determined values are therefore used.

With the above-determined coefficients the theoretical course of the driving torque can be determined, which results in the following equation, for a non-cavitating cutting process:

$$M = 1763 \rightarrow 2246 \frac{v_s^2}{n_o} \cdot A \quad (7.13)$$

In figures 7.24 to 7.32 are shown:

1. The hydraulic and mechanical losses.
2. The theoretical course of the driving torque as a function of the layer-thickness h_i . In these figures two lines are shown, the lower line is valid for a c_1 value of 0.37 and for m_{gc} of 0.82. The upper line is valid for a c_1 value of 0.42 and for m_{gc} of 0.92.
3. The measured driving torques.

In general the correlation between the measured torques and the theoretical determined torques is reasonable. Immediately has to be remarked that the spread in the measured torques is large. A cause for this spread could be the reproducibility of the sandbed. Although the sandbed is prepared according the in chapter 3 discussed method, it is not known what influence a preceding cut has on the sand distribution. The accompanying spread of the soil mechanical parameters is unfortunately not known.

Striking are the extremely high driving torques for the layer-thickness of approximately 15 mm. These can be explained with the "bulldozer" effect (Miedema [56]). The passage between two blades is approximately 26 mm, with a radius of 235 mm (Derks [81]). A layer of 15.2 mm is deformed during the cutting process to 26 mm thickness on the blade, at a dynamic blade angle of 32° and a shear angle of 30° . An increasing haul velocity causes thicker layers, which can not pass through two succeeding blades. The dredging wheel does not cut anymore but acts like a "bulldozer". This "bulldozer" limit is however also dependent on the dynamic blade angle and the shear angle and therefore of the geometry of the blade and the soil mechanical parameters. This implies that the danger of the "bulldozer" effect can occur in a range around the layer-thickness of 15 mm, in the performed model tests. The size of this range can be easily determined as far as the geometry of the cutting process is concerned. In the used model dredging wheel this area is however very small, in other words for a certain number of revolutions the "bulldozer" effect occurs all along the cutting edge for approximately the same haul velocity. The influence of the soil mechanical parameters on the "bulldozer" limit can be well estimated theoretically. The variation of the soil mechanical parameters itself is however hard to estimate, certainly with the earlier remark on the reproducibility of the sandbed. This is therefore not about the accuracy of the

soil mechanical parameters but the reproducibility of the sandbed.

If a variation of the angle of internal friction and the soil/steel angle of friction of $\pm 5^\circ$ is assumed then the shear angle varies with approximately $\pm 4^\circ$ according to table 2.2 ($h_b/h_i = 1$). This results in a starting range of the "bulldozer" effect between 13.4 mm and 15.9 mm for the initial layer-thickness.

[Back to top](#)

This is a translation of the dissertation of Dr.ir. S.A. Miedema, dated September 15th 1987 .
The dissertation was originally published in Dutch by the:
Delft University of Technology
Faculty of Mechanical Engineering and Marine Technology
Chair of Dredging Technology
Mekelweg 2
2628 CD, Delft
The Netherlands

It is advised to also read the papers following this dissertation, since the theory developed has been refined and extended.

Last modified Monday May 29, 2000 by: [Sape A. Miedema](#)

Translation by: [Laurens de Jonge](#)

Figures, equations and tables by: [Erik Miedema](#)

Copyright © May, 2000 Dr.ir. S.A. Miedema



[Download Adobe Acrobat Reader V4.0](#)

7.07 Conclusions.

The cutting torques and the cutting forces on the cutterhead correlate well with the in chapter 4 developed theory, if the effects of the bottom blades on the cutterhead loads are included in the verification and if the experimentally determined coefficients c_1 and c_2 are used for the determination of the force in the haul direction, because of, among other things, the different blade shape of the circumference blades.

The hydraulic and mechanical losses can be neglected in these tests because of the low numbers of revolution. The cutting torques on the dredging wheel are reasonably predictable with the in chapter 5 developed theory. It is however necessary to include the mechanical and hydraulic losses in the determination of the total driving torque. As a result of different scale rules for the cutting process and for the hydraulic losses, must be counted on proportionally different hydraulic losses for the prototype.

The in chapter 4 and 5 developed calculation models can be used as a basis for the calculation model of a three-dimensional moving cutterhead.

[Back to top](#)

This is a translation of the dissertation of Dr.ir. S.A. Miedema, dated September 15th 1987 .

The dissertation was originally published in Dutch by the:
Delft University of Technology
Faculty of Mechanical Engineering and Marine Technology
Chair of Dredging Technology
Mekelweg 2
2628 CD, Delft
The Netherlands

It is advised to also read the papers following this dissertation, since the theory developed has been refined and extended.

Last modified Monday May 29, 2000 by: [Sape A. Miedema](#)

Translation by: [Laurens de Jonge](#)

Figures, equations and tables by: [Erik Miedema](#)

Copyright © May, 2000 Dr.ir. S.A. Miedema



[Download Adobe Acrobat Reader V4.0](#)

7.03 Figures Cutterhead Tests.

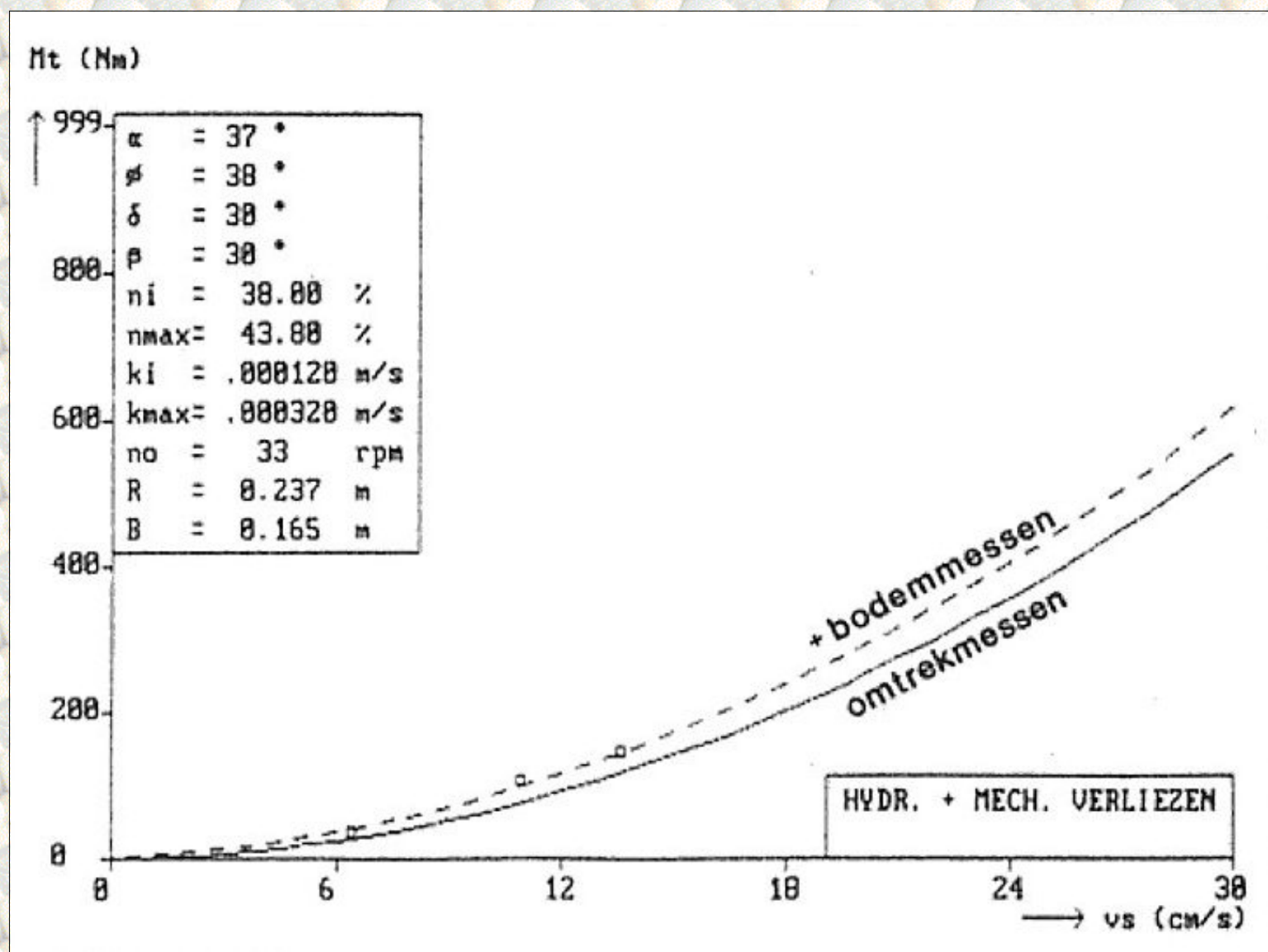


Figure 7.7 : The drive torque M_t of the disc bottom cutterhead. Experiments in 200 μm sand, overcutting at 33 rpm as a function of the swing velocity v_s .

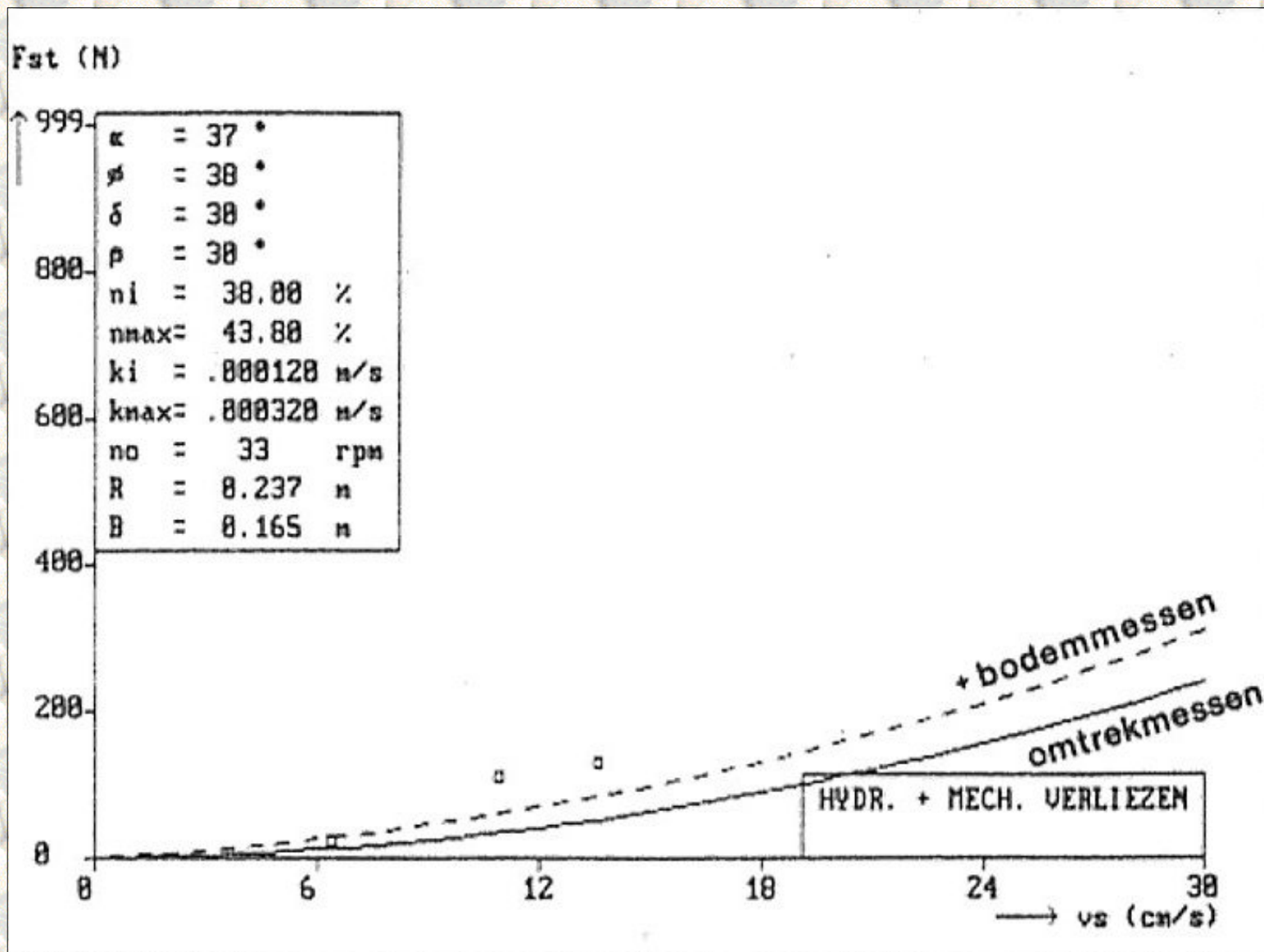


Figure 7.8 : The force in the swing direction F_{st} on the disc bottom cutterhead. Experiments in 200 μ m sand, overcutting at 33 rpm as a function of the swing velocity v_s .

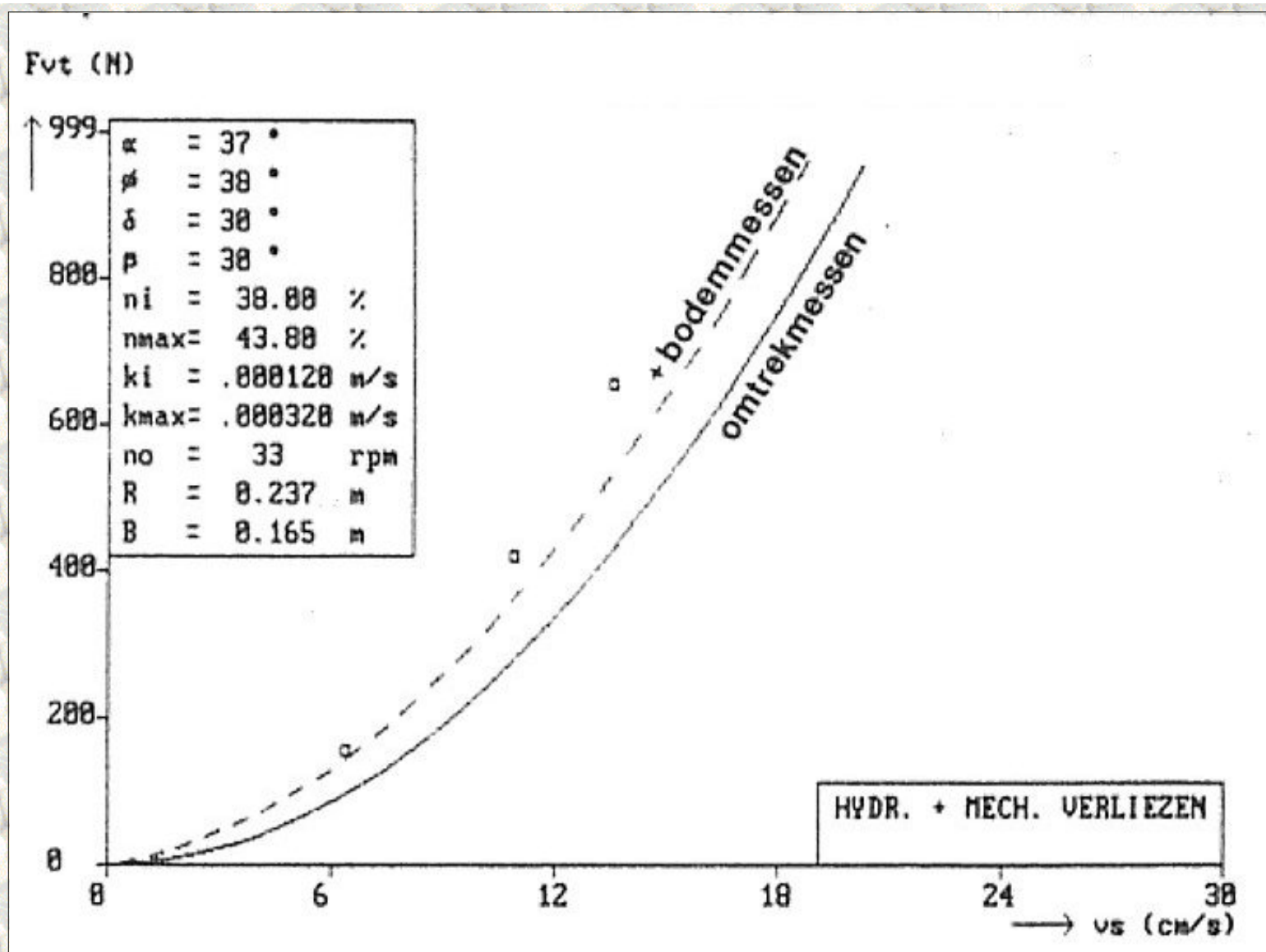


Figure 7.9 : The force perpendicular to the swing direction F_{vt} on the disc bottom cutterhead. Experiments in 200 μm sand, overcutting at 33 rpm as a function of the swing velocity v_s .

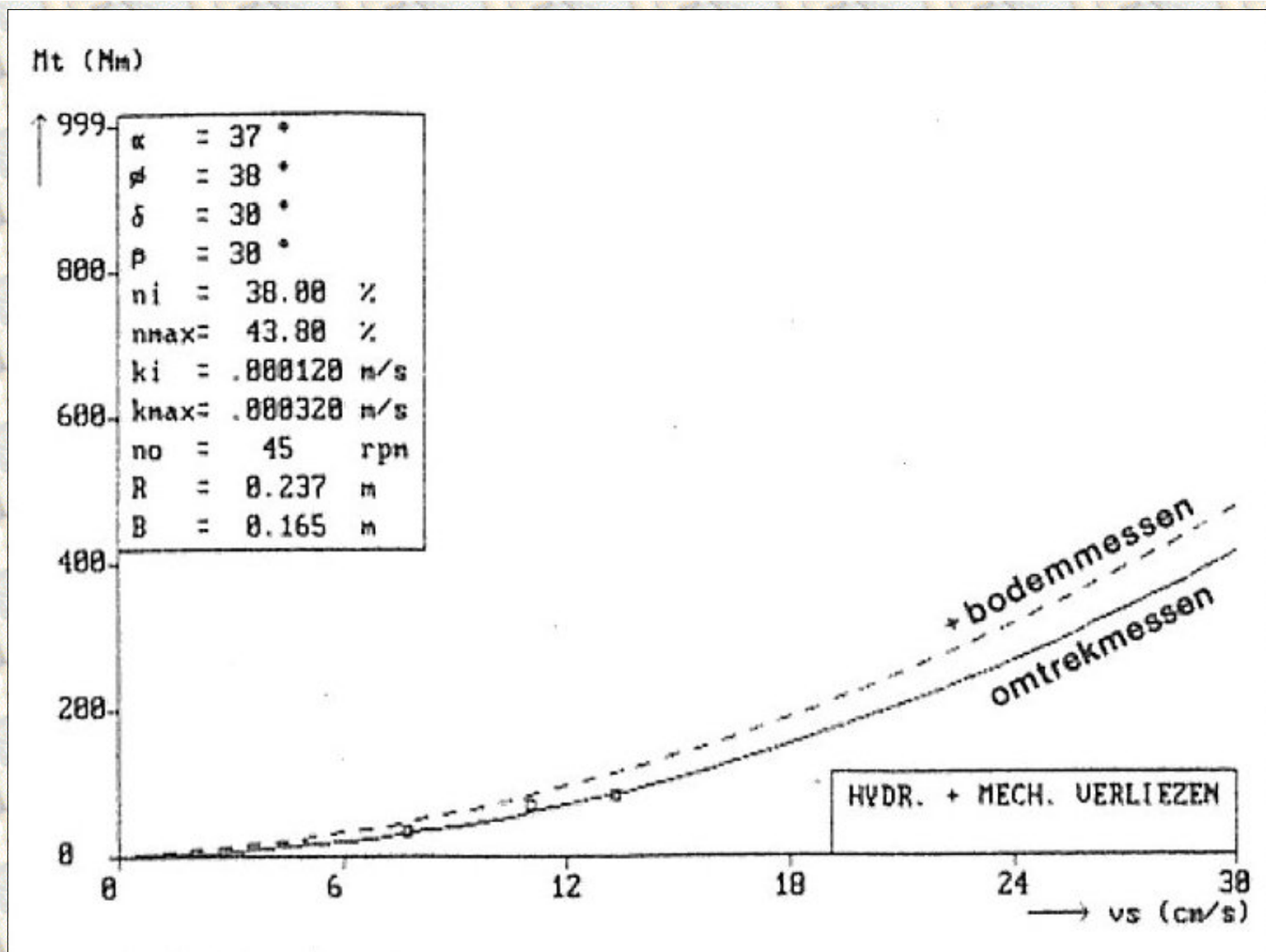


Figure 7.10 : The drive torque M_t of the disc bottom cutterhead. Experiments in 200 μ m sand, overcutting at 45 rpm as a function of the swing velocity v_s .

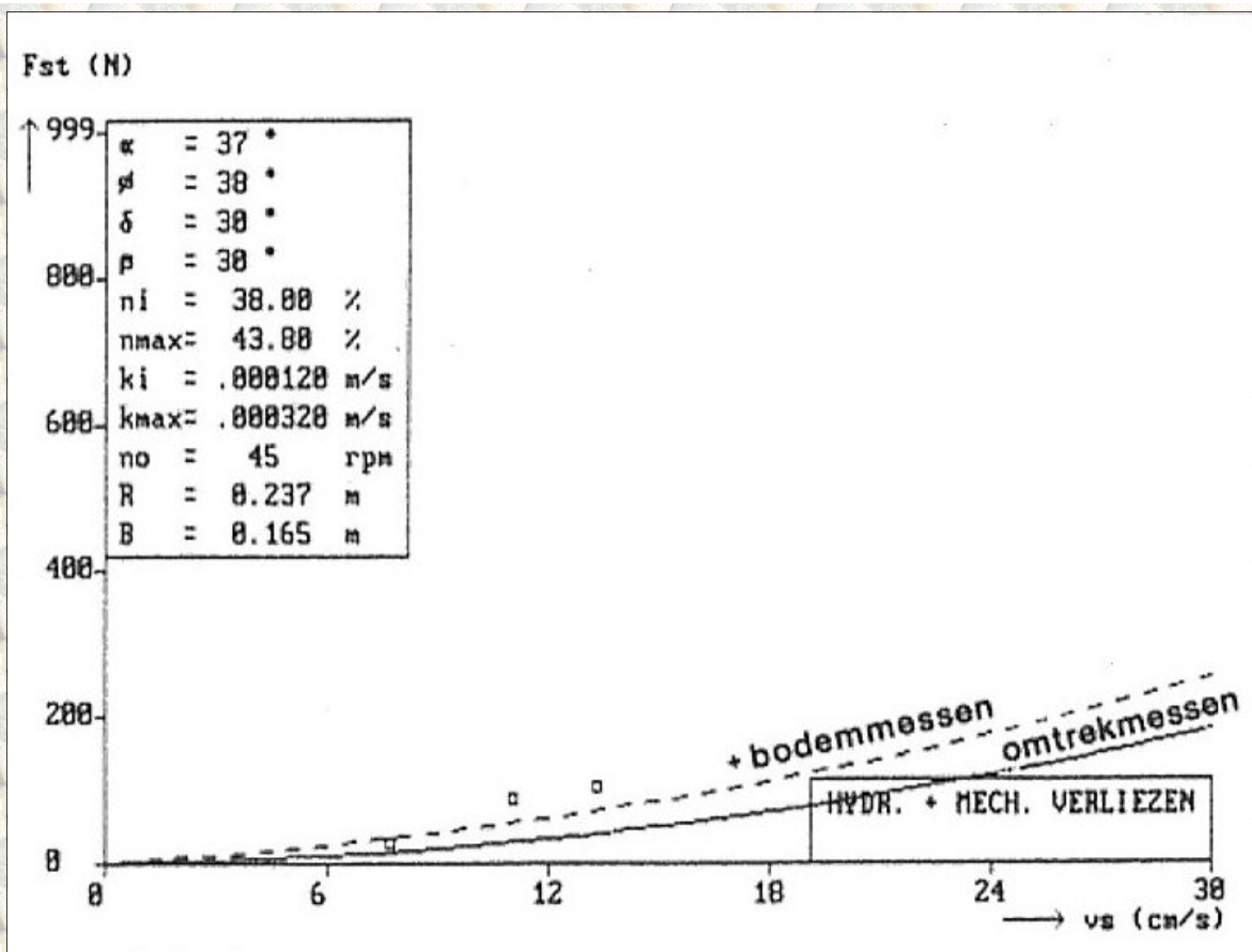


Figure 7.11 : The force in the swing direction F_{st} on the disc bottom cutterhead. Experiments in 200 μ m sand, overcutting at 45 rpm as a function of the swing velocity v_s .

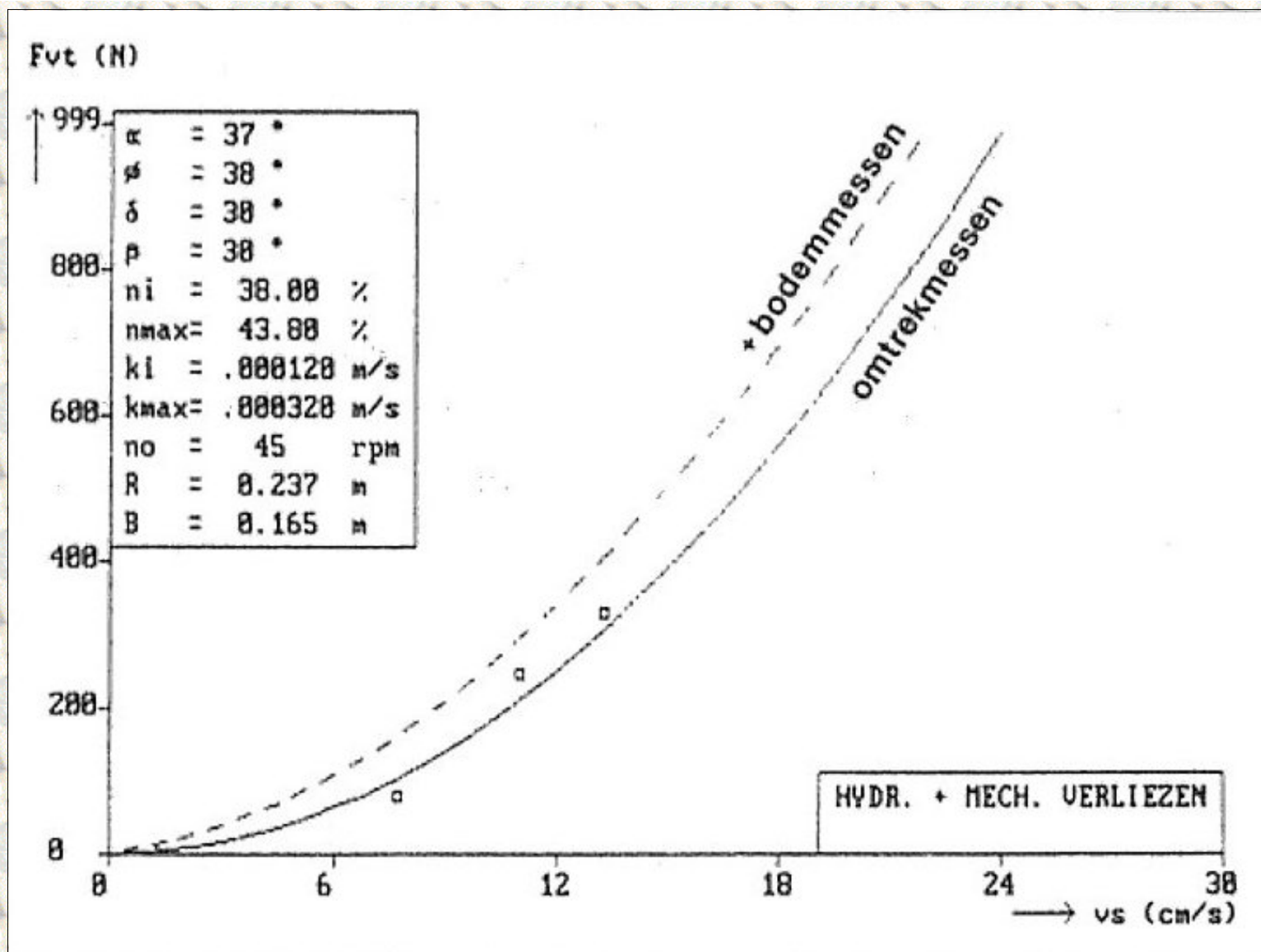


Figure 7.12 : The force perpendicular to the swing direction F_{vt} on the disc bottom cutterhead. Experiments in 200 μ m sand, overcutting at 45 rpm as a function of the swing velocity v_s .

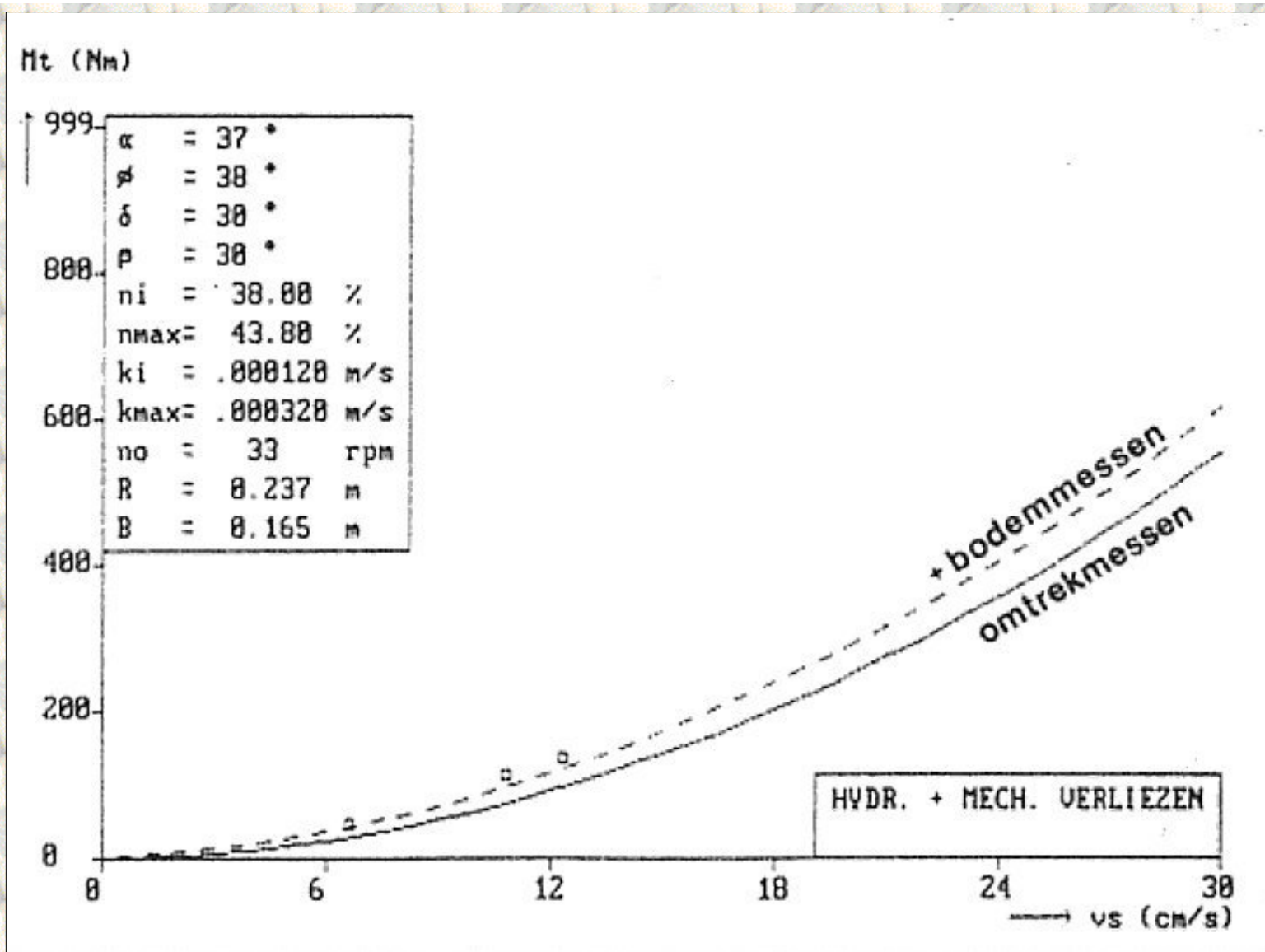


Figure 7.13 : The drive torque M_t of the disc bottom cutterhead. Experiments in 200 μm sand, undercutting at 33 rpm as a function of the swing velocity v_s .

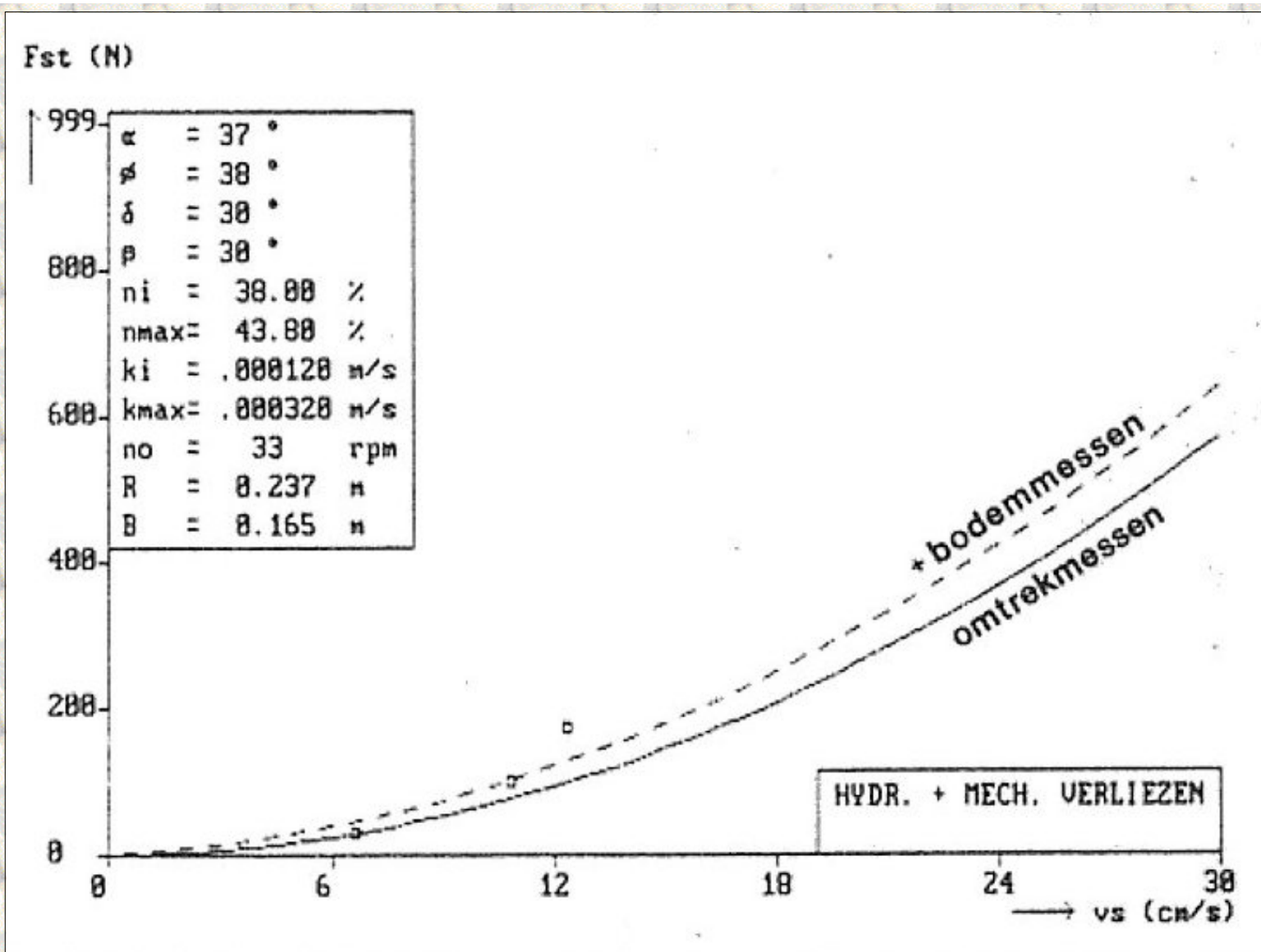


Figure 7.14 : The force in the swing direction F_{st} on the disc bottom cutterhead. Experiments in $200 \mu\text{m}$ sand, undercutting at 33 rpm as a function of the swing velocity v_s .

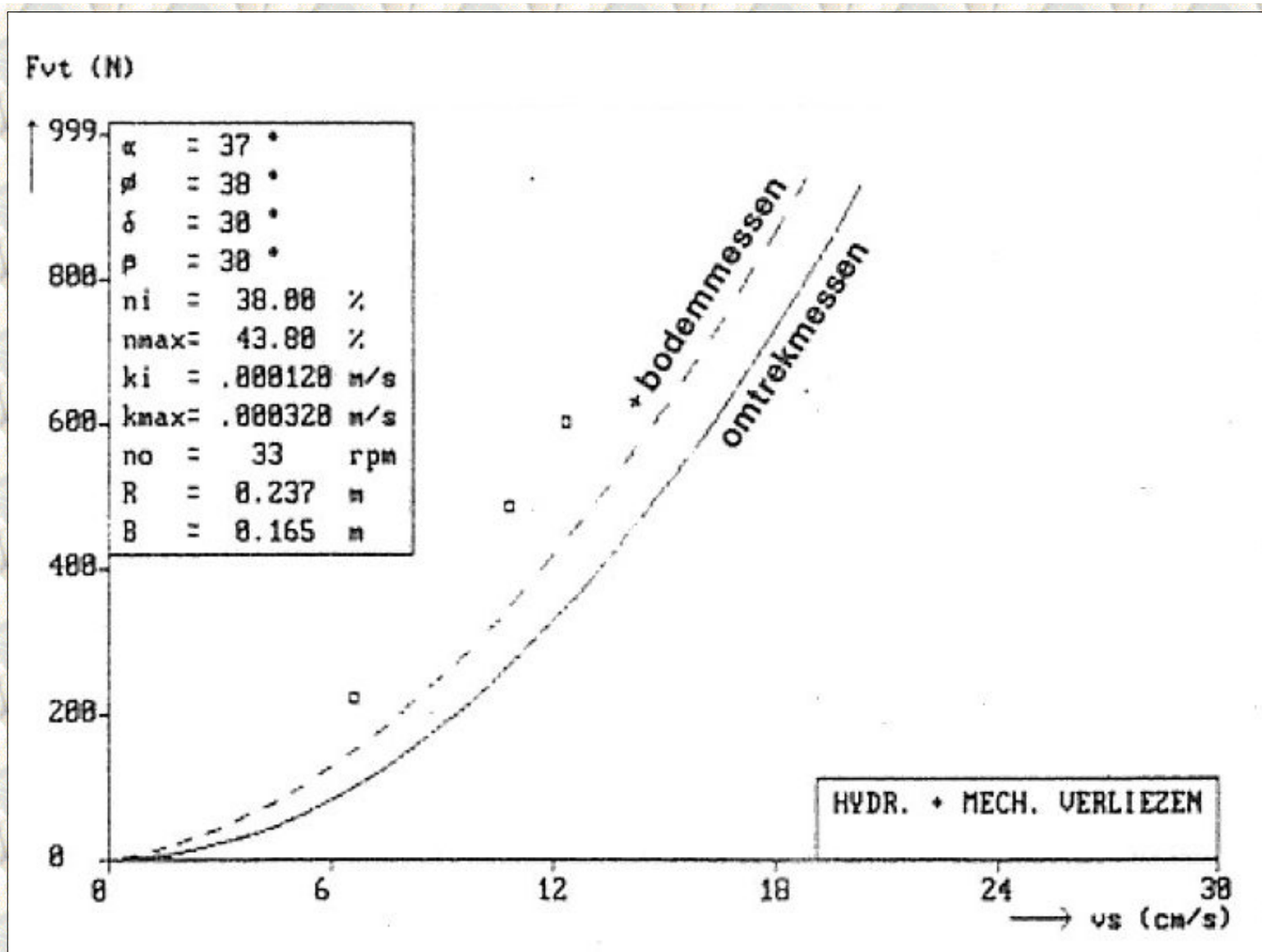


Figure 7.15 : The force perpendicular to the swing direction F_{vt} on the disc bottom cutterhead. Experiments in 200 μ m sand, undercutting at 33 rpm as a function of the swing velocity v_s .

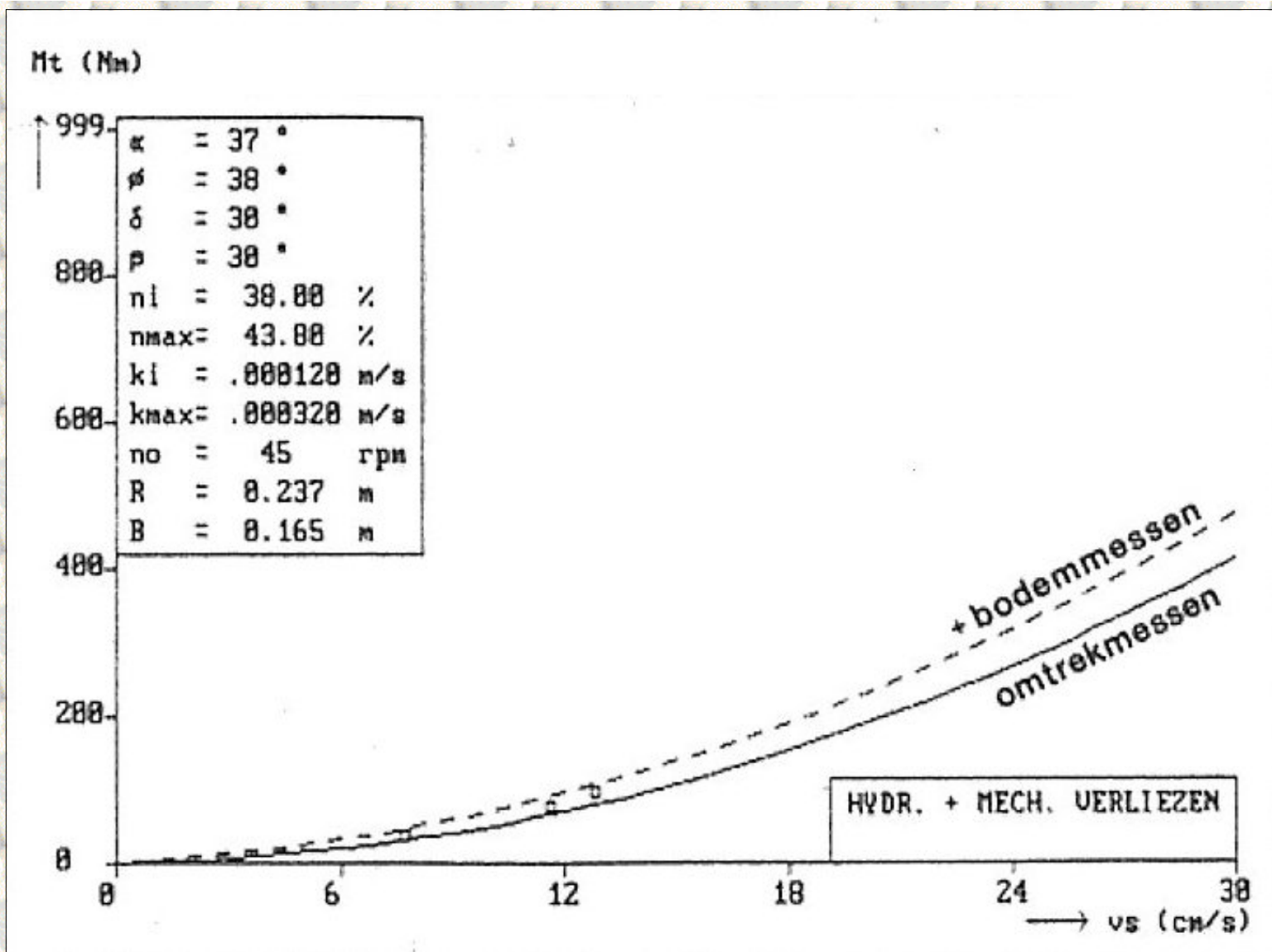


Figure 7.16 : The drive torque M_t of the disc bottom cutterhead. Experiments in $200 \mu\text{m}$ sand, undercutting at 45 rpm as a function of the swing velocity v_s .

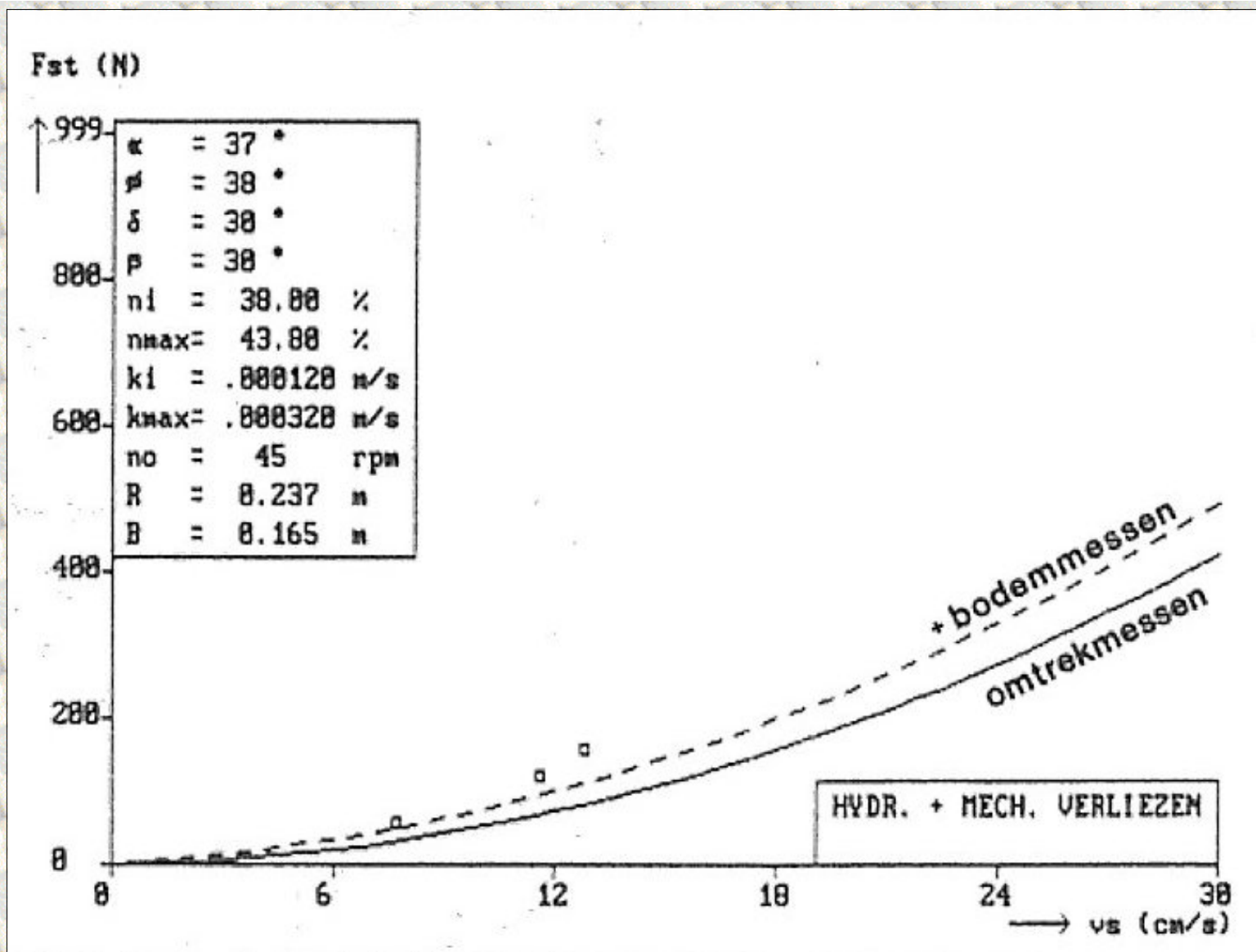


Figure 7.17 : The force in the swing direction F_{st} on the disc bottom cutterhead. Experiments in 200 μm sand, undercutting at 45 rpm as a function of the swing velocity v_s .

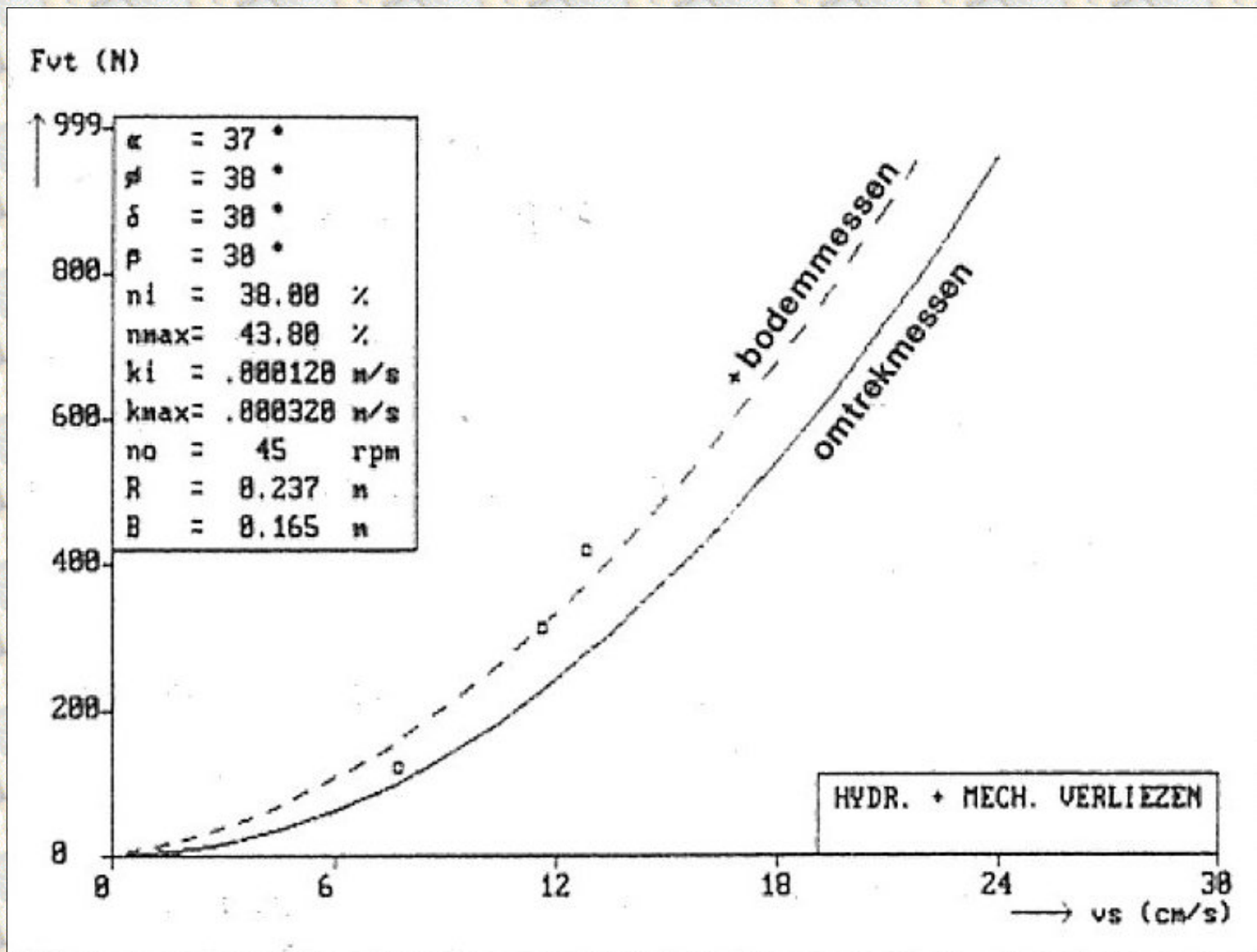


Figure 7.18 : The force perpendicular to the swing direction F_{vt} on the disc bottom cutterhead. Experiments in 200 μm sand, undercutting at 45 rpm as a function of the swing velocity v_s .

[Back to top](#)

This is a translation of the dissertation of Dr.ir. S.A. Miedema, dated September 15th 1987 .
 The dissertation was originally published in Dutch by the:
 Delft University of Technology
 Faculty of Mechanical Engineering and Marine Technology
 Chair of Dredging Technology
 Mekelweg 2
 2628 CD, Delft
 The Netherlands

It is advised to also read the papers following this dissertation, since the theory developed has been refined and extended.

Last modified Monday May 29, 2000 by: [Sape A. Miedema](#)

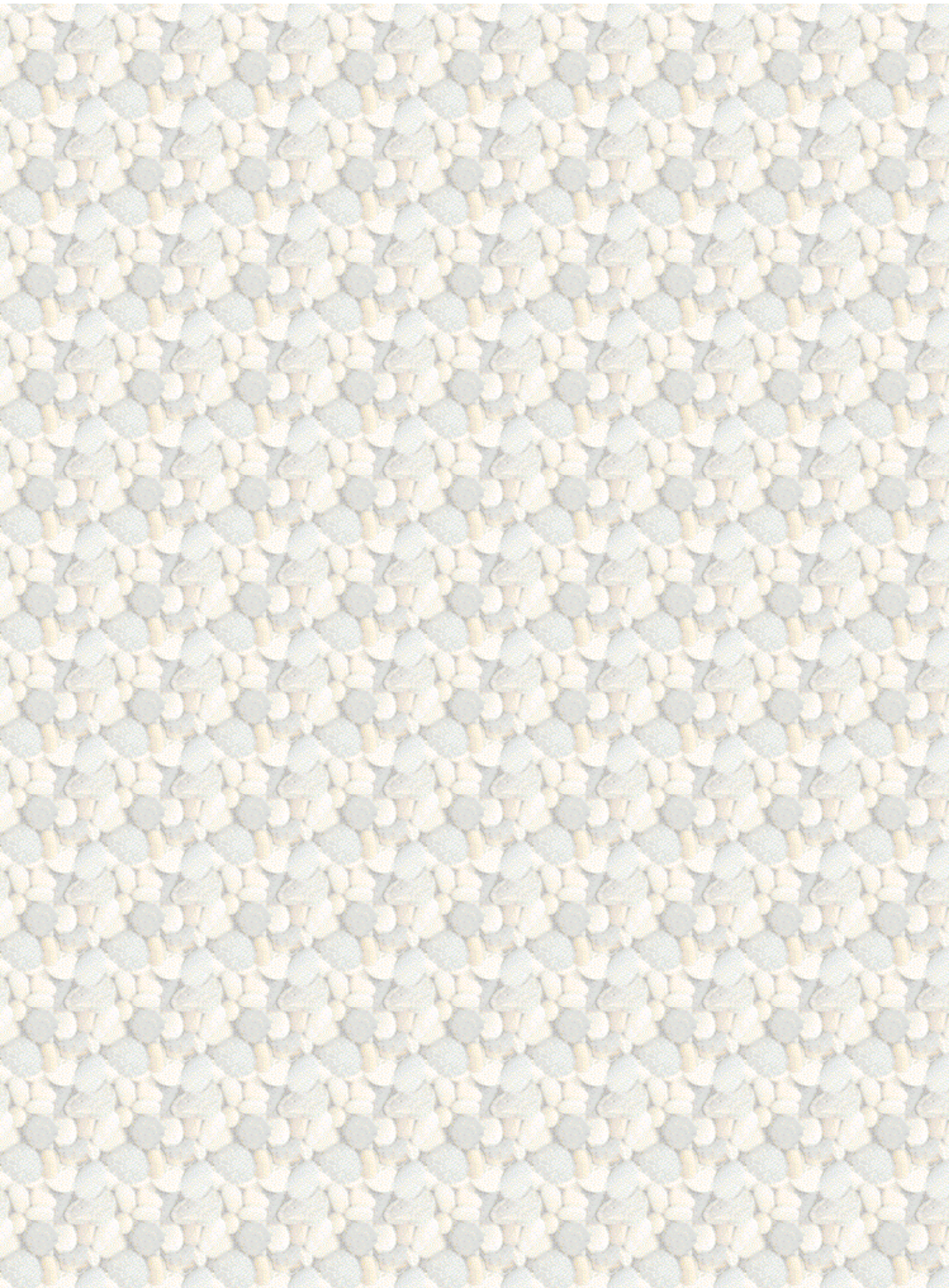
Translation by: [Laurens de Jonge](#)

Figures, equations and tables by: [Erik Miedema](#)

Copyright © May, 2000 Dr.ir. S.A. Miedema



[Download Adobe Acrobat Reader V4.0](#)



7.07 Figures Dredging Wheel Tests.

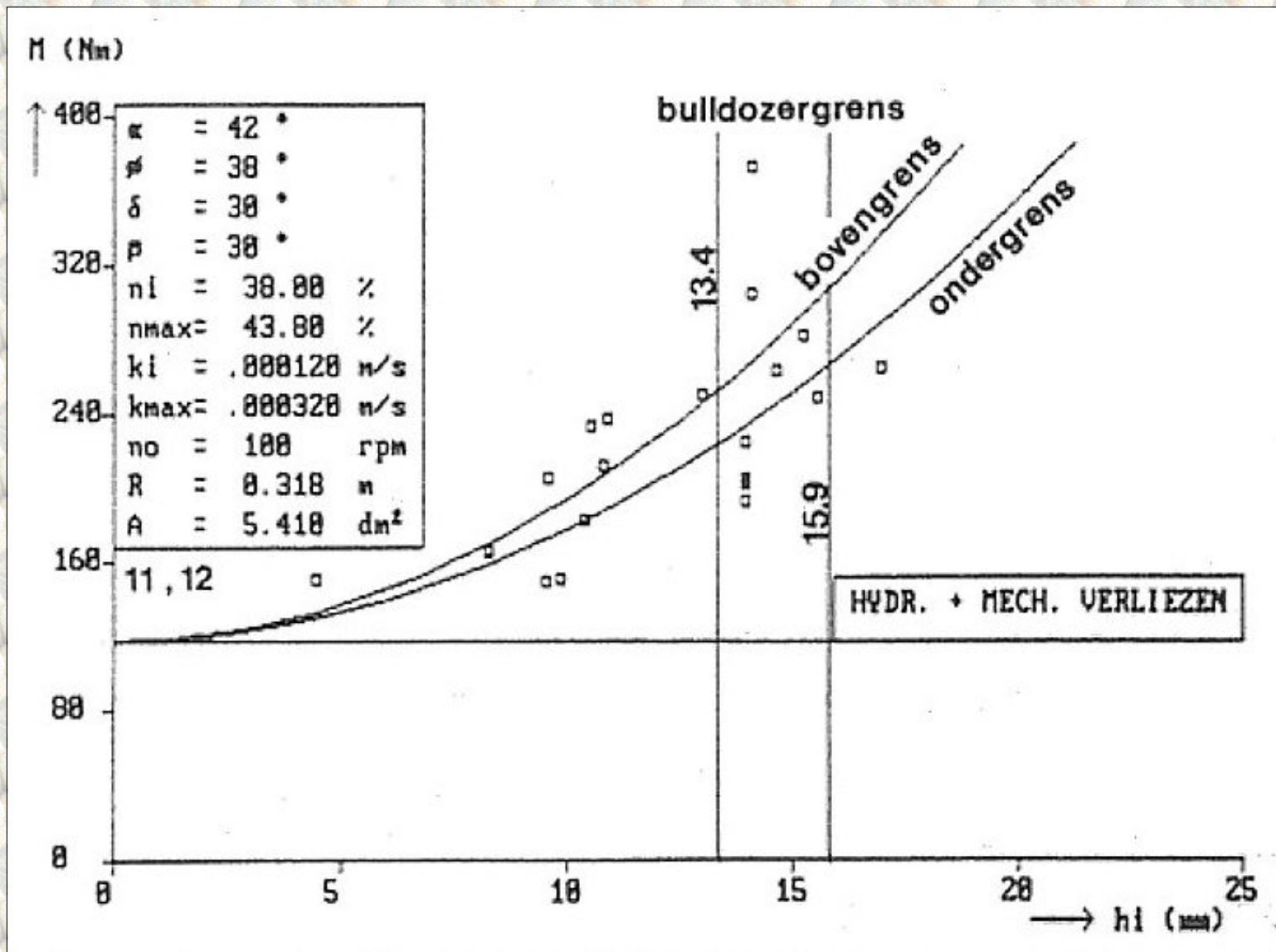


Figure 7.24: The drive torque M of the dredging wheel. Experiments in $200 \mu\text{m}$ sand, undercutting at 100 rpm and a cross sectional area A of 5.41 dm^2 . (bulldozergrans=bulldozer limit, bovengrens=upper limit, ondergrens=lower limit, verliezen=losses)

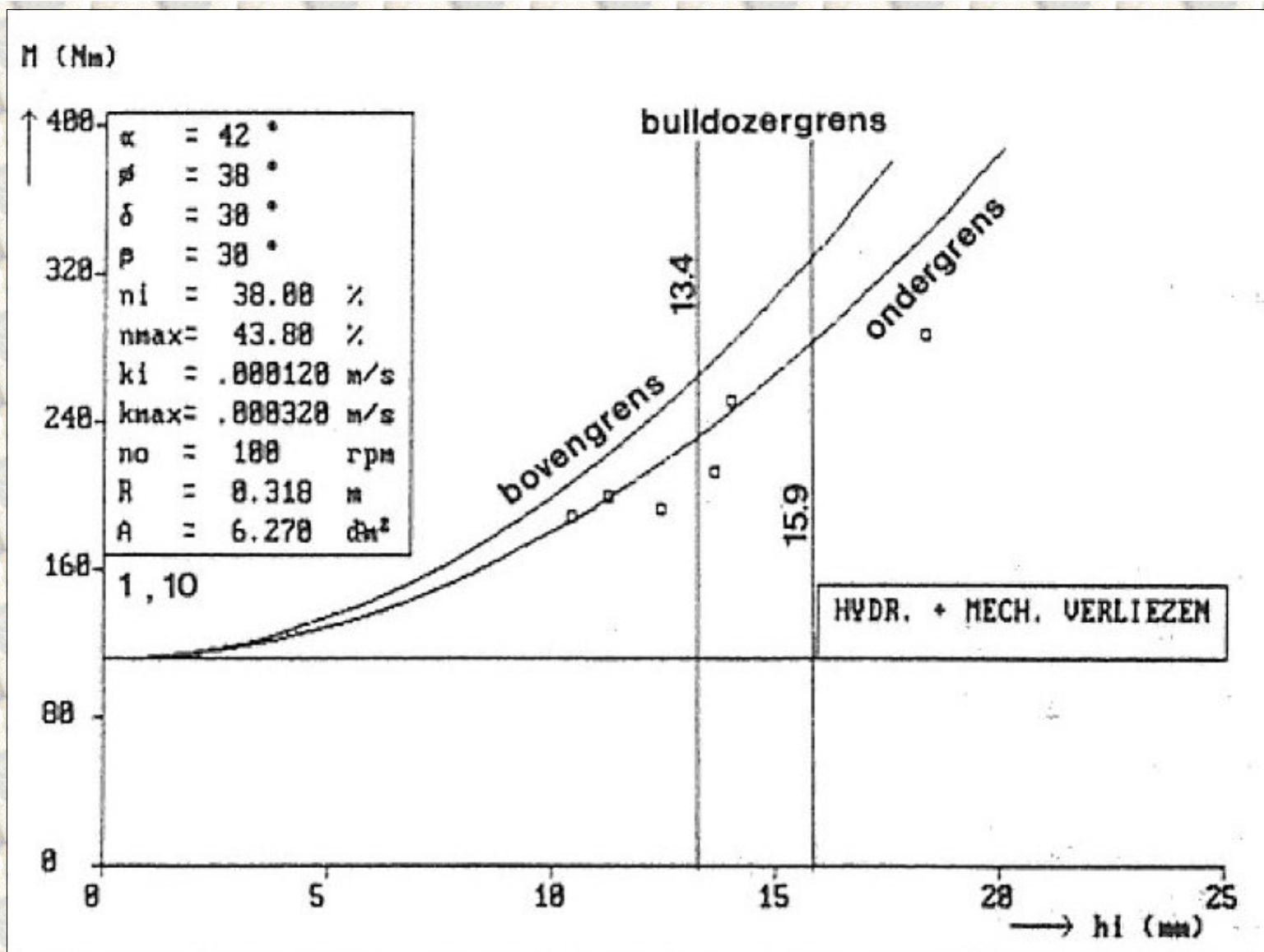


Figure 7.25: The drive torque M of the dredging wheel. Experiments in $200 \mu\text{m}$ sand, undercutting at 100 rpm and a cross sectional area A of 6.27 dm^2 . (bulldozergrrens=bulldozer limit, bovengrens=upper limit, ondergrens=lower limit, verliezen=losses)

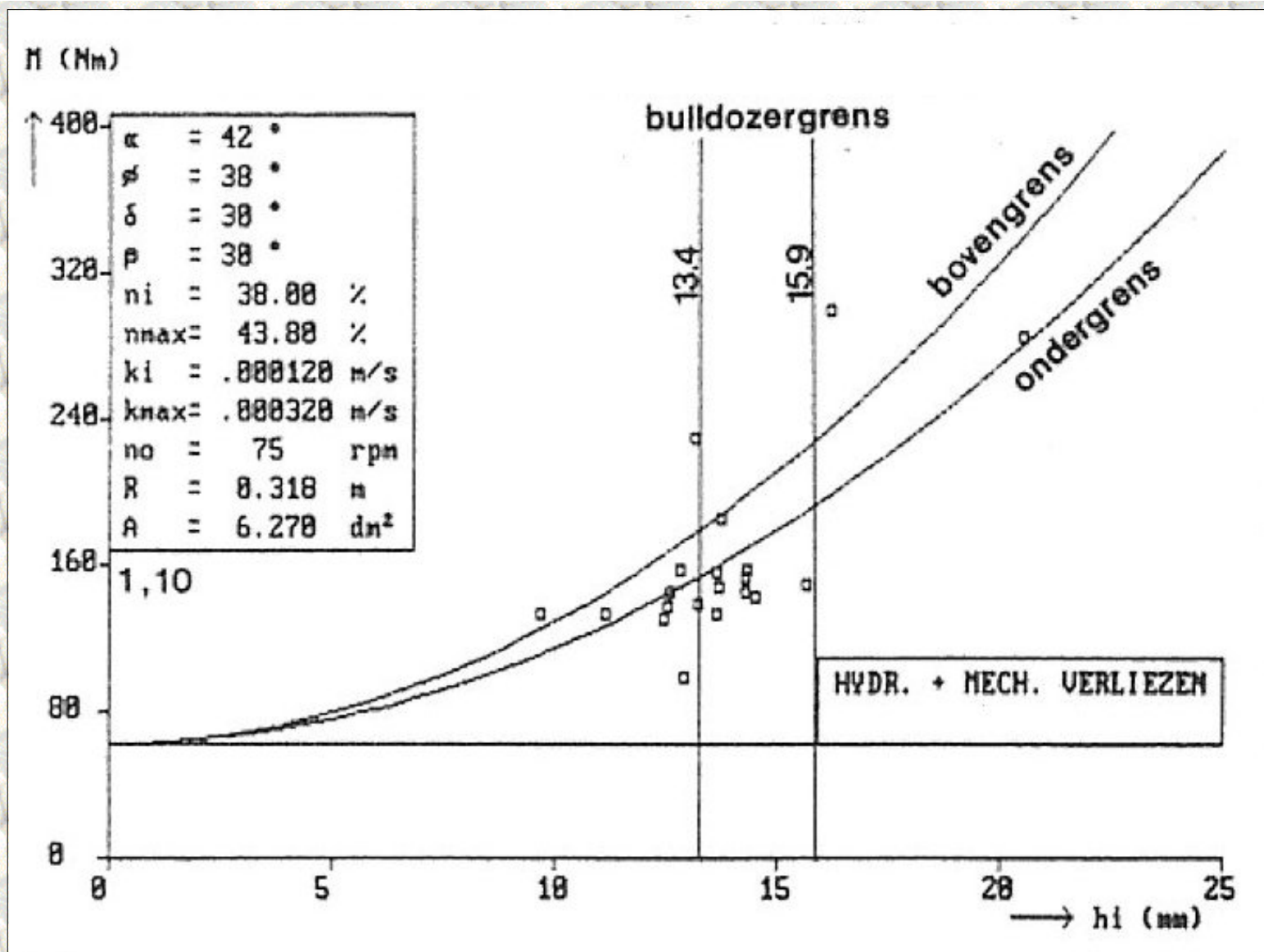


Figure 7.26: The drive torque M of the dredging wheel. Experiments in $200 \mu\text{m}$ sand, undercutting at 75 rpm and a cross sectional area A of 6.27 dm^2 . (bulldozergrens=bulldozer limit, bovengrens=upper limit, ondergrens=lower limit, verliezen=losses)

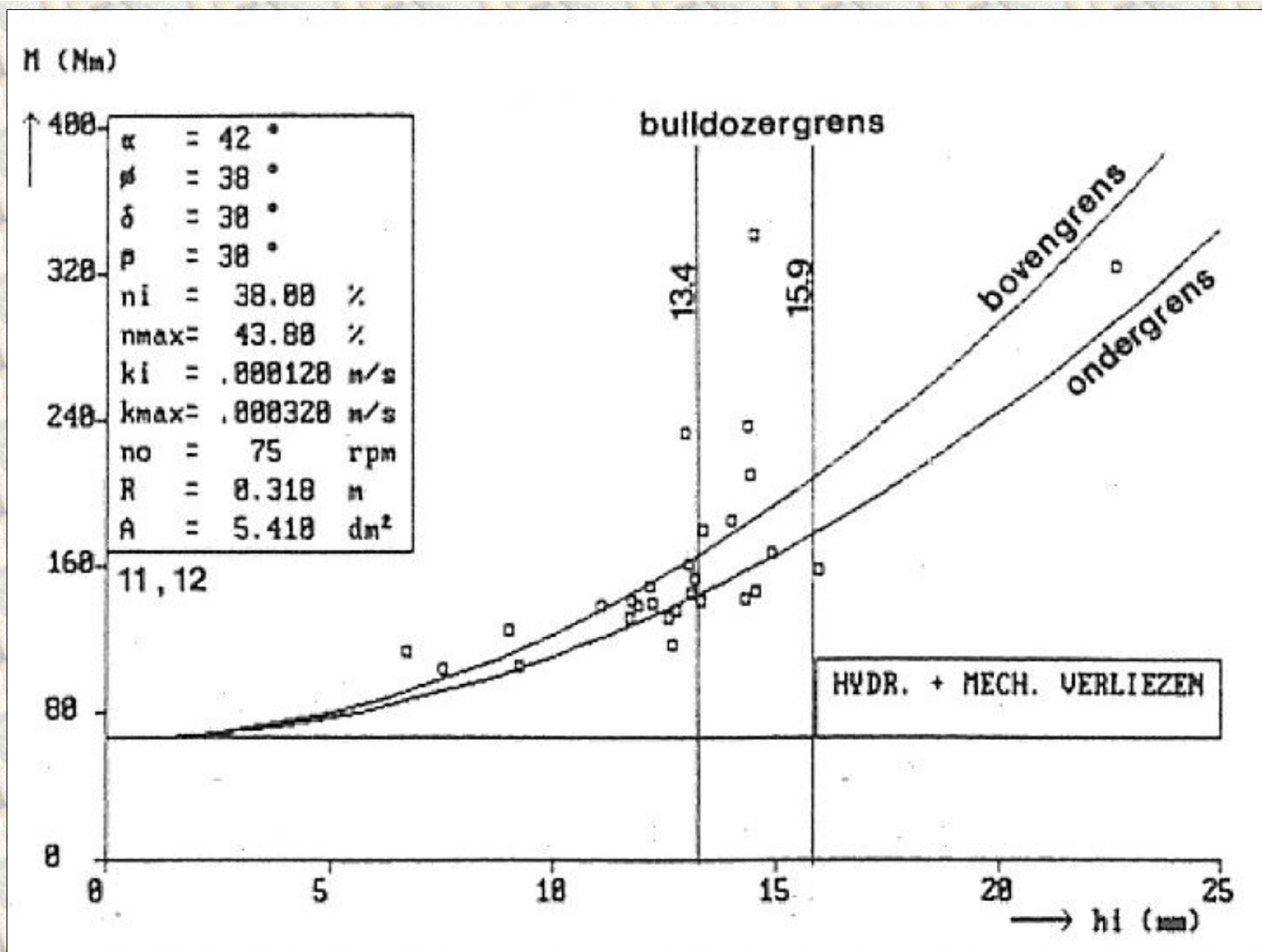


Figure 7.27: The drive torque M of the dredging wheel. Experiments in $200 \mu\text{m}$ sand, undercutting at 75 rpm and a cross sectional area A of 5.41 dm^2 . (bulldozergrens=bulldozer limit, bovengrens=upper limit, ondergrens=lower limit, verliezen=losses)

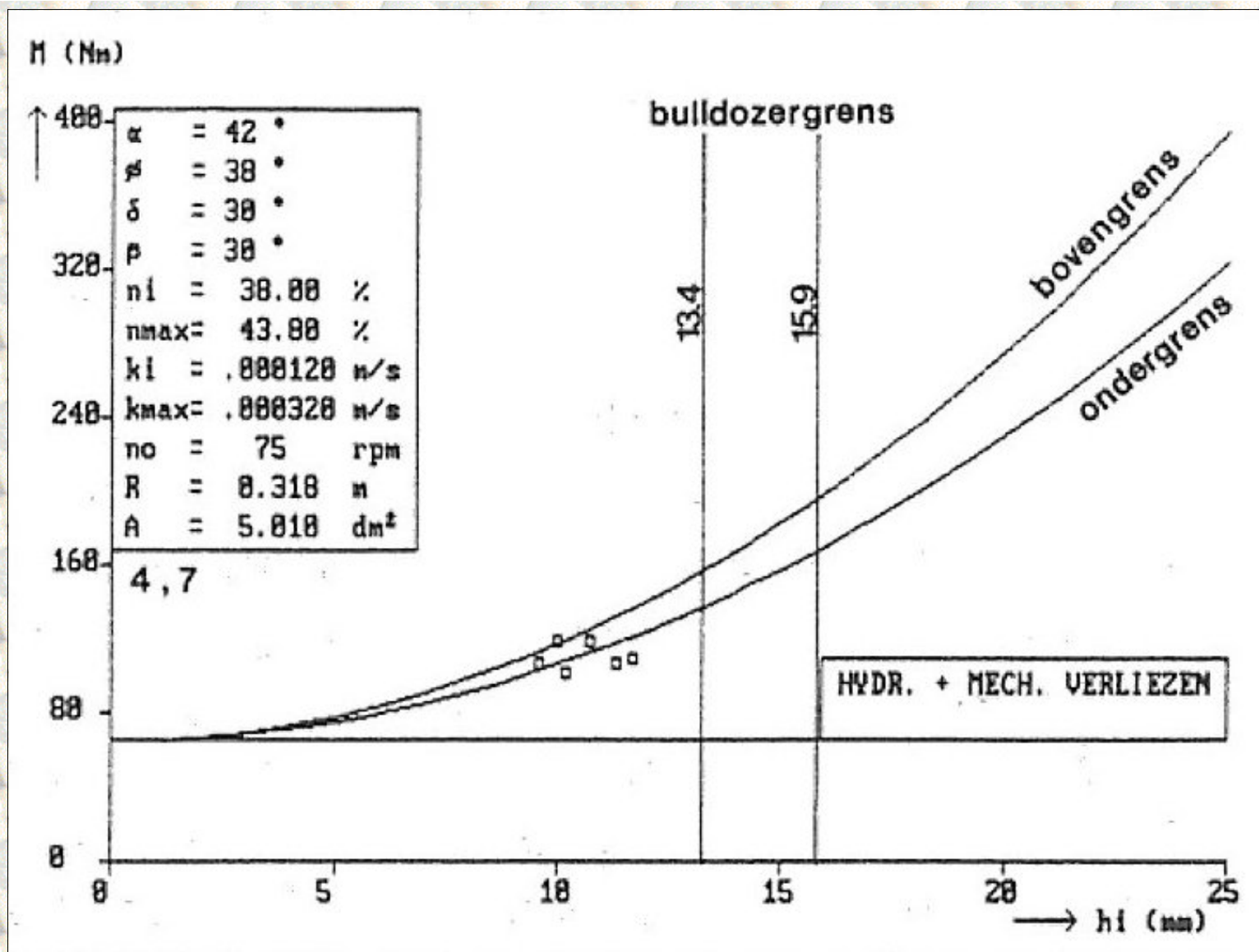


Figure 7.28: The drive torque M of the dredging wheel. Experiments in $200 \mu\text{m}$ sand, undercutting at 75 rpm and a cross sectional area A of 5.01 dm^2 . (bulldozergrrens=bulldozer limit, bovengrens=upper limit, ondergrens=lower limit, verliezen=losses)

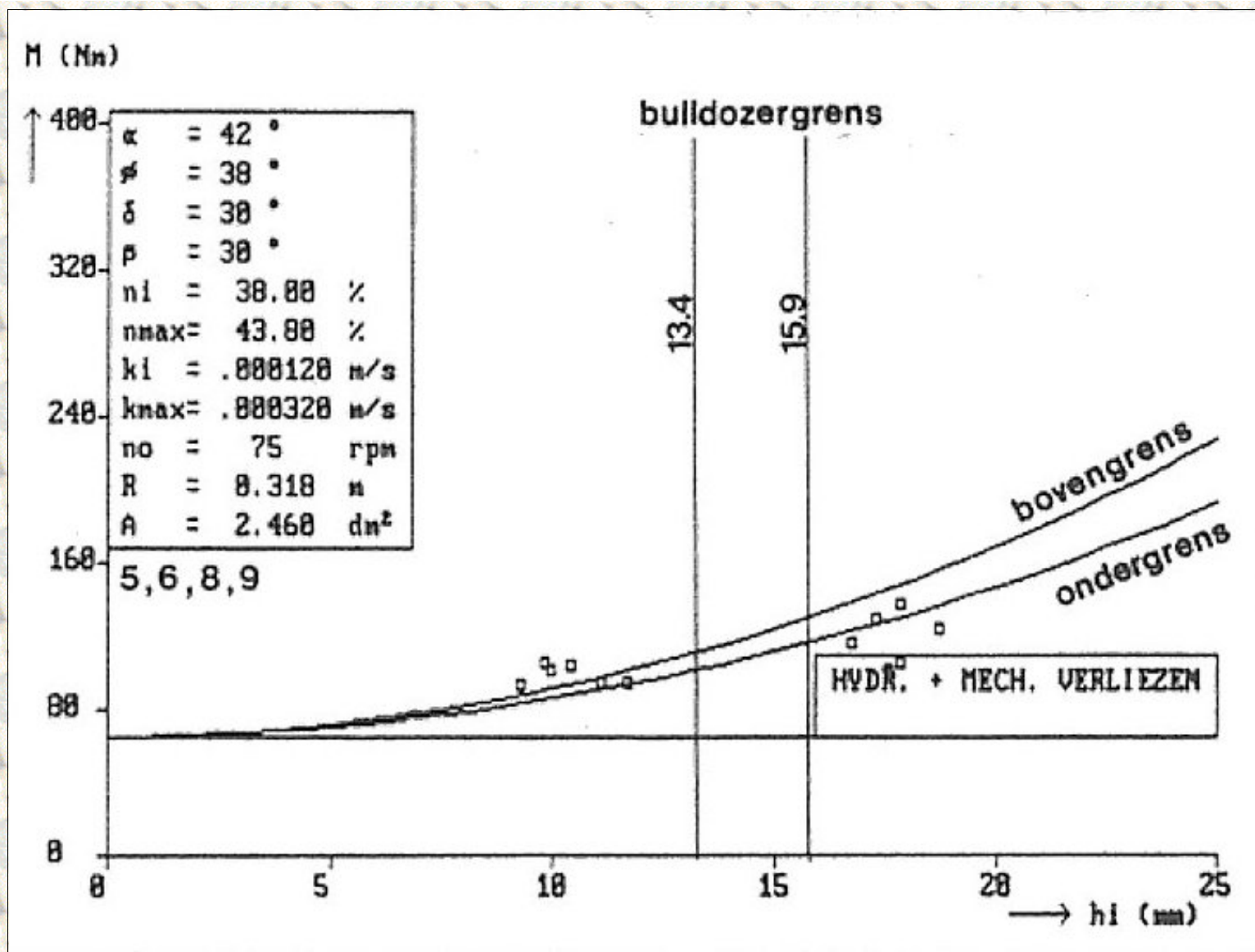


Figure 7.29: The drive torque M of the dredging wheel. Experiments in $200 \mu\text{m}$ sand, undercutting at 75 rpm and a cross sectional area A of 2.46 dm^2 . (bulldozer grens=bulldozer limit, bovengrens=upper limit, ondergrens=lower limit, verliezen=losses)

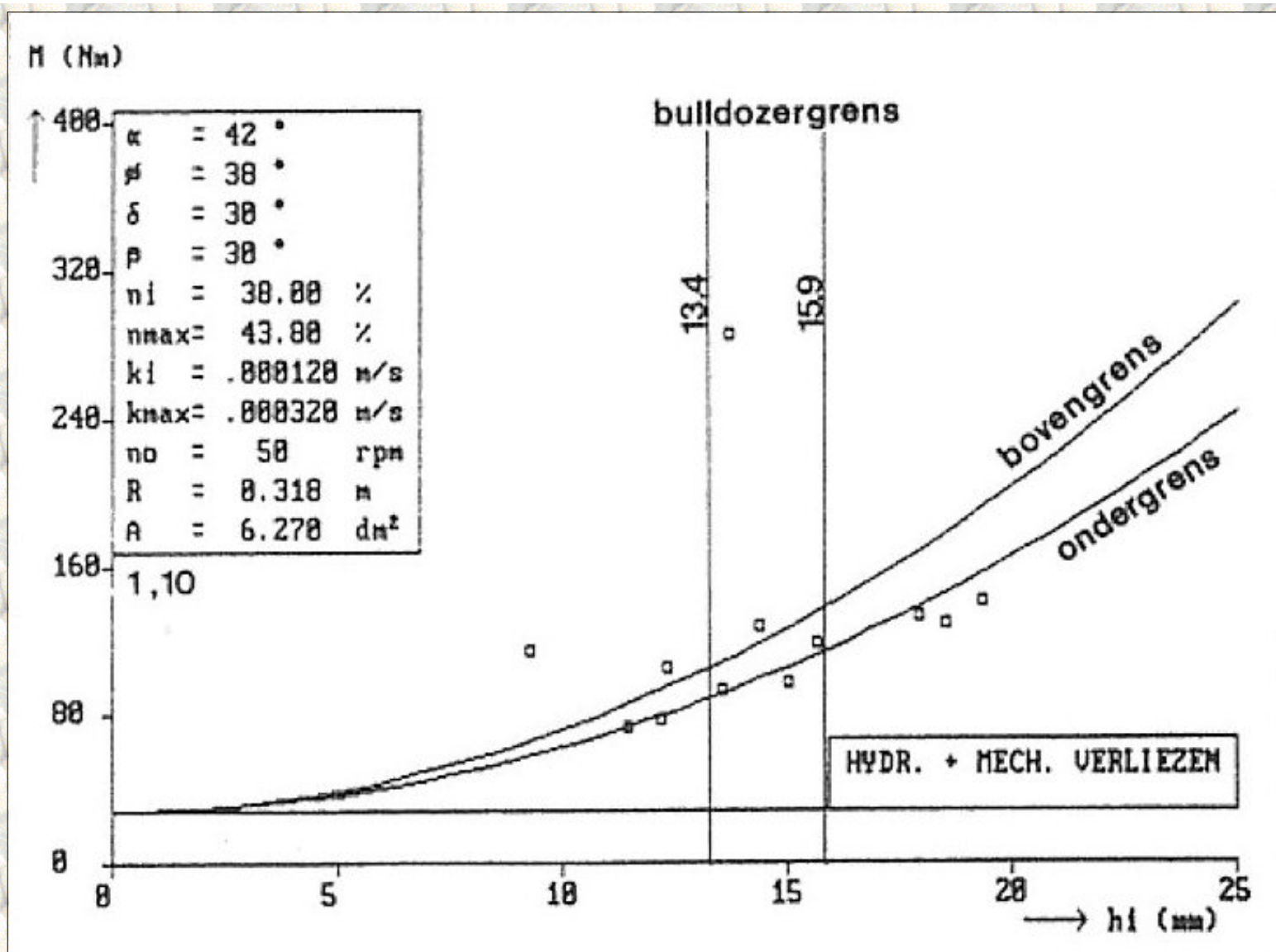


Figure 7.30: The drive torque M of the dredging wheel. Experiments in $200 \mu\text{m}$ sand, undercutting at 50 rpm and a cross sectional area A of 6.27 dm^2 . (bulldozergrens=bulldozer limit, bovengrens=upper limit, ondergrens=lower limit, verliezen=losses)

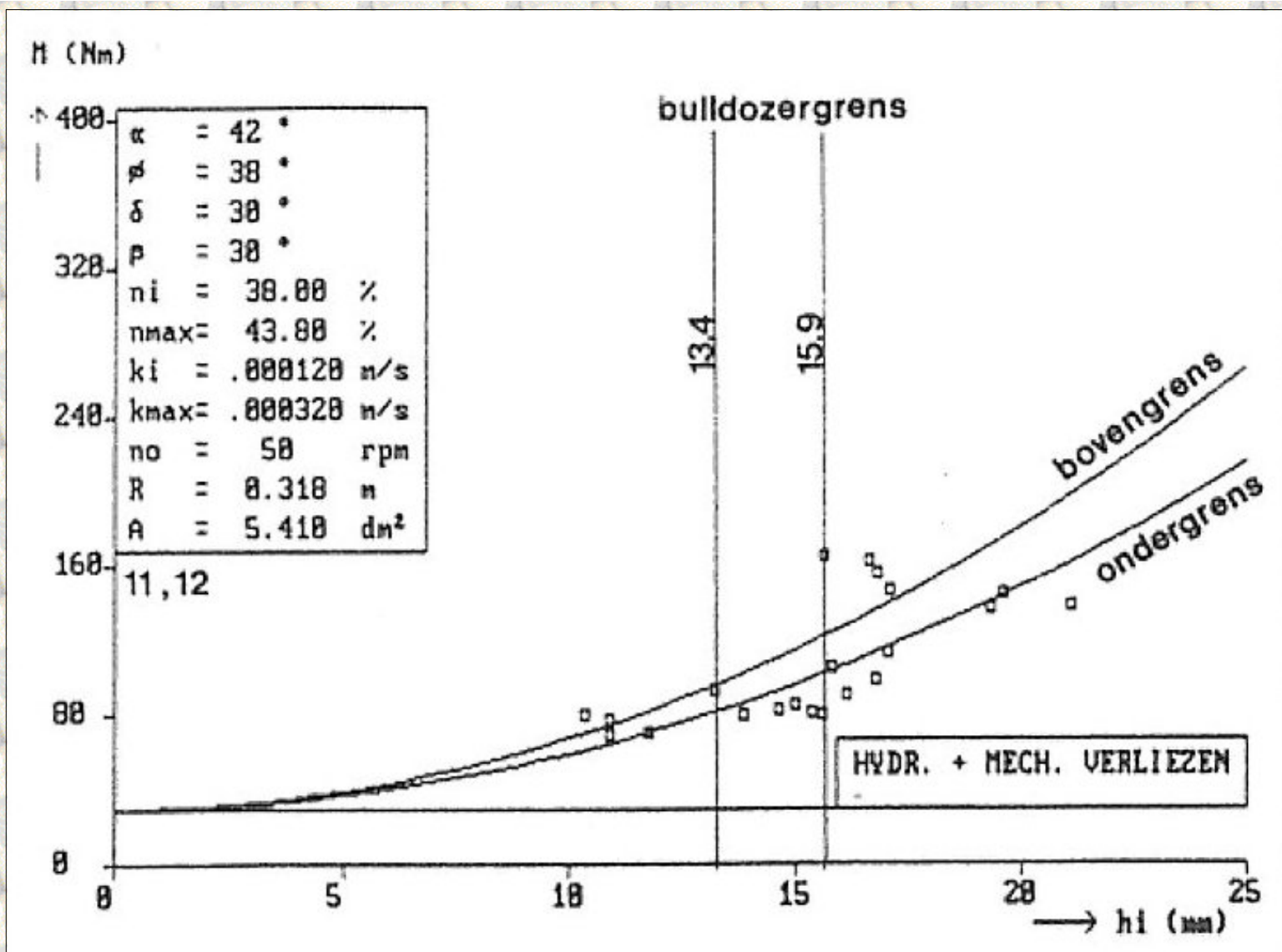


Figure 7.31: The drive torque M of the dredging wheel. Experiments in $200 \mu\text{m}$ sand, undercutting at 50 rpm and a cross sectional area A of 5.41 dm^2 . (bulldozergrrens=bulldozer limit, bovengrens=upper limit, ondergrens=lower limit, verliezen=losses)

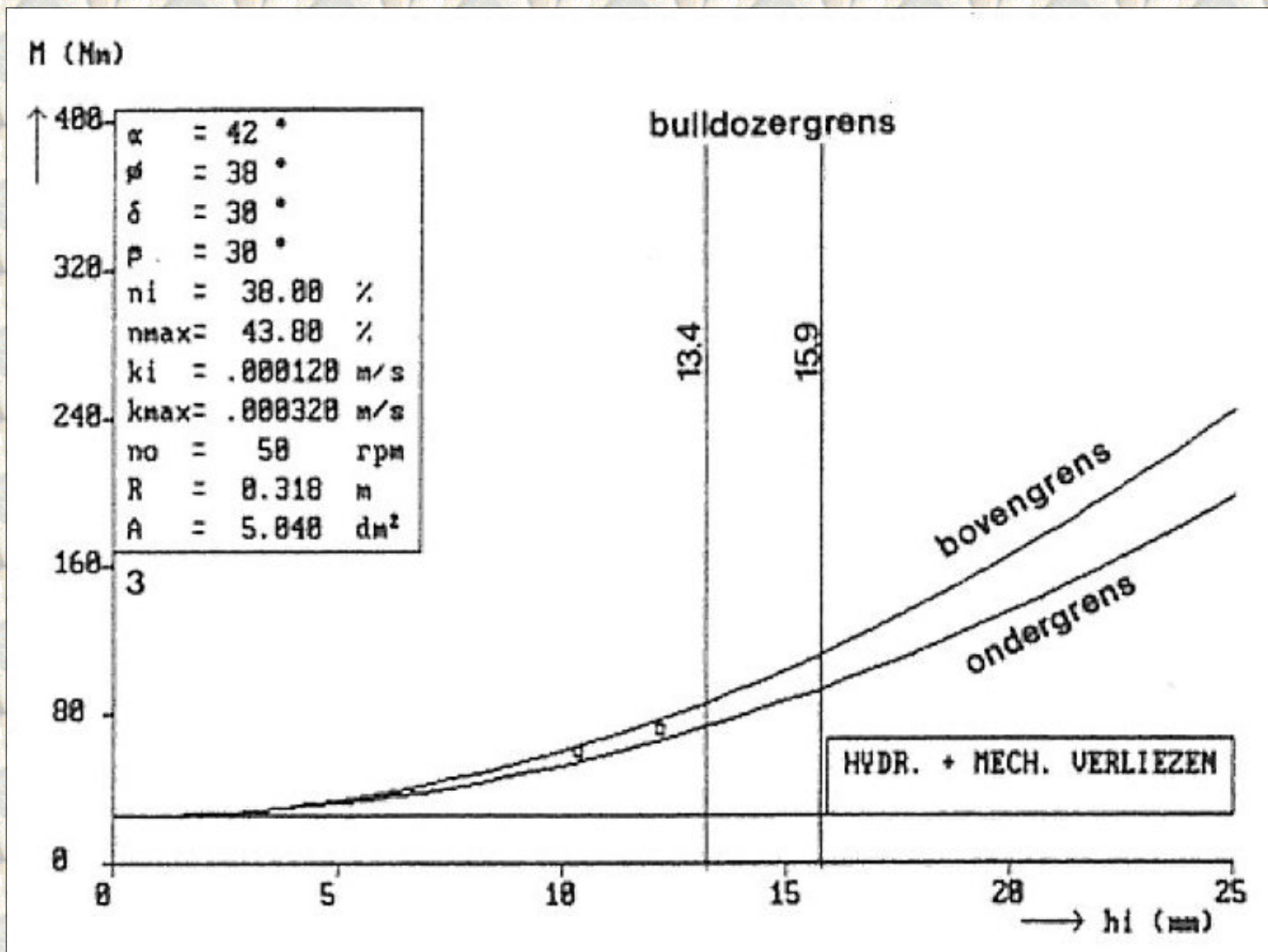


Figure 7.32: The drive torque M of the dredging wheel. Experiments in 200 μ m sand, undercutting at 50 rpm and a cross sectional area A of 5.04 dm². (bulldozergrens=bulldozer limit, bovengrens=upper limit, ondergrens=lower limit, verliezen=losses)

[Back to top](#)

This is a translation of the dissertation of Dr.ir. S.A. Miedema, dated September 15th 1987.

The dissertation was originally published in Dutch by the:

Delft University of Technology

Faculty of Mechanical Engineering and Marine Technology

Chair of Dredging Technology

Mekelweg 2

2628 CD, Delft

The Netherlands

It is advised to also read the papers following this dissertation, since the theory developed has been refined and extended.

Last modified Monday May 29, 2000 by: [Sape A. Miedema](#)

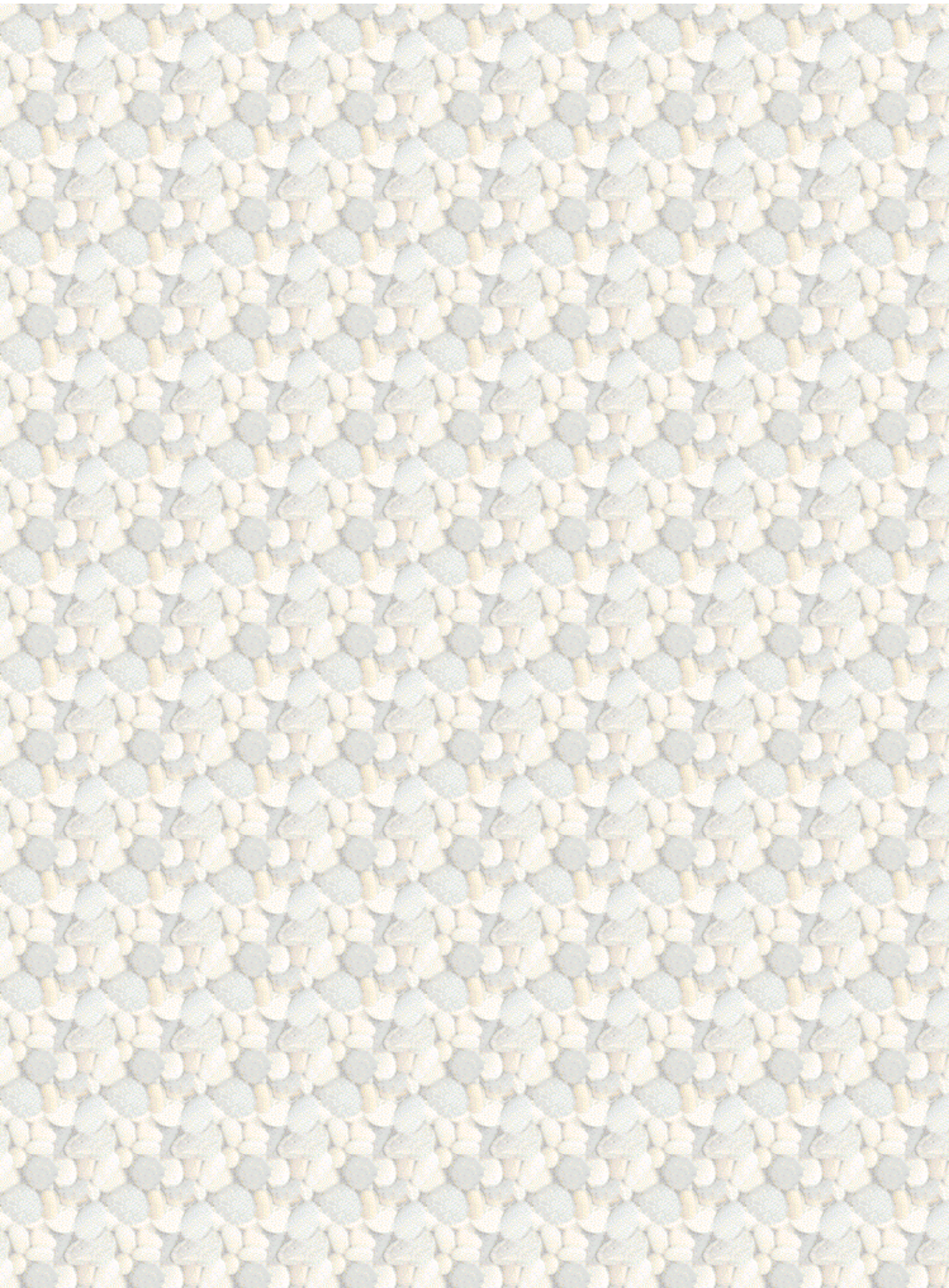
Translation by: [Laurens de Jonge](#)

Figures, equations and tables by: [Erik Miedema](#)

Copyright © May, 2000 Dr.ir. S.A. Miedema



[Download Adobe Acrobat Reader V4.0](#)



8.01 Introduction.

In chapter 4 and 5 the analytical models are derived for the determination of the forces and the driving torque on a cutterhead and a dredging wheel. In these models a few aspects of the cutting process are neglected, that is:

1. Inertia forces.
2. Gravity force.
3. Water resistance.
4. Cohesion and adhesion.
5. Side effects.
6. Wear and bluntness of the blades.

Besides the analytical models are only suitable for densely packed and water saturated sand. In this chapter a description is given of the momentary geometry of a three-dimensional moving blade element, of an arbitrary excavating element. This implies that with this description the course of the loads in time and space can be determined. The average loads on the excavating element can be determined by integrating the loads in time and space. The 6 above-mentioned aspects can be included in the numerical model, if a mathematical description is available. The loads for other types of soil (clay and rock) can in principle, also be determined with this method, if fundamental calculation methods become available for these types of soil

[Back to top](#)

This is a translation of the dissertation of Dr.ir. S.A. Miedema, dated September 15th 1987 .
The dissertation was originally published in Dutch by the:
Delft University of Technology
Faculty of Mechanical Engineering and Marine Technology
Chair of Dredging Technology
Mekelweg 2
2628 CD, Delft
The Netherlands

It is advised to also read the papers following this dissertation, since the theory developed has been refined and extended.

Last modified Monday May 29, 2000 by: [Sape A. Miedema](#)

Translation by: [Laurens de Jonge](#)

Figures, equations and tables by: [Erik Miedema](#)

Copyright © May, 2000 [Dr.ir. S.A. Miedema](#)



[Download Adobe Acrobat Reader V4.0](#)

8.02 Definitions.

For the numerical forces model a vector space has to be defined in which blade elements, velocities and forces are represented by vectors. Because it is impossible to define a blade element simply as a rectangular plane for the three-dimensional blades, the following solution is chosen:

A blade is defined by two space curves, that is the blade edge (cutting edge) and the backside of the blade plane (figure 8.1). These space curves are discretized in the model by a number of points along the curves, connected with straight lines. In figure 8.1 a side view and a top view of a cutterhead are shown. A point along the blade edge is defined by a radius r_i , a height H_i and a sweep angle sw_i , similar to a point on the back side of the cutting plane of the blade, where the cut sand leaves the blade. A blade element is defined as the distance between two points along the blade edge. The coordinates of a point can be determined with the following three equations:

$$x_i = r_i \cdot \cos(sw_i) \quad (8.1)$$

$$y_i = r_i \cdot \sin(sw_i) \quad (8.2)$$

$$z_i = H_i \quad (8.3)$$

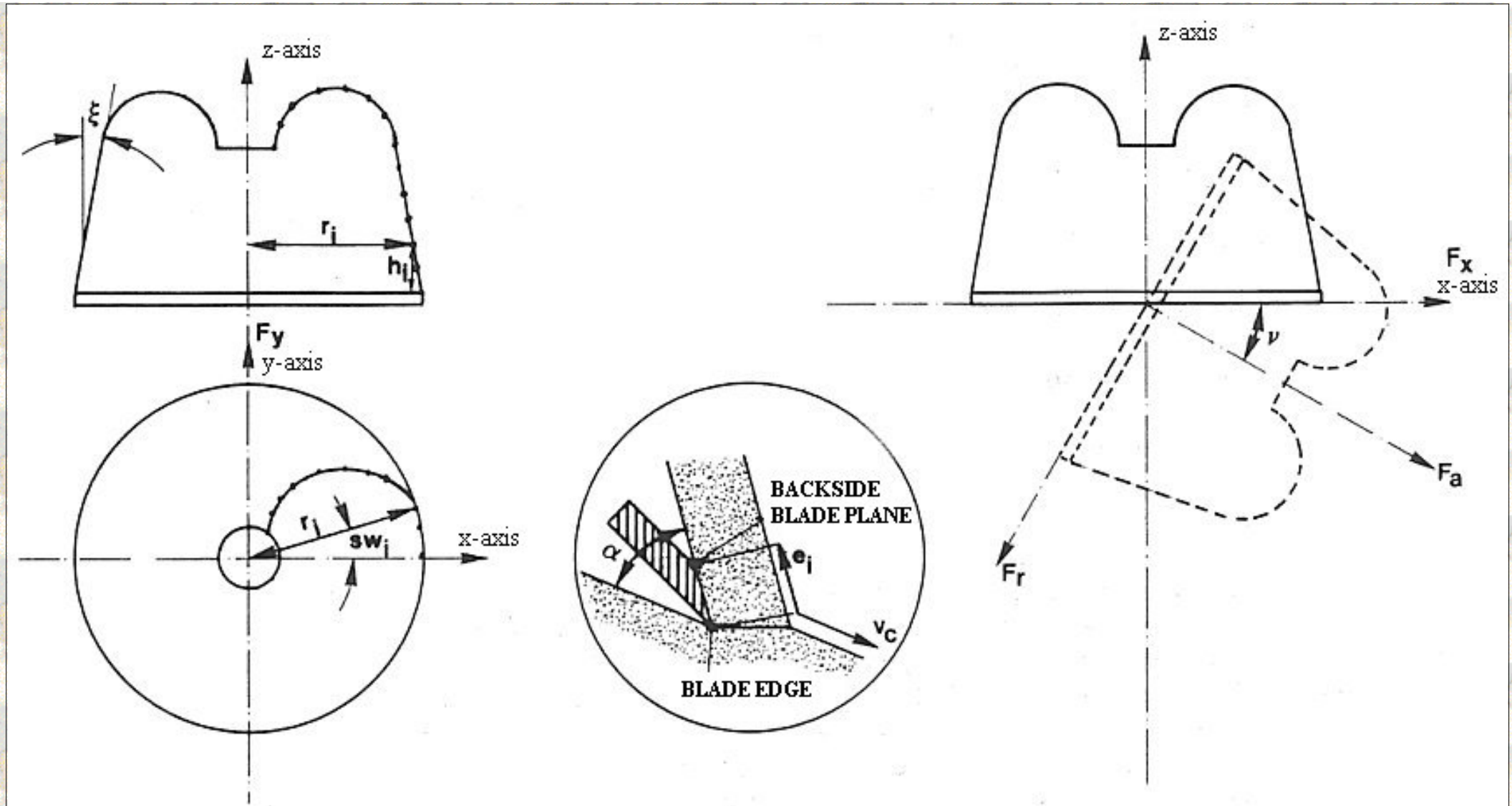


Figure 8.1: Definition of points along the edge of the blade and the backside of the blade plane.

In the next equations a point or vector is represented by a lower-case letter, e.g. a_i , where the index k represents the direction ($k = 1 = x, 2 = y$ en $3 = z$). The indices i or j indicate the serial number of the point or element. The following vectors can now be defined:

a_i - radius vector of a point along the blade edge

b_i - direction vector along the blade edge

c_j - radius vector of a point along the back side of the blade plane

d_j - direction vector along the back side of the blade plane

e_i - direction vector perpendicular to the blade edge to the blade plane

The relations between these vectors are as follows:

$$\vec{b}_i = \vec{a}_{i+1} - \vec{a}_i \quad (8.4)$$

and

$$\vec{d}_j = \vec{c}_{j+1} - \vec{c}_j \quad (8.5)$$

The vector e_i is determined as follows:

The vector b_i is the normal vector on an auxiliary plane in the point, of which a_i is the radius vector. Those coefficients c_j en d_j have to be looked for, for which d_j intersects the plane. This intersection point lies between c_j en c_{j+1} . This can be represented in vectors by:

$$\vec{p}_i = \vec{c}_j + f \cdot \vec{d}_j \quad (8.6)$$

Where the scalar f needs to have a value between 0 and 1. The earlier mentioned plane has the vector representation:

$$\vec{b}_i \cdot \vec{p}_i = \vec{b}_i \cdot \vec{a}_i \quad (8.7)$$

Eliminating the vector \vec{p}_i derives:

$$f = \frac{\vec{a}_i \cdot \vec{b}_i - \vec{b}_i \cdot \vec{c}_j}{\vec{b}_i \cdot \vec{d}_j} \quad (8.8)$$

thus:

$$\vec{e}_i = \vec{p}_i - \vec{a}_i = \vec{c}_j + f \cdot \vec{d}_j - \vec{a}_i \quad (8.9)$$

These vectors are indicated in figure 8.2.

A blade element is now fixed by the point \vec{a}_i and the direction vector \vec{b}_i along the blade edge and \vec{e}_i perpendicular to that (height direction).

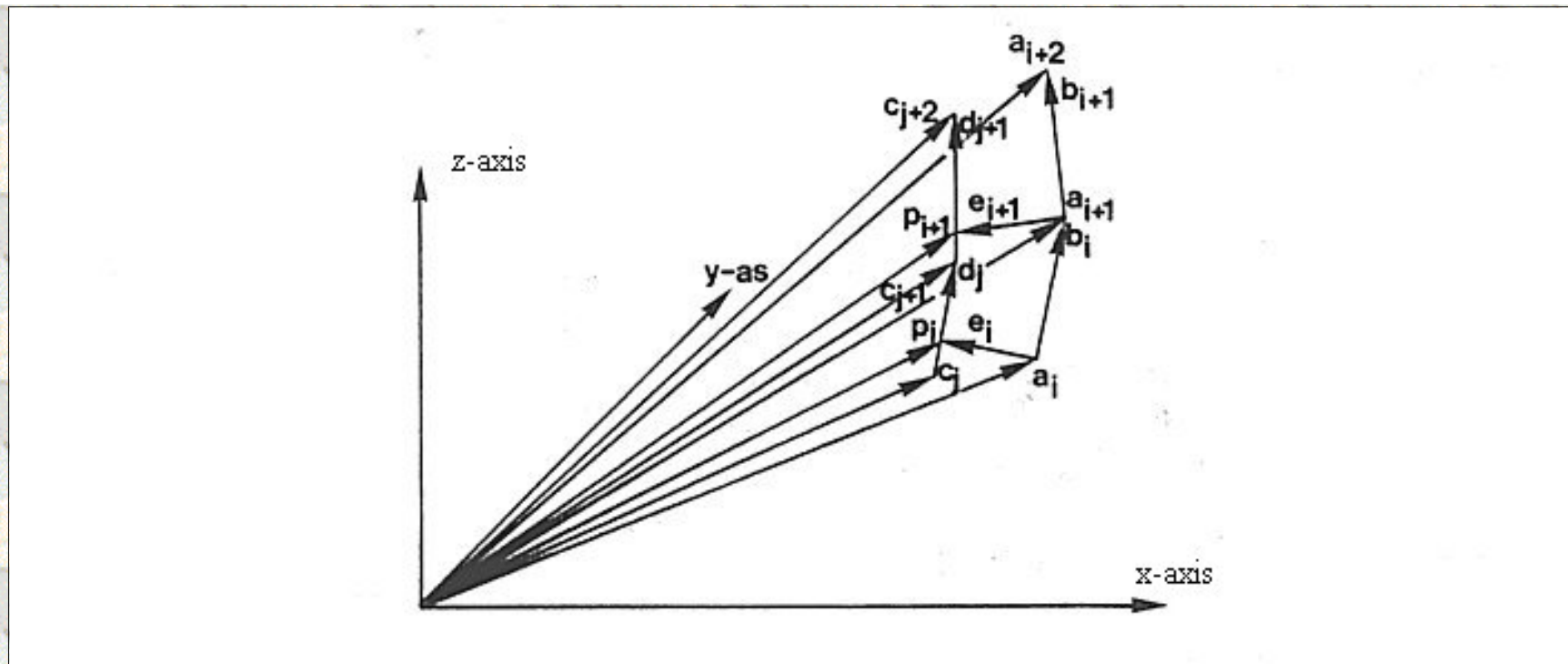


Figure 8.2: The vectors describing a blade element.

a_i , b_i and a_{i+1} the blade edge (cutting edge).

c_j , d_j and c_{j+1} the backside of the blade.

e_i the direction perpendicular on the blade edge.

p_i auxiliary vector

[Back to top](#)

This is a translation of the dissertation of Dr.ir. S.A. Miedema, dated September 15th 1987 .

The dissertation was originally published in Dutch by the:

Delft University of Technology

Faculty of Mechanical Engineering and Marine Technology

Chair of Dredging Technology

Mekelweg 2

2628 CD, Delft

The Netherlands

It is advised to also read the papers following this dissertation, since the theory developed has been refined and extended.

Last modified Monday May 29, 2000 by: [Sape A. Miedema](#)

Translation by: [Laurens de Jonge](#)

Figures, equations and tables by: [Erik Miedema](#)

Copyright © May, 2000 Dr.ir. S.A. Miedema



[Download Adobe Acrobat Reader V4.0](#)

8.03 Transformations.

The direction vectors have to be transformed to determine the forces for a certain time and with a certain ladder angle. The direction vectors used so far are in a coordinate system with the excavation element placed in the ring as in figure 8.3. If the excavation element has run-through an angle Ω , a rotation around the z-axis, the next transformation is used:

$$x_t = x \cdot \cos(\Omega) - y \cdot \sin(\Omega) \quad (8.10)$$

$$y_t = x \cdot \sin(\Omega) + y \cdot \cos(\Omega) \quad (8.11)$$

$$z_t = z \quad (8.12)$$

The transformation to the ladder angle ν (figure 8.1), a rotation around the y-axis, gives:

$$x_{tt} = x_t \cdot \cos(\pi/2 + \nu) + z_t \cdot \sin(\pi/2 + \nu) \quad (8.13)$$

$$y_{tt} = y_t \quad (8.14)$$

$$z_{tt} = z_t \cdot \cos(\pi/2 + \nu) - x_t \cdot \sin(\pi/2 + \nu) \quad (8.15)$$

The concerned vectors will be, like b_i , indicated with the index "tt" to indicate that the transformed coordinate system is used.

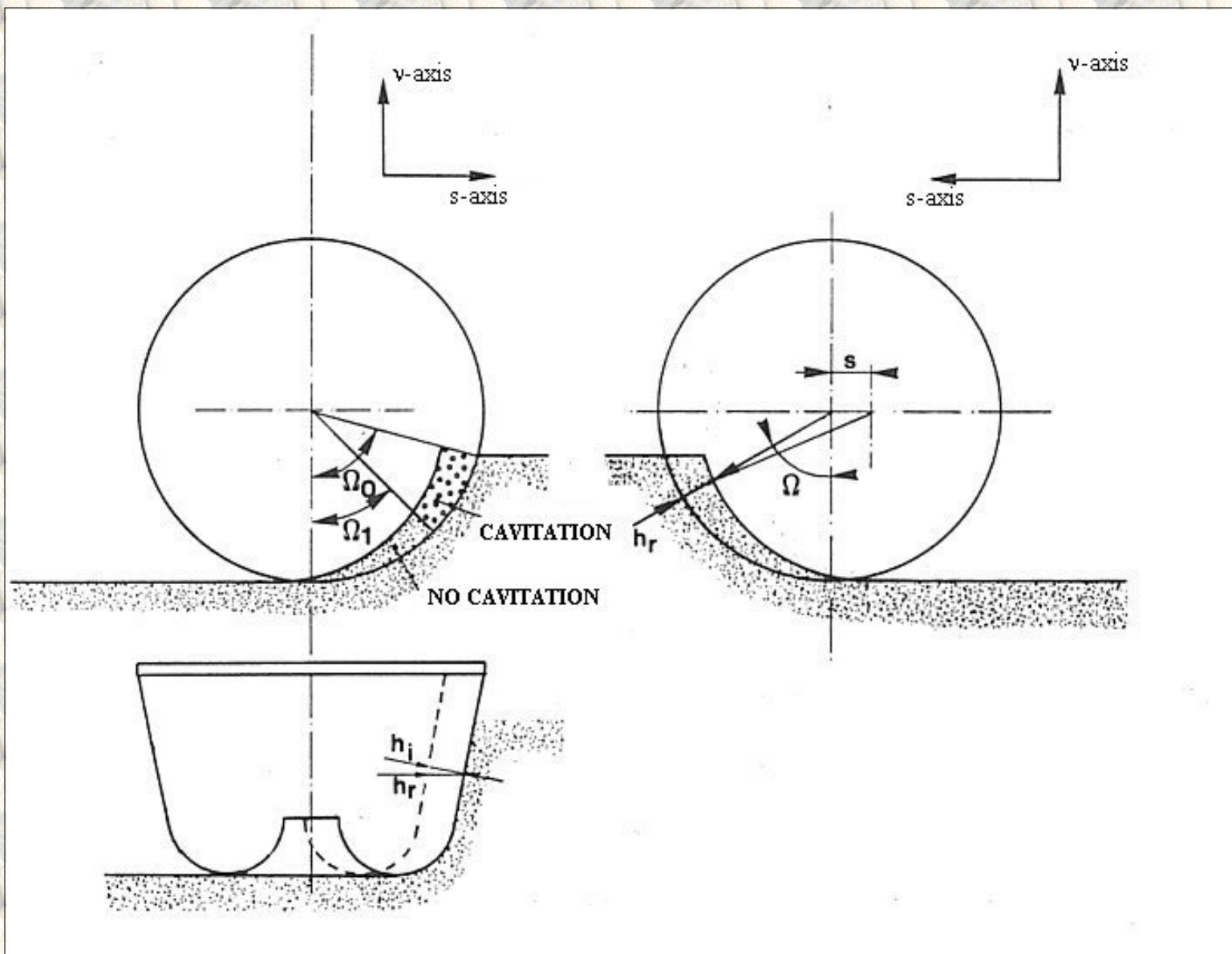


Figure 8.3: Definition of Ω , Ω_0 and Ω_1 and the layer thicknesses h_i and h_r .

[Back to top](#)

This is a translation of the dissertation of Dr.ir. S.A. Miedema, dated September 15th 1987 .

The dissertation was originally published in Dutch by the:
Delft University of Technology
Faculty of Mechanical Engineering and Marine Technology
Chair of Dredging Technology
Mekelweg 2
2628 CD, Delft
The Netherlands

It is advised to also read the papers following this dissertation, since the theory developed has been refined and extended.

Last modified Monday May 29, 2000 by: [Sape A. Miedema](#)

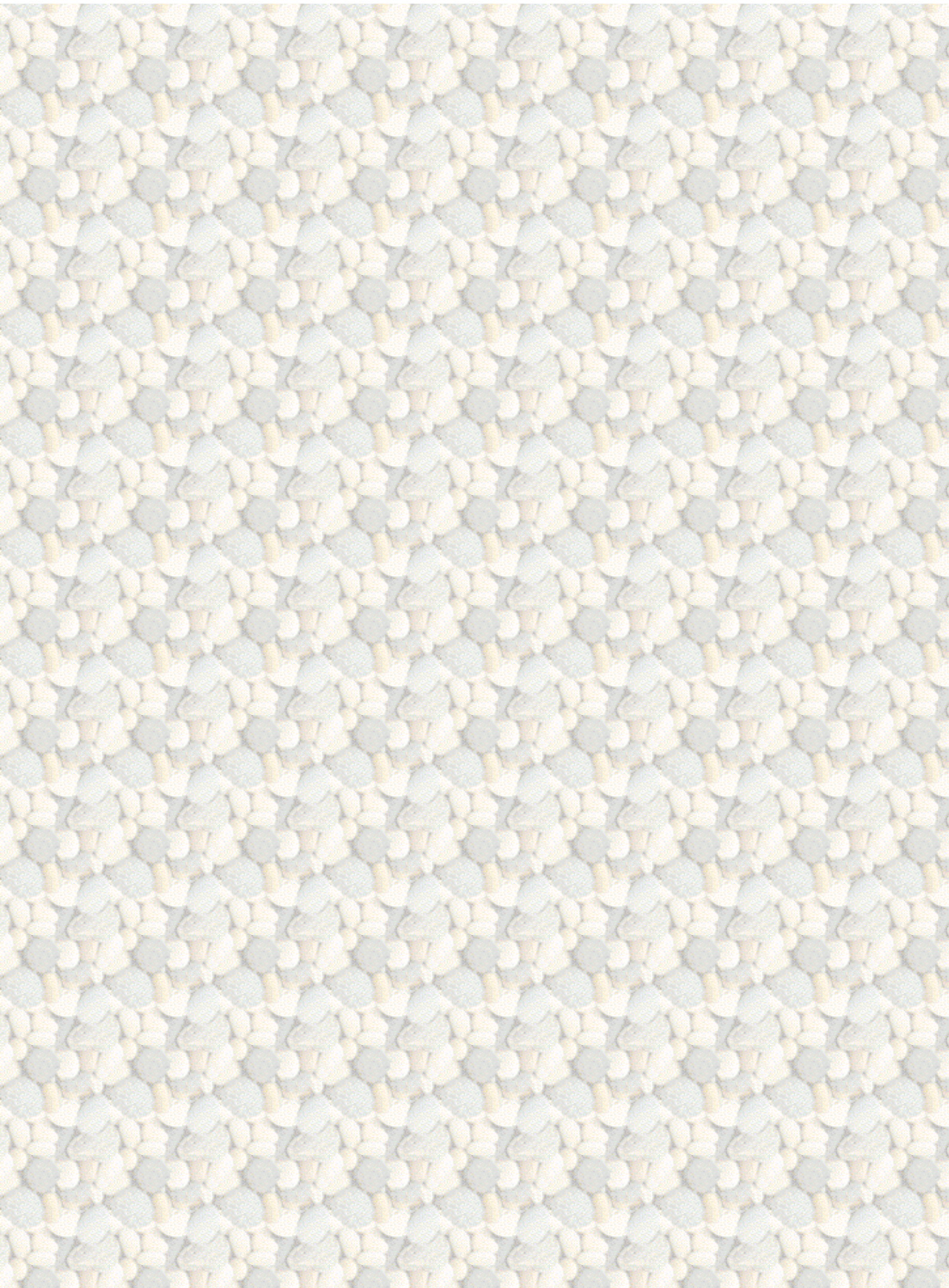
Translation by: [Laurens de Jonge](#)

Figures, equations and tables by: [Erik Miedema](#)

Copyright © May, 2000 Dr.ir. S.A. Miedema



[Download Adobe Acrobat Reader V4.0](#)



8.04 Velocity vectors.

For the peripheral velocity of the cutterhead can be written:

$$\vec{V}_{ci} = \frac{2 \cdot \pi \cdot n_0 \cdot \vec{r}_i}{60} = \omega \cdot \vec{r}_i \quad (8.16)$$

The transformation to the run-through angle Ω , a rotation around the z-axis, gives:

$$V_{xt} = -V_{ci} \cdot \sin(\Omega + \text{sw}_i) \quad (8.17)$$

The haul velocity v_s has to be added to the velocity component in the y-direction (haul direction):

$$V_{yt} = +V_{ci} \cdot \cos(\Omega + \text{sw}_i) + V_s \quad (8.18)$$

The axial velocity v_{ax} has to be added to the velocity component in the z-direction (axial direction):

$$V_{zt} = V_{ax} \quad (8.19)$$

The second transformation of the ladder angle ν , a rotation around the y-axis, gives:

$$V_{xtt} = +V_{xt} \cdot \cos(\pi/2 + \nu) + V_{zt} \cdot \sin(\pi/2 + \nu) \quad (8.20)$$

$$V_{ytt} = +V_{yt} \quad (8.21)$$

$$V_{ztt} = -V_{xt} \cdot \sin(\pi/2 + \nu) + V_{zt} \cdot \cos(\pi/2 + \nu) \quad (8.22)$$

To work with an average situation over an element the radius r_i and the sweep angle sw_i are averaged over an element. The total direction vector will from now on be indicated with \vec{v}_t . Now the momentary direction vectors of the blade element and the momentary velocity vector are known. To determine the cutting forces the velocities perpendicular to and along the blade edge have to be known. The velocity component along the blade edge is:

$$\vec{v}_1 = \frac{\vec{b}_{tt,i} \cdot \vec{v}_t}{|\vec{b}_{tt,i}|} \vec{b}_{tt,i} \quad (8.23)$$

The velocity component perpendicular to the blade edge is now:

$$\vec{v}_c = \vec{v}_t - \vec{v}_1 \quad (8.24)$$

[Back to top](#)

This is a translation of the dissertation of Dr.ir. S.A. Miedema, dated September 15th 1987 .
 The dissertation was originally published in Dutch by the:
Delft University of Technology
Faculty of Mechanical Engineering and Marine Technology
Chair of Dredging Technology
Mekelweg 2
2628 CD, Delft
The Netherlands

It is advised to also read the papers following this dissertation, since the theory developed has been refined and extended.

Last modified Monday May 29, 2000 by: [Sape A. Miedema](#)

Translation by: [Laurens de Jonge](#)

Figures, equations and tables by: [Erik Miedema](#)

Copyright © May, 2000 Dr.ir. S.A. Miedema



[Download Adobe Acrobat Reader V4.0](#)

8.05 Layer thickness, blade angle and blade height.

For the determination of the layer-thickness a subdivision has to be made between the radial (cutterhead) and axial (dredging wheel) cutting process. A derivation for the layer-thickness for the radial cutting process follows first:

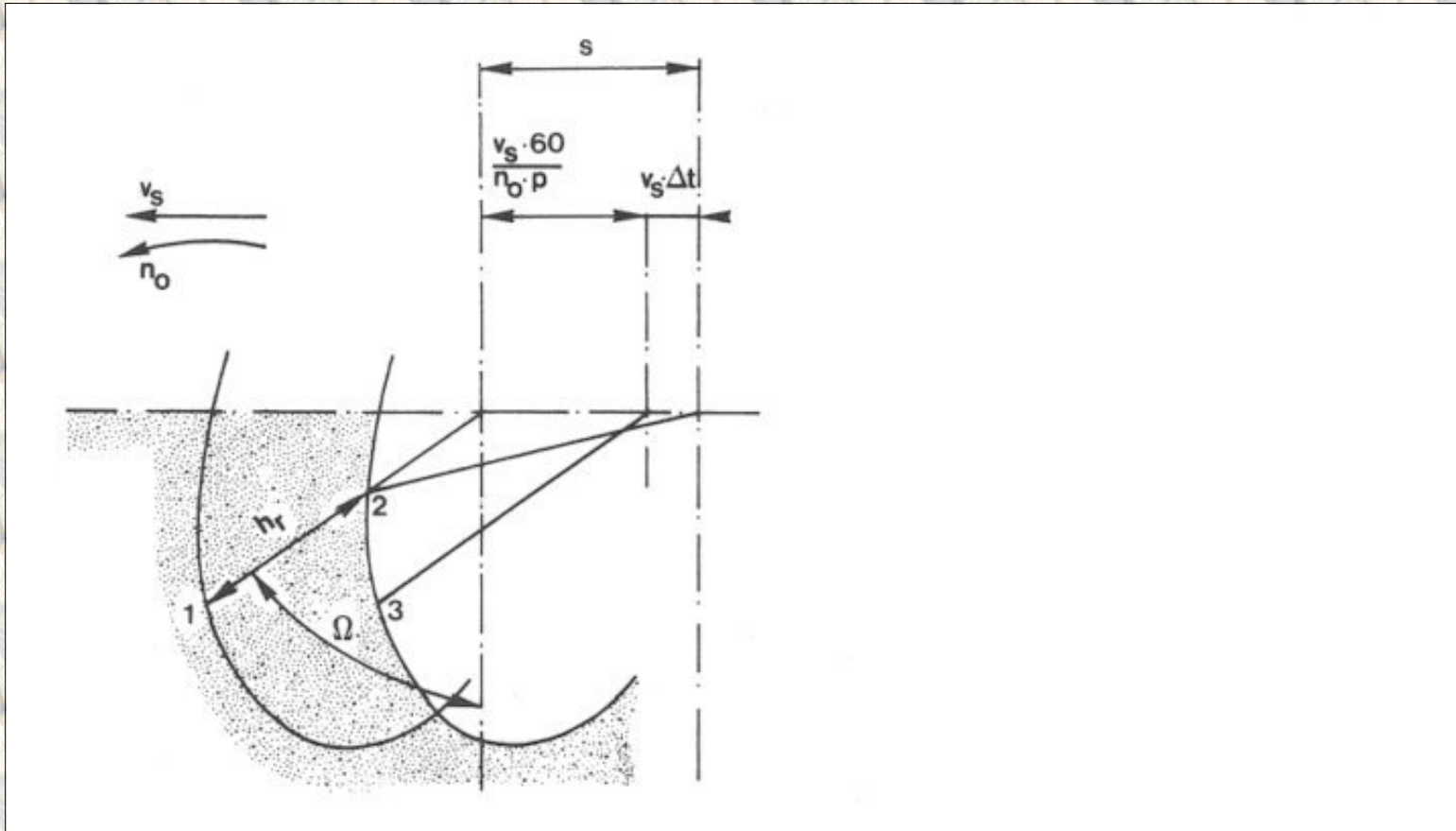


Figure 8.4: The radial layer thickness.

The time needed to go from 2 to 3, if translation and rotation are accounted for:

$$\Delta t = \frac{v_s \cdot 60}{n_o \cdot p} \cdot \left(\frac{\cos(\Omega)}{\omega \cdot r_1 - v_s \cdot \cos(\Omega)} \right)$$

With:

$$S = v_s \cdot \Delta t + \frac{v_s \cdot 60}{n_o \cdot p}$$

The momentary radial layer-thickness can be determined with the following equation, according figure 8.4:

$$S = \frac{v_s \cdot 2 \cdot \pi}{\omega \cdot p} \cdot \left(\frac{\omega \cdot r_1}{\omega \cdot r_1 - v_s \cdot \cos(\Omega)} \right) \quad (8.25)$$

In which s is the distance covered by the excavation element since the passage of the previous blade (under cutting $v_s < 0$, over cutting $v_s > 0$). For the radial layer-thickness h_r can now be derived (see also equation (5.4)):

$$h_r = s \cdot \sin(\Omega) + r_1 \cdot \left[1 - \sqrt{1 - \cos^2(\Omega) \cdot \frac{s^2}{r_1^2}} \right] \quad (8.26)$$

This layer-thickness is indicated in figure 8.3 and will be corrected for the curvature angle ξ according to:

$$h_{ir} = h_r \cdot \cos(\xi) \quad (8.27)$$

The axial layer-thickness h_a for the axial cutting process can be described as:

$$h_a = \frac{v_{ax} \cdot 60}{n_o \cdot p} \cdot \frac{v_{ci}}{\sqrt{(v_{ci}^2 + v_{ax}^2)}} \quad (8.28)$$

with:

$$v_{ci} = \frac{2\pi \cdot n_o \cdot r_1}{60} \quad (8.29)$$

The axial layer-thickness is corrected for the curvature angle ξ according:

$$h_{ia} = h_a \cdot \sin(\xi) \quad (8.30)$$

The total layer-thickness can now be determined by summing the radial and the axial layer-thickness:

$$h_i = h_{ir} + h_{ia} \quad (8.31)$$

For the dynamic blade angle can be derived (see figure 8.1):

$$a' = -\arccos \left(\frac{\vec{v}_c \cdot \vec{e}_{tt,i}}{|\vec{v}_c| |\vec{e}_{tt,i}|} \right) \quad (8.32)$$

The blade height is:

$$h_b = |\vec{e}_{tt,i}| \sin(\alpha) \quad (8.33)$$

[Back to top](#)

This is a translation of the dissertation of Dr.ir. S.A. Miedema, dated September 15th 1987 .
The dissertation was originally published in Dutch by the:
Delft University of Technology
Faculty of Mechanical Engineering and Marine Technology
Chair of Dredging Technology
Mekelweg 2
2628 CD, Delft
The Netherlands

It is advised to also read the papers following this dissertation, since the theory developed has been refined and extended.

Last modified Monday May 29, 2000 by: [Sape A. Miedema](#)

Translation by: [Laurens de Jonge](#)

Figures, equations and tables by: [Erik Miedema](#)

Copyright © May, 2000 Dr.ir. S.A. Miedema



[Download Adobe Acrobat Reader V4.0](#)

8.06 Forces in densely packed saturated sand.

Contents

Because the soil/steel angle of friction, acting in the plane perpendicular to the blade edge, is determinative for the equilibrium of the cut layer, a correction on this angle has to be used due to the sliding velocity of the sand along the blade element. This phenomenon is known as the snowplough effect. The following is, in principle, sufficient:

$$\vec{v}_r = \left| \vec{v}_c \right| \cdot \frac{\sin(\beta)}{\sin(\alpha + \beta)} \cdot \frac{\vec{e}_{tt,i}}{\left| \vec{e}_{tt,i} \right|} \quad (8.34)$$

This is the relative velocity of the sand over the blade. The effective soil/steel angle of friction δ_e is now:

$$\delta_e = \text{atn} \left(\frac{\left| \vec{v}_r \right|}{\sqrt{\left(\vec{v}_r \cdot \vec{v}_r + (1 - f_0)^2 \cdot \vec{v}_1 \cdot \vec{v}_1 \right)}} \cdot \tan(\delta) \right) \quad (8.35)$$

Because the shear angle β is dependent on the effective soil/steel angle of friction δ_e an iterative solution has to be found. In chapter 2.11 is however indicated that the coefficient f_0 is approximately 1, so that initially the nominal soil/steel angle of friction can be used.

The coefficients c_1 , c_2 , d_1 and d_2 can be determined, with the found values for h_i , h_b , δ , α , and ϕ , from the tables in chapter 2 by interpolation or extrapolation. For the blade width $|b_{tt,i}|$ and for the cutting velocity $|v_s|$ is used.

With the equations from chapter 2 the cutting forces F_h en F_v for the

non-cavitating and the cavitating case can be determined. As a criterion for cavitation is used:

If the horizontal force F_h in the non-cavitating case is larger than in the cavitating case than cavitation takes place.

The friction force in the transversal direction of the blade edge can be determined as follows:

$$F_w = F_h \cdot \cos(\alpha) - F_v \cdot \sin(\alpha) \quad (\text{see also equation (2.58)}) \quad (8.36)$$

$$F_1 = F_w \cdot \frac{\left| \begin{array}{c} \rightarrow \\ V_1 \end{array} \right|}{\left| \begin{array}{c} \rightarrow \\ V_r \end{array} \right|} \cdot (1 - f_0) \quad (\text{see also equation (2.59)}) \quad (8.37)$$

[Back to top](#)

This is a translation of the dissertation of Dr.ir. S.A. Miedema, dated September 15th 1987 .

The dissertation was originally published in Dutch by the:

Delft University of Technology

Faculty of Mechanical Engineering and Marine Technology

Chair of Dredging Technology

Mekelweg 2

2628 CD, Delft

The Netherlands

It is advised to also read the papers following this dissertation, since the theory developed has been refined and extended.

Last modified Monday May 29, 2000 by: [Sape A. Miedema](#)

Translation by: [Laurens de Jonge](#)

Figures, equations and tables by: [Erik Miedema](#)

Copyright © May, 2000 Dr.ir. S.A. Miedema



[Download Adobe Acrobat Reader V4.0](#)

8.07 Transformation of the forces to the space fixed coordinate system.

Contents

The forces in the three directions on the blade element are now known. For transformation to the coordinate system of the excavating element also the direction of F_v has to be known. This can be determined by the vector product of the direction vector along the blade edge $b_{tt,i}$ and velocity vector v_c .

$$\vec{n} = \frac{\vec{b}_{tt,i} \times \vec{v}_c}{\left| \vec{b}_{tt,i} \times \vec{v}_c \right|} \quad (8.38)$$

This gives the inward aimed normal vector on the plane, formed by the blade edge and the direction of the cutting velocity v_c .

Now the spatial forces follow from:

$$F_k = \frac{F_h \cdot \vec{v}_{c,k}}{\left| \vec{v}_c \right|} - \frac{F_v \cdot \vec{n}_k}{\left| \vec{n} \right|} - \frac{F_l \cdot \vec{b}_{tt,i,k}}{\left| \vec{b}_{tt,i} \right|} \quad (8.39)$$

The driving torque can now be derived from the dot product of the force vector F and the peripheral velocity vector v_{ci} , multiplied with the radius of the element.

$$M = \frac{\vec{F} \cdot \left(\vec{v}_t - \vec{v}_s \right) r_i}{\left| \vec{v}_t - \vec{v}_s \right|} \quad (8.40)$$

Summation of these forces and this torque over the run-through angle and the number of elements and dividing by the number of angle elements derives the average forces and the average torque on the excavating element. This implies, that the run-through angle has to be known for every blade element. Furthermore it has to be known which part of the element in the width direction is in contact with the breach of every blade element.

[Back to top](#)

This is a translation of the dissertation of Dr.ir. S.A. Miedema, dated September 15th 1987 .
The dissertation was originally published in Dutch by the:
Delft University of Technology
Faculty of Mechanical Engineering and Marine Technology
Chair of Dredging Technology
Mekelweg 2
2628 CD, Delft
The Netherlands

It is advised to also read the papers following this dissertation, since the theory developed has been refined and extended.

Last modified Monday May 29, 2000 by: [Sape A. Miedema](#)

Translation by: [Laurens de Jonge](#)

Figures, equations and tables by: [Erik Miedema](#)

Copyright © May, 2000 Dr.ir. S.A. Miedema



[Download Adobe Acrobat Reader V4.0](#)

9.01 Introduction.

In the analytical models a number of simplifications are assumed compared to the theory of chapter 2. In the introduction of chapter 8 a number of these simplifications are already mentioned. These are about load components that are not caused by the two-dimensional dilatancy model. Within the two-dimensional dilatancy model, however, a number of simplifications are used. These simplifications are:

1. Constant values of the coefficients c_1 , c_2 , d_1 and d_2 are assumed, with a varying haul velocity and/or number of revolutions.
2. Constant values of the coefficients c_1 , c_2 , d_1 and d_2 are assumed, with a varying layer-thickness (as function of the run-trough angle), for a certain haul velocity and a certain number of revolutions.
3. It is assumed that the dynamic blade angle is a constant, both as a function of the run-through angle as for a varying haul velocity and/or number of revolutions.
4. It is assumed that the blade height h_b is a constant, both as a function of the run-through angle as for a varying haul velocity and/or number of revolutions.
5. A constant ratio h_b/h_i is assumed in connection with the assumptions under 3 and 4.

The dynamic blade angle is not a constant, but varies with the run-through angle and is also dependent on the ratio between the number of revolutions and the haul velocity. As a direct result, the blade height also varies. For a cutterhead the layer-thickness varies with the run-through angle, while for the cutter-wheel the layer-thickness slightly varies with the radius at which a blade element is located. As a result of these variations the ratio h_b/h_i also varies. To determine the coefficients c_1 , c_2 , d_1 and d_2 , the values of the dynamic blade angle and the blade-height / layer-thickness ratio are needed. Since these values vary with the run-through angle and the radius as well as the haul velocity and the number of revolutions, the coefficients c_1 , c_2 , d_1 and d_2 vary. The theoretical relation between the loads, the haul velocity and the number of revolutions will therefore not be exactly correct. Also the mutual ratios

between the forces and the forces in relation to the torque can differ from the theory of chapter 4 and 5. In short this implies that the loads will not be exactly proportional to the square of the haul velocity and not inversely proportional to the number of revolutions.

In [46,52] we proposed to use the following approximation:

$$F_{ci} = C_i \cdot \left(\frac{60 \cdot v_s}{n_o \cdot p} \right)^{(1 + \alpha_2)} \cdot \left(\frac{2\pi \cdot n_o \cdot R}{60} \right)^{\alpha_1} \quad (9.1)$$

In which: C_i = coefficient containing variables like c_i , $\rho_w \cdot g$, b and e/k_m . (see also equation (4.6)).

For the torque a similar approximation equation can be used. The second factor in equation (9.1) is the maximum layer-thickness and the third factor is the peripheral velocity of the cutterhead (approximately the cutting velocity).

In [46] the values are given of the coefficients α_1 en α_2 for seven different cutterheads. The values of α_1 and α_2 vary roughly between 0.5 and 1.5. A closer analysis of the loads on the, in chapter 7 mentioned, disc bottom cutterhead using the numerical model of chapter 8 gives a more detailed impression of the coefficients α_1 and α_2 .

[Back to top](#)

This is a translation of the dissertation of Dr.ir. S.A. Miedema, dated September 15th 1987 .

The dissertation was originally published in Dutch by the:

Delft University of Technology

Faculty of Mechanical Engineering and Marine Technology

Chair of Dredging Technology

Mekelweg 2

2628 CD, Delft

The Netherlands

It is advised to also read the papers following this dissertation, since the theory developed has been refined and extended.

Last modified Tuesday May 30, 2000 by: [Sape A. Miedema](#)

Translation by: [Laurens de Jonge](#)

Figures, equations and tables by: [Erik Miedema](#)

Copyright © May, 2000 Dr.ir. S.A. Miedema



[Download Adobe Acrobat Reader V4.0](#)

9.02 Numerical calculations of the forces on a disc bottom cutterhead.

To check the analytical model of the cutterhead a series of calculations is performed with the numerical forces model and the theory from chapter 2. In the numerical model from chapter 8 both the loads caused by the dilatancy as by the inertia forces are taken into account. The loads caused by the bottom blades are however not taken into account in these calculations. The results of these calculations can be found in the figures B10.1 to B10.9 (see Appendix B10). In these figures the upper and lower limit of the loads are shown, as determined according the method of chapter 7. Assumed is here, however, a run-through angle of 180° , for which the following coefficients are valid:

Chapter 4 gives: General

$f_1 = 0.00$	$g_1 = c_1$
$f_2 = 1.33$	$g_2 = c_2$
$f_5 = 1.57$	$g_5 = 0$

Chapter 2 gives:

Lower limit	Upper limit
$c_1 = 0.35$	$c_1 = 0.48$
$c_2 = 0.17$	$c_2 = 0.15$

Also the results of the numerical model are indicated as measuring points. It has to be beard in mind that the upper and lower limit are determined for hauling velocities between 6.4 cm/sec and 13.6 cm/sec. In this range the results of the numerical model are between the upper and lower limit of the analytical model. The method for the determination of an upper and lower limit, according chapter 7, is therefore sufficient.

The force F_s in the numerical model deviates slightly from the analytical model for haul velocities higher than 13.6 cm/sec. In this calculation example the force F_s is only dependent on the coefficient c_2 . With higher haul velocities the dynamic blade angle in particular is decreased. As a result the coefficient c_2 increases, so that the force F_s increases per ratio, with an increasing haul velocity.

For the force F_v the case is opposite. A smaller dynamic blade angle gives a smaller value for c_1 , so that F_v decreases per ratio, with an increasing haul velocity. This relative decrease is smaller than the relative increase of the force F_s since the coefficient c_1 is less sensitive for variations of the dynamic blade angle than the coefficient c_2 . Roughly the same applies for the torque M as for the force F_v .

The powers with which the loads are proportional to the number of revolutions and the haul velocity can be found in the tables 9.1 to 9.3.

Table 9.1 gives the power, with which the loads are proportional to the number of revolutions at a constant haul velocity. A clear increase in absolute value can be observed with an increasing haul velocity. The theoretical assumed inversely proportionality of the loads with the number of revolutions, in the analytical model, is only partly true. It is clear from the table that, with a relatively high haul velocity, the absolute powers become larger than 1 and even approach 2. This can be explained with the in the analytical model adopted assumption that the haul velocity \ll cutting velocity. This assumption is violated by the in this example used haul velocities of > 0.10 to 0.15 m/sec. Tables 9.2 and 9.3 give the powers, with which the loads are proportional to the haul velocity. Table 9.2 shows the powers to a haul velocity of 0.30 m/sec, while table 9.3 is limited to a haul velocity of 0.15 m/sec (in accordance with chapter 7). Here it is also observed that, though these powers vary less than the powers of the number of revolutions, the quadratic relation, assumed in the analytical model, is not exactly correct. It is remarkable that the tendency for higher powers at a higher number of revolutions that can be seen with the lower haul velocities, is not present with the higher haul velocities. Here the opposite can be seen.

An explanation for this phenomenon has to be found in the earlier mentioned variations of the coefficients c_1 and c_2 (or d_1 and d_2 if there is cavitation) and in the drift of the layer-thickness as a function of the haul velocity (chapter 8.5).

When the haul velocity increases, the layer-thickness increases less in proportion (equation (8.25)), so that the power, with which the haul velocity is proportional to the loads, will decrease. In particular when the haul velocity can not be neglected compared to the peripheral velocity this effect becomes very important.

**This is a translation of the dissertation of Dr.ir. S.A. Miedema, dated September 15th 1987 .
The dissertation was originally published in Dutch by the:
Delft University of Technology
Faculty of Mechanical Engineering and Marine Technology
Chair of Dredging Technology
Mekelweg 2
2628 CD, Delft
The Netherlands**

It is advised to also read the papers following this dissertation, since the theory developed has been refined and extended.

Last modified Tuesday May 30, 2000 by: [Sape A. Miedema](#)

Translation by: [Laurens de Jonge](#)

Figures, equations and tables by: [Erik Miedema](#)

Copyright © May, 2000 Dr.ir. S.A. Miedema



[Download Adobe Acrobat Reader V4.0](#)

9.03 Conclusions.

The determination of an upper and lower limit for the loads on a cutterhead in the analytical model from chapter 4 is in accordance with the results of the calculations with the numerical model. It is however required that the correct haul velocity and the correct number of revolutions is used for the determination of the upper and lower limit.

The deviations observed in the measurements of the quadratic relation between the loads and the haul velocity and the inverse proportionality of the loads with the number of revolutions, can partly be explained using the calculations of the numerical model. It appears that a number of assumptions exert quite a large influence on the mentioned proportionalities.

For an indication of the magnitude order of the loads the analytical models can however be used all right.

Certain tendencies can be predicted more accurate with the numerical model, although it remains uncertain if such an accuracy can be reached in the model tests, considering the reproducibility of the sandbed.

Equation (9.1) can give an accurate approximation of the loads within a small range of variations of the haul velocity and the number of revolutions.

The powers α_1 and α_2 will however change, if the loads have to be predicted over a larger range, as indicated in the calculation example. One needs to be aware of this when interpreting model tests.

v_s	M	F_v	F_s
0.05	-0.73	-0.69	-0.85
0.10	-0.83	-0.80	-1.01
0.15	-0.92	-0.84	-1.19
0.20	-1.00	-0.87	-1.41
0.25	-1.13	-0.90	-1.68
0.30	-1.34	-0.91	-2.07

Table 9.1: The power α_1 , with which the loads on the disc bottom cutterhead are proportional to the number of revolutions n_o , for several values of the haul velocity v_s .

n_o	M	F_v	F_s
25	2.04	1.88	2.44
33	1.92	1.85	2.21
45	1.86	1.81	2.07

Table 9.2: The power $(1+\alpha_2)$, with which the loads on the disc bottom cutterhead are proportional with the haul velocity v_s ($v_s < .30$ m/s), for several values of the number of revolutions n_o .

n_o	M	F_v	F_s
25	1.81	1.70	2.10
33	1.96	1.85	2.29
45	2.12	2.01	2.48

Table 9.3: The power $(1+\alpha_2)$, with which the loads on the disc bottom cutterhead are proportional with the haul velocity v_s ($v_s < .15$ m/s), for several values of the number of revolutions n_o .

[Back to top](#)

This is a translation of the dissertation of Dr.ir. S.A. Miedema, dated September 15th 1987 .

The dissertation was originally published in Dutch by the:

Delft University of Technology

Faculty of Mechanical Engineering and Marine Technology

Chair of Dredging Technology

Mekelweg 2

2628 CD, Delft

The Netherlands

It is advised to also read the papers following this dissertation, since the theory developed has been refined and extended.

Last modified Tuesday May 30, 2000 by: [Sape A. Miedema](#)

Translation by: [Laurens de Jonge](#)

Figures, equations and tables by: [Erik Miedema](#)

Copyright © May, 2000 Dr.ir. S.A. Miedema



[Download Adobe Acrobat Reader V4.0](#)



9.03 Figures Numerical Model Tests.

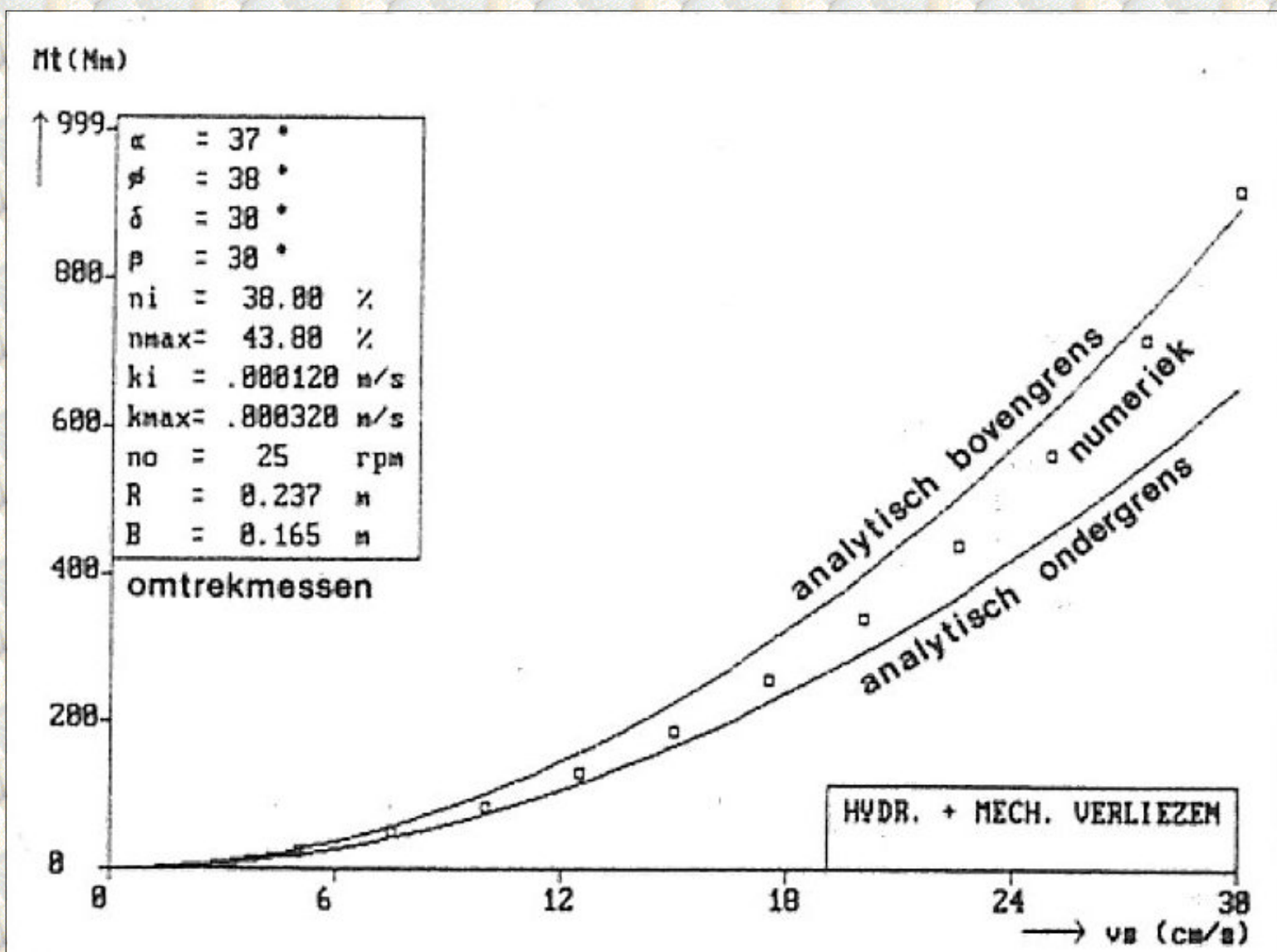


Figure 9.1: The drive torque M_t on the disc bottom cutterhead. Analytical versus numerical model, for the 200 μ m sand at 25 rpm, as a function of the swing velocity v_s . (numeriek=numerical, bovengrens=upper limit, ondergrens=lower limit, omtrekmessen=circumferential blades, verliezen=losses)

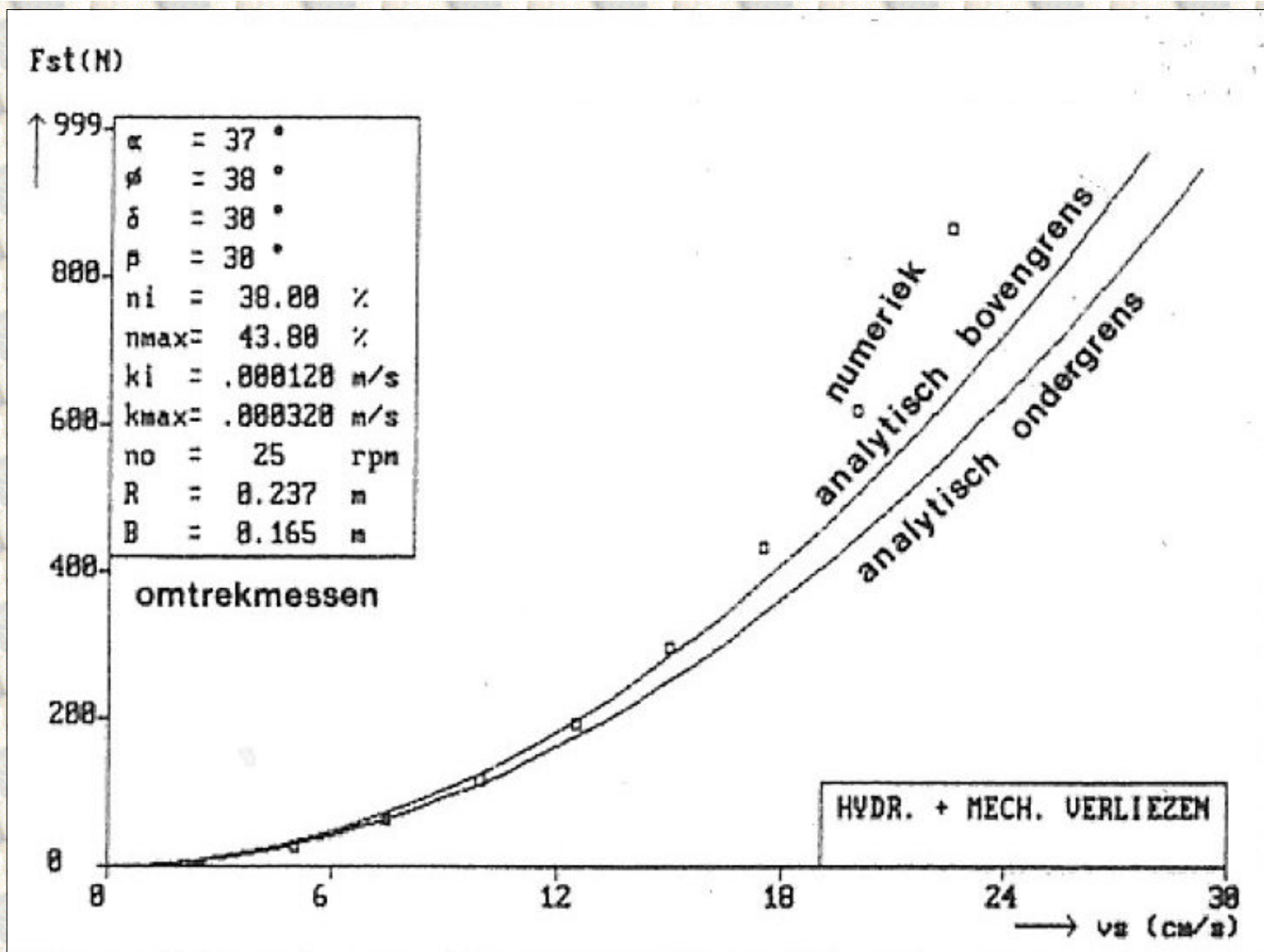


Figure 9.2: The force in the swing direction F_{st} on the disc bottom cutterhead. Analytical versus numerical model, for the 200 μ m sand at 25 rpm, as a function of the swing velocity v_s . (numeriek=numerical, bovengrens=upper limit, ondergrens=lower limit, omtrek-messen=circumferential blades, verliezen=losses)

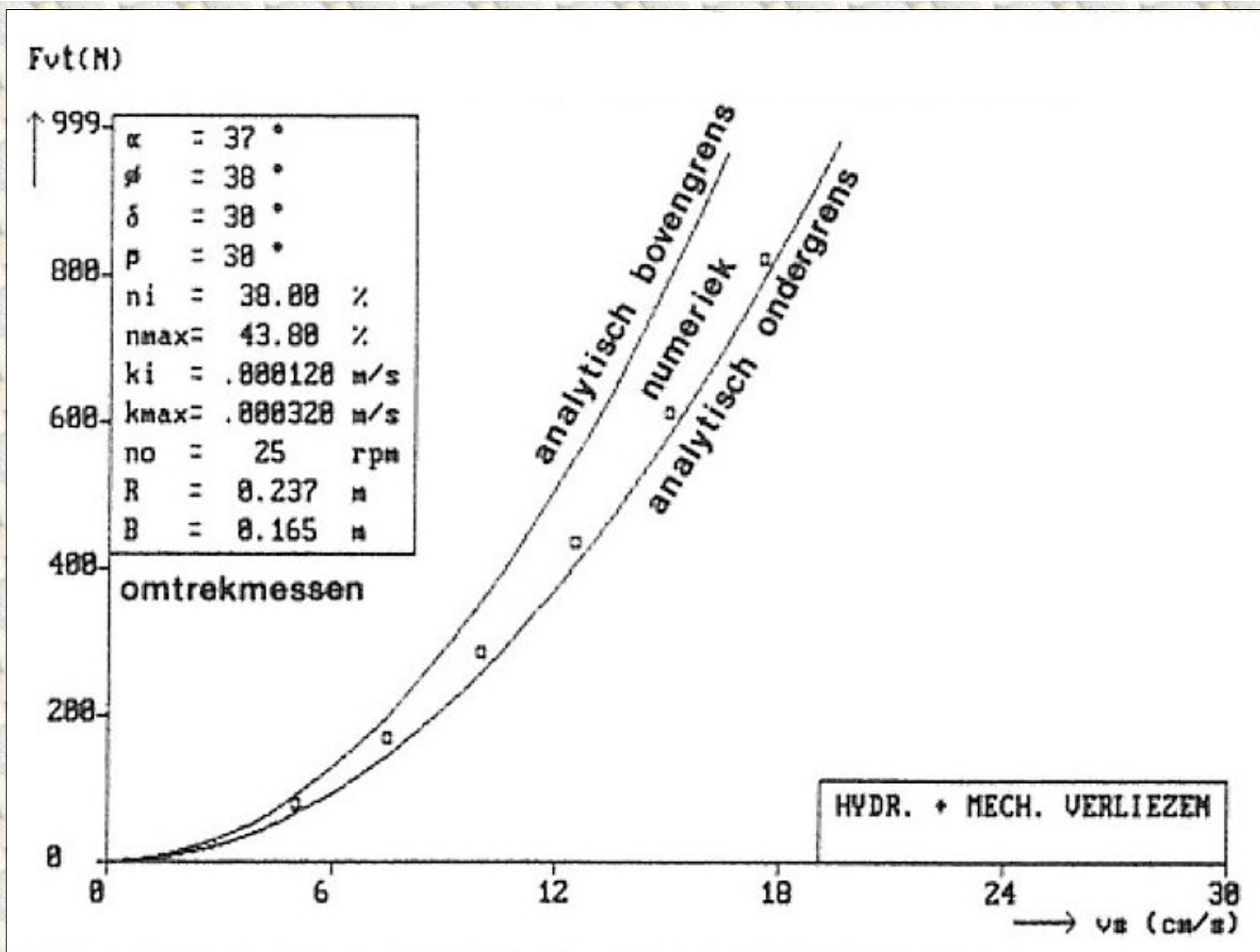


Figure 9.3: The force perpendicular to the swing direction F_{vt} on the disc bottom cutterhead. Analytical versus numerical model, for the 200 μ m sand at 25 rpm, as a function of the swing velocity v_s . (numeriek=numerical, bovengrens=upper limit, ondergrens=lower limit, omtrekmessen=circumferential blades, verliezen=losses)

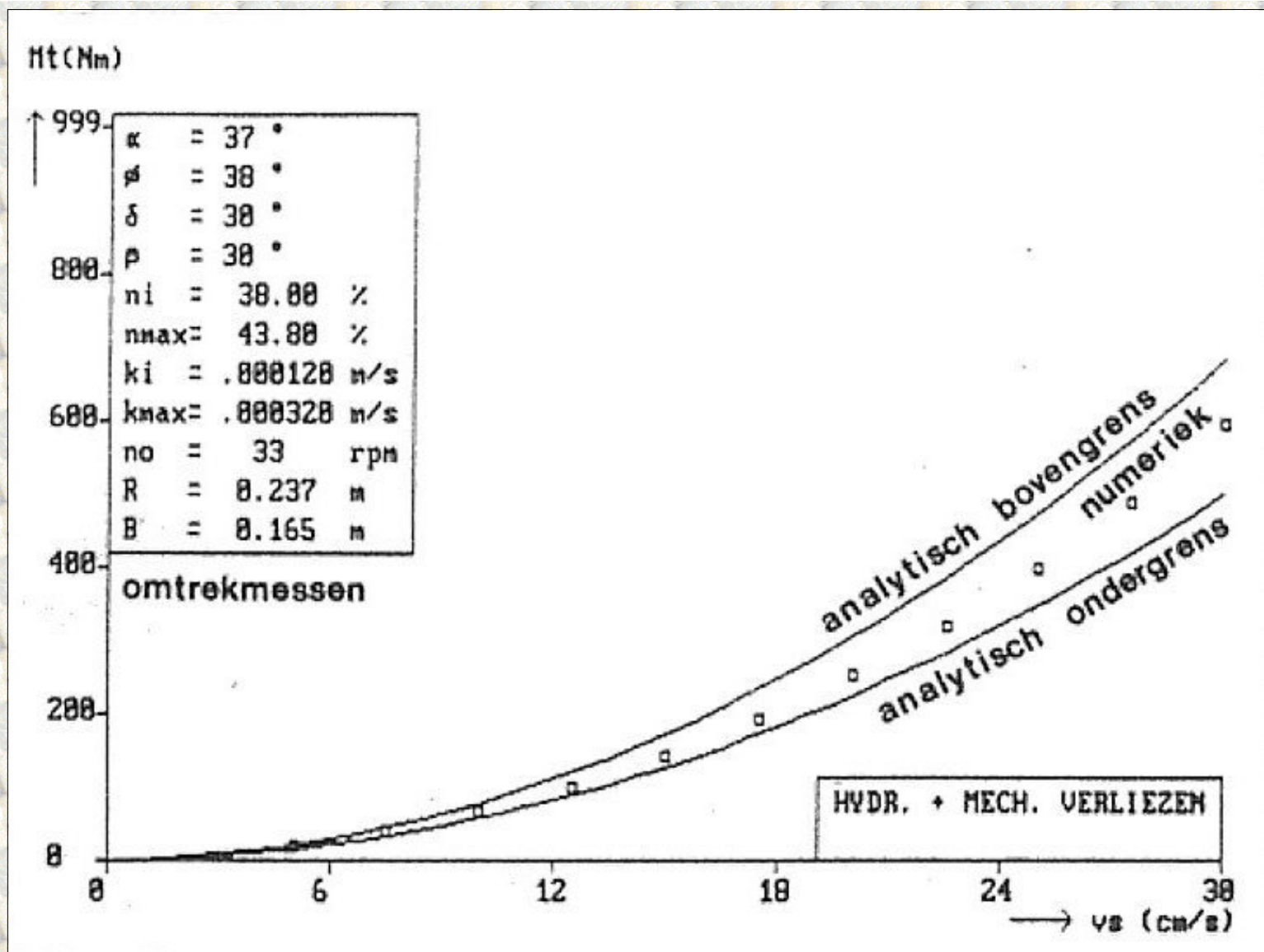


Figure 9.4: The drive torque M_t on the disc bottom cutterhead. Analytical versus numerical model, for the 200 μm sand at 33 rpm, as a function of the swing velocity v_s . (numeriek=numerical, bovengrens=upper limit, ondergrens=lower limit, omtremessen=circumferential blades, verliezen=losses)

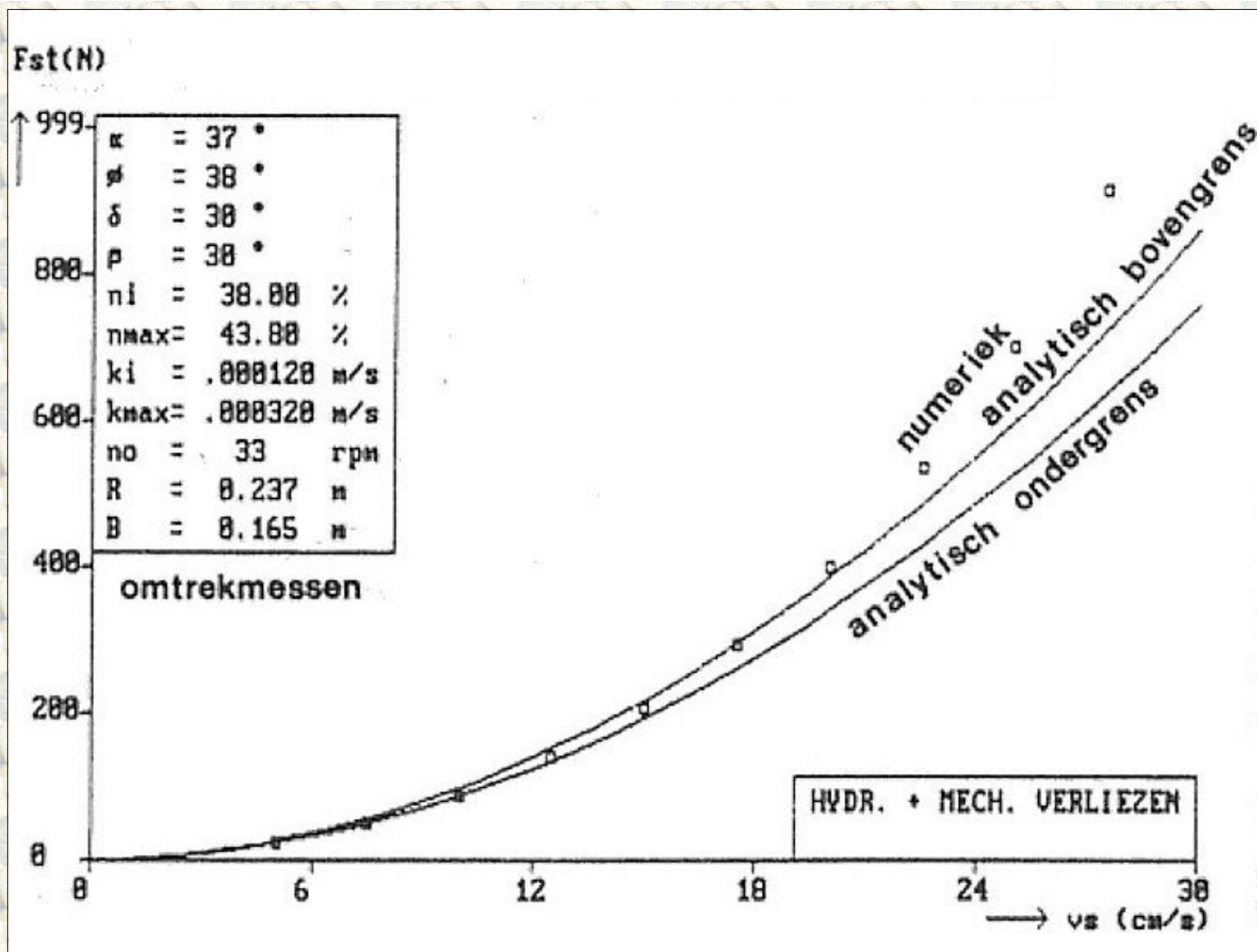


Figure 9.5: The force in the swing direction F_{st} on the disc bottom cutterhead. Analytical versus numerical model, for the 200 μm sand at 33 rpm, as a function of the swing velocity v_s . (numeriek=numerical, bovengrens=upper limit, ondergrens=lower limit, omtrekmessen=circumferential blades, verliezen=losses)

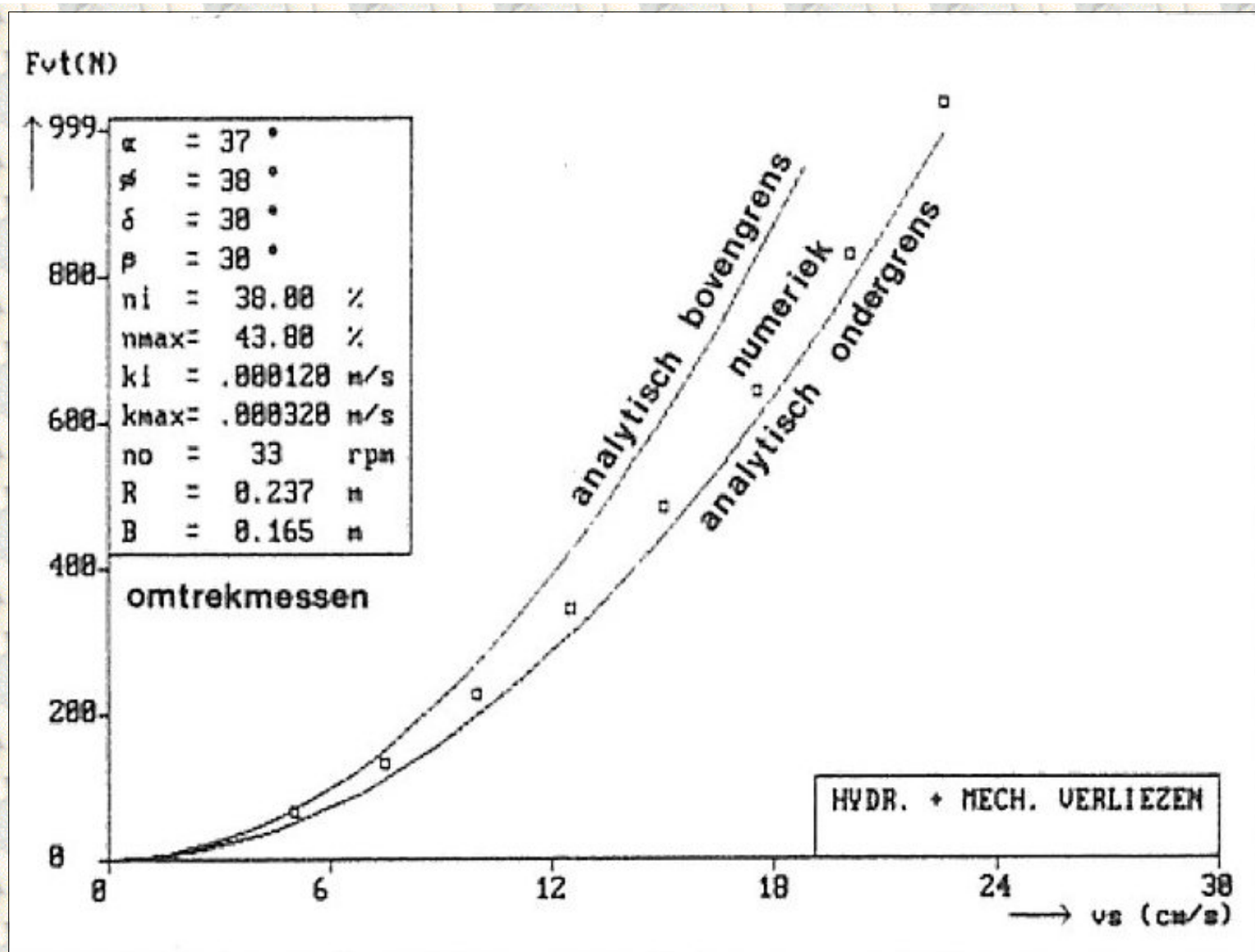


Figure 9.6: The force perpendicular to the swing direction F_{vt} on the disc bottom cutterhead. Analytical versus numerical model, for the 200 μm sand at 33 rpm, as a function of the swing velocity v_s .

(numeriek=numerical, bovengrens=upper limit, ondergrens=lower limit, omtrekmessen=circumferential blades, verliezen=losses)

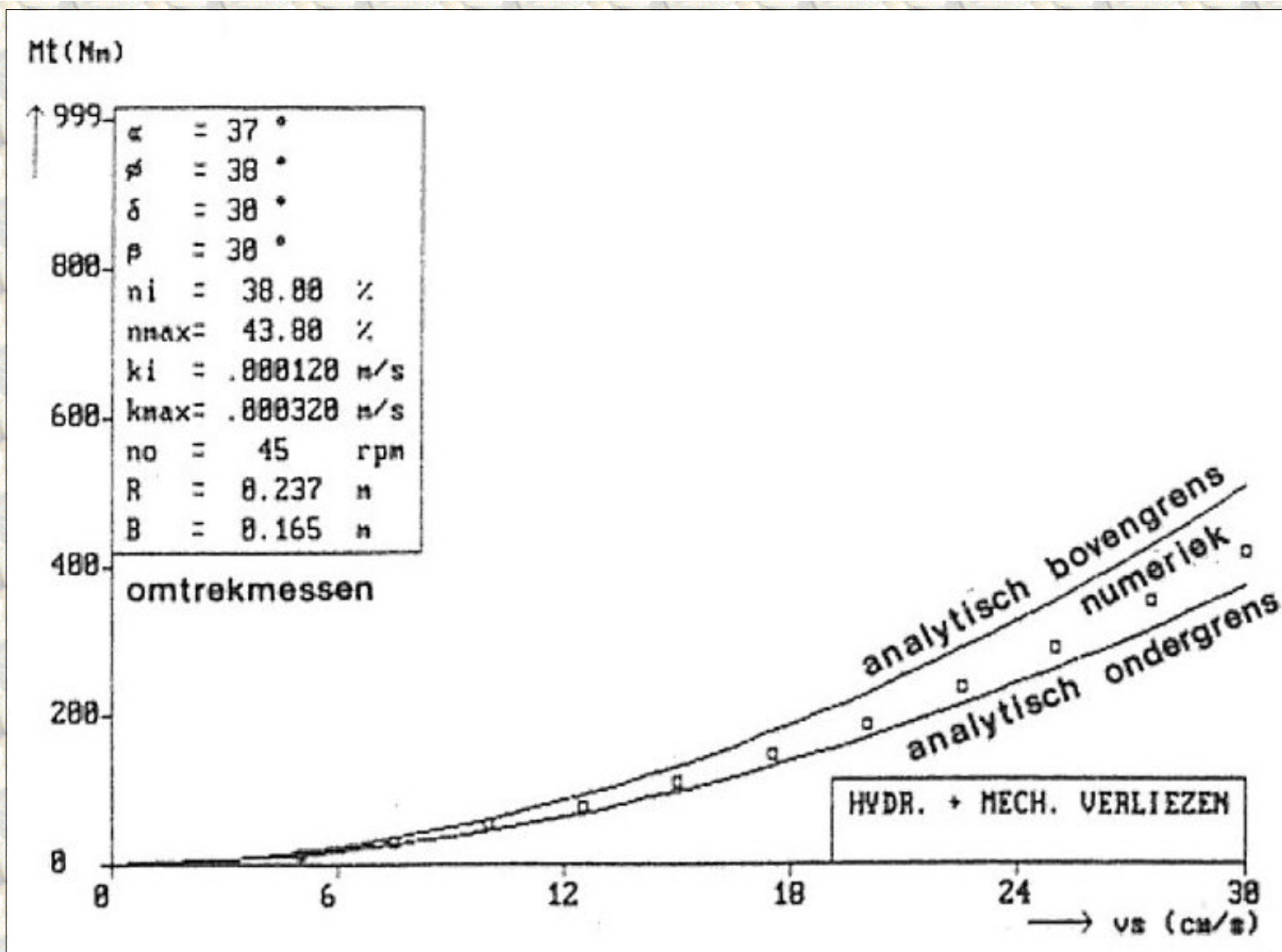


Figure 9.7: The drive torque M_t on the disc bottom cutterhead. Analytical versus numerical model, for the 200 μm sand at 45 rpm, as a function of the swing velocity v_s . (numeriek=numerical, bovengrens=upper limit, ondergrens=lower limit, omtrekmessen=circumferential blades, verliezen=losses)

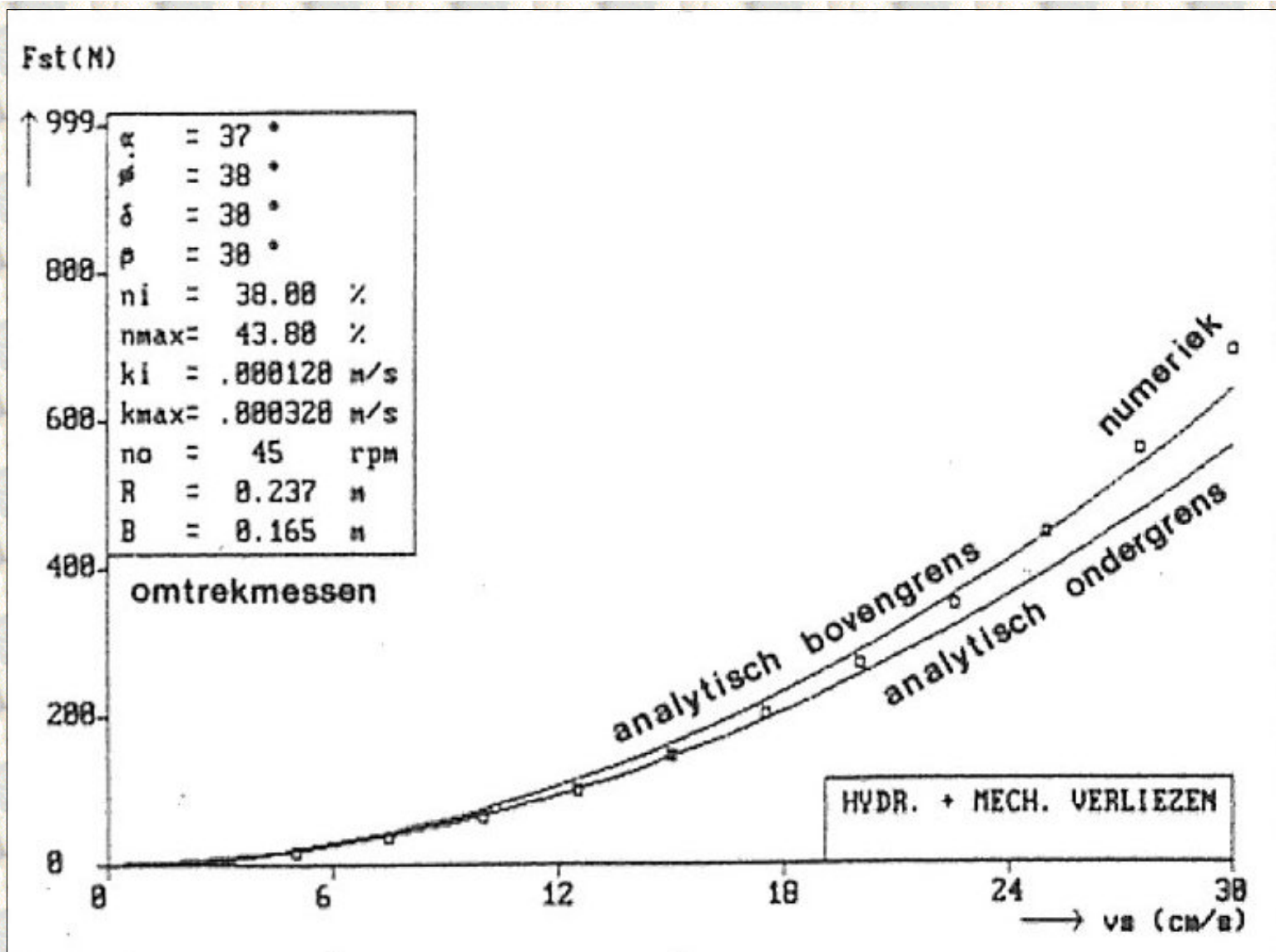


Figure 9.8: The force in the swing direction F_{st} on the disc bottom cutterhead. Analytical versus numerical model, for the $200 \mu\text{m}$ sand at 45 rpm, as a function of the swing velocity v_s . (numeriek=numerical, bovengrens=upper limit, ondergrens=lower limit, omtrekmessen=circumferential blades, verliezen=losses)

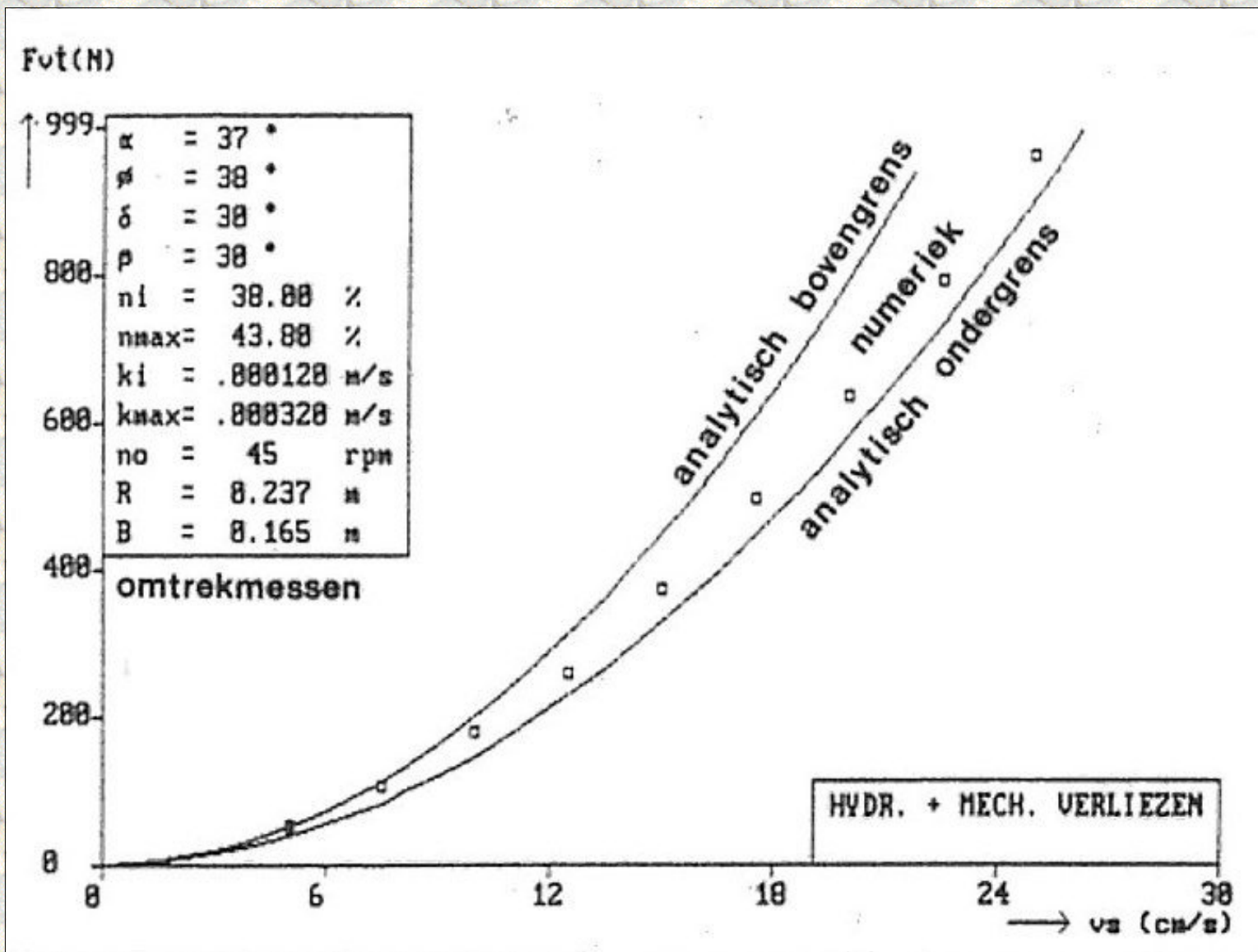


Figure 9.9: The force perpendicular to the swing direction F_{vt} on the disc bottom cutterhead. Analytical versus numerical model, for the 200 μm sand at 45 rpm, as a function of the swing velocity v_s .

(numeriek=numerical, bovengrens=upper limit, ondergrens=lower limit, omtrekmessen=circumferential blades, verliezen=losses)

[Back to top](#)

This is a translation of the dissertation of Dr.ir. S.A. Miedema, dated September 15th 1987 .
The dissertation was originally published in Dutch by the:
Delft University of Technology
Faculty of Mechanical Engineering and Marine Technology
Chair of Dredging Technology
Mekelweg 2
2628 CD, Delft
The Netherlands

It is advised to also read the papers following this dissertation, since the theory developed has been refined and extended.

Last modified Tuesday May 30, 2000 by: [Sape A. Miedema](#)

Translation by: [Laurens de Jonge](#)

Figures, equations and tables by: [Erik Miedema](#)

Copyright © May, 2000 Dr.ir. S.A. Miedema



[Download Adobe Acrobat Reader V4.0](#)

10.01 Introduction.

For the determination of the forces on a three-dimensional moving cutterhead (as a result of swell) the following starting-points and assumptions will be used.

1. The assumptions from chapter 4, Analytical forces model cutterhead.
2. The assumptions from chapter 5, Analytical forces model cutter-wheel.
3. Assumed will be a cylindrical cutterhead with radial bottom blades, the so-called disc bottom cutterhead.
A cutter-wheel is in this perspective the same as a disc bottom cutterhead, rotated 90° .
4. The in chapter 1 mentioned conditions for the modeling within the structure of the DREDMO program.
5. The results of calculations with DREDMO concerning a swell compensated cutter-suction dredger [4,48,49].
6. A pure cutting process, that is a cutting process with sharp blades and a positive clearance angle.

A cutterhead is able to move in three dimensions as a result of the following motions of the cutter-suction dredger:

1. Radial in the haul direction as a result of the sway, roll and yaw of the ship (the s-axis).
2. Radial perpendicular to the haul direction as a result of the surge, pitch and heave of the ship and as a result of the rotation of the ladder around the ladder hinge (the v -axis).
3. Axial as a result of the surge, pitch and heave of the ship (the a-axis).

In this chapter the influence of radial motions, perpendicular to the haul direction, on the cutterhead loads is discussed. Research showed (Miedema [46,47,51]) that the cutting forces as a result of both radial motions of the cutterhead can be determined with the theory of chapter 4. The influence of axial motions on the cutterhead loads is also discussed in this chapter. The axial force as a result of the axial motions of the cutterhead can be determined with

the theory from chapter 5.

Important for the cutting process of a three-dimensional moving cutterhead are, however, also the shape and size of the cut breach. The determination of the breach shape and the dimensions are discussed in chapter 10.2.

[Back to top](#)

This is a translation of the dissertation of Dr.ir. S.A. Miedema, dated September 15th 1987 .

The dissertation was originally published in Dutch by the:

Delft University of Technology

Faculty of Mechanical Engineering and Marine Technology

Chair of Dredging Technology

Mekelweg 2

2628 CD, Delft

The Netherlands

It is advised to also read the papers following this dissertation, since the theory developed has been refined and extended.

Last modified Tuesday May 30, 2000 by: [Sape A. Miedema](#)

Translation by: [Laurens de Jonge](#)

Figures, equations and tables by: [Erik Miedema](#)

Copyright © May, 2000 Dr.ir. S.A. Miedema



[Download Adobe Acrobat Reader V4.0](#)

10.02 Determination of the bank shape and the bank dimensions.

Similar to the division between the axial and the radial motions of the cutterhead, a division can be made between the axial and the radial breach shape. Starting-points are:

1. A cylindrical cutterhead, with bottom blades.
2. A breach as shown in figure 10.1.

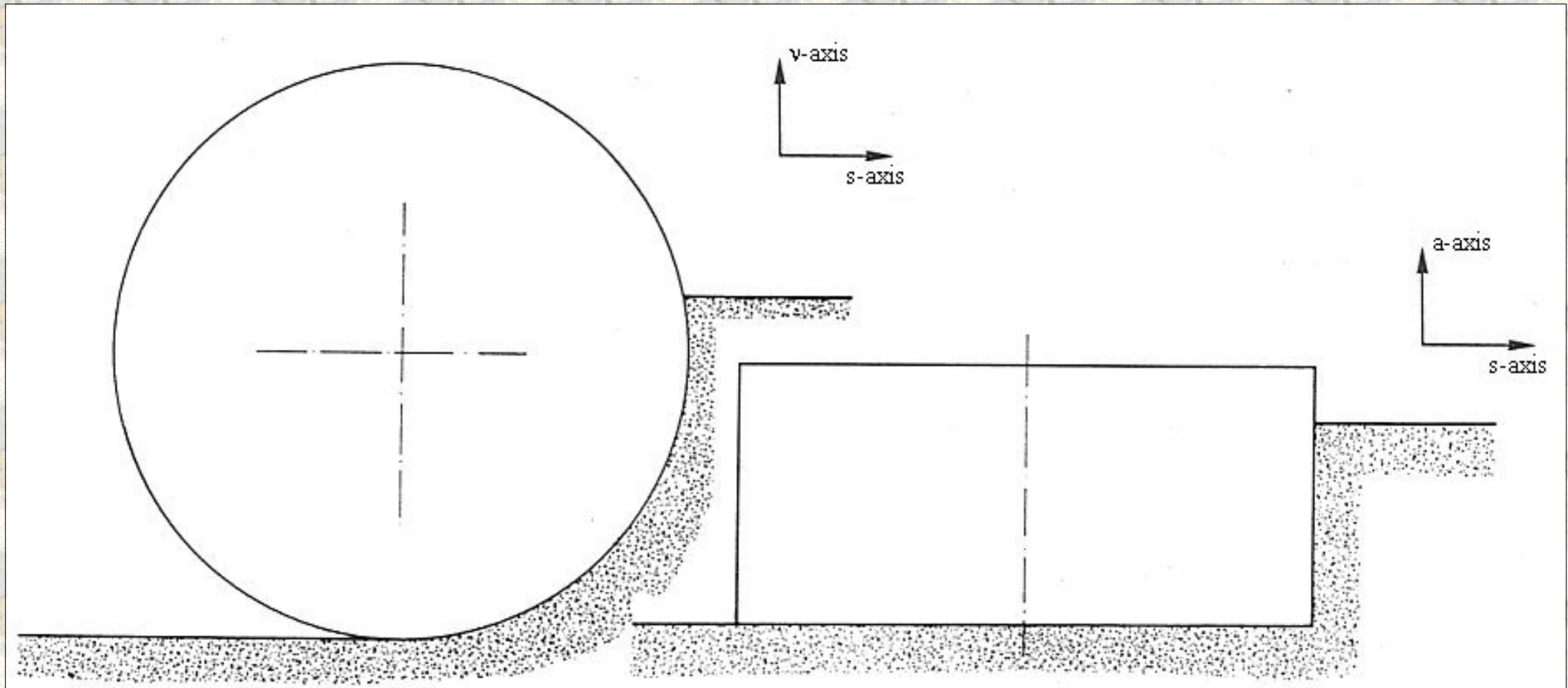


Figure 10.1: The axial and radial bank shapes.

From literature [46,47] it is known that the loads on the cutterhead are largely dependent on the already dredged profile of the breach. This shows from a strong motion-frequency dependency. In chapter 11 this is discussed. The determination of the shape and the dimensions of the breach part in contact with the cutterhead is based on a mask. A mask in this case is the cross-section of the breach in a certain plane. In figure 10.2 and 10.3 the possible masks are shown for the plane determined by the cutterhead-axis (a-axis) and the haul direction (s-axis) and the plane determined by the haul direction (s-axis) and the axis perpendicular to the haul-direction (v -axis).

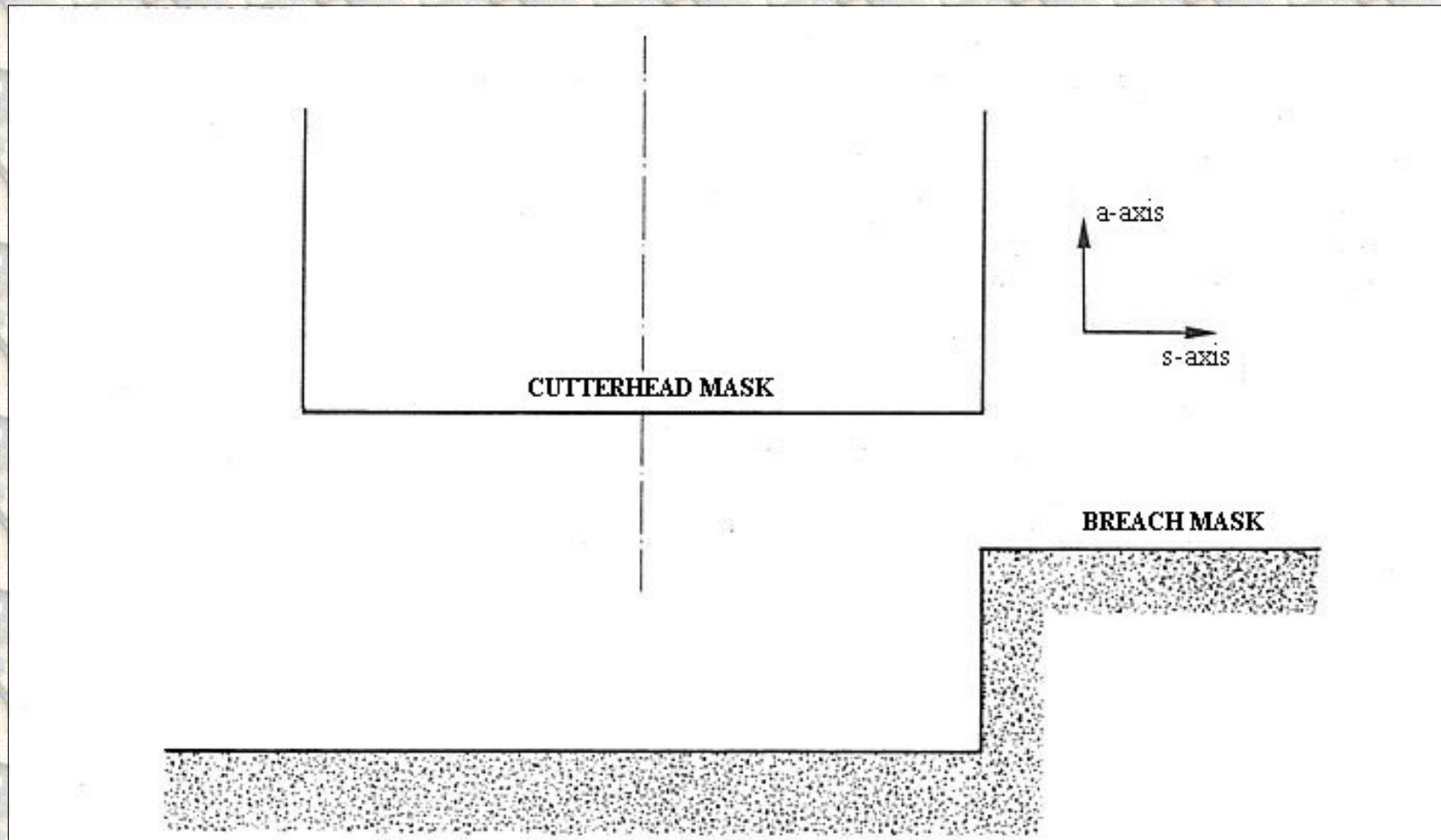


Figure 10.2: Possible axial bank and cutterhead masks (initial).

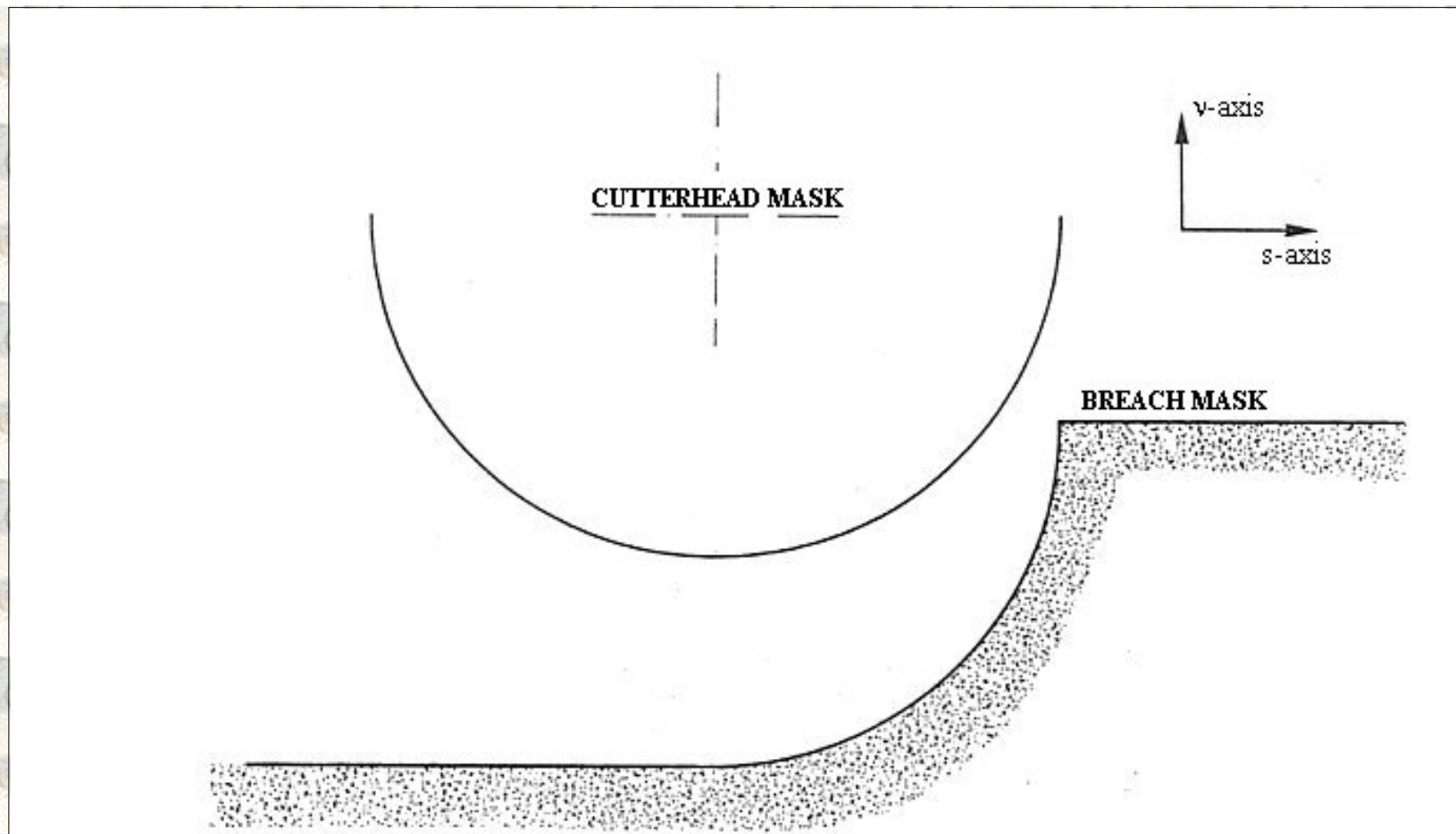


Figure 10.3: Possible radial bank and cutterhead masks (initial).

In this context the cutterhead can also be approximated by a couple of masks, in the same two planes. These masks are also shown in the figures 10.2 and 10.3. The two masks of the breach, the breach profiles, change continuously in time due to the motions of the cutterhead. In figures 10.4 and 10.5 is shown how the breach masks depend on the motions of the cutterhead for sinusoidal motions of the cutterhead.

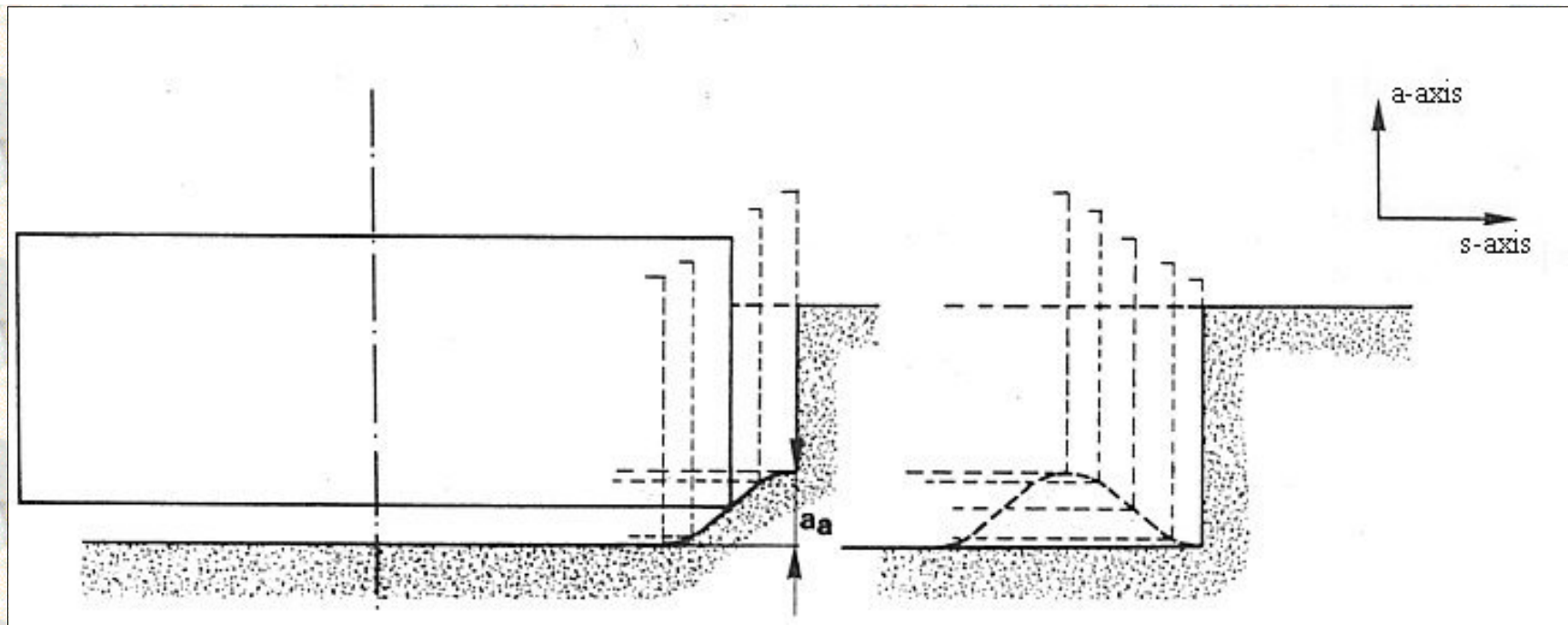


Figure 10.4: The axial bank mask as a function of time.

($v_s = 0.1$ m/s, $\omega_a = \pi$ rad/s, $a_a = 0.03$ m, $b = 0.165$ m).

Using these masks it can be determined at any time which part of the cutterhead is in contact with the breach. It is also possible to give the initial breach an irregular shape to simulate the profile, dredged during the previous cut. This method is useful for both regular and irregular motions of the cutterhead (or the cutter-wheel). This method requires however a numerical approach that increases the calculation time.

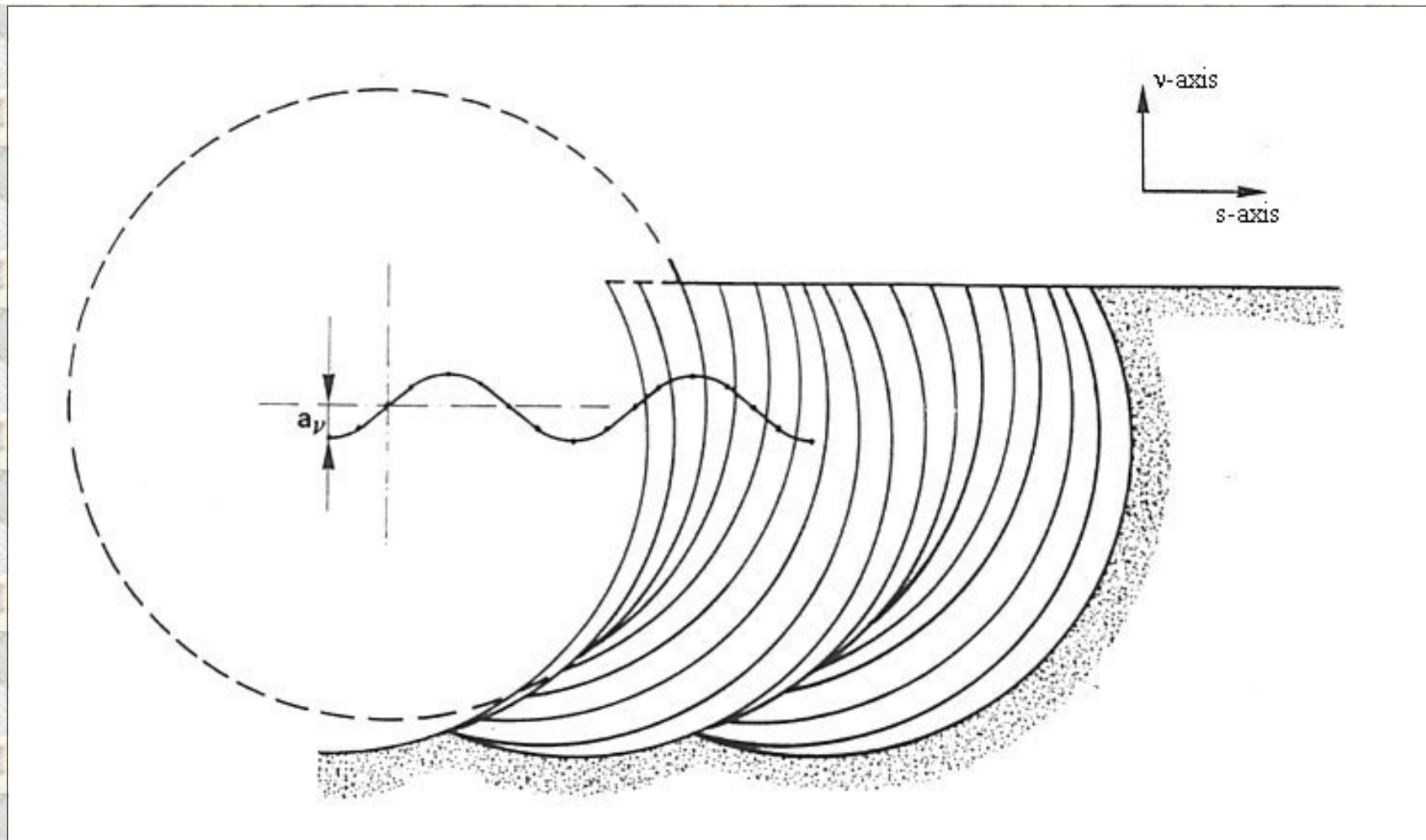


Figure 10.5: The radial bank mask as a function of time.

($v_s = 0.1$ m/s, $\omega_a = \pi$ rad/s, $a_a = 0.03$ m, $R = 0.475$ m).

Besides for a non-constant haul velocity interpolation techniques have to be used. Under certain conditions it is, however, possible to make some analytical predictions of the behavior of the loads that act on the three-dimensional cutterhead.

These conditions are:

1. The cutterhead makes a sinusoidal motion, axial or radial.

2. The initial breach has a smooth surface.
3. The axial and radial motions are unlinked and therefore do not influence each other.
4. The wavelength of the motion is smaller than the width of the bottom blades.
5. The sum of the breach height and the amplitude of the axial motion is smaller than the width of the blades on the circumference of the blades.
6. The sum of the step and the amplitude of the radial motion is smaller than the diameter of the cutterhead.

[Back to top](#)

This is a translation of the dissertation of Dr.ir. S.A. Miedema, dated September 15th 1987 .

The dissertation was originally published in Dutch by the:

Delft University of Technology

Faculty of Mechanical Engineering and Marine Technology

Chair of Dredging Technology

Mekelweg 2

2628 CD, Delft

The Netherlands

It is advised to also read the papers following this dissertation, since the theory developed has been refined and extended.

Last modified Tuesday May 30, 2000 by: [Sape A. Miedema](#)

Translation by: [Laurens de Jonge](#)

Figures, equations and tables by: [Erik Miedema](#)

Copyright © May, 2000 Dr.ir. S.A. Miedema



[Download Adobe Acrobat Reader V4.0](#)

10.03 The influence of radial velocity variations on the cutterhead loads.

[Contents](#)

If the cutterhead has only radial velocity variations, the axial force caused by the bottom blades will be equal to zero since for that case the bottom blades have no contact with the breach, except for the contribution mentioned in chapter 7 for the used model disc bottom cutterhead. It will be clear from chapter 4 that a varying haul velocity influences the loads on the cutterhead in magnitude, while a varying radial velocity perpendicular to the haul direction also influences the mutual relations between the loads. Since the effects of a varying haul velocity can be determined with the theory from chapter 4 (and 5), the effects of a varying radial velocity perpendicular to the haul direction (figure 10.6) will be discussed in this chapter.

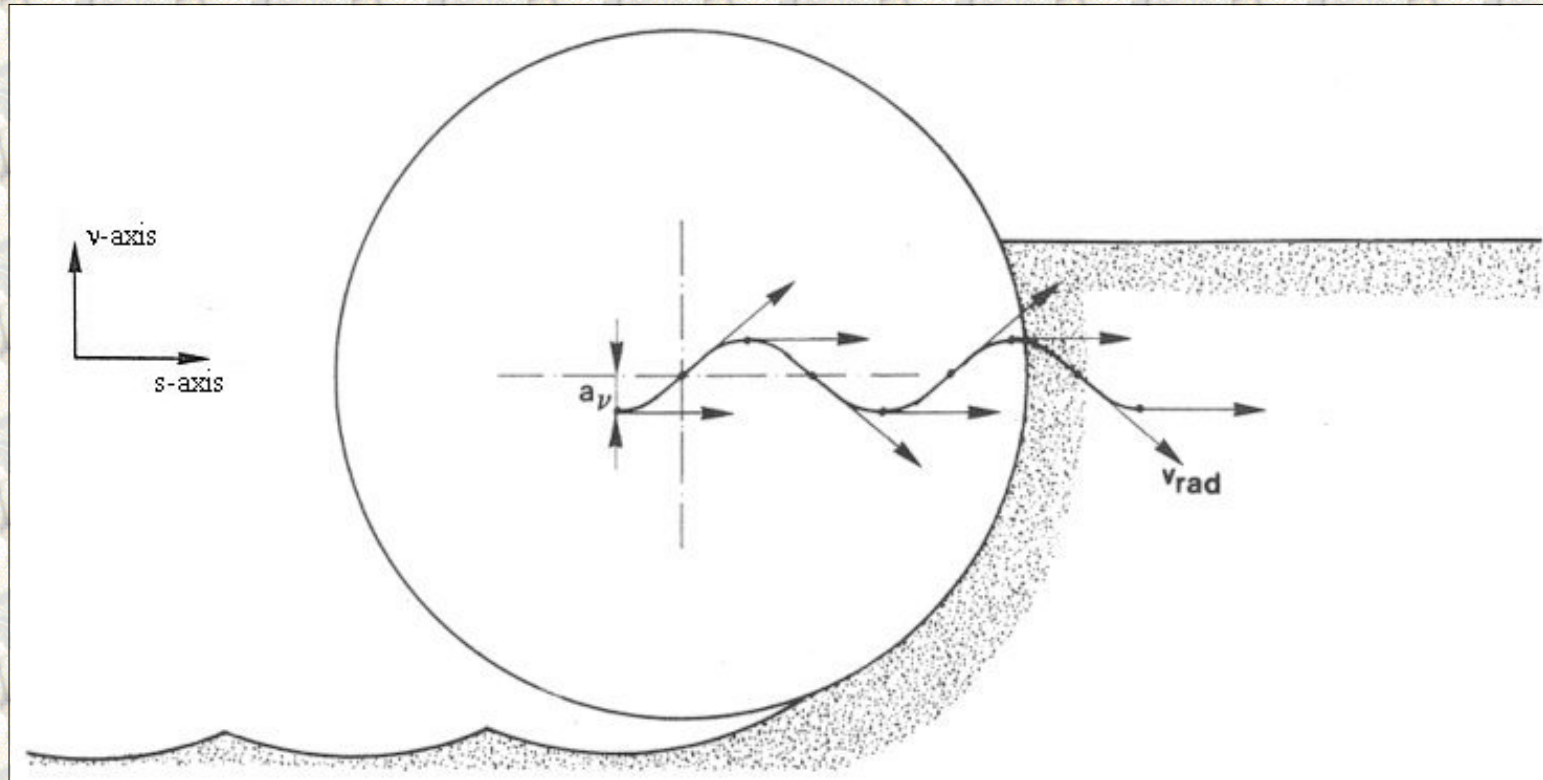


Figure 10.6: The direction of the radial velocity as a function of time.
($v_s = 0.1$ m/s, $\omega_a = \pi$ rad/s, $a_a = 0.03$ m, $R = 0.475$ m).

The effect of the radial velocity variations is dual. On the one hand the direction of the total radial velocity changes continuously, on the other hand the run-through angle varies continuously in time. If the cutterhead makes a radial sinusoidal motion with amplitude a_v and an angular frequency ω_v , the following equations can be derived for the radial velocity and the run-through angle. For the radial covered path perpendicular to the haul velocity can be derived:

$$v(t) = a_v \cdot \sin(\omega_v \cdot t) \quad (10.1)$$

The radial velocity is now:

$$v_v(t) = a_v \cdot \omega_v \cdot \cos(\omega_v \cdot t) \quad (10.2)$$

For the angle between the momentary velocity direction and the haul directions is valid:

$$\Omega'_0(t) = \arctan\left(\frac{v_v(t)}{v_s}\right) = \arctan\left(\frac{a_v \cdot \omega_v \cdot \cos(\omega_v \cdot t)}{v_s}\right) \quad (10.3)$$

The run-through angle is determined by both the radial covered path as by the radial velocity, with the total run-through angle related to the momentary velocity direction. For the run-through angle as a function of the radial covered path can be written:

$$\Omega''_0(t) = \arccos\left(1 - \frac{B_v + a_v \cdot \sin(\omega_v \cdot t)}{R}\right) \quad (10.4)$$

The correction that has to be used for the radial velocity is the angle Ω'_0 , so that for the total run-through angle can be written:

$$\Omega_0(t) = \Omega'_0(t) + \Omega''_0(t) - \Omega_{0c} \quad (10.5)$$

In which: Ω_{0c} = the correction for the already cutaway breach.

With of course the restriction that the total run-through angle can never be larger than 180° and with the complication that the cut profile has to allow for the correction with Ω_0 . Figure 10.7 shows this problem.

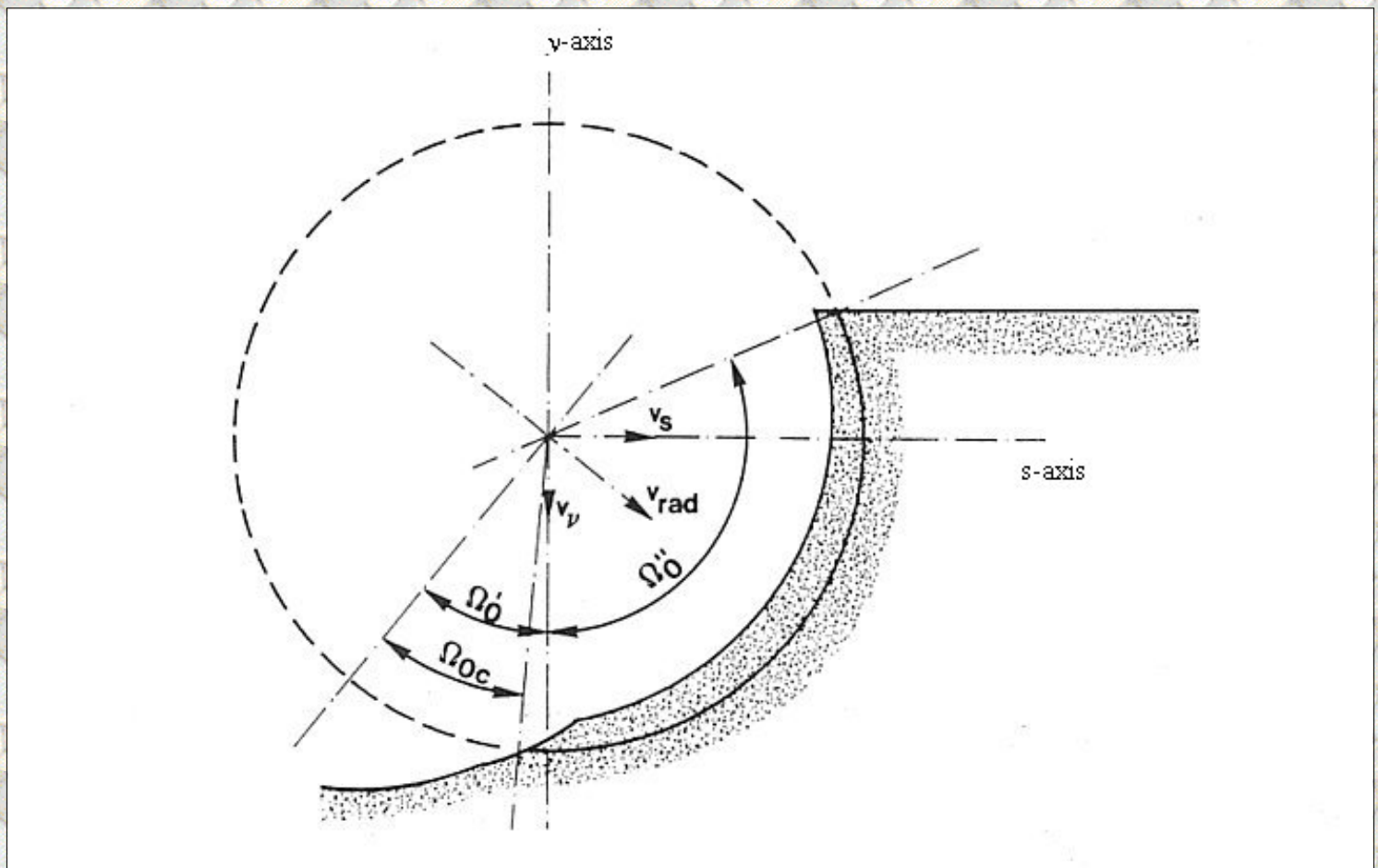


Figure 10.7: The total run-through angle $\Omega_0 = \Omega'_0 + \Omega''_0 - \Omega_{0c}$ corrected for the bank cut.

Dependent on the frequency and the amplitude of the motion forced upon the cutterhead, a situation can occur where over a part of the run-through angle, as determined above, the breach is already cut (figure 10.7). A correction has to be made for the concerning part of the run-through angle Ω_{0c} . The easiest way to implement this correction is to determine first the forces for the run-through angle according equation (10.5) and subtract from these the loads that occur for a run-through angle Ω_{0c} according figure 10.7. This last angle can only be determined according the method described in chapter 10.2.

From equations (10.3) and (10.4) can be derived that the total run-through angle depends on the radial covered path and on the radial velocity. This means that the total run-through angle will reach a maximum between the point where the radial velocity reaches a maximum breach inward and where the radial covered path reaches a maximum breach inward. The total run-through angle will reach a minimum between the point where the radial covered path reaches a maximum and the point where the radial velocity reaches a maximum breach outward.

Since the loads on the cutterhead show a more or less proportionality with the square of the total radial velocity and also a proportionality with the run-through angle, the loads will reach a maximum between the point where the total radial velocity reaches a maximum and the point where the run-through angle reaches a maximum. The loads will reach a minimum between the point where the total radial velocity reaches a minimum (and therefore equal to the haul velocity) and the point where the run-through angle reaches a minimum.

On the basis of these considerations it can be expected that the maximum of the loads will occur somewhat later than the maximum radial velocity.

The loads can be determined with the equations (4.40) to (4.43) from chapter 4. It has to be remarked, however, that the velocity v_s in equation (4.31) is derived from equation (4.1) for the layer-thickness. This layer-thickness is build up during a certain time, according the next equation:

$$\Delta t = \frac{60}{n_o \cdot p} \quad (10.6)$$

With a varying velocity, this means that the velocity has to be integrated over Δt to determine the layer-thickness. This means for the effective radial velocity:

$$v_{vc}(t) = \frac{a_v}{\Delta t} \cdot (\sin(\omega_v \cdot t) - \sin(\omega_v(t - \Delta t))) \quad (10.7)$$

Now can be derived that a phase haul takes place between the development of the total radial velocity and the layer-thickness. This phase haul is:

$$\epsilon = \frac{\Delta t \cdot \omega_r}{2} \quad (10.8)$$

Where the development of the layer-thickness lags on the development of the velocity. This phase

haul will also result in a phase haul between the loads and the development of the radial velocity, besides the already mentioned phase haul.

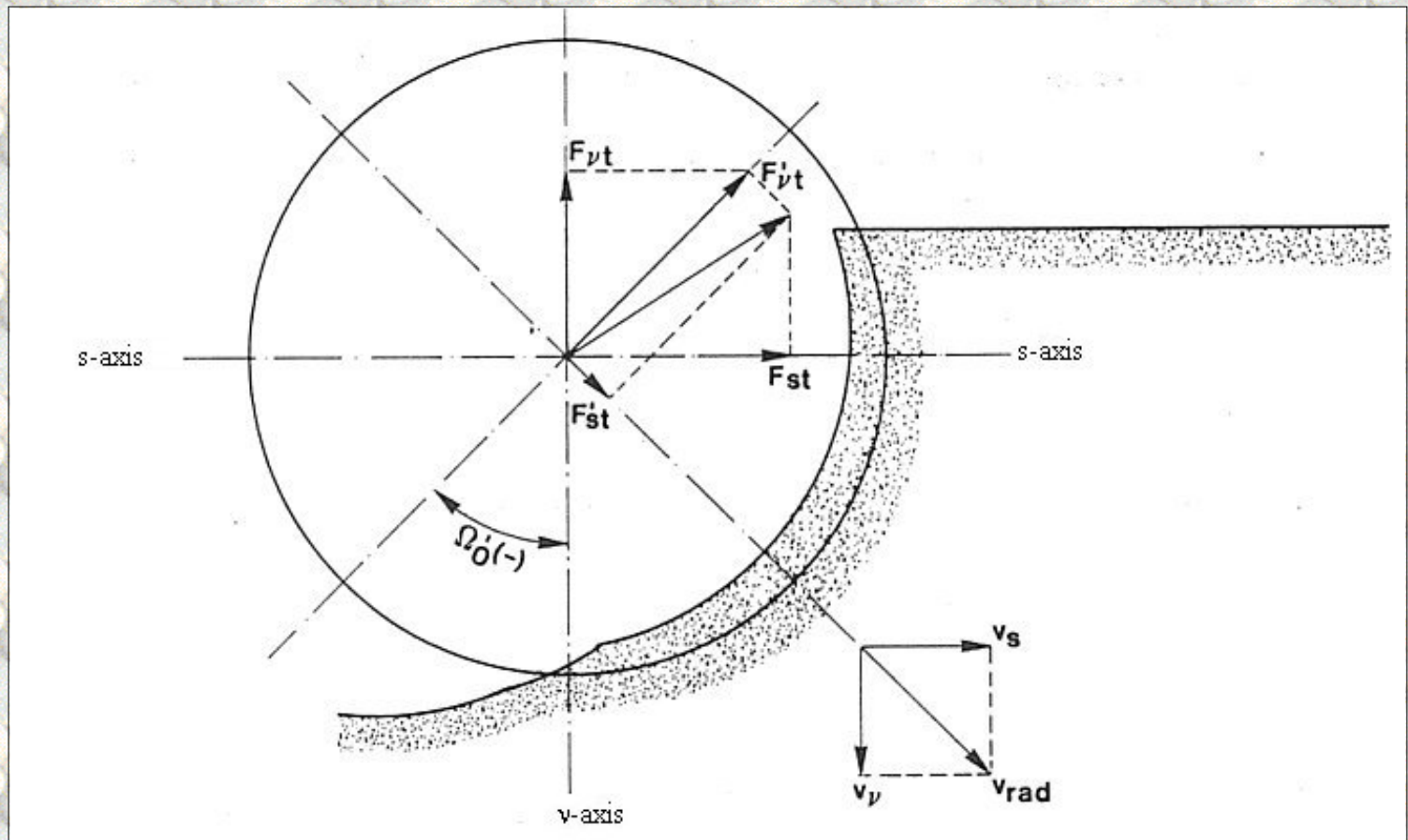


Figure 10.8: The momentary force directions at a bank inward radial velocity, where Ω_0 is negative.

The loads are determined in a coordinate system, where the total radial velocity is one of the axis. This means that the direction of the forces F_{st} and F_{vt} (figure 10.8) has to be corrected. If the momentary forces are indicated with a ', then the forces in the fixed coordinate system become:

$$F_{st} = F'_{st} \cdot \cos(\Omega'_0) - F'_{vt} \cdot \sin(\Omega'_0) \quad (10.9)$$

and

$$F_{vt} = F'_{st} \cdot \sin(\Omega'_0) + F'_{vt} \cdot \cos(\Omega'_0) \quad (10.10)$$

[Back to top](#)

This is a translation of the dissertation of Dr.ir. S.A. Miedema, dated September 15th 1987 .
The dissertation was originally published in Dutch by the:
Delft University of Technology
Faculty of Mechanical Engineering and Marine Technology
Chair of Dredging Technology
Mekelweg 2
2628 CD, Delft
The Netherlands

It is advised to also read the papers following this dissertation, since the theory developed has been refined and extended.

Last modified Tuesday May 30, 2000 by: [Sape A. Miedema](#)

Translation by: [Laurens de Jonge](#)

Figures, equations and tables by: [Erik Miedema](#)

Copyright © May, 2000 [Dr.ir. S.A. Miedema](#)



[Download Adobe Acrobat Reader V4.0](#)

10.04 The influence of axial velocity variations on the cutterhead loads.

[Contents](#)

Axial velocity variations cause a sliding velocity on the blades on the circumference of the cutterhead. Also the cutting blade width will vary. In chapter 2.11 is noted that the effects of a sliding velocity are negligible. The effect of a varying cutting blade width can be accounted for with the substitution of:

$$b_{pr}(t) = B_a + a_a \cdot \sin(\omega_a \cdot t) \quad (10.11)$$

in the equations (4.31) and/or (4.32).

If there are axial velocity variations the bottom blades will also participate periodically in the cutting process. The cutting behavior of the bottom blades is similar to the cutting behavior of a cutter-wheel according chapter 5, where the axial velocity, breach inward, equals the haul velocity of a cutter-wheel. The loads on the bottom blades can be determined with the equations (5.30) to (5.33), for the non-cavitating cutting process and with the equations (5.34) t/m (5.37) for the cavitating process.

The axial velocity breach inward has to be substituted in the equations (5.16) and (5.25) for the haul velocity with the restriction that also for the axial motion the layer-thickness has to be determined by integrating the axial velocity over a time Δt . For the axial velocity can be written:

$$v_a(t) = a_a \cdot \omega_a \cdot \cos(\omega_a \cdot t) \quad (10.12)$$

The axial layer-thickness can be determined with the effective axial velocity:

$$v_{ac}(t) = \frac{a_a}{\Delta t} \cdot (\sin(\omega_a \cdot t) - \sin(\omega_a (t - \Delta t))) \quad (10.13)$$

The axial layer-thickness will therefore also have a phase haul compared to the axial velocity, as is derived in chapter 10.3 for the radial layer-thickness. Still unknown is the shape and the size of the cutaway surface.

In figure 10.9 the covered path in the s-direction is indicated, for the breach inward motion, for a point along the circumference of the cutterhead, from the time the cutterhead is positioned on the same a-coordinate for the breach outward motion.

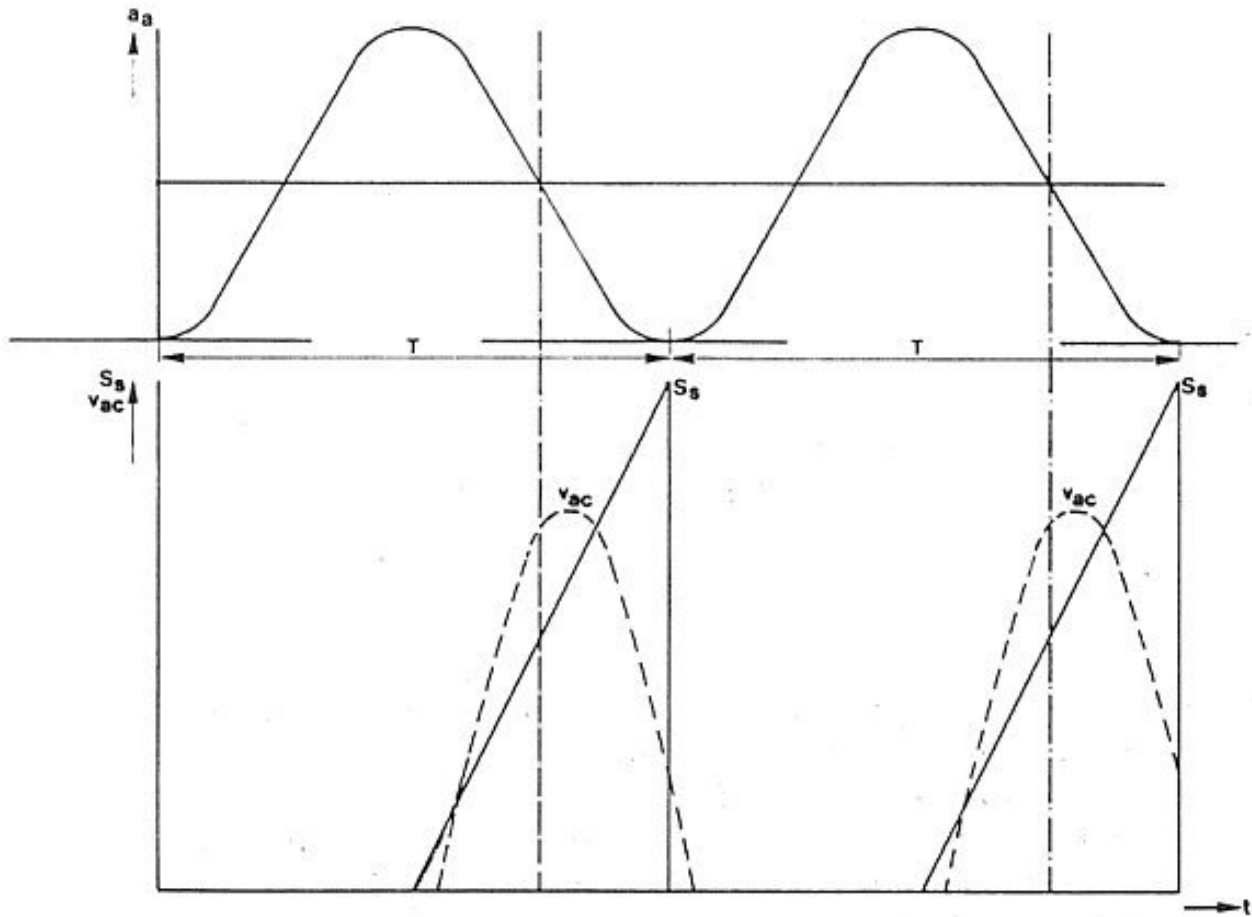


Figure 10.9: The step S_s and the effective axial layer thickness v_{ac} during two periods of the axial motions.

The fact that the covered path is similar for every point along the circumference of the cutterhead, implies also that the cutaway surface is similar to the cutaway surface on which the theory in chapter 5 is based. This implies that this covered path can be substituted for the step size for the cutter-wheel. In figure 10.9 a sinus shaped axial motion of the cutterhead is assumed. For an irregular motion basically the same conclusions are valid.

For this covered path S_s , for a sinus shaped axial motion, can be derived:

For the wave length:

$$\lambda_a(\omega) = \frac{2 \cdot \pi \cdot v_s}{\omega_a} \quad (10.14)$$

And for the path covered:

$$s(t) = v_s \cdot t \quad (10.15)$$

this gives:

$$S_s(t) = 2 \cdot \left(s(t) - \frac{\lambda_a(\omega)}{4} - n \cdot \lambda_a(\omega) \right) \quad (10.16)$$

for:

$$\frac{\lambda_a(\omega)}{4} + n \cdot \lambda_a(\omega) < s(t) < \frac{3 \cdot \lambda_a(\omega)}{4} + n \cdot \lambda_a(\omega)$$

and

$$S_s(t) = 0 \text{ voor } -\frac{\lambda_a(\omega)}{4} + n \cdot \lambda_a(\omega) < s(t) < \frac{\lambda_a(\omega)}{4} + n \cdot \lambda_a(\omega) \quad (10.17)$$

With n the number of periods. With the aid of the found values for $S_s(t)$ and the step of the cutterhead in the v -direction B_v (figure 10.9) the surface $A(t)$ in the equations (5.30) to (5.37) can be determined.

This results in:

$$A(t) = S_s(t) \cdot B_v \quad (10.18)$$

By substituting equation (10.14) in the above mentioned equations the part of the loads on the cutterhead caused by the bottom blades can be determined. These considerations give the impression that, for the axial velocity variations as well, the loads reach a maximum after the axial velocity reaches a maximum breach inward and before the cutterhead reaches a maximum cutting depth.

The effects of radial velocity variations on the loads that occur on the bottom blades, can be neglected if the radial velocity variations can be neglected compared to the peripheral velocity of the cutterhead. Accounting for effects, not covered by the analytical models from chapter 4 and 5, can be done in the numerical model of chapter 8. For the application of the cutting theory for the three-dimensional moving cutterheads in the DREDMO program it is important to use the dominating tendencies as described in this chapter.

[Back to top](#)

This is a translation of the dissertation of Dr.ir. S.A. Miedema, dated September 15th 1987 .

The dissertation was originally published in Dutch by the:

Delft University of Technology

Faculty of Mechanical Engineering and Marine Technology

Chair of Dredging Technology

Mekelweg 2

2628 CD, Delft

The Netherlands

It is advised to also read the papers following this dissertation, since the theory developed has been refined and extended.

Last modified Sunday December 31, 2000 by: [Sape A. Miedema](#)

Translation by: [Laurens de Jonge](#)

Figures, equations and tables by: [Erik Miedema](#)

Copyright © December, 2000 Dr.ir. S.A. Miedema



[Download Adobe Acrobat Reader V4.0](#)

10.05 The specific energy and conclusions.

The specific cutting energy, emerging from a three-dimensional moving cutterhead (or cutter-wheel), will vary in time, similar to the loads on the cutterhead. Here as well a division can be made between specific energy emerging from the blades along the circumference of the cutterhead and the bottom blades. For the determination of the specific cutting energy emerging at the blades along the circumference of the cutterhead, equation (4.54) can be used, corrected for the total radial velocity:

$$V_{\text{rad}}(t) = \sqrt{(V_s \cdot V_s + V_{vc}(t) \cdot V_{vc}(t))} \quad (10.19)$$

Substitution of equation (10.19) for the haul velocity in equation (4.54) results in the specific cutting energy, as a function of time, needed for the cutting process of the blades along the circumference of the cutterhead. However, a correction has to be made for the real run-through angle.

For the determination of the specific cutting energy arising from the bottom blades, equations (5.40) can be used for the non-cavitating cutting process and equation (5.41) for the cavitating cutting process. For a fully cavitating cutting process, the specific cutting energy is constant according equation (5.41). This is similar to the hypothetical case where a fully cavitating cutting process arises on the circumference blades (equation (4.54)). When there is a non-cavitating cutting process, the specific cutting energy can be determined by substituting the effective axial velocity for the haul velocity (for a cutter-wheel) in equation (5.40).

The coefficient m_{gc} from these equations can be determined from the tables 5.1 to 5.5 (see appendix B8), for known values of $S_s(t)$ and B_v .

The specific cutting energy varies in time and can therefore not be a basis for the determination of the loads on a three-dimensional moving cutterhead.

The modeling in this chapter meets the demands that are required by the solution method of DREDMO, within the limitations set in chapter 10.2. Indicated is how effective velocities can be determined by integrating over a time Δt for time domain calculations. Within this solution method it is also possible to introduce an irregular breach profile. When the limitations set in

chapter 10.2 are no longer satisfied, the modeling from chapter 4 and 5 can no longer be used as such for a basis for the determination of the loads. Some goniometric effort is then required to come to a satisfying formulation of the loads.

[Back to top](#)

This is a translation of the dissertation of Dr.ir. S.A. Miedema, dated September 15th 1987 .
The dissertation was originally published in Dutch by the:
Delft University of Technology
Faculty of Mechanical Engineering and Marine Technology
Chair of Dredging Technology
Mekelweg 2
2628 CD, Delft
The Netherlands

It is advised to also read the papers following this dissertation, since the theory developed has been refined and extended.

Last modified Tuesday May 30, 2000 by: [Sape A. Miedema](#)

Translation by: [Laurens de Jonge](#)

Figures, equations and tables by: [Erik Miedema](#)

Copyright © May, 2000 Dr.ir. S.A. Miedema



[Download Adobe Acrobat Reader V4.0](#)

11.01 Description of the test stand.

The chapters 11.1 to 11.7 give a summary of the content of the already published articles in [36,44,45,46,47,50,51].

Chapters 11.8 and further contain the verification of the modeling from chapter 10.

The tests are performed in the old laboratory GV that is described in chapter 3.1. The properties of the sand in this test stand can be found in appendix B3. A number of facilities are installed on the main carriage for this research:

An auxiliary carriage, carrying the cutterhead installation (figure 11.1), can move transverse of the concrete tank on the main carriage.

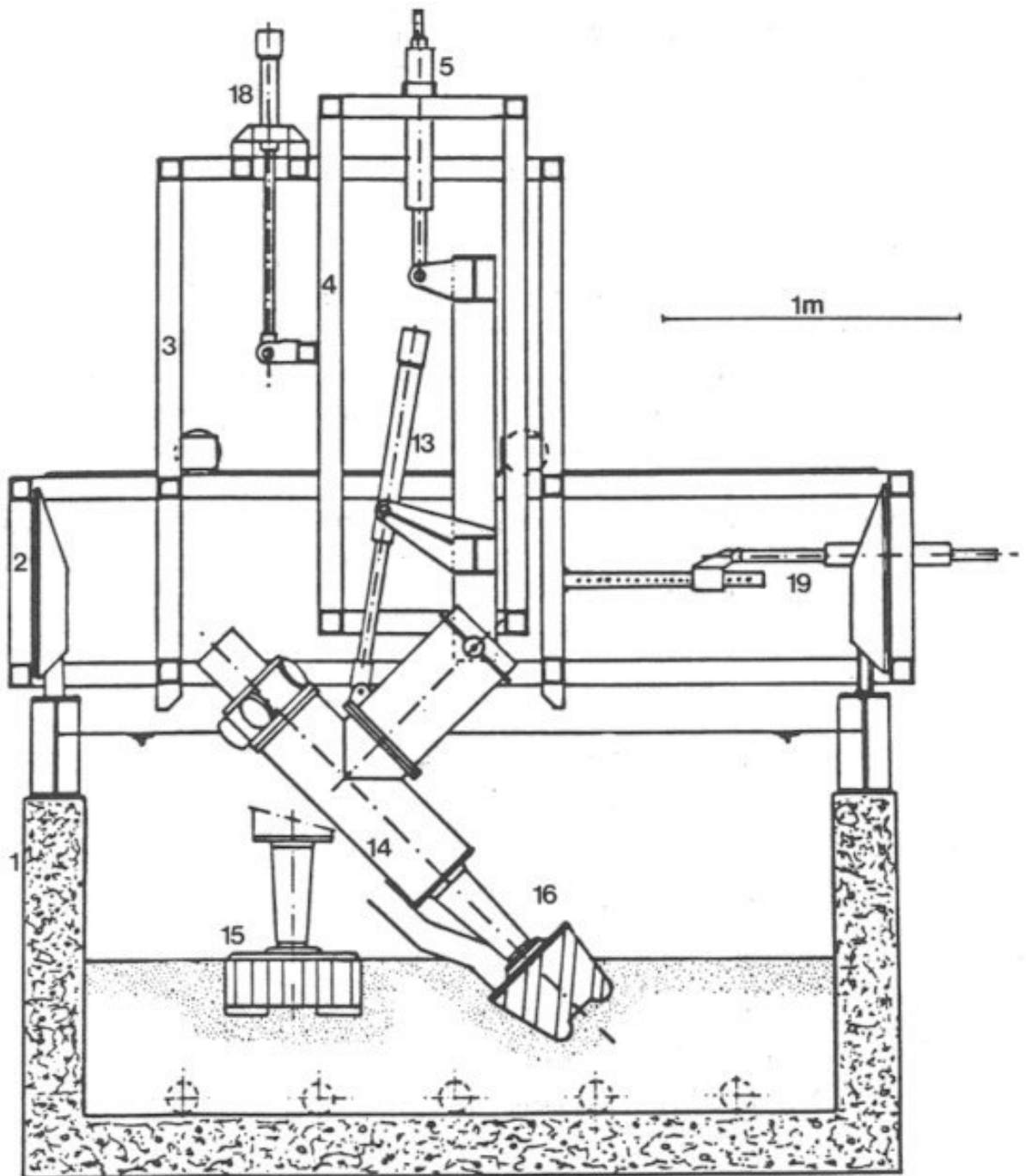


Figure 11.1: The test stand, with:

1. The concrete tank
2. The main carriage
3. The auxiliary carriage
4. An auxiliary frame
5. Hydraulic cylinder for vertical positioning
13. Hydraulic cylinder for positioning ladder angle
14. Ladder
15. Disc bottom cutterhead
16. Helix cutterhead
18. Hydraulic servo actuator for vertical wave simulation
19. Hydraulic servo actuator for horizontal wave simulation

Hydraulic cylinders are used to adjust the nominal cutting depth and the ladder angle. Two electronic controlled servo-actuators are used to enforce a vertical and/or horizontal motion to the cutterhead. The cutterhead has a hydraulic drive of 20 kW, with which the number of revolutions can be varied between 0 and 180 rev/min. The dredging pump is positioned on the main carriage and is driven by an electric drive of 15 kW, which makes a slurry velocity of 1.5 to 4.0 m/sec possible in the suction and pressure piping. These pipes have a diameter of 100 mm.

The dredged slurry is transported to a settling basin. The overflow of this tank is connected with the concrete tank. The sand that stays in the settling basin is weighed continuously. When a test is finished the sand from the settling basin is transported back to the concrete tank with a second dredging pump to recondition the sand bed to the initial sand level. The sand is then raked loose, scraped plane and vibrated firm. A drainage system on the bottom of the concrete tank makes it possible to give the sand a higher density during the vibration.

[Back to top](#)

This is a translation of the dissertation of Dr.ir. S.A. Miedema, dated September 15th 1987 .
The dissertation was originally published in Dutch by the:
Delft University of Technology
Faculty of Mechanical Engineering and Marine Technology
Chair of Dredging Technology
Mekelweg 2
2628 CD, Delft
The Netherlands

It is advised to also read the papers following this dissertation, since the theory developed has been refined and extended.

Last modified Tuesday May 30, 2000 by: [Sape A. Miedema](#)

Translation by: [Laurens de Jonge](#)

Figures, equations and tables by: [Erik Miedema](#)

Copyright © May, 2000 Dr.ir. S.A. Miedema



[Download Adobe Acrobat Reader V4.0](#)

11.02 The experiments.

The tests are performed with an experimental disc bottom cutterhead. The disc bottom cutterhead has a diameter of 475 mm, a height of 184 mm, 8 vertical blades along the circumference and 8 blades in the bottom. This cutterhead is chosen for the research because of the geometry, so that influences caused by the horizontal and vertical motions of the cutterhead can be determined independently. Also tests on a helix cutterhead are performed. These tests are however not suitable for the verification of the theory from chapter 10 since the cutterhead was equipped with tooth.

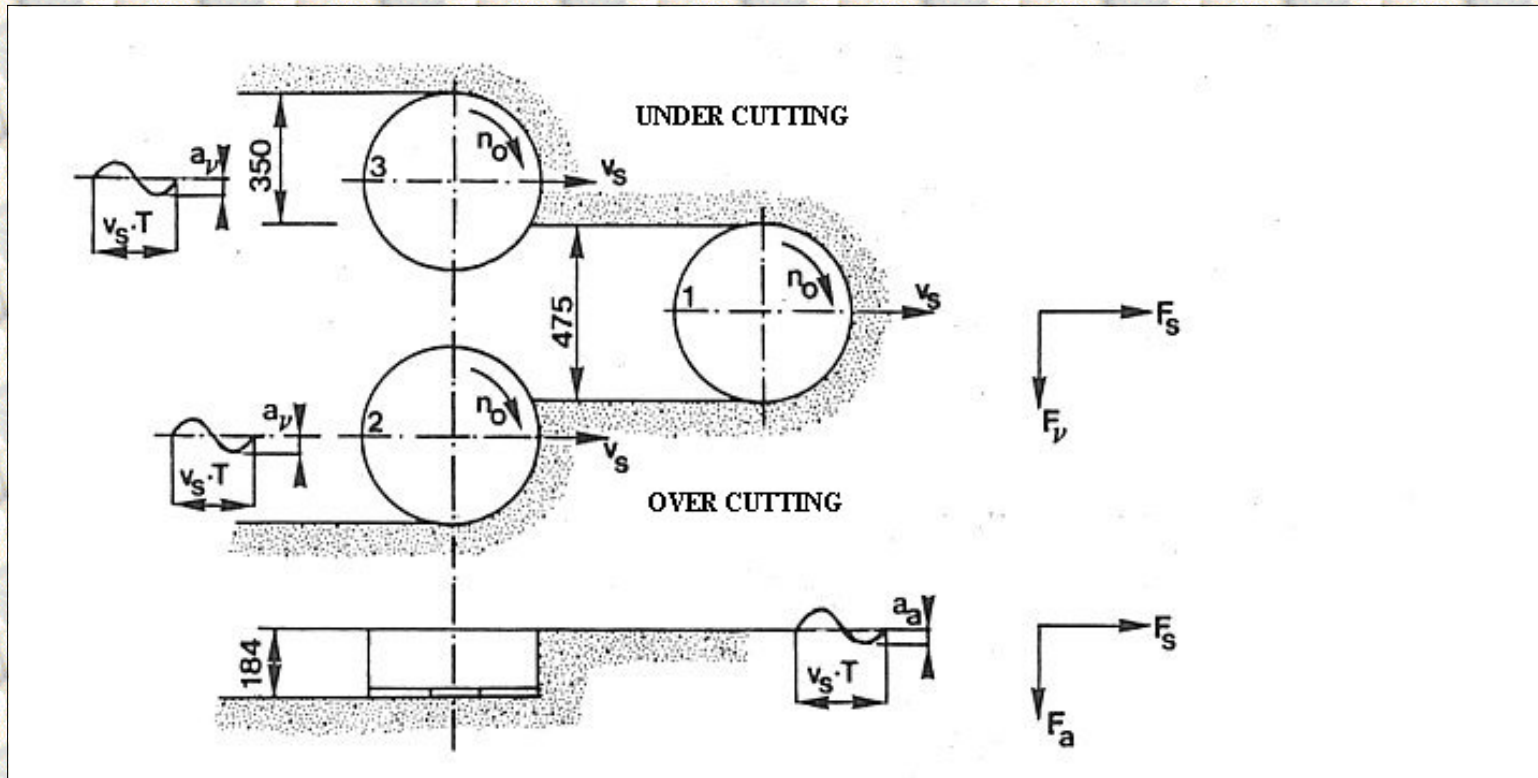


Figure 11.2: The cutting pattern.

For the simulated swell response on the cutterhead, a maximum amplitude of 40 mm on model scale is assumed with a wave period of 2 to 4 seconds. The tests with the disc bottom cutterhead are performed according the cutting pattern in figure 11.2. The length of the cut was 10 meters, of which only the middle 4.5 meters where used as the measuring area. In the tests with the disc bottom cutterhead the first cut was a breach forming cut, without enforcement of an oscillating motion on the cutterhead. For this cut always the same haul velocity and the same cutterhead number of revolutions is used, to create the same initial conditions for every test. In a series of tests with the disc bottom cutterhead of 23 over cutting and 23 under cutting tests, the following parameters are varied:

cutterhead number of revolutions: 25, 33 and 45 revolutions per minute

haul velocity: 60, 90 and 120 mm/sec

wave period: 4, 3.3, 2.5 and 2 sec

wave amplitude: 20, 30 and 40 mm

This is a translation of the dissertation of Dr.ir. S.A. Miedema, dated September 15th 1987 .
The dissertation was originally published in Dutch by the:
Delft University of Technology
Faculty of Mechanical Engineering and Marine Technology
Chair of Dredging Technology
Mekelweg 2
2628 CD, Delft
The Netherlands

It is advised to also read the papers following this dissertation, since the theory developed has been refined and extended.

Last modified Tuesday May 30, 2000 by: [Sape A. Miedema](#)

Translation by: [Laurens de Jonge](#)

Figures, equations and tables by: [Erik Miedema](#)

Copyright © May, 2000 Dr.ir. S.A. Miedema



[Download Adobe Acrobat Reader V4.0](#)

11.03 The measured signals.

The following signals are measured:

1. The number of revolutions of the cutterhead.
2. The haul velocity.
3. The oscillating motion of the cutterhead.
4. The radial force F_v , the surge force.
5. The force in the haul direction F_s , the haul force.
6. The axial force F_a , the heave force.
7. The drive torque M .

For the tests with the disc bottom cutterhead the surge force was equal to the radial force, perpendicular to the haul direction and the heave force was equal to the axial force, since the cutterhead axis had a vertical position.

The time history of the seven signals is recorded analogue during the tests. A further analysis of these signals was possible with the aid of several computer programs (Miedema [44,45]), developed within the framework of this research.

[Back to top](#)

This is a translation of the dissertation of Dr.ir. S.A. Miedema, dated September 15th 1987 .

The dissertation was originally published in Dutch by the:

Delft University of Technology

Faculty of Mechanical Engineering and Marine Technology

Chair of Dredging Technology

Mekelweg 2

2628 CD, Delft

The Netherlands

It is advised to also read the papers following this dissertation, since the theory developed has been refined and extended.

Last modified Tuesday May 30, 2000 by: [Sape A. Miedema](#)

Translation by: [Laurens de Jonge](#)

Figures, equations and tables by: [Erik Miedema](#)

Copyright © May, 2000 Dr.ir. S.A. Miedema



[Download Adobe Acrobat Reader V4.0](#)

11.04 The processing of the data measured.

Because high frequencies have limited influence on the motions of a moored ship and because it is required by the numerical processing method (mirror effect in a Fourier transformation), the measured signals is first filtered with a 12 dB "Low Pass" Butterworth filter with a toggle frequency of 20 Hz. Next the filtered signals are sampled during 20 seconds (of the measuring area), with a sampling frequency of 50 Hz so that every measuring signal is represented by 1001 samples. Since the swell response on the cutterhead is simulated by enforcing a sinusoidal motion, it can be expected that the measuring signals will have a periodical character with a period equal to this motion. To get a good impression of the history of the measuring signals during a period of the, on the cutterhead, enforced sinusoidal motion, a discrete Fourier transformation is chosen for the processing.

This results in a description of the periodic part of every measuring signal by a Fourier series. The general shape for the description of a signal $f(t)$ with a period T by a Fourier series is:

$$f(t) = \sum_{k=1}^{\infty} \left[a_k \cdot \cos(k \cdot 2 \cdot \pi \cdot t / T) + b_k \cdot \sin(k \cdot 2 \cdot \pi \cdot t / T) \right] + a_0 \quad (11.1)$$

For every measuring signal the constants a_0 , a_k and b_k are determined with a computer program, specially developed for this purpose. With this the periodic part of every measuring signal is determined deterministic and therefore reconstructable. From the processing of the measuring signals of in total 65 over cutting and 65 under cutting tests it is determined that only the first 6 terms of the Fourier series are relevant for the behavior of the measuring signals, so that the previous equation changes to:

$$f(t) = \sum_{k=1}^6 \left[a_k \cdot \cos(k \cdot 2 \cdot \pi \cdot t / T) + b_k \cdot \sin(k \cdot 2 \cdot \pi \cdot t / T) \right] + a_0 \quad (11.2)$$

[Back to top](#)

This is a translation of the dissertation of Dr.ir. S.A. Miedema, dated September 15th 1987 .
 The dissertation was originally published in Dutch by the:
Delft University of Technology
Faculty of Mechanical Engineering and Marine Technology
Chair of Dredging Technology

**Mekelweg 2
2628 CD, Delft
The Netherlands**

It is advised to also read the papers following this dissertation, since the theory developed has been refined and extended.

Last modified Tuesday May 30, 2000 by: [Sape A. Miedema](#)

Translation by: [Laurens de Jonge](#)

Figures, equations and tables by: [Erik Miedema](#)

Copyright © May, 2000 Dr.ir. S.A. Miedema



[Download Adobe Acrobat Reader V4.0](#)

11.05 Macroscopic cutting behavior.

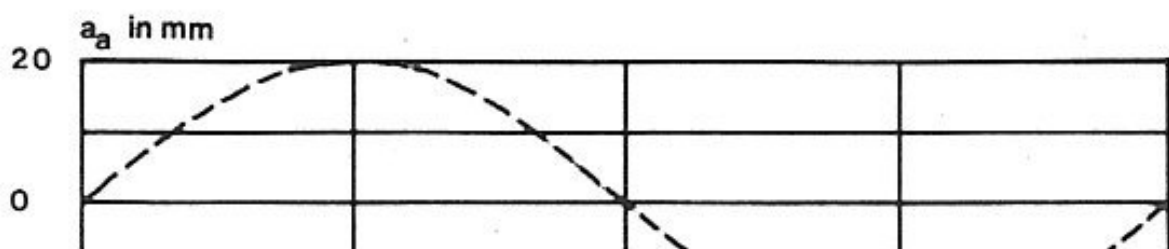
The history of the cutterhead loads during a period of the axial and the radial oscillation is shown in figure 11.3 (axial) and 11.4 (radial), for two representable tests with a disc bottom cutterhead. The history shows, as can be seen in these figures, in general a slowly increasing load, from the moment that the axial velocity of the cutterhead is aimed towards the breach. As the axial velocities increases, all loads on the cutterhead increase.

The loads remain increasing to a maximum value that is positioned in time between the moment where the axial velocity is maximal and the moment where the cutting depth is maximal. The loads decrease quickly from the moment on which the loads are maximal to the moment where the cutting depth is maximal. After this the axial velocity turns around (the cutterhead starts to move outward of the breach) and the loads decrease further to a minimum, that is positioned between the moment where the axial velocity is aimed maximal off the breach and the moment where the cutting depth is minimal. The moment on which the load is maximal can slightly differ in time for the various loads.

In the tests with the disc bottom cutterhead it is observed that the maximum for the heave force appears obviously later than the maxima in the drive torque and the surge force, while for the sway force this was not clearly present. This is probably caused by the horizontal bottom blades. It has to be remarked that during the tests with the disc bottom cutterhead the ladder made a 90° angle with the horizontal, so that the surge and heave forces were equal to the radial and axial forces. The experiments with the disc bottom cutterhead showed that the size of the maxima of the driving torque, the sway force and the radial force perpendicular to the haul direction are strongly dependent on the velocity with which the cutterhead axially enters the breach and the reached cutting depth. On the other hand they showed that the size of the maximum of the axial force mainly depends on the cutting depth and the profile of the breach part where the cutterhead cuts. This last influence quantity can be quantified by the ratio of the wave length of the oscillation and the cutterhead diameter. Also the haul velocity and the number of revolutions of the cutterhead have a role in the size of the maximal emerging loads.

The haul velocity and the number of revolutions of the cutterhead show also a characteristic history path during a period of the oscillating motion of the cutterhead. While over cutting the haul velocity increases when the cutterhead is pushed into the breach. This is caused by the fact that the cutterhead starts to drive the main carriage in the haul direction. While under cutting the opposite happens when the main carriage is slowed down. In both cases the number of revolutions of the cutterhead decreases when the cutterhead is pushed into the breach.

Since the cutterhead loads are inversely proportional to the number of revolutions of the cutterhead, a decrease of the number of revolutions will result in an increase of the loads, which is followed by a further decrease of the number of revolutions. Therefore a new equilibrium between the torque characteristic of the cutterhead drive and the drive torque required by the cutting process will develop.



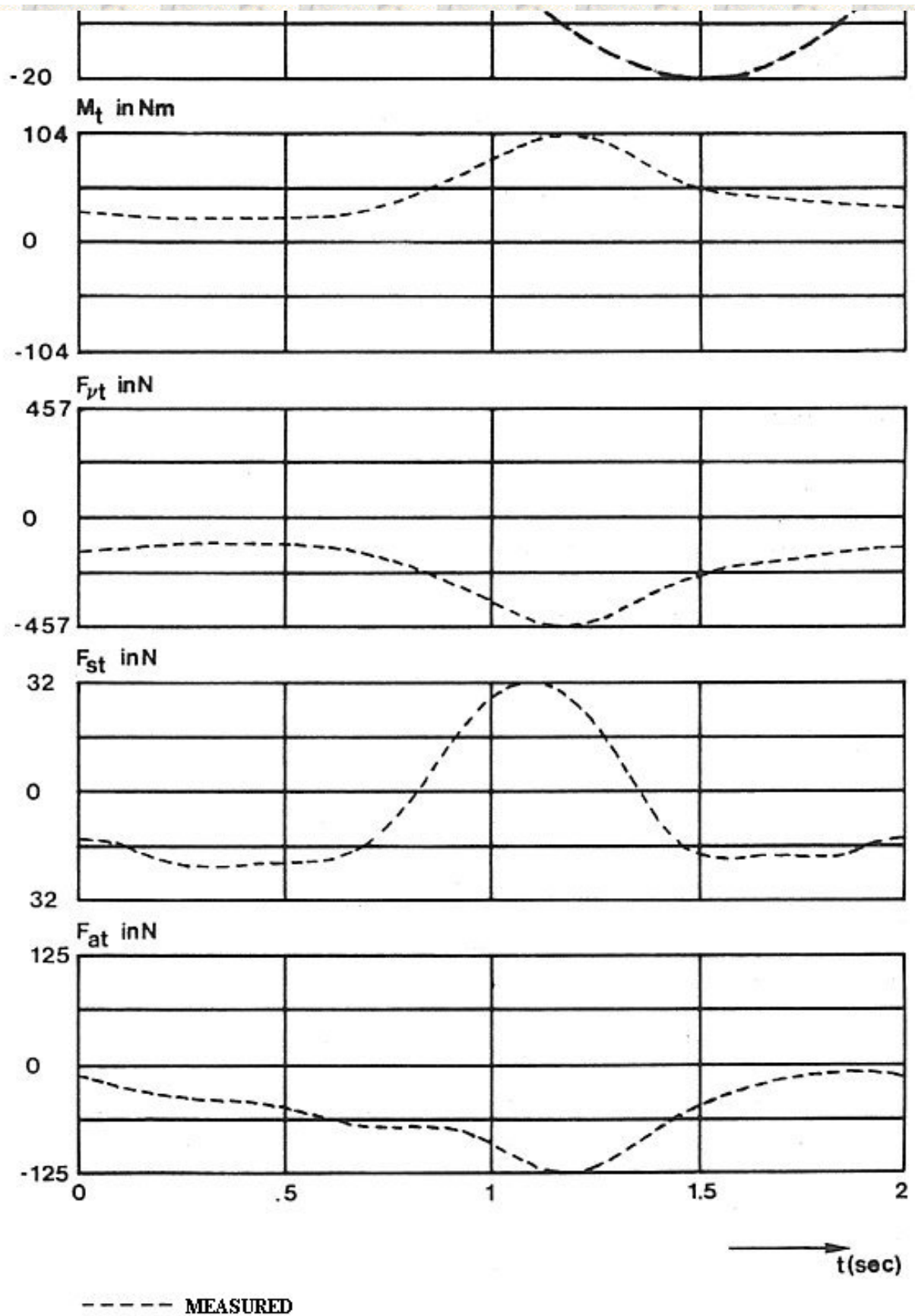


Figure 11.3: The measured forces F_{st} , F_{vt} and F_{at} and the measured torque M_t on the disc bottom cutterhead for an axial oscillation with a period T of 2 seconds, an amplitude a_a of 20 mm, a haul velocity v_s of 0.089 m/s, a number of revolutions n_0 of 45 rpm and an over cutting cutting process.

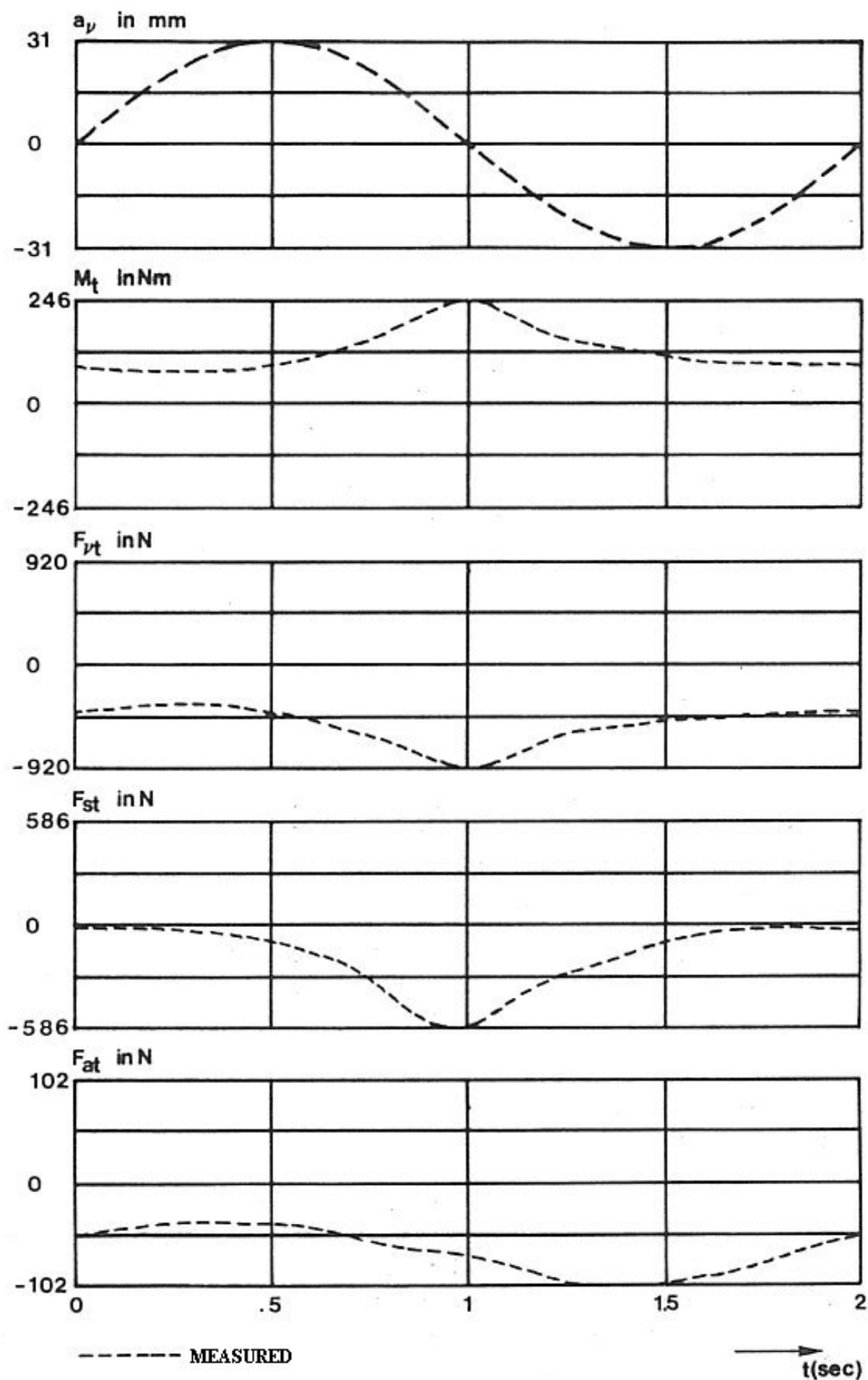


Figure 11.4: The measured forces F_{st} , F_{vt} and F_{at} and the measured torque M_t on the disc bottom

cutterhead for a radial oscillation with a period T of 2 seconds, an amplitude a_v of 31 mm, a haul velocity v_s of 0.108 m/s, a number of revolutions n_0 of 34 rpm and an under cutting cutting process.

[Back to top](#)

This is a translation of the dissertation of Dr.ir. S.A. Miedema, dated September 15th 1987 .

The dissertation was originally published in Dutch by the:

Delft University of Technology

Faculty of Mechanical Engineering and Marine Technology

Chair of Dredging Technology

Mekelweg 2

2628 CD, Delft

The Netherlands

It is advised to also read the papers following this dissertation, since the theory developed has been refined and extended.

Last modified Tuesday May 30, 2000 by: [Sape A. Miedema](#)

Translation by: [Laurens de Jonge](#)

Figures, equations and tables by: [Erik Miedema](#)

Copyright © May, 2000 Dr.ir. S.A. Miedema



[Download Adobe Acrobat Reader V4.0](#)

11.06 Influence parameters.

The qualitative and quantitative image of the history of the cutterhead loads as a result of the oscillating motions of the cutterhead mainly depends on the following influence parameters:

$$\frac{v_s \cdot 60}{2 \cdot \pi \cdot n_o} \quad (11.3)$$

This influence parameter gives an impression of the layer-thickness and the clearance angle of the blades (tooth) as a result of the uniform motion of the cutterhead in the haul direction.

$$\frac{2 \cdot \pi \cdot n_o}{60} \quad (11.4)$$

This influence parameter is an approximation of the cutting velocity of the blades.

$$\frac{v_s \cdot 60}{\omega_a \cdot D} \quad \frac{v_s \cdot 60}{\omega_v \cdot D} \quad (11.5)$$

This influence parameter gives the ratio between the wave length of the oscillation enforced on the cutterhead and the diameter of the cutterhead. This gives an impression of the partly dredged profile in which the cutterhead is dredging.

$$\frac{a_a}{B_a} \quad (11.6)$$

This influence parameter gives the ratio between the amplitude of the axial oscillating motion and the nominal cutting depth. It gives therefore an impression of the relative variation in the cutterhead loads.

$$\frac{\omega_a \cdot a_a \cdot 60}{n_o \cdot R} \quad (11.7)$$

This influence parameter gives an impression of the influence of the axial velocity of the cutterhead on the layer-thickness and the clearance angle of the bottom blades.

[Back to top](#)

This is a translation of the dissertation of Dr.ir. S.A. Miedema, dated September 15th 1987 .

The dissertation was originally published in Dutch by the:

Delft University of Technology

Faculty of Mechanical Engineering and Marine Technology

Chair of Dredging Technology

Mekelweg 2

2628 CD, Delft

The Netherlands

It is advised to also read the papers following this dissertation, since the theory developed has been refined and extended.

Last modified Tuesday May 30, 2000 by: [Sape A. Miedema](#)

Translation by: [Laurens de Jonge](#)

Figures, equations and tables by: [Erik Miedema](#)

Copyright © May, 2000 Dr.ir. S.A. Miedema



[Download Adobe Acrobat Reader V4.0](#)

11.07 Conclusions macroscopic behavior.

It can be posed that an oscillating motion of the cutterhead in the axial direction can lead to a strong momentary increase of the cutterhead loads. For an amplitude of the oscillation of only 10%-20% of the cutting depth, this can already lead to a multiplication of the cutterhead loads. The choice of the haul velocity and the number of revolutions of the cutterhead have a main influence on this. It also has to be remarked that the loads have a characteristic history relative to the cutterhead related coordinate system.

In the body related coordinate system of the cutter-suction dredger the loads can have a more irregular course, in which the load can even change sign in a certain direction (Miedema [47]). The turn around of the direction of the surge or heave force can have an influence on the design of a swell compensation system due to the characteristic of such a system. The best thing to do is to design a system that compensates in radial and in axial direction and therefore independent of the ladder angle. Such a system is described by Miedema [48,49,51].

[Back to top](#)

This is a translation of the dissertation of Dr.ir. S.A. Miedema, dated September 15th 1987 .

The dissertation was originally published in Dutch by the:

Delft University of Technology

Faculty of Mechanical Engineering and Marine Technology

Chair of Dredging Technology

Mekelweg 2

2628 CD, Delft

The Netherlands

It is advised to also read the papers following this dissertation, since the theory developed has been refined and extended.

Last modified Tuesday May 30, 2000 by: [Sape A. Miedema](#)

Translation by: [Laurens de Jonge](#)

Figures, equations and tables by: [Erik Miedema](#)

Copyright © May, 2000 Dr.ir. S.A. Miedema



[Download Adobe Acrobat Reader V4.0](#)

[Contents](#) **11.08 Verification radial velocity variations.**

In chapter 7.3 simplified equations are derived for the loads on the used experimental disc bottom cutterhead. Included in these equations are the influences of the loads on the circumference blades and the loads as a result of the 19 mm, cut by the bottom blades. For the verification of the loads in the radial velocity variations the coefficients, mentioned in chapter 7, will be assumed. In chapter 10.3 is indicated how the loads on a cutterhead, as a result of the radial velocity variations, can be determined. With the aid of a computer program these loads are determined for those tests, where the cutting process was more or less pure. The figures 11.5 and 11.6 show the measured loads and the calculated loads during a period of radial oscillation.

From this simulation can be concluded:

1. The level of the loads is approximated well, while the history path of the measured loads agree well with the theory.
2. At a number of revolutions of 33 rev/min the measured loads are in proportion larger compared to the theory than at a number of revolutions of 45 rev/min.
3. The phase haul between the loads and the cutterhead motion agree with the phase haul, mentioned in chapter 10.

A few aspects, except for the simplifications that are necessary within the analytical models of chapter 4 and 5, that can explain conclusion 2 have not been discussed yet. In the modeling of the cutting process has always been assumed that the cutting process was pure, that is a cutting process where the backside of the blade is clear from the cut sand. The construction of the disc bottom cutterhead is however such, that certain parts of the cutterhead (for instance the ring) "bulldozer". The effect of this on the measured loads is not clear, but is probably larger with lower number of revolutions.

In the development of the theory a constant haul velocity and a constant number of revolutions of the cutterhead are assumed. Deviations from the constant haul velocity and the constant number of revolutions of the cutterhead have already been observed in chapter 11.5. These deviations are caused by the drive mechanisms of the test stand and are very hard to model. Here it can also be assumed that the effects are larger with lower numbers of revolutions, but it can also be assumed that in this case there is a difference between over and under cutting dredging due to the direction of the force F_s .

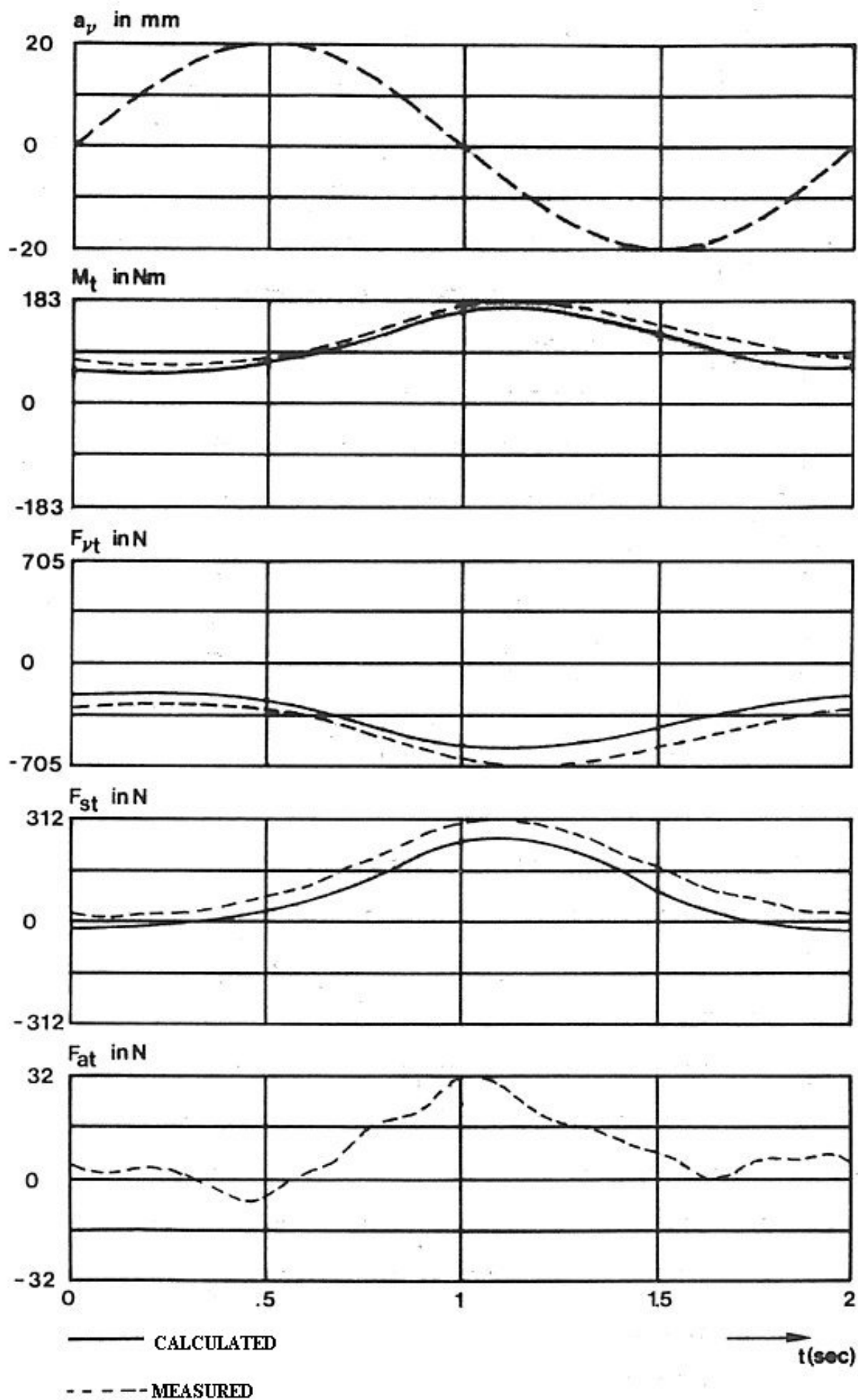
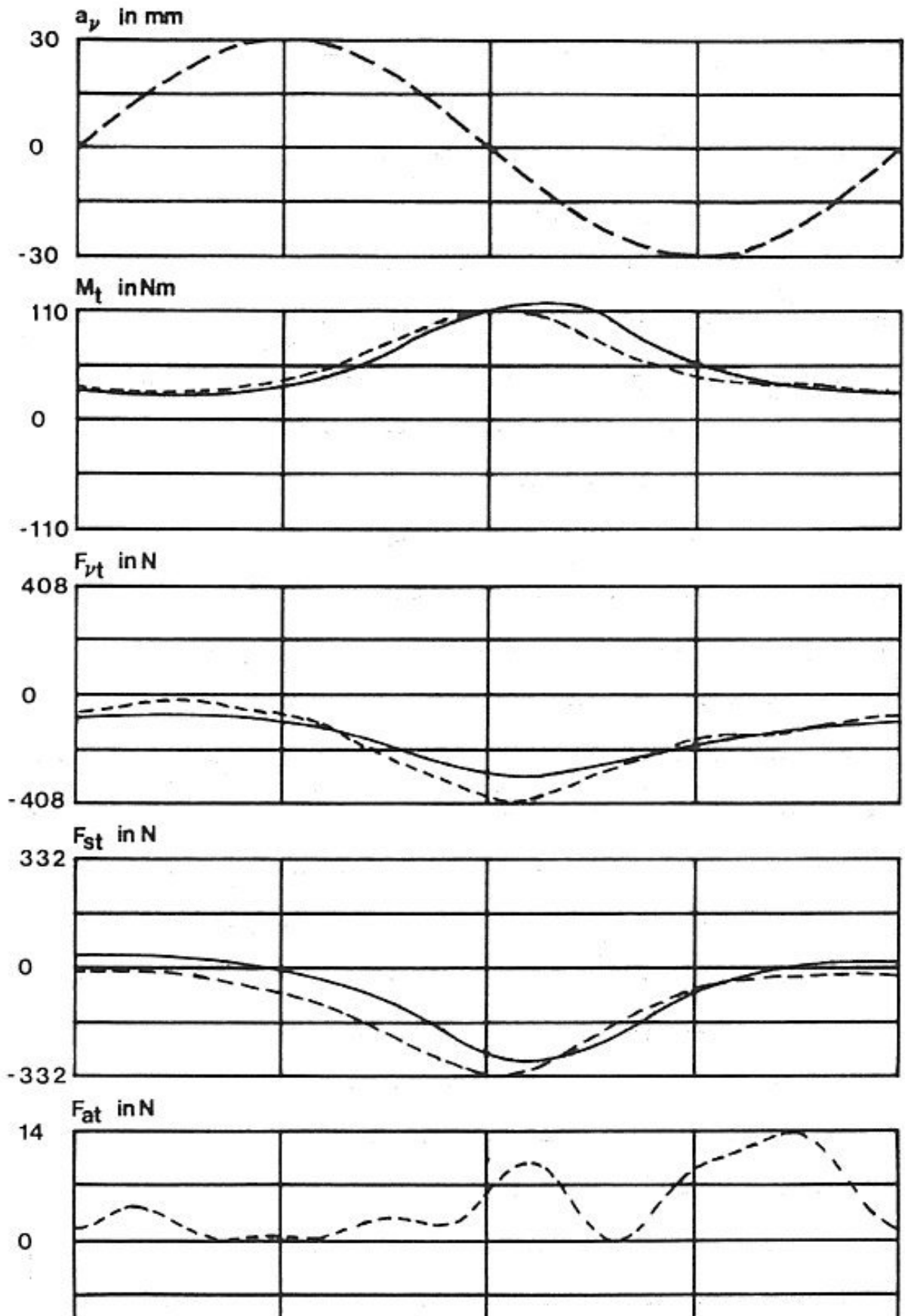


Figure 11.5: The measured forces F_{st} , F_{vt} and F_{at} and the measured torque M_t on the disc bottom cutterhead for a radial oscillation with a period T of 2 seconds, an amplitude a_v of 20 mm, a haul velocity v_s of 0.109 m/s, a number of revolutions n_0 of 33 rpm and an over cutting cutting process (dashed line). Also the according chapter 10 determined forces F_{vt} and F_{st} and the torque M_t are shown with a solid line.



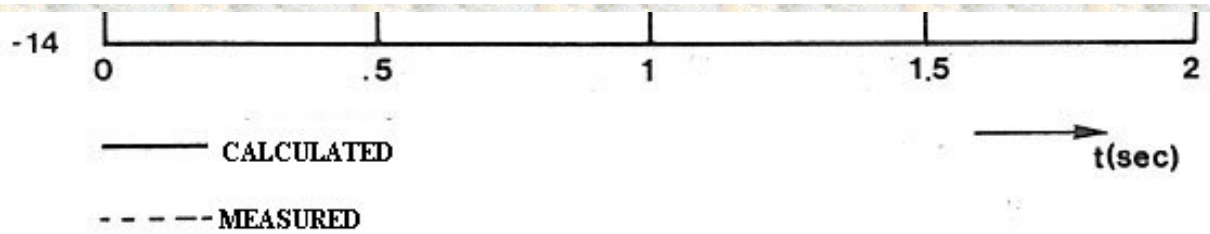


Figure 11.6: The measured forces F_{st} , F_{vt} and F_{at} and the measured torque M_t on the disc bottom cutterhead for a radial oscillation with a period T of 2 seconds, an amplitude a_v of 30 mm, a haul velocity v_s of 0.079 m/s, a number of revolutions n_0 of 44 rpm and an under cutting cutting process (dashed line). Also the according chapter 10 determined forces F_{vt} and F_{st} and the torque M_t are shown with a solid line.

[Back to top](#)

This is a translation of the dissertation of Dr.ir. S.A. Miedema, dated September 15th 1987 .
 The dissertation was originally published in Dutch by the:
 Delft University of Technology
 Faculty of Mechanical Engineering and Marine Technology
 Chair of Dredging Technology
 Mekelweg 2
 2628 CD, Delft
 The Netherlands

It is advised to also read the papers following this dissertation, since the theory developed has been refined and extended.

Last modified Tuesday May 30, 2000 by: [Sape A. Miedema](#)

Translation by: [Laurens de Jonge](#)

Figures, equations and tables by: [Erik Miedema](#)

Copyright © May, 2000 Dr.ir. S.A. Miedema



[Download Adobe Acrobat Reader V4.0](#)

11.09 Verification axial velocity variations.

In a closer analysis of the tests, where a sinusoidal axial motion is enforced on the cutterhead, it appeared that the bottom plate of the cutterhead made contact with the breach ("bulldozer") for lower numbers of revolutions (25 and 33 rev/min). Although the history of the loads in these tests agree qualitatively with the theory from chapter 10, which is mainly a result of the history of the axial velocity in time, maximum loads are found which are twice to three times as could be expected from theory. Figure 11.7 gives an impression.

During the tests with a number of revolutions of 45 rev/min the bottom plate stayed clear of the breach, while the bottom blades participated in the cutting process. The theoretic determination of the loads on the bottom blades in chapter 10 is based on the analytical cutter-wheel model. The layer-thickness is, in contrast to the cutter-wheel with constant haul velocity, for the disc bottom cutterhead with an axial oscillating motion not constant, but varies corresponding equation (10.13). This implies that the coefficients c_1 and c_2 are also not constant.

For these coefficients two approximation equations are formulated, by means of extrapolation:

$$c_1 = 1.32 \cdot \left(\frac{h_b}{h_i} \right)^{0.307} \quad (11.8)$$

$$c_2 = -.40 \cdot \left(\frac{h_b}{h_i} \right)^{0.485} \quad (11.9)$$

The figures 11.8 and 11.9 show the measured loads and the, according the theory of chapter 10, calculated loads. The measured loads agree well, both qualitative as quantitative, with the calculated loads.

Also the theoretical expected phase haul can be observed clearly in the measurements. However it has to be accounted for that the figures 11.8 and 11.9 each show the result of a test and that the present spread of the soil mechanical parameters will influence the history of the loads and the mutual ratio's of the loads.

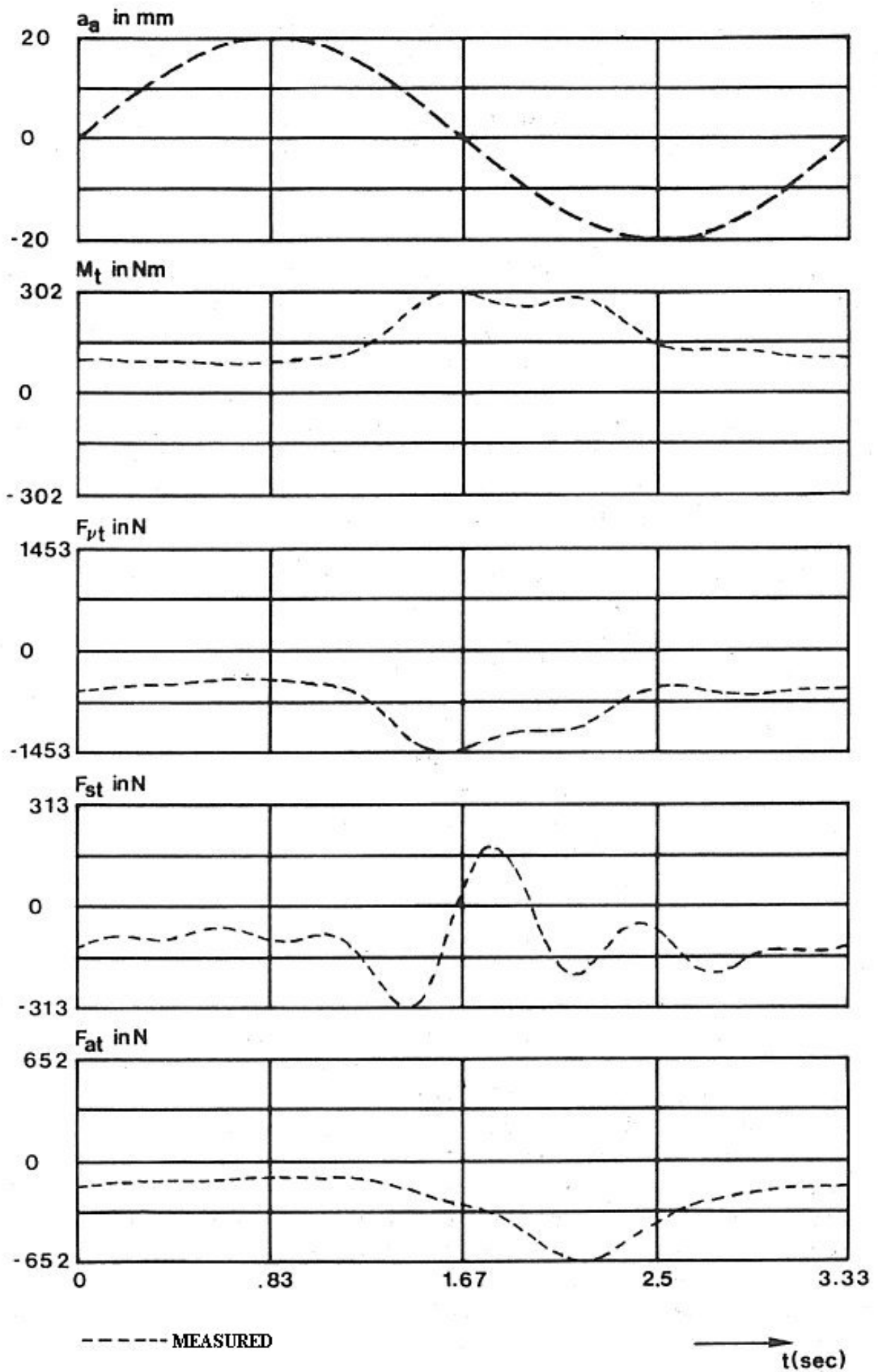
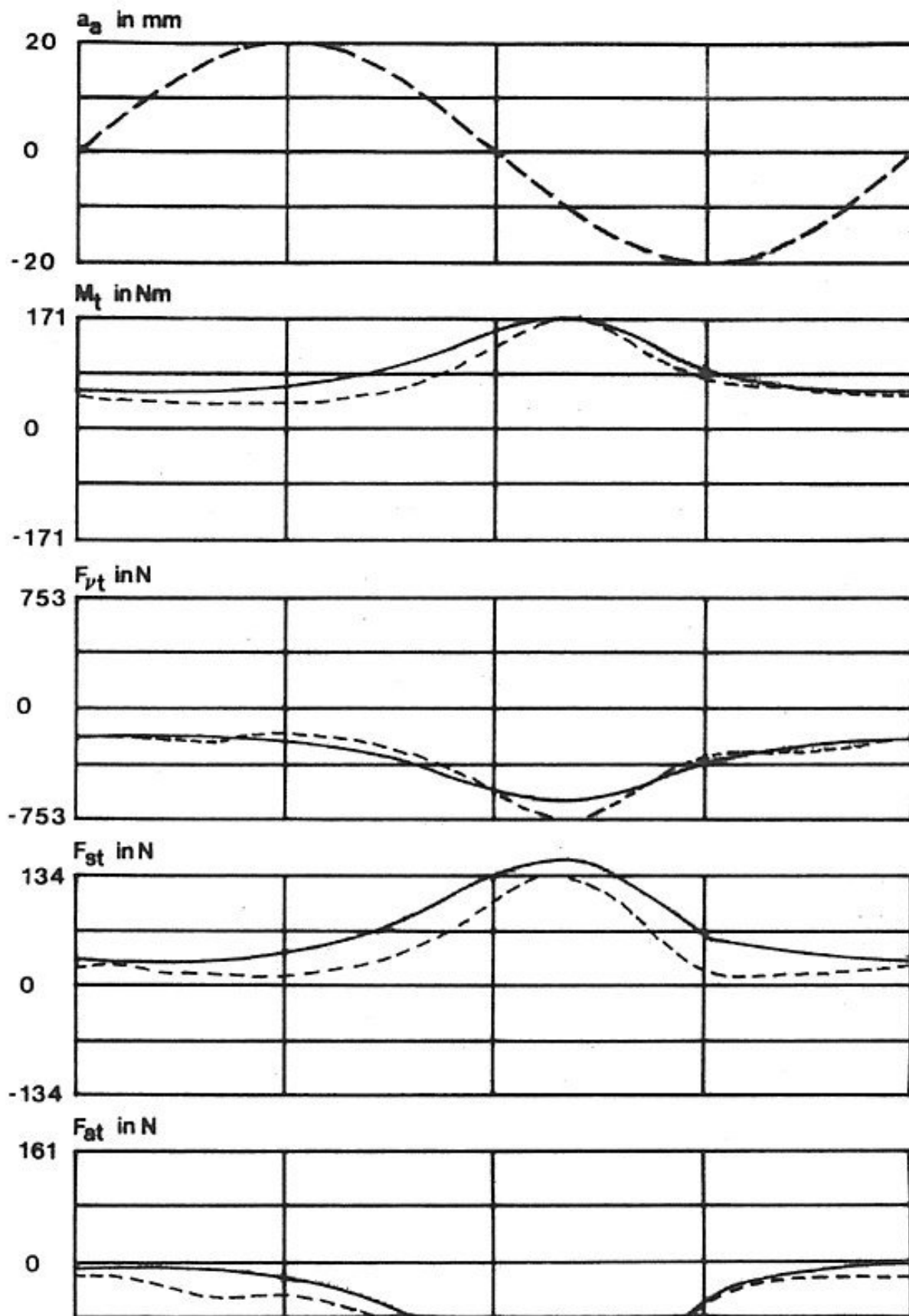


Figure 11.7: The measured forces F_{st} , F_{vt} and F_{at} and the measured torque M_t on the disc bottom cutterhead for an axial oscillation with a period T of 3.33 seconds, an amplitude a_v of 20 mm, a haul velocity v_s of 0.113 m/s, a number of revolutions n_0 of 23 rpm and an over cutting cutting process (dashed line). As a result of the rubbing of the bottom of the cutterhead a deviating path of the loads is seen while the peak loads are extremely high.



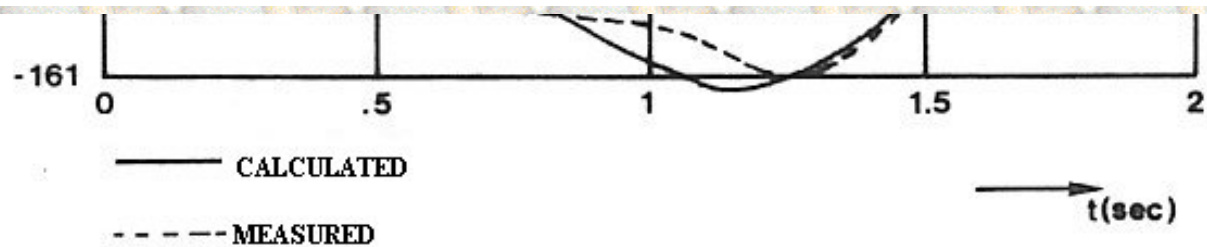
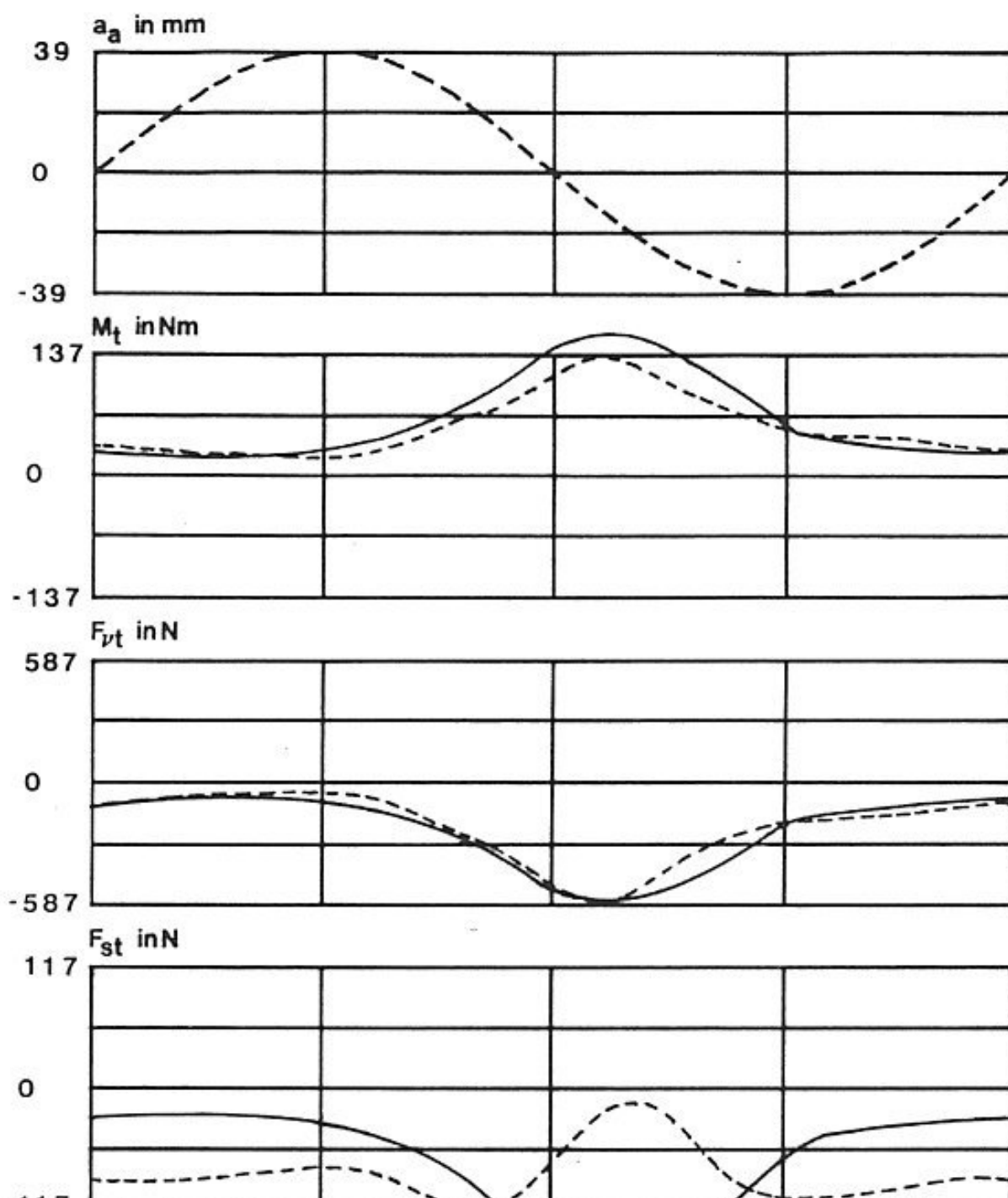


Figure 11.8: The measured forces F_{st} , F_{vt} and F_{at} and the measured torque M_t on the disc bottom cutterhead for an axial oscillation with a period T of 2 seconds, an amplitude a_v of 20 mm, a haul velocity v_s of 0.110 m/s, a number of revolutions n_0 of 44 rpm and an over cutting cutting process (dashed line). Also the according chapter 10 determined forces F_{vt} and F_{st} and the torque M_t are shown with a solid line.



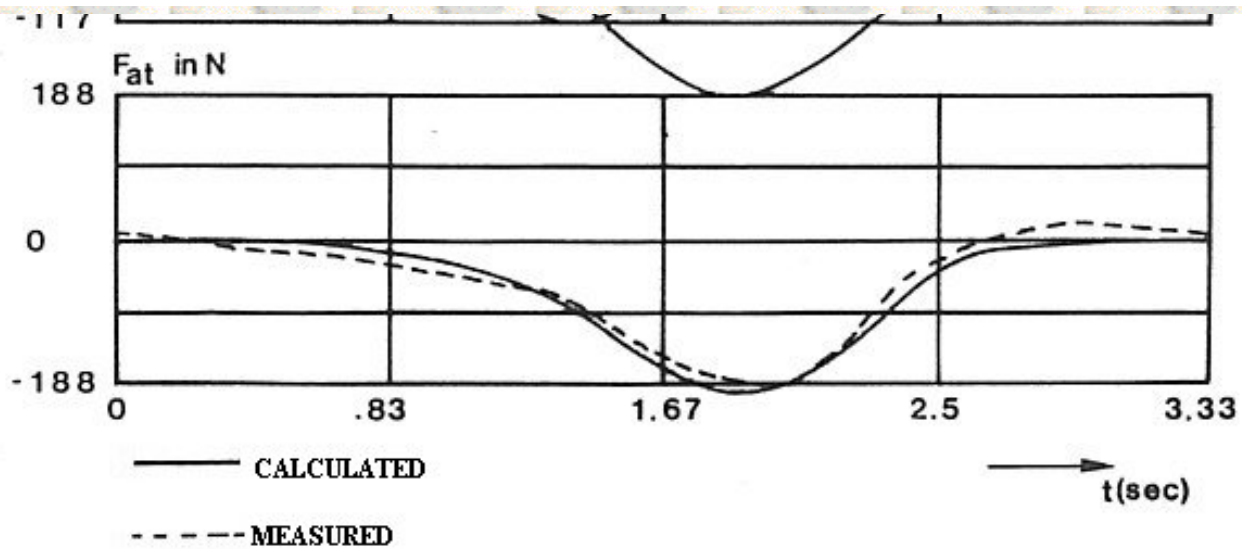


Figure 11.9: The measured forces F_{st} , F_{vt} and F_{at} and the measured torque M_t on the disc bottom cutterhead for an axial oscillation with a period T of 3.33 seconds, an amplitude a_v of 39 mm, a haul velocity v_s of 0.074 m/s, a number of revolutions n_0 of 45 rpm and an under cutting cutting process (dashed line). Also the according chapter 10 determined forces F_{vt} and F_{st} and the torque M_t are shown with a solid line.

[Back to top](#)

This is a translation of the dissertation of Dr.ir. S.A. Miedema, dated September 15th 1987 .

The dissertation was originally published in Dutch by the:

Delft University of Technology

Faculty of Mechanical Engineering and Marine Technology

Chair of Dredging Technology

Mekelweg 2

2628 CD, Delft

The Netherlands

It is advised to also read the papers following this dissertation, since the theory developed has been refined and extended.

Last modified Tuesday May 30, 2000 by: [Sape A. Miedema](#)

Translation by: [Laurens de Jonge](#)

Figures, equations and tables by: [Erik Miedema](#)

Copyright © May, 2000 Dr.ir. S.A. Miedema



[Download Adobe Acrobat Reader V4.0](#)

[Contents](#)

11.10 Conclusions.

The loads on a periodic axial or radial moving disc bottom cutterhead can be predicted well with the theory, derived in chapter 10, if a pure cutting process can be assumed. It turned out to be essential in this research, that for the construction of a model cutterhead and for the determination of values to be applied of the number of revolutions, the haul velocity and the frequency and amplitude of the oscillating motion in model tests, this has to be taken into account.

[Back to top](#)

This is a translation of the dissertation of Dr.ir. S.A. Miedema, dated September 15th 1987 .
The dissertation was originally published in Dutch by the:
Delft University of Technology
Faculty of Mechanical Engineering and Marine Technology
Chair of Dredging Technology
Mekelweg 2
2628 CD, Delft
The Netherlands

It is advised to also read the papers following this dissertation, since the theory developed has been refined and extended.

Last modified Tuesday May 30, 2000 by: [Sape A. Miedema](#)

Translation by: [Laurens de Jonge](#)

Figures, equations and tables by: [Erik Miedema](#)

Copyright © May, 2000 Dr.ir. S.A. Miedema



[Download Adobe Acrobat Reader V4.0](#)

12.01 Conclusion verification two-dimensional cutting theory.

1. The water resistance are negligible within the applied range of the cutting velocity.
2. Side influences lead to more downward aimed forces, while these do not unambiguously influence the magnitude of the forces. No sliding forces were clearly present on the side blades.
3. As a result of a slightly increasing density with a greater depth in proportion larger cutting forces are observed for larger blade dimensions. As a result larger cutting forces in relation to the theory have also been observed with the thicker layers and therefore with smaller blade-height/layer-thickness ratios.
4. In relation to the theory the cutting forces decrease with an increasing blade angle. This is observed in two types of sand.
5. The cutting forces agree approximately well with the theory, both in size and in direction.
6. The point of application of the cutting forces is positioned closer to the blade tip for a smaller blade-height / layer-thickness ratio.
7. As a result of wear the cutting forces are slightly aimed more upward, although it has to be remarked that the extent will totally depend on the wear image.
8. The measured water under-pressures agrees also well with the theory, although the water under-pressures are a little smaller in relation to the theory as the cutting forces.
9. The application of a horizontal wear face behind the blade tip did not lead to the initially expected increase of the water under-pressures, but showed approximately the same image as the tests without the wear face. From this it is concluded that the sand behind the blade tip comes slightly up (dilatancy?) which always gives a certain scraping of the sand against the clearance section.
10. In the transition region between the non-cavitating and the cavitating

cutting process a flattening of the pore pressure profile on the blade can be observed. This phenomenon has a progressive character, which causes the water under-pressures on the blade to increase almost continuously linear to the point where full cavitation on the blade occurs. As a result the direction of the cutting force changes.

11. Behind the blade large under-pressures are observed, these under-pressures determine to a large extent the value of the angle of internal friction as this can be derived from the cutting process.
12. From the determination of the angle of internal friction from the cutting tests it showed that the applicable value of this angle for the cutting process is 3 to 4 degrees higher than the values determined with undrained triaxial tests.
13. Summarizing it can be posed that the theory is well applicable for the cutting of water saturated sand with straight blades, if the above mentioned conclusions and remarks are taken in consideration.

[Back to top](#)

This is a translation of the dissertation of Dr.ir. S.A. Miedema, dated September 15th 1987 .

The dissertation was originally published in Dutch by the:

Delft University of Technology

Faculty of Mechanical Engineering and Marine Technology

Chair of Dredging Technology

Mekelweg 2

2628 CD, Delft

The Netherlands

Last modified Wednesday May 24, 2000 by: [Sape A. Miedema](#)

Translation by: [Laurens de Jonge](#)

Figures, equations and tables by: [Erik Miedema](#)

Copyright © May, 2000 Dr.ir. S.A. Miedema



[Download Adobe Acrobat Reader V4.0](#)

12.02 Conclusions verification cutterhead and dredging wheel.

Contents

1. The loads on the disc bottom cutterhead with bottom blades are well approximated with the theory, both in magnitude and the mutual ratios. From the mutual ratios of the loads can be derived that the coefficients c_1 and c_2 have slightly different values than is predicted with the theory, which is probably caused by the deviant shape of the circumference blades.
2. The comparison between the analytical model and the numerical model, as far as the loads on the disc bottom cutterhead are concerned, show little changes in the proportionalities between the loads on one hand and the haul velocity and the number of revolutions on the other hand. The simplifications and the neglects within the analytical model cause these changes.
3. By choosing low haul velocities and low numbers of revolutions the hydraulic and the mechanical losses are negligible on the disc bottom cutterhead, which should not allow the conclusion that this can always be done.
4. On the dredging-wheel the hydraulic losses and mechanical losses are surely not negligible. This is caused by the choice of high numbers of revolutions and haul velocities on the one hand and on the other hand mainly by the shape of the cutting edges on the dredging-wheel.
5. The loads on the dredging-wheel can be predicted fairly well, although the model tests showed a large spread.
6. The so-called "bulldozer limit" is observed clearly. With the aid of the in the tables mentioned shear angles and dimensionless forces, optimization of the construction of the cutting edges with regard to the size of the loads and the possible occurrence of the "bulldozer effect" is possible.
7. The occurrence of wear of the cutting edges can be the cause that for small blade angles the dredging-wheel does not drive itself in the haul direction but rather has to be driven.
8. Summarizing it can be posed that the theoretical models for the cutterhead

and the dredging-wheel agree reasonable to well with the loads measured during the model tests. These models are used as a starting point for the determination of the loads on a three-dimensional moving cutterhead.

[Back to top](#)

This is a translation of the dissertation of Dr.ir. S.A. Miedema, dated September 15th 1987 .

The dissertation was originally published in Dutch by the:

Delft University of Technology

Faculty of Mechanical Engineering and Marine Technology

Chair of Dredging Technology

Mekelweg 2

2628 CD, Delft

The Netherlands

Last modified Wednesday May 24, 2000 by: [Sape A. Miedema](#)

Translation by: [Laurens de Jonge](#)

Figures, equations and tables by: [Erik Miedema](#)

Copyright © May, 2000 Dr.ir. S.A. Miedema



[Download Adobe Acrobat Reader V4.0](#)

12.03 Conclusions verification 3D moving cutterhead.

[Contents](#)

1. The conversion of the two-dimensional cutting theory, using the models for the cutterhead and the dredging-wheel, to a three-dimensional moving cutterhead or dredging-wheel is mainly a geometric occurrence, where the macroscopic behavior of the loads is still determined by the fundamental process.
2. The loads are both qualitative and quantitative well predictable, if the requirements for a pure cutting process are met, that is a cutting process with a sharp blade and a positive clearance angle.
3. Deviations of the theory can be the result of the scraping of the sand against the bottom or against the hub in axial motions or the scraping of the ring of the cutterhead in radial motions.
4. During the construction of the cutterhead and for the determination of a test program this has to be accounted for.

[Back to top](#)

This is a translation of the dissertation of Dr.ir. S.A. Miedema, dated September 15th 1987 .

The dissertation was originally published in Dutch by the:

Delft University of Technology

Faculty of Mechanical Engineering and Marine Technology

Chair of Dredging Technology

Mekelweg 2

2628 CD, Delft

The Netherlands

Last modified Wednesday May 24, 2000 by: [Sape A. Miedema](#)

Translation by: [Laurens de Jonge](#)

Figures, equations and tables by: [Erik Miedema](#)

Copyright © May, 2000 Dr.ir. S.A. Miedema



[Download Adobe Acrobat Reader V4.0](#)

12.04 Conclusions, possible further research.

[Contents](#)

1. Research of the under-pressure behind the blade for the two-dimensional cutting process, in order to establish a better formulation of this under-pressure as a function of the process parameters.
2. Research of the influence of the wear on the size and the direction of the cutting forces for several wear mechanisms to quantify the concept of wear.
3. Research of the loads on tooth and tooth equipped excavating elements.
4. Research of the cutting forces at higher cutting velocities and higher pressures, in order to verify the expected occurrence of full cavitation and the expected proportionalities with the water depth.
5. Research of the possibility to develop a model disc bottom cutterhead, with which the characteristic soil parameters Π_1 and Π_2 can be determined.
6. Research of the scale rules belonging to the hydraulic and the mechanical losses, occurring in the cutting process of a dredging-wheel and a cutterhead, to improve the insight in the possibility to scale-up the results from model tests to prototype.
7. Research of the occurring forces in other soils than sand (clay and rock).
8. Addition of a soil module for dredging-wheel dredgers to DREDMO.
9. Research of a refinement of the integration and the iteration methods in DREDMO.
10. Besides the above mentioned possibilities for further research there are numerous aspects to which attention can be paid. For the choice of research in the field of hydraulic earthworks however, the practical applicability has to be the first objective.

[Back to top](#)

This is a translation of the dissertation of Dr.ir. S.A. Miedema, dated September 15th 1987 .

The dissertation was originally published in Dutch by the:
Delft University of Technology
Faculty of Mechanical Engineering and Marine Technology
Chair of Dredging Technology
Mekelweg 2
2628 CD, Delft
The Netherlands

Last modified Wednesday May 24, 2000 by: [Sape A. Miedema](#)

Translation by: [Laurens de Jonge](#)

Figures, equations and tables by: [Erik Miedema](#)

Copyright © May, 2000 Dr.ir. S.A. Miedema



[Download Adobe Acrobat Reader V4.0](#)

Bibliography.

1. Akerboom, P.G.A.M., "Studie naar een flexibele verankeringsmogelijkheid voor een snijkopzuiger t.b.v. het buitengaatse baggeren". Proc. Baggerdag 9/11/1985, T.H. Delft 1984.
2. Biot, M.A., "General theory of three dimensional consolidation". Journal of Applied Physics, Vol. 12, pp. 155-164, 1941.
3. Bishop, A.W., "The strength of soils as engineering materials". Geotechnique, Vol. 16, No. 2, pp. 91-128, 1966.
4. Blaazer, J.G., "De deining gecompenseerde schijfbodem snijkopzuiger". Proc. Baggerdag 9/11/1984, T.H. Delft 1984.
5. Brakel, J.D., "Mathematisch model voor de krachten op een roterende snijkop van een in zeegang werkende snijkopzuiger". Sco/80/96. T.H. Delft 1981.
6. Boer, T.J.M. de, "De Cutter". Scriptie Sc0/77/81, T.H. Delft 1977.
7. Boer, T.J.M. de, "Metingen aan een verticale cutter". Laboratoriumverslag La0/77/73, T.H. Delft 1977.
8. Boer, T.J.M. de, "Ontwerp van een deiningscompensator voor een cutterzuiger". Rapport Nr. CO/77/93, T.H. Delft 1977.
9. Boom, H. van den, "Verankeringskrachten op een snijkopzuiger in zeegang". Vijfde jaars cursuswerk, T.H. Delft 1979.
10. Boom, H. van den, "Verankering van een snijkopzuiger in zeegang". Ingenieurswerk, T.H. Delft 1980.
11. Butterfield, R. & Andrawes, K.Z., "On the angles of friction between sand and plane surfaces". Journal of Terramechanics, Vol.8, No. 4, pp. 15-23, 1972.
12. Cuvelier, C. & Segal, A., "Eindige elementen methode in de stromingsleer". PATO cursus, T.H.Delft 1983.
13. Cummins, W.E., "The Impulse Response Function and Ship Motions". Schiffstechnik B.D. 9-1962 Heft 47, pp. 101-109.

14. Drimmelen, N.J. van, t'Hoen, J.P.T.A., Willigen, F.A. and Eygenraam J.A., "Development and First Production Unit of the IHC Beaver Wheel Dredger". Proc., Wodcon 1983 Singapore 1983.
15. Engelshoven, R.P.V.A. van, "Het statisch en dynamisch gedrag van een zelfdrijvende persleiding in zeegang". Proc. Baggerdag 9/11/1985, T.H. Delft 1984.
16. Gerritsma, J., "Scheepsbewegingen en sturen". Collegedictaat k16, T.H. Delft 1974.
17. Groot, A.K. de, "Een snijkopzuiger met deiningsgecompenseerde ladder". Proc. Baggerdag 19/11/1982, T.H. Delft 1982.
18. Hatamura, Y. and Chijiiwa, K., "Analyses of the mechanism of soil cutting".
1st report, Bulletin of the JSME, vol. 18, no. 120, June 1975.
2st report, Bulletin of the JSME, vol. 19, no. 131, May 1976.
3st report, Bulletin of the JSME, vol. 19, no. 139, Nov. 1976.
4st report, Bulletin of the JSME, vol. 20, no. 139, January 1977.
5st report, Bulletin of the JSME, vol. 20, no. 141, March 1977.
19. Hansen, B., "Line ruptures regarded as narrow rupture zones. Basic equations based on kinematic considerations". Proc. Conf. Earth Pressure Problems, Brussels, 1, pp.39-48, 1958.
20. Hettiaratchi, D.R.P. & Witney, B.D. & Reece, A.R., "The calculation of passive pressure in two dimensional soil failure". Journal Agric. Engng. Res. 11 (2), pp. 89-107, 1966.
21. Hettiaratchi, D.R.P. and Reece, A.R., "Symmetrical Three-Dimensional Soil Failure". J. Terramech. 1967, 4 (3) pp. 45-67.
22. Hettiaratchi, D.R.P., "The mechanics of soil cultivation". AES, paper No. 3/245/C/28, 1967.
23. Hettiaratchi, D.R.P. & Reece, A.R., "The calculation of passive soil resistance". Geotechnique 24, No. 3, pp. 289-310, 1974.
24. Hettiaratchi, D.R.P. and Reece, A.R., "Boundary Wedges in Two Dimensional Passive Soil Failure". Geotechnique 25, No 2, pp. 197-220, 1975.

25. Hogben, and Lumb,. "Ocean Wave Statistics". 1967.
26. Joanknecht, L.F.W., "Mechanisch graafonderzoek onder water". T.H. Delft, Febr. 1973.
27. Joanknecht, L.W.F., "Cutting Forces in Submerged Soils". T.H.Delft, 1974, The Netherlands.
28. Joanknecht, L.W.F., "Results of Tests on Two Cutterheads operating in Sand". First Int. Symp. Dredging Technology, Canterbury, England, 1975.
29. Joanknecht, L.F.W., "A Review of Dredge Cutterhead Modelling and Performance". Proc. WODCON VII, San Francisco, 1976.
30. Journee, J.M.J. and Vis, F.C., "Compensatie van de bewegingen van een cutterzuiger op zee". 1e Interim rapport. T.H. Delft 1979.
31. Journee, J.M.J. and Vis, F.C. and Keuning, P.J., "Compensatie van de bewegingen van een cutterzuiger op zee". 2e Interim rapport. T.H. Delft 1980.
32. Journee, J.M.J. and Miedema, S.A. and Keuning, J.A. "Dredmo, A Computer Programm for the Calculation of the Behaviour of a Cutter Suction Dredger Operating in Irregular Waves". T.U. Delft & Delft Hydraulics Laboratory, Delft 1983.
33. Josselin de Jong, G. de, "Rowe's stress-dilatancy relation based on friction". Geotechnique 26, No. 3, pp. 527-534, 1976.
34. Keuning, J.A. & Beukelman, W., "Hydrodynamic coefficients of rectangular barges in shallow water". Proc. BOSS, Cranfield, UK, 1979.
35. Keuning, P.J. & Journee, J., "Calculation Method for the Behaviour of a Cutter Suction Dredger Operating in Irregular Waves". Proc. Wodcon X, Singapore 1983.
36. Koning, J de & Miedema, S.A. & Zwartbol, A., "Soil/Cutterhead Interaction under Wave Conditions". Proc. WODCON X, Singapore, 1983.
37. Lambe, T.W. & Whitman, R.V., "Soil mechanics, SI version". John Wiley & Sons, New York 1979.

38. Lanting, D., "Cutterproeven met cilindrische snijkoppen in aangetrild zand". Laboratoriumverslag LaO/81/97, T.H. Delft 1977.
39. Leussen, W. van & Nieuwenhuis J.D., "Soil Mechanics Aspects of Dredging". Geotechnique 34 No.3, pp. 359-381.
40. Leussen, W. van & Os, A.G. van, "Basic Research On Cutting Forces In Saturated Sand". Paper submitted for publication in proceedings ASCE. Delft Hydraulics Laboratory, Delft July 1986 (beschikbaar 28 Augustus 1986).
41. Meijer, K.L. & Os, A.G. van, "Pore pressures near moving underwater slope". Geotech. Engng. Div. ASCE 102, No. GT4, pp. 361-372
42. Meijer, K.L., "Berekening van spanningen en deformaties in verzadigde grond". Rapport R 914, deel 1, Waterloopkundig Laboratorium, 1981.
43. Meijer, K.L., "Computation of stresses and strains in saturated soil". Proefschrift T.H. Delft 1985.
44. Miedema, S.A., "De grondreactiekrachten op een kroonsnijkop die via een ladder is opgehangen in een deiningscompensator". LaO/81/97, T.H.Delft 1981.
45. Miedema, S.A., "Computerprogramma ter bepaling van de reactiekrachten op de snijkop, als gevolg van de bewegingen van de snijkop". Stagerapport Waterloopkundig Laboratorium 1981 Delft.
46. Miedema, S.A., "De modellering van de grondreacties op een snijkop en het operationeel maken van het computerprogramma DREDMO. CO/82/125, T.H.Delft 1982.
47. Miedema, S.A., "De interactie tussen snijkop en grond in zeegang". Proc. Baggerdag 19/11/1982, T.H. Delft, 1982.
48. Miedema, S.A., "Principe ontwerp van een deiningsgecompenseerde snijkopzuiger met axiale en radiale compensatie op de snijkop". CO/82/134, T.H.Delft 1983.
49. Miedema, S.A., "Snijkopzuiger voor het buitengaatse baggeren met een deiningsgecompenseerde ladder". IO/83/107, T.H.Delft 1983.

50. Miedema, S.A., "Computersimulatie baggerschepen". De Ingenieur, Dec. 1983. (Kivi/Misset).
51. Miedema, S.A., "Mathematische modelvorming t.a.v. een snijkopzuiger in zeeegang". T.H. Delft 1984. (Kivi September 1984), The Netherlands.
52. Miedema, S.A., "The cutting of densely compacted sand under water". Terra et Aqua No. 28, October 1984 pp. 4-10.
53. Miedema, S.A., "Dwarsscheepse en langsscheepse deiningscompensatie van een snijkopzuiger". Proc. Baggerdag 9/11/1984, T.H. Delft 1984.
54. Miedema, S.A., "Mathematical Modelling of the Cutting of Densely Compacted Sand Under Water". Dredging & Port Construction, July 1985, pp. 22-26.
55. Miedema, S.A., "Derivation of the Differential Equation for Sand Pore Pressures". Dredging & Port Construction, September 1985, pp. 35.
56. Miedema, S.A., "The Application of a Cutting Theory on a Dredging Wheel". Proc. WODCON XI, Brighton 1986.
57. Miedema, S.A., "Underwater soil cutting: a study in continuity". Dredging & Port Construction, June 1986, pp. 47-53.
58. Miedema, S.A., "SAMTEXT & SAMBASE, wetenschappelijk tekstbewerkingssysteem voor Personal Computers". Delft 1986.
59. Nieuwenhuis, J.D., "Failure of sands in plain strain tests". LGM - Mededelingen deel XXI, no.2 1980, pp. 171-177.
60. Ofuji, I. & Katoh, M. & Amemiya, S. & Matsui, A. & Kitanaka, S., "Studies on Cutter Suction Dredger for Deep and Rough Seas". Proc. WODCON XI, Brighton, England, 1986.
61. Oortmerssen, G. van, "The motions of a moored ship in waves". N.S.B.M. Publication No. 510, Wageningen 1976.
62. Os, A.G. van, "Behaviour of Soil when Excavated Underwater". International Course Modern Dredging. June 1977, The Hague, The Netherlands.
63. Os, A.G. van, "Snelle deformatie van korrelvormig materiaal onder

- water". pt-p 31 (1976) nr.12, pp. 735-741. pt-b 32 (1977) nr. 8, pp. 461-467.
64. Osman, M.S., "The mechanics of soil cutting blades". J.A.E.R. 9 (4) pp. 313-328, 1964.
 65. Raalte, G.H. van & Zwartbol, A., "The Disc Bottom Cutterhead: A Report on Laboratory and Field Tests". Proc. WODCON XI, Brighton, England, 1986.
 66. Reece, A.R., "The Fundamental Equation Of Earth Moving Machinery". Proc. Symp. Earth Moving Machinery, Inst. of Mech. Eng. London 1965.
 67. Rowe, P.W., "The Stress Dilatancy Relation for Static Equilibrium of an Assembly of Particles in Contact". Proc. Roy. Soc. A269, pp.500-527, 1962.
 68. Shiraki, Y. & Saito, M. & Kajita, E. & Tahara, S., "On Design Problems of a Cutter Suction Dredger Operated in Waves". Proc. WODCON XI, Brighton, England, 1986.
 69. Segal, G., "Septra Analysis, Programmers Guide, Standard Problems and Users Manual". Ingenieursbureau Septra, Leidschendam, The Netherlands 1984.
 70. Slump, G.F., "Bulldozertests under water in sand and stones". LaO/79/87, T.H. Delft 1979.
 71. Sohne, W., "Some basic considerations of soil mechanics as applied to agricultural engineering". Grundlagen der Landtechnik (7), 11-27, 1956.
 72. Steeghs, H., "Snijden van zand onder water (I & II)". Ports & Dredging No. 121, June 1985. Ports & Dredging No. 123, November 1985.
 73. Steeghs, H., "Snijden van zand onder water; een theoretisch model". Rapport: GR 37-IIB * MTI-Holland, Kinderdijk, 1986.
 74. Terzaghi, K. and Peck, R.B., "Soil Mechanics in Engineering Practice". John Wiley & Sons, Inc. 1967.
 75. Vermeer, P.A., "Materiaalmodellen in de grondmechanica". T.H.Delft, 1983, The Netherlands (collegedictaat).

76. Verruijt, A., "Grondmechanica". Delftse uitgevers maatschappij, Nederland, 1983.
77. Wichers, J.E.W., "On the Forces on a Cutter Suction Dredger in Waves". Proc. WODCON IX, Vancouver, B.C., Canada, 1980
78. Wichers, J.E.W. and Drimmelen, N.J. van, "On the forces on the cutterhead and the spud of a cutter suction dredger, operating in waves". Proc. WODCON X, Singapore 1983.
79. Wismer, R.D. & Luth, H.J., "Performance of plane soil cutting blades in sand". Trans. ASEA No. 69-115, 1969.
80. Wismer, R.D. & Luth, H.J., "Rate effects in soil cutting". Journal of Terramechanics, Vol. 8, No. 3, pp. 11-21, 1972
81. Derks, J.C.M., "Model tests in relation with mixture formation in a dredge wheel". Rapport Nr. CO/83/143, T.H.Delft 1984.
82. Anoniem, "DREDMO, Dredger response to waves and current". Users Manual. Waterloopkundig Laboratorium Delft, Delft, December 1986.
83. Lambert, J.D., "Computational methods in ordinary differential equations". London, Wiley, 1972.
84. Belytschko, T. & Hughes, T.J.R., "Computational Methods for Transient Analysis". Elsevier Science Publishers B.V. 1983.

[Back to top](#)

This is a translation of the dissertation of Dr.ir. S.A. Miedema, dated September 15th 1987 .
The dissertation was originally published in Dutch by the:
Delft University of Technology
Faculty of Mechanical Engineering and Marine Technology
Chair of Dredging Technology
Mekelweg 2
2628 CD, Delft
The Netherlands

Last modified Wednesday May 24, 2000 by: [Sape A. Miedema](#)

Translation by: [Laurens de Jonge](#)

Figures, equations and tables by: [Erik Miedema](#)

Copyright © May, 2000 Dr.ir. S.A. Miedema



[Download Adobe Acrobat Reader V4.0](#)

[Contents](#)

General List Of Symbols Used.

a	adhesion	kPa
$a_{0,k}$	coefficient Fourier series	-
a_1, a_2	weigh factors k-value (permeability)	-
a_a	amplitude axial oscillation	m
a_v	amplitude radial oscillation	m
A	surface	m ²
A	adhesive force	kN
b	width of blade of blade element	m
b_{ca}	coefficient cutting force cavitating, dredging wheel	kN/m
b_{gc}	coefficient cutting force non-cavitating, dredging wheel	kN/m ²
b_k	coefficient Fourier series	m
b_{pr}	projected width of the blade perpendicular to the velocity direction	m
B	bank height	m
B_a	axial bank height	m
B_v	radial bank height	m
c_{ca}	coefficient cutting force cavitating, cutter head	kN
c_{gc}	coefficient cutting force non-cavitating, cutter head	kN
c_i, c_1, c_2	coefficients (non-cavitating cutting process)	-
c_r	coefficient side effects	-
c_s	wear coefficient	-
c_t	coefficient total cutting force (non-cavitating cutting process)	-
c_{ts}	coefficient total cutting force including wear effects	-
c_{tr}	coefficient total cutting force including side effects	-
c	cohesion	kPa
C	cohesive force	kN
C	coefficient	-

d_i, d_1, d_2	coefficients (cavitating cutting process)	-
d_r	coefficient side effects	-
d_s	wear coefficient	-
d_t	coefficient total cutting force (cavitating cutting process)	-
d_{ts}	coefficient total cutting force including wear	-
d_{tr}	coefficient total cutting force including side effects	-
D	diameter excavating element	m
e	volume strain	%
E	specific cutting energy	kN/m ²
E_{gc}	specific cutting energy (no cavitation)	kN/m ²
E_{ca}	specific cutting energy (full cavitation)	kN/m ²
$f(t)$	signal	-
f_0	coefficient longitudinal force	kN
$f_{1..6}$	coefficients cutting forces on cutter head	-
$f_{x,y,zca}$	coefficients cutting forces on dredging wheel	-
$f_{x,y,zgc}$	coefficients cutting forces on dredging wheel	-
F_{ci}	cutting force (general)	kN
F_{cit}	total cutting force (general)	kN
F_a	axial cutting force	kN
F_h	horizontal cutting force (parallel to the cutting speed)	kN
F_l	cutting force parallel to the edge of the blade	kN
F_n	normal force	kN
F_r	radial cutting force	kN
F_s	cutting force in the swing direction	kN
F_t	tangential cutting force	kN
F_v	vertical cutting force (perpendicular to the cutting velocity)	kN
F_w	friction force	kN
F_x	cutting force in x-direction (longitudinal)	kN
F_{xt}	total cutting force in x-direction (longitudinal)	kN

F_y	cutting force in y-direction (transversal)	kN
F_{yt}	total cutting force in y-direction (transversal)	kN
F_z	cutting force in z-direction (vertical)	kN
F_{zt}	total cutting force in z-direction (vertical)	kN
F_v	cutting force in v direction	kN
g	gravitational acceleration	m/s ²
$g_{1..6}$	coefficients cutting forces on cutter head	-
G	gravitational force	kN
h_a	axial layer thickness without curvature	m
h_i	initial layer thickness	m
h_{ia}	axial layer thickness	m
h_{ir}	radial layer thickness	m
h_r	radial layer thickness without curvature	m
h_{igc}	characteristic layer thickness (no cavitation)	m
h_{ica}	characteristic layer thickness (cavitation)	m
h_{def}	thickness deformed layer	m
h_b	blade height	m
k	counter Fourier series	-
k	permeability	m/s
k_i	initial permeability	m/s
k_{max}	maximum permeability	m/s
k_m	effective permeability	m/s
K_1	grain force on the shear zone	kN
K_2	grain force on the blade	kN
l	length of the shear zone	m
$m_{gc,ca}$	coefficients drive torque dredging wheel	-
M	drive torque	kNm
M_t	average drive torque	kNm
n	normal on an edge	m
n	number of periods	-

n_o	number of revolutions excavating element	rpm
n_i	initial pore percentage	%
n_{\max}	maximum pore percentage	%
N_1	normal force on the shear zone	kN
N_2	normal force on the blade	kN
p	number of blades excavating element	-
p	pressure (water pressure)	kPa
P_{atm}	atmospheric pressure	kPa
P_{ber}	calculated dimensionless pressure (water pore pressure)	-
P_{damp}	saturated water pore pressure (12 cm w.k.)	kPa
P_{werk}	real pore pressure (water pore pressure)	kPa
P_{1m}	average pore pressure in the shear zone	-
P_{2m}	average pore pressure on the blade	-
P_{3m}	average pore pressure behind the blade	-
P_t	drive power excavating element	kW
q, q_1, q_2	specific flow	m/s
Q	flow per unit of blade width	m ² /s
r	radius	m
R	radius excavating element	m
$r_{gc \gg ca}$	radius transition cavitating versus non-cavitating cutting process	m
r_{cor}	characteristic radius dredging wheel	m
s	length of a stream line	m
s	measure for the layer thickness	m
S	step	m
S_s	step in radial velocity direction	m
S_1	shear force on the shear zone	kN
S_2	shear force on the blade	kN
t	time	s
Δt	time interval	s

T	inertial force	kN
T	period	s
v_{ax}	axial velocity	m/s
v_c	cutting velocity perpendicular to the edge of the blade	m/s
v_{ci}	circumferential velocity	m/s
v_s	swing velocity	m/s
v_r	relative velocity between blade and sand	m/s
v_l	velocity component parallel to the edge of the blade	m/s
v_{rad}	total radial velocity	m/s
v_t	total blade velocity	m/s
v_v	radial velocity	m/s
v_{vc}	effective radial velocity	m/s
v_{ac}	effective axial velocity	m/s
V	volume strain per unit of blade width	m ²
W_1	pore pressure force on the shear zone	kN
W_2	pore pressure force on the blade	kN
W_3	pore pressure force behind the blade	kN
W_4	water resistance on the layer cut	kN
x	coordinate	m
y	coordinate	m
z	coordinate	m
z	water depth	m
α	blade angle	rad
$\alpha_{1,2}$	coefficients	-
β	shear angle	rad
ε	phase shift	rad
φ	angle of internal friction	rad
δ	soil/steel interface friction angle	rad
δ_e	effective soil/steel interface friction angle	rad
ι	sweep angle blade	rad
θ_r	rotation force vector as a result of side effects	rad

θ_s	rotation force vector as a result of wear	rad
θ_t	rotation force vector with respect to the velocity vector	rad
θ_{ts}	angle of force vector with respect to the velocity vector including wear effects	rad
θ_{tr}	angle of force vector with respect to the velocity vector including side effects	rad
γ	angle of velocity vector with the horizontal	rad
ρ_g	wet density of the sand	ton/m ³
ρ_s	dry density of the sand	ton/m ³
ρ_w	density of water	ton/m ³
ν	ladder angle	rad
ω	angular frequency	rad/s
ω_a	angular frequency axial oscillation	rad/s
ω_v	angular frequency radial oscillation	rad/s
ξ	angle blade with axis excavating element, curvature angle	rad
ζ	difference static and dynamic blade angle	rad
Ω	angle passed of blade with excavating element	rad
Ω_0	total angle passed (cutter head)	rad
Ω'_0	angle between velocity direction and swing direction	rad
Ω''_0	angle passed as a result of oscillation	rad
Ω_{0c}	correction on total angle passed	rad
Ω_1	angle passed, marking the beginning of cavitation (cutter head)	rad
$\Omega_{0,1,2}$	angle passed (dredging wheel)	rad
λ_a	wave length axial oscillation	m
λ_c	scale factor absolute pressure (water height + 10m)	-
λ_l	scale factor length scale	-
Π_1	coefficient	s/m
Π_2	coefficient	s/m
::	proportionality sign	
m	index model	

p index prototype

[Back to top](#)

**This is a translation of the dissertation of Dr.ir. S.A. Miedema, dated September 15th 1987 .
The dissertation was originally published in Dutch by the:
Delft University of Technology
Faculty of Mechanical Engineering and Marine Technology
Chair of Dredging Technology
Mekelweg 2
2628 CD, Delft
The Netherlands**

Last modified Wednesday May 24, 2000 by: [Sape A. Miedema](#)

Translation by: [Laurens de Jonge](#)

Figures, equations and tables by: [Erik Miedema](#)

Copyright © May, 2000 Dr.ir. S.A. Miedema



[Download Adobe Acrobat Reader V4.0](#)

[Contents](#)

List Of Symbols Used In Chapter 1.

a	frequency dependent added mass matrix	kg $\text{kg}\cdot\text{m}^2$
A	acceleration vector	m/s^2 rad/s^2
b	frequency dependent damping matrix	$\text{N}\cdot\text{s}/\text{m}$ $\text{N}\cdot\text{m}\cdot\text{s}/\text{rad}$
C	hydrostatic spring matrix	N/m $\text{N}\cdot\text{m}/\text{rad}$
D	damping vector	N $\text{N}\cdot\text{m}$
F	load vector	N $\text{N}\cdot\text{m}$
F'	load vector dependent part	N $\text{N}\cdot\text{m}$
F''	load vector independent part	N $\text{N}\cdot\text{m}$
I	unity matrix	-
K	retardation functions	N/m $\text{N}\cdot\text{m}/\text{rad}$
m	frequency independent added mass matrix	kg $\text{kg}\cdot\text{m}^2$
M	mass matrix	kg $\text{kg}\cdot\text{m}^2$
N	inverse mass matrix	$1/\text{kg}$ $1/\text{kg}\cdot\text{m}^2$
r_{t0}	relaxation factor initial damping	-
r_{it}	relaxation factor iteration process	-
r_{sp}	relaxation factor block functions	-
t	time	s
V	velocity vector	m/s rad/s
X	displacement vector	m

		rad
α	dummy variable	
ε	convergence criterium	m/s ²
		rad/s ²
θ	theta (0 - 1)	-
τ	time	s
ω	wave frequency	rad/s
ϕ	roll angle	rad
φ	pitch angle	rad
ψ	yaw angle	rad

Indices.

i	incoming vector
j	degree of freedom of motion
k	degree of freedom of motion
n	time step
m	iteration step
u	outgoing vector

[Back to top](#)

This is a translation of the dissertation of Dr.ir. S.A. Miedema, dated September 15th 1987 .
The dissertation was originally published in Dutch by the:
Delft University of Technology
Faculty of Mechanical Engineering and Marine Technology
Chair of Dredging Technology
Mekelweg 2
2628 CD, Delft
The Netherlands

Last modified Wednesday May 24, 2000 by: [Sape A. Miedema](#)

Translation by: [Laurens de Jonge](#)

Figures, equations and tables by: [Erik Miedema](#)

Copyright © May, 2000 Dr.ir. S.A. Miedema



[Download Adobe Acrobat Reader V4.0](#)

[Contents](#)

List Of Symbols Used In Chapter 8.

a_i	vector point cutting edge	m
b_i	vector cutting edge	m
c_i	vector point rear blade surface	m
d_i	vector parallel to rear blade surface	m
e_i	vector height direction blade surface	m
f	factor	-
F	force vector	kN
F_h	force vector parallel to v_c	kN
F_v	force vector perpendicular to v_c and v_l	kN
F_l	force vector parallel to v_l	kN
F_j	force component in j-direction	kN
F_w	friction force on surface formed by v_c and e	kN
H_i	height blade element	m
h_a	axial layer thickness without correction ξ	m
h_{ia}	axial layer thickness with correction ξ	m
h_r	radial layer thickness without correction ξ	m
h_{ir}	radial layer thickness with correction ξ	m
h_i	layer thickness	m
M	moment	kNm
n	normal on surface formed by v_c and v_l	m
p_i	vector arbitrary point	m
r_i	radius	m
s	distance covered between two subsequent blades	m
sw_i	sweep angle	rad
v_{ax}	axial velocity	m/s
v_l	longitudinal velocity vector	m/s
v_c	velocity vector perpendicular to the cutting edge	m/s
v_r	relative velocity vector of sand with respect to the blade	m/s

V_s	swing velocity	m/s
V_{xt}	velocity in x-direction after transformation angle passed	m/s
V_{xtt}	velocity in x-direction after transformation ladder angle	m/s
V_{yt}	velocity in y-direction after transformation angle passed	m/s
V_{ytt}	velocity in y-direction after transformation ladder angle	m/s
V_{zt}	velocity in z-direction after transformation angle passed	m/s
V_{ztt}	velocity in z-direction after transformation ladder angle	m/s
V_t	total blade velocity	m/s
x_i	x-coordinate	m
x_t	x-coordinate after transformation angle passed	m
x_{tt}	x-coordinate after transformation ladder angle	m
y_i	y-coordinate	m
y_t	y-coordinate after transformation angle passed	m
y_{tt}	y-coordinate after transformation ladder angle	m
z_i	z-coordinate	m
z_t	z-coordinate after transformation angle passed	m
z_{tt}	z-coordinate after transformation ladder angle	m
δ_e	effective soil/steel interface friction angle	rad

[Back to top](#)

This is a translation of the dissertation of Dr.ir. S.A. Miedema, dated September 15th 1987 .

The dissertation was originally published in Dutch by the:

Delft University of Technology

Faculty of Mechanical Engineering and Marine Technology

Chair of Dredging Technology

Mekelweg 2

2628 CD, Delft

The Netherlands

Last modified Wednesday May 24, 2000 by: [Sape A. Miedema](#)

Translation by: [Laurens de Jonge](#)

Figures, equations and tables by: [Erik Miedema](#)

Copyright © May, 2000 Dr.ir. S.A. Miedema



[Download Adobe Acrobat Reader V4.0](#)

B1.01 The space fixed coordinate systems.

A cutter-suction dredger has 6 degrees of freedom, three translations and three rotations. The motions of the cutter-suction dredge are looked upon as oscillating motions with small amplitudes in comparison with the stationary position of the cutter-suction dredge. Two right-handed coordinate systems are used:

- 1.a. A space fixed coordinate system X, Y, Z in which the origin is positioned in the mass center of gravity of the cutter-suction dredge in stationary condition. The Z -axis is aimed vertically upwards, while the X -axis is positive in the headway direction of the dredging vessel.
- 1.b A body fixed coordinate system fixed to the dredging vessel in which the origin coincides with the mass center of gravity of the cutter-suction dredger. This coordinate system coincides with the space fixed coordinate system in stationary condition.

The body fixed coordinate system is shown in figure B1.1.

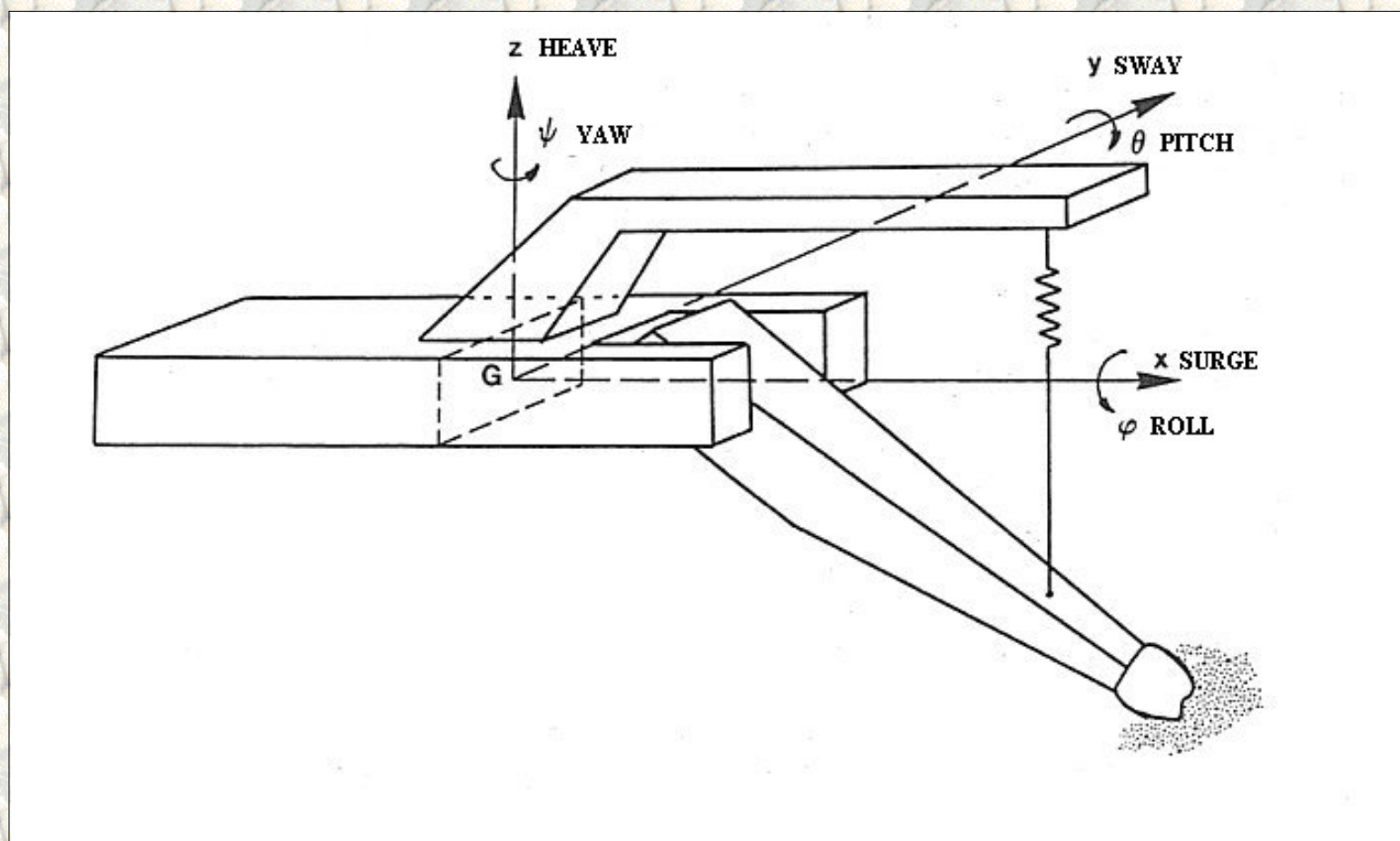


Figure B1.1: The body fixed coordinate system of the cutter-suction dredger.

The six motions are called:

1. Surge, translation in the X -direction.
2. Sway, translation in the Y -direction.
3. Heave, translation in the Z -direction.
4. Roll (ϕ), rotation around the x -axis.

5. Pitch (θ), rotation around the y-axis.

6. Yaw (ψ), rotation around the z-axis.

The transformation of the coordinate systems can be linearized for angles of rotation smaller than 0.1 radial, using the following relation:

$$\begin{bmatrix} X \\ Y \\ Z \end{bmatrix} = \begin{bmatrix} 1 & \psi & \Theta \\ \psi & 1 & -\varphi \\ -\Theta & \varphi & 1 \end{bmatrix} \cdot \begin{bmatrix} X \\ Y \\ Z \end{bmatrix} \quad (\text{B1.1})$$

The six degrees of freedom can be divided in symmetrical and anti-symmetrical motions. The symmetrical motions are motions in which a point at port and the similar point on starboard move symmetrical to the symmetrical plane along the length of the ship. The symmetrical motions are the surge, the heave and the pitch, also called the ships longitudinal motions. The anti-symmetrical motions are the sway, roll and the yaw, also called the athwartships motions. Within the linear theory the symmetrical motions are mutual coupled and the anti-symmetrical motions are mutual coupled. The symmetrical and anti-symmetrical motions are mutual uncoupled. For a cutter-suction dredger however, the symmetrical and the anti-symmetrical motions are coupled by the mooring and the ladder with the excavating element.

In this dissertation the body fixed coordinate system is used.

[Back to top](#)

This is a translation of the dissertation of Dr.ir. S.A. Miedema, dated September 15th 1987 .

The dissertation was originally published in Dutch by the:

Delft University of Technology

Faculty of Mechanical Engineering and Marine Technology

Chair of Dredging Technology

Mekelweg 2

2628 CD, Delft

The Netherlands

Last modified Wednesday May 24, 2000 by: [Sape A. Miedema](#)

Translation by: [Laurens de Jonge](#)

Figures, equations and tables by: [Erik Miedema](#)

Copyright © May, 2000 Dr.ir. S.A. Miedema



[Download Adobe Acrobat Reader V4.0](#)

B1.02 The ladder related local coordinate system.

[Contents](#)

A cutter-suction dredger has a seventh degree of freedom of motion, that is the rotation of the ladder around the ladder hinge. The cutterhead, positioned at the end of the ladder, has motions in three directions, with the assumption that the axis of the cutterhead coincides with the longitudinal axis of the ladder. These directions are:

1. The a-axis, this is the longitudinal axis of the ladder. The motions of the cutterhead in the a-direction are caused by the surge, heave and pitch of the cutter-suction dredger.
2. The v-axis, this is the athwart direction perpendicular to the longitudinal direction of the ladder. The motions of the cutterhead in the v-direction are caused by the surge, heave and pitch of the cutter-suction dredger and by the rotation of the ladder around the ladder hinge.
3. The s-axis, this axis coincides with the y-axis of the body fixed coordinate system. The motions of the cutterhead in the s-direction are caused by the sway, roll and yaw of the cutter-suction dredger.

This coordinate system is shown in figure B1.2.

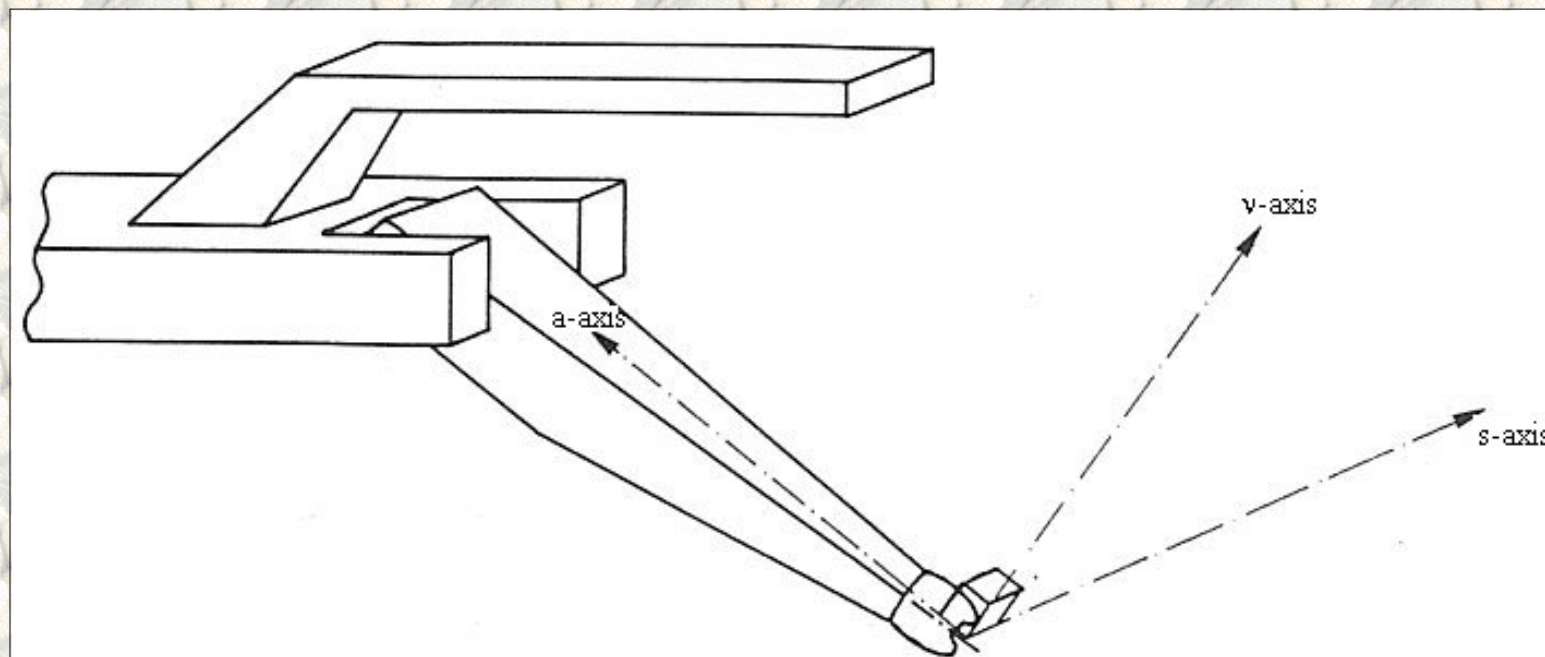


Figure B1.2: The ladder related coordinate system.

[Back to top](#)

This is a translation of the dissertation of Dr.ir. S.A. Miedema, dated September 15th 1987 .

The dissertation was originally published in Dutch by the:

Delft University of Technology

Faculty of Mechanical Engineering and Marine Technology

Chair of Dredging Technology

Mekelweg 2

2628 CD, Delft

The Netherlands

Last modified Wednesday May 24, 2000 by: [Sape A. Miedema](#)

Translation by: [Laurens de Jonge](#)

Figures, equations and tables by: [Erik Miedema](#)

Copyright © May, 2000 Dr.ir. S.A. Miedema



[Download Adobe Acrobat Reader V4.0](#)

B1.03 The cutterhead related local coordinate system.

[Contents](#)

A cutterhead consists of a number of cutting edges (blades), attached to a ring on one side and to the hub on the other side. The hub is connected with an electrical or hydraulic drive through the cutterhead-axis, which gives the rotation of the cutterhead around the cutterhead-axis. To determine the momentary loads on a cutting edge from the cutting theory of the straight blades subjected to a straightforward motion, a coordinate system is defined related to the momentary position of the cutting edge. This coordinate system is shown in figure B1.3.

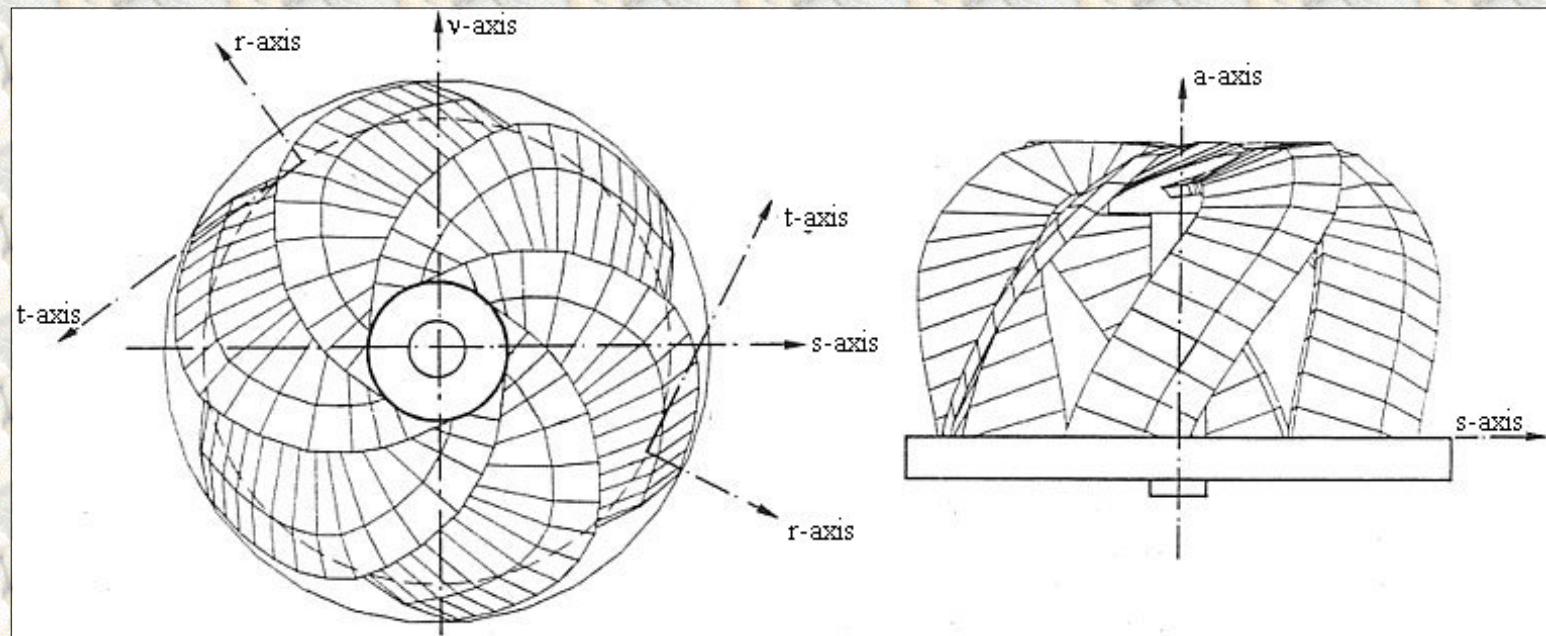


Figure B1.3: The cutterhead related coordinate system.

The coordinate system consists of a radial, a tangential and an axial axis, where the axial axis coincides with the axial axis from the ladder related coordinate system. The radial axis is positive in the outward direction. The tangential axis is positive opposite to the rotation direction of the cutterhead. The axial axis is directed positively from the ring towards the hub.

[Back to top](#)

This is a translation of the dissertation of Dr.ir. S.A. Miedema, dated September 15th 1987 .

The dissertation was originally published in Dutch by the:
Delft University of Technology
Faculty of Mechanical Engineering and Marine Technology
Chair of Dredging Technology
Mekelweg 2
2628 CD, Delft
The Netherlands

Last modified Wednesday May 24, 2000 by: [Sape A. Miedema](#)

Translation by: [Laurens de Jonge](#)

Figures, equations and tables by: [Erik Miedema](#)

Copyright © May, 2000 Dr.ir. S.A. Miedema



[Download Adobe Acrobat Reader V4.0](#)

B1.04 The dredging wheel related local coordinate system.

Contents

The cutting process of the dredging wheel takes place with a standing cut or a bank cut. In the cutting process with the standing cut the body fixed coordinate system is used while in the cutting process with the bank cut the ladder related local coordinate system is used. This is shown in figure B1.4.

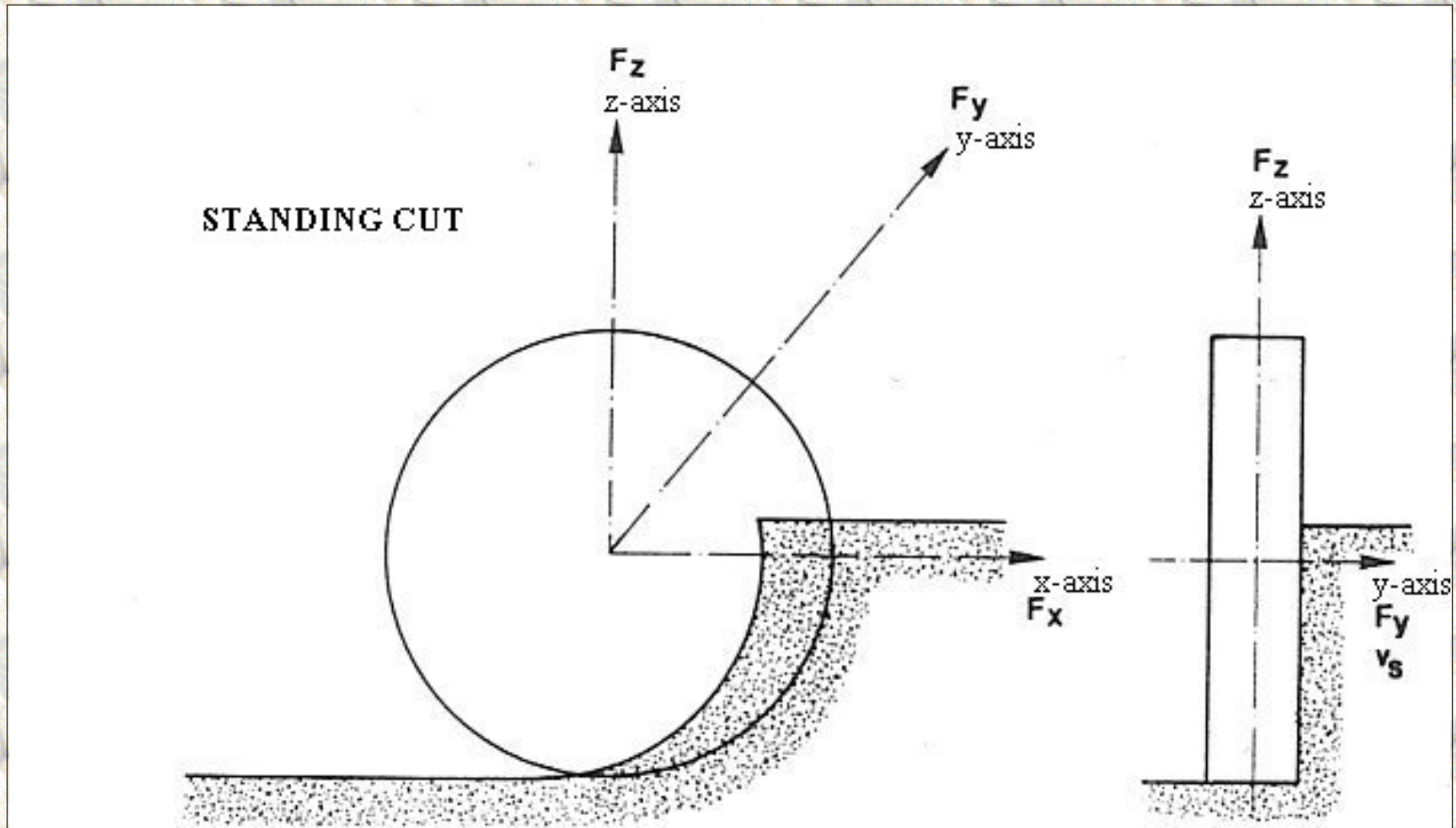


Figure B1.4a: The dredging wheel related coordinate system.

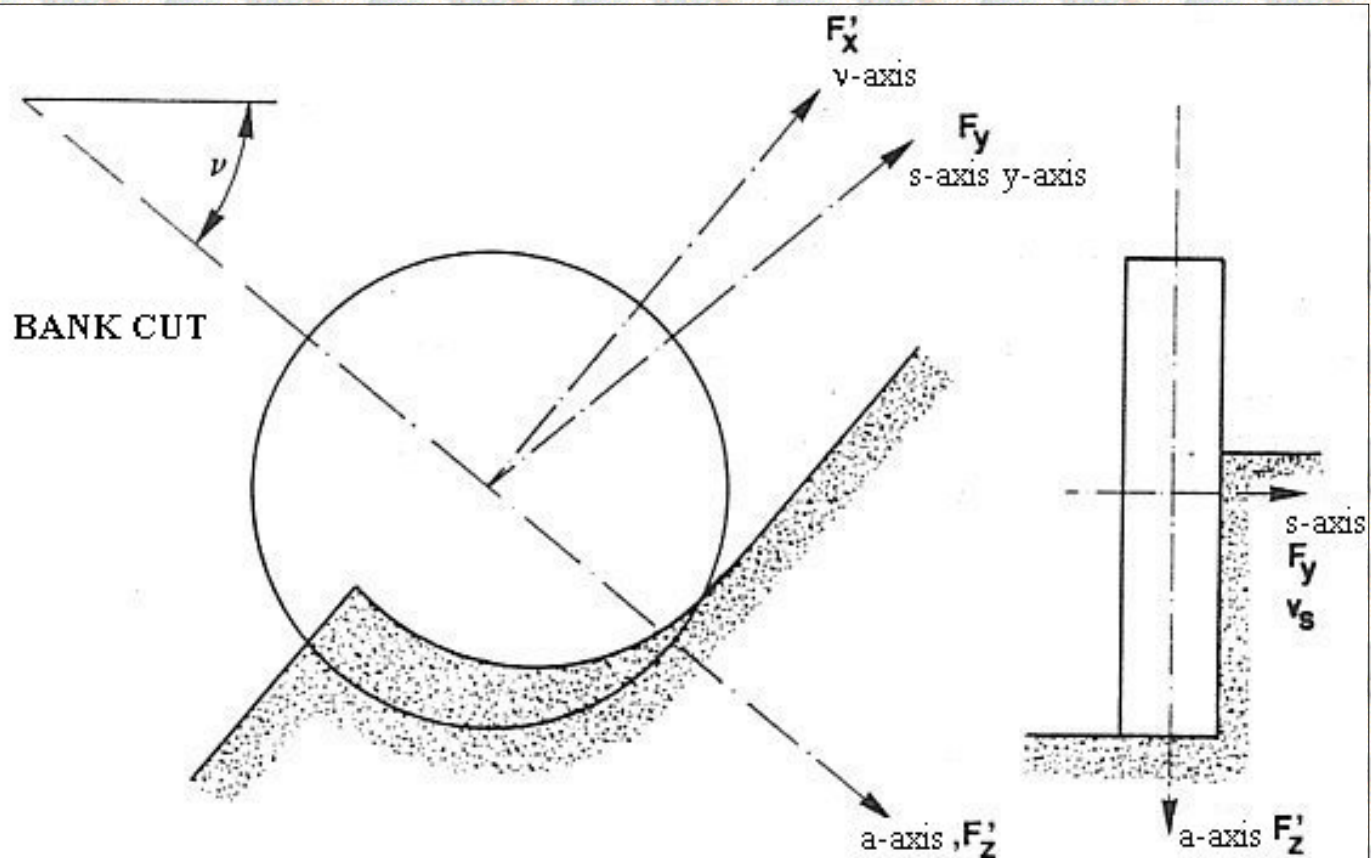


Figure B1.4b: The dredging wheel related coordinate system.

[Back to top](#)

This is a translation of the dissertation of Dr.ir. S.A. Miedema, dated September 15th 1987 .
The dissertation was originally published in Dutch by the:
Delft University of Technology
Faculty of Mechanical Engineering and Marine Technology
Chair of Dredging Technology
Mekelweg 2
2628 CD, Delft
The Netherlands

Last modified Wednesday May 24, 2000 by: [Sape A. Miedema](#)

Translation by: [Laurens de Jonge](#)

Figures, equations and tables by: [Erik Miedema](#)

Copyright © May, 2000 Dr.ir. S.A. Miedema



[Download Adobe Acrobat Reader V4.0](#)

B1.05 The blade motions related local coordinate system.

[Contents](#)

For a straight blade subjected to a straightforward uniform motion, a coordinate system can be defined related to the motion direction. Figure B1.5 shows this. Distinguished can be the axis parallel to the velocity direction (h-axis), the axis perpendicular to the velocity direction and perpendicular to the blade edge (v -axis) and the axis parallel to the blade edge (l-axis). In figure B1.5 also shows the positive directions of the loads.

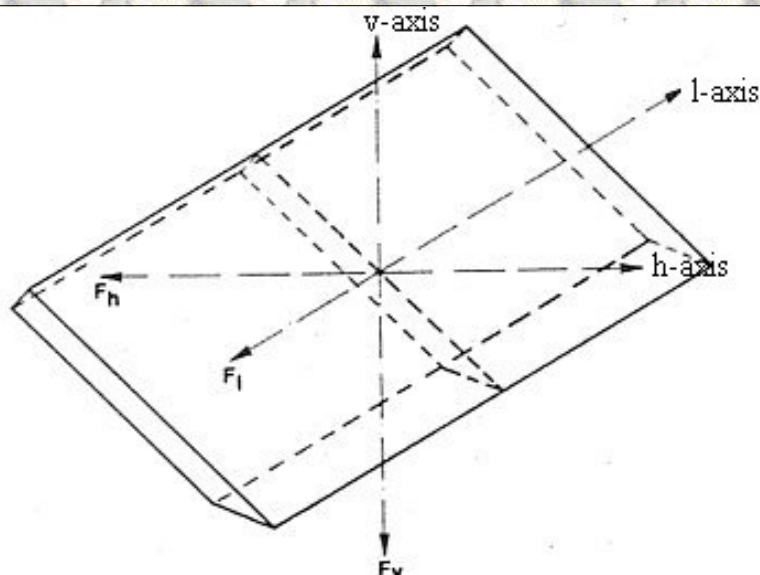


Figure B1.5: The blade motions related coordinate system.

[Back to top](#)

This is a translation of the dissertation of Dr.ir. S.A. Miedema, dated September 15th 1987 .

The dissertation was originally published in Dutch by the:

Delft University of Technology

Faculty of Mechanical Engineering and Marine Technology

Chair of Dredging Technology

Mekelweg 2

2628 CD, Delft

The Netherlands

Last modified Wednesday May 24, 2000 by: [Sape A. Miedema](#)

Translation by: [Laurens de Jonge](#)

Figures, equations and tables by: [Erik Miedema](#)

Copyright © May, 2000 Dr.ir. S.A. Miedema



[Download Adobe Acrobat Reader V4.0](#)

B2.01 The theta integration method.

The theta integration method (Lambert [83]) is a modification of the trapezoidal rule, in which the integration is not performed by multiplying the average of two function values with the step size, but by taking a weighed average of the two function values according to:

$$\int_{(n-1)\Delta t}^{n\Delta t} f(t) \cdot dt = \theta \cdot \Delta t \cdot f((n-1) \cdot \Delta t) + (1-\theta) \cdot \Delta t \cdot f(n \cdot \Delta t) \quad (\text{B2.1})$$

In which: $f(t)$ = an arbitrary function of the time.

The value of θ can be chosen between 0 and 1. within DREDMO a value of approximately 0.45 is used. This value is determined experimentally on the basis of a minimization of numerical instabilities and an optimization of the convergence velocity. With the aid of the theta method the following integration equations are found.

In the prediction step applies for the acceleration vector A_i :

$$A_{i,n,1} = A_{i,n-1} + \Delta A_{i,n,1} \quad (\text{B2.2})$$

In the iteration process applies for the acceleration vector A_i :

$$A_{i,n,m} = A_{i,n,m-1} + \Delta A_{i,n,m} \quad (\text{B2.3})$$

In the next equations the prediction step is obtained by substituting 1 for the index "m". The velocity vector V_i can be derived, by integrating A_i :

$$V_{i,n,m} = V_{i,n-1} + \theta \cdot \Delta t \cdot A_{i,n-1} + (1-\theta) \cdot \Delta t \cdot A_{i,n,m} \quad (\text{B2.4})$$

The displacement vector X_i can be derived by integrating V_i :

$$X_{i,n,m} = X_{i,n-1} + \theta \cdot \Delta t \cdot V_{i,n-1} + (1-\theta) \cdot \Delta t \cdot V_{i,n,m} \quad (\text{B2.5})$$

[Back to top](#)

**This is a translation of the dissertation of Dr.ir. S.A. Miedema, dated September 15th 1987 .
The dissertation was originally published in Dutch by the:
Delft University of Technology
Faculty of Mechanical Engineering and Marine Technology
Chair of Dredging Technology
Mekelweg 2
2628 CD, Delft
The Netherlands**

Last modified Wednesday May 24, 2000 by: [Sape A. Miedema](#)

Translation by: [Laurens de Jonge](#)

Figures, equations and tables by: [Erik Miedema](#)

Copyright © May, 2000 Dr.ir. S.A. Miedema



[Download Adobe Acrobat Reader V4.0](#)

B2.02 The prediction step.

Dividing the change of the velocity vector between the end value of the preceding time-step and the prediction of the actual time-step (equation (B2.6)) in a part that is independent of the change of the actual acceleration vector (equation (B2.7)) and a part that is dependent of the change of the actual acceleration vector (equation (B2.8)), gives:

$$V_{i,n,1} - V_{i,n-1} = \Delta V_{i,n} + \frac{\partial V_i}{\partial A_i} \cdot \Delta A_{i,n,1} \quad (B2.6)$$

For the first term in the right hand side of the equation (B2.6) applies:

$$\Delta V_{i,n} = V_{i,n-1} - V_{i,n-2} + \theta \cdot \Delta t \cdot (A_{i,n-1} - A_{i,n-2}) \quad (B2.7)$$

For the second term in the right hand side of equation (B2.6) applies in the prediction step:

$$\frac{\partial V_i}{\partial A_i} \cdot \Delta A_{i,n,1} = (1 - \theta) \cdot \Delta t \cdot (A_{i,n,1} - A_{i,n-1}) \quad (B2.8)$$

Dividing the change of the displacement vector between the end value of the preceding time-step and the value in the prediction step (equation (B2.9)) in a part that is independent of the change of the actual velocity vector and acceleration vector (equation (B2.10)), in a part that is dependent of the change of the independent part of the velocity vector (equation (B2.11)) and a part that is dependent of the change of the actual acceleration vector (equation (B2.12)), gives:

$$X_{i,n,1} - X_{i,n-1} = \Delta X_{i,n} + \frac{\partial X_i}{\partial V_i} \cdot \Delta V_{i,n} + \frac{\partial X_i}{\partial V_i} \cdot \frac{\partial V_i}{\partial A_i} \cdot \Delta A_{i,n,1} \quad (B2.9)$$

For the first term in the right hand side of the equation (B2.9) applies:

$$\Delta X_{i,n} = X_{i,n-1} - X_{i,n-2} + \theta \cdot \Delta t \cdot (V_{i,n-1} - V_{i,n-2}) \quad (B2.10)$$

For the second term in the right hand side of the equation (B2.9) applies:

$$\frac{\partial X_i}{\partial V_i} \cdot \Delta V_{i,n} = (1-\theta) \cdot \Delta t \cdot \left[V_{i,n-1} - V_{i,n-2} + \theta \cdot \Delta t \cdot (A_{i,n-1} - A_{i,n-2}) \right] \quad (\text{B2.11})$$

For the third term in the right hand side of the equation (B2.10) applies in the prediction step:

$$\frac{\partial X_i}{\partial V_i} \cdot \frac{\partial V_i}{\partial A_i} \cdot \Delta A_{i,n,1} = (1-\theta)^2 \cdot \Delta t^2 \cdot (A_{i,n,1} - A_{i,n-1}) \quad (\text{B2.12})$$

[Back to top](#)

This is a translation of the dissertation of Dr.ir. S.A. Miedema, dated September 15th 1987 .

The dissertation was originally published in Dutch by the:

Delft University of Technology

Faculty of Mechanical Engineering and Marine Technology

Chair of Dredging Technology

Mekelweg 2

2628 CD, Delft

The Netherlands

Last modified Wednesday May 24, 2000 by: [Sape A. Miedema](#)

Translation by: [Laurens de Jonge](#)

Figures, equations and tables by: [Erik Miedema](#)

Copyright © May, 2000 Dr.ir. S.A. Miedema



[Download Adobe Acrobat Reader V4.0](#)

B2.03 The correction step.

Within the iteration process the velocity vector V_i and the displacement vector X_i are only dependent on the actual acceleration vector A_i . For the change of the velocity vector V_i between two successive iteration steps is found:

$$V_{i,n,m} - V_{i,n,m-1} = \frac{\partial V_i}{\partial A_i} \cdot \Delta A_{i,n,m} \quad (\text{B2.13})$$

For the term in the right hand side of equation (B2.13) the following applies in the correction step:

$$\frac{\partial V_i}{\partial A_i} \cdot \Delta A_{i,n,m} = (1-\theta) \cdot \Delta t \cdot (A_{i,n,m} - A_{i,n,m-1}) \quad (\text{B2.14})$$

For the change of the displacement vector X_i between two successive iteration steps is found:

$$X_{i,n,m} - X_{i,n,m-1} = \frac{\partial X_i}{\partial V_i} \cdot \frac{\partial V_i}{\partial A_i} \cdot \Delta A_{i,n,m} \quad (\text{B2.15})$$

For the term in the right hand side of equation (B2.15) the following applies in the correction step:

$$\frac{\partial X_i}{\partial V_i} \cdot \frac{\partial V_i}{\partial A_i} \cdot \Delta A_{i,n,m} = (1-\theta)^2 \cdot \Delta t^2 \cdot (A_{i,n,m} - A_{i,n,m-1}) \quad (\text{B2.16})$$

**Mekelweg 2
2628 CD, Delft
The Netherlands**

Last modified Wednesday May 24, 2000 by: [Sape A. Miedema](#)

Translation by: [Laurens de Jonge](#)

Figures, equations and tables by: [Erik Miedema](#)

Copyright © May, 2000 Dr.ir. S.A. Miedema



[Download Adobe Acrobat Reader V4.0](#)

B2.04 The convolution integral.

In chapter 1, equation (1.2), the potential damping in the equilibrium equations of motion is integrated in the form of a convolution integral of the retardation functions and the velocity history. Since DREDMO works with discrete time-steps, this integral will have to be solved using a numerical integration method. The trapezoidal rule is chosen:

$$\int_{(n-1) \cdot \Delta t}^{n \cdot \Delta t} f(t) \cdot dt = 0.5 \cdot [f((n-1) \cdot \Delta t) + f(n \cdot \Delta t)] \cdot \Delta t \quad (B2.17)$$

In which: $f(t)$ = an arbitrary function of the time.

For the convolution integral can be written:

$$D_k = \int_{-\infty}^t K_{jk}(t-\tau) \cdot V_j(\tau) \cdot d\tau \quad (B2.18)$$

Assuming that DREDMO starts at $t=0$, this can be written as, using equation (B2.17):

$$D_k = \sum_{j=1}^6 \left[\sum_{i=0}^n 0.5 \cdot [K_{jk,n-i} \cdot V_{j,i} + K_{jk,n-i+1} \cdot V_{j,i-1}] \right] \cdot \Delta t \quad (B2.19)$$

This can be transformed into:

$$D_k = \sum_{j=1}^6 \left[\sum_{i=1}^{n-1} [K_{jk,n-i} \cdot V_{j,i}] + 0.5 \cdot K_{jk,n} \cdot V_{j,0} + 0.5 \cdot K_{jk,0} \cdot V_{j,n} \right] \cdot \Delta t \quad (B2.20)$$

In chapter 1.1 the convolution integral is classified in the momentarily partly independent loads. Dividing equation (B2.20) into an independent and an interactive part derives for the independent part:

$$D_k'' = \sum_{j=1}^6 \left[\sum_{i=1}^{n-1} [K_{jk,n-i} \cdot V_{j,i}] + 0.5 \cdot K_{jk,n} \cdot V_{j,0} \right] \cdot \Delta t \quad (B2.21)$$

While for the interactive part it can be written:

$$D'_k = \sum_{j=1}^6 0.5 \cdot K_{jk,0} \cdot V_{j,n} \cdot \Delta t \quad (B2.22)$$

[Back to top](#)

This is a translation of the dissertation of Dr.ir. S.A. Miedema, dated September 15th 1987 .
The dissertation was originally published in Dutch by the:
Delft University of Technology
Faculty of Mechanical Engineering and Marine Technology
Chair of Dredging Technology
Mekelweg 2
2628 CD, Delft
The Netherlands

Last modified Wednesday May 24, 2000 by: [Sape A. Miedema](#)

Translation by: [Laurens de Jonge](#)

Figures, equations and tables by: [Erik Miedema](#)

Copyright © May, 2000 Dr.ir. S.A. Miedema



[Download Adobe Acrobat Reader V4.0](#)

B3.00 Soil mechanical properties of the 200 μm sand.

[Contents](#)

The sand in the old laboratory GV, with a d_{50} of 200 μm , is examined for the following soil mechanical parameters:

1. The minimum and the maximum density, table B3.1.
2. The dry critical density, table B3.1.
3. The saturated critical density, table B3.1.
4. The permeability as a function of the density, table B3.2.
5. The angle of internal friction as a function of the density, table B3.3.
6. The d_{50} as a function of the time, table B3.4.
7. The cone resistance per test.
8. The density in the test stand in combination with the cone resistance.

The points 7 and 8 need some explanation. With the aid of a Troxler density measuring set density measurements are performed in situ, that is in the test stand. During each measurement the cone resistance is determined at the same position. In this way it is possible to formulate a calibration formula for the density as a function of the cone resistance. The result is:

$$n = \frac{65.6}{C_p^{0.082}} \quad (n \text{ in } \%, C_p \text{ in kPa}) \quad (\text{B3.1})$$

In which the cone resistance is determined in a top layer of 18 cm, where the cone resistance was continuously increasing and almost proportional with the depth. The value to be used in equation (B3.1) is the cone resistance for the 18 cm depth.

With the aid of equation (B3.1) it was possible to determine the density for each cutting test from the cone resistance measurements. The result was an average pore percentage of 38.53% over 367 tests.

By interpolating in table B3.2 can be derived that a pore percentage of 38.53% corresponds to a permeability of 0.000165 m/s. By extrapolating in table B3.2 can also be derived that the maximum pore percentage of 43.8% corresponds to a permeability of approximately 0.00032 m/s. At the start of the cutting tests the pore percentage was averaged 38%, which corresponds to a permeability of 0.00012 m/s.

Minimal density	43.8%
Maximum density	32.7%
Dry critical density	39.9%

Wet critical density	40.7%-41.7%
Initial density	38.5%

Table B3.1: Pore percentages.

Pore percentages	Permeability (m/s)
36.97%	0.000077
38.48%	0.000165
38.98%	0.000206
39.95%	0.000240
40.88%	0.000297
41.84%	0.000307
43.07%	0.000289
43.09%	0.000322

Table B3.2: Permeabilities.

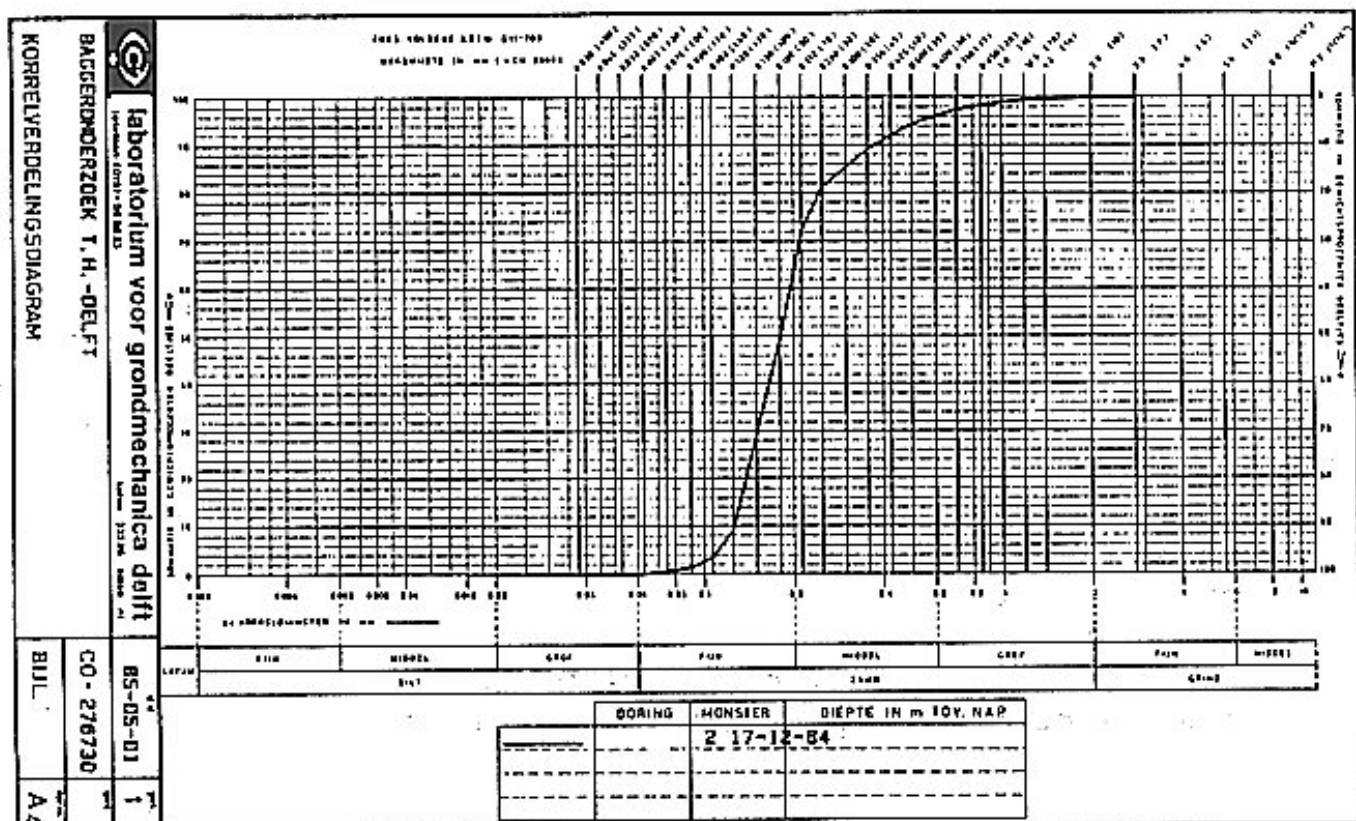


Figure B3.1: The grain distribution of the 200 µm sand.

Date	d ₅₀ (mm)
22-09-1982	0.175
17-12-1984	0.180
02-01-1985	0.170
08-01-1985	0.200
14-01-1985	0.200
21-01-1985	0.200
28-01-1985	0.195
04-02-1985	0.205
26-02-1985	0.210

Tabel B3.3: The d₅₀ of the sand as a function of time.

Pore percentage	Cell pressure kPa	Angle of internal friction
Dry		
43.8%	50	35.1 °
41.2%	50	36.0 °
39.9%	50	38.3 °
Wet undrained		
43.8%	100	30.9 °
42.1%	10	31.2 °
42.1%	50	31.2 °
42.1%	100	31.6 °
42.2%	100	32.0 °
41.8%	10	33.1 °
41.3%	10	31.9 °
41.2%	50	32.2 °
41.1%	50	30.1 °
41.1%	100	31.3 °
41.1%	100	33.7 °
41.0%	100	35.2 °
40.5%	10	33.8 °
40.3%	50	33.7 °
40.4%	100	33.1 °
39.8%	10	34.1 °

39.2%	10	33.8 °
39.2%	50	33.8 °
39.2%	100	33.9 °
38.2%	10	35.2 °
38.1%	50	35.3 °
38.1%	100	35.0 °
37.3%	10	37.4 °
37.0%	10	38.6 °
37.0%	50	37.3 °
36.9%	100	36.8 °
36.2%	100	38.0 °

Tabel B3.4: The angle of internal friction as a function of the pore percentage.

[Back to top](#)

This is a translation of the dissertation of Dr.ir. S.A. Miedema, dated September 15th 1987 .

The dissertation was originally published in Dutch by the:

Delft University of Technology

Faculty of Mechanical Engineering and Marine Technology

Chair of Dredging Technology

Mekelweg 2

2628 CD, Delft

The Netherlands

Last modified Wednesday May 24, 2000 by: [Sape A. Miedema](#)

Translation by: [Laurens de Jonge](#)

Figures, equations and tables by: [Erik Miedema](#)

Copyright © May, 2000 Dr.ir. S.A. Miedema



[Download Adobe Acrobat Reader V4.0](#)

B4.00 The soil mechanical properties of the 105 μm sand.

Contents

The sand in the new laboratory GV, with a d_{50} of 105 μm , is examined for the following soil mechanical parameters:

1. The minimum and the maximum density, table B4.1.
2. The saturated critical density, table B4.1.
3. The permeability as a function of the density, table B4.2.
4. The angle of internal friction as a function of the density, table B4.3.
5. The d_{50} as a function of the time, table B4.4.
6. The cone resistance per test.
7. The density in the test stand in combination with the cone resistance.

The points 6 and 7 need some explanation. As with the 200 μm sand density measurements are performed in situ with the aid of a Troxler density measuring set. The calibration formula for the 105 μm sand is:

$$n = \frac{69.9}{C_p^{0.068}} \quad (n \text{ in } \%, C_p \text{ in kPa}) \quad (\text{B4.1})$$

In which the cone resistance is determined in a top layer of 12 cm, where the cone resistance was continuously increasing and almost proportional with the depth. The value to be used in equation (B3.1) is the cone resistance for the 12 cm depth.

With the aid of equation (B4.1) it was possible to determine the density for each cutting test from the cone resistance measurements. As, however, new sand was used, the density showed changed in time. The sand was more loose in the first tests than in the last tests. This resulted in different average initial densities for the different test series. The test with a 45° blade were performed first with an average pore percentage of 44.9%. The tests with the 60° blade were performed with an average pore percentage of 44.2%. The tests with the 30° blade were performed with an average pore percentage of 43.6%. Because of the consolidation of the sand a relatively large spread was found in the first tests. Table B4.2 lists the permeabilities corresponding to the mentioned pore percentages. By extrapolation in table B4.2 a permeability of 0.00017 m/s is derived for the maximum pore percentage of 51.6%.

The sandbed is flushed after the linear tests because of the visibility in the water above the sand. In the tables is indicated which soil mechanical parameters are determined after the flushing of the sandbed.

Minimal density	51.6%
Maximum density	38.3%

Initial density 30 °	43.6%
Initial density 45 °	44.9%
Initial density 60 °	44.2%
After flushing the sand	
Minimal density	50.6%
Maximum density	37.7%
Wet critical density	44.5%

Table B4.1: Pore percentages. Indicated are the average measured densities for the various blade angles.

Pore percentages	Permeability (m/s)
42.2%	0.000051
45.6%	0.000082
47.4%	0.000096
49.4%	0.000129
Initial	
43.6%	0.000062
44.2%	0.000067
44.9%	0.000075
After flushing the sand	
39.6%	0.000019
40.7%	0.000021
41.8%	0.000039
43.8%	0.000063
45.7%	0.000093
48.3%	0.000128

Table B4.2: Permeabilities. Indicated are the average permeabilities for the various blade angles.

Date	d ₅₀ (mm)
06-08-1986	0.102
06-08-1986	0.097
06-08-1986	0.104
06-08-1986	0.129

06-08-1986	0.125
06-08-1986	0.123
29-08-1986	0.105
29-08-1986	0.106
29-08-1986	0.102
16-09-1986	0.111
16-09-1986	0.105
16-09-1986	0.107

Table B4.3: The d_{50} of the sand as a function of time.

Pore percentage	Cell pressure kPa	Angle of internal friction
Wet undrained		After flushing the sand
44.7%	100	33.5 °
44.9%	200	33.3 °
44.5%	400	32.8 °
42.6%	100	35.0 °
42.1%	200	35.5 °
42.2%	400	34.8 °
39.8%	100	38.6 °
39.9%	200	38.3 °
39.6%	400	37.9 °

Table B4.4: The angle of internal friction as a function of the pore percentage.

[Back to top](#)



http://dutw1127/dredging/miedema/1987_Dissertation/Appendix04_e/b400.htm (4 of 4) [31/12/2000 08:04:13]

B5.01 The measured horizontal and vertical cutting forces

additional to table 3.4, chapter 3.7,
scaled to a blade with $b=200$ mm and $h=200$ mm.

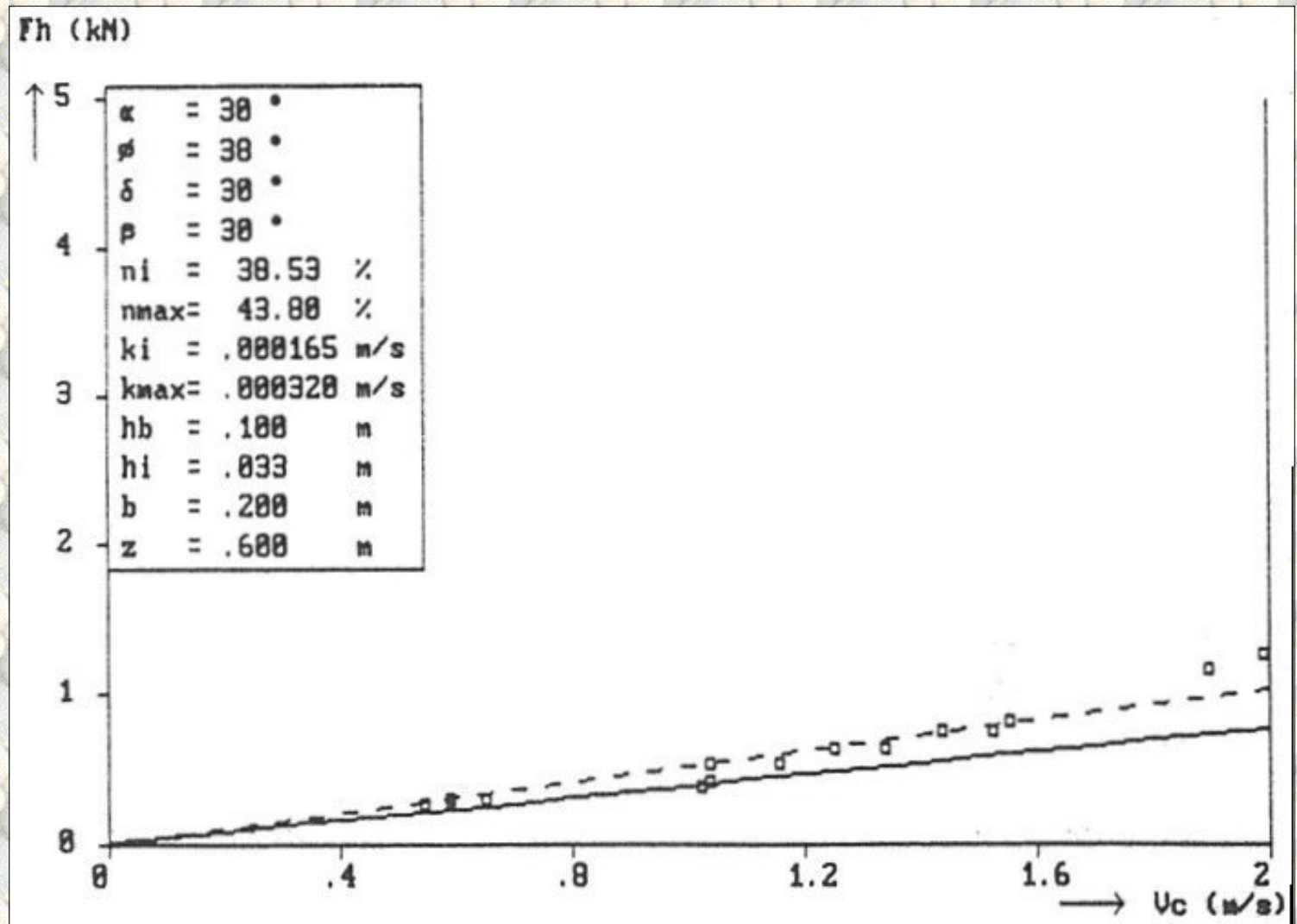
[Contents](#)


Figure B5.1: The horizontal force F_h as a function of the cutting velocity v_c , at a blade angle of 30° for the non-cavitating cutting process and a layer thickness of 33 mm, in the 200 μ m sand.

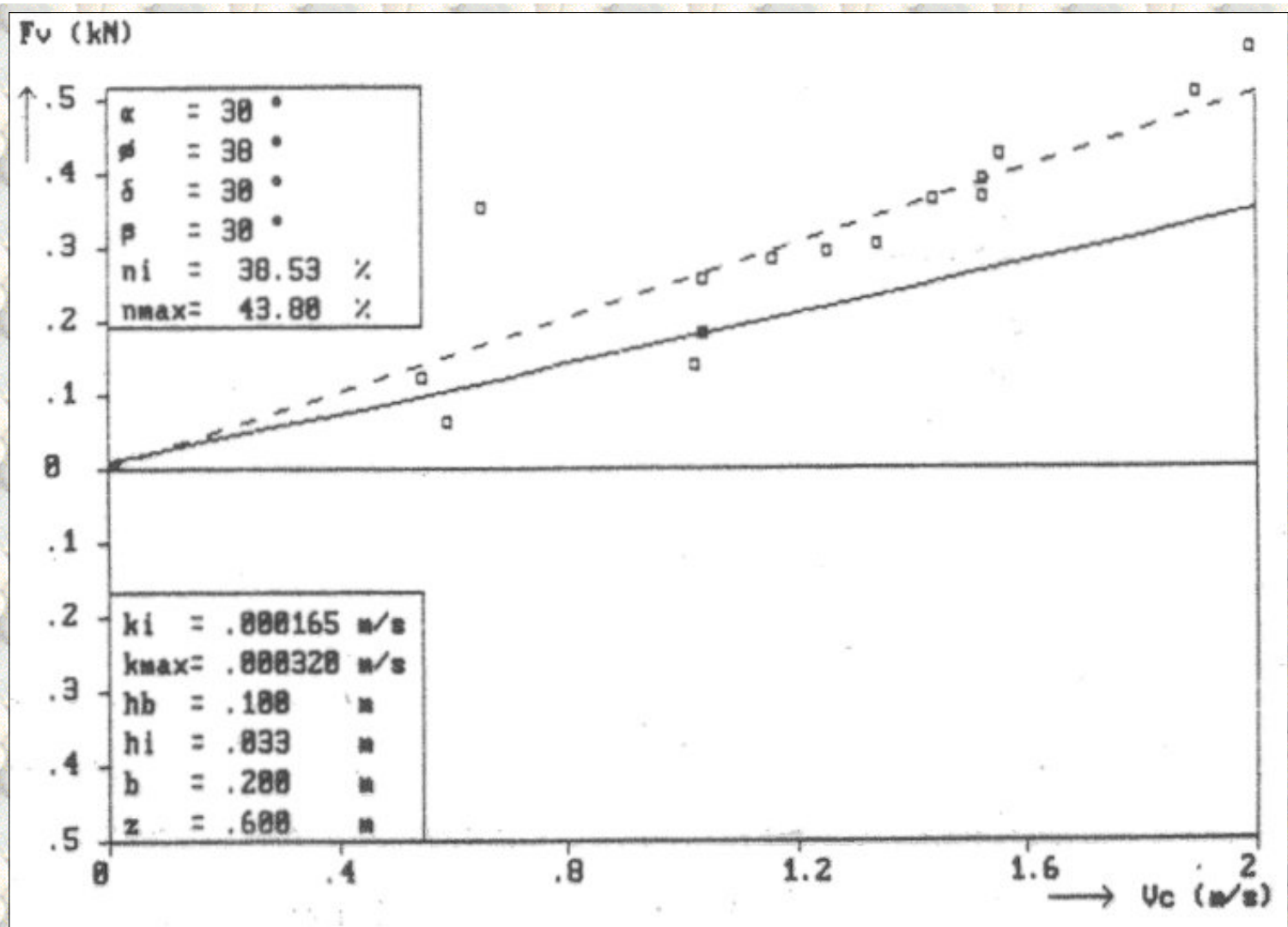


Figure B5.2: The vertical force F_v as a function of the cutting velocity v_c , at a blade angle of 30° for the non-cavitating cutting process and a layer thickness of 33 mm, in the 200 μm sand.

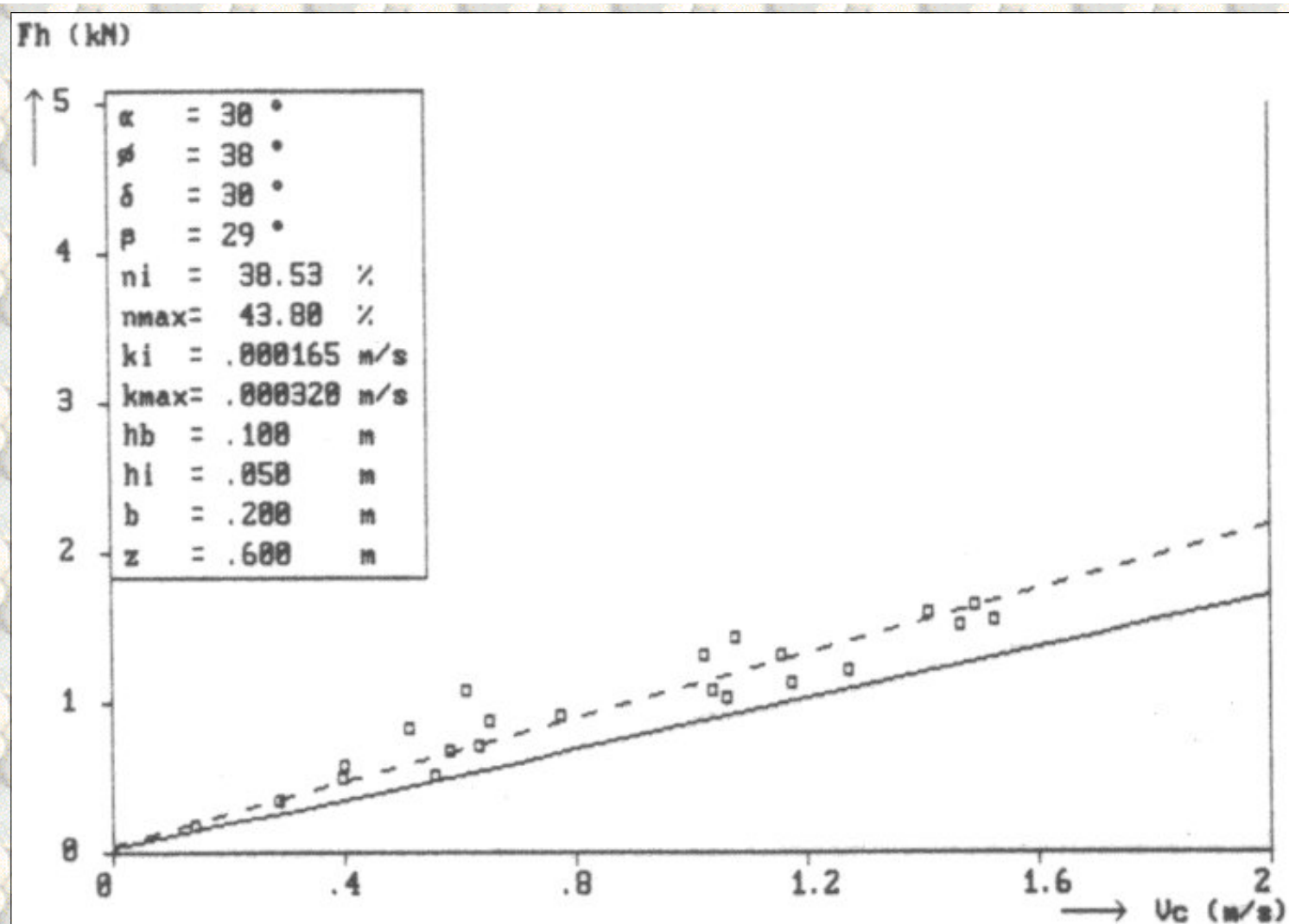


Figure B5.3: The horizontal force F_h as a function of the cutting velocity v_c , at a blade angle of 30° for the non-cavating cutting process and a layer thickness of 50 mm, in the 200 μm sand.

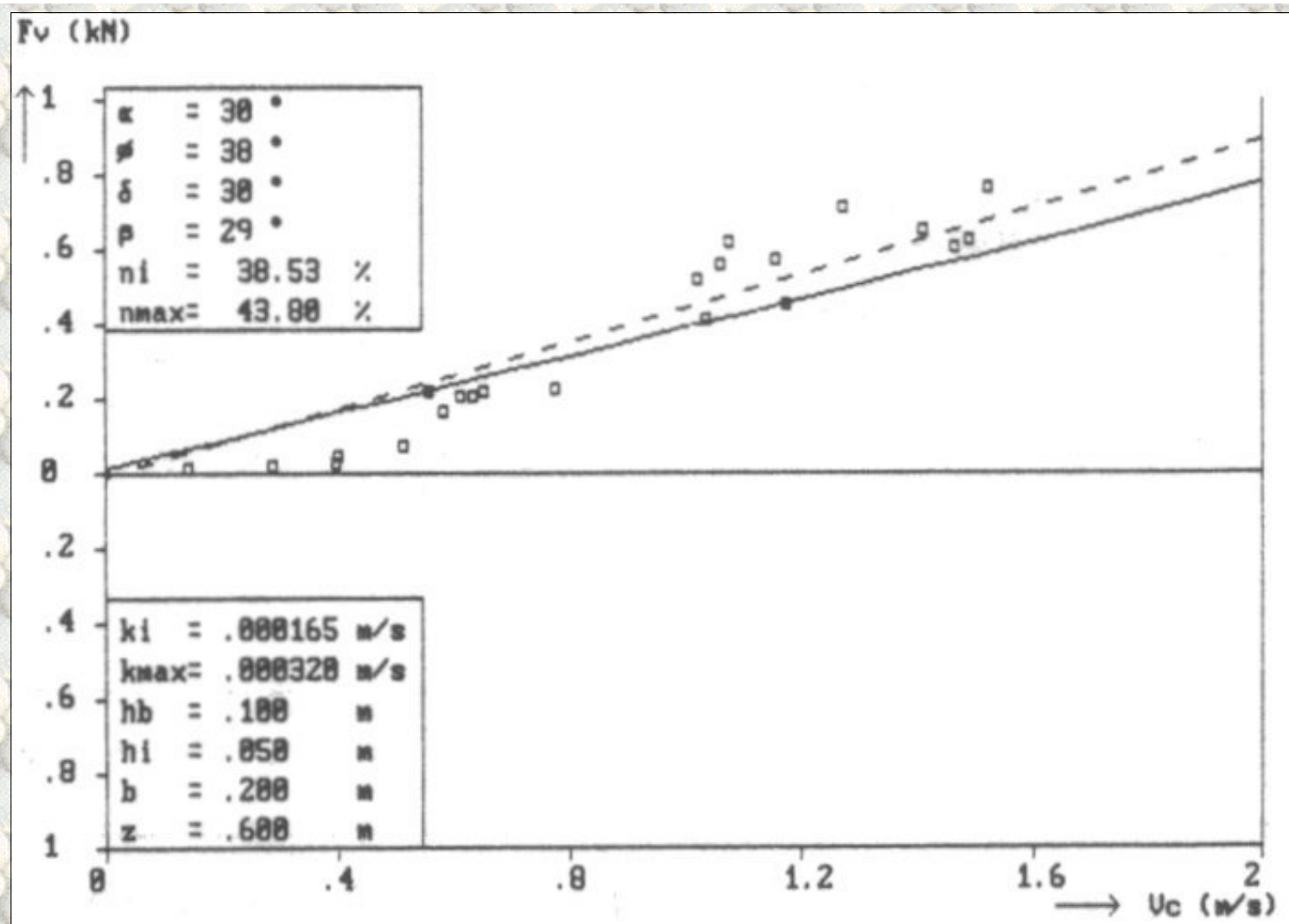


Figure B5.4: The vertical force F_v as a function of the cutting velocity v_c , at a blade angle of 30° for the non-cavitating cutting process and a layer thickness of 50 mm, in the 200 μm sand.

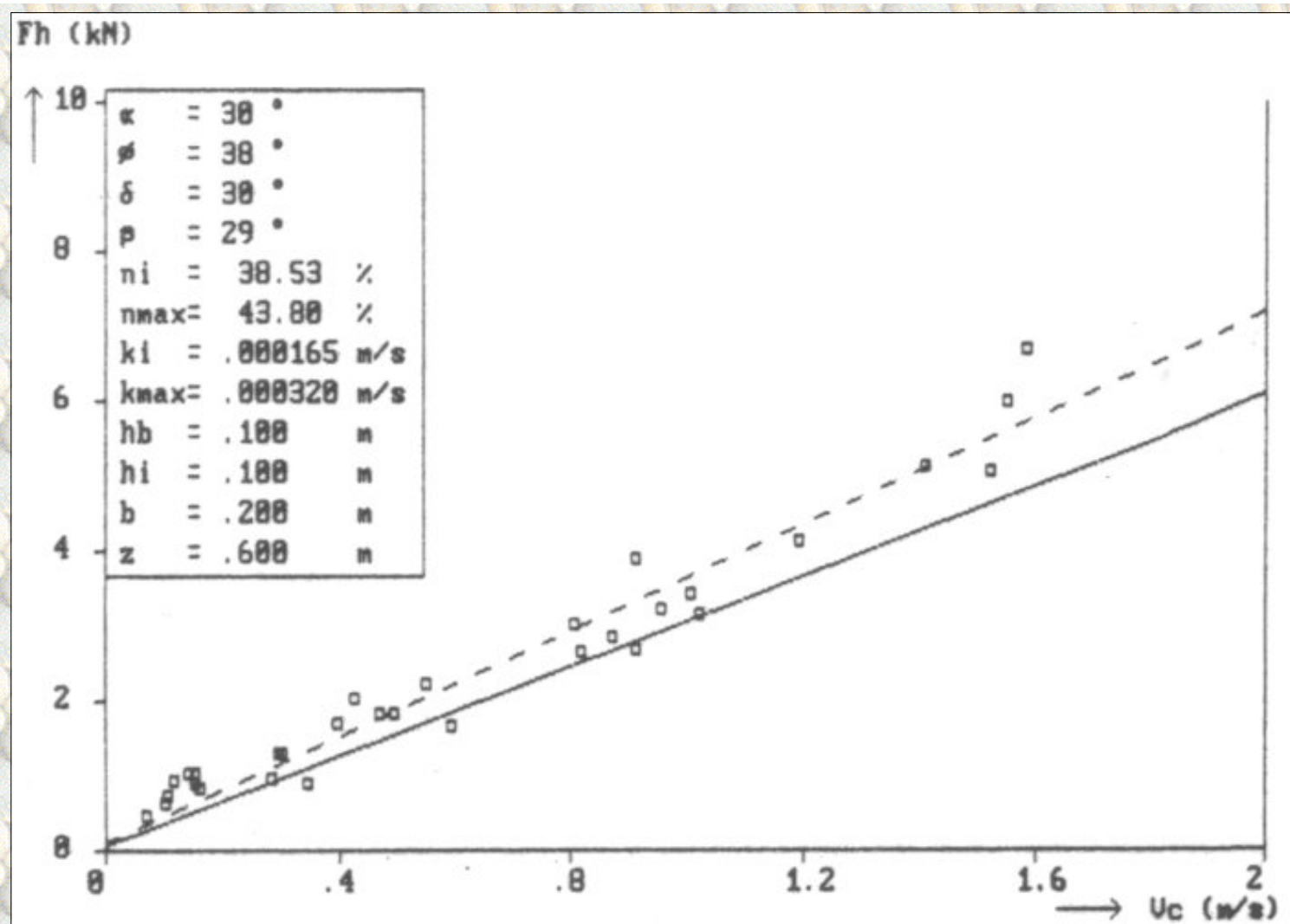


Figure B5.5: The horizontal force F_h as a function of the cutting velocity v_c , at a blade angle of 30° for the non-cavating cutting process and a layer thickness of 100 mm, in the 200 μm sand.

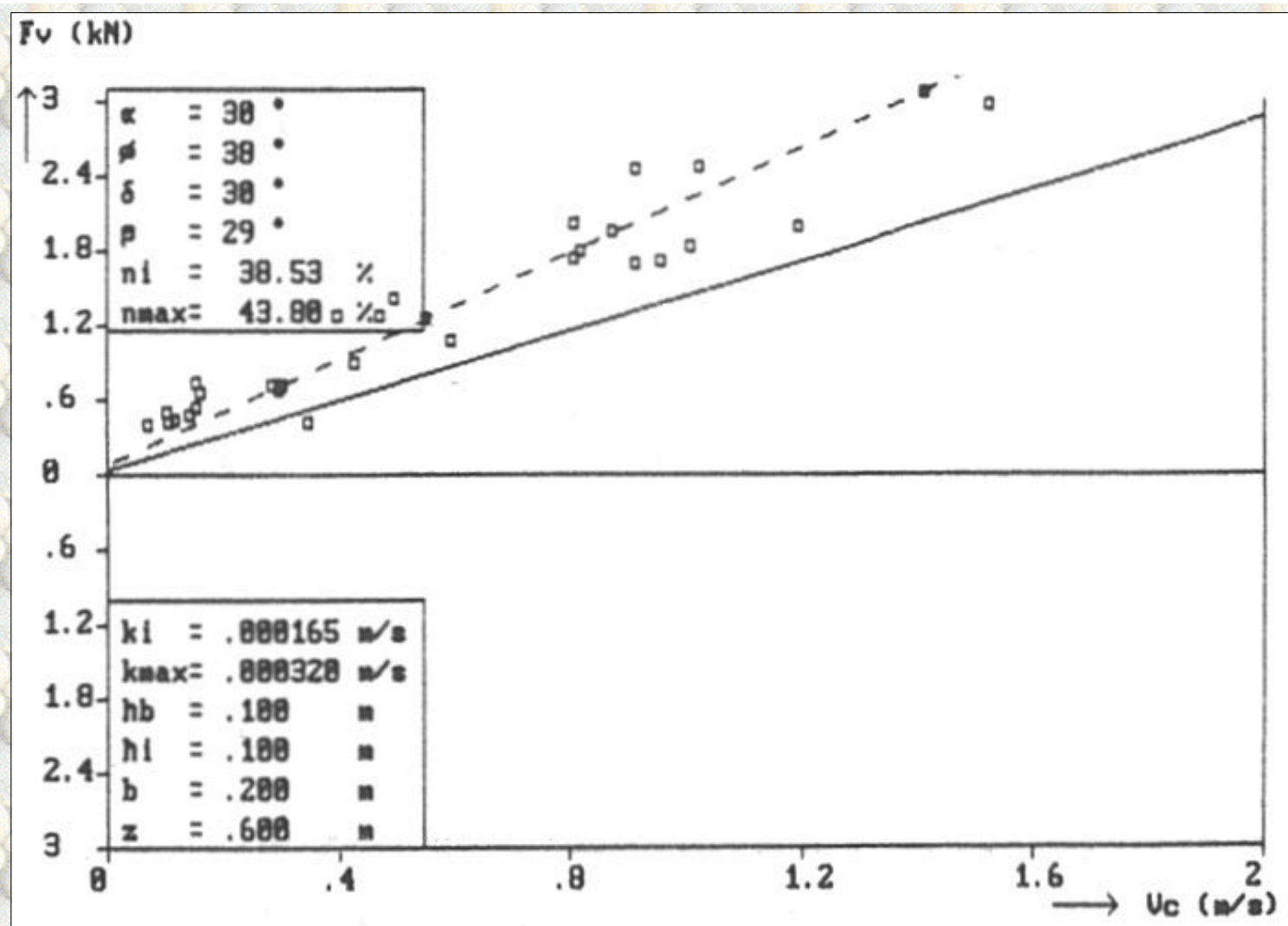


Figure B5.6: The vertical force F_v as a function of the cutting velocity v_c , at a blade angle of 30° for the non-cavitating cutting process and a layer thickness of 100 mm, in the 200 μm sand.

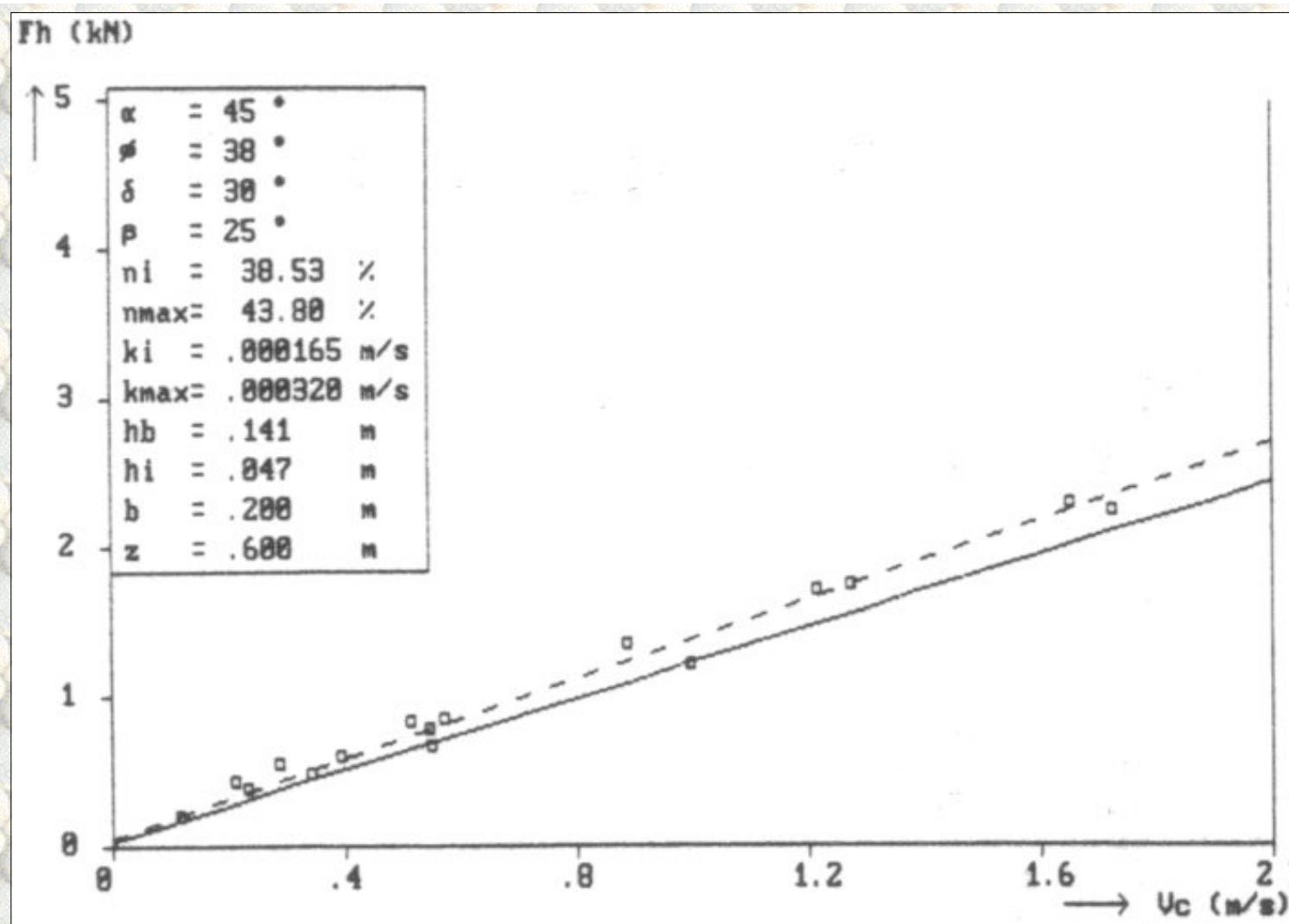


Figure B5.7: The horizontal force F_h as a function of the cutting velocity v_c , at a blade angle of 45° for the non-cavitating cutting process and a layer thickness of 47 mm, in the 200 μm sand.

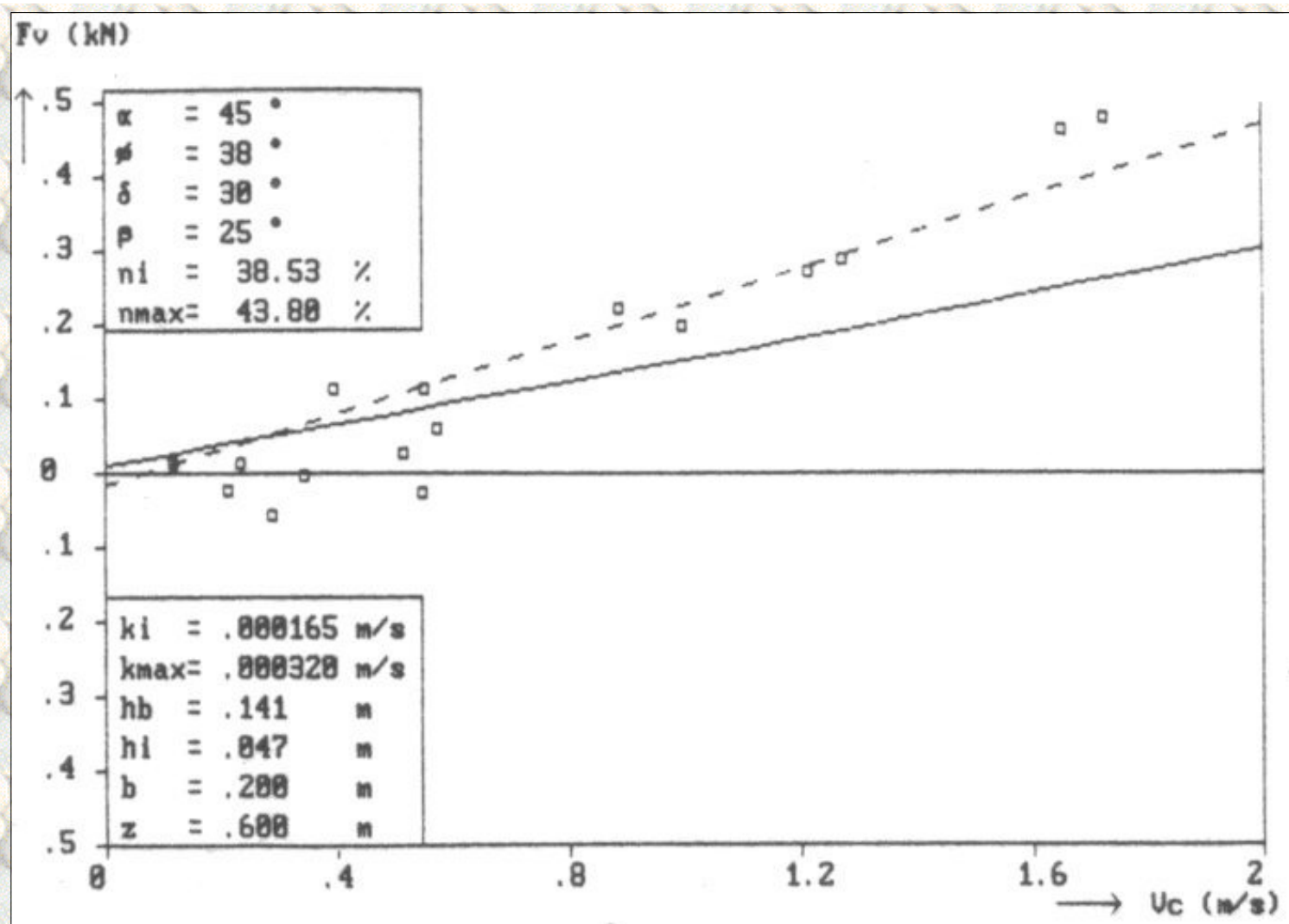


Figure B5.8: The vertical force F_v as a function of the cutting velocity v_c , at a blade angle of 45° for the non-cavitating cutting process and a layer thickness of 47 mm, in the 200 μm sand.

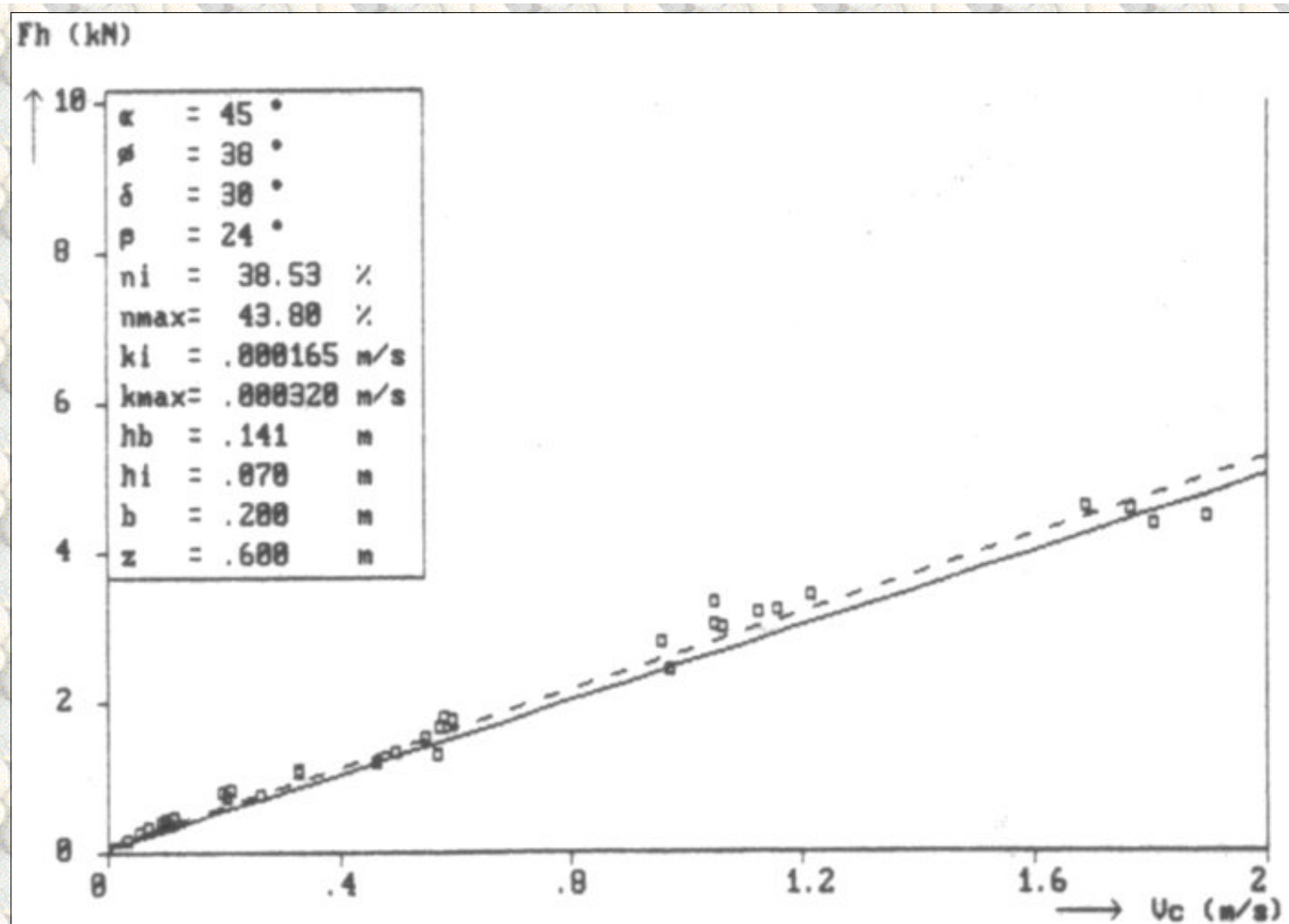


Figure B5.9: The horizontal force F_h as a function of the cutting velocity v_c , at a blade angle of 45° for the non-cavitating cutting process and a layer thickness of 70 mm, in the 200 μm sand.

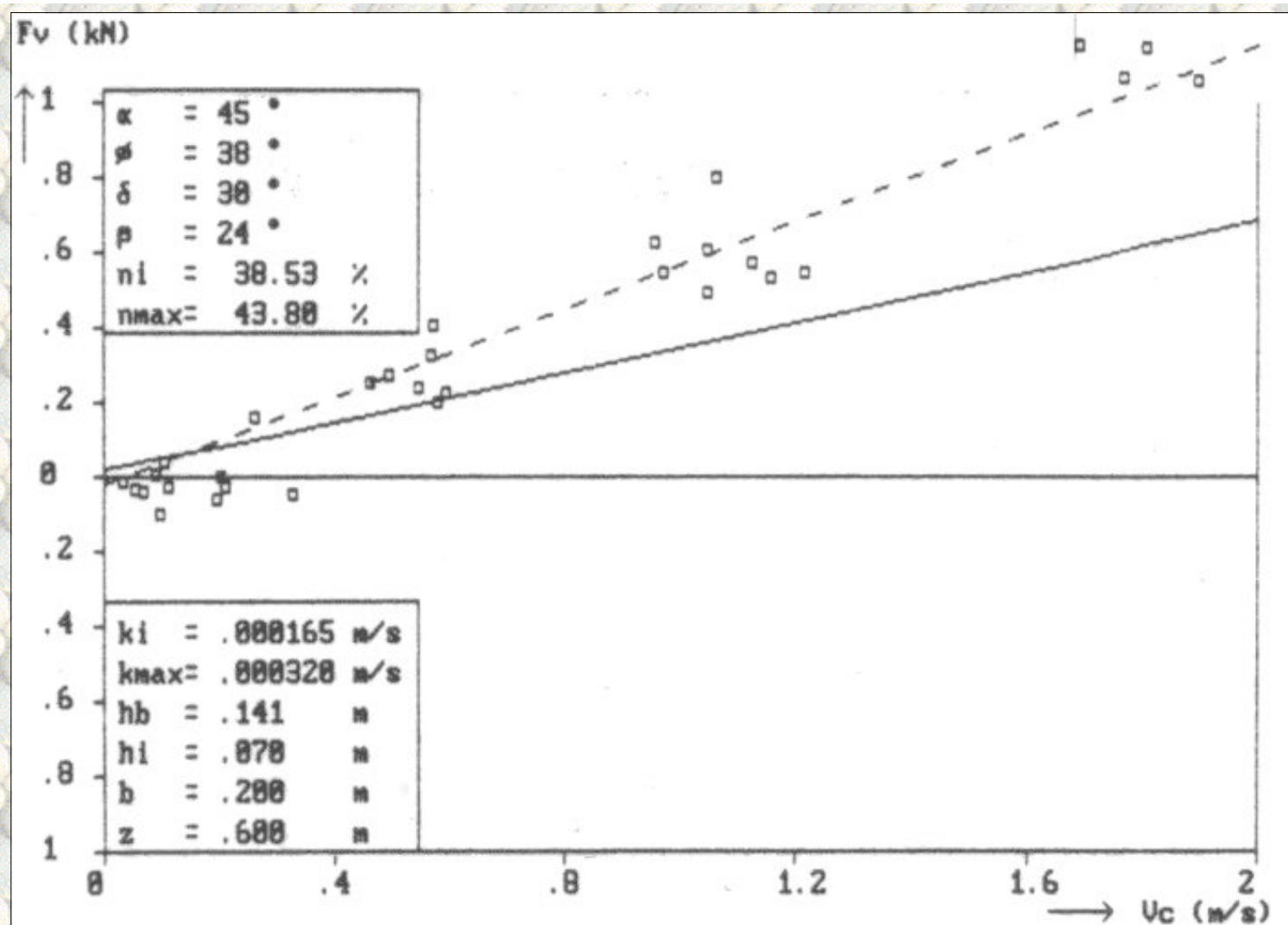


Figure B5.10: The vertical force F_v as a function of the cutting velocity v_c , at a blade angle of 45° for the non-cavitating cutting process and a layer thickness of 70 mm, in the 200 μm sand.

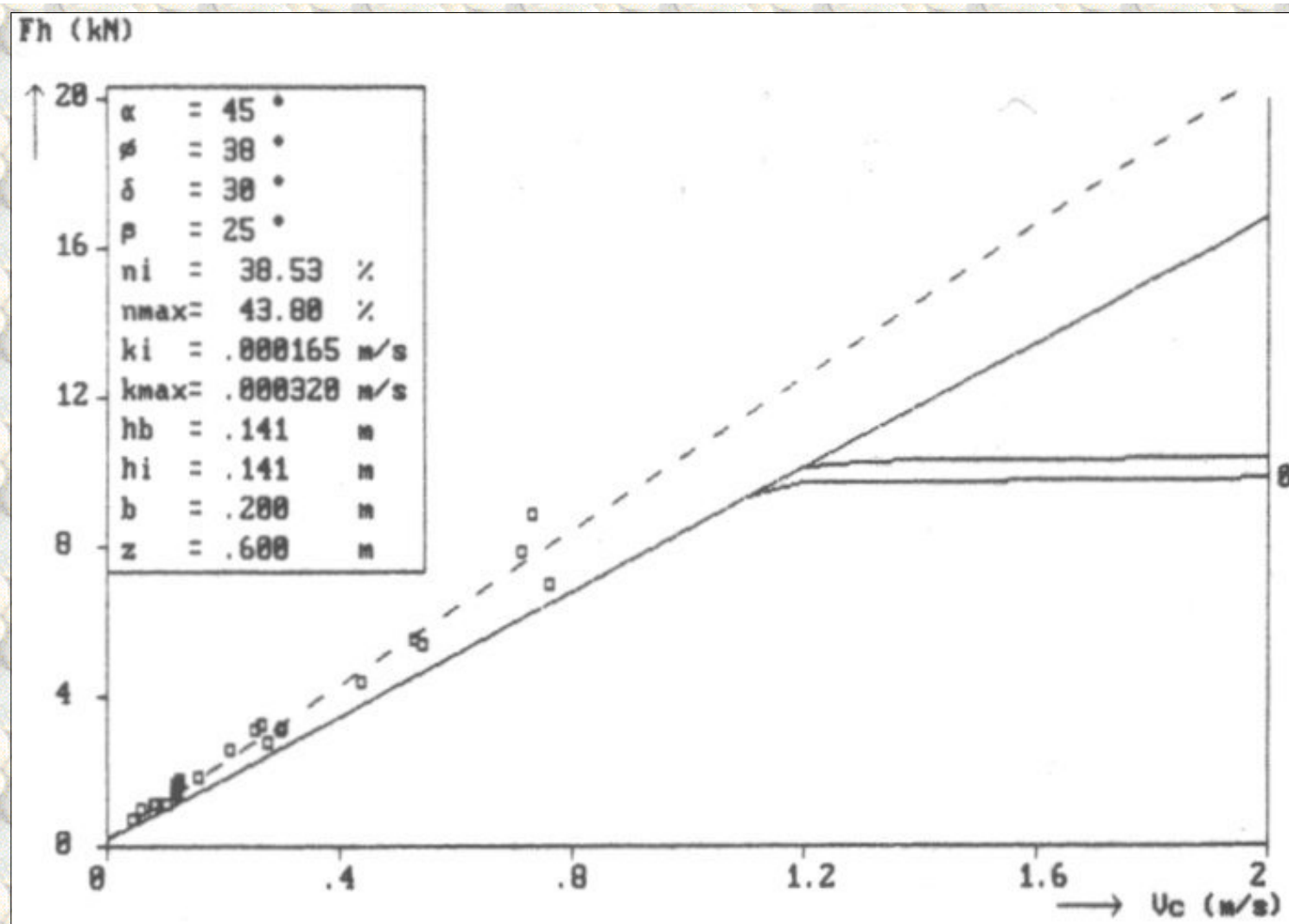


Figure B5.11: The horizontal force F_h as a function of the cutting velocity v_c , at a blade angle of 45° for the non-cavitating cutting process and a layer thickness of 141 mm, in the 200 μm sand.

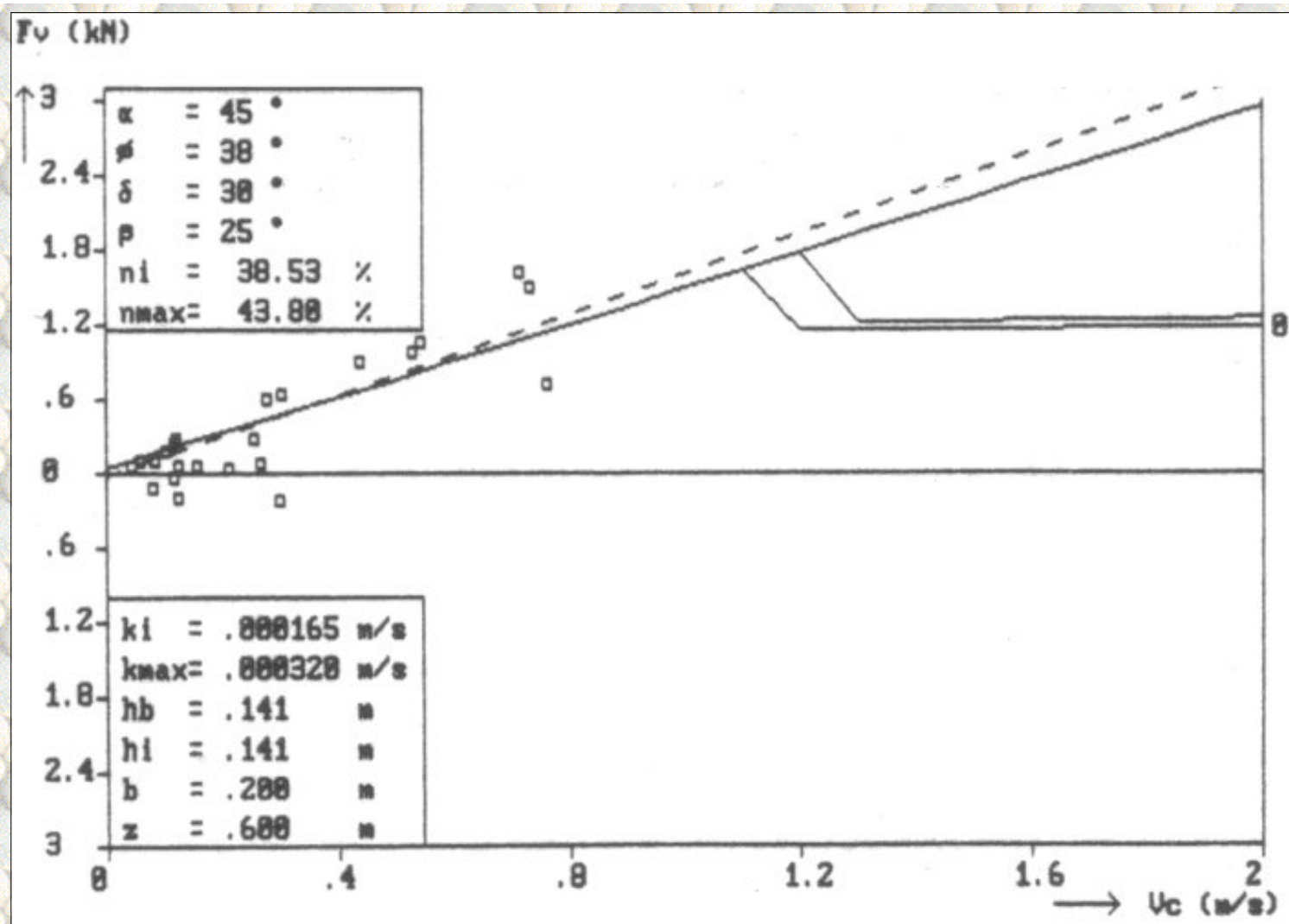


Figure B5.12: The vertical force F_v as a function of the cutting velocity v_c , at a blade angle of 45° for the non-cavitating cutting process and a layer thickness of 141 mm, in the 200 μm sand.

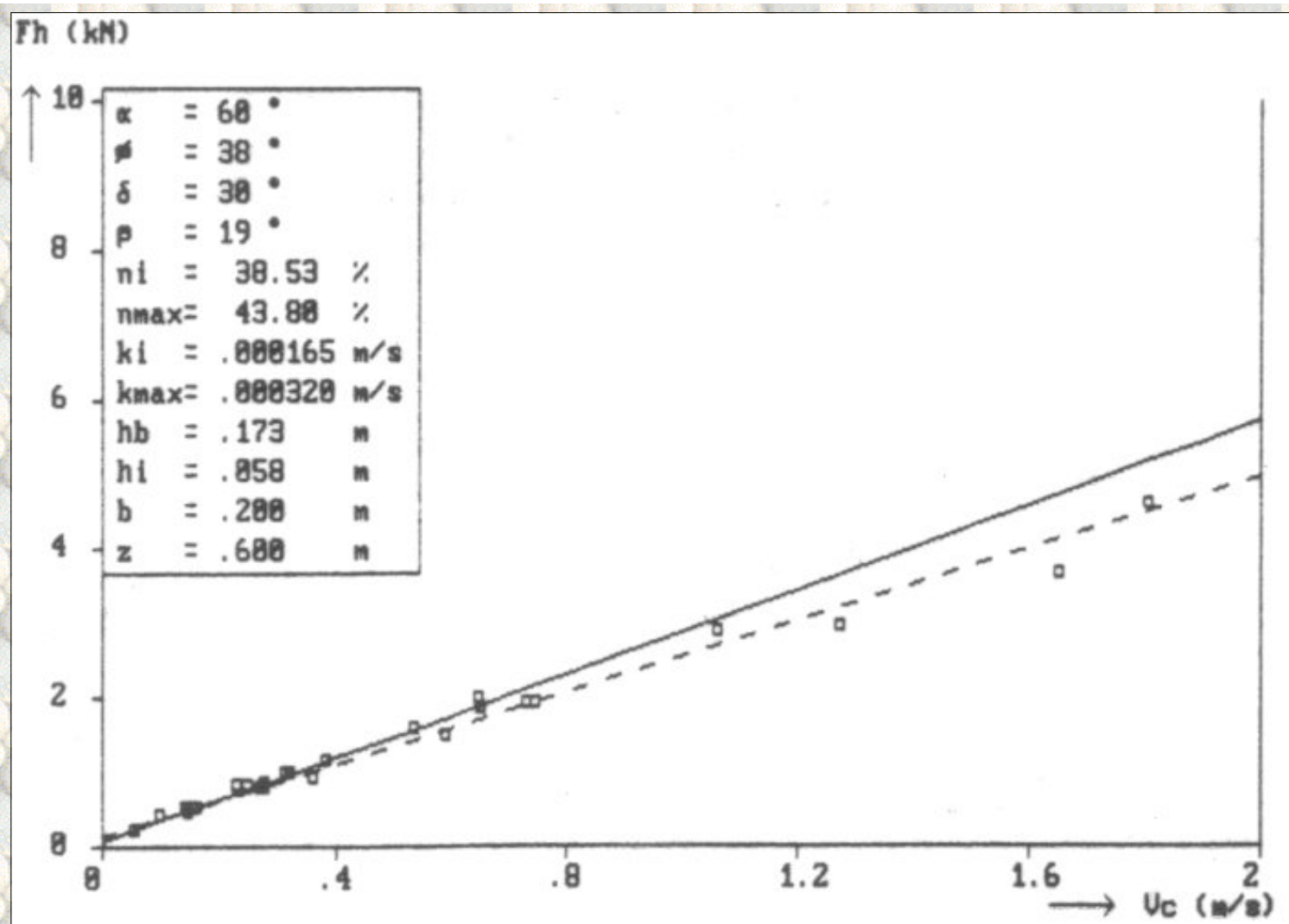


Figure B5.13: The horizontal force F_h as a function of the cutting velocity v_c , at a blade angle of 60° for the non-cavating cutting process and a layer thickness of 58 mm, in the 200 μm sand.

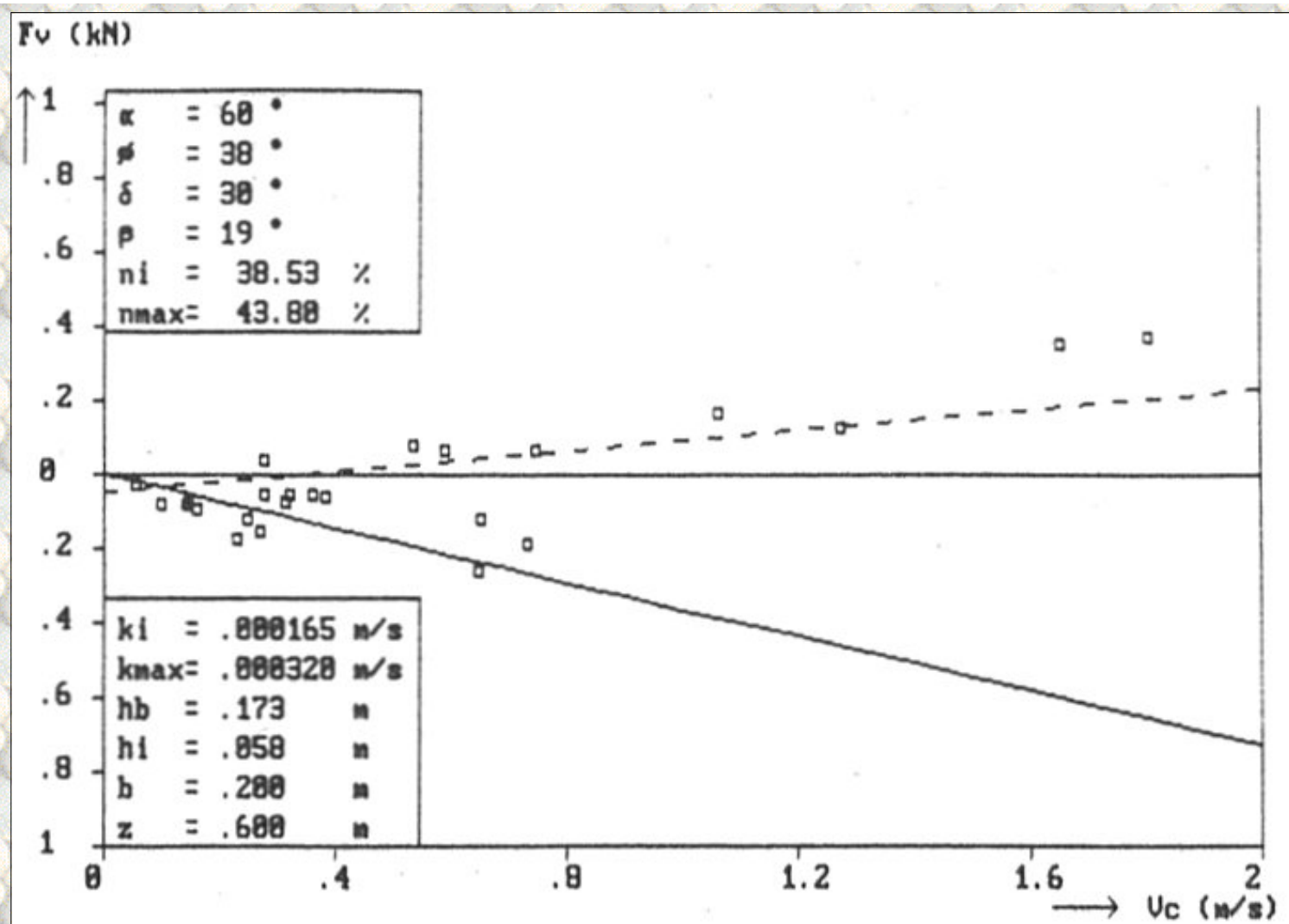


Figure B5.14: The vertical force F_v as a function of the cutting velocity v_c , at a blade angle of 60° for the non-cavitating cutting process and a layer thickness of 58 mm, in the 200 μm sand.

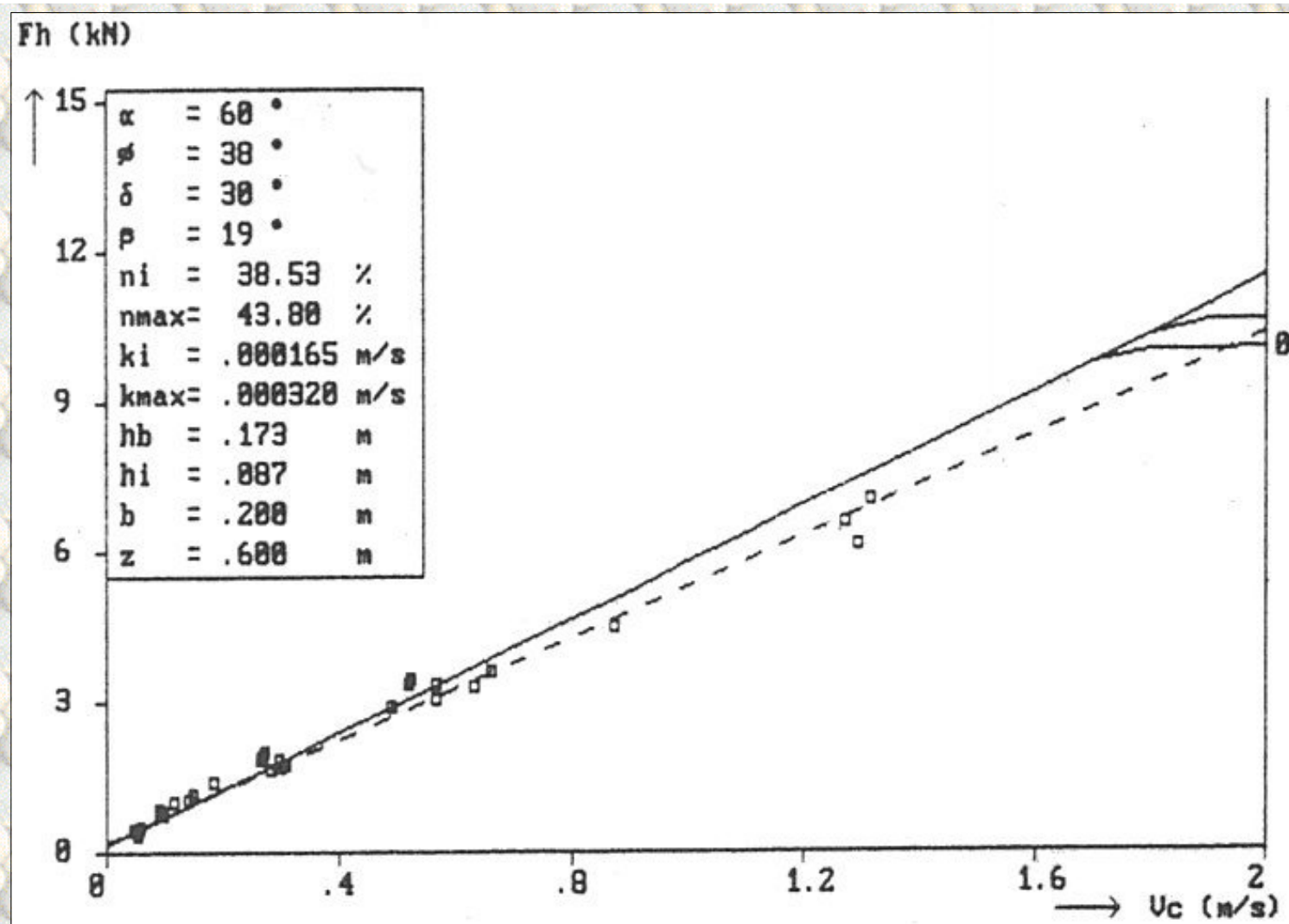


Figure B5.15: The horizontal force F_h as a function of the cutting velocity v_c , at a blade angle of 60° for the non-cavitating cutting process and a layer thickness of 87 mm, in the 200 μm sand.

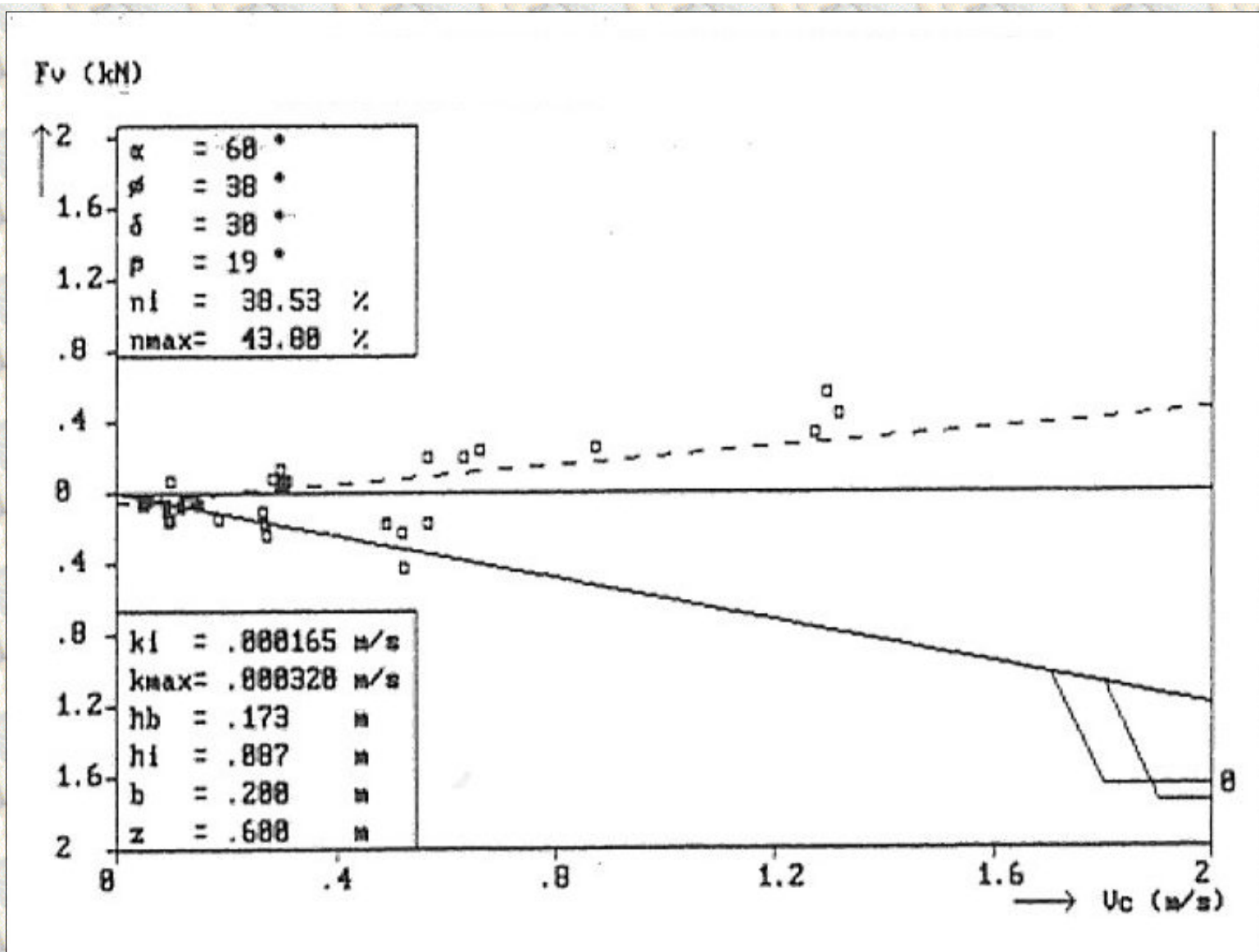


Figure B5.16: The vertical force F_v as a function of the cutting velocity v_c , at a blade angle of 60° for the non-cavitating cutting process and a layer thickness of 87 mm, in the 200 μm sand.

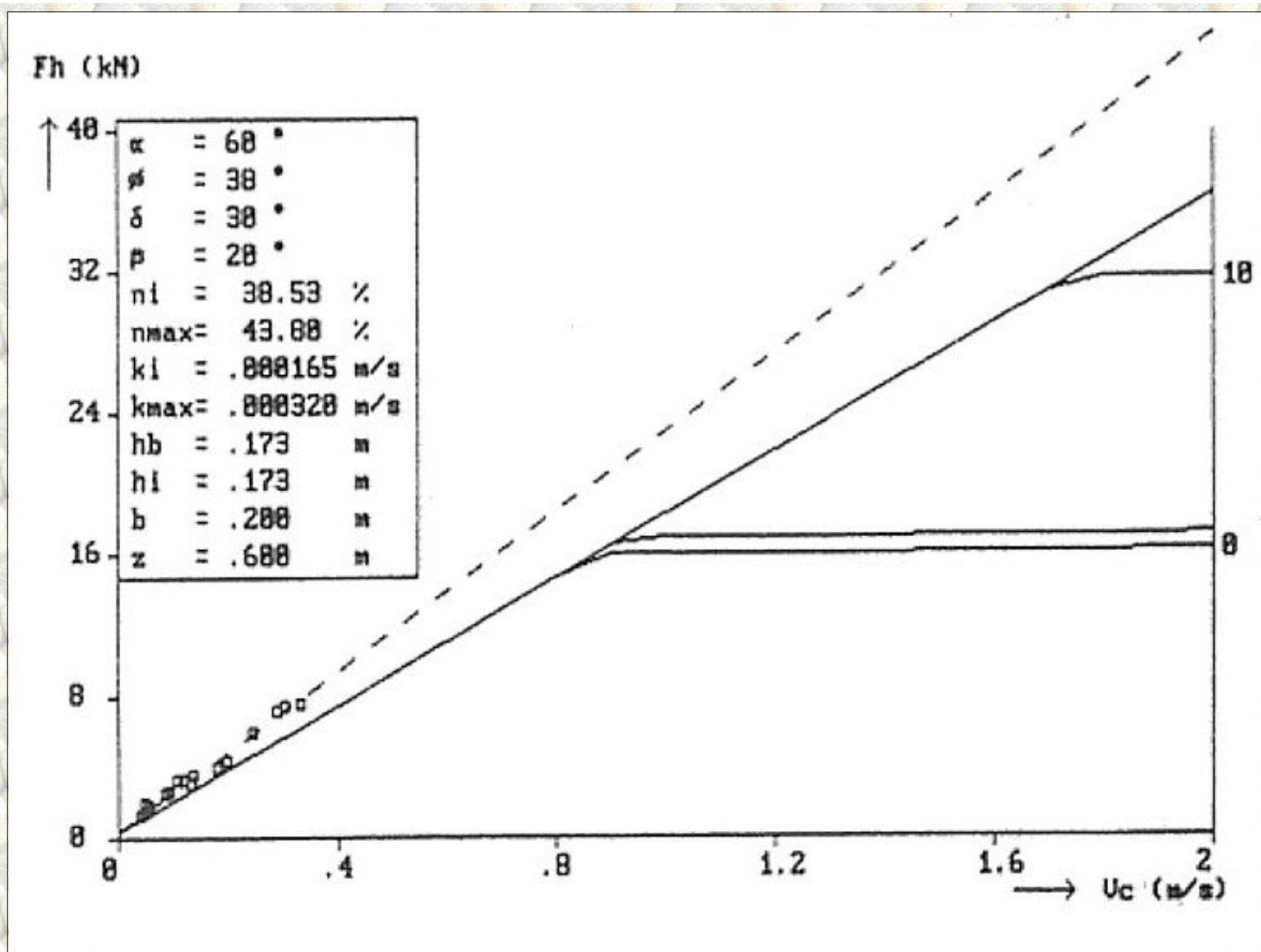


Figure B5.17: The horizontal force F_h as a function of the cutting velocity v_c , at a blade angle of 60° for the non-cavating cutting process and a layer thickness of 173 mm, in the 200 μm sand.

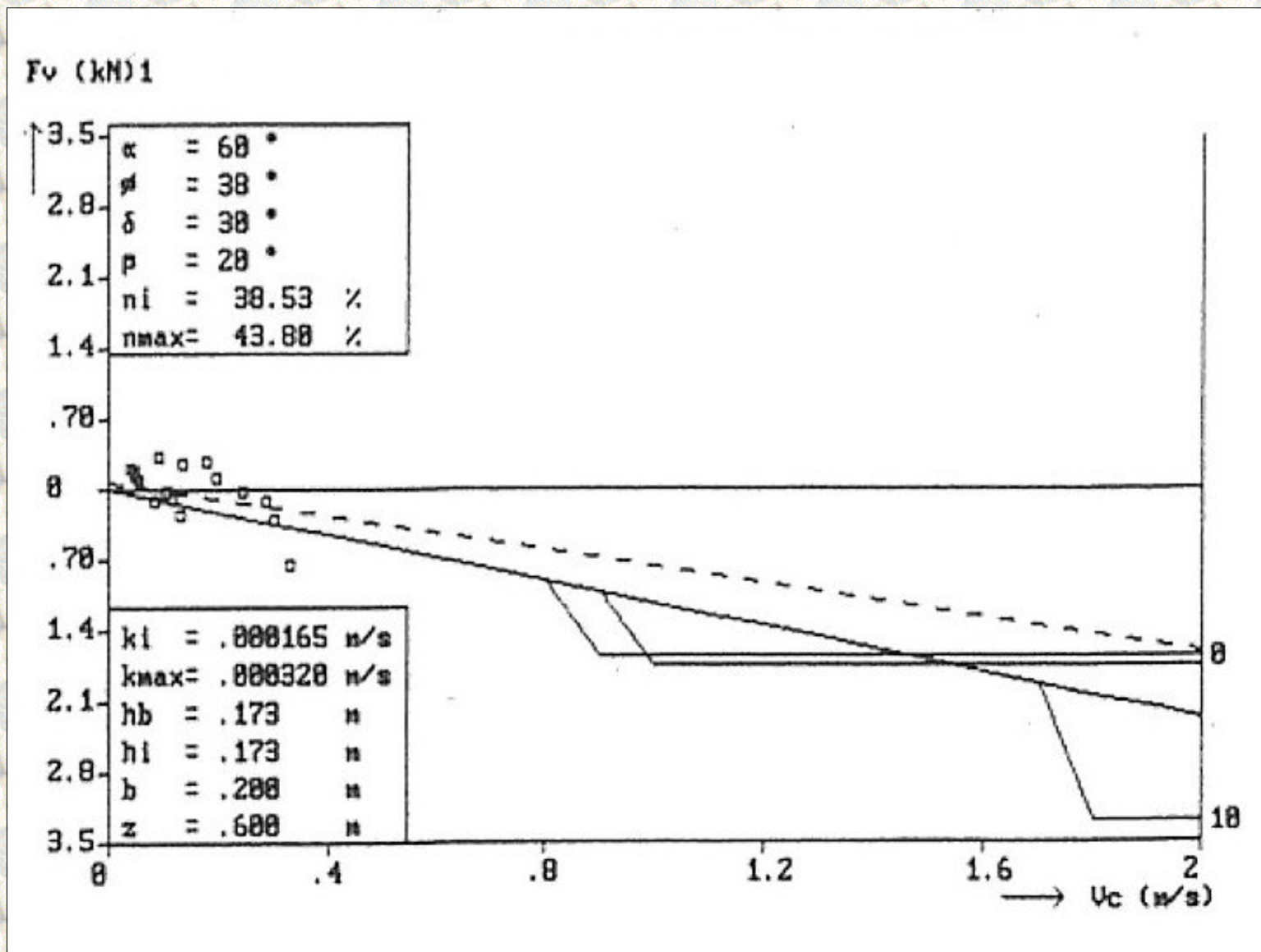


Figure B5.18: The vertical force F_v as a function of the cutting velocity v_c , at a blade angle of 60° for the non-cavitating cutting process and a layer thickness of 173 mm, in the 200 μm sand.

[Back to top](#)

This is a translation of the dissertation of Dr.ir. S.A. Miedema, dated September 15th 1987.

The dissertation was originally published in Dutch by the:

Delft University of Technology

Faculty of Mechanical Engineering and Marine Technology

Chair of Dredging Technology

Mekelweg 2

2628 CD, Delft

The Netherlands

Last modified Wednesday May 24, 2000 by: [Sape A. Miedema](#)

Translation by: [Laurens de Jonge](#)

Figures, equations and tables by: [Erik Miedema](#)

Copyright © May, 2000 Dr.ir. S.A. Miedema



[Download Adobe Acrobat Reader V4.0](#)

B5.02 The measured horizontal and vertical cutting forces

additional to table 3.2, chapter 3.5,
scaled to a blade with $b=200$ mm and $h=200$ mm.

[Contents](#)

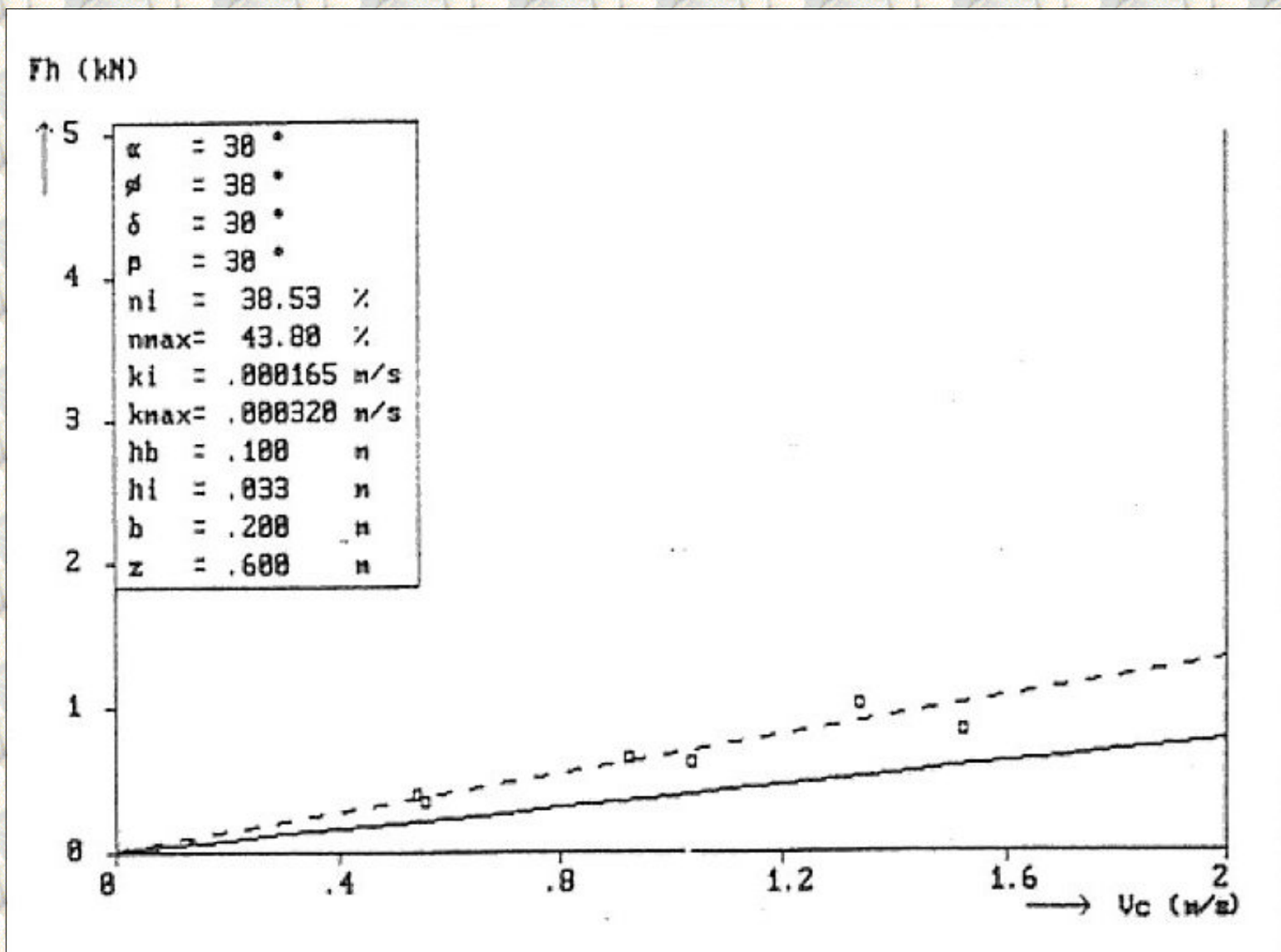


Figure B5.19: The horizontal force F_h as a function of the cutting velocity v_c , at a blade angle of 30° for the non-cavitating cutting process and a layer thickness of 33 mm, in the 200 μ m sand.

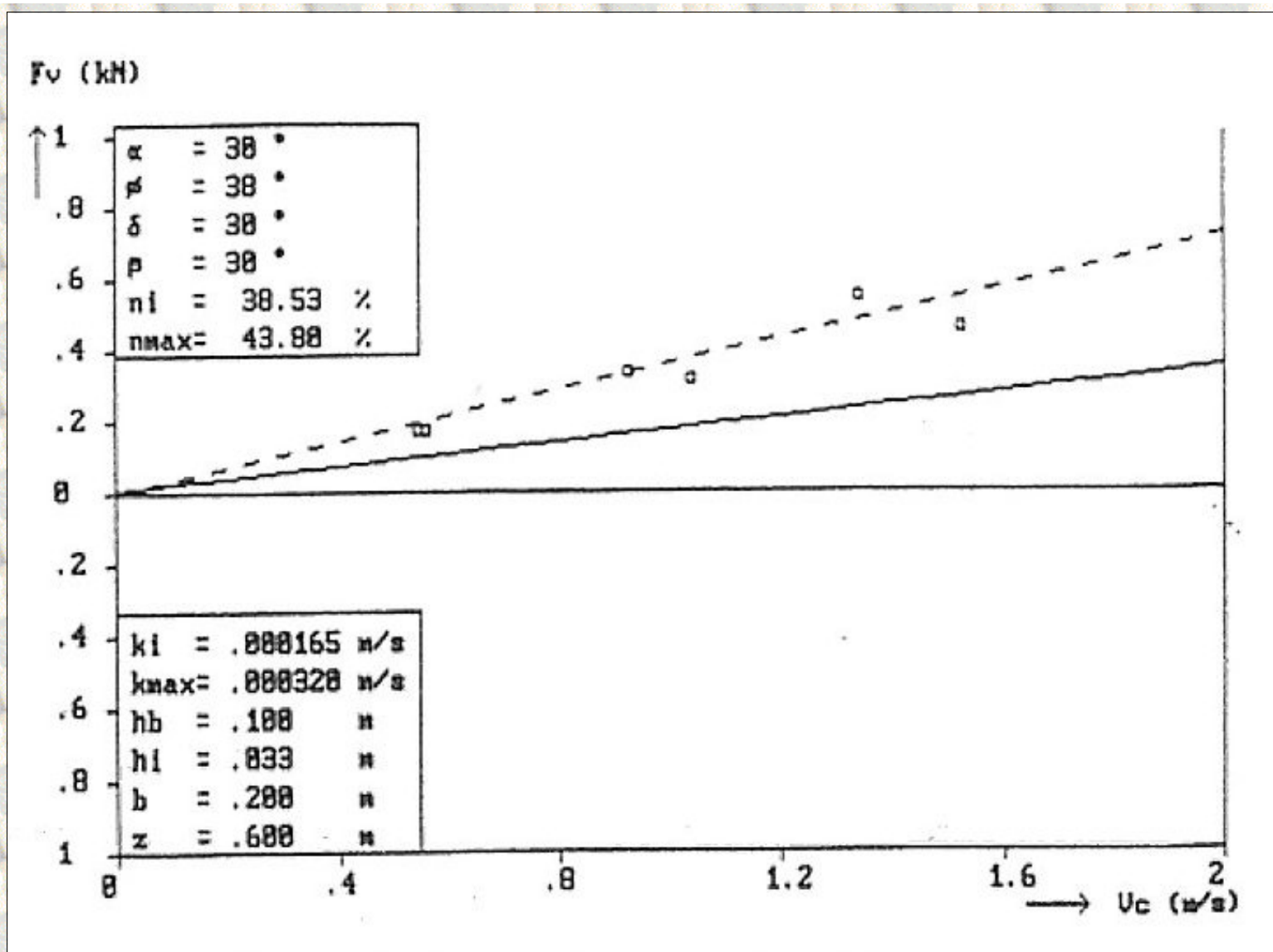


Figure B5.20: The vertical force F_v as a function of the cutting velocity v_c , at a blade angle of 30° for the non-cavitating cutting process and a layer thickness of 33 mm, in the 200 μm sand.

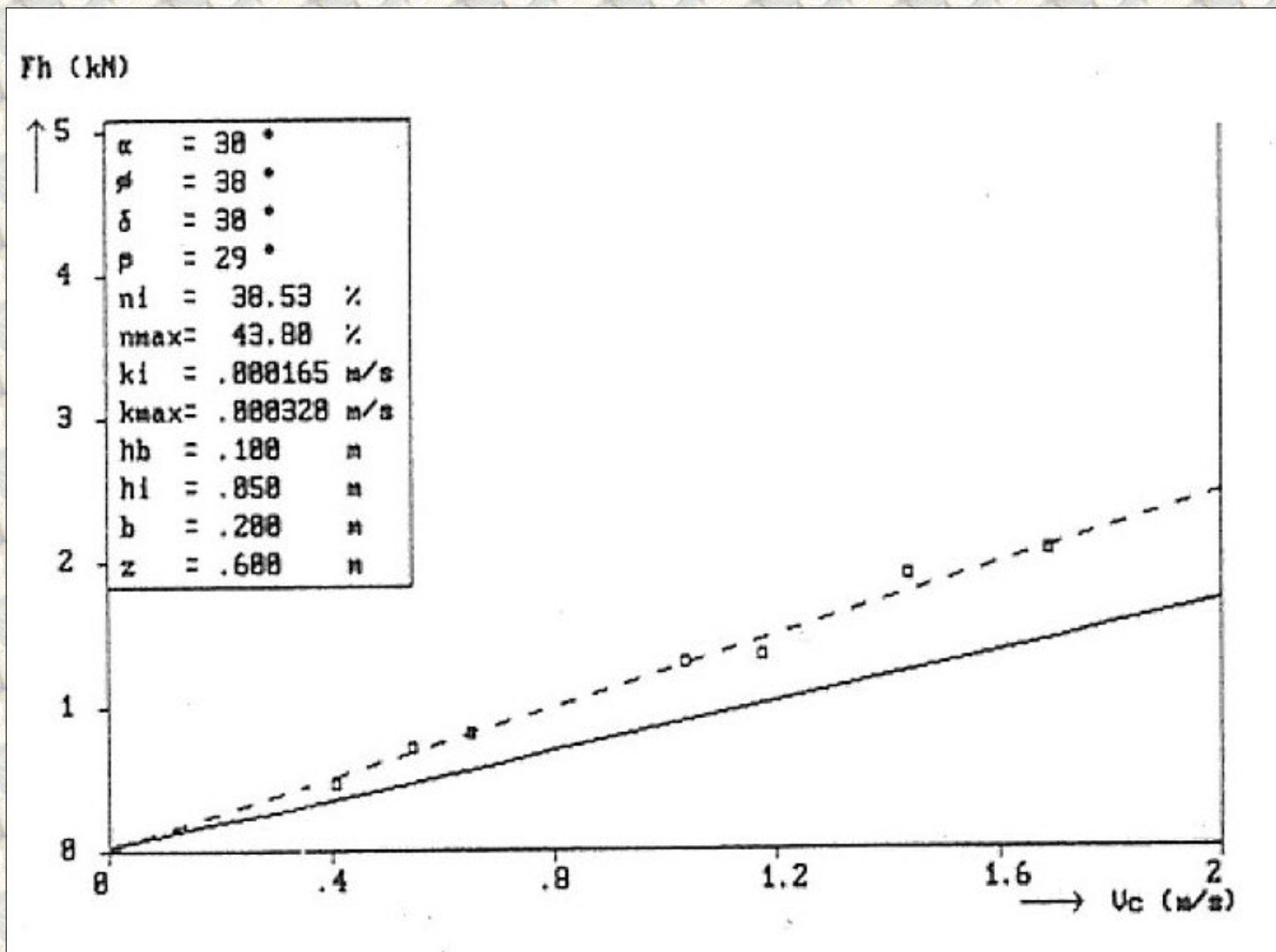
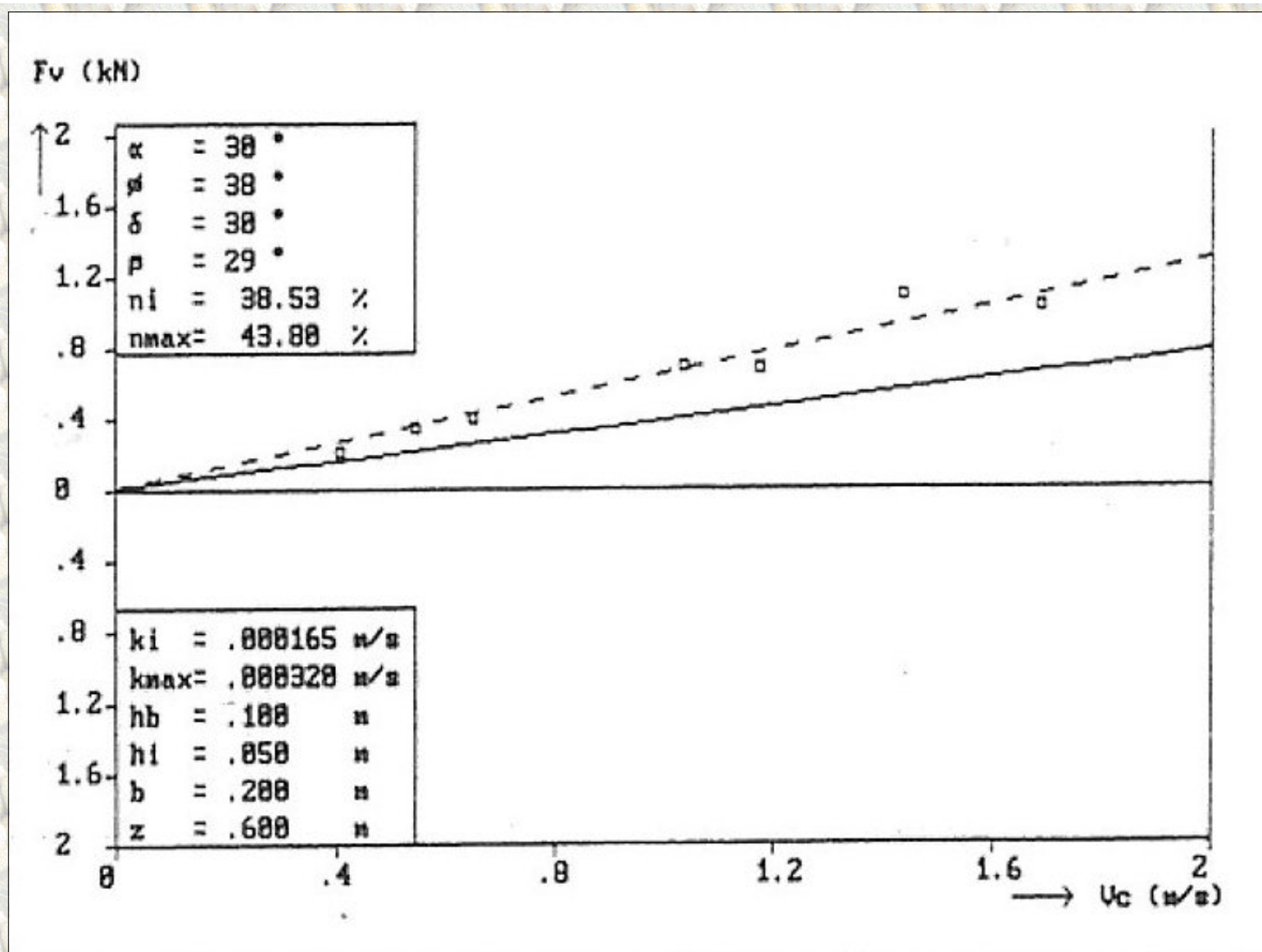


Figure B5.21: The horizontal force F_h as a function of the cutting velocity v_c , at a blade angle of 30° for the non-cavitating cutting process and a layer thickness of 50 mm, in the 200 μ m sand.



Figuur B5.22: The vertical force F_v as a function of the cutting velocity v_c , at a blade angle of 30° for the non-cavating cutting process and a layer thickness of 50 mm, in the 200 μm sand.

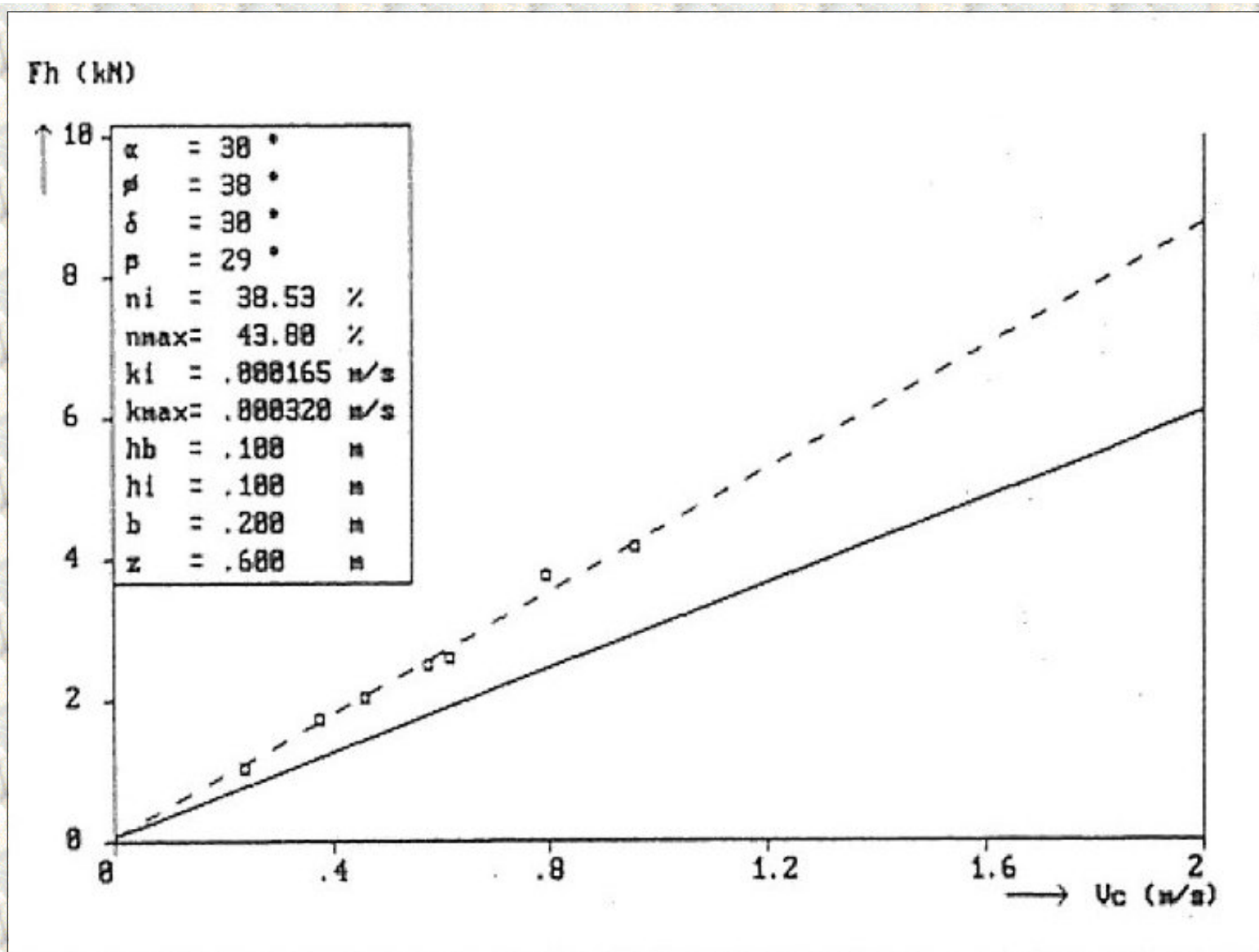


Figure B5.23: The horizontal force F_h as a function of the cutting velocity v_c , at a blade angle of 30° for the non-cavitating cutting process and a layer thickness of 100 mm, in the 200 μm sand.

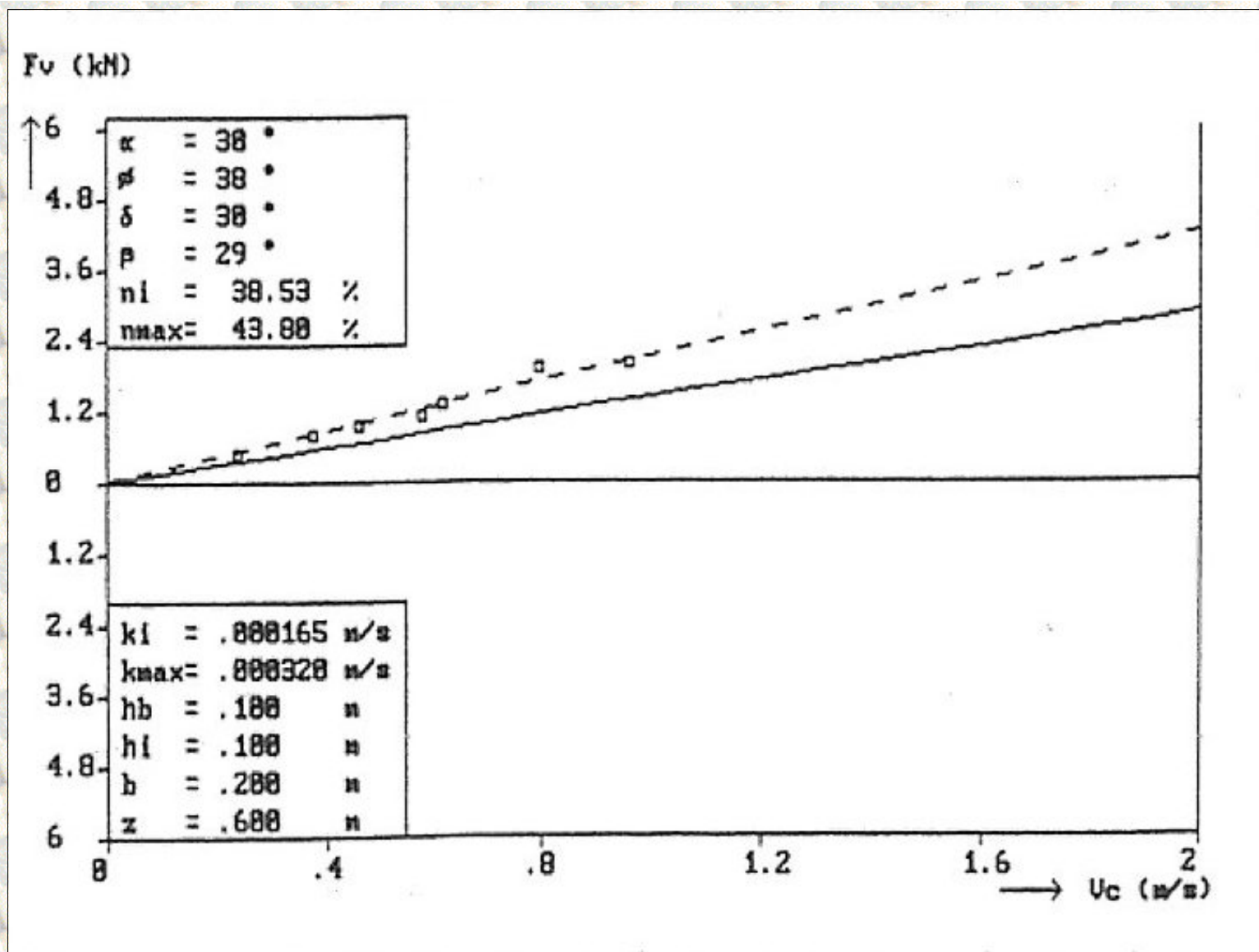


Figure B5.24: The vertical force F_v as a function of the cutting velocity v_c , at a blade angle of 30° for the non-cavitating cutting process and a layer thickness of 100 mm, in the 200 μm sand.

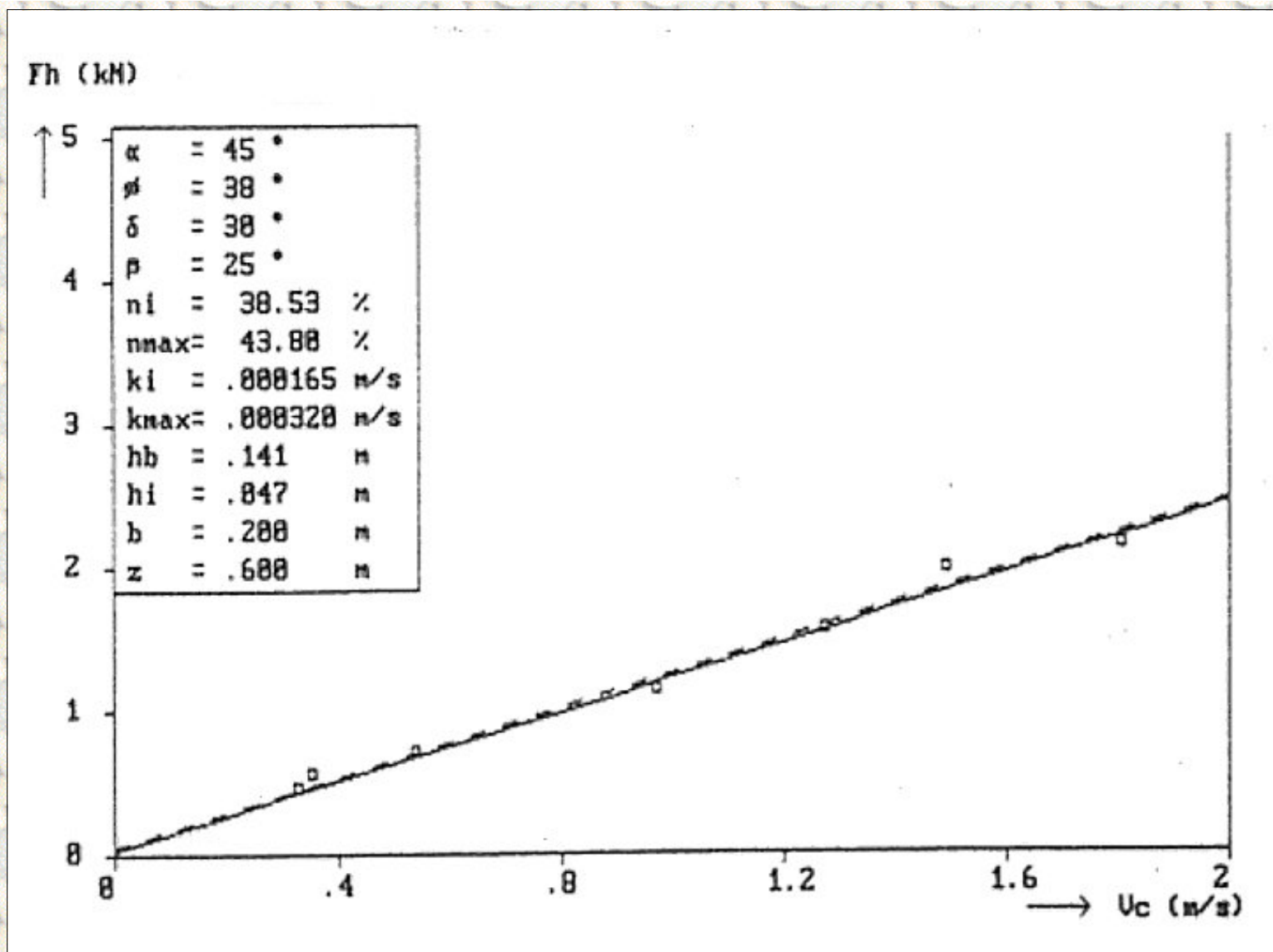


Figure B5.25: The horizontal force F_h as a function of the cutting velocity v_c , at a blade angle of 45° for the non-cavitating cutting process and a layer thickness of 47 mm, in the 200 μm sand.

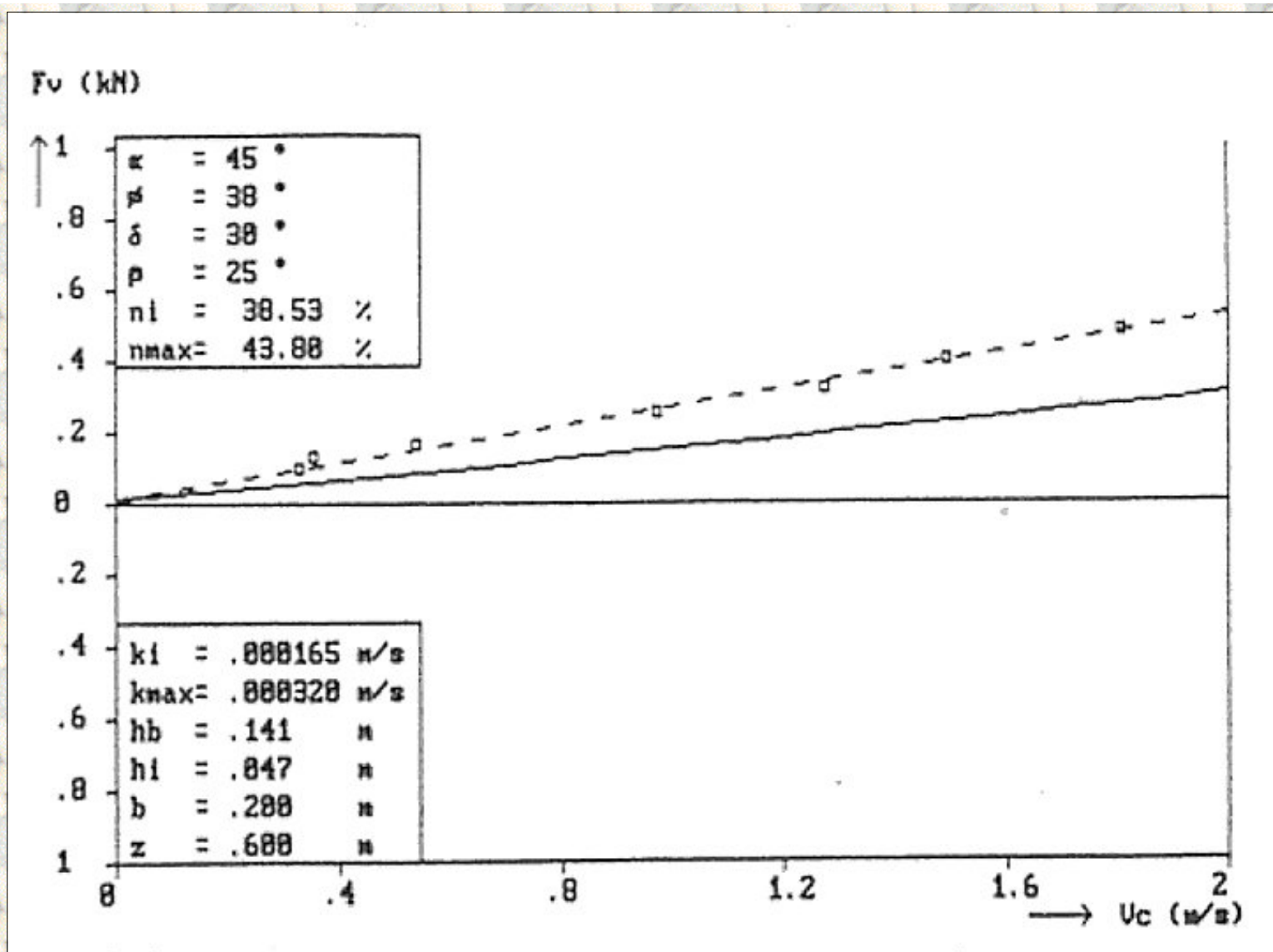


Figure B5.26: The vertical force F_v as a function of the cutting velocity v_c , at a blade angle of 45° for the non-cavitating cutting process and a layer thickness of 47 mm, in the 200 μm sand.

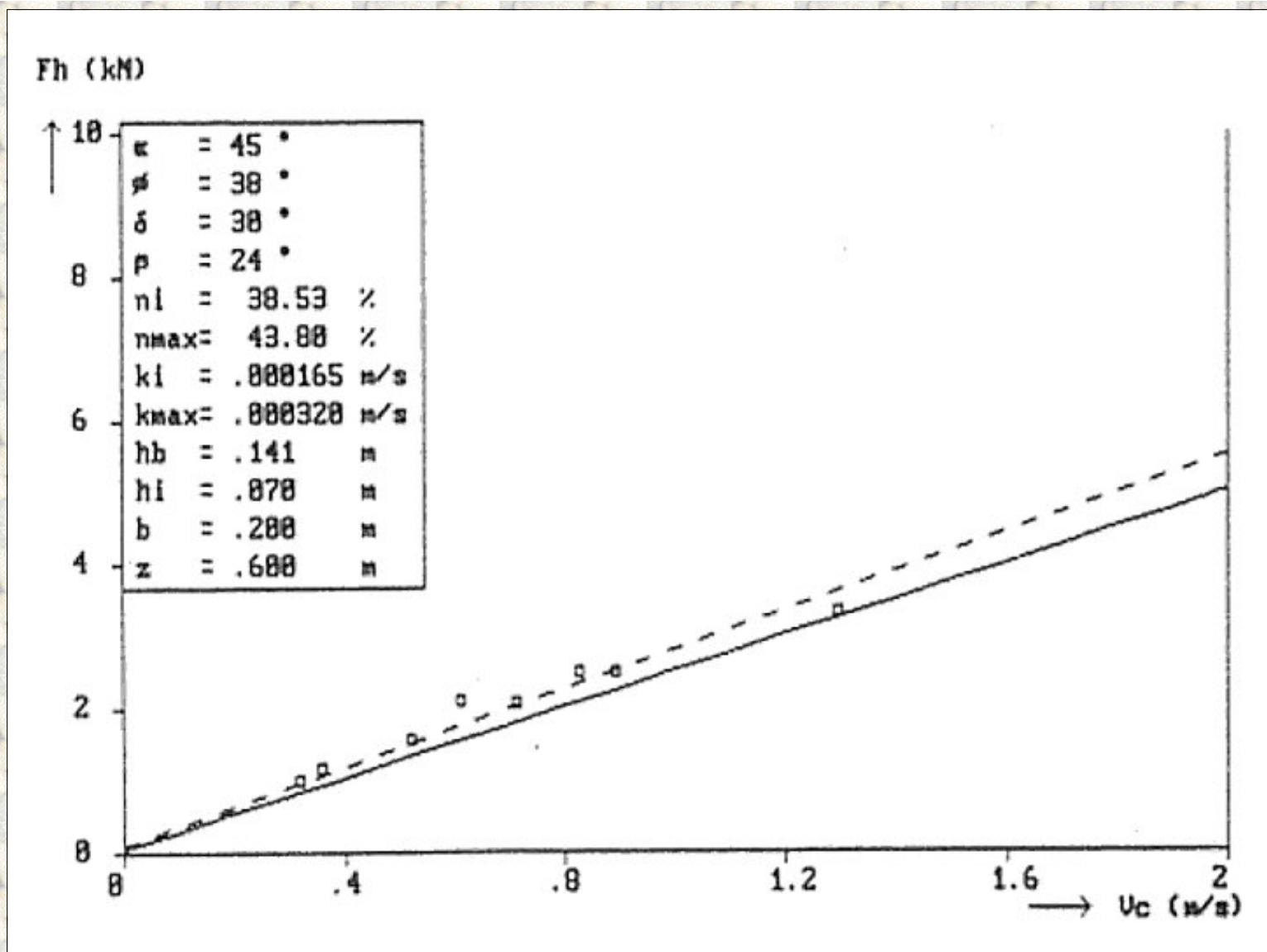


Figure B5.27: The horizontal force F_h as a function of the cutting velocity v_c , at a blade angle of 45° for the non-cavitating cutting process and a layer thickness of 70 mm, in the 200 μm sand.

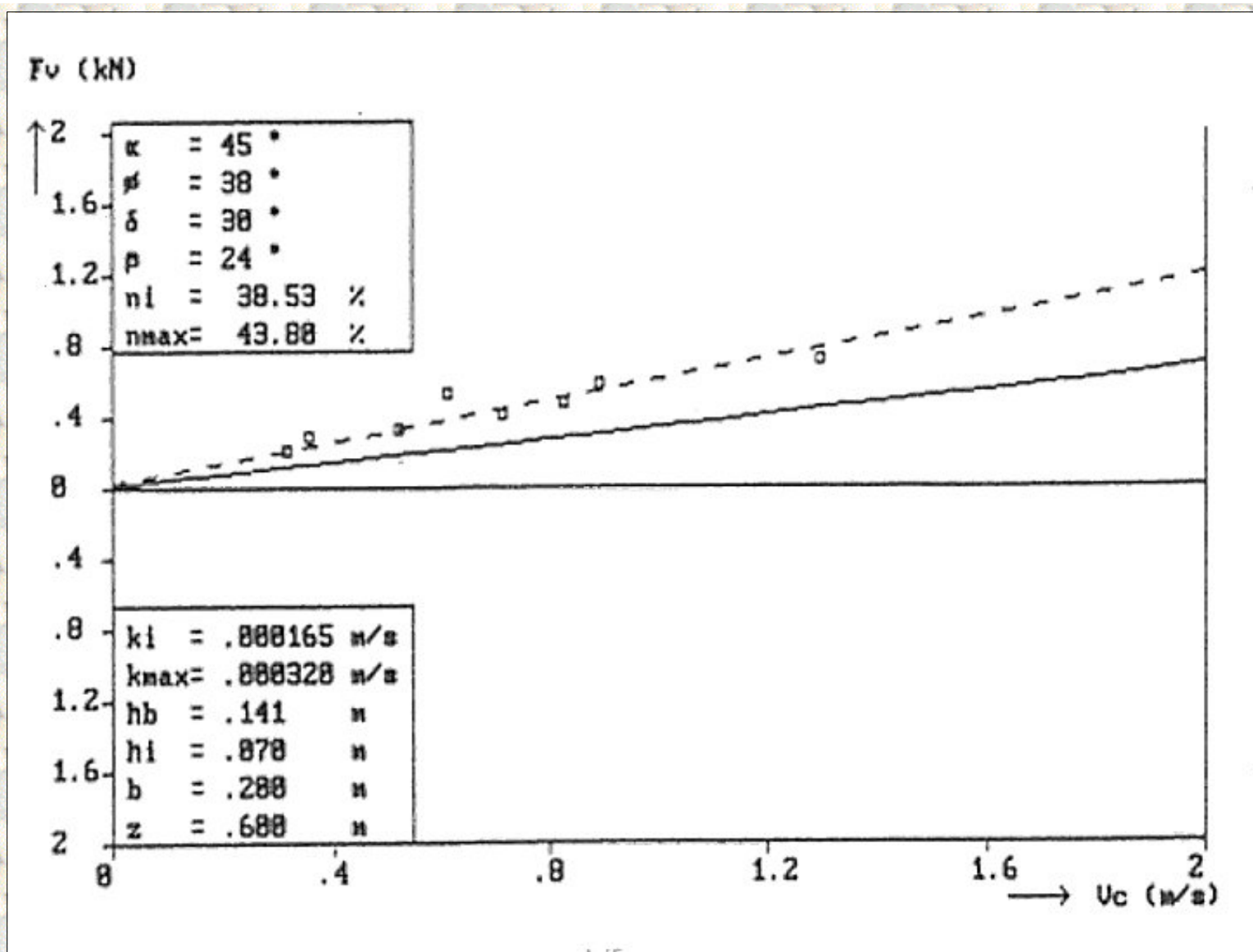


Figure B5.28: The vertical force F_v as a function of the cutting velocity v_c , at a blade angle of 45° for the non-cavitating cutting process and a layer thickness of 70 mm, in the 200 μm sand.

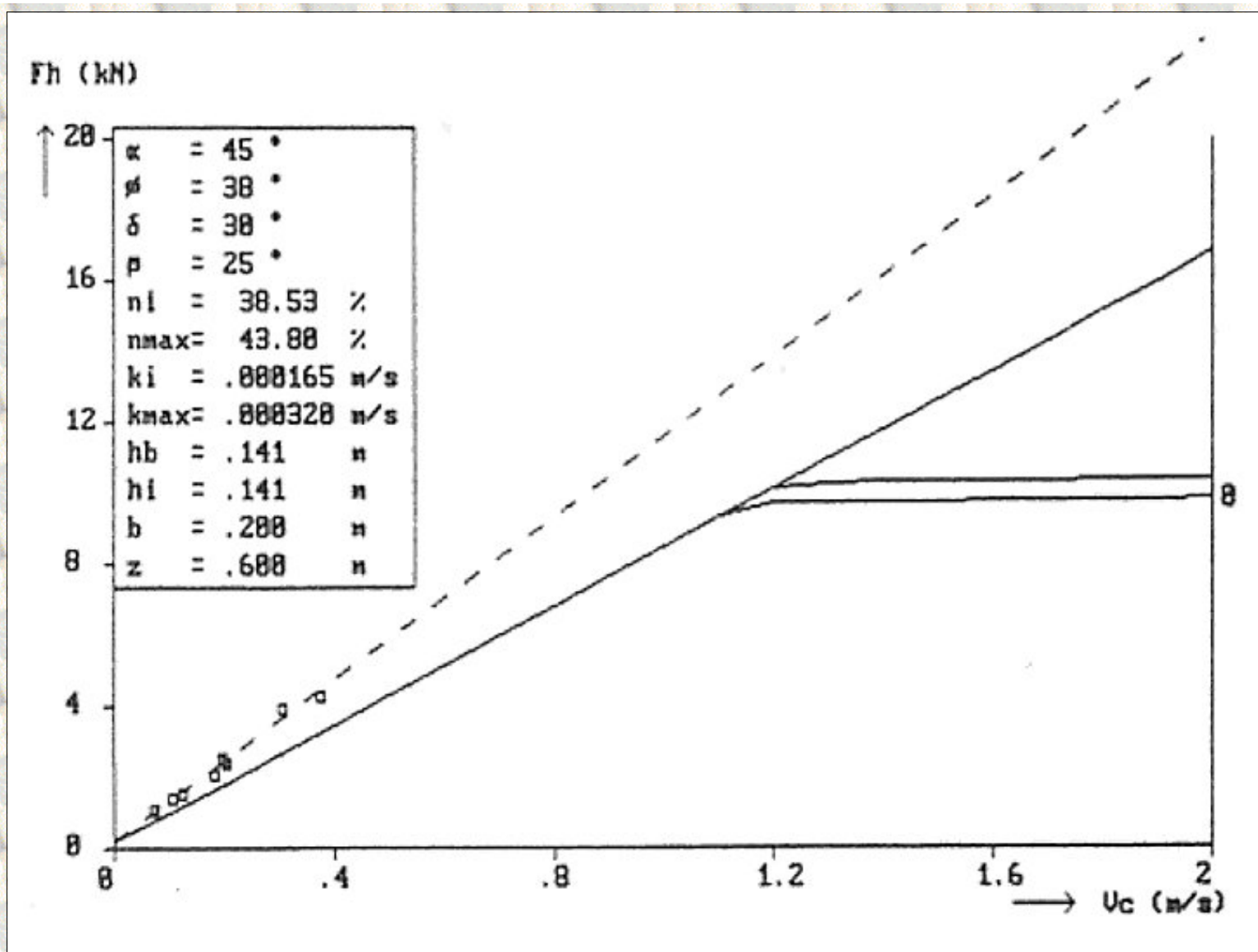


Figure B5.29: The horizontal force F_h as a function of the cutting velocity v_c , at a blade angle of 45° for the non-cavitating cutting process and a layer thickness of 141 mm, in the 200 μm sand.

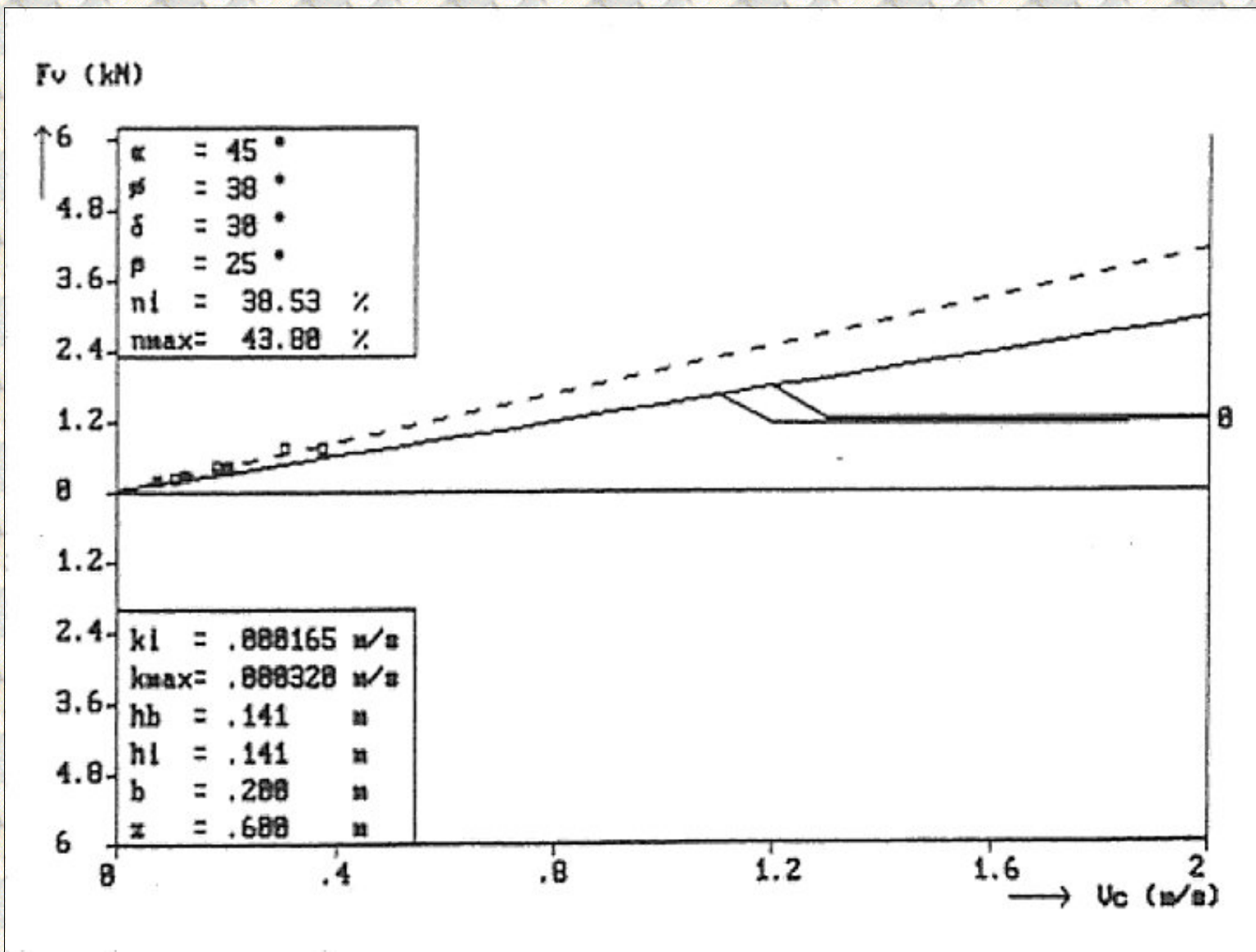


Figure B5.30: The vertical force F_v as a function of the cutting velocity v_c , at a blade angle of 45° for the non-cavating cutting process and a layer thickness of 141 mm , in the 200 μm sand.

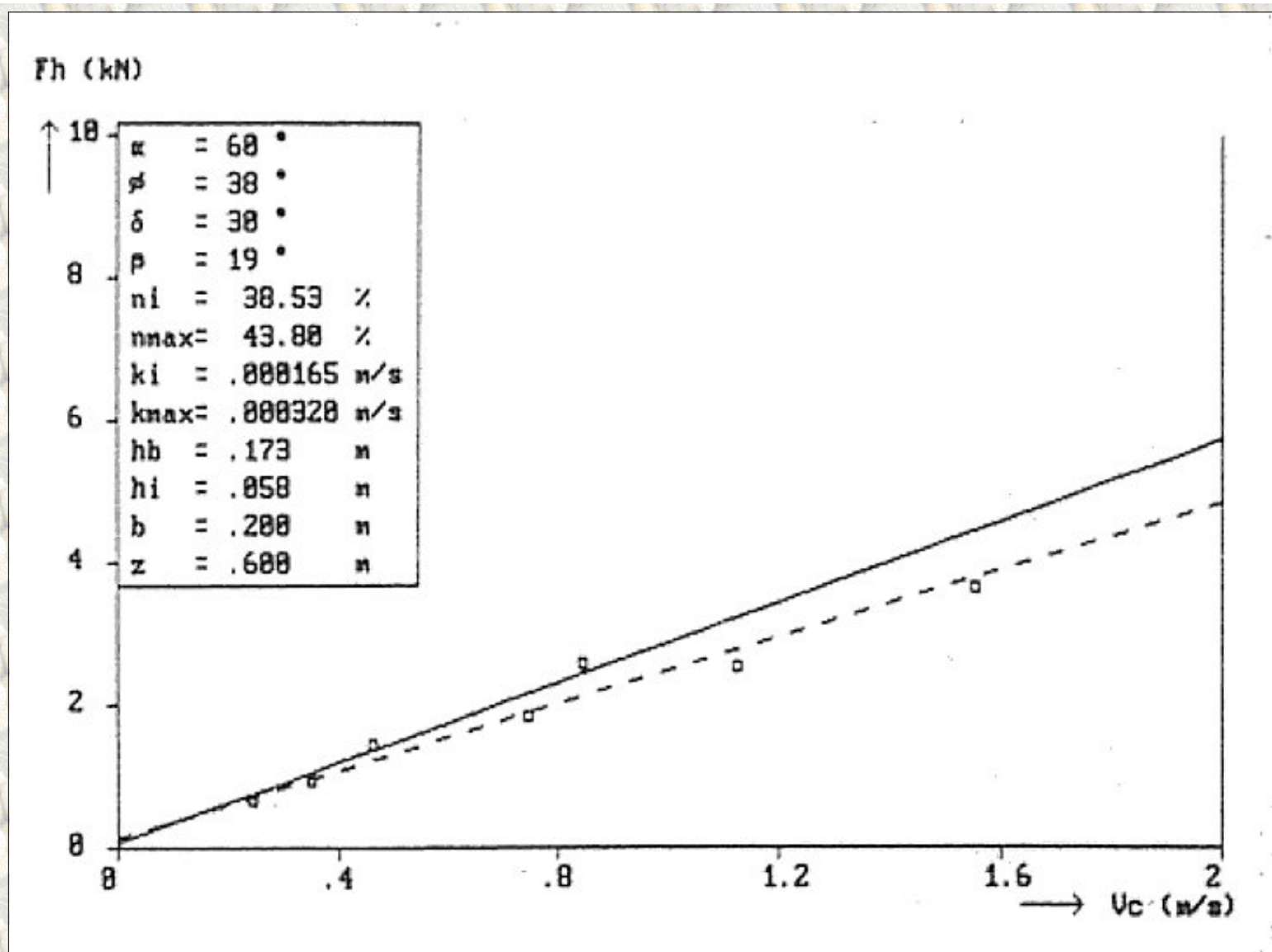


Figure B5.31: The horizontal force F_h as a function of the cutting velocity v_c , at a blade angle of 60° for the non-cavitating cutting process and a layer thickness of 58 mm, in the 200 μm sand.

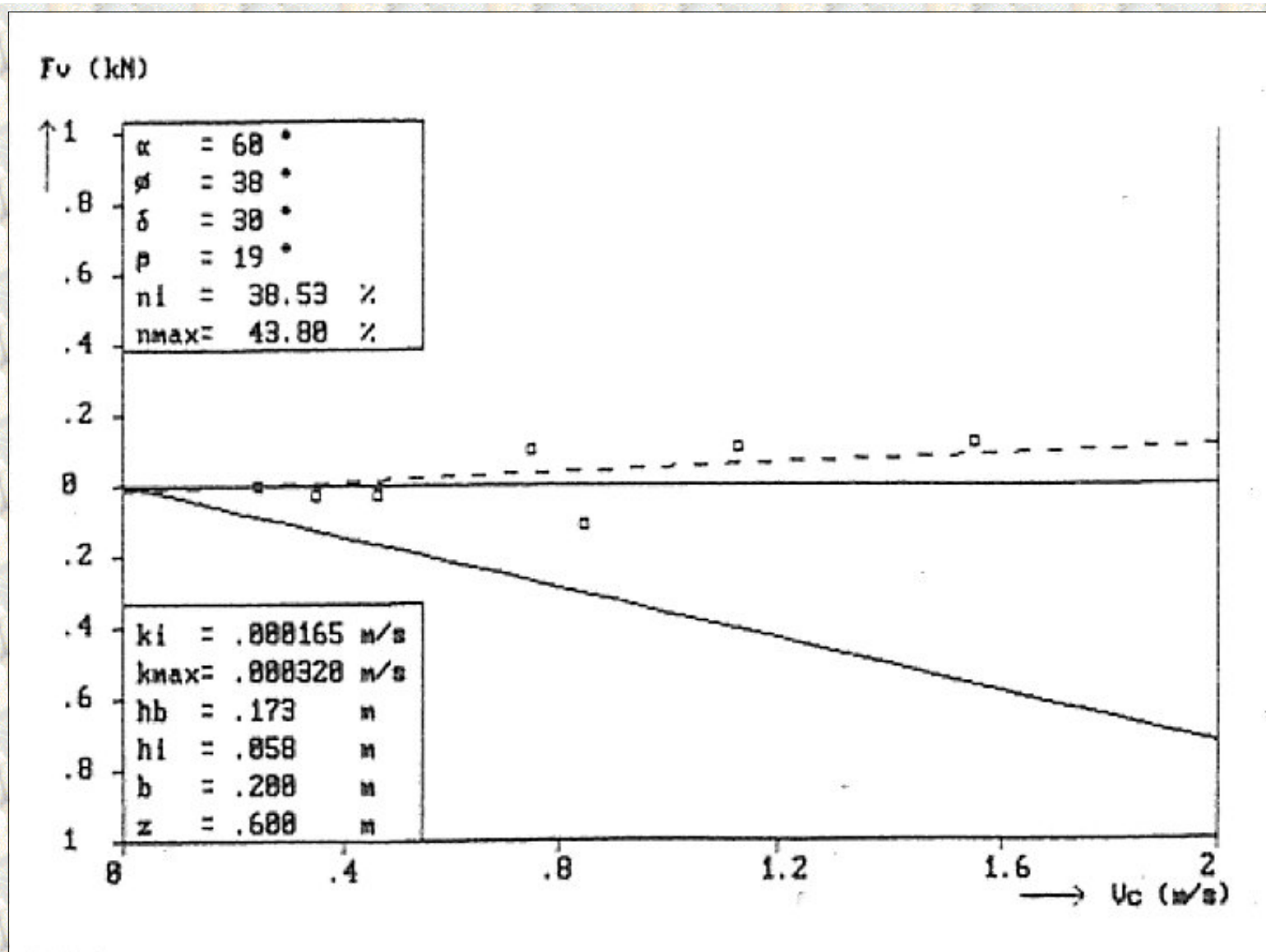


Figure B5.32: The vertical force F_v as a function of the cutting velocity v_c , at a blade angle of 60° for the non-cavitating cutting process and a layer thickness of 58 mm, in the 200 μm sand.

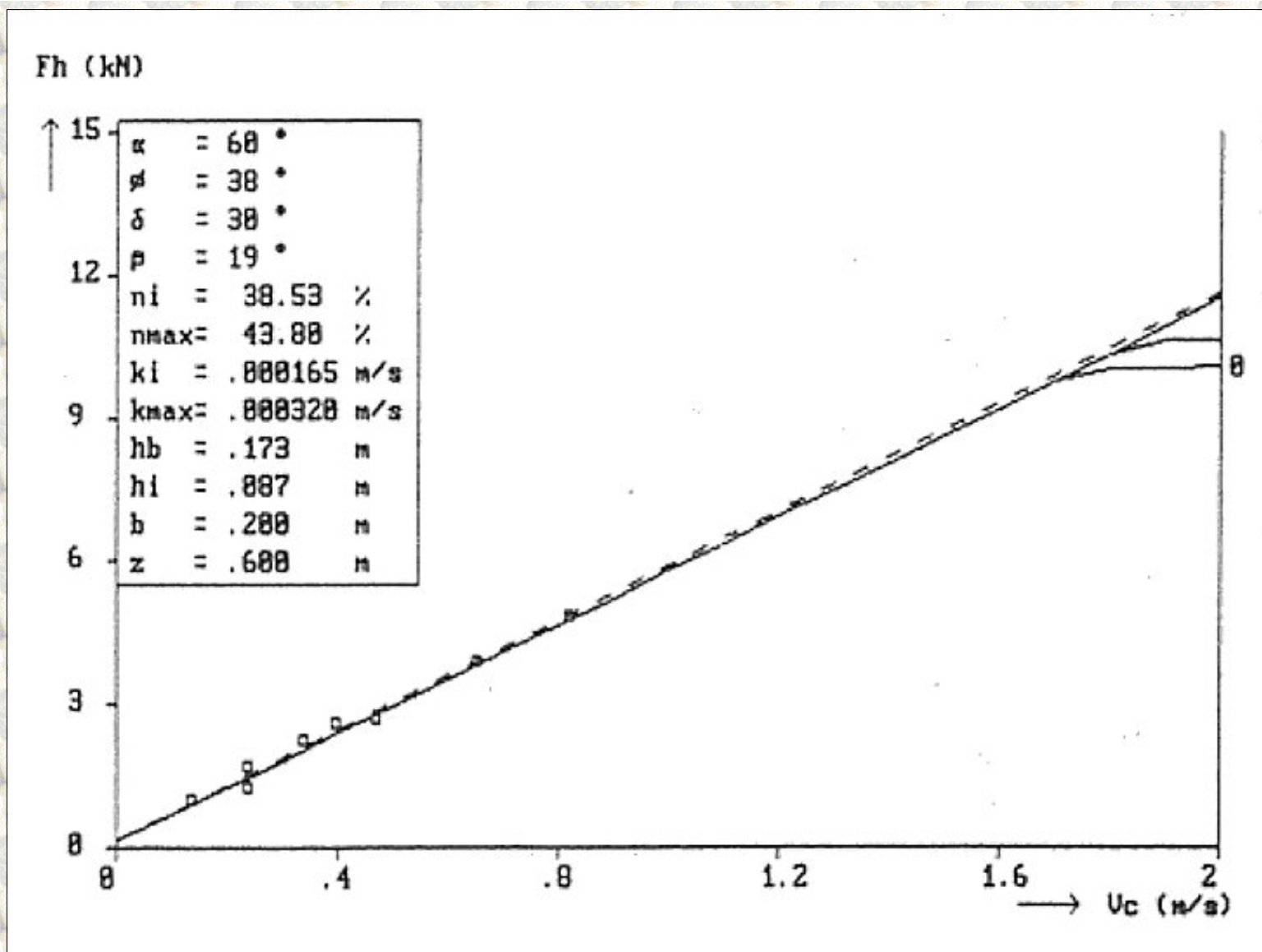


Figure B5.33: The horizontal force F_h as a function of the cutting velocity v_c , at a blade angle of 60° for the non-cavitating cutting process and a layer thickness of 87 mm, in the 200 μm sand.

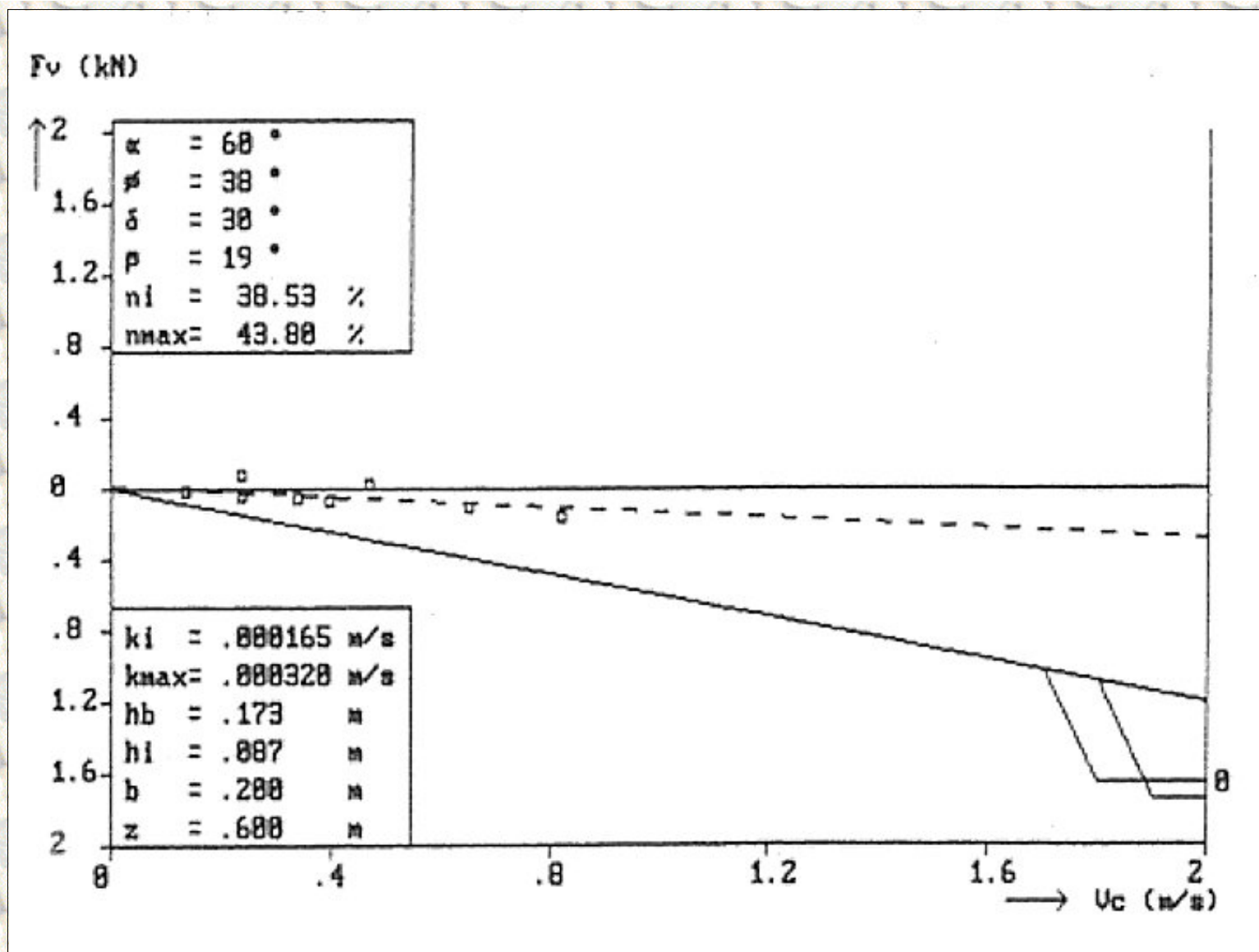


Figure B5.34: The vertical force F_v as a function of the cutting velocity v_c , at a blade angle of 60° for the non-cavating cutting process and a layer thickness of 87 mm, in the 200 μm sand.

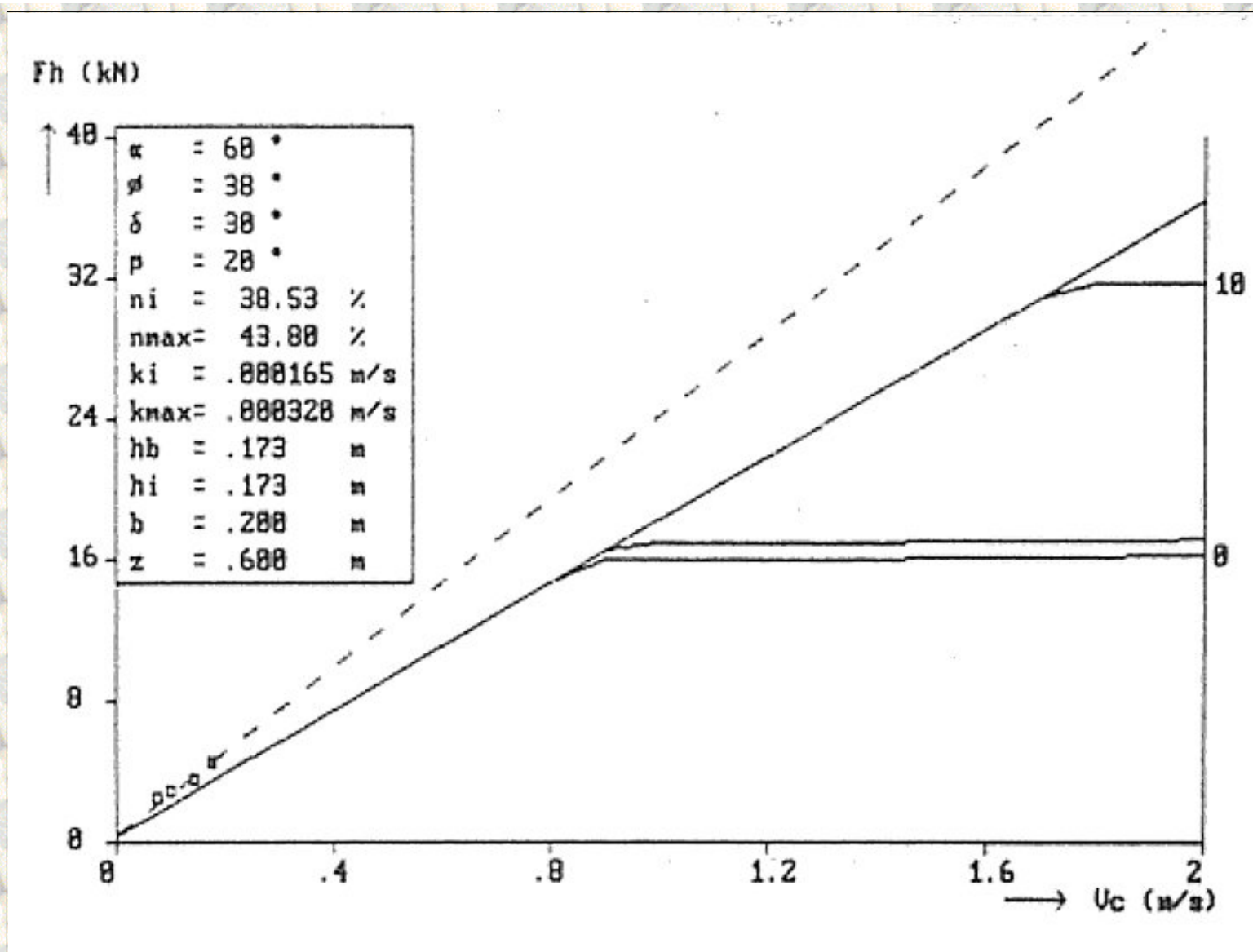


Figure B5.35: The horizontal force F_h as a function of the cutting velocity v_c , at a blade angle of 60° for the non-cavating cutting process and a layer thickness of 173 mm, in the 200 μm sand.

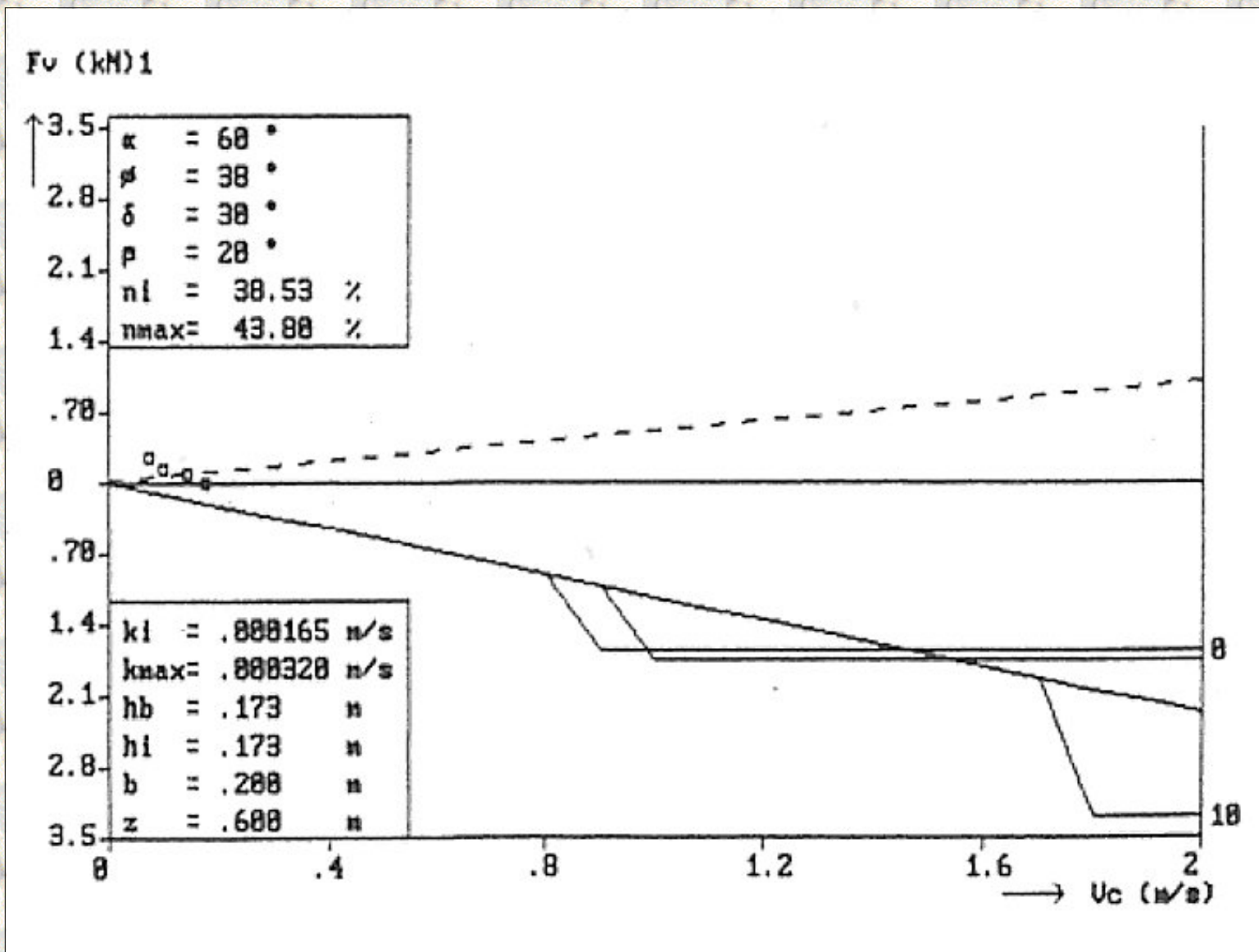


Figure B5.36: The vertical force F_v as a function of the cutting velocity v_c , at a blade angle of 60° for the non-cavitating cutting process and a layer thickness of 173 mm, in the 200 μm sand.

[Back to top](#)

This is a translation of the dissertation of Dr.ir. S.A. Miedema, dated September 15th 1987.

The dissertation was originally published in Dutch by the:

Delft University of Technology

Faculty of Mechanical Engineering and Marine Technology

Chair of Dredging Technology

Mekelweg 2

2628 CD, Delft

The Netherlands

Last modified Wednesday May 24, 2000 by: [Sape A. Miedema](#)

Translation by: [Laurens de Jonge](#)

Figures, equations and tables by: [Erik Miedema](#)

Copyright © May, 2000 Dr.ir. S.A. Miedema



[Download Adobe Acrobat Reader V4.0](#)

B5.03 The measured horizontal and vertical cutting forces

additional to table 3.7-3.8, chapter 3.9,
scaled to a blade with $b=200$ mm and $h=200$ mm.

[Contents](#)

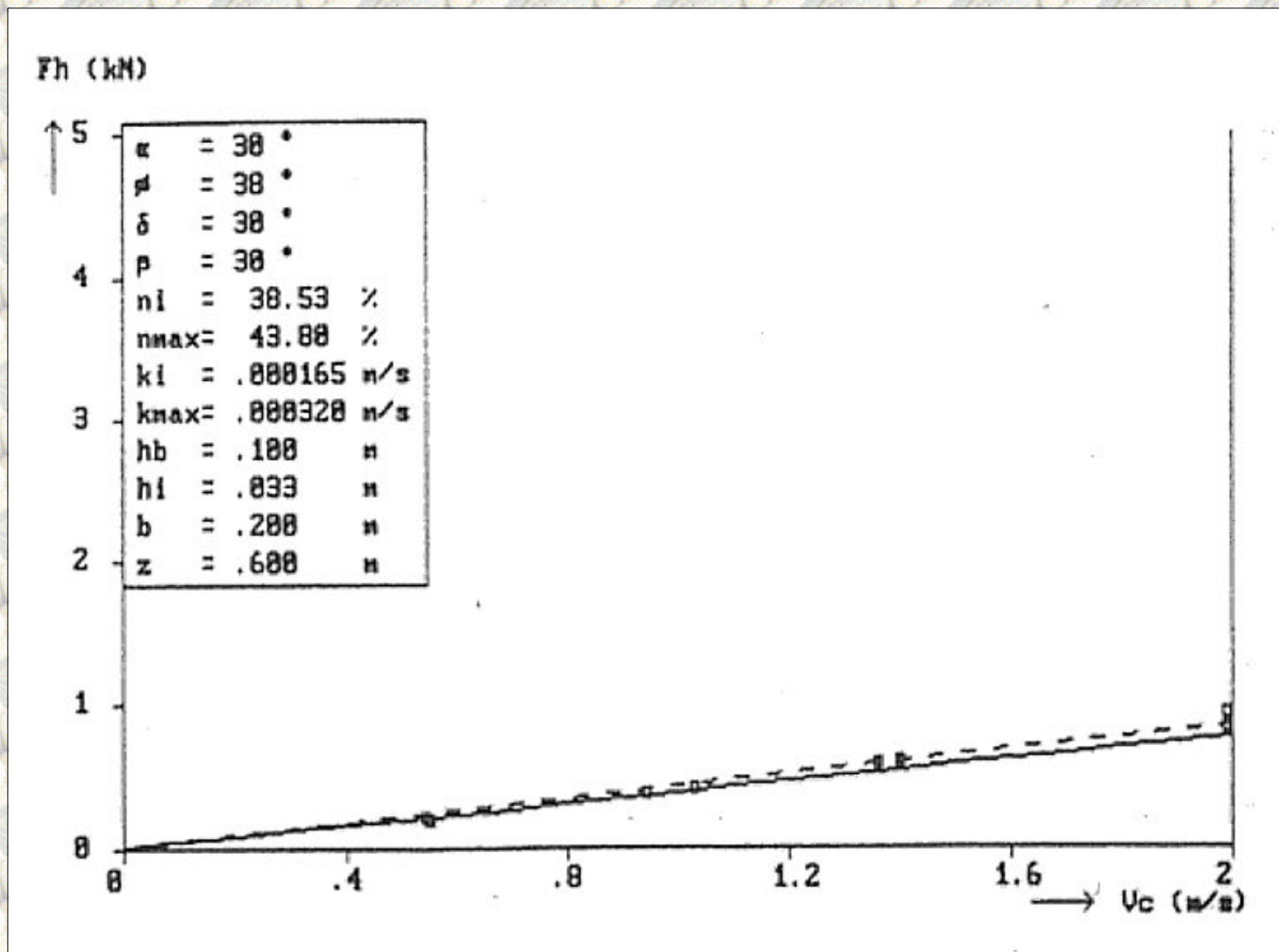


Figure B5.37: The horizontal force F_h as a function of the cutting velocity v_c , at a blade angle of 30° for the non-cavitating cutting process and a layer thickness of 33 mm, in the 200 μ m sand.

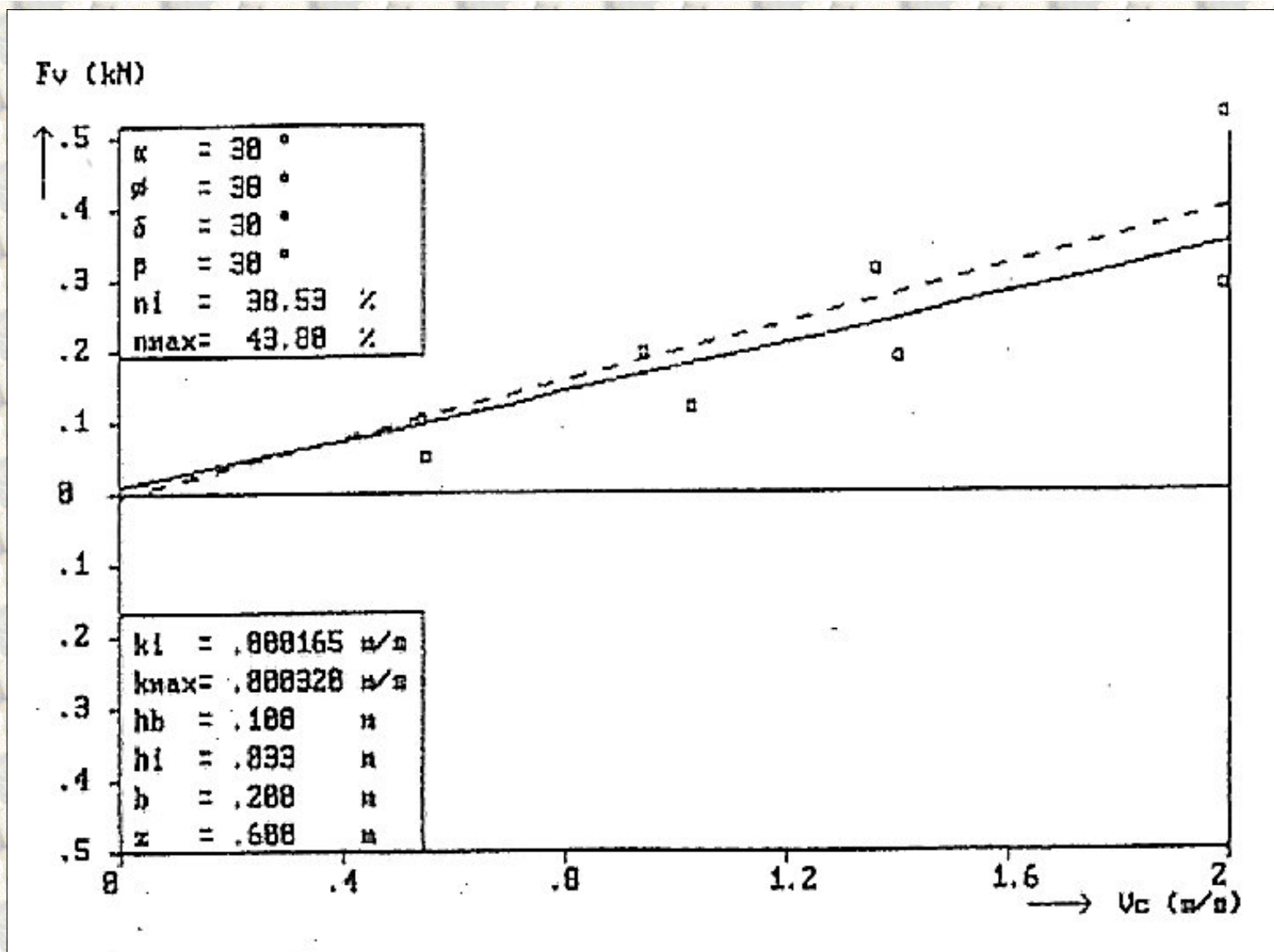


Figure B5.38: The vertical force F_v as a function of the cutting velocity v_c , at a blade angle of 30° for the non-cavitating cutting process and a layer thickness of 33 mm, in the 200 μ m sand.

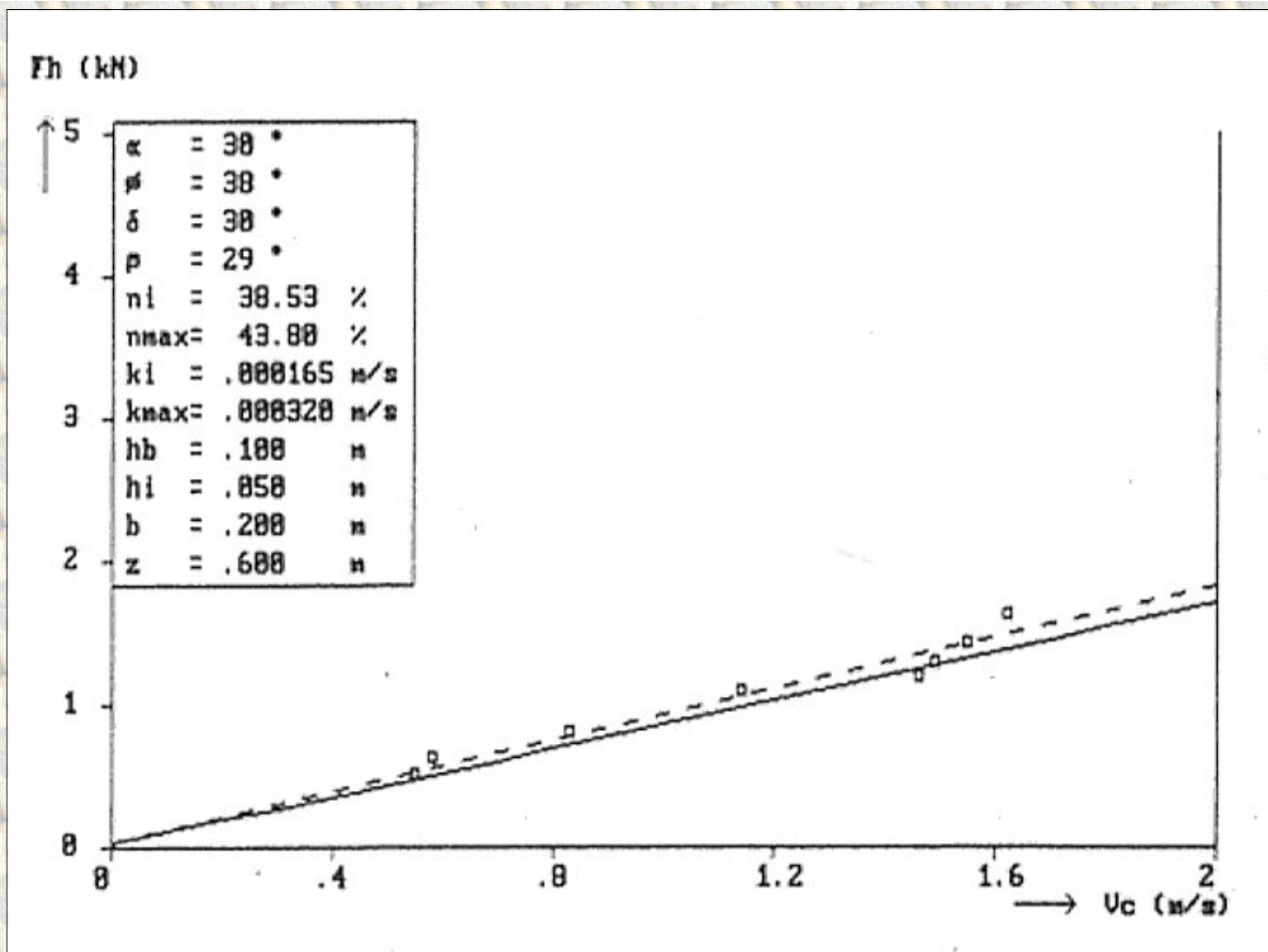


Figure B5.39: The horizontal force F_h as a function of the cutting velocity v_c , at a blade angle of 30° for the non-cavitating cutting process and a layer thickness of 50 mm, in the 200 μm sand.

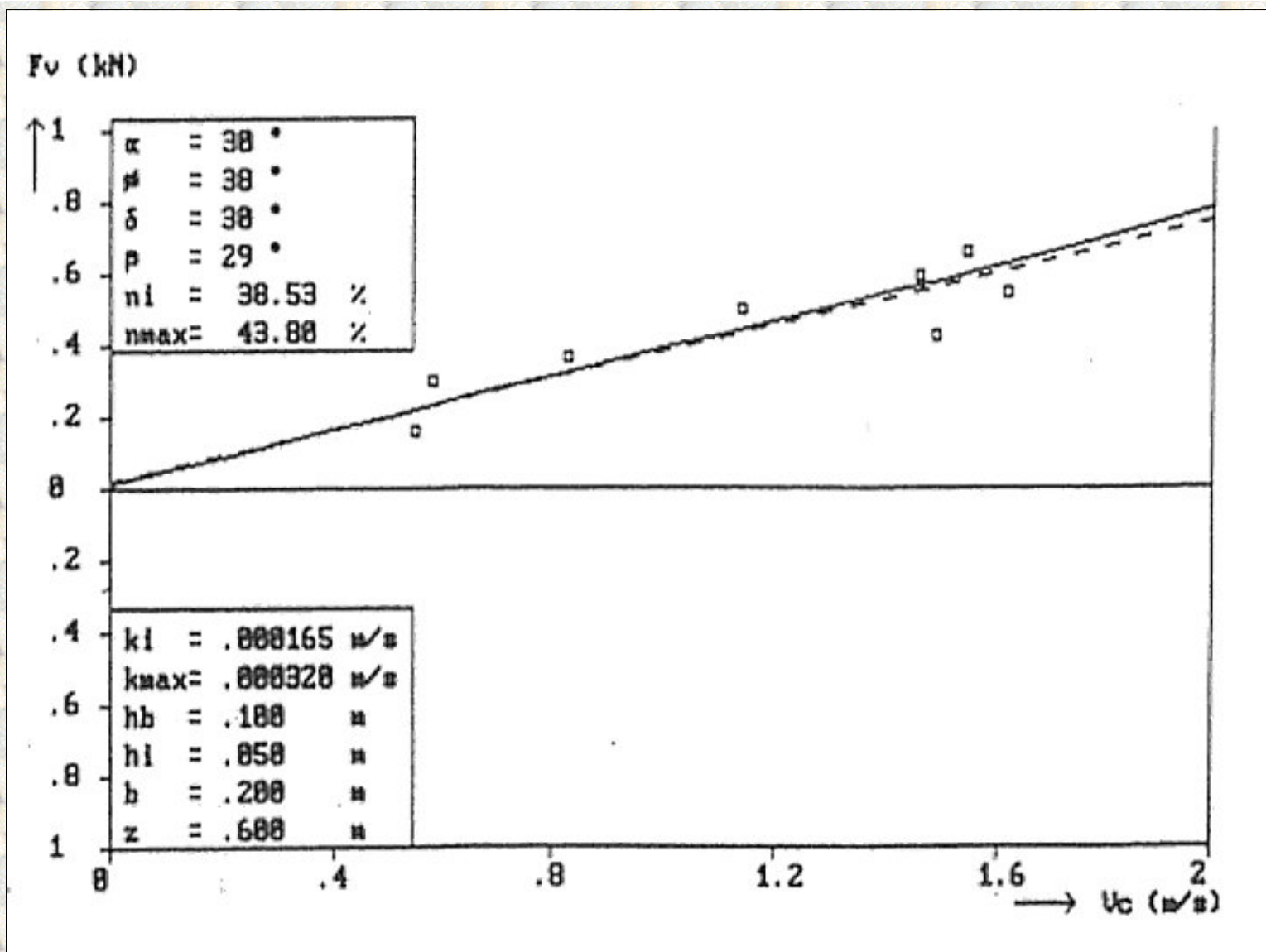


Figure B5.40: The vertical force F_v as a function of the cutting velocity v_c , at a blade angle of 30° for the non-cavitating cutting process and a layer thickness of 50 mm, in the 200 μm sand.

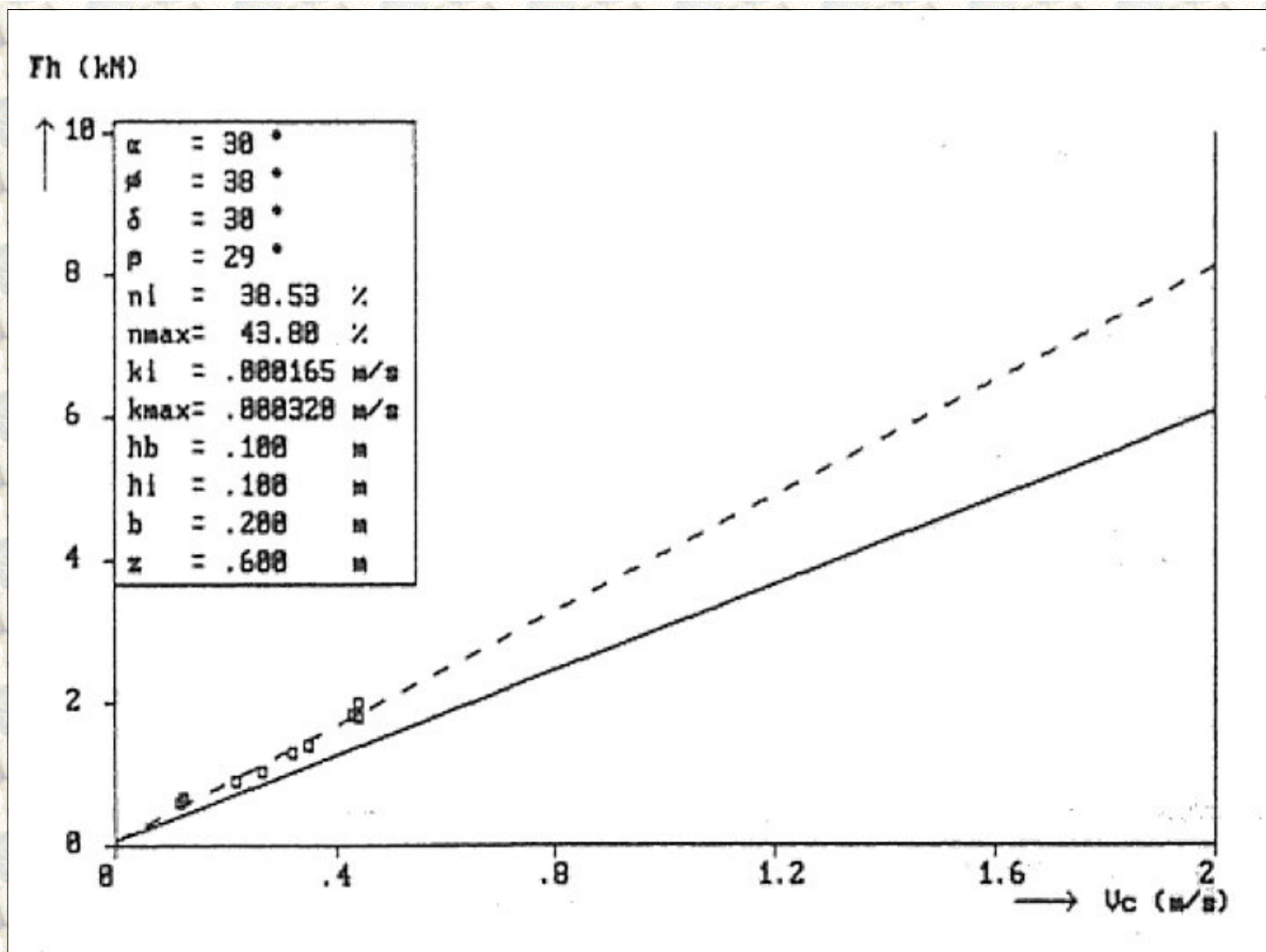


Figure B5.41: The horizontal force F_h as a function of the cutting velocity v_c , at a blade angle of 30° for the non-cavitating cutting process and a layer thickness of 100 mm, in the 200 μm sand.

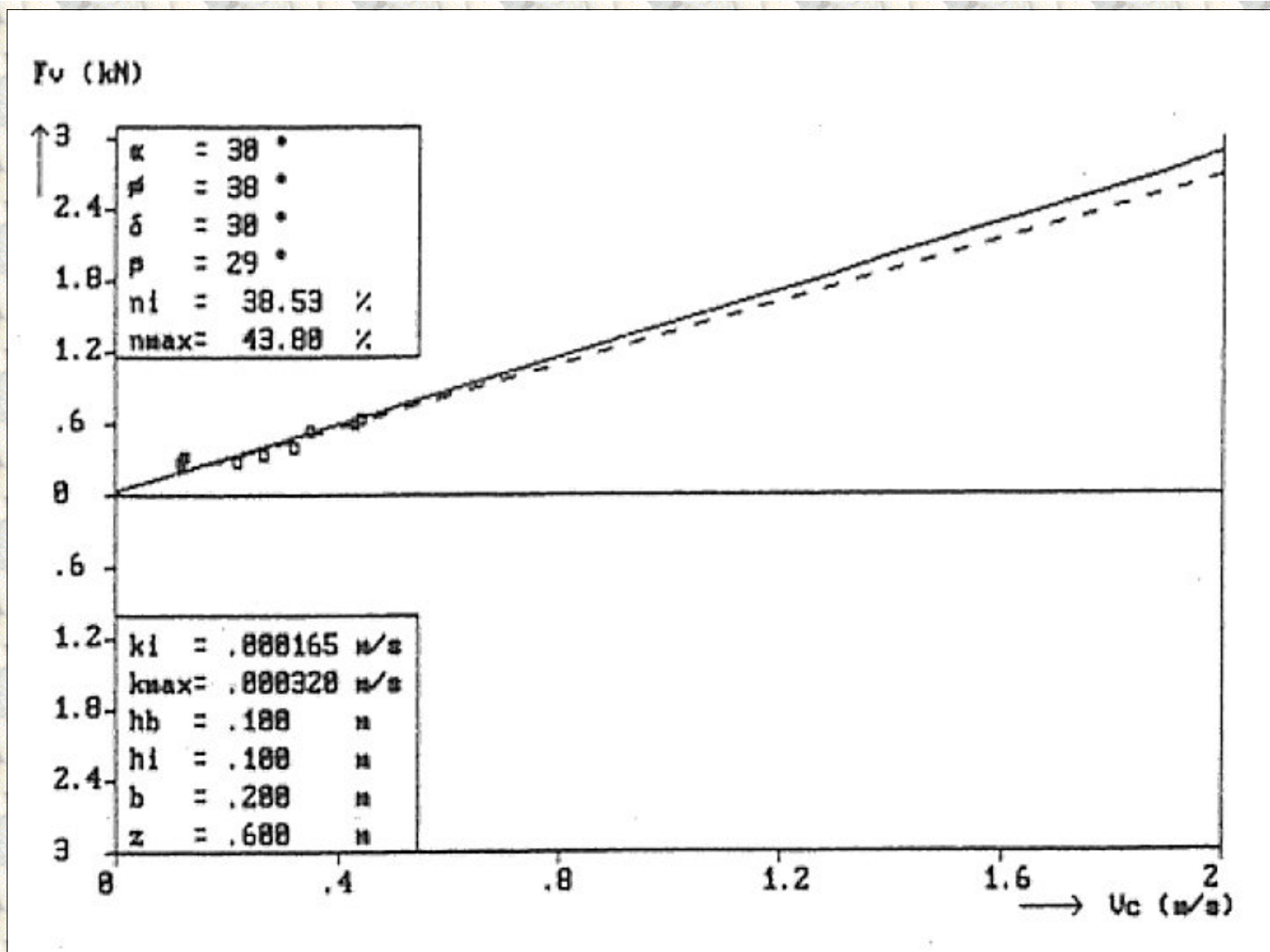


Figure B5.42: The vertical force F_v as a function of the cutting velocity v_c , at a blade angle of 30° for the non-cavitating cutting process and a layer thickness of 100 mm , in the 200 μ m sand.

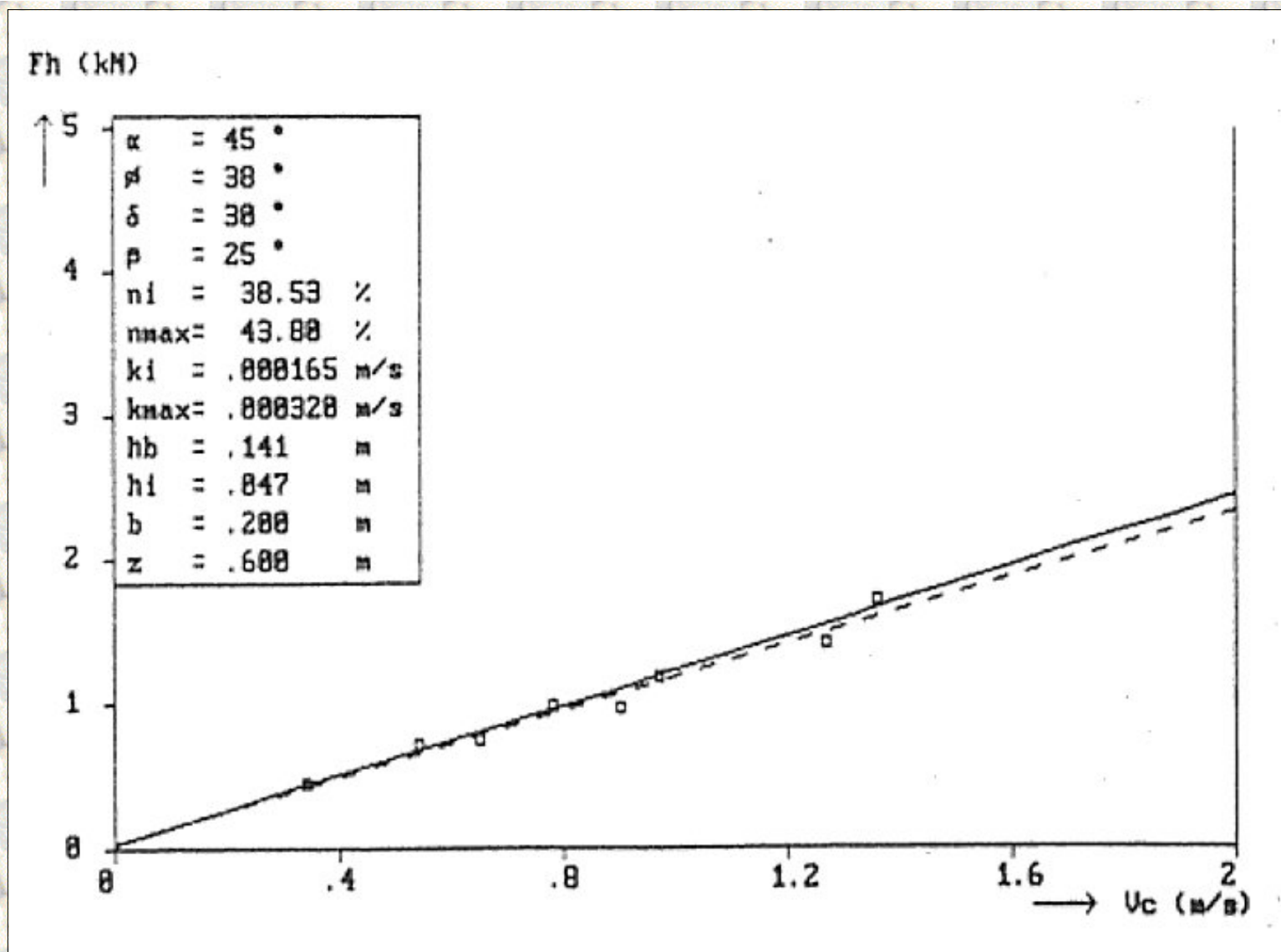


Figure B5.43: The horizontal force F_h as a function of the cutting velocity v_c , at a blade angle of 45° for the non-cavitating cutting process and a layer thickness of 47 mm, in the 200 μm sand.

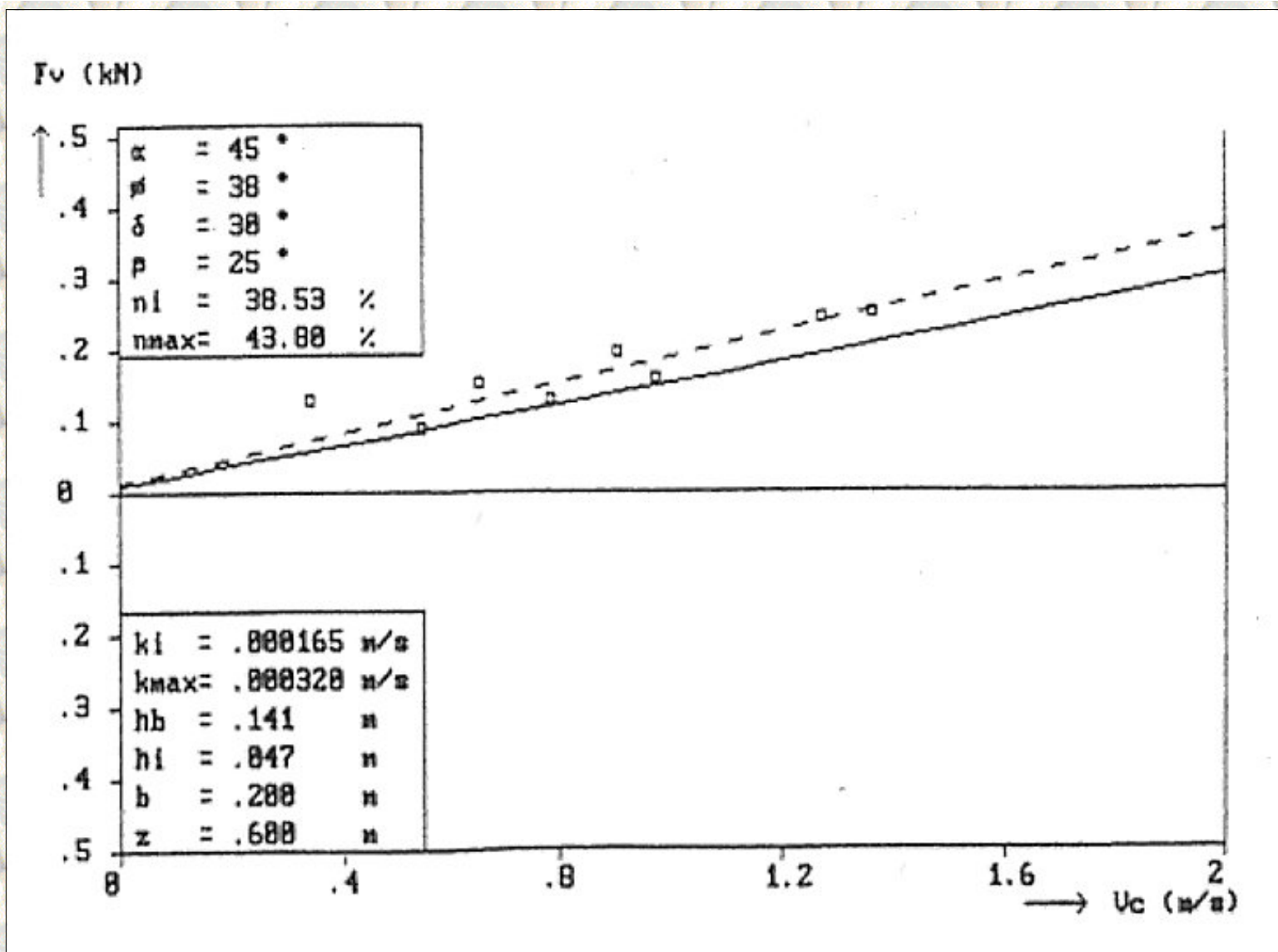


Figure B5.44: The vertical force F_v as a function of the cutting velocity v_c , at a blade angle of 45° for the non-cavitating cutting process and a layer thickness of 47 mm, in the 200 μm sand.

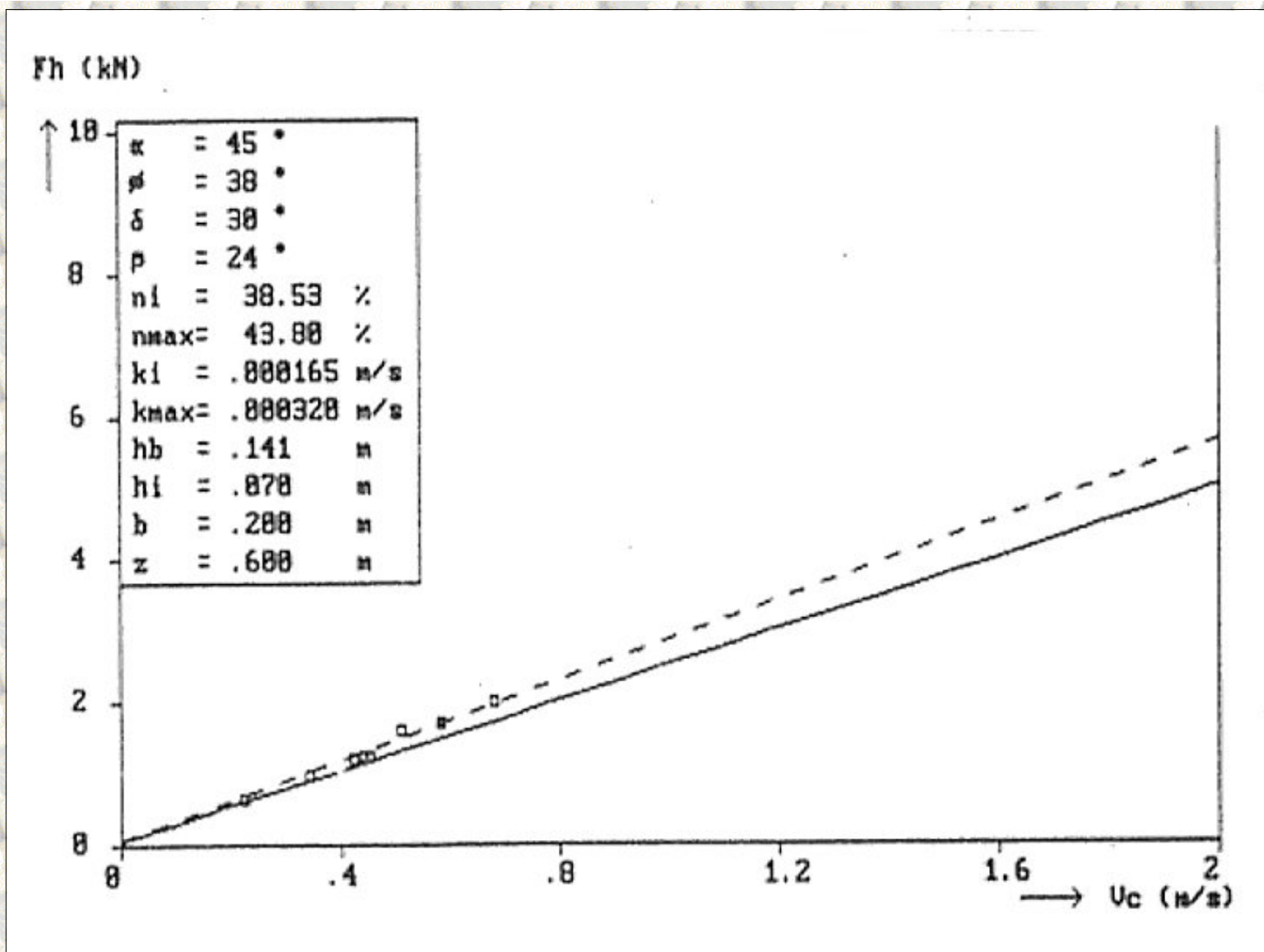


Figure B5.45: The horizontal force F_h as a function of the cutting velocity v_c , at a blade angle of 45° for the non-cavitating cutting process and a layer thickness of 70 mm, in the 200 μm sand.

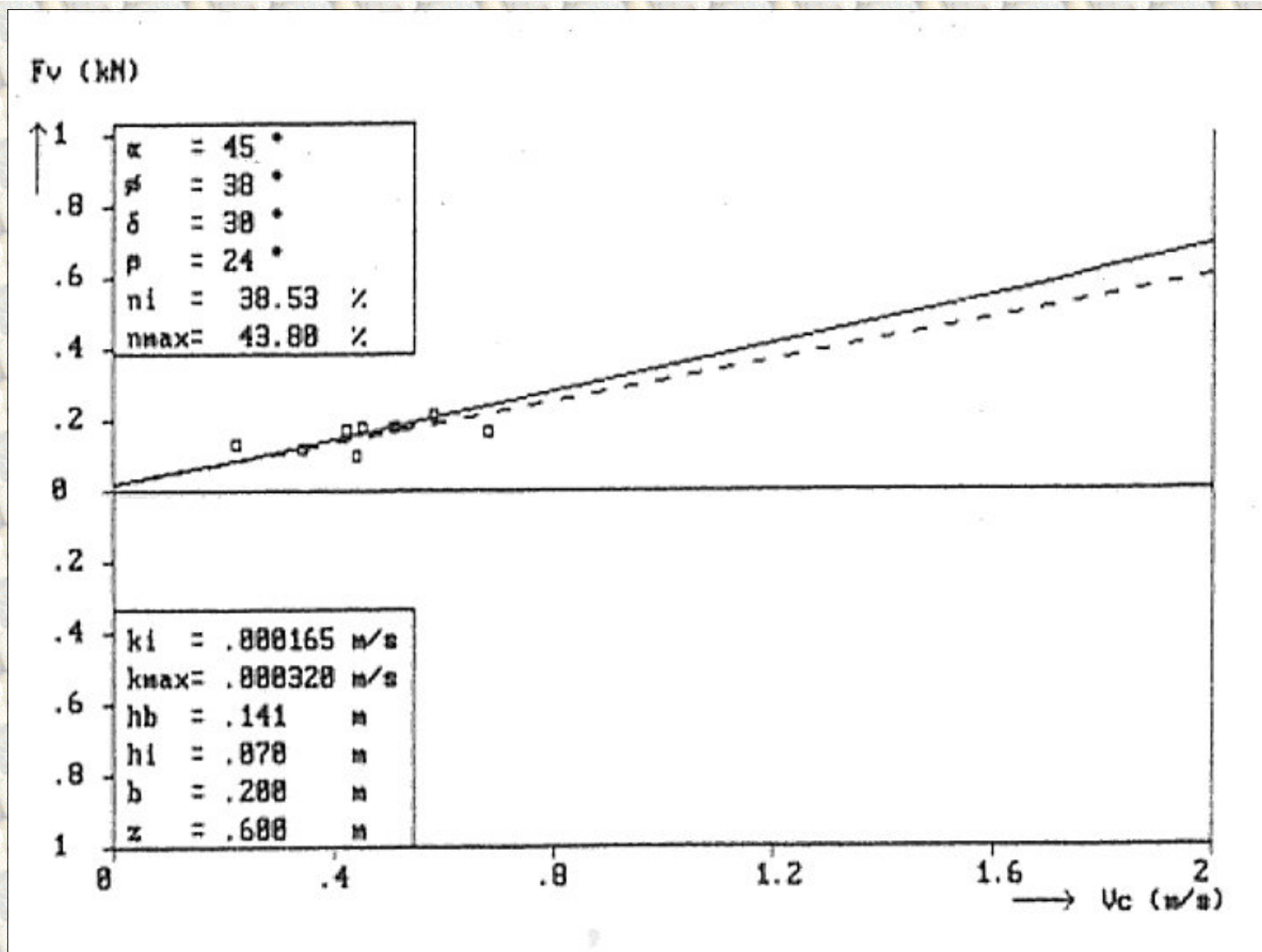


Figure B5.46: The vertical force F_v as a function of the cutting velocity v_c , at a blade angle of 45° for the non-cavitating cutting process and a layer thickness of 70 mm, in the 200 μm sand.

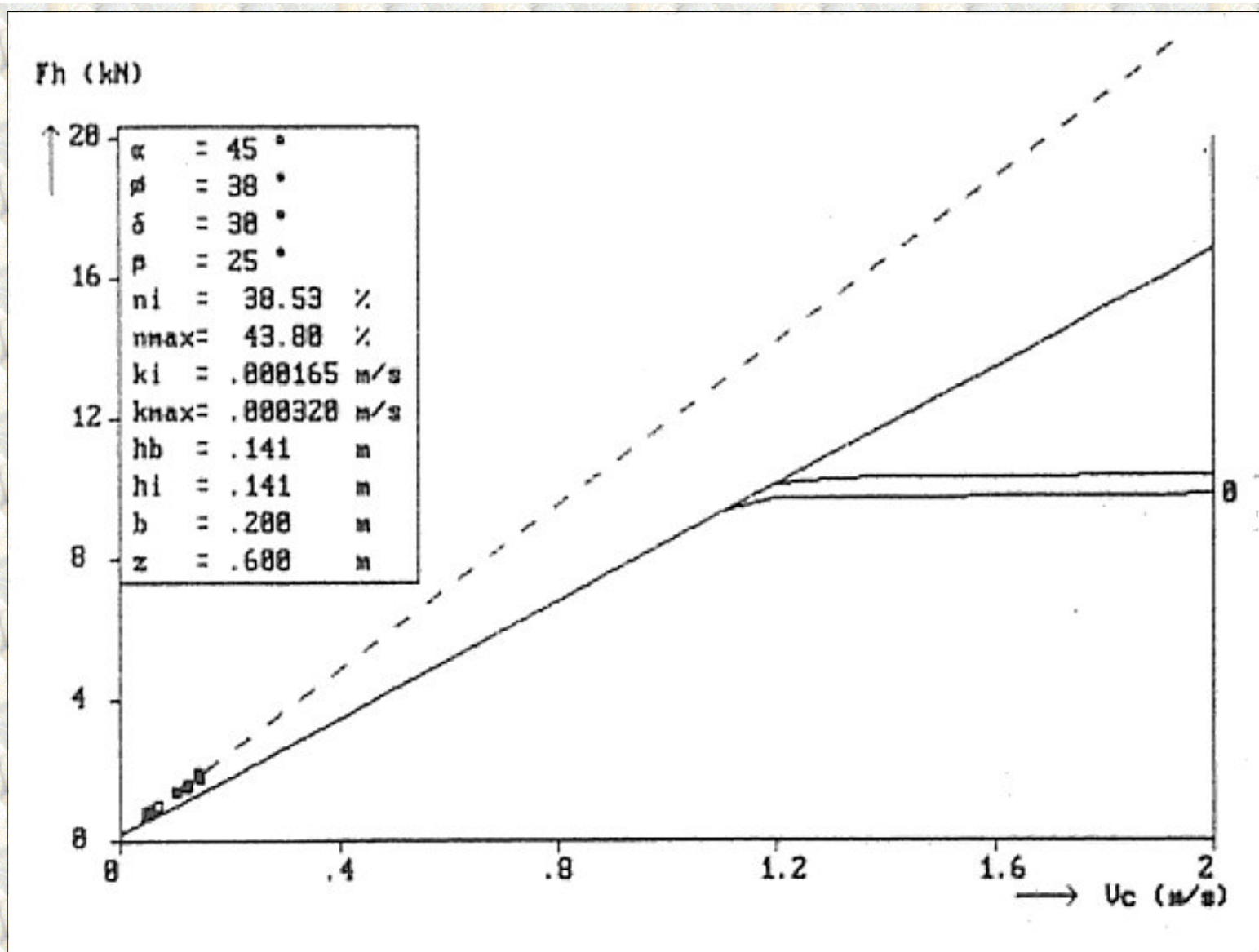


Figure B5.47: The horizontal force F_h as a function of the cutting velocity v_c , at a blade angle of 45° for the non-cavitating cutting process and a layer thickness of 141 mm, in the $200\ \mu\text{m}$ sand.

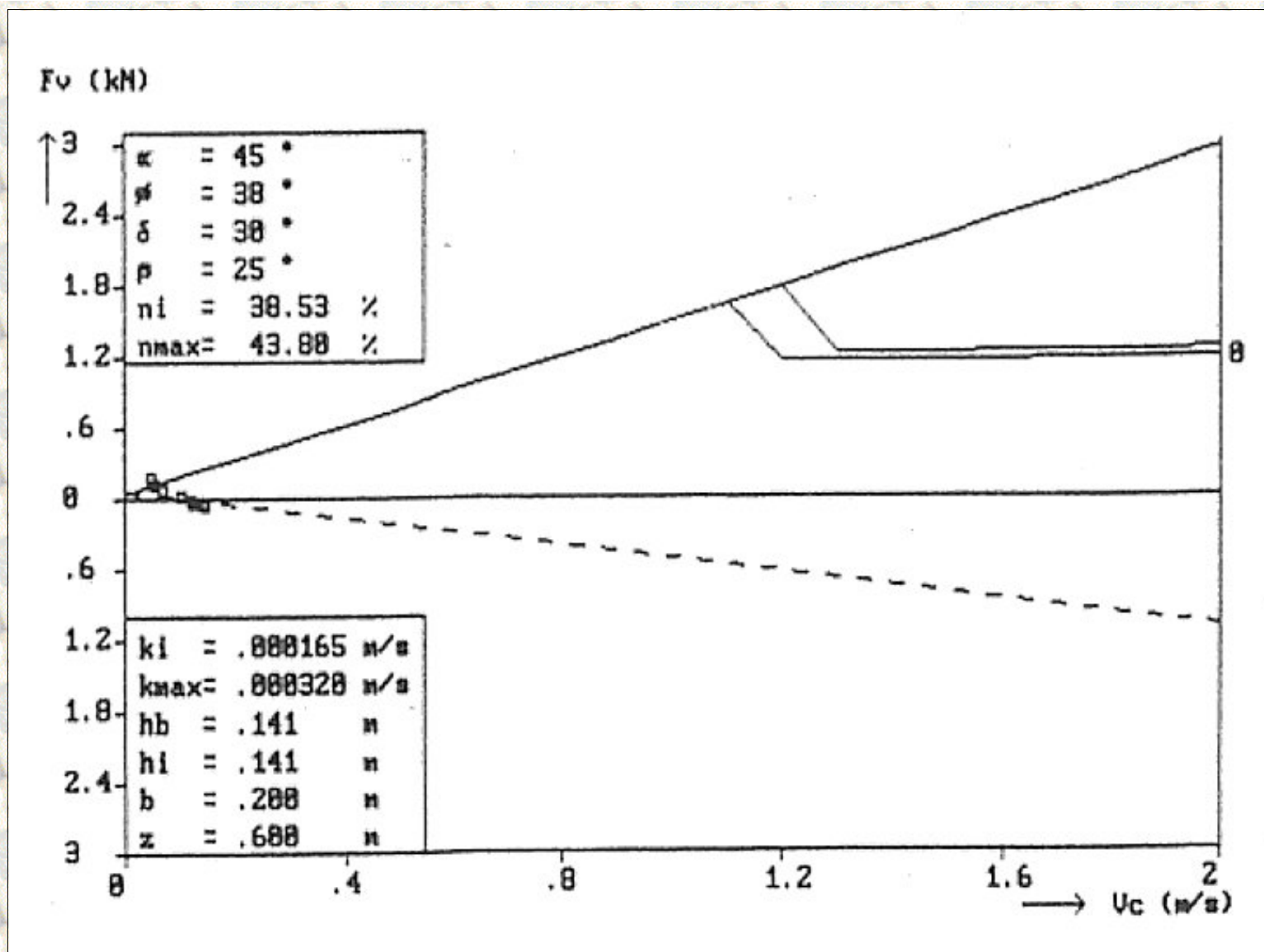


Figure B5.48: The vertical force F_v as a function of the cutting velocity v_c , at a blade angle of 45° for the non-cavitating cutting process and a layer thickness of 141 mm, in the 200 μm sand.

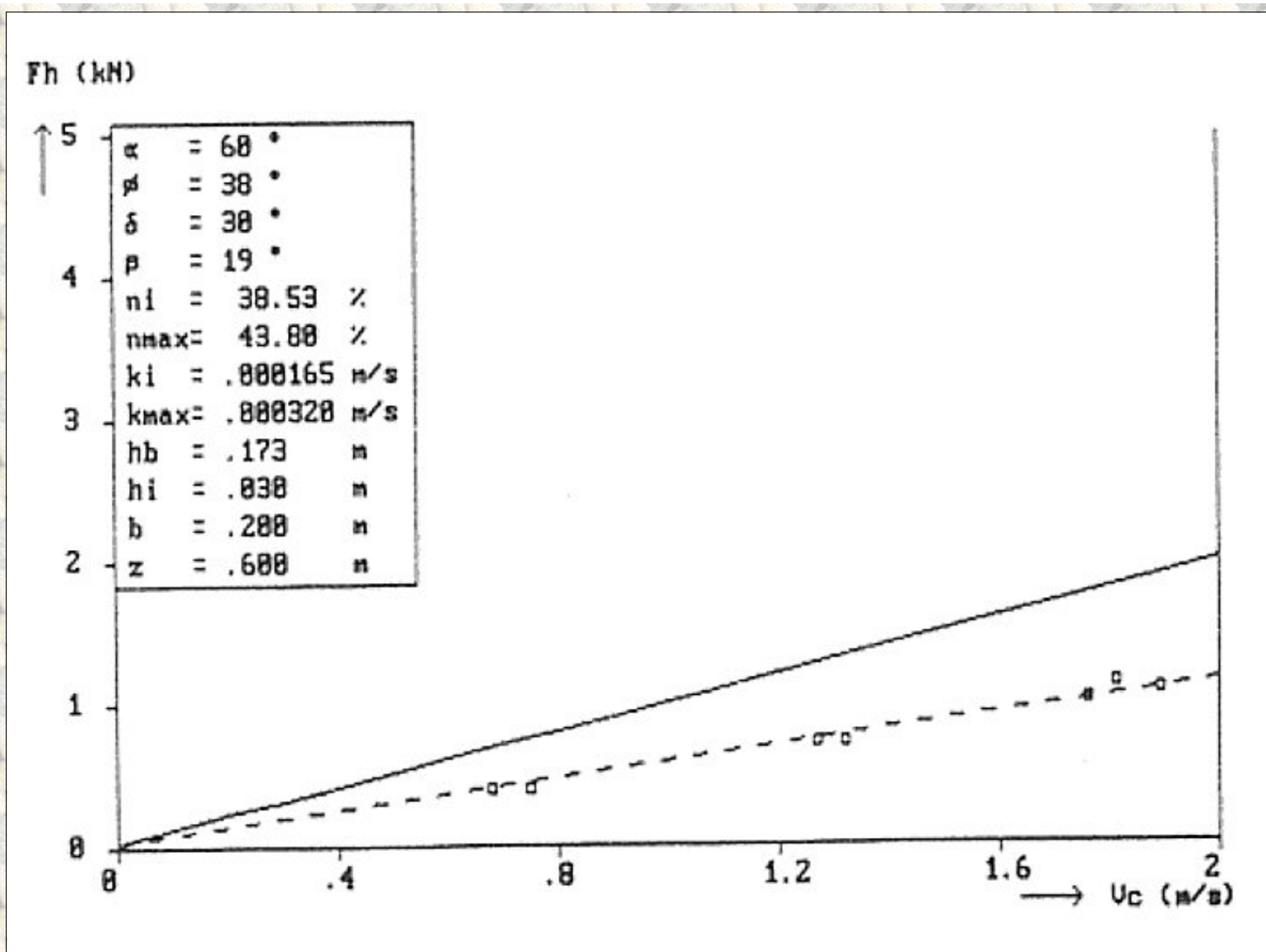


Figure B5.49: The horizontal force F_h as a function of the cutting velocity v_c , at a blade angle of 60° for the non-cavitating cutting process and a layer thickness of 58 mm, in the 200 μm sand.

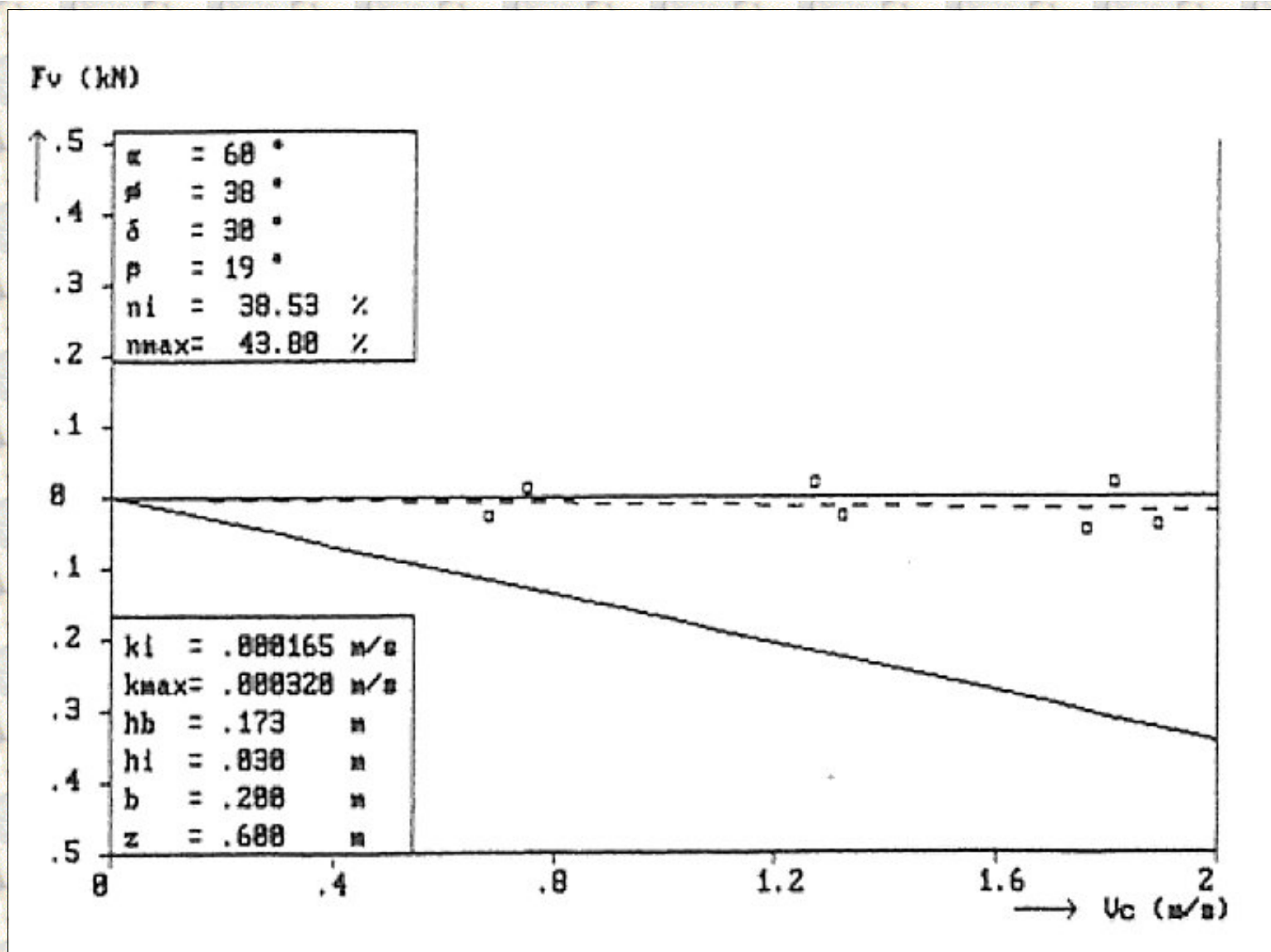


Figure B5.50: The vertical force F_v as a function of the cutting velocity v_c , at a blade angle of 60° for the non-cavitating cutting process and a layer thickness of 58 mm, in the 200 μm sand.

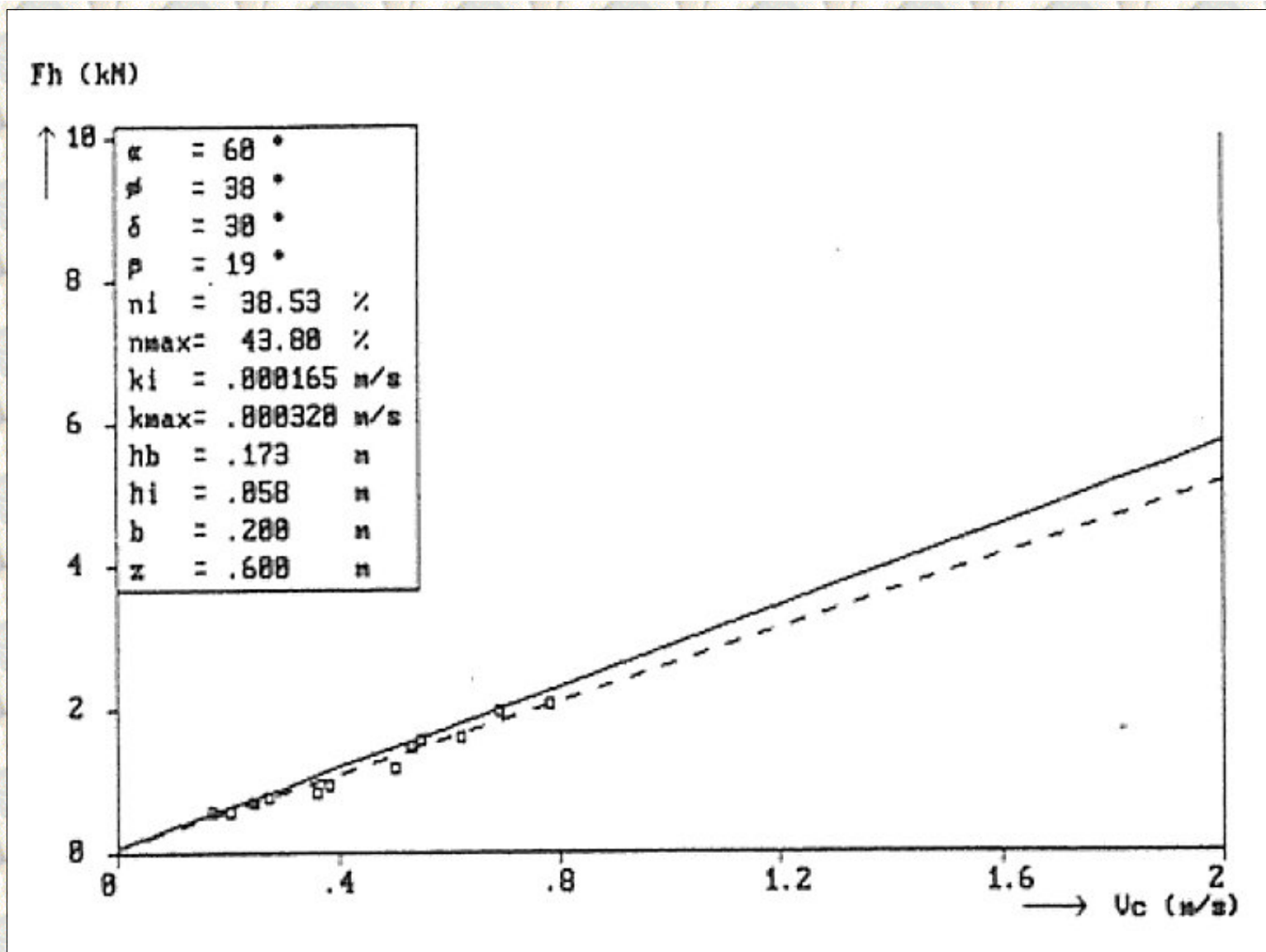


Figure B5.51: The horizontal force F_h as a function of the cutting velocity v_c , at a blade angle of 60° for the non-cavitating cutting process and a layer thickness of 87 mm, in the 200 μm sand.

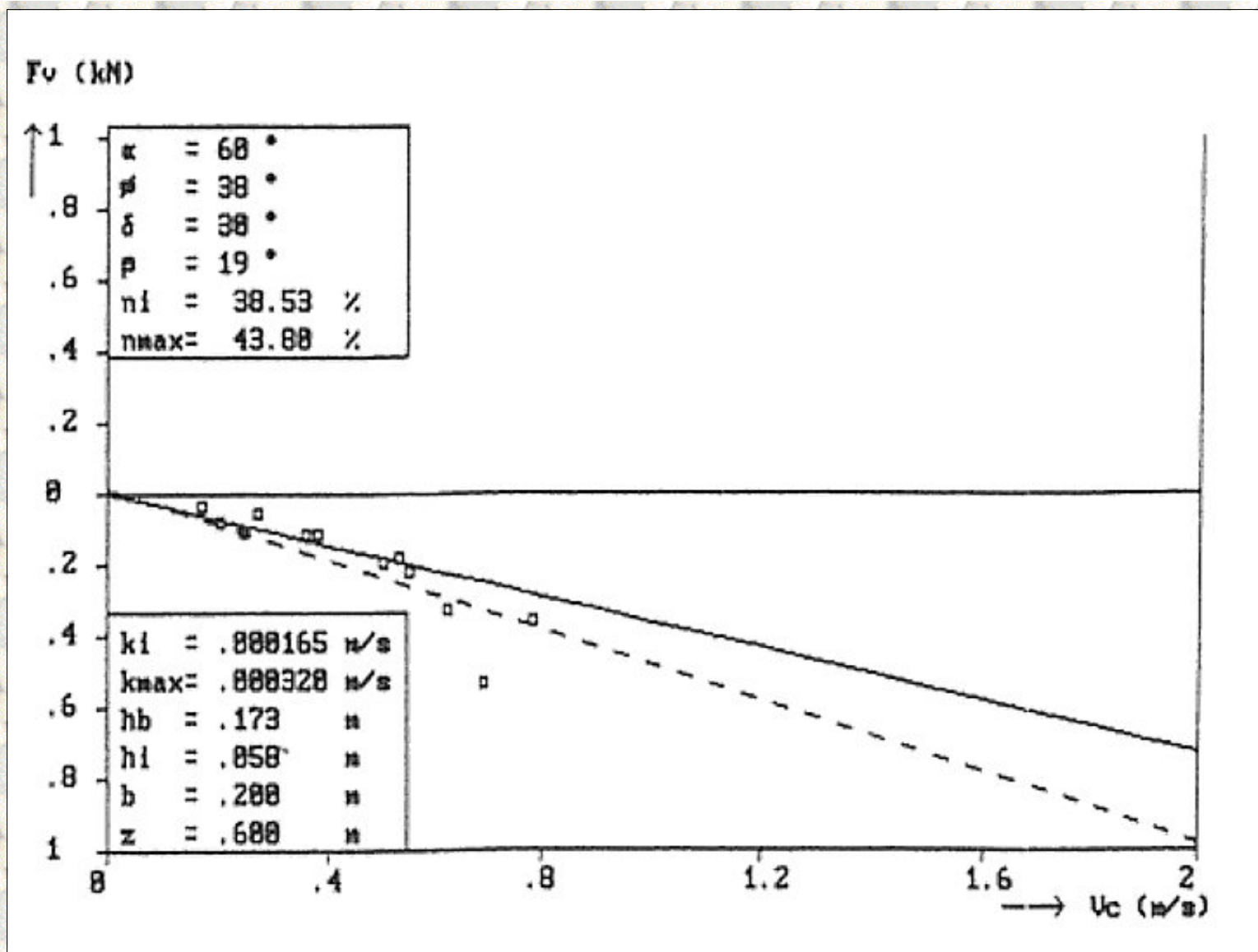


Figure B5.52: The vertical force F_v as a function of the cutting velocity v_c , at a blade angle of 60° for the non-cavitating cutting process and a layer thickness of 87 mm, in the 200 μm sand.

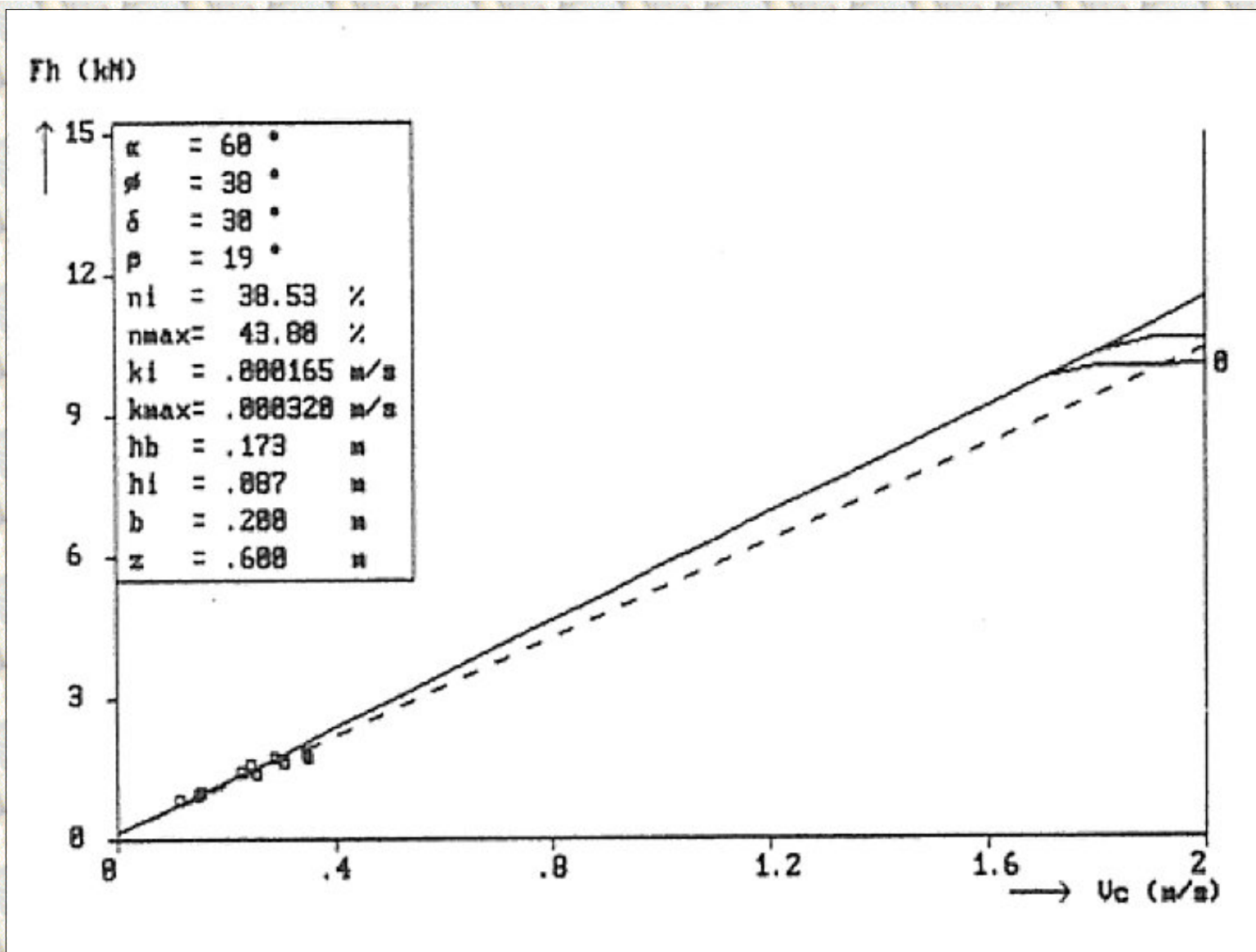


Figure B5.53: The horizontal force F_h as a function of the cutting velocity v_c , at a blade angle of 60° for the non-cavating cutting process and a layer thickness of 173 mm, in the 200 μ m sand.

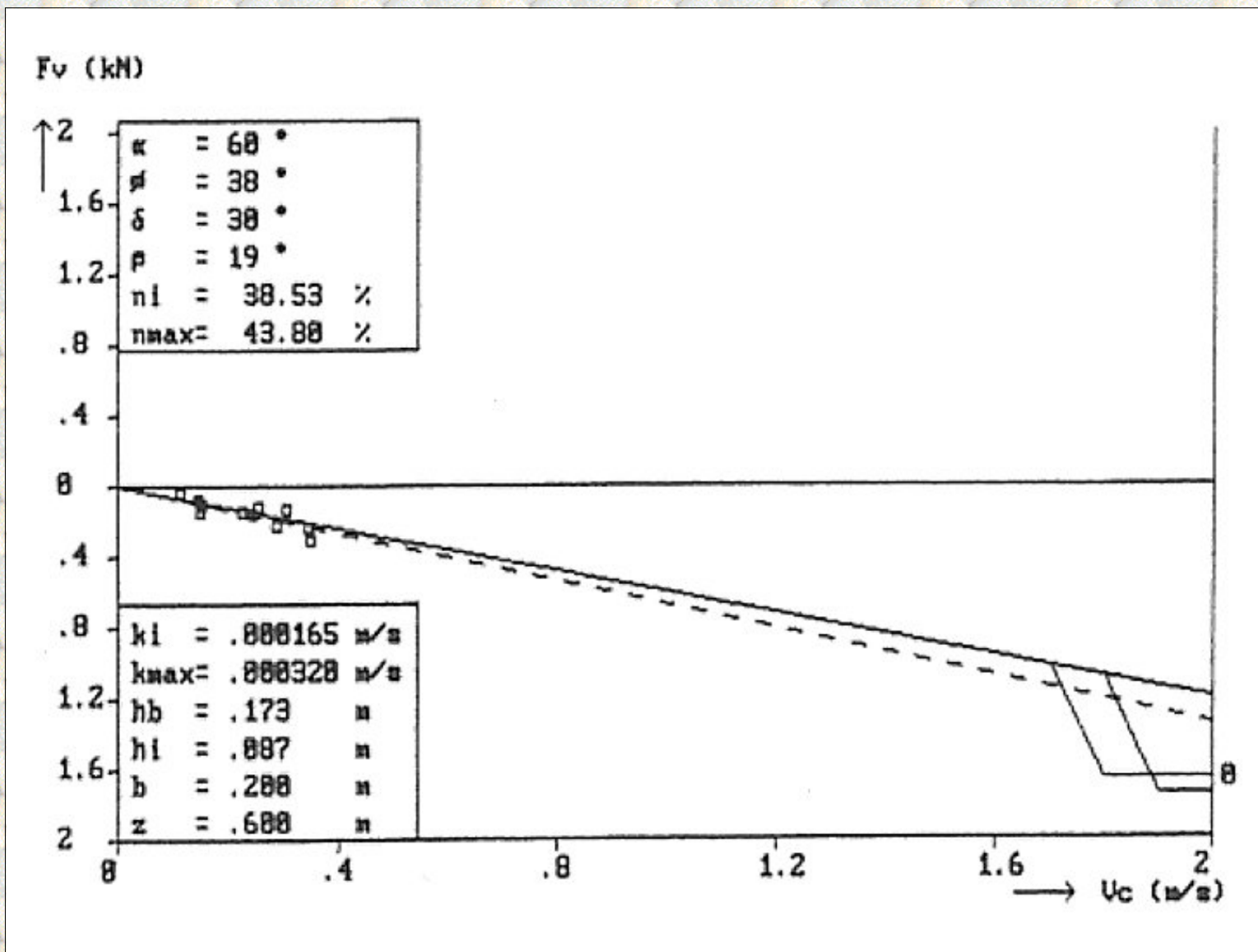


Figure B5.54: The vertical force F_v as a function of the cutting velocity v_c , at a blade angle of 60° for the non-cavitating cutting process and a layer thickness of 173 mm, in the 200 μm sand.

[Back to top](#)

This is a translation of the dissertation of Dr.ir. S.A. Miedema, dated September 15th 1987.

The dissertation was originally published in Dutch by the:

Delft University of Technology

Faculty of Mechanical Engineering and Marine Technology

Chair of Dredging Technology

Mekelweg 2

2628 CD, Delft

The Netherlands

Last modified Wednesday May 24, 2000 by: [Sape A. Miedema](#)

Translation by: [Laurens de Jonge](#)

Figures, equations and tables by: [Erik Miedema](#)

Copyright © May, 2000 Dr.ir. S.A. Miedema



[Download Adobe Acrobat Reader V4.0](#)

Curriculum Vitae.

Curriculum Vitae

08 November 1955 Born in Giekerk (Friesland).

1962 - 1968 Primary education in Leeuwarden.

1968 - 1974 Athenaeum-B in Leiden.

1974 - 1983 T.H. Delft, Afdeling der Werktuigbouwkunde (faculty of mechanical engineering), section "De Techniek van het Grondverzet" (Dredging Technology). The final thesis consisted of the development of a computer program (DREDMO) to simulate the motions of a cutter suction dredger in swell and the development of a swell compensated ladder using the DREDMO program. This study was concluded cum laude under the direction of Prof. Ir. J. de Koning.

1983 - 1987 Employed at the T.U. Delft in the faculty of Mechanical Engineering, section Transport Technology, O&O group Dredging as a Ph.D. student. The research performed in this period is described in this dissertation and consists of the further development of DREDMO with the emphasis on the numerical methods and the modeling of the cutterhead / soil interaction. Also since 1985 member of the administrative board and the section board of the section Transport Technology and member of several work committees.

1987 - At present employed at the T.U. Delft in the faculty of Mechanical engineering, section Transport Technology, Dredging Technology as an Assistant Professor and since 92 Associate Professor, among other things responsible for the stimulation and assistance of staff, AIO's and students concerning computer usage.

1996 - present Director of education of Mechanical Engineering and Marine Technology at the Delft University of Technology.

[Back to top](#)

**This is a translation of the dissertation of Dr.ir. S.A. Miedema, dated September 15th 1987 .
The dissertation was originally published in Dutch by the:
Delft University of Technology
Faculty of Mechanical Engineering and Marine Technology**

Chair of Dredging Technology
Mekelweg 2
2628 CD, Delft
The Netherlands

Last modified Wednesday May 24, 2000 by: [Sape A. Miedema](#)

Translation by: [Laurens de Jonge](#)

Figures, equations and tables by: [Erik Miedema](#)

Copyright © May, 2000 [Dr.ir. S.A. Miedema](#)



[Download Adobe Acrobat Reader V4.0](#)

1. The compensation of the motions of a helix cutterhead of a cutter suction dredger in swell for the under cutting process gives complications owing to the force-path relation in the soil, this in contrast to the upper cutting process. From this it can be concluded that the cutting process for a swell compensated bucket wheel dredger is preferably performed upper cutting, in contrast to the customary undercutting process.
2. The prediction step in the solution of the equations of motion of ships can be looked upon as an iteration step, in which time dependent effects are included.
3. The uncoupling, often used in the solution of the equations of motion for ship motions, between the motions along the length of the ship and athwartships, cannot be used for a cutter suction dredger or an bucket wheel dredger, because in these cases the soil reactions on the cutterhead or the bucket wheel cause a coupling between these motions.
4. The phase shift, present between the motions of the cutterhead and the loads on the cutterhead, will lead to a less quick presence of resonance in the swing direction in the simulation of the motions of the cutter suction dredger in swell, than is currently used in the modeling within the DREDMO computer program.
5. Modeling is the attempt to describe reality without containing the pretension to be the reality.
6. The significance that can be attached to the results of a calculation has to be related to the modeling that forms the basis of the calculation method.
7. The accuracy of the results of a calculation is never more accurate than the accuracy of the input data of a calculation. This statement does, however, not imply that it is useless to calculate more accurate within a calculation than the input data would suggest, because certain tendencies can take place within the accuracy of the input data.
8. Just like the introduction of pocket calculators has replaced the calculation by hand and with that has taken away the feeling for numbers, the feeling for the syntax of the language is taken away by the spelling check and the automatic hyphenation in text editors.

9. An obstacle in the development of criteria, based upon the syntax of the language, for the hyphenation of words is the joining point of compound words.
10. The difficulty in the execution of a policy, as a result of the hierarchical structure within the T.U. Delft, leads to stagnation in the scientific research.
11. The economy measures in the scientific education have lead to a control system, in which the available funds have to be accounted for, in such a way that the ratio between the time spend on education and research compared to the time spend on the time accounting grows crooked. In other words one has to account for the things that could have been done in the time spend on the accounting.
12. The crooked grow of the age distribution, by among other things the years long vacancy stop, within the T.U. Delft has serious consequences for the function of the Technical University within the fast developing information society.

S.A. Miedema, 15-09-1987.

Calculation of the cutting forces when cutting water saturated sand.

Basic theory and applications for 3-dimensional blade movements and periodically varying velocities for, in dredging commonly used excavating means.

[Back to top](#)

This is a translation of the dissertation of Dr.ir. S.A. Miedema, dated September 15th 1987 .

The dissertation was originally published in Dutch by the:

Delft University of Technology

Faculty of Mechanical Engineering and Marine Technology

Chair of Dredging Technology

Mekelweg 2

2628 CD, Delft

The Netherlands

Last modified Wednesday May 24, 2000 by: [Sape A. Miedema](#)

Translation by: [Laurens de Jonge](#)

Figures, equations and tables by: [Erik Miedema](#)

Copyright © May, 2000 Dr.ir. S.A. Miedema



[Download Adobe Acrobat Reader V4.0](#)